General Disclaimer

One or more of the Following Statements may affect this Document

- This document has been reproduced from the best copy furnished by the organizational source. It is being released in the interest of making available as much information as possible.

- This document may contain data, which exceeds the sheet parameters. It was furnished in this condition by the organizational source and is the best copy available.

- This document may contain tone-on-tone or color graphs, charts and/or pictures, which have been reproduced in black and white.

- This document is paginated as submitted by the original source.

- Portions of this document are not fully legible due to the historical nature of some of the material. However, it is the best reproduction available from the original submission.

CR 73275

AVAILABLE TO THE PUBLIC

BOEING

COMMERCIAL
AIRPLANE DIVISION

AN ANALYSIS OF METHODS FOR PREDICTING THE STABILITY CHARACTERISTICS OF AN ELASTIC AIRPLANE

APPENDIX B
METHODS FOR DETERMINING STABILITY DERIVATIVES

BY

Members of the Aerodynamics
and Structures Research Organizations

D6-20659-3

November 1968

Prepared Under Contract No. NAS 2-3662 by

The Boeing Company
Commercial Airplane Division
P.O. Box 707
Renton, Washington

for

AMES RESEARCH CENTER
NATIONAL AERONAUTICS AND SPACE ADMINISTRATION

TABLE OF CONTENTS

FIGURES

FIGURES (Continued)

FIGURES (Continued)

FIGURES (Continued)

TABLES

TABLES

1. INTRODUCTION

This appendix presents the details of the theoretical, semi-empirical, and experimental techniques used to calculate stability derivatives. The purpose is to evaluate methods for estimating stability derivatives of rigid and elastic airplanes.

As reported in app. A, airplane stability derivatives are not all equally important. For example, the derivative C_{m_α} is generally accepted to be of considerably more importance to stability and control than is the derivative C_{D_q}. Also, the accuracy with which stability derivatives can be estimated under the current state of the art varies considerably between derivatives. Table 1 shows an estimate of relative importance and prediction accuracy under the current state of the art from a qualitative viewpoint.

To calculate the stability derivatives (in the widest sense of the word), it may be necessary to use several mathematical models to represent the airplane. For a thorough understanding of the mathematical models — their limitations and applications — the connection between models must be established. The following discussion provides this connection and identifies the location and interrelationship of material presented in this report.

It will be assumed that the completely elastic airplane has $6 + 6n$ degrees of freedom, where n denotes the number of elastically connected mass elements used to represent the airplane. There are six rigid-body (or equivalent elastic airplane) degrees of freedom and $6n$ "elastic degrees of freedom". If the c.g. is considered as a mass point, this mass could be considered as one of the n elastically connected mass elements and the $6 + 6n$ "elastic degrees of freedom" could be reduced to $6n$. However, it is more convenient to use $6 + 6n$ when considering the rigid, equivalent elastic, and structural relationships. Although the number n is infinitely large, in practical applications it is limited by computer capacity.

Appendix A also proved that the coupling between rigid-body degrees of freedom and elastic degrees of freedom occurs only in the generalized forces. The structural degrees of freedom were found to be most conveniently described in terms of the normal modes that were shown to arise from an eigenvalue problem, the corresponding eigenvectors being the mode shapes.

TABLE 1.–RELATIVE IMPORTANCE AND PREDICTION ACCURACY OF STABILITY DERIVATIVES

Longitudinal			Lateral-directional		
Derivative	Relative importance	Estimated accuracy*	Derivative	Relative importance	Estimated accuracy*
C_{L_α}	Primary	Good	C_{n_β}	Primary	Good
C_{m_α}	Primary	Good	C_{l_β}	Primary	Good
C_{m_q}	Primary	Good	C_{l_p}	Primary	Good
C_{m_u}	Primary	Good	C_{n_r}	Primary	Fair
$C_{m_{\dot\alpha}}$	Primary	Fair	C_{n_p}	Primary	Poor
C_{D_u}	Primary	Good	C_{l_r}	Primary	Poor
C_{D_α}	Secondary	Good	C_{Y_β}	Primary	Good
C_{L_u}	Secondary	Good	C_{Y_p}	Secondary	Poor
$C_{L_{\dot\alpha}}$	Secondary	Poor	$C_{n_{\dot\beta}}$	Secondary	Poor
C_{L_q}	Secondary	Good	C_{Y_r}	Secondary	Fair
$C_{D_{\dot\alpha}}$	Minor	Poor	$C_{Y_{\dot\beta}}$	Minor	Poor
C_{D_q}	Minor	Fair	$C_{l_{\dot\beta}}$	Minor	Poor

*Estimated prediction accuracy assumes use of theoretical, handbook, and wind tunnel data.

As a consequence, the structural degrees of freedom are represented in the equations of motion as products of eigenvectors (mode shapes) and time-dependent functions. These time-dependent functions are used as the generalized coordinates. An important consequence of using these normal mode shapes was shown to be a practical reduction in the number of degrees of freedom needed to adequately describe aerodynamic forces generated by structural dynamics.

Now, if it is assumed that there is sufficient accuracy that it is reasonable to speak of, say, 100 modes, then the following question arises: How important are all these structural degrees of freedom to stability and control problems? The answer to this question depends to a large extent on the type of problem. For example, it has been found that flutter (structural stability) calculations require that many normal modes be included. In airplane performance problems, it is very unlikely that any of the normal modes play a significant role. To the performance analyst, only the steady-state elastic deformation is important. The stability and control engineer and flight-control-systems designer operate somewhere between these extremes. To the stability and control engineer, who is mainly interested in the motions of the center of mass, the number of important normal modes is generally very small and can sometimes even be disregarded. In the latter case, the elastic airplane reduces to the so-called equivalent elastic airplane for which loads and deformations are always assumed to be in phase. This means that only the steady-state elastic behavior is to be considered and the problem of (elastic) airplane stability and control reduces to one of six degrees of freedom. To the stability and control engineer interested in handling and ride qualities of a large flexible airplane, the motions of the structure as experienced at the pilots station can be very significant. In that case, the number of structural degrees of freedom to be accounted for is definitely not zero, but probably consists only of low-frequency normal modes. This assumes that the high-frequency normal modes contribute little to deformations, a condition that is usually satisfied. (S7)

The flight-control systems designer should account for the interaction between control systems, sensors, and structure in solving the problems of aircraft c.g. control, gust-response control (which is a combination of c.g.

and structural mode control), and modal-response control. In these problems, the number of structural degrees of freedom to be accounted for can be large, but will not usually be as large as required by the flutter engineer.

The interrelationships among the various mathematical models of the airplane as discussed here are shown in fig. 1. The mathematical model selected by the engineer to solve a certain problem depends strongly on that problem. This is illustrated also by fig. 2, which shows the relative frequency range associated with a number of typical problem areas.

For each of the applications mentioned so far, the engineer must decide what mathematical airplane model to use to obtain a satisfactory representation of the physical problem involved. If it is decided to use only 10 normal modes out of, say, n = 100 available, then another important decision must be made. The m = 90 modes that are neglected have quasi-static deflections that may or may not be negligible. If all n = 100 dynamic modes are neglected, it has already been shown that the mathematical airplane model reduces to that of the equivalent elastic airplane (fig. 1). This means that the stability derivatives of the rigid degrees of freedom are corrected for the steady-state aeroelastic effects by assuming that all loads and deformations are in phase with each other. Neglecting only m instead of all n normal modes does not alter the fact that there exist nonnegligible steady-state aeroelastic effects corresponding to these m modes. A method exists for correcting the rigid degree-of-freedom stability derivatives to account for the steady-state aeroelastic effects of the m modes that are left out of the mathematical model. This model is based on the residual flexibility theory indicated in fig. 1.

Evaluation of methods for predicting stability derivatives implies a comparison of theoretical and experimental results. This can be done only on specific configurations. Two airplane configurations have been selected for this study: the Boeing 707-320B and a typical variable sweep SST configuration referred to as the SST. The SST data presented in this study are not necessarily related to the Boeing Model B2707, but are based on one of many SST study configurations considered by Boeing. Three views of the configurations used for the evaluation are presented in Sec. 7.

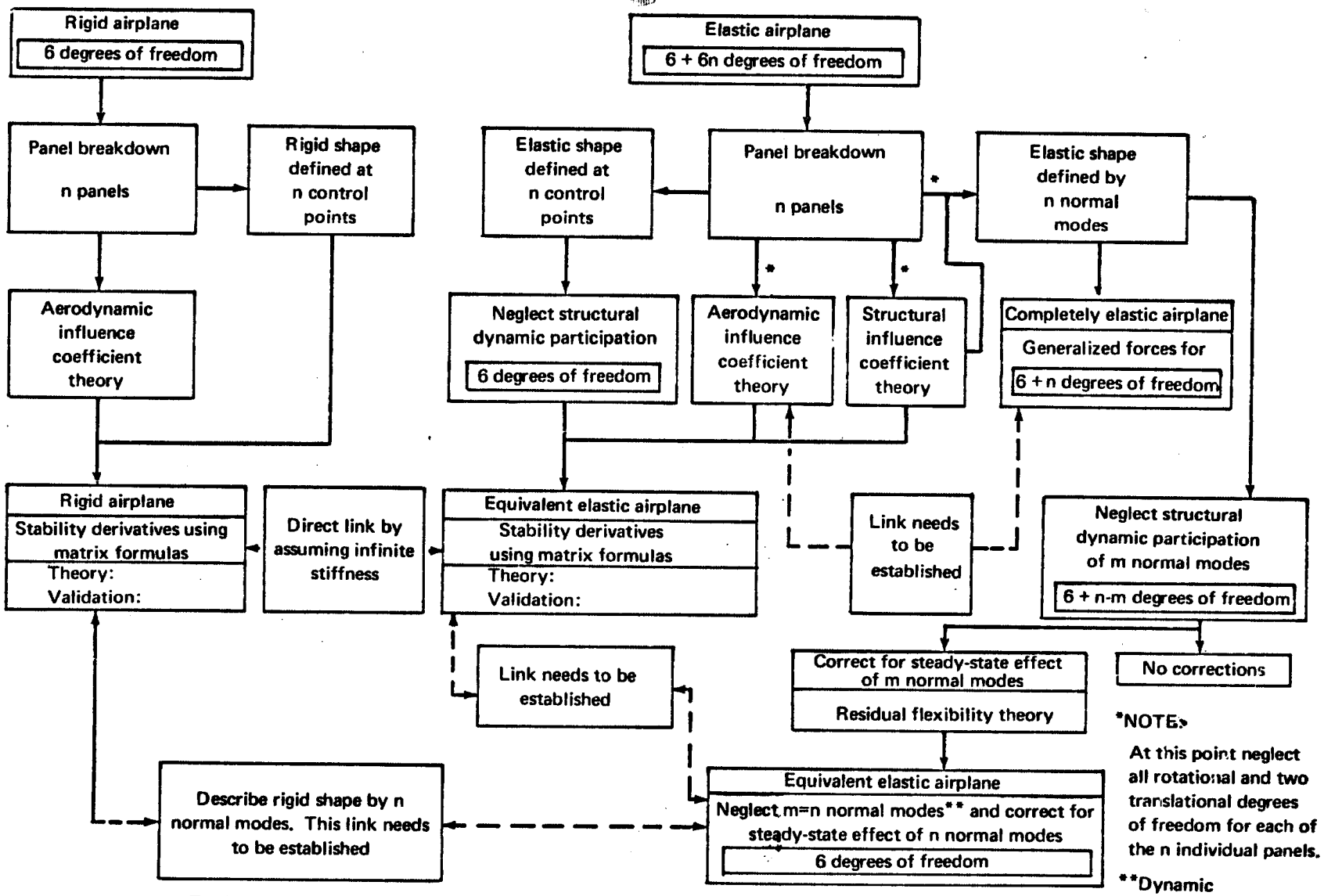

FIGURE 1. – INTERRELATION OF MATHEMATICAL MODELS FOR RIGID AND ELASTIC AIRPLANES

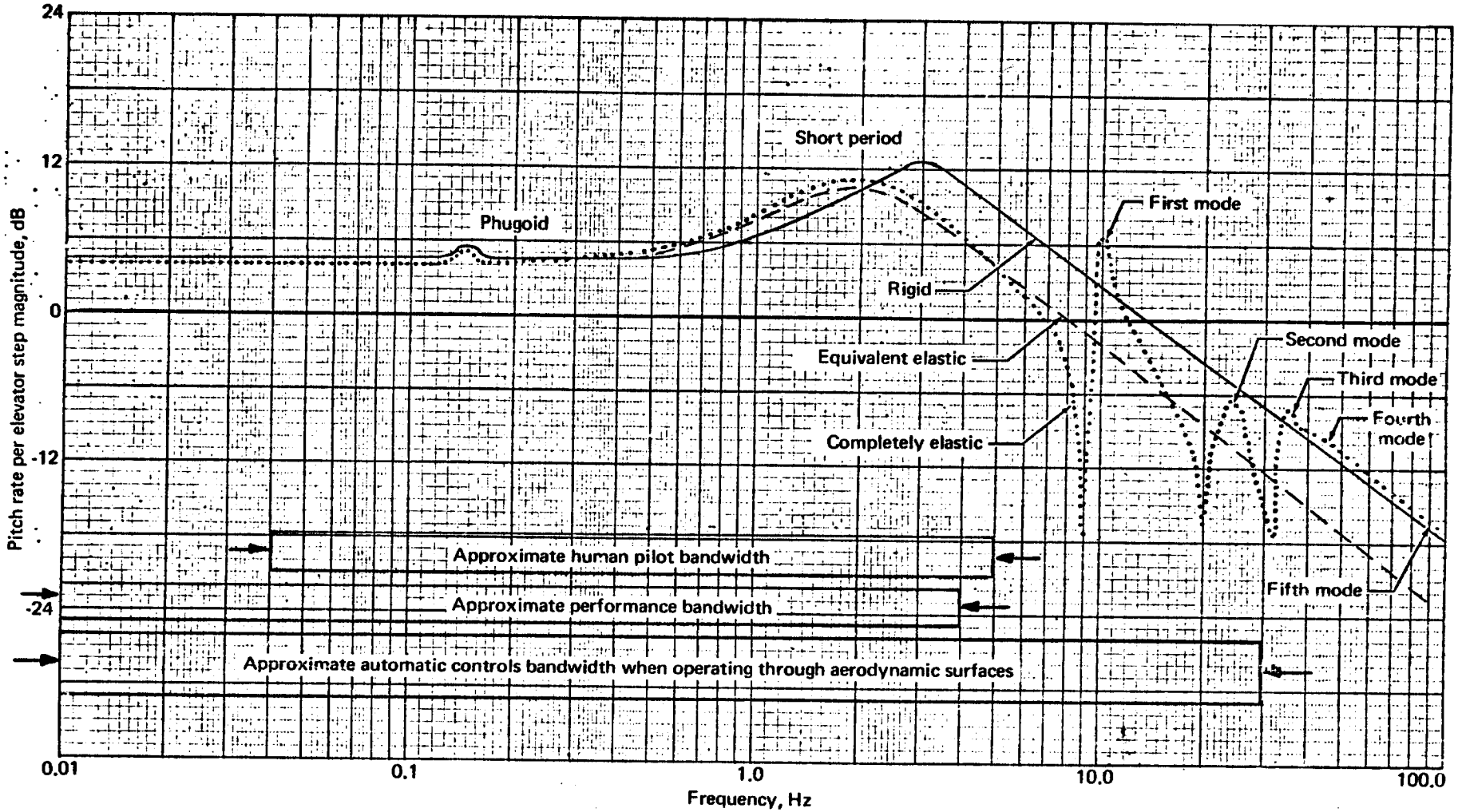

FIGURE 2.– BODE PLOT OF THE PITCH RATE TO ELEVATOR TRANSFER FUNCTION OF A TYPICAL ELASTIC AIRPLANE

Section 2 presents a list of symbols used in this report. The list is the same for each appendix and therefore not all the symbols shown are used in this appendix.

Section 3 lists the complete set of assumptions used in this report; not all are important to this appendix. All assumptions are numbered (XXX) and are inserted at appropriate places in the text. Where they affect conclusions, restrictions, or techniques, their number is placed in a circle in the margin.

Section 4 presents the theoretical methods used to calculate stability derivatives. Primary emphasis is placed upon lifting surface theory applied to thin (flat plate) bodies. A discussion of one "thick" wing-body technique is presented.

Section 5 presents the semi-empirical techniques presently used to calculate the stability derivatives. Primary emphasis is placed upon the United States Air Force Stability and Control Handbook (ref. 6).

In Sec. 6 the experimental techniques of wind tunnel and flight test stability derivative analysis are outlined.

Section 7 contrasts the theoretical, semi-empirical, and experimental techniques used to calculate stability derivatives for the equivalent elastic and the rigid mathematical models of an elastic aircraft. A typical SST configuration and the Boeing 707-320B are used in the analysis. Experimental results, when available, are used as a basis in the discussion of the accuracy of the various techniques.

Conclusions and recommendations for further work are given in Sec. 8.

References 1 through 76 for the entire report are listed in Sec. 9. For convenience in working with the summary handbook and the other appendixes, the reference list numbering was standardized for all volumes of this report.

It is anticipated that the discussion will (1) outline the most accurate technique for each derivative, (2) define the assumptions required by each technique to evaluate each stability derivative, (3) imply which technique holds the greatest promises for future development, and (4) provide increased understanding of each of the mathematical models used to represent the elastic

airplane in flight. In all cases, it is assumed the reader is relatively familiar with the notation of refs. 4, 26, and 27, and the significance of each of the axis systems used to describe the structural and aerodynamic effects.

2. SYMBOLS

This list includes the symbols found in the Summary and appendixes. In different technologies some of the symbols have different meanings. For example, ϵ means downwash angle to an aerodynamicist, but strain to a structural engineer. In these cases the several definitions have been listed after the symbol.

General

AR	Aspect ratio, nondimensional
[A]	Steady aerodynamic influence coefficients matrix, meters^2/radian
[δA]	Unsteady aerodynamic influence coefficients matrix, meter^2-seconds/radian
[A_1], [A_2], [A_3], [A_4], [A_5]	Aerodynamic matrices, newtons, newton-meters
a	Root of characteristic equation, second^{-1}; lift curve slope, radian^{-1}
a_∞	Speed of sound, meters/second
$\bar{a}_v$	Vertical tail elastic to rigid lift ratio, nondimensional
$\ddot{a}$	Acceleration, meters/second^2
b	Wingspan, meters
$C_{1/2}$	Cycles to damp to half amplitude, nondimensional
C_2	Cycles to double amplitude, nondimensional
C_D	Drag coefficient, $D/\bar{q}S$, nondimensional
C_{D_i}	Induced drag coefficient, $D_i/\bar{q}S$, nondimensional
C_L	Lift coefficient, $L/\bar{q}S$, nondimensional
C_l	Rolling moment coefficient, $M_x/\bar{q}Sb$, nondimensional

C_m	Pitching moment coefficient, $M_y / \bar{q}S\bar{c}$, nondimensional
C_N	Normal pressure force coefficient, $N / \bar{q}S$, nondimensional
C_n	Yawing moment coefficient, $M_z / \bar{q}Sb$, nondimensional
C_p	Pressure coefficient, $(P - P_\infty)/\bar{q}_\infty$, nondimensional
C_T	Thrust coefficient, $T / \bar{q}S$, nondimensional
C_Y, C_y	Side force coefficient, $F_y / \bar{q}S$, nondimensional
$[C]$	Flexibility matrix with reference point fixed, meters/newton
$[C_o]$	Flexibility matrix with reference point fixed and with reference point rows and columns removed, meters/newton
$[\bar{C}]$	Flexibility matrix with reference point free, meters/newton
$[\bar{C}_R]$	Residual flexibility matrix, meters/newton
c	Wing chord, meters
c_R	Root chord, meters
$\bar{c}$	Mean aerodynamic chord, meters
c_{ref}	$\bar{c}$ for the 707 and c_R for the SST, meters
D	Drag, newtons
D_i	Induced drag, newtons
$[D]$	Transformation matrix from fluid to stability axis system, nondimensional
$\bar{d}$	Elastic displacement, meters
$\{d_i\}$	Column matrix of elastic displacement components at the i^{th} element, meters
$\{d_p\}$	Matrix of elastic displacement perturbation, meters
E	Total airplane perturbation energy, newton-meters; Young's modulus, newtons/meter^2; induced drag efficiency factor, nondimensional; energy, newton-meters

e	Internal energy density, newton-meters^4/kilogram
F	Energy decay parameter, nondimensional
$\vec{F}$	Force, newtons; surface stress vector, newtons/meter^2
$\{F\}$	Total force matrix, newtons
$\{F_A\}$	Aerodynamic force matrix, newtons
$[F_d]$	Flexibility matrix relating changes in panel centroid deflections to unit loads, meters/newton
$\{F_i\}$	Generalized forces at i^{th} element, arbitrary dimensions
$\{F_T\}$	Thrust force matrix, newtons
$[F_\theta]$	Flexibility matrix relating panel slopes to unit loads, radians/newton
f_{ij}	Aerodynamic influence coefficients (subsonic), newtons/radian
$\vec{f}$	Perturbation force, newtons; perturbation surface stress vector, newtons/meter^2
$\{f\}$	Perturbation force matrix, newtons
$\{f_A\}$	Aerodynamic perturbation force matrix, newtons
$\{f_T\}$	Thrust perturbation force matrix, newtons
G	Shear modulus, newtons/meter^2
GW	Gross weight, newtons
$\bar{\bar{G}}$	Structural influence functions in diadic form with reference point free, meters^3/newton
g_{ij}	Aerodynamic influence coefficients (supersonic), newtons/radian
$\vec{g}$	Acceleration due to gravity, meters/second^2
$\vec{g}_i$	Unit base vector, nondimensional
h	Altitude, meters; specific enthalpy, newton-meters/kilogram; center-of-gravity position, nondimensional

h_m	Maneuver point position, nondimensional
h_n	Neutral point position, nondimensional
$(h_n - h)$	Static margin, nondimensional
$\dot{h}_p$	Velocity of panel normal to the streamwise direction, meters/second
I_{xx}, I_{xy}, I_{xz} I_{yy}, I_{yz}, I_{zz}	Moments and products of inertia, kilogram-meters^2
[I], $[I_3]$	Identity matrix, nondimensional
i_H	Horizontal tail deflection, degrees
$\hat{i}, \hat{j}, \hat{k}$ $\underline{i}, \underline{j}, \underline{k}$	Unit base vectors, nondimensional
J	Torsional constant, meters^4/radian
K	Angular deflection at the exposed horizontal tail due to a unit load at the tail, radians/newton
K_{ij}	Structural stiffness coefficient, newtons/meter
K_N	Ratio of aircraft nose lift to aircraft wing lift, nondimensional
$K_{\dot{p}}$	Effective change in vertical tail angle of sideslip due to a unit change in rolling acceleration measured at the exposed vertical tail, degrees/radian/second^2
$K_{\dot{r}}$	Effective change in vertical tail angle of sideslip due to a unit change in yawing acceleration measured at the exposed vertical tail, degrees/radian/second^2
$K_{\ddot{y}}$	Effective change in vertical tail angle of sideslip due to a unit change in side acceleration measured at the exposed vertical tail, degrees/meter/second^2
$K'_{B(W)}$	Effect of lift carryover on the body due to the wing, nondimensional
$K'_{W(B)}$	Effect of lift carryover on the wing due to the body, nondimensional
[K]	Stiffness matrix with respect to fixed reference point, newtons/meter

$[K]_i$	Element stiffness matrix, newtons/meter
$[\bar{K}]$	Stiffness matrix with respect to free reference point, newtons/meter
$[\![\bar{K}]\!]$	Generalized stiffness matrix with free reference point, newtons/meter
k	Thermal conductivity, newton-meters/second-meter-degrees Celsius; elastic constant, newtons/meter^2; Strouhal number, nondimensional
$[K], [\![K]\!]$	Corrector matrix for influence coefficients, nondimensional
L	Lift, newtons
l	Moment arm, meters; characteristic length, meters; pressure difference across surface, newtons/meter^2
l_H	Wing $c_{ref}/4$ to horizontal tail $c_{ref}/4$, meters
l_v	Wing $c_{ref}/4$ to vertical tail $c_{ref}/4$, meters
l_1, l_2, l_3	Direction cosines, nondimensional
M	Mach number, nondimensional; mass of the airplane, kilograms
$\bar{M}$	Moment, meter-newtons
$[M]$	Inertial matrix, kilograms, kilogram-meters^2
$[\![M]\!]$	Generalized mass matrix, kilograms
m_1, m_2, m_3	Direction cosines, nondimensional
$\bar{m}$	Perturbation moment, meter-newtons
$[m]$	Mass matrix, kilograms
$[\![m]\!]$	Diagonal mass matrix, kilograms
N	Yawing moment, meter-newtons
$\bar{N}$	Normal force, newtons
n	Load factor, nondimensional; number of elastically connected mass elements used to represent the airplane, nondimensional

n_1, n_2, n_3	Direction cosines of the normal surface, nondimensional
$\bar{n}$	Unit vector normal to the surface, nondimensional
$[n]$	Diagonal matrix of panel unit normal vectors, nondimensional
P	Period, seconds
P, Q, R	Components of the angular velocity $\bar{\omega}$ in the body axis system, radians/second
P_t	Total pressure, newtons/meter^2
$\{P\}$	Aerodynamic panel pressure forces, newtons
p	Static pressure, newtons/meter^2; roll rate, radians/second
p, q, r	Perturbation components of angular velocity $\bar{\omega}_p$ in the body axis system, radians/second
Q_i	Generalized force, arbitrary dimensions*
$\{Q\}$	Matrix of generalized aerodynamic and thrust forces, arbitrary dimensions*
q	Pitch rate, radians/second; rate of internal heat energy addition, newton-meters/second
q_i	Generalized coordinates, arbitrary dimensions*
$\bar{q}$	Dynamic pressure, newtons/meter^2
$\hat{q}$	Pitch rate, $qc_{ref}/2V_{c_1}$, nondimensional
$\{q\}$	Matrix of generalized coordinates, arbitrary dimensions*
$\{\tilde{q}\}$	Matrix of generalized coordinates of elastic free vibration, arbitrary dimensions*
$\{\bar{\tilde{q}}\}$	Cantilever eignvectors, nondimensional

*The units of a generalized force times the generalized coordinates must be newton-meters.

R	Universal gas constant, newton-meters/kilogram-degrees Kelvin; magnitude of position vector, meters; region of XY plane not covered by the airplane or wake, nondimensional
Re	Reynolds number, nondimensional
$\vec{R}$	Position vector at an initial instant of time, meters; body force per unit volume, newtons/meter^3
r	Reference distance, meters; magnitude of the position vector, meters
$\hat{r}$	Yaw rate component, $rb/2V_{c_l}$, nondimensional
$\vec{r}$	Position vector relative to the body axis system, meters; position vector relative to the fluid axis system, meters
$\vec{r}_o$	Position vector of the center of gravity relative to the fluid axis system, meters
$\vec{r}_s$	Position vector relative to the stability axis system, meters
$\vec{r}'$	Position vector relative to inertial space, meters
$\vec{r}'_o$	Position vector of the center of gravity relative to the inertial space, meters
$\vec{\bar{r}}_s$	Position vector in the undeformed airplane relative to the body axis system, meters
$\{ r'_{o_p} \}$	Matrix of airplane position and orientation perturbations, meters, radians
S	Reference area, meters^2; airplane's projection on the XY plane, nondimensional
$[S]$	Diagonal matrix of panel areas, meters^2
s	Complex frequency function, 1/seconds
T	Kinetic energy, newton-meters; thrust, newtons; time, seconds
$T_{1/2}$	Time to damp to ½ amplitude, seconds
	Time to double the amplitude, seconds

$-1/T_r$	Rolling convergence mode root, 1/seconds
$-1/T_s$	Spiral mode root, 1/seconds
t	Time, seconds; airfoil thickness, meters
t*	Nondimensionalizing time factor, seconds
U	Potential energy, newton-meters
U, V, W	Components of velocity $\vec{V}_c$ in the body axis system, meters/second
u, v, w	Perturbation components of the velocity in the body axis system, meters/second
u_i	Generalized coordinates, nondimensional
$\hat{u}$	Forward velocity component, u/V_{c_1}, nondimensional
$\{u\}, \{u_p\}$	Generalized elastic displacements, meters
V	Lyapunov function, nondimensional; volume, meters^3
V_E	Equivalent airspeed, meters/second
$\vec{V}_c$	Velocity vector of the airplane center of gravity, meters/second
$\vec{V}$	Velocity vector, meters/second
$\vec{V}_{c_p}$	Perturbation velocity vector of the airplane center of gravity meters/second
$\{V_p\}$	Matrix of airplane linear and rotational rate perturbations, meters/second, radians/second
$\{\dot{V}_p\}$	Matrix of airplane linear and rotational acceleration perturbations, meters/second^2, radians/second^2
W	Weight, newtons; airplane's wake projection on the XY plane, nondimensional
$\{X\}$	Matrix of panel centroid distances to the reference point, meters
X, Y, Z x, y, z	Body-fixed-axis system (app. A); fluid axis system (app. B)

X_B, Y_B, Z_B; x_B, y_B, z_B	Body-fixed-axis system
X_o, Y_o, Z_o	Axis system fixed to a material point
X', Y', Z'; x', y', z'	Earth-fixed-axis system
Y	Side force, newtons
$\lceil \Delta y \rfloor$	Matrix of spanwise panel widths, meters
Z_R	Vertical displacement of structural reference point, meters
$\{z\}$	Matrix of vertical displacements of each panel from equilibrium, meters
$[\ ]$	Square matrix
$\{\ \}$	Column matrix
$[\ ]$	Row matrix
$\lceil \rfloor$	Diagonal matrix
$[\ ]^T, \{\ \}^T$	Transposed matrix
$[\ ]^{-1}$	Matrix inverse
$\|[\ ]\|$	Determinant of a matrix
$[0]$	All zero elements
$\{1\}$	Column matrix of ones
$[\![\ ]\!]$	"Jump" in enclosed quantity

Greek Symbols

α	Angle of attack, radians
α_R	Angular rotation of structural reference point, radians
α_{ref}	Angle between X body axis and $\bar{V}_{c_l}$, radians
$\{\alpha\}$	Matrix of panel slopes, radians

β	Angle of sideslip, radians
β^2	$(M^2 - 1)$, nondimensional
Γ	Circulation, meters^2/second
$\bar{\Gamma}_o$	Structural influence functions with reference point fixed in diadic form, meters^3/newton
γ	Flight path angle, radians; ratio of specific heats for air, nondimensional
Δ	Finite change in some parameter, nondimensional
δ	Control surface deflection, radians; arbitrarily small number, nondimensional; Dirac's function, nondimensional; thickness ratio, nondimensional
$\{\delta\}$	Matrix of displacements relative to a space-fixed inertial system, meters
$\{\delta_s\}$	Matrix of flexible displacements relative to the structural axis system, meters
ϵ	Downwash angle, radians; arbitrarily small number, nondimensional; strain, meters/meter
ϵ_α	Change in downwash angle at the stabilizer per unit change in wing angle of attack, $\partial\epsilon/\partial\alpha$, radians/radian
ζ	Damping ratio, nondimensional; nondimensionalized coordinate, nondimensional; dummy variable, nondimensional
η	Efficiency factor, nondimensional; coordinate, nondimensional; dummy variable, nondimensional
Θ	Euler angle, radians
θ	Perturbed Euler angle, radians
Θ_s	Streamwise rotation of panel, radians
$\Theta_{ix}, \Theta_{iy}, \Theta_{iz}$	Node rotations, radians
$\dot{\Theta}$	Rate of change of Euler angle, radians/second

$\dot{\theta}_{ei}$	Rotational rate of paneled airplane about axis of rotation, radians/second
$\bar{\theta}$	Rigid-body rotation about center of gravity, radians
$[\theta]$	Angle mode matrix, radians/meter
λ	Eigenvalue, nondimensional; taper ratio, nondimensional; bulk modulus, newtons/meter^2; Lame's constant, newtons/meter^2; sweep angle, degrees
λ_i	Roots of characteristic equation, 1/seconds
μ	Reduced mass parameter, nondimensional; Lame's constant, newtons/meter^2; extent of influence region, nondimensional
$\{\mu\}$	Cantilever mode shape matrix, nondimensional
$[\mu]$	Matrix of all cantilever modes, nondimensional
ν	Poisson's ratio, nondimensional
ξ,η,ζ	Coordinates, nondimensional; dummy variables, nondimensional
π	Constant, 3.14159. . ., nondimensional
ρ	Density, kilograms/meter^3
σ	Normal stress, newtons/meter^2; density ratio, nondimensional; real root of characteristic equation, 1/seconds
σ_R	Rotation of structural reference axis system, radians
σ_T	Rectilinear translation of structural reference axis system, meters
τ	Coefficient of viscosity, kilograms/meter-second; shear stress, newtons/meter^2; time, nondimensional
Φ	Total velocity potential, meters^2/second; Euler angle, radians
$[\Phi_n]$	Normalized natural free vibration modes of the airplane, nondimensional

Φ	Perturbation velocity potential, meters; perturbed Euler angle radians
$\dot{\Phi}$	Rate of change of Euler angle, radians/second
$[\phi]$	Free-vibration mode shape matrix, nondimensional
$[\bar{\phi}]$	Rigid-body mode shape matrix, nondimensional
$\overline{\phi}$	Stress diadic, newtons/meter^2
$\vec{\phi}_\alpha$	Normal mode of generalized coordinate, nondimensional
φ	Velocity potential, nondimensional
$\varphi(t)$	Arbitrary positive function of time, arbitrary dimension
Ψ	Euler angle, radians
ψ	Perturbed Euler angle, radians
$\dot{\psi}$	Rate of change of Euler angle, radians/second
$\overline{\psi}$	Inertia diadic
Ω	Phase angle, radians
ω	Frequency, radians/second; imaginary part of a pair of complex roots, 1/seconds
ω_n	Undamped natural frequency, radians/second
$\vec{\omega}_p$	Perturbed angular velocity, radians/second

Subscripts

A	Aerodynamic; airplane; aileron
a	Aerodynamic
ac	Aerodynamic center
b	Body reference axis system

c.g.	Center of gravity
cp	Center of pressure
D	Dutch roll mode
E	Equivalent elastic (Formulation II); elevator
$\bar{E}$	Equivalent elastic (Formulation I)
Eff	Effective
EqEl	Equivalent elastic
exp	Experimental
F	Flutter
HB	Handbook methods
h, ht	Horizontal tail
I	Inertia relief
l	Lower surface
L.E., LE	Leading edge
ls	Lifting surface theory method
P	Phugoid mode
R	Rigid; rudder
r	Rolling convergence root mode
S	Spiral root
sp	Short period
s	Stability axis system; spiral mode

$_{sl}$	Sea level
t	Tip; total
u	Upper surface
v, vert, V.T.	Vertical tail
W	Wing
WB	Wing-body
WBT	Wing-body-tail
WT	Wind tunnel
0	At $\alpha = \delta_E = i_h = 0^o$; initial state
1	Steady state motion variables; trimmed condition
$_{\infty}$	Undisturbed condition

3. ASSUMPTIONS

Assumptions used in developing the equations and methods are listed here for reference. Where appropriate in the summary report, pertinent assumptions used in obtaining a result or equation are given. However, discussions of the assumptions as they come into the developments are given in the appendixes. Further descriptions and justifications are included in those discussions.

General Assumptions

- (G1) Airplane mass and mass distribution are constant with time
- (G2) No thermoelastic effects considered
- (G3) No electromagnetic effects considered
- (G4) Symmetric airplane
- (G5) Variation of air density with altitude is negligible
- (G6) No gust effects considered
- (G7) Gravitational forces on the field are negligible
- (G8) Small perturbation theory
- (G9) Large perturbation theory
- (G10) Origin of coordinate system is at the center of mass
- (G11) Arbitrary perturbations

Aerodynamic Assumptions

- (A1) Potential flow theory
- (A2) Thin body
- (A3) Slender body
- (A4) High aspect ratio
- (A5) Prandtl boundary layer approximation
- (A6) Perfect gas, thermally nonconducting and chemically nonreacting
- (A7) Isentropic flow
- (A8) Steady flow

(A9) Unsteady flow

(A10) Inviscid flow

(A11) Quasi-steady flow

(A12) Aerodynamic influence coefficients for nonzero sideslip

(A13) Continuum flow

(A14) No finite shock waves

(A15) Velocity field is irrotational

Structural Assumptions

(S1) Hooke's law applies

(S2) Only small strain and displacement gradients are considered

(S3) Structural damping is negligible

(S4) Structural perturbations can be represented by normal modes

(S5) Completely elastic math model of elastic airplane

(S6) Residual elastic math model of elastic airplane

(S7) Equivalent elastic math model of elastic airplane

(S8) Rigid math model of elastic airplane

(S9) Airplane displacement vector field is such that the center of gravity does not displace or rotate

(S10) X component of elastic deflection is negligible

(S11) Y component of elastic deflection is negligible

(S12) The structure can be adequately represented with beams

(S13) Inertia of each finite mass element about its center of gravity is negligible

Dynamic Assumptions

(D1)	Free flight only
(D2)	No spinning rotors
(D3)	Steady-state curvilinear flight
(D4)	Steady-state rotation is small
(D5)	Zero-lag thrust derivatives
(D6)	$C_{L_{\ddot{\theta}}}$ is negligible
(D7)	$C_{Y_{\dot{P}_I}}$, $C_{Y_{\dot{r}_I}}$, $C_{\ell_{\ddot{Y}_I}}$, and $C_{n_{\ddot{Y}_I}}$ are negligible
(D8)	C_{D_q} is negligible
(D9)	Steady-state rectilinear motion
(D10)	Stick-fixed-and-unaugmented airplane
(D11)	Thrust perturbation forces are negligible
(D12)	Steady state, wings level, and zero sideslip
(D13)	Level flight (steady state)
(D14)	Linear aerodynamic stability derivatives
(D15)	Two-degree-of-freedom longitudinal motion

4. THEORETICAL METHODS FOR CALCULATING STABILITY DERIVATIVES

4.1 Introduction

The six-degree-of-freedom problem associated with the calculation of the airplane's flight path, the control power necessary to obtain the desired optimum flight path, and the stability of the airplane about that flight path has been well defined and discussed in the classical textbooks (refs. 4, 15, and 55). Additional refinements have been suggested by many authors (refs. 12 and 23) and in app. A.

Central to this six-degree-of-freedom problem is the discussion of airplane center-of-gravity motion equations in terms of "stability derivatives." Consequently, evaluation of these stability derivatives to a high degree of accuracy is required. Since the stability derivatives are a function of airplane geometry (structural dynamics) and aerodynamic theory (inviscid and viscid), accuracy becomes a function of the degree of sophistication used in both the geometric and aerodynamic definition of the airplane. (G8)

The development of structural influence coefficient theory using a beam idealization of the airplane (ref. 1), when combined with recent advances in unsteady aerodynamic theory (ref. 28), suggests a large improvement in the theoretical calculation of stability derivatives may be obtainable. By a proper formulation of the boundary conditions imposed upon the inviscid fluid dynamic equations in terms of time-dependent c.g. motion variables and structural coefficients, the stability derivatives for any existing mathematical model of an elastic airplane may be calculated. (S12) (A9)

This section of app. B will summarize and discuss briefly stability and control equations derived in app. A for the motion of the c.g. of a completely elastic airplane undergoing small disturbances. The associated aerodynamic and structural equations will then be derived and boundary conditions on the airplane surface will be related to time-dependent motion variables such as $\alpha(t)$, $q(t)$, $u_n(t)$, etc. The stability derivatives associated with these time-dependent motions, i.e., C_{z_α}, C_{x_α}, C_{m_α}, $C_{z_{\dot{u}_n}}$, etc., will then be evaluated using a frequency expansion of the force equations written in terms of the stability derivatives and using the inviscid, first order in thickness velocity potential.

Three different coordinate systems (shown in the following sketch) must be introduced because the development makes use of concepts from three different technologies: aerodynamics, stability and control, and structures. The three coordinate systems, all of which are rectangular cartesian, are:

x, y, z: fluid axis system, translating with a constant velocity relative to an earth-fixed system of axes (inertial system)

x_S, y_S, z_S: stability axis system, body fixed and in unrestricted motion relative to the x, y, z system (noninertial)

x_B, y_B, z_B: body axis system, body fixed and used in the specification of the airplane's structural, mass, and geometric properties (noninertial)

The body axis system and the stability axis system are related by a rigid-body translation and rotation. The structural, mass, and geometric properties of the airplane will be regarded as being expressed in the stability axis system as, indeed, they may be by introducing the transformation of coordinates. Thus, the surface of the airplane will be represented as:

$G_S(x_S, y_S, z_S, t) = 0$ in the stability axis system

$G(x, y, z, t) = 0$ in the fluid axis system

Further, to be precise and avoid misinterpretation, a number of definitions must be introduced. Most of these are included in the section of symbols, but they are repeated here for convenience to this development. They are:

$\vec{r}_s$ - spatial position relative to the stability axis system

$\vec{r}$ - spatial position relative to the inertial fluid axis system

$\vec{R}_S$ - Spatial position of a mass particle of the airplane relative to the stability axis system at the reference instant of time t_o

$\vec{R}$ - spatial position of a fluid particle relative to the fluid axis system at the instant of time t_o

$\vec{r}_s = \vec{r}_s(\vec{R}_S, t)$ - position relative to the stability axis system at time t of the airplane's mass particle at $\vec{R}_S$ at time t_o (this is the motion of an arbitrary airplane mass particle)

$\vec{r} = \vec{r}(\vec{R}, t)$ - position relative to the fluid axis system at time t of the fluid particle at R at time t_o (this is the motion of an arbitrary fluid particle)

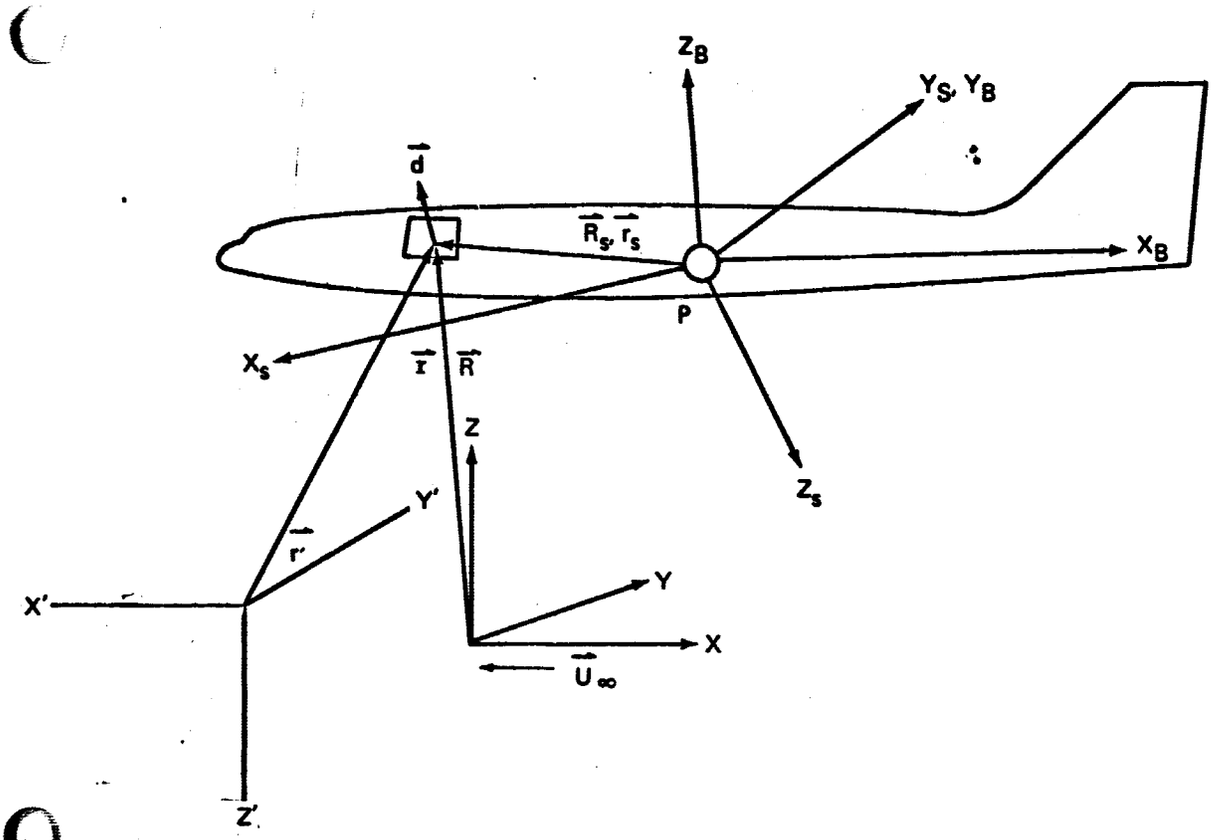

X'Y'Z' earth-fixed axis

XYZ fluid axis system, translating with a constant velocity relative to the earth-fixed axis.

X_s Y_s Z_s stability axis system: body fixed and in unrestricted motion relative to the XYZ system.

X_B Y_B Z_B body axis system: body fixed and used in the specification of the airplane's structural, mass, and geometric properties.

The following differentiations with respect to time are required:

$\left.\frac{D}{Dt}\right|_{\vec{R}_s}$ - time rate of change apparent to an airplane's mass particle

$\left.\frac{D}{Dt}\right|_{\vec{R}}$ - time rate of change apparent to a fluid particle

These differentiations may be performed on the expressions representing motion to find the following velocities:

$\vec{v} = \left.\frac{D\vec{r}(\vec{R},t)}{Dt}\right|_{\vec{R}} = \left.\frac{\partial \vec{r}}{\partial t}\right|_{\vec{R}}$ - velocity (or time rate of change of position) of the arbitrary fluid particle R relative to the fluid axis system

$\dot{\vec{d}} = \left.\frac{D\vec{r}_s(\vec{R}_s,t)}{Dt}\right| = \left.\frac{\partial \vec{r}_s}{\partial t}\right|_{\vec{R}_s}$ - velocity (or time rate of change of position) of the arbitrary airplane mass particle $\vec{R}_s$ relative to the stability axis system

$$\vec{v}_s \equiv \frac{D}{Dt}\,\vec{r}_s\left(r(\vec{R},t),t\right)\Big|_{\vec{R}}$$

$$= \left.\frac{\partial \vec{r}_s}{\partial t}\right|_{\vec{r},\vec{R}} + \left.\frac{\partial \vec{r}_s}{\partial \vec{r}}\right|_t \cdot \left.\frac{\partial \vec{r}}{\partial t}\right|_{\vec{R}}$$

$$= -\vec{v}_R - \vec{\omega} \times \vec{r}_s + \left.\frac{\partial \vec{r}_s}{\partial \vec{r}}\right|_t \cdot \vec{v}$$ - velocity (or time rate of change of position) of the arbitrary fluid particle R relative to the stability axis system

$\vec{r}_o = (\vec{r} - \vec{r}_s)$ - position of the origin of the stability axis system relative to the fluid axis system

$\vec{v}_R = \frac{\partial \vec{r}_o}{\partial t}$ - velocity of the origin of the stability axis system relative to the fluid axis system

$\left.\frac{\partial \vec{r}_s}{\partial t}\right|_{\vec{r},\vec{R}} = -\vec{v}_R - \vec{\omega} \times \vec{r}_s$ - velocity relative to the stability axis system of a point fixed relative to the fluid axis system

$\vec{\omega}$ - rate of rotation of stability axis system relative to stability axis system

The above notation is somewhat ambiguous because it is difficult to indicate that the scalar product

$$\left.\frac{\partial \vec{r}_s}{\partial \vec{r}}\right|_t \cdot \vec{v}$$

has the meaning

$$\left.\frac{\partial \vec{r}_s}{\partial \vec{r}}\right|_t \cdot \vec{v} = \left.\frac{\partial \vec{r}_s}{\partial x}\right|_t v_x + \left.\frac{\partial \vec{r}_s}{\partial y}\right|_t v_y + \left.\frac{\partial \vec{r}_s}{\partial z}\right|_t v_z$$

. and not

$$\left.\frac{\partial x_s}{\partial \vec{r}}\right|_t \vec{i}_s \cdot \vec{v} + \left.\frac{\partial y_s}{\partial \vec{r}}\right|_t \vec{j} \cdot \vec{v} + \left.\frac{\partial z_s}{\partial \vec{r}}\right|_t \vec{k}_s \cdot \vec{v}$$

This ambiguity may be overcome by introducing matrix notation. Let the following matrix definitions be introduced:

$$\vec{r} = \begin{Bmatrix} x \\ y \\ z \end{Bmatrix} \qquad \vec{v} = \begin{Bmatrix} \left.\frac{\partial x}{\partial t}\right|_{\vec{R}} \\ \left.\frac{\partial y}{\partial t}\right|_{\vec{R}} \\ \left.\frac{\partial z}{\partial t}\right|_{\vec{R}} \end{Bmatrix}$$

$$\vec{r}_s = \begin{Bmatrix} x_s \\ y_s \\ z_s \end{Bmatrix} \qquad \vec{v}_s = \begin{Bmatrix} \left.\frac{\partial x_s}{\partial t}\right|_{\vec{R}_s} \\ \left.\frac{\partial y_s}{\partial t}\right|_{\vec{R}_s} \\ \left.\frac{\partial z_s}{\partial t}\right|_{\vec{R}_s} \end{Bmatrix}$$

$$\frac{\partial \vec{r}_s}{\partial \vec{r}} = \begin{bmatrix} \frac{\partial x_s}{\partial x} & \frac{\partial x_s}{\partial y} & \frac{\partial x_s}{\partial z} \\ \frac{\partial y_s}{\partial x} & \frac{\partial y_s}{\partial y} & \frac{\partial y_s}{\partial z} \\ \frac{\partial z_s}{\partial x} & \frac{\partial z_s}{\partial y} & \frac{\partial z_s}{\partial z} \end{bmatrix}$$

$$\vec{\omega} \times \vec{r}_s = \begin{bmatrix} 0 & z_s & -y_s \\ -z_s & 0 & x_s \\ y_s & -x_s & 0 \end{bmatrix} \begin{Bmatrix} p \\ q \\ r \end{Bmatrix}$$

$$\vec{\omega} = \begin{Bmatrix} p \\ q \\ r \end{Bmatrix}$$

The need for the vector operator for the gradient will be required. This operator is related to the matrix definitions as

$$\vec{\nabla} \equiv \frac{\partial}{\partial \vec{r}} \equiv \left\{ \begin{matrix} \frac{\partial}{\partial x} \\ \frac{\partial}{\partial y} \\ \frac{\partial}{\partial z} \end{matrix} \right\}$$

and

$$\vec{\nabla}_s \equiv \frac{\partial}{\partial \vec{r}_s} \equiv \left\{ \begin{matrix} \frac{\partial}{\partial x_s} \\ \frac{\partial}{\partial y_s} \\ \frac{\partial}{\partial z_s} \end{matrix} \right\}$$

where

$$\vec{\nabla} = \frac{\partial}{\partial \vec{r}} = \left(\frac{\partial \vec{r}_s}{\partial \vec{r}} \right)^T \frac{\partial}{\partial \vec{r}_s}$$

$$= \begin{bmatrix} \frac{\partial x_s}{\partial x} & \frac{\partial y_s}{\partial x} & \frac{\partial z_s}{\partial x} \\ \frac{\partial x_s}{\partial y} & \frac{\partial y_s}{\partial y} & \frac{\partial z_s}{\partial y} \\ \frac{\partial x_s}{\partial z} & \frac{\partial y_s}{\partial z} & \frac{\partial z_s}{\partial z} \end{bmatrix} \left\{ \begin{matrix} \frac{\partial}{\partial x_s} \\ \frac{\partial}{\partial y_s} \\ \frac{\partial}{\partial z_s} \end{matrix} \right\}$$

$$= \left(\frac{\partial \vec{r}_s}{\partial \vec{r}} \right)^T \vec{\nabla}_s$$

Now, if the preceding and the following equations are interpreted in terms of the matrix expressions, the ambiguity should be resolved, while the useful physical appeal associated with vectors is retained. Furthermore, the matrix formulation is essential for the lumped parametric representation of the airplane. Having introduced the matrices at this point will facilitate that formulation.

4.2 Derivation of Significant Equations

4.2.1 Small disturbance equations. —The equations of motion describing the small-disturbance motion of an aircraft's c.g. from a reference flight condition were derived in app. A. It is advantageous to extend the development of these equations to a coefficient representation of forces and moments (stability derivatives) and then to suggest the form of their solution. Detailed solution techniques are presented in app. C. These results will later be required to evaluate the aerodynamic boundary conditions and the small-disturbance forces in terms of the inviscid velocity potential.

It may be recalled from app. A that forces are expressed individually for each panel. The total airplane forces are a linear summation of the individual panel forces associated with the independent motion variables characterizing a particular flight mode. The usual motion variables considered are: (1) those associated with the aircraft's cg motion, i.e., u(t), v(t), w(t), p(t), q(t), r(t), $\dot{u}(t)$, . . ., $\dot{r}(t)$ and (2) those associated with panel elastic motion, i.e., $u_1(t)$, $u_2(t)$, . . ., $u_{3n-6}(t)$. Thus, it is sufficient to calculate the force coefficient for each panel while accounting for the induced effects of other panels.

It was shown in app. A that the equations of dynamics describing both the airplane cg motion and elastic motion are in their most general form for the "completely elastic" mathematical model of an elastic airplane. The "residual elastic," "equivalent elastic," and "rigid" mathematical models are special cases contained in the completely elastic equations. Therefore, it is most advantageous to define stability derivatives as they are associated with "completely elastic" airplane forces.

4.2.1.1 The stability derivatives: Consider the form of the aircraft's c.g. dynamic equation (6.118) and the internal equilibrium equation (6.166) derived in app. A for small perturbations from a reference flight path.

$$[M]\frac{\partial}{\partial t}\{v\} + [M][M_1]\{v_p\} + [M][M_2]\{r_{cp}\} = [\phi]^T\{f\}$$

(6.118, app. A)

N69-12906

$$[\bar{K}]\{u_p\} + [\bar{m}]\{\ddot{u}_p\} = [\phi]^T\{f\} \qquad \text{(6.166, app, A)}$$

$$[M] = \begin{bmatrix} M & & & & & \\ & M & & & & \\ & & M & & & \\ & & & I_x & & -I_{xz} \\ & & & & I_y & \\ & & & -I_{xz} & & I_z \end{bmatrix} \qquad \text{(6.115, app. A)}$$

$$\{V_p\} = \begin{bmatrix} u \\ v \\ w \\ p \\ q \\ r \end{bmatrix}, \qquad \{\dot{r}_{o_p}\} = \begin{bmatrix} \dot{x}_{o_p} \\ \dot{y}_{o_p} \\ \dot{z}_{o_p} \\ \dot{\phi} \\ \dot{\theta} \\ \dot{\psi} \end{bmatrix} \qquad \text{(6.116, app. A)} \qquad \text{(6.117, app. A)}$$

$$[M_2] = \begin{bmatrix} 0 & 0 & 0 & 0 & W_1 & -V_1 \\ 0 & 0 & 0 & -W_1 & 0 & U_1 \\ 0 & 0 & 0 & V_1 & -U_1 & 0 \\ 0 & 0 & 0 & A & B & C \\ 0 & 0 & 0 & D & E & F \\ 0 & 0 & 0 & G & H & I \end{bmatrix} \qquad \text{(6.120a, app. A)}$$

$$[M_2] = \begin{bmatrix} 0 & 0 & 0 & 0 & g\cos\theta_1 & 0 \\ 0 & 0 & 0 & -g\cos\theta_1\cos\phi_1 & g\sin\theta_1\sin\phi_1 & 0 \\ 0 & 0 & 0 & g\cos\theta_1\sin\phi_1 & g\sin\theta_1\cos\phi_1 & 0 \\ 0 & 0 & 0 & 0 & 0 & 0 \\ 0 & 0 & 0 & 0 & 0 & 0 \\ 0 & 0 & 0 & 0 & 0 & 0 \end{bmatrix}$$

(6.120b, app. A)

$$[\phi] = \begin{bmatrix} [\phi_1] \\ [\phi_2] \\ \vdots \\ [\phi_m] \end{bmatrix} \qquad \text{(6.113, app. A)}$$

$$[\phi_i] = \begin{bmatrix} 1 & 0 & 0 & 0 & z_i & -y_i \\ 0 & 1 & 0 & -z_i & 0 & x_i \\ 0 & 0 & 1 & y_i & -x_i & 0 \end{bmatrix} \quad \text{(6.112, app. A)}$$

$$\{d_p\} = [\phi]\{u_p\} \quad \text{(6.136, app. A)}$$

where

$$[\bar{K}] = [\phi]^T[\bar{K}][\phi] \quad \text{(6.157, app. A)}$$

is the generalized stiffness matrix, and $[\bar{K}]$ is the stiffness matrix for the free-free airplane defined in equation (6.147, app A)

$$[\bar{m}] = [\phi]^T[m][\phi] \quad \text{(6.158, app. A)}$$

is the generalized mass matrix

$$[\phi] = [\{\phi_1\}\{\phi_2\}\{\phi_3\} \cdots \{\phi_{3n-6}\}] \quad \text{(6.156, app. A)}$$

is the free vibration mode shape matrix

$$\{f\} = \lfloor f_{1x}\ f_{1y}\ f_{1z}\ f_{2x}\ f_{2y}\ f_{2z} \cdots f_{nx}\ f_{ny}\ f_{nz} \rfloor^T$$

where, for example, f_{i_x} is the force on the i^{th} panel in the x direction due to the aerodynamics associated with the aircraft's c.g. motion or elastic motion

It is the intent of this section to indicate the form of $\{f\}$ in terms of individual panel stability derivatives and/or force perturbations and then refer the reader to several numerical calculation techniques.

The aerodynamic forces associated with the small-disturbance, time-dependent motions can be expanded in a Taylor series about their reference value. Consider the total force acting on the airplane F_z:

$$F_z = f_{z_0} + f_z\left(u, v, w, p, q, r, \dot{u}, \ldots, \dot{r}, u_{p_1}, \ldots, u_{p_{3n-6}}, \dot{u}_{p_1}, \ldots, \dot{u}_{p_{3n-6}}, \ddot{u}_{p_1}, \ldots, \ddot{u}_{p_{3n-6}}\right) \quad \text{(4.1)}$$

where f_{z_1} is the steady-state force

f_z is the small-disturbance (perturbation) force

where the parenthesis notation (. . .), means f_z is a function of the small quantities (ref. 31).

Performing a Taylor series expansion as in ref. 4 separates components of f_z associated with each motion variable.

$$F_z(t) = f_{z_1} + f_{z_u} u(t) + f_{z_v} v(t) + f_{z_w} w(t) + f_{z_p} p(t) + f_{z_q} q(t) + f_{z_r} r(t)$$
$$+ f_{z_{\dot{u}}} \dot{u}(t) + \cdots + f_{z_{\dot{r}}} \dot{r}(t) + f_{z_{u_1}} u_{p_1}(t) + \cdots + f_{z_{u_{p_{3n-6}}}} u_{p_{3n-6}}(t)$$
$$+ f_{z_{\dot{u}_{p_1}}} \dot{u}_{p_1}(t) + \cdots + f_{z_{\dot{u}_{p_{3n-6}}}} \dot{u}_{p_{3n-6}}(t) + f_{z_{\ddot{u}_{p_1}}} \ddot{u}_{p_1}(t) + \cdots + f_{z_{\ddot{u}_{p_{3n-6}}}} \ddot{u}_{p_{3n-6}}(t)$$

Developing a similar representation of the f_X, f_Y, M_X, M_Y, and M_Z aerodynamic forces and moments on the aircraft and writing the equations in the matrix notation results in the following equation in which higher order terms are neglected:

$$\{f_a\} = \begin{Bmatrix} F_x - f_{x_0} \\ F_y - f_{y_0} \\ F_z - f_{z_0} \\ M_x - M_{x_0} \\ M_y - M_{y_0} \\ M_z - M_{z_0} \end{Bmatrix} = [A_1^a]\{v_a\} + [A_2^a]\{\dot{v}_a\} + [A_3^a]\{u_a\} + [A_4^a]\{\dot{u}_a\} + [A_5^a]\{\ddot{u}_a\} \tag{4.2a}$$

where

$$\{v_p\} = \lfloor u \; v \; w \; p \; q \; r \rfloor^T \qquad (4.2b)$$

$$\{\dot{v}_p\} = \lfloor \dot{u} \; \dot{v} \; \dot{w} \; \dot{p} \; \dot{q} \; \dot{r} \rfloor^T \qquad (4.2c)$$

$$\{u_p\} = \lfloor u_{p_1} \; u_{p_2} \cdots u_{p_{3n-6}} \rfloor^T \qquad (4.2d)$$

$$\{\dot{u}_p\} = \lfloor \dot{u}_{p_1} \; \dot{u}_{p_2} \cdots \dot{u}_{p_{3n-6}} \rfloor^T \qquad (4.2e)$$

$$\{\ddot{u}_p\} = \lfloor \ddot{u}_{p_1} \; \ddot{u}_{p_2} \cdots \ddot{u}_{p_{3n-6}} \rfloor^T \qquad (4.2f)$$

$$[A_1^*] = \begin{bmatrix} f_{x_u} & f_{x_v} & f_{x_w} & f_{x_p} & f_{x_q} & f_{x_r} \\ f_{y_u} & f_{y_v} & \cdot & \cdot & \cdot & f_{y_r} \\ f_{z_u} & \cdot & \cdot & \cdot & \cdot & f_{z_r} \\ M_{x_u} & \cdot & \cdot & \cdot & \cdot & M_{x_r} \\ M_{y_u} & \cdot & \cdot & \cdot & \cdot & M_{y_r} \\ M_{z_u} & \cdot & \cdot & \cdot & \cdot & M_{z_r} \end{bmatrix} \qquad (4.2g)$$

$$[A_2^*] = \begin{bmatrix} f_{x_{\dot{u}}} & f_{x_{\dot{v}}} & f_{x_{\dot{w}}} & f_{x_{\dot{p}}} & f_{x_{\dot{q}}} & f_{x_{\dot{r}}} \\ f_{y_{\dot{u}}} & \cdot & \cdot & \cdot & \cdot & f_{y_{\dot{r}}} \\ \cdot & \cdot & \cdot & \cdot & \cdot & \cdot \\ \cdot & \cdot & \cdot & \cdot & \cdot & \cdot \\ \cdot & \cdot & \cdot & \cdot & \cdot & \cdot \\ M_{z_{\dot{u}}} & \cdot & \cdot & \cdot & \cdot & M_{z_{\dot{r}}} \end{bmatrix} \qquad (4.2h)$$

$$[A_3^*] = \begin{bmatrix} f_{x_{u_{p_1}}} & f_{x_{u_{p_2}}} & \cdot & \cdot & \cdot & f_{x_{u_{p_{3n-6}}}} \\ f_{y_{u_{p_1}}} & \cdot & \cdot & \cdot & \cdot & f_{y_{u_{p_{3n-6}}}} \\ \cdot & \cdot & \cdot & \cdot & \cdot & \cdot \\ \cdot & \cdot & \cdot & \cdot & \cdot & \cdot \\ \cdot & \cdot & \cdot & \cdot & \cdot & \cdot \\ M_{z_{u_{p_1}}} & \cdot & \cdot & \cdot & \cdot & M_{z_{u_{p_{3n-6}}}} \end{bmatrix} \qquad (4.2i)$$

$$[A_4^*] = \begin{bmatrix} f_{z\ddot{u}_{\rho_1}} & f_{z\ddot{u}_{\rho_2}} & \cdots & f_{z\ddot{u}_{\rho_{3n-6}}} \\ f_{y\ddot{u}_{\rho_1}} & \cdots & \cdots & f_{y\ddot{u}_{\rho_{3n-6}}} \\ \vdots & \vdots & \vdots & \vdots \\ M_{z\ddot{u}_{\rho_1}} & \cdots & \cdots & M_{z\ddot{u}_{\rho_{3n-6}}} \end{bmatrix} \quad (4.2j)$$

$$[A_5^*] = \begin{bmatrix} f_{x\ddot{u}_{\rho_1}} & f_{x\ddot{u}_{\rho_2}} & \cdots & f_{x\ddot{u}_{\rho_{3n-6}}} \\ f_{y\ddot{u}_{\rho_1}} & \cdots & \cdots & f_{y\ddot{u}_{\rho_{3n-6}}} \\ \vdots & \vdots & \vdots & \vdots \\ M_{z\ddot{u}_{\rho_1}} & \cdots & \cdots & M_{z\ddot{u}_{\rho_{3n-6}}} \end{bmatrix} \quad (4.2k)$$

By definition, $$\{f_a\} \equiv [\bar{\phi}]^T \{f\}$$

Two examples will be considered to illustrate the form of [A*] :

(1) A rigid airplane

(2) An elastic airplane of n number of lumped masses

The rigid airplane. — In the case of a rigid airplane, the elements of [A3*] , [A4*] , and [A5*] are equal to zero (by definition) and equation (4.2a) simplifies:

$$\{f_{a_{RIGID}}\} = [A_1^*]\{v_\rho\} + [A_2^*]\{\dot{v}_\rho\}$$

It remains to express the elements in [A1*] and [A2*] in the usual stability derivative form.

Recall from ref. 4:

$$f_x = C_x \bar{q} S \qquad M_x = C_l \bar{q} S b$$
$$f_y = C_y \bar{q} S \qquad M_y = C_m \bar{q} S \bar{c}_{ref.}$$
$$f_z = C_z \bar{q} S \qquad M_z = C_n \bar{q} S b$$

where $q = \frac{1}{2}\rho\left[(U_1+u)^2 + (V_1+v)^2 + (W_1+w)^2\right]$

$C_x = C_x([u, v, w, \ldots, \dot{r}])$

$C_y = C_y([u, v, w, \ldots, \dot{r}])$

.
.
.

$C_n = C_n([u, v, w, \ldots, \dot{r}])$

S is the reference area

b is wing span

c_{ref} is the reference wing chord

As examples, consider f_{x_u}, f_{x_w}, and M_{x_v} for the case of zero initial sideslip, i.e., $V_1 = 0$.

$$f_{x_u} = \frac{\partial}{\partial u}(f_x) = \frac{\partial}{\partial u}(\bar{q} S C_x)$$
$$= \frac{1}{2}\rho S\left[C_{x_u}\left((U_1+u)^2 + v^2 + (W_1+w)^2\right) + 2(U_1+u)C_x\right]$$
$$= \frac{1}{2}\rho S\left[C_{x_u}(U_1^2 + W_1^2) + 2U_1 C_x\right] + \text{terms of Order } u, u^2, v^2, w^2$$
$$\doteq \frac{\rho}{2} S\left[C_{x_u}(U_1^2 + W_1^2) + 2C_x U_1\right]$$

$$f_{x_w} = \frac{1}{V_{c_1}} \frac{\partial}{\partial \alpha} (f_x)$$

$$= \frac{1}{V_{c_1}} \frac{\rho}{2} S \left[C_{x_\alpha} \left((U_1 + u)^2 + v^2 + (W_1 + w)^2 \right) + 2 (W_1 + \dot{w}) C_x \right]$$

$$\doteq \frac{1}{V_{c_1}} \frac{\rho}{2} S \left[C_{x_\alpha} (U_1^2 + W_1^2) + 2 W_1 C_x \right]$$

$$M_{z_v} = \frac{\partial}{\partial v} (M_z) = \frac{1}{V_{c_1}} \frac{\partial}{\partial \beta} (M_z)$$

$$= \frac{1}{V_{c_1}} \frac{\rho}{2} bS \left[C_{l_\beta} (U_1^2 + W_1^2) + 2 v C_l \frac{\partial v}{\partial \beta} \right]$$

$$\doteq \frac{1}{V_{c_1}} \frac{\rho}{2} bS (U_1^2 + W_1^2) C_{l_\beta}$$

where

$$V_{c_1} = \left[U_1^2 + W_1^2 \right]^{1/2}$$

and where the derivative in each case is evaluated at the reference flight condition.

Since wind tunnel tests are often used to numerically evaluate the stability derivatives, it is helpful to define C_x and C_z forces in terms of a wind-oriented axis system shown in the sketch below. The y and y_S axes are into the paper.

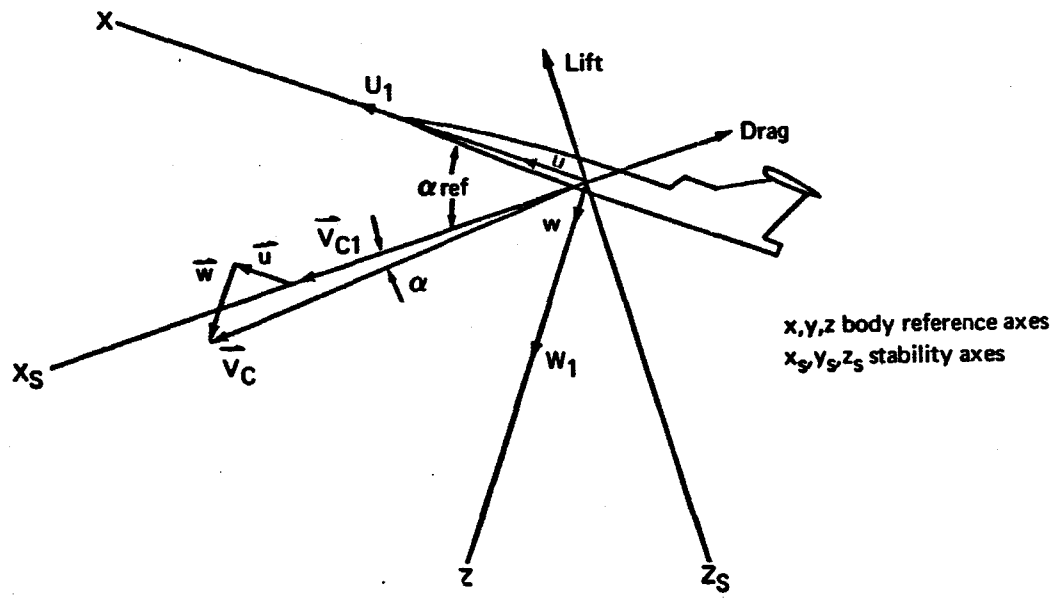

By definition:

$$V_c = \left[(U_1 + u)^2 + (V_1 + v)^2 + (W_1 + w)^2\right]^{1/2}$$

$$V_{c_1} = \left[U_1^2 + V_1^2 + W_1^2\right]^{1/2}$$

$$\alpha_{ref.} = \tan^{-1}\frac{W_1}{V_{c_1}} \doteq \frac{W_1}{V_{c_1}}$$

$$\beta_{ref.} = \tan^{-1}\frac{V_1}{V_{c_1}} \doteq \frac{V_1}{V_{c_1}}$$

$$\alpha = \tan^{-1}\frac{w}{V_c} \doteq \tan^{-1}\frac{w}{V_{c_1}} \doteq \frac{w}{V_{c_1}}$$

$$\beta = \tan^{-1}\frac{v}{V_c} \doteq \tan^{-1}\frac{v}{V_{c_1}} \doteq \frac{v}{V_{c_1}}$$

where u, v, w are the small-disturbance c.g. velocities referred to a body reference axis system x, y, z.

For the usual case of zero initial sideslip, $V_1 = 0$, the C_X and C_Z forces become:

$$C_x = -C_D \cos(\alpha_{ref.} + \alpha) + C_L \sin(\alpha_{ref.} + \alpha)$$

$$C_z = -C_D \sin(\alpha_{ref.} + \alpha) - C_L \cos(\alpha_{ref.} + \alpha)$$

where $L = C_L \bar{q} S$ is perpendicular to V_c

$D = C_D \bar{q} S$ is parallel and opposite to V_c

Defining the remaining elements in $[A_1^*]$ and $[A_2^*]$ in terms of the stability derivatives, as has been done for f_{x_u}, f_{x_w}, and M_{x_v}, results in a complete set of dynamic equations resembling those of ref. 4. It should be noted, however, that ref. 4 uses a body-fixed axis system that is the "stability axis system ($W_1 = 0$)," while this development has been in the "body reference axis system ($W_1 \neq 0$)."

An elastic airplane of n lumped masses. —The "completely elastic" mathematical model of an elastic airplane assumes the airplane can be

represented dynamically by the dynamics of lumped masses n in number. The masses are elastically connected to one another through a mathematical idealization of the aircraft's structure. Associated with each of the n-lumped masses is a panel description of the aircraft's surface. The aerodynamic forces associated with airplane c.g. motion and elastic distortion are then calculated using the value of the velocity of each panel relative to an inertial, fluid axis system.

It will be assumed that the individual panel pressures associated with the perturbation aerodynamic forces $\{f_a\}$ are a function only of the perturbation motion variables, and not geometric parameters such as wing thickness and camber, body thickness and camber, wing and tail dihedral, etc. This assumption means we must use the linear aerodynamic flow equation, boundary conditions, and pressure coefficient.

Consider the perturbation pressure force of an individual panel:

$$\vec{f}_i = f_{i_x}\hat{i} + f_{i_y}\hat{j} + f_{i_z}\hat{k}$$
$$= \vec{f}_i\left(u, v, w, \ldots, \dot{r}, u_{p_1}, \ldots, u_{p_{3n-6}}, \ldots, \ddot{u}_{p_{3n-6}}\right)$$

where i = 1, 2, 3, . . ., n and where i,j,k are the unit base vectors in the body reference system.

Note that the functional relationship of individual panel forces to the perturbation-motion variables is exactly the same as that for the aerodynamic forces of the complete airplane. This suggests that each panel force can be expanded in a form resembling equation (4.2a). For latter convenience the Taylor-series expansion of $\vec{f}_i$ will include the free vibration mode shapes $\vec{\phi}_j$ where

$$\vec{d}_{p_j} = \sum_{j=1}^{3n-6} \vec{\phi}_j\, u_j(t) \qquad \text{for n masses.}$$

Performing the Taylor-series expansion of each panel force, ignoring the same higher order terms ignored in equation (4.2a), and writing the resulting n-vector equations in component form, results in the following 3n equations:

(4.3a)

$$\{f\} = [A_1]\{v_p\} + [A_2]\{\dot{v}_p\} + [A_3][\phi]\{u_p\} + [A_4][\phi]\{\dot{u}_p\} + [A_5][\phi]\{\ddot{u}_p\}$$

where $\{f\} = \begin{bmatrix} f_{1_x} & f_{1_y} & f_{1_z} & f_{2_x} & f_{2_y} & f_{2_z} & \cdots & f_{n_x} & f_{n_y} & f_{n_z} \end{bmatrix}^T$ (4.3b)

$\{v_p\}$ as in equation (4.2b)

$\{\dot{v}_p\}$ as in equation (4.2c)

$\{u_p\}$ as in equation (4.2d)

$\{\dot{u}_p\}$ as in equation (4.2e)

$\{\ddot{u}_p\}$ as in equation (4.2f)

ϕ is the free-free mode shape matrix and is 3n x 3n-6.

$$[\phi] = \begin{bmatrix} \phi_{11_x} & \phi_{12_x} & \phi_{13_x} & \cdots & \phi_{1\,3n-6_x} \\ \phi_{11_y} & \phi_{12_y} & \phi_{13_y} & \cdots & \phi_{1\,3n-6_y} \\ \phi_{11_z} & \phi_{12_z} & \phi_{13_z} & \cdots & \phi_{1\,3n-6_z} \\ \phi_{21_x} & \phi_{22_x} & \phi_{23_x} & \cdots & \phi_{1\,3n-6_x} \\ \vdots & \vdots & \vdots & \cdots & \vdots \\ \phi_{n1_z} & \phi_{n2_z} & \cdots & \cdots & \phi_{n\,3n-6_z} \end{bmatrix} \quad (4.3c)$$

where, for example, ϕ_{ij_x} is the magnitude of the x component of the j^{th} mode shape evaluated at the control point of the i^{th} panel.

$$[A_i] = \begin{bmatrix} f_{1z_u} & f_{1z_v} & f_{1z_w} & f_{1z_p} & f_{1z_q} & f_{1z_r} \\ f_{1y_u} & \cdots & \cdots & \cdots & \cdots & f_{1y_r} \\ f_{1x_u} & \cdots & \cdots & \cdots & \cdots & f_{1x_r} \\ f_{2x_u} & \cdots & \cdots & \cdots & \cdots & f_{2x_r} \\ \vdots & \vdots & \vdots & \vdots & \vdots & \vdots \\ f_{nz_u} & \cdots & \cdots & \cdots & \cdots & f_{nz_r} \end{bmatrix} \quad (4.3d)$$

where, for example, f_{jx_u} is the variation in the x component of the force on the j^{th} panel due to the airplane's velocity perturbation u.

$$[A_2] = \begin{bmatrix} f_{1x_{\ddot{u}}} & f_{1x_{\ddot{v}}} & f_{1x_{\ddot{w}}} & f_{1x_{\dot{p}}} & f_{1x_{\dot{q}}} & f_{1x_{\dot{r}}} \\ f_{1y_{\ddot{u}}} & f_{1y_{\ddot{v}}} & \cdot & \cdot & \cdot & f_{1y_{\dot{r}}} \\ f_{1z_{\ddot{u}}} & \cdot & \cdot & \cdot & \cdot & f_{1z_{\dot{r}}} \\ f_{2x_{\ddot{u}}} & \cdot & \cdot & \cdot & \cdot & f_{2x_{\dot{r}}} \\ \cdot & \cdot & \cdot & \cdot & \cdot & \cdot \\ \cdot & \cdot & \cdot & \cdot & \cdot & \cdot \\ f_{nx_{\ddot{u}}} & \cdot & \cdot & \cdot & \cdot & f_{nx_{\dot{r}}} \end{bmatrix} \qquad (4.3e)$$

where, for example, $f_{jz_{\dot{p}}}$ is the variation of the z component of the force on the j^{th} panel due to the airplane's rotational acceleration $\dot{p}$.

The definition of the elements of $[A_3]$, $[A_4]$, and $[A_5]$ is more difficult because of the necessary separation of the $[\phi]$ matrix from the $[A_3^*]$, $[A_4^*]$, and $[A_5^*]$ matrices. The best approach is to use a simple example to illustr te the physical meaning of the elements.

Consider the case of a 3-mass, 3-panel airplane. By definition $\bar{d}_p$, $\{d_p\}$, $\{f\}$, $[\phi]$, and $[\bar{\phi}]^T$ become:

$$\vec{d}_p = \sum_{j=1}^{3n-6+3} \phi_j u_{p_i}(t) = d_{p_x}\hat{i} + d_{p_y}\hat{j} + d_{p_z}\hat{k}$$

$$d_{p_x} = \phi_{1x} u_1 + \phi_{2x} u_2 + \phi_{3x} u_3$$
$$d_{p_y} = \phi_{1y} u_1 + \phi_{2y} u_2 + \phi_{3y} u_3$$
$$d_{p_z} = \phi_{1z} u_1 + \phi_{2z} u_2 + \phi_{3z} u_3$$

$$\{d_p\} = \begin{Bmatrix} d_{p_{1x}} \\ d_{p_{1y}} \\ d_{p_{1z}} \\ d_{p_{2x}} \\ d_{p_{2y}} \\ d_{p_{2z}} \\ d_{p_{3x}} \\ d_{p_{3y}} \\ d_{p_{3z}} \end{Bmatrix} \qquad \{f\} = \begin{Bmatrix} f_{1x} \\ f_{1y} \\ f_{1z} \\ f_{2x} \\ f_{2y} \\ f_{2z} \\ f_{3x} \\ f_{3y} \\ f_{3z} \end{Bmatrix} .$$

where, for example,

$d_{p_{jy}}$ is the y component of the deformation of the j^{th} panel.

f_{jy} is the y component of the perturbation aerodynamic force acting on the j^{th} panel.

f_{jy} =

$$f_{jy} = f_{jy}\left(u, v, w, \ldots, \dot{r}, u_{p_1}, \ldots, \ddot{u}_{p_{3n-6}}\right)$$

$$[\phi] = \begin{bmatrix} \phi_{11_x} & \phi_{12_x} & \phi_{13_x} \\ \phi_{11_y} & \phi_{12_y} & \phi_{13_y} \\ \phi_{11_z} & \phi_{12_z} & \phi_{13_z} \\ \phi_{21_x} & \phi_{22_x} & \phi_{23_x} \\ \phi_{21_y} & \phi_{22_y} & \phi_{23_y} \\ \phi_{21_z} & \phi_{22_z} & \phi_{23_z} \\ \phi_{31_x} & \phi_{32_x} & \phi_{33_x} \\ \phi_{31_y} & \phi_{32_y} & \phi_{33_y} \\ \phi_{31_z} & \phi_{32_z} & \phi_{33_z} \end{bmatrix}$$

where, for example, ϕ_{jk_z} is the magnitude of the z component (evaluated at the control point of the j^{th} panel) of the k^{th} mode shape.

$$[\phi]^T = \left[\begin{array}{ccc|ccc|ccc} 1 & 0 & 0 & 1 & 0 & 0 & 1 & 0 & 0 \\ 0 & 1 & 0 & 0 & 1 & 0 & 0 & 1 & 0 \\ 0 & 0 & 1 & 0 & 0 & 1 & 0 & 0 & 1 \\ 0 & -z_1 & y_1 & 0 & -z_2 & y_2 & 0 & -z_3 & y_3 \\ z_1 & 0 & -x_1 & z_2 & 0 & -x_2 & z_3 & 0 & -x_3 \\ -y_1 & x_1 & 0 & -y_2 & x_2 & 0 & -y_3 & x_3 & 0 \end{array}\right]$$

where, for example, x_j is the x component of a vector from the aircraft's moment reference point to the control point of the j^{th} panel when the aircraft is flying its reference trajectory.

Arbitrarily defining $[A_3]$ for this 3-mass, 3-panel case:

$$[A_3] = \begin{bmatrix} A_{11} & A_{12} & A_{13} & A_{14} & A_{15} & A_{16} & A_{17} & A_{18} & A_{19} \\ A_{21} & A_{22} & \cdot & \cdot & \cdot & \cdot & \cdot & \cdot & A_{29} \\ A_{31} & \cdot & \cdot & \cdot & \cdot & \cdot & \cdot & \cdot & A_{39} \\ \vdots & \vdots & \vdots & \vdots & \vdots & \vdots & \vdots & \vdots & \vdots \\ \vdots & \vdots & \vdots & \vdots & \vdots & \vdots & \vdots & \vdots & \vdots \\ \vdots & \vdots & \vdots & \vdots & \vdots & \vdots & \vdots & \vdots & \vdots \\ A_{91} & A_{92} & \cdot & \cdot & \cdot & \cdot & \cdot & \cdot & A_{99} \end{bmatrix}$$

It is required to assign a physical meaning to the elements of $[A_3]$. This can be done by forming the product $[\phi]^T [A_3][\phi]$, equating the product to $[A_3^*]$ of equation (4.2a), and then equating elements. Recall:

$$\{f_a\} = [\bar{\phi}]^T\{f\} = [A_1^*]\{v_o\} + [A_2^*]\{\dot{v}_o\} + [A_3^*]\{u_o\} + [A_4^*]\{\dot{u}_o\} + [A_5^*]\{\ddot{u}_o\} \tag{4.2a}$$

Substituting equation (4.3a) into the equation above:

$$\{f_a\} = [\bar{\phi}]^T\left\{[A_1]\{v_o\} + [A_2]\{\dot{v}_o\} + [A_3][\phi]\{u_o\} + [A_4][\phi]\{\dot{u}_o\} + [A_5][\phi]\{\ddot{u}_o\}\right\}$$

therefore,

$$[A_1^*] = [\bar{\phi}]^T [A_1]$$
$$[A_2^*] = [\bar{\phi}]^T [A_2]$$
$$[A_3^*] = [\bar{\phi}]^T [A_3][\phi]$$
$$[A_4^*] = [\bar{\phi}]^T [A_4][\phi]$$
$$[A_5^*] = [\bar{\phi}]^T [A_5][\phi]$$

Consider the $f_{xu_{p_1}}$ element of $[A_3^*]$ from equation (4.2i) and the corresponding element of $[\bar{\phi}]^T [A_3] [\phi]$ as an example.

$$f_{xu_{p_1}} = \left(A_{11}\phi_{11_x} + A_{12}\phi_{11_y} + A_{13}\phi_{11_z} + A_{14}\phi_{21_x} + \cdots + A_{19}\phi_{31_z}\right)$$
$$\left(+ A_{41}\phi_{11_x} + A_{42}\phi_{11_y} + \cdots + A_{49}\phi_{31_z}\right)$$
$$\left(+ A_{71}\phi_{11_x} + A_{72}\phi_{11_y} + \cdots + A_{79}\phi_{31_z}\right)$$

where $f_{xu_{p_1}} = \frac{\partial f_x}{\partial u_{p_1}}$, is the change in the x component of aerodynamic force due to a change in u_{p_1}.

where the first parenthesis contains the contribution of the first panel to $f_{xu_{p_1}}$.

where the second parenthesis contains the contribution of the second panel to $f_{xu_{p_1}}$.

where the third parenthesis contains the contribution of the third panel to $f_{xu_{p_1}}$.

In more detail, the contribution to $f_{xu_{p_1}}$ of each component of mode shape 1 can be separated. For example:

$(A_{11}+A_{41}+A_{71})\phi_{11x}$ ~ contribution of panel 1, 2, and 3 to $f_{xu_{p_1}}$ due to the magnitude of the x component of the first mode shape evaluated at the control point of panel 1.

$(A_{12}+A_{42}+A_{72})\phi_{11y}$ ~ contribution of panel 1, 2, and 3 to $f_{xu_{p_1}}$ due to the magnitude of the y component of the first mode shape evaluated at the control point of panel 1.

$(A_{19}+A_{49}+A_{79})\phi_{31z}$ contribution of panel 1, 2, and 3 to $f_{xu_{p_1}}$ due to the magnitude of the z component of the first mode shape evaluated at the control point of panel 3.

Finally, each element of $[A_3]$ can be defined:

$$[A_3] = \begin{bmatrix} X_{11x1} & X_{11y1} & X_{11z1} & X_{12x1} & X_{12y1} & X_{12z1} & X_{13x1} & \dot{X}_{13y1} & X_{13z1} \\ Y_{11x2} & Y_{11y2} & Y_{11z2} & Y_{12x2} & \cdot & \cdot & \cdot & \cdot & Y_{13z2} \\ Z_{11x3} & Z_{11y3} & Z_{11z3} & \cdot & \cdot & \cdot & \cdot & \cdot & Z_{13z3} \\ X_{21x1} & X_{21y1} & X_{21z1} & \cdot & \cdot & \cdot & \cdot & \cdot & X_{23z1} \\ Y_{21x2} & \cdot & \cdot & \cdot & \cdot & \cdot & \cdot & \cdot & Y_{23z2} \\ Z_{21x3} & \cdot & \cdot & \cdot & \cdot & \cdot & \cdot & \cdot & Z_{23z3} \\ X_{31x1} & \cdot & \cdot & \cdot & \cdot & \cdot & \cdot & \cdot & X_{33z1} \\ Y_{31x2} & \cdot & \cdot & \cdot & \cdot & \cdot & \cdot & \cdot & Y_{33z2} \\ Z_{31x3} & \cdot & \cdot & \cdot & \cdot & \cdot & \cdot & \cdot & Z_{33z3} \end{bmatrix}$$

where now the elements of $[A_3]$ have been assigned the following definitions:

$$\begin{aligned} A_{11} &= X_{11x1} \\ A_{12} &= X_{11y1} \\ &\vdots \\ A_{99} &= Z_{33z3} \end{aligned}$$

where, for example, Y_{ijzk} is the y component of the aerodynamic force on panel i due to the magnitude (evaluated at the control point of each panel j) of the z deformation component of mode number k.

A similar definition for the elements of $[A_4]$ and $[A_5]$ holds:

$$[A_4] = \begin{bmatrix} \dot{X}_{11x1} & \dot{X}_{11y1} & \dot{X}_{11z1} & \cdots & \dot{X}_{13z1} \\ \dot{Y}_{11x2} & \dot{Y}_{11y2} & \dot{Y}_{11z2} & \cdots & \dot{Y}_{13z2} \\ \vdots & \vdots & \vdots & & \vdots \\ \dot{Z}_{31x3} & \dot{Z}_{31y3} & \dot{Z}_{31z3} & \cdots & \dot{Z}_{33z3} \end{bmatrix} \qquad (4.3a)$$

where, for example, Y_{ijzk} is the y component of the aerodynamic force on panel i due to the magnitude (evaluated at the control point of panel j) of the z-velocity component of mode number k.

$$[A_6] = \begin{bmatrix} \ddot{X}_{11z1} & \ddot{X}_{11y1} & \ddot{X}_{11\theta1} & \cdots & \ddot{X}_{1j\theta1} \\ \ddot{Y}_{11z1} & \ddot{Y}_{11y1} & \ddot{Y}_{11\theta1} & \cdots & \ddot{Y}_{1j\theta1} \\ \vdots & \vdots & \vdots & & \vdots \\ \ddot{Z}_{j1z1} & \ddot{Z}_{11y1} & \ddot{Z}_{11\theta1} & \cdots & \ddot{Z}_{jn\theta1} \end{bmatrix} \qquad (4.3h)$$

where, for example, Y_{ijzk} is the y component of the aerodynamic force on panel i due to the magnitude (evaluated at the control point of panel j) of the z-acceleration component of mode number k.

The generalization of the $[A_j]$ to the case of an n-mass, n-panel mathematical model of an airplane is direct. Elements within each of these matrices are interpreted the same as the general elements of the 3-mass-panel case.

Although the general formulation of the $[A_j^*]$ and $[A_j]$ matrices (where j = 1, 2, 3, 4, and 5) is complete and elements are suitably defined, the numerical evaluation of the matrices for a general case is difficult. The numerical evaluation of the u, w, p, and q elements of $[A_1]$ and $[A_2]$ for a "thin airplane" and the u and w elements for a slender-body, thin-wing airplane are presented in par. 4.4 of this appendix. In addition, several semi-empirical and experimental methods to evaluate the elements of the $[A_1^*]$ and $[A_2^*]$ matrices are presented in Secs. 5 and 6. References 4 and 26 contain methods to evaluate the elements of $[A_3^*]$, $[A_4^*]$, and $[A_5^*]$ matrices.

4.2.1.2 Form of the dynamic solution: Applying the usual small-disturbance assumptions listed in app. A or ref. 4 uncouples the force and moment equations into two sets, describing either the longitudinal small disturbance or the lateral-directional small disturbances. The longitudinal and lateral-directional equations can be solved independently and in each case the solution of the equations is of the form,

$$r_p(t) = r_{p_0} e^{at} \qquad (4.4)$$

where $v_p(t)$ is some small-disturbance motion variable, i.e., $\alpha(t)$, $u(t)$, $u_{p_{3n-6}}(t)$, etc.

v_{p_0} is some initial amplitude of the small-disturbance motion, i.e., α_1, u_1, $u_{p_{1_{3n-6}}}$, etc.

a is a complex number of the form $a = a_1 + ia_2$ reflecting a damped oscillation. If $a_1 = 0$, motion is circularly harmonic; if $a_2 = 0$, motion is nonoscillatory divergent or convergent

Details of the development of the longitudinal and lateral-directional equations and their solution for the small-disturbance variables, u, β, α, p, q, r, u_p, $\dot{u}_p$, $\ddot{u}_p$, are contained in app. C and ref. 4.

Equations (4.3a) and (4.4) will be used later in this section when the completely elastic airplane problem is formulated to include structural and aerodynamic terms in the stability derivative definition of the small perturbation forces on the airplane.

4.2.2 Inviscid fluid dynamic equations. — The inviscid fluid dynamic equations and associated boundary conditions on the airplane's surface and its wake will be developed. It is assumed that the body is experiencing a small-amplitude, time-dependent motion from its equilibrium value (determined by the balance of aerodynamic, inertial, and gravitational forces). Particular attention will be paid to the boundary condition applied at the surface of the airplane, G = 0.

The basis of the inviscid flow equations lies in the conservation laws (refs. 27 and 56). Observe that for small perturbations of an airplane from an optimum flight path, six important assumptions can be applied to simplify the representation of the velocity field surrounding the airplane.

(A13) Continuum flow ($L << 1$)

(A10) Inviscid flow ($\tau = 0$)

(A6) Adiabatic flow ($\dot{q} = 0$, no chemical reactions)

(A14) No finite shock waves

(G3) (G7) External body forces ($\vec{g}$, M.H.D., etc.) have little effect

(A15) The velocity field is irrotational ($\nabla \times \vec{v} = 0$)

Applying these assumptions to the conservation laws simplifies them to

Mass: $$\left.\frac{D\rho}{Dt}\right|_{\vec{R}} + \rho \nabla \cdot \vec{v} = 0 \qquad (4.5)$$

Momentum: $$\left.\frac{D\vec{v}}{Dt}\right|_{\vec{R}} + \frac{1}{\rho} \nabla p = 0 \qquad (4.6)$$

and implies the isentropic equation of state,

$$\frac{p}{p_0} = \left(\frac{\rho}{\rho_0}\right)^{\gamma} \qquad (4.7)$$

The usual definitions of p, ρ, $\vec{v}$, and γ apply. It is important to note that the velocity $\vec{v}$ must be fluid velocity measured relative to an inertial axis system.

It is also important to note at this point in the development that the assumptions applied to the conservation laws to develop equations (4.5), (4.6), and (4.7) do not apply to hypersonic flow. Precise limits of applicability cannot be placed upon these equations because the onset of hypersonic flow depends upon the shape of the body, the particular gas involved, and upon the region of the flow considered (ref. 34). Hypersonic flow characteristics are observed at $M_\infty = 3.0$ on some blunt bodies but not until $M_\infty = 10.0$ on some thin bodies. For supersonic jet type airplanes which are relatively slender, significant hypersonic flow effects do not occur below $M_\infty = 5.0$. The flow equations used in this report will be assumed valid up to M = 5.0 for the study SST configuration.

The characteristics used to define the onset of hypersonic flow are either hydrodynamic or physical and chemical in nature. Highly rarified gas conditions may invalidate assumptions (A6) and (A13) . Entropy gradients, produced by strong, curved shocks, make the classical isentropic, irrotational approach inapplicable by invalidating assumptions (A14) and (A15) . In many cases the boundary layer can influence the inviscid, external flow field and assumption (A10) will not apply. Other chemical reaction effects, unusual to supersonic flow, are outlined in ref. 34.

As a further consequence of the assumptions above, several useful relationships can be developed to reduce the seven equations of (4.5), 4.6), and (4.7) to a single equation in terms of a velocity potential. Listing these relationships:

(1) The irrotationality of the flow implies

$$\vec{V} = \vec{\nabla} \Phi \tag{4.8}$$

where Φ is the velocity potential (ft^2/sec)

(2) The isentropic state equation implies

$$a^2 = \frac{dp}{d\rho} \tag{4.9}$$

(3) The assumptions imply that the flow is "barotropic," i.e.,

$$P = P(\rho) \tag{4.10}$$

Applying equations (4.8) through (4.10) to equations (4.5) through (4.7) and following the pattern developed in Miles (ref. 28) or Ward (ref. 30), the inviscid flow equations simplify to

$$a_\infty^2 \nabla^2 \Phi = (\gamma - 1) \nabla^2 \Phi \left[\frac{\partial \Phi}{\partial t} + \frac{1}{2} (\nabla \Phi)^2 - \frac{U_\infty^2}{2} \right] + \frac{D}{Dt} \left[\frac{\partial \Phi}{\partial t} + \frac{1}{2} (\nabla \Phi)^2 \right] \tag{4.11}$$

Additionally, from the momentum equation, the pressure can be related to the velocity potential as

$$\frac{\partial \Phi}{\partial t} + \frac{1}{2} (\nabla \Phi)^2 + \left(\frac{\gamma}{\gamma - 1} \right) \frac{P_0}{\rho_0} \left[\left(\frac{P}{P_0} \right)^{\frac{\gamma - 1}{\gamma}} - 1 \right] = 0 \tag{4.12}$$

The problem is completely specified by assigning boundary conditions to the body and the wake. From Lamb (ref. 3), the boundary conditions are as follows:

On the wing: $$\left. \frac{DG}{Dt} \right|_{\vec{R}} = \left. \frac{\partial G}{\partial t} \right|_{\vec{r}} + \vec{V} \cdot \nabla G = 0 \tag{4.13a}$$

where $G(x, y, z, t) = 0$ defines the surface and where $\vec{V} = \nabla \Phi$

On the wake: the jump in pressure is zero

$$[C_p] = C_{p_{UPPER}} - C_{p_{LOWER}} = 0 \tag{4.13b}$$

Equations (4.11) and (4.12) describe the inviscid flow about an arbitrarily shaped body. When combined with relations 4.13, equations (4.11) through (4.13) are a complete statement of the problem and it is exact within the listed assumptions. No approximations relating to smallness of terms have been applied at this point.

Next, consider bodies that are thin and whose mean thickness δ is such that

$$\begin{aligned} \delta &\ll AR \\ \delta &\ll \tau \\ \delta &\ll b/2 \end{aligned} \qquad (4.14)$$

Proceeding with the development as found in Miles, the velocity potential can be approximated by a series expansion of Φ in terms of the perturbation quantity δ. Assume:

$$\Phi = u\left(x + \delta\phi^{(1)} + \delta^2\phi^{(2)} + \delta^3\phi^{(3)} + \cdots\right) \qquad (4.15)$$

where $u\phi^{(1)}$ - main stream velocity

$u\phi^{(1)}$ - first order in thickness perturbation of the flow

.

.

.

etc.

By substituting the series for Φ into the flow equation (4.11) the pressure equation (4.12), and the boundary conditions (4.13) and collecting terms of like order in δ, a series representation of the exact equations is generated. Higher order terms of δ represent increasingly more accurate approximations to the exact equations, providing the series converge. Consider:

(1) The flow equation (4.11)

$$\left[\frac{1}{M^2}\nabla^2\phi^{(1)} - \frac{1}{U^2}\phi^{(1)}_{tt} - \frac{2}{U}\phi^{(1)}_{xt} - \phi^{(1)}_{xx}\right]\delta$$
$$+ \delta^2\left[\frac{1}{M^2}\nabla^2\phi^{(2)} - \frac{1}{U^2}\phi^{(2)}_{tt} - \frac{2}{U}\phi^{(2)}_{xt} - \phi^{(2)}_{xx} + f(\phi^{(1)})\right]$$
$$+ \cdots = 0 \qquad (4.16)$$

(2) The pressure equation (4.12)

$$\delta\left\{u^2\frac{\partial\phi^{(1)}}{\partial x}+u\frac{\partial\phi^{(1)}}{\partial t}+\frac{1}{2}u^2+\frac{u^2}{2}\left(\nabla\phi^{(1)}\right)^2 -\left(\frac{\gamma}{\gamma-1}\right)\frac{P_\infty}{\rho}\left[1-\left(\frac{P}{P_\infty}\right)^{\frac{\gamma-1}{\gamma}}\right]\right\}+\delta^2\{\ \}+\cdots=0 \tag{4.17}$$

(3) The boundary conditions (4.13)

(a) On the wing, $\left.\frac{DG}{Dt}\right|_{\vec{k}} = \left.\frac{\partial G}{\partial t}\right|_{\vec{r}} + \vec{V}\cdot\nabla G = 0$ (4.18a)

where $\vec{V} = \nabla\Phi = u\left(\hat{i}+\delta\nabla\phi^{(1)}+\delta^2\nabla\phi^{(2)}+\cdots\right)$ (4.18b)

(b) On the wake, the same as equation (4.13b) (4.18c)

One further assumption — the usual one found in the literature — is required to simplify equations (4.16) through (4.18) to a more easily solvable set. Assume that:

(A2) the body is sufficiently thin such that the velocity field is adequately represented by first-order terms in thickness, e.g., ignore terms of δ^2 or higher order.

Define

$$\Phi = U\left(x+\delta\phi^{(1)}\right)+O\underbrace{(\delta^2)}_{\text{small}\approx 0} = U\left(x+\phi\right) \tag{4.19}$$

Equations (4.16) through (4.18) simplify to flow equation:

$$\beta^2\phi_{xx}-\phi_{yy}-\phi_{zz}+\frac{2M}{a_\infty}\phi_{xt}+\frac{1}{a_\infty^2}\phi_{tt}=0 \tag{4.20}$$

where $\beta^2 = M^2 - 1$

pressure: $$u^2\phi_x+u\phi_t+\frac{1}{2}u^2=\frac{\gamma}{\gamma-1}\left(\frac{P_\infty}{\rho_\infty}\right)\left[1-\left(\frac{P}{P_\infty}\right)^{\frac{\gamma-1}{\gamma}}\right] \tag{4.21}$$

B.C.: On the wing, $\left.\frac{\partial G}{\partial t}\right|_{\vec{r}}+u\left(\hat{i}+\nabla\phi\right)\cdot\nabla G=0$ (4.22a)

On the wake, the same as equation (4.14b) (4.22b)

By a proper definition of terms, the pressure equation (4.21) can be written in terms of a pressure coefficient for an arbitrary spatial point and instant of time. Another immediate result is the boundary condition of the wake of the body, $[C_p] = 0$. First, define mainstream conditions denoted by the subscript ∞, where $\phi_t = \nabla\phi = \phi = 0$ by definition. Evaluating equation (4.21) at "infinity,"

$$\frac{1}{2} u_\infty^2 = \frac{\gamma}{\gamma-1}\left(\frac{p_\infty}{\rho_\infty}\right)\left[1-\left(\frac{p_\infty}{p_0}\right)^{\frac{\gamma-1}{\gamma}}\right] \qquad (4.23)$$

then, subtracting (4.23) from (4.21) and simplifying it follows that

$$u_\infty^2 \phi_x + u_\infty \phi_t = \frac{\gamma}{\gamma-1}\frac{p_\infty}{\rho_\infty}\left[\left(\frac{p_\infty}{p_0}\right)^{\frac{\gamma-1}{\gamma}} - \left(\frac{p}{p_0}\right)^{\frac{\gamma-1}{\gamma}}\right] \qquad (4.24)$$

$$= \frac{\gamma}{\gamma-1}\frac{p_\infty}{\rho_\infty}\left(\frac{p_\infty}{p_0}\right)^{\frac{\gamma-1}{\gamma}}\left[1-\left(1+\frac{\bar{p}}{p_\infty}\right)^{\frac{\gamma-1}{\gamma}}\right]$$

where $\bar{p} = p - p_\infty$, static pressure difference.

$$\bar{p}/p_\infty << 1 \qquad \text{(G8)}$$

Expanding the terms in parentheses (equation (4.24)) into a binomial series and ignoring higher order terms,

$$-C_p = -\frac{\bar{p}}{q_\infty} \doteq 2\left[\frac{1}{u_\infty}\phi_t + \phi_x\right] \qquad (4.25)$$

where $q_\infty = 1/2\ \rho v^2$

and where products of the perturbation velocity potential are assumed small, e.g., $(\nabla \phi)^2 \doteq 0$ (G8)

Equation (4.25) relates the pressure coefficient at any point to the derivatives of the velocity potential evaluated at that point. For a thin body, Miles has shown that the jump in pressure between upper and lower body surfaces is defined by

$$[C_p]_{WING} = C_{p_u} - C_{p_l} = -l \qquad \text{(A2)}$$

Alternatively,

$$l = -4\left(\phi_x + \frac{1}{u_\infty}\phi(t)\right)_{0^+} \qquad (4.26)$$

where ϕ_x and ϕ_t are to be evaluated at the upper surface of the body.

The boundary condition on the body's wake is evaluated by substituting equation (4.26) into equation (4.13b).

$$[C_p]_{WAKE} = 0 \qquad \left(\phi_x + \frac{1}{u_\infty}\phi_t\right)_{WAKE} = 0 \qquad (4.27)$$

where ϕ_x and ϕ_t are evaluated on either the upper or lower surface of the wake.

It is advantageous to evaluate wing and wake boundary conditions at a spatial position that is time independent. The usual technique applied in the literature (refs. 28 and 41) is to expand the boundary conditions and velocity potential about a plane containing the time-averaged body trajectory. For rigid-

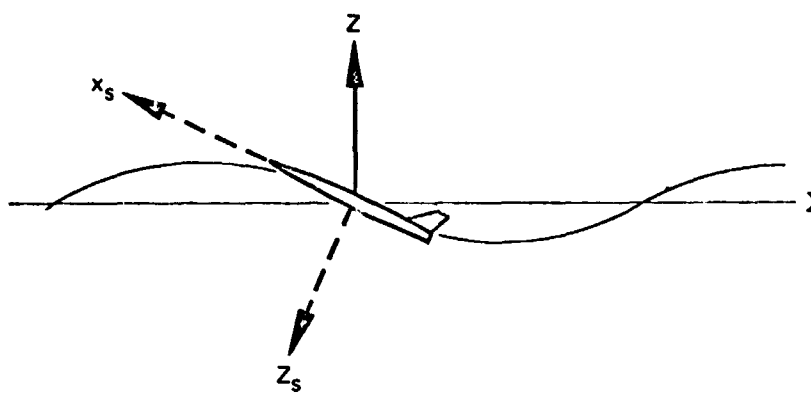

Mean plane for c.g. motion only

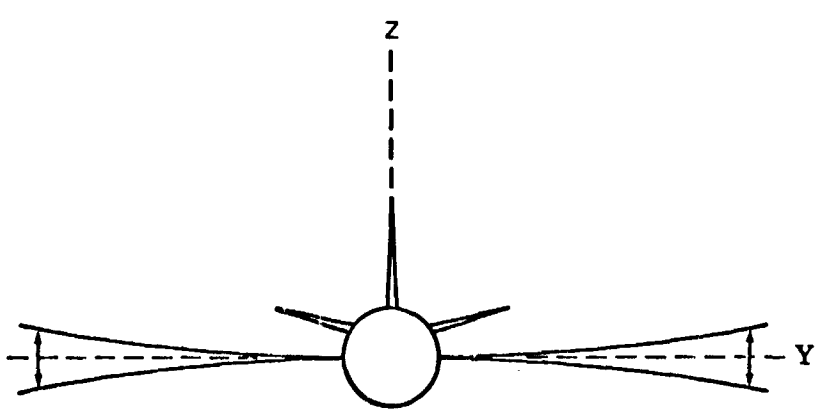

Mean plane for elastic motion only

airplane motion, the plane is that about which the small disturbance motion takes place. For flutter or other structural dynamics, the plane is that about which elastic deflections occur.

The difficulty in choosing the expansion plane when elastic motion is superimposed on airplane c.g. motion is apparent. Fortunately, the small-disturbance equation, (4.2) is written so that the stability derivatives are evaluated for one motion variable at a time (i.e., to evaluate α (t) derivatives, the only surface motion occurring relative to the fluid axis system translating at u_∞ is that due to a change in surface angle of attack). Consequently, although a single mean plane cannot be specified for the general boundary condition on the wing, one does exist for each stability derivative and it can be defined as the z = 0 plane. Details will be presented later in this section and illustrated by sample.

In the z = 0 plane in which the potential flow singularities will be placed, three distinct regions are defined, i.e., S, W, and R (ref. 28), and in each the boundary conditions are different.

Define S - the airplane's projection on the xy plane; the singularity position on the z = 0 plane

W - the airplane's wake projection on the xy plane

R - "remainder" of the xy plane

where xyz - is the axis system in which the flow equation and boundary conditions are written

x_B, y_B, z_B - is a body fixed axis system in which the body's surface is defined

x_S, y_S, z_S - is a body fixed axis system in which the usual stability and control small-disturbance equations are written; the "stability axes"

The boundary conditions then simplify (ref. 28) to

$$\frac{DG}{Dt}_{\vec{R}} = \frac{\partial G}{\partial t} + \vec{V} \cdot \nabla G = 0 \qquad \text{on } S \qquad (4.28a)$$

$$\left(\phi_z + \frac{1}{u_\infty}\phi_t\right)_{z=0} = 0 \qquad \text{on } W \qquad (4.28b)$$

$$\phi\big|_{z=0} = 0 \qquad \text{on } R \qquad (4.28c)$$

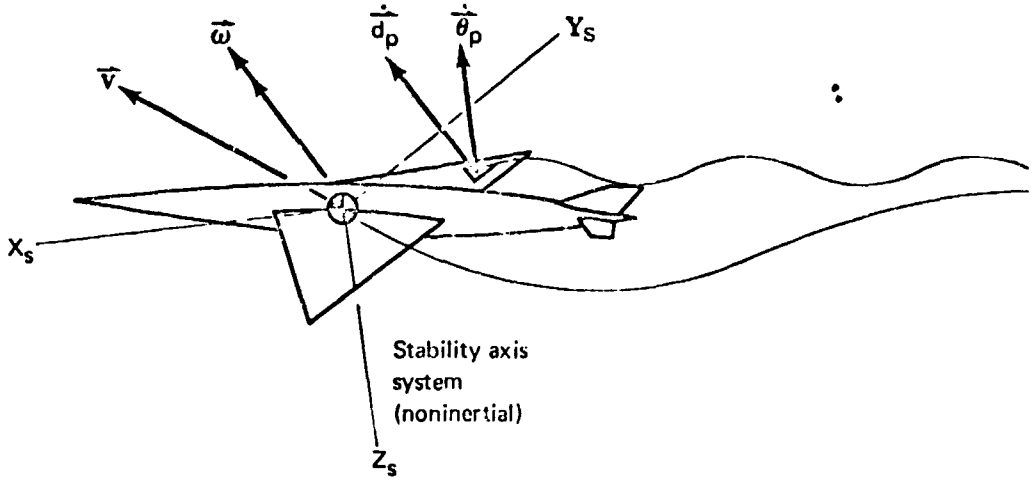
$\vec{\omega}$
$\dot{\vec{d}}_p$
$\dot{\vec{\theta}}_p$
Y_S
$\vec{V}$
X_S
Stability axis
system
(noninertial)
Z_S

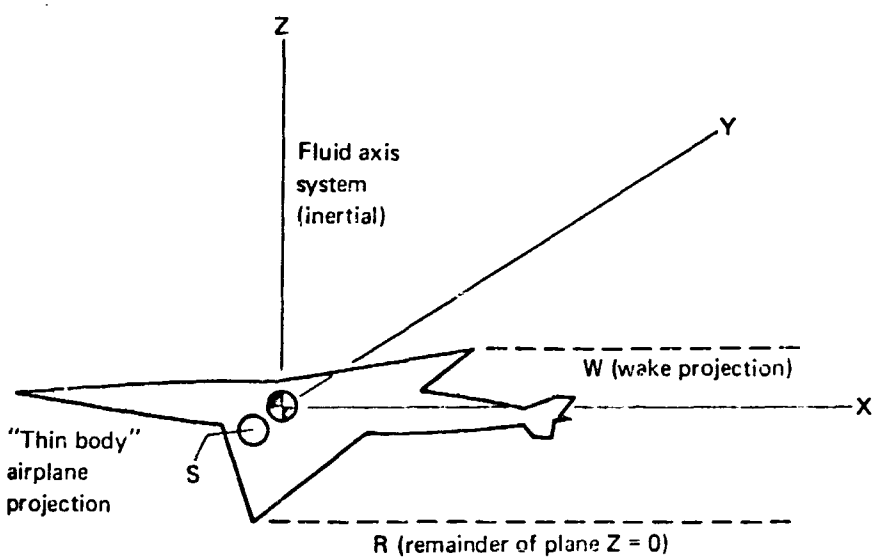
Z
Fluid axis
system
(inertial)
Y
W (wake projection)
X
"Thin body"
airplane
projection
S
R (remainder of plane Z = 0)

4.2.3 Structural theory — general considerations. —

4.2.3.1 Introduction: The fundamental considerations in the development (A1) of the structural theory are continuity (essentially conservation of mass), conservation of momentum, and Hooke's law. The consideration of continuity follows from an investigation of the deformation of a continuous body. Conservation of momentum follows from Newton's laws of motion, and Hooke's law relates deformation of the continuous body to forces acting on the body. The object of this introduction is to outline the basis of structural theories used in relating the elastic deformation of an airplane to the applied loads. This outline will briefly follow the development of the internal equilibrium equation with only sufficient detail as is required to point out the approximations included in the theory.

As shown by refs. 8 and 57, if two neighboring points in a body are separated by the differential distance ds_0 before deformation and by the differential distance ds after deformation, the following exact relationship is satisfied by the components of the displacement vector $\vec{d}$:

$$(ds)^2 - (ds_0)^2 = 2\left[(d\vec{r}\cdot\vec{\nabla})\vec{d}\,\right]\cdot d\vec{r} + \left[(d\vec{r}\cdot\vec{\nabla})\vec{d}\right]\cdot\left[(d\vec{r}\cdot\vec{\nabla})\vec{d}\right] \tag{4.30}$$

where

$$(ds_0)^2 \equiv d\vec{r}\cdot d\vec{r}$$

The strain in the direction of the ds_0 is defined as

$$\varepsilon \equiv \frac{ds - ds_0}{ds_0} \tag{4.31}$$

and it follows that

$$(ds)^2 - (ds_0)^2 = (2\varepsilon + \varepsilon^2)(ds_0)^2 \tag{4.32}$$

If the strains are sufficiently small, then $\varepsilon^2 << 2\varepsilon$ and equation (4.32) (S2) reduces to

$$\varepsilon \approx \frac{1}{2}\left[\frac{(ds)^2 - (ds_0)^2}{(ds_0)^2}\right] \tag{4.33}$$

This relationship may be used to relate strain to arbitrary displacement gradients by equating equation (4.33) to equation (4.30). If the displacement gradients are sufficiently small, then equations (4.30) and (4.33) may be used to

write

$$\varepsilon \approx \frac{1}{(ds_0)^2}\left[(d\vec{r}\cdot\vec{\nabla})\vec{d}\right]\cdot d\vec{r} \tag{4.34}$$

Letting $d\vec{r}=dx\vec{i}$, $d\vec{r}=dy\vec{j}$, $d\vec{r}=dz\vec{k}$ in sequence, the following small strain-small displacement gradient relations are obtained.

$$\varepsilon_x = \frac{\partial u}{\partial x} \qquad \varepsilon_y = \frac{\partial v}{\partial y} \qquad \varepsilon_z = \frac{\partial w}{\partial z} \tag{4.35a}$$

where $\vec{d} = u\vec{i} + v\vec{j} + w\vec{k}$

Considerations similar to the above regarding the change in angle between infinitesimal fibers in the solid due to deformation leads to the small strain-small displacement gradient relations

$$\gamma_{xy} = \frac{\partial v}{\partial x} + \frac{\partial u}{\partial y} \qquad \gamma_{xz} = \frac{\partial w}{\partial x} + \frac{\partial u}{\partial z} \qquad \gamma_{yz} = \frac{\partial w}{\partial y} + \frac{\partial v}{\partial z} \tag{4.35b}$$

and the small rotation-small displacement gradient relations

$$\omega_{xy} = \frac{1}{2}\left(\frac{\partial v}{\partial x} - \frac{\partial u}{\partial y}\right) \qquad \omega_{xz} = \frac{1}{2}\left(\frac{\partial u}{\partial x} - \frac{\partial w}{\partial z}\right) \qquad \omega_{yz} = \frac{1}{2}\left(\frac{\partial w}{\partial y} - \frac{\partial v}{\partial z}\right) \tag{4.36}$$

If the displacement field $\vec{d}(x, y, z, t)$ is specified so that the displacement components are continuous functions of the coordinates, then the strains may be computed using equations (4.35). If the strains are specified, then it may or may not be possible to integrate equations (4.35) to obtain a set of compatible displacement components. The specified strains must satisfy compatibility relations (ref. 8). This is mentioned here for completeness only, as the technique of structural analysis to be considered here will deal only with specified displacements that are continuous interior to elements of the structure.

Conservation of momentum has been expressed in app. A by the two equations

$$\int_V \rho_A \frac{d^2\vec{r}}{dt^2}\, dV = \int_V \vec{R}\, dV + \int_S \vec{F}\, dS \tag{4.37}$$

for conservation of linear momentum and

$$\int_V \rho_A\, \vec{r} \times \frac{d^2\vec{r}}{dt^2}\, dV = \int_V \vec{r} \times \vec{R}\, dV + \int_S \vec{r} \times \vec{F}\, dS \tag{4.38}$$

for conservation of angular momentum.

The surface traction $\vec{F}$ ds must be related to forces internal to the structure. This is accomplished (ref. 8) by introducing the concept of internal stress. The stress vector $\vec{F}$ is expanded as

$$\vec{F} = \sum_{i=1}^{3}\sum_{j=1}^{3} \sigma_{ij}\, n_i\, \vec{g}_j \tag{4.39}$$

where n_i are the components of the unit normal vector $\vec{n}$ at the surface S, and $\vec{g}_j$ are the unit base vectors. Thus,

$$\vec{n} = n_x \vec{i} + n_y \vec{j} + n_z \vec{k}$$

$$\equiv n_1 \vec{g}_1 + n_2 \vec{g}_2 + n_3 \vec{g}_3$$

$$\vec{n} = \sum_{i=1}^{3} n_i \vec{g}_i \qquad (4.40)$$

The quantities σ_{ij} are the components of the stress tensor. As shown by ref. 8 they are related to a more familiar notation as

$$\sigma_{11} \equiv \sigma_x \qquad \sigma_{12} \equiv \tau_{xy} \qquad \sigma_{13} \equiv \tau_{xz}$$

$$\sigma_{21} \equiv \tau_{yx} \qquad \sigma_{22} \equiv \sigma_y \qquad \sigma_{23} \equiv \tau_{yz} \qquad (4.41)$$

$$\sigma_{31} \equiv \tau_{zx} \qquad \sigma_{23} \equiv \tau_{zy} \qquad \sigma_{33} \equiv \sigma_z$$

where σ_x, σ_y, σ_z are the components of normal stress and τ_{xy}, τ_{xz}, τ_{yx}, τ_{yz}, τ_{zx}, τ_{zy} are the components of shear stress.

In terms of the stress tensor and on using the divergence theorem such that

$$\int_S \sum_{i=1}^{3} \sum_{j=1}^{3} \sigma_{ij} n_i \vec{g}_j \, dS = \int_V \sum_{i=1}^{3} \sum_{j=1}^{3} \frac{\partial \sigma_{ij}}{\partial x_i} \vec{g}_j \, dV$$

equation (4.38) becomes

$$\int_V \left[\rho_A \frac{d^2 \vec{r}'}{dt^2} - \vec{R} - \frac{\partial \sigma_{ij}}{\partial x_i} \vec{g}_j \right] dV = 0$$

Thus, the result vanishes only if the integrand vanishes. Hence,

$$\rho_A = \frac{d^2 \vec{r}'}{dt^2} - \vec{R} - \frac{\partial \sigma_{ij}}{\partial x_i} \vec{g}_j = 0 \qquad (4.42)$$

As shown by ref. 8, a similar set of operations on equation (4.39) leads to the result

$$\sigma_{ij} = \sigma_{ji} \qquad (4.43)$$

The stress tensor is symmetric and in the notation of equation (4.41)

$$\tau_{xy} = \tau_{yx} \,, \quad \tau_{xz} = \tau_{zx} \,, \quad \tau_{yz} = \tau_{zy}$$

(S1) Hooke's law is given by ref. 8 as (S1)

$$\varepsilon_x = \frac{1}{E}\left[\sigma_x - \nu(\sigma_y + \sigma_z)\right]$$
$$\varepsilon_y = \frac{1}{E}\left[\sigma_y - \nu(\sigma_x + \sigma_z)\right]$$
$$\varepsilon_z = \frac{1}{E}\left[\sigma_z - \nu(\sigma_y + \sigma_x)\right] \qquad (4.44)$$
$$\gamma_{xy} = \frac{1}{G}\tau_{xy} \qquad \gamma_{xz} = \frac{1}{G}\tau_{xz} \qquad \gamma_{yz} = \frac{1}{G}\tau_{yz}$$

where
$$G = \frac{E}{2(1+\nu)}$$

The constants are identified as E: Young's modulus, G: shear modulus, and ν : Poisson's ratio. The introduction of Hooke's law represents an assumption that differs in a sense from those preceding. Hooke's law describes the behavior of a hypothetical material that is homogeneous, isotropic, and linearly elastic. No terms from a more exact expression have been discarded as small in obtaining equations (4.46). They, in fact, represent a definition and, if the structure of the airplane is constructed of a material with a behavior exactly described by equations (4.44), then there is no approximation involved. However, aircraft structures are neither homogeneous, isotropic, nor linearly elastic; they have these characteristics only approximately.

Hooke's law and the strain-displacement relations may be used to write the equilibrium equations, equations (4.42), in terms of the displacement components as (ref. 8):

$$\frac{E}{2(1+\nu)(1-2\nu)}\frac{\partial e}{\partial x} + G\nabla^2 u = \rho_A a_x - R_x$$
$$\frac{E}{2(1+\nu)(1-2\nu)}\frac{\partial e}{\partial y} + G\nabla^2 v = \rho_A a_y - R_y \qquad (4.45)$$
$$\frac{E}{2(1+\nu)(1-2\nu)}\frac{\partial e}{\partial z} + G\nabla^2 w = \rho_A a_z - R_z$$

where

$$e \equiv \frac{\partial u}{\partial x} + \frac{\partial v}{\partial y} + \frac{\partial w}{\partial z} = \vec{\nabla}\cdot\vec{d}$$
$$\nabla^2 \equiv \frac{\partial^2}{\partial x^2} + \frac{\partial^2}{\partial y^2} + \frac{\partial^2}{\partial z^2}$$

and

$$a \equiv \frac{d^2\vec{r}}{dt}$$

Equations (4.45) are referred to as the Navier equations and in the theory of elasticity they have a role which is analogous to the Navier-Stokes equation of fluid dynamics.

The structural influence functions $\vec{\Gamma}$ introduced by Bisplinghoff (ref. 1) and used extensively in this report are obtained from a supposed inverse to the Navier equations. The inverse leads to an integral equation that is equivalent to the Navier equations. It contains the boundary conditions at the surface of the structure and the condition that the structure is a free body and is given by

$$\vec{d} - \vec{d}_o - \tfrac{1}{2}(\nabla \times \vec{d})_o \times \vec{r} = \int_V \vec{\Gamma}_o \cdot [\vec{e} - \rho_A \vec{a} + \delta(\vec{r} - \vec{r}_s)\vec{F}]\, dV \quad (4.46)$$

This equation appears in app. A and is referred to as the internal equilibrium equation. The vectors $\vec{d}_o$ and $\frac{1}{2}(\vec{\nabla} \times \vec{d})_o$, which appear in equation (4.46), are introduced out of necessity. The airplane is a free structure with only stress boundary conditions at the surface. To invert the Navier equations, a single displacement boundary condition must be added. This consists of clamping a reference point chosen here to be the c.g. As shown in app. A $\vec{d}_o$ and $\frac{1}{2}(\vec{\nabla} \times \vec{d})_o$ represent the displacement and rotation of the material point relative to the c.g. when the airplane is allowed to be free.

During the past twenty years, considerable research has been directed toward constructing the influence coefficients, $\vec{\Gamma}$, for complex structures such as that of an airplane (refs. 1, 26, 39, 43, and 58). The advent of large, high-speed digital computers has provided the impetus for this research. The theoretical basis for analyzing a complex structure such as that of an airplane has existed for over fifty years. However, the number of numerical calculations required limited application to relatively simple structures and usually employed relaxation techniques as illustrated by the work of R. V. Southwell in "Relaxation Methods in Engineering Science," Clarendon Press, Oxford, 1940.

The methods of structural analyses now being developed employ detailed analyses of the elements of the structure, i.e., spar and rib caps, webs, cover plates, etc. The analysis of an element takes into consideration the interaction with other elements of the structure. This is accomplished by requiring compatibility or continuity of displacements and equilibrium of stresses interior to the structural elements and across boundaries of the structural elements.

Neither the displacements n or the stresses at the element boundaries are precisely the actual displacements and stresses that occur at those boundaries in the structure. They may, however, be excellent approximations to the displacement and stresses in the structural elements at a short distance from the intersecting boundaries. The displacement and stress fields at intersecting boundaries are in general complicated functions of the coordinates. These are local effects and, in accordance with Saint-Venant's principle (ref. 8), they have little effect on the overall structural behavior.

The terms "generalized displacements" and "generalized forces" have been applied to the values of the displacements and the summation of the forces at the intersecting boundaries. The term "structural node," not to be confused with "vibration nodes," has been used to identify the intersections. The values of these quantities are treated as unknowns in the structural problem.

There are two alternate approaches to the structural analysis. They may be denoted as the displacement method and the force method. In the displacement method the displacement fields are specified for each element and their intensities are functions of the generalized displacements at the nodes. An element stiffness matrix is formed and denoted by $[K]_i$. The elements of the element stiffness matrix relate the generalized forces at the nodes, denoted as $\{F\}_i$ for the i^{th} element, to the magnitudes of the generalized displacements at the nodes, denoted by $\{d\}_i$. This is written as

$$\{F\}_i = [K]_i \{d\}_i \qquad (4.47)$$

and an example derivation for this relation is carried out in the following section for a beam-type element.

When equations of the form of equation (4.47) are written for all of the n elements of a complex structure, they may be combined into a single matrix equation as

$$\begin{Bmatrix} \{F\}_1 \\ \vdots \\ \{F\}_n \end{Bmatrix} = \begin{bmatrix} [K]_1 & & 0 \\ & \ddots & \\ 0 & & [K]_n \end{bmatrix} \begin{Bmatrix} \{d\}_1 \\ \vdots \\ \{d\}_n \end{Bmatrix} \qquad (4.48)$$

The stiffness matrix contained in equation (4.48) is usually of very large order, but the nonzero elements are concentrated along the diagonal. Special techniques for manipulating matrices of this type have been developed that lead to economical computer-storage usage. Also, there are methods for reducing the order of the stiffness matrix so that only those nodes where the displacements and forces are related to the exterior-applied loads and enforced displacements are retained. Both considerations exceed the scope required for this discussion. The discussion here is centered on the approximations and not on the detailed problems involved in efficient computation.

The approximations involved in the force method need not differ from those contained in the displacement method. Both methods make use of Saint-Venant's principle. The degree of accuracy in any application is limited only in the degree of sophistication used in the representation of the displacement or stress fields used in the analysis of the elements. Certain advantages accrue in the mechanization for the computer through the use of one method or the other. But, again, a discussion of these advantages and disadvantages exceeds the present scope. It is important to realize only that the influence $\bar{\Gamma}_0$ may be obtained to any degree of desired accuracy within practical limits. However, the result is a set of influence coefficients in lieu of influence functions.

4.2.3.2 Calculation of structural influence matrices from beam theory: This paragraph deals with the generation of structural influence coefficients using a beam structural idealization of the airplane. Two sets of structural coefficients are of special interest. One relates vertical loads to the resulting streamwise angular distortions, and the other relates vertical loads to the resulting vertical displacements.

(S9) For calculation of structural influence coefficients, the airplane is assumed to have some point fixed in space. This point is sometimes assumed to be the wing-body intersection; but, as will be shown later, the point that must be fixed is entirely arbitrary.

Mathematical model: The purpose of this paragraph is to depict an airplane by a set of beams and to list the assumptions that are involved in the beam analysis.

The assumptions involved are:

(S3) The material is perfectly elastic.

(S2) The deflections are small compared to the size of the structure, and secondary deflections caused by interaction between applied forces and primary deflections are negligible.

(S12) The structure can be adequately represented with beams.

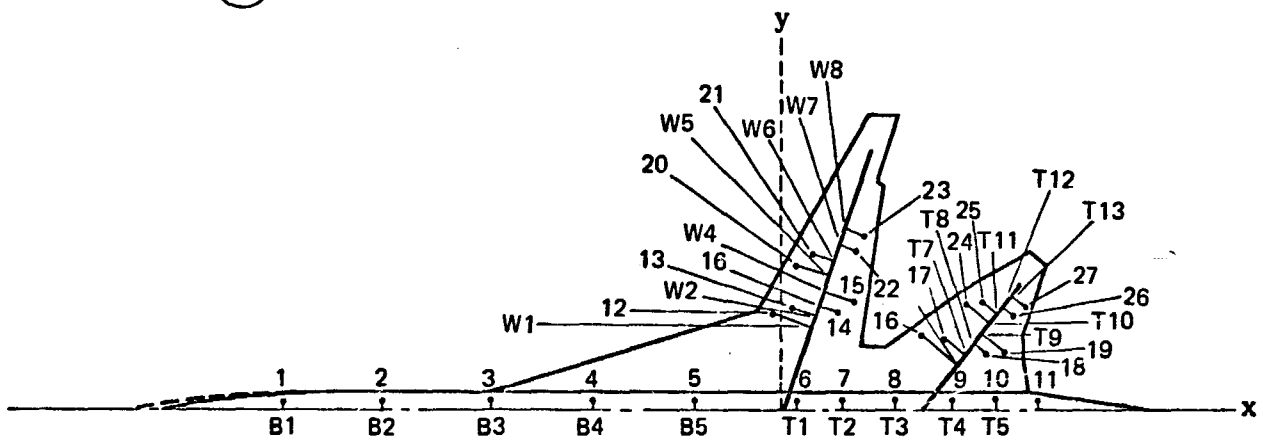

FIGURE 3.– BEAM REPRESENTATION OF AN AIRPLANE

Figure 3 is a typical beam representation of an airplane. The elastic axis representing the body connects points B1, B2, etc.; the wing axis W1, W2, etc.; and the tail axis T1, T2, etc. There are other beams connecting the control points, 1, 2, 3, 4, etc., to the elastic axis points. The input required for computation of influence coefficients requires two quantities. These are the structural beam components and the coordinate positions of control points. The beams connecting the control points to the elastic axis are considered to be infinitely stiff compared to the elastic axis stiffness. There is no requirement as to where the control point must be attached to the elastic axis.

The attachment point is left to the discretion of the engineer. As will be shown later, the attachment points are eliminated from the solution so that only influence coefficients at the control points are retained.

Development of equations to generate structural coefficient matrix: There are several methods that can be used for generating the structural influence matrix using beam theory. The method presented herein is a continuation of the direct stiffness generation method presented in par. 4.2.3.1 of this appendix.

Consider a beam element connecting points 1 and 2 in fig. 4. This beam may be an element of a larger beam in the total structure.

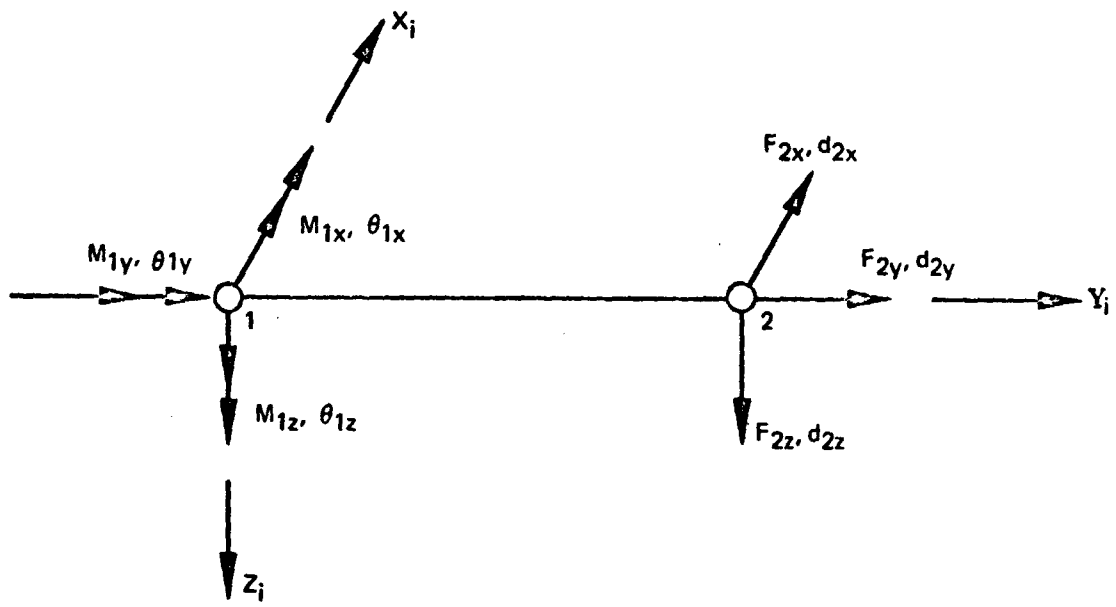

FIGURE 4. – TYPICAL BEAM ELEMENT

The coordinate system is as shown in fig. 4 and is repeated from app. A. The general stiffness matrix for the beam element is

$$
[K]_i = \begin{array}{c}
\begin{matrix} U_1 & V_1 & W_1 & \theta_{1x} & \theta_{1y} & \theta_{1z} & U_2 & V_2 & W_2 & \theta_{2x} & \theta_{2y} & \theta_{2z} \end{matrix} \\
\begin{bmatrix}
\frac{12EI_y}{L^3} & & & & & & & & & & & \\
0 & \frac{AE}{L} & & & & & & & & & & \\
0 & 0 & \frac{12EI_x}{L^3} & & & & & \text{(SYMMETRIC)} & & & & \\
0 & 0 & \frac{6EI_x}{L^2} & \frac{4EI_x}{L} & & & & & & & & \\
0 & 0 & 0 & 0 & \frac{GJ}{L} & & & & & & & \\
-\frac{6EI_z}{L^2} & 0 & 0 & 0 & 0 & \frac{4EI_z}{L} & & & & & & \\
-\frac{12EI_z}{L^3} & 0 & 0 & 0 & 0 & \frac{6EI_z}{L^2} & \frac{12EI_z}{L^3} & & & & & \\
0 & -\frac{AE}{L} & 0 & 0 & 0 & 0 & 0 & \frac{AE}{L} & & & & \\
0 & 0 & -\frac{12EI_x}{L^3} & -\frac{6EI_x}{L^2} & 0 & 0 & 0 & 0 & \frac{12EI_z}{L^3} & & & \\
0 & 0 & -\frac{6EI_x}{L^2} & \frac{2EI_x}{L} & 0 & 0 & 0 & 0 & -\frac{6EI_x}{L^2} & \frac{4EI_x}{L} & & \\
0 & 0 & 0 & 0 & \frac{GJ}{L} & 0 & 0 & 0 & 0 & 0 & \frac{GJ}{L} & \\
-\frac{6EI_z}{L^2} & 0 & 0 & 0 & 0 & \frac{2EI_z}{L} & \frac{6EI_z}{L^2} & 0 & 0 & 0 & 0 & \frac{4EI_z}{L}
\end{bmatrix}_i
\end{array}
$$

The force-deflection relation for the i^{th} beam is then given as

$$\{F\}_i = [K]_i \{d\}_i \qquad (4.47)$$

where $\{d\}_i$ and $\{F\}_i$ can be considered to include rotations and moments as well as longitudinal displacements and applied forces.

Equation (4.47) is written in the local coordinate axis system shown in fig. 4; however, we generally deal with problems in which the beam has an arbitrary orientation in space and the forces and displacements are required in a specified axis system.

A transformation matrix that changes displacements and forces oriented to the local axis of the beam into another general axis system is developed as follows:

Consider the case of an arbitrary orientation of a beam as in fig. 5.

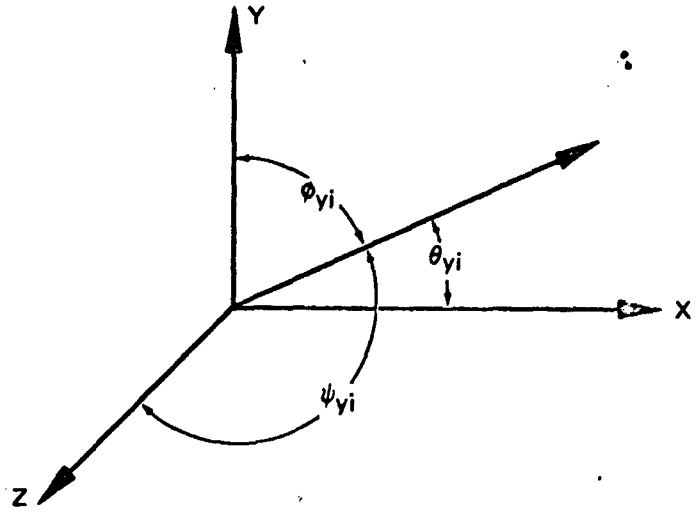

FIGURE 5. – LOCAL BEAM AXIS SYSTEM

A deflection in the y_i direction can be written as,

$$d_{y_i} = d_x \cos \theta_{y_i} + d_y \cos \phi_{y_i} + d_z \cos \psi_{y_i} \qquad (4.49)$$

and a force as,

$$F_{y_i} = F_x \cos \theta_{y_i} + F_y \cos \phi_{y_i} + F_z \cos \psi_{y_i} \qquad (4.50)$$

Moment forces can be transformed in the same fashion. Although rotations are not vectors, it is possible to use the same transformation on rotations provided the rotations are small. This assumption is justified in the case of structural displacement. All of the components transform in an analogous fashion, thus giving

$$\begin{Bmatrix} d_{x_i} \\ d_{y_i} \\ d_{z_i} \end{Bmatrix} = \begin{bmatrix} a_x & b_x & c_x \\ a_y & b_y & c_y \\ a_z & b_z & c_z \end{bmatrix} \begin{Bmatrix} d_x \\ d_y \\ d_z \end{Bmatrix} = [\lambda]_i \{d\} \qquad (4.51)$$

and

$$\begin{Bmatrix} F_{x_i} \\ F_{y_i} \\ F_{z_i} \end{Bmatrix} = \begin{bmatrix} a_x & b_x & c_x \\ a_y & b_y & c_y \\ a_z & b_z & c_z \end{bmatrix} \begin{Bmatrix} F_x \\ F_y \\ F_z \end{Bmatrix} = [\lambda]_i \{F\} \qquad (4.52)$$

where a, b, and c are respective direction cosines. The column of forces and moments in equation (4.47) can then be written as

$$\{F\}_i = [T]_i \{F\} = \begin{bmatrix} \lambda & 0 & 0 & 0 \\ 0 & \lambda & 0 & 0 \\ 0 & 0 & \lambda & 0 \\ 0 & 0 & 0 & \lambda \end{bmatrix} \cdot \begin{Bmatrix} F_1 \\ M_1 \\ F_2 \\ M_2 \end{Bmatrix} \quad (4.53)$$

In a similar manner the deflection matrix in equation (4.47) becomes

$$\{d\}_i = [T]_i \{d\} \quad (4.54)$$

Since the transformation $[T]_i$ is an orthogonal transformation, its inverse is equal to its transpose; thus, equation (4.52) can be rewritten using (4.53) and becomes,

$$\{F\}_i = [T]_i^T [K]_i [T] \{d\} = [K] \{d\} \quad (4.55)$$

where

$$[K] = [T]_i^T [K]_i [T]_i \quad (4.56)$$

The stiffness of a beam element is now known in terms of some general axis system where the direction cosines between local and general coordinates can be determined from the position of the ends of the element and the orientation of its principal axis with respect to the general axis system.

The general coordinates considered for the airplane analysis of interest herein are the body fixed reference, x_s, y_s, z_s coordinates described in the previous sections. The origin is generally at the wing-body intersection point, with x_s positive forward, y_s positive on the right side of the airplane, and z_s positive downward; however, there is nothing special about the choice of origin.

The stiffness for the entire airplane is computed by combining the stiffness of each individual element. For example, a dummy stiffness matrix for the entire structure can be formulated with all elements of the matrix equal to zero. Then the stiffness contribution of each element is added in turn to the dummy matrix until all elements of the structure have been included.

Each of the displacement and force terms are meant to represent all of the nodal forces or moments in that particular direction. For example, F_z is a column of forces in the z direction at each of the 1 through n node points. Thus, [K*] in equation (4.63) is a 6n x 6n matrix.

The desired quantities are generally the displacements in the z direction due to a set of loads in the z direction and the θ_y angle change due to a load in the z direction. By using certain of the assumptions that are made regarding the beam representation of the airplane, equation (4.63) can be reduced to obtain the desired stiffness matrix.

Displacements d_y, d_x, and θ_z are assumed to be zero for a longitudinal analysis and all forces and moments except F_{z_i} are assumed to be zero. (S10) (S11)

Expanding equation (4.63) using the above assumptions gives

$$\begin{Bmatrix} F_z \\ 0 \\ 0 \end{Bmatrix} = [K_1^*] \begin{Bmatrix} d_z \\ \theta_x \\ \theta_y \end{Bmatrix} \tag{4.64}$$

Inverting $[K_1^*]$ yields

$$\begin{Bmatrix} d_z \\ \theta_x \\ \theta_y \end{Bmatrix} = [C] \begin{Bmatrix} F_z \\ 0 \\ 0 \end{Bmatrix} \tag{4.65}$$

[C] can be partitioned in equation (4.65) to give

$$\left[\begin{array}{c} d_z \\ \hline \theta_x \\ \hline \theta_y \end{array}\right] = \left[\begin{array}{c|c|c} C_{11} & C_{12} & C_{13} \\ \hline C_{21} & C_{22} & C_{23} \\ \hline C_{31} & C_{32} & C_{33} \end{array}\right] \left[\begin{array}{c} F_z \\ \hline 0 \\ \hline 0 \end{array}\right] \tag{4.66}$$

Expanding (4.66) and retaining the quantities of interest gives

$$\{d_z\} = [C_{11}]\{F_z\} \tag{4.67a}$$

and

$$\{\theta_y\} = [C_{31}]\{F_z\} \tag{4.67b}$$

The method presented here for determining influence coefficients is a restriction of a more general method of structural analysis. As listed in the assumptions, one must be able to describe the airplane as a set of beams. There

is no pat answer as to when one should not describe the structure with beams. Generally, it is assumed that high-aspect-ratio wings (such as the 707) can be represented by beams and that delta wings such as the B-58 cannot.

The structural analysis method presented will work with beams or any other structural elements desired or any degree of indeterminate structure. The accuracy of the results is bounded primarily by the engineer's resourcefulness.

Figure 6 is a flow diagram for programming the previous analysis.

4.2.3.3 Free-free mode shapes: It was shown in app. A that the equation of motion describing the deformation of an airplane can be described in matrix form as

$$\{d_p\} = -[\bar{C}][[m]\left(\frac{\partial^2}{\partial t^2}\{d_p\} + [\bar{\phi}]\frac{\partial}{\partial t}\{v_p\} + [\bar{\phi}][M_2]\{v_p\} + [\bar{\phi}][M_2]\{r'_{op}\}\right) - \{f\}]$$

(6.132, app. A)

where $\{d_p\}$ is the column matrix describing the deflections of all panel control points due to aerodynamic and inertial loads

$[\bar{c}]$ is the stiffness matrix

$[m]$ is the diagonal matrix of lumped masses

$[\phi]$, $[M_1]$, $[M_2]$, $\{r'_{op}\}$, $\{f\}$ are as defined in par. 4.2.1 of this appendix

By definition, the free-free mode shapes will be defined as $[\phi]$, which satisfy equation (6.132, app. A) when the resulting forces and moments are equal to zero. This implies that $\{f\} = \frac{\partial}{\partial t}\{v_p\} = \{v_p\} = 0$. Applying these simplifications to equation (6.132, app. A) results in the free-free motion equation of the form

$$\{\ddot{d}_p\} = -[\bar{C}][m]\frac{\partial^2}{\partial t^2}\{d_p\} \qquad (4.68)$$

Following the suggestion of app. A and ref. 26, the deflection matrix $\{d_p\}$ can be written

$$\{d_p\} = [\phi]\{u_{3n-6}(t)\} \qquad (4.69)$$

where $[\phi]$ are the normalized natural free vibration modes of the airplane and are eigenfunctions of the integral equation.

$$\phi = \omega_i^2 \iint_S C(x, y_i, \xi, \eta)\,\phi_i(\xi, \eta)\,\rho(\xi, \eta)\,d\xi\,d\eta$$

and where $\{u_{3n-6}(t)\}$ is the time variation of the mode shapes.

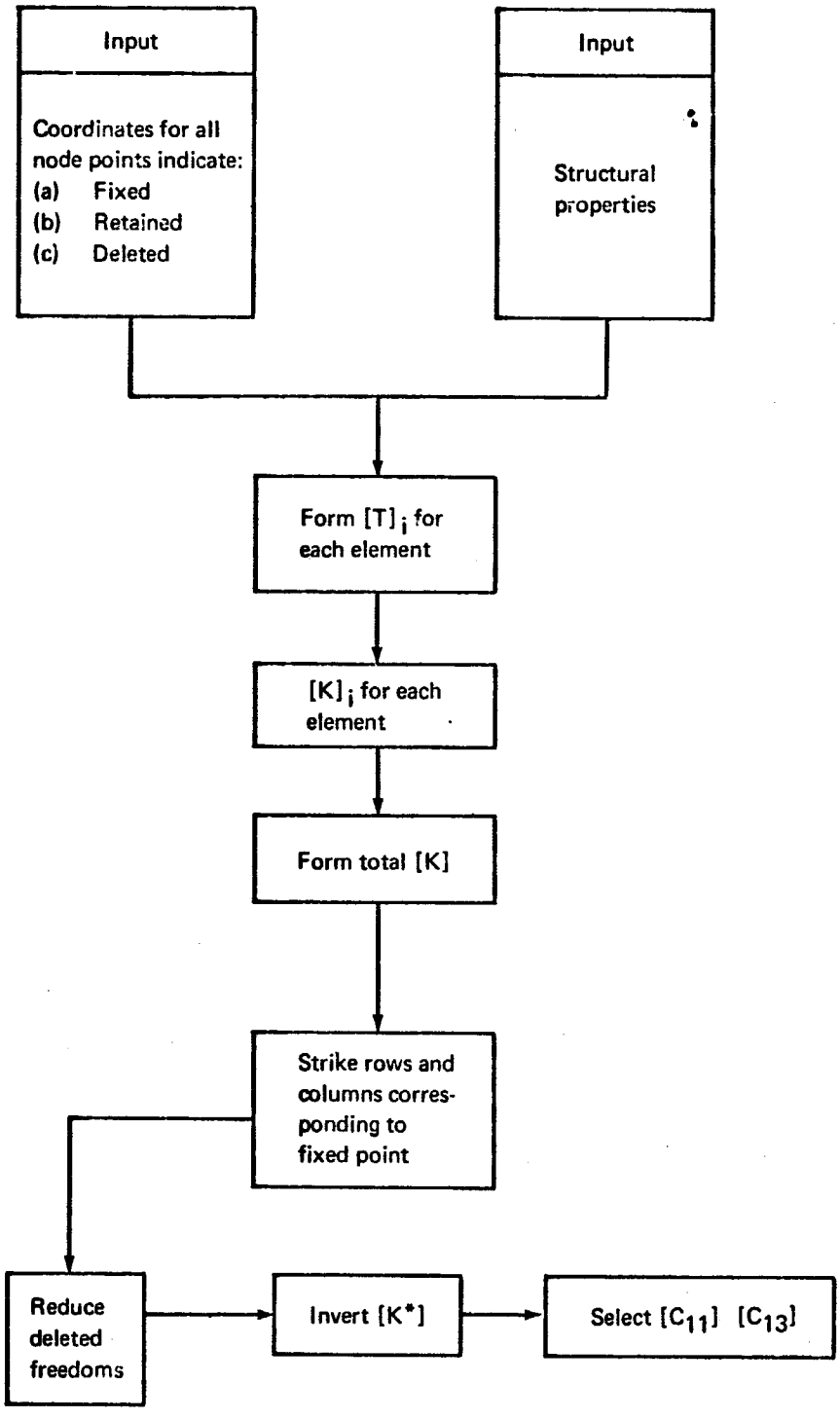

FIGURE 6.–FLOW DIAGRAM FOR A BEAM STRUCTURAL ANALYSIS

Equation (4.69) is a series representation of the deflection of each lumped mass. The value of $\{d_p\}$ becomes increasingly more accurate as the number of mode shapes, 3n-6, goes to infinity.

Substituting for $\{d_p\}$ in (4.68) using (4.69),

$$[\phi]\{u(t)\} = -[\bar{C}][m][\phi]\frac{\partial^2}{\partial t^2}\{u(t)\}$$
$$= -[\bar{C}][m][\phi]\{\ddot{u}(t)\} \qquad (4.70)$$

Applying the separation of variables technique to (4.70) results in two eigenvalue equations of the form,

$$\{\phi\} = [\bar{C}][m]\{\phi\}\omega^2 \qquad (4.71a)$$

$$\ddot{u} + \omega^2 u = 0 \qquad (4.71b)$$

Equation (4.71a) represents an eigenvalue problem with 3n-6 solutions given by the 3n-6 eigenvectors $\{\phi\}_i$ corresponding to the 3n-6 eigenvalues ω_i^2. From equation (4.71b) it is clear that the time dependence is simple harmonic with frequencies ω_i. Arranging the eigenvectors (referred to as mode shapes) as columns of the matrix $[\phi]$, the result is termed the elastic mode matrix. The deflected shape may be obtained as a linear sum of the mode shapes, i.e.,

$$\{d_p\} = \{\phi\}_1 u_1 + \{\phi\}_2 u_2 + \cdots + \{\phi\}_{3n} u_{3n-6}$$

where the time-varying coefficients are obtained from equation (4.71b). Hence, in matrix form

$$\{d_p\} = [\phi]\{u\} \qquad (4.72)$$

Introduce equation (4.72) into equation (6.132, app. A). The result is

$$[m][\phi]\frac{\partial^2}{\partial t^2}\{u\} + [\bar{K}][\phi]\{u\} =$$
$$-[m][\bar{\phi}]\left(\frac{\partial}{\partial t}\{V_p\} + [M]\{V_p\} - [M_2][r_p']\right) + \{f\} \qquad (4.73)$$

Multiplying this expression by $[\phi]^T$, one may use the property of the mode shapes being orthogonal with respect to the mass and stiffness matrices, i.e.,

$$[\bar{M}] \equiv [\phi]^T[m][\phi] \qquad (4.74a)$$

$$[\bar{K}] \equiv [\phi]^T[\bar{K}][\phi] \qquad (4.74b)$$

to find

$$[\bar{M}]\frac{\partial^2}{\partial t^2}\{u\} + [\bar{K}]\{u\} = [\phi]^T\{f\} \tag{4.75}$$

In a dynamic analysis not all of the mode shapes are included. In fact, one of the valuable assets of using the mode shapes is that some may be dropped from the analysis, thereby reducing the number of degrees of freedom. Here the coordinates u_i are separated into two sets:

$\{u_f\}$: included as degrees of freedom

$\{u_e\}$: excluded as degrees of freedom

Similarly, the modal matrix is partitioned as

$$[\phi] = \left[[\phi_f]\,[\phi_e]\right] \tag{4.76}$$

so

$$\{d_p\} = [\phi_f]\{u_f\} + [\phi_e]\{u_e\} \tag{4.77}$$

Also, the generalized mass and stiffness matrices may be partitioned.

$$\begin{bmatrix}[\phi_1]^T\\ [\phi_2]^T\end{bmatrix}[m]\,[\phi_1]\,[\phi_2] = \left[\begin{array}{c|c} [\phi_1]^T[m][\phi_1] & 0 \\ \hline 0 & [\phi_2]^T[m][\phi_2] \end{array}\right] \equiv \begin{bmatrix}[\bar{M}_1] & 0\\ 0 & [\bar{M}_2]\end{bmatrix} \tag{4.78}$$

and

$$\begin{bmatrix}[\phi_1]^T\\ [\phi_2]^T\end{bmatrix}[\bar{K}]\,[\phi_1]\,[\phi_2] = \left[\begin{array}{c|c} [\phi_1]^T[\bar{K}][\phi_1] & 0 \\ \hline 0 & [\phi_2]^T[\bar{K}][\phi_2] \end{array}\right] \equiv \begin{bmatrix}[\bar{M}_1] & 0\\ 0 & [\bar{M}_2]\end{bmatrix} \tag{4.79}$$

Now, ignoring the inertial and damping forces arising from the elastic displacements

$$\{d_e\} = [\phi_e]\{u_e\} \tag{4.80}$$

Equation (4.75) may be partitioned into two equations

$$[\bar{M}_f]\frac{\partial^2}{\partial t^2}\{u_f\} + [\bar{K}_f]\{u_f\} = [\phi_f]^T\{f\} \qquad (4.81a)$$

which describes the elastic motion associated with those terms of the completely elastic airplane motion equations that are of dynamic importance and

$$[\bar{K}_e]\{u_e\} = [\phi_e]^T\{f\} \qquad (4.81b)$$

which describes the elastic motion associated with those terms of the completely elastic airplane equations that are unimportant dynamically (residual flexibility).

4.3 Problem Formulation

Previous sections have considered the c.g. small-disturbance equations (4.1) through (4.5), the inviscid fluid-dynamic equations (4.29), and the structural equations (4.81a) and (4.81b) as independent sets. An aircraft in free flight is simultaneously described with respect to the fluid by all three sets of equations, so some means of uniting them must be developed to calculate the stability derivatives. In this section the three sets of equations will be united through the aerodynamic boundary condition on the wing applied in the region of the S domain of the plane of potential flow singularities. Stability derivatives describing force perturbations can then be related to the velocity potential $\phi(x,y,z,t)$ by the pressure-force equation (4.29e). Moment derivatives are calculated directly from the force derivatives. Singularities in the normal velocity at the subsonic leading and side edges of the thin body are neglected in the analysis.

4.3.1 The boundary condition at the surface. — The plane of singularities $z = 0$, representing the time-dependent thin-body motion, has been obtained from the surface description, $G(x,y,z,t) = 0$. The boundary condition that is satisfied in the neighborhood of region S in the $z = 0$ plane was given by

$$\left.\frac{DG}{Dt}\right|_{\vec{R}} = \left.\frac{\partial G}{\partial t}\right|_{\vec{r}} + \vec{v}\cdot\nabla G = 0 \quad \text{on } G(x,y,z,t) = 0 \qquad (4.13a)$$

where all terms have been defined in par. 4.1. It states that the mass flux through the surface $G = 0$ is zero. Thus, the fluid is moving tangentially to the surface. The notation $\vec{v}$ for the fluid velocity implies that it is the velocity

measured relative to the inertial fluid axis system (x, y, z) used to express the fluid-flow equations. Therefore, to be consistent with definition of the substantial derivative, the surface G = 0 must be described in terms of this inertial axis system (x, y, z).

The stability and control small-disturbance equations of motion and the structural equations are written in a noninertial, body-fixed axis system (x_s, y_s, z_s) that may be undergoing acceleration and rotation relative to inertial space. The problem of bringing these two inertial and noninertial axis systems into consistency is the main objective of the following analysis.

Additionally, for simplicity of operation and to improve the clarity of the presentation, it is desirable to formulate the boundary condition in the neighborhood of the region S for the elastic airplane as defined in par. 4.2.3. Then, by a simple elimination or alternation of terms, the restricted mathematical models representing a residual elastic, completely elastic, equivalent elastic, or a rigid airplane in a stability derivative analysis can be generated. It is also anticipated that the elimination of airplane c.g. motion from the boundary condition on G = 0 will simplify equations (4.29) to the flutter equations developed in the literature (refs. 1, 26 and 42). These equations will be required to evaluate the stability derivatives associated with the elastic-motion variables ($u_n(t)$, $\dot{u}_n(t)$, and $\ddot{u}_n(t)$) of the completely elastic and residual elastic mathematical model of an elastic aircraft.

It should be noted that the development of the boundary condition on the surface G = 0 and its wake given in equations (4.13) implied that a plane of singularities has been defined, about which the boundary conditions (B.C.) given in equations (4.29) have been expanded in a Maclaurin or Taylor series. This plane of singularities, z = 0, is that containing the reference surface motion or the time-averaged c.g. trajectory. In order to preserve generality, the implication will be continued in this paragraph, and no further mathematical effort will be expended to define the plane of singularities. The reader should note that in the subsequent analysis each stability derivative will have its unique set of boundary conditions that are developed from equations (4.29b, c, d).

Consider each term of equation (4.13a), i.e.,

$$\left.\frac{DG}{Dt}\right|_{\vec{R}} = \left.\frac{\partial G}{\partial t}\right|_{\vec{r}} + \vec{v}\cdot\nabla G = 0 \qquad \text{on } G=0 \qquad (4.13a)$$

where, as noted in par. 4.1,

$\left.\frac{DG}{Dt}\right|_{\vec{R}}$ is the time rate of change of the surface apparent to a fluid particle on G = 0 at the time t, when no blowing, suction, or fluid cavitation occurs.

The surface G(x,y,z,t) = 0 is the continuous infinity of spatial points that are adjacent to both fluid particles and particles of the airplane's skin at the instant of time t. The preceding relation is the condition that must be satisfied if fluid particles do not penetrate or separate from this surface. The terms have the following physical interpretation:

$\left.\frac{\partial G}{\partial t}\right|_{\vec{r}}$ is the time rate of change of G(z,y,z,t) = 0 apparent to a spatial point at the surface.

$\vec{v}\cdot\nabla G$ is the component of fluid velocity normal to the surface multiplied by $|\vec{\nabla} G|$ where $\vec{v}$ is the fluid velocity relative to the x,y,z system.

Particles of the airplane's skin, also, must not penetrate the surface G(x,y,z,t) = 0. Thus, the velocity of skin particles at the surface must satisfy the relation

$$\left.\frac{DG}{Dt}\right|_{\vec{R}_s} = \left.\frac{\partial G}{\partial t}\right|_{\vec{r}} + \left(\left.\frac{\partial \vec{r}}{\partial t}\right|_{\vec{R}_s}\right)\cdot\nabla G = 0 \qquad \text{on } G(x,y,z,t)=0$$

Again, $\left.\frac{\partial G}{\partial t}\right|_{\vec{r}}$ is the time rate of change of G(x,y,z,t) = 0 apparent to a spatial point at the surface,

but

$\left.\frac{\partial \vec{r}}{\partial t}\right|_{\vec{R}_s}$ is the velocity of a skin particle at the surface at time t, and

$\left(\left.\frac{\partial \vec{r}}{\partial t}\right|_{\vec{R}_s}\right)\cdot\nabla G$ is the normal component multiplied by $|\vec{\nabla} G|$.

The two relations may be combined to give

$$\left[\vec{v} - \left(\left.\frac{\partial \vec{r}}{\partial t}\right|_{\vec{R}_s}\right)\right]\cdot\vec{\nabla} G = 0 \qquad \text{on} \quad G(x,y,z,t)=0 \qquad (4.82)$$

Usually, the definition of the surface is in some body-fixed-axis system x_B, y_B, z_B that is related to the stability axis system x_s, y_s, z_s by a transfer of the origin and direction cosines once the reference flight condition is specified. These axis systems are translating with velocity $\vec{v}_p$, and have a rotation rate

$\vec{\omega}$ relative to the (x, y, z) fluid axis system. A point in the undeformed airplane has position $\vec{\tilde{r}}$ relative to the origin of the stability axis system (i.e., the airplane's c.g.). At the instant of time t under consideration, it is displaced elastically as $\vec{d}_p$ and is undergoing further elastic displacement with the rate $\dot{\vec{d}}_p$ as shown in the following sketch.

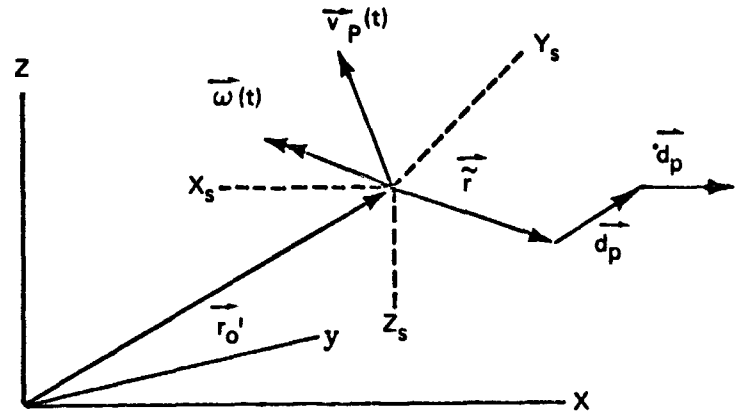

The velocity of the skin particle relative to the (x, y, z) fluid axis system is

$$\left(\frac{\partial \vec{r}}{\partial t}\bigg|_{\vec{R}_s}\right) = \vec{v}_p + \vec{\omega} \times \left(\vec{\tilde{r}} + \vec{d}_p\right) + \dot{\vec{d}}_p \qquad (4.83)$$

Letting the airplane's surface be represented by a system of panels consistent with the structural representation of par. 4.2.3, the elastic displacement rate is a consequence of translation and rotation rate of the panel so that

$$\dot{\vec{d}}_p = \dot{\vec{d}}_i + \dot{\vec{\theta}}_{e_i} \times \vec{r}_{e_i}$$

where i - denotes an artibrary panel

$\dot{\vec{d}}_i$ - is the translation rate of that panel due to elastic deformation

$\dot{\vec{\theta}}_i$ - is the rotation rate of that panel due to elastic deformation

$\vec{r}_{e_i}$ - is the position of the point under consideration relative to the reference point on the panel (usually its centroid)

Further, letting

$\vec{\tilde{r}}_i$ - be the position of the panel relative to the c.g. in the undeformed airplane

$\vec{d}_i$ - be the current elastic displacement of the panel reference point

it follows that

$$\left(\frac{\partial \vec{r}}{\partial t}\bigg|_{\vec{R}_s}\right) = \vec{v}_p + \vec{\omega} \times \left(\vec{r}_i + \vec{d}_i\right) + \dot{\vec{d}}_i + \left(\vec{\omega} + \dot{\vec{\theta}}_{e_i}\right) \times \vec{r}_{e_i} \qquad (4.84)$$

Combining this with the previous result (4.82) gives

$$\left[\vec{v} - \vec{v}_p - \vec{\omega} \times \left(\vec{r}_i + \vec{d}_i\right) - \dot{\vec{d}}_i - \left(\vec{\omega} + \dot{\vec{\theta}}_{e_i}\right) \times \vec{r}_{e_i}\right] \cdot \vec{\nabla} G = 0$$

$$\text{on } G(x,y,z,t) = 0$$

The velocity of the fluid is given by

$$\vec{v} = u_\infty \left(\vec{i} + \vec{\nabla}\phi\right) \qquad (4.85)$$

so on combining (4.85) with the previous result gives

$$-\left\{\vec{v}_p + \dot{\vec{d}}_i + \left(\vec{\omega} + \dot{\vec{\theta}}_{e_i}\right) \times \vec{r}_{e_i} + \vec{\omega} \times \left(\vec{r}_i + \vec{d}_i\right)\right\} \cdot \vec{\nabla} G$$

$$+ \left[u_\infty \left(\vec{i} + \vec{\nabla}\phi\right)\right] \cdot \vec{\nabla} G = 0 \qquad \text{on } G(x,y,z,t) = 0 \qquad (4.86)$$

The components appearing in the first term are usually written in terms of the stability axis system. To account for this in our matrix notation equation (4.86) must be written as

$$\left[\dot{\vec{d}}_i + \left(\vec{\omega} + \dot{\vec{\theta}}_{e_i}\right) \times \vec{r}_{e_i} + \vec{\omega} \times \left(\vec{r}_i + \vec{d}_i\right)\right]^T \left(\frac{\partial \vec{r}_s}{\partial \vec{r}}\right) \vec{\nabla} G$$

$$+ \left[\left(\frac{\partial \vec{r}_s}{\partial \vec{r}}\right)^T \vec{v}_p - u_\infty \left(\vec{i} + \vec{\nabla}\phi\right)\right]^T \vec{\nabla} G = 0 \qquad \text{on } G(x,y,z,t) = 0$$

Further, to take cognizance of the fact that the surface is most conveniently described in terms of a body-fixed-axis system, let

$$G_s(x_s, y_s, z_s, t) = G(x_s(x,y,z,t), y_s(x,y,z,t), z_s(x,y,z,t), t) = 0$$

so that

$$\vec{\nabla} G = \left(\frac{\partial \vec{r}_s}{\partial \vec{r}}\right)^T \vec{\nabla}_s G_s \qquad (4.87)$$

Hence, on noting that the coordinate transformation is an orthogonal one, it follows that

$$\left[\dot{\vec{d}}_i + \left(\vec{\omega} + \dot{\vec{\theta}}_{e_i}\right) \times \vec{r}_{e_i} + \vec{\omega} \times \vec{r}_i\right] \vec{\nabla}_s G_s$$

$$+ \left[\left(\frac{\partial \vec{r}_s}{\partial \vec{r}}\right)^T \vec{v}_p - u_\infty \left(\vec{i} + \vec{\nabla}\phi\right)\right] \left(\frac{\partial \vec{r}_s}{\partial \vec{r}}\right) \vec{\nabla}_s G_s = 0 \qquad \text{on } G(x,y,z,t) = 0 \qquad (4.88)$$

Equation (4.88) is the exact boundary condition on G = 0 relating stability and control and structural variables to the velocity potential.

It is usual, in defining stability derivatives, to relate inertial and noninertial space by the Euler angle transform (refs. 4 and 33). The transform between the space described by the stability axis (x_{s_i}) and the fluid axis (x_i) is given in par. 4.1:

$$\left(\frac{\partial r_s}{\partial r}\right) = [D] = \begin{bmatrix} (\cos\phi\cos\theta) & (\sin\psi\cos\theta) & (-\sin\theta) \\ \begin{pmatrix}-\sin\psi\cos\theta \\ +\cos\psi\sin\theta\sin\phi\end{pmatrix} & \begin{pmatrix}\cos\psi\cos\phi \\ +\sin\psi\sin\theta\sin\phi\end{pmatrix} & (\cos\theta\sin\phi) \\ \begin{pmatrix}\sin\psi\sin\phi \\ +\cos\psi\sin\theta\cos\phi\end{pmatrix} & \begin{pmatrix}-\cos\psi\sin\phi \\ +\sin\psi\sin\theta\cos\phi\end{pmatrix} & (\cos\theta\cos\phi) \end{bmatrix} \tag{4.89}$$

where

$$\psi = \int_o^t \left(Q\sin\phi + R\cos\phi\right)\sec\theta\, dt \tag{4.90a}$$

$$\theta = \int_o^t \left(Q\cos\phi - R\sin\phi\right) dt \tag{4.90b}$$

$$\phi = \int_o^t \left(P + Q\sin\phi\tan\theta + R\cos\phi\tan\theta\right) dt \tag{4.90c}$$

where

$Q = Q_1 + q\,(t)$

$R = R_1 + r\,(t)$

$P = P_1 + p\,(t)$ and usually $Q_1 = R_1 = P_1 = 0$

In applying equation (4.88) to specific cases discussed in the literature, the choice of the mathematical model used to represent the elastic airplane may simplify the boundary condition applied to the surface G = 0. It is of interest to consider these models: (1) the completely elastic airplane, (2) the residual elastic airplane, (3) the equivalent elastic airplane, and (4) the rigid airplane. Also, as a check of equation (4.88) the case of flutter should be obtainable by setting c.g. motion equal to zero.

4.3.1.1 The completely elastic airplane: The completely elastic airplane used in stability derivative analysis is characterized by elastic surface motion and thin-body c.g. motion of different frequency. In general, the total number of elastic mode shapes used to represent the elastic deflections is equal to the number of lumped masses representing the body's structure and they are

limited only by computer capacity. If there are n lumped masses, 6n-6 motion equations due to elastic motion variables arise. As is usual, the elastic rotational degrees of freedom are neglected and the 6n-6 equations simplify to 3n-3. Since elastic derivatives arise from elastic position, velocity, and acceleration terms, 9n-9 stability derivatives due to elastic motion must be evaluated. If one now includes the small-disturbance c.g. motion, three-force plus three-moment equations and m number of control surface equations also arise. Ignoring the control surface equations, the resulting six c.g. equations each have six motion variables that contribute stability derivatives attributable to position, velocity, and acceleration. By choosing a "stability axis" system some of these derivatives due to position vanish. Hence, there remain approximately 84 stability derivatives associated with the body's c.g. Finally, combining the c.g. small-disturbance stability derivatives with the elastic stability derivatives results in approximately 9n + 75 stability derivatives to be evaluated. Fortunately, most of these can be shown to be negligible in usual stability and control analysis.

All 9n + 75 stability derivatives can be evaluated using equations (4.29) and (4.88). Since the c.g. motion and elastic motions are treated independently, the problem is split into derivatives associated with elastic motion and those associated with c.g. motion. The stability derivatives dependent on c.g. motion are exactly the same as those for the rigid airplane.

As equation (4.88) was developed for the most general case, the completely elastic airplane, the boundary condition on G = 0 is as stated in equation (4.88).

S6 4.3.1.2 The residual elastic airplane: The potential use and application of residual flexibility theory by stability and control engineers may be discerned by considering certain practical aspects of the preceding analysis. The completely elastic airplane representation constitutes the most precise mathematical model for assessing the dynamic stability of an elastic airplane. However, the limitations of computers that will be available in the foreseeable future to carry out the numerical computations limit its use because of the large number of elastic degrees of freedom involved in describing the elastic airplane adequately.

A discussion of the number of free-vibration-mode shapes required for the airplane's representation is included in par. 4.2.1. In that discussion it is

pointed out that the stability and control engineer is usually concerned with dynamic participation of only a small number of vibration modes. This follows from the fact that he is primarily concerned with the six-degree-of-freedom-motion of the airplane c.g. A free vibration mode is excited dynamically by the airplane c.g. motion if the natural frequency of the free vibration mode is nearly equal to the frequency of the c.g. motion. The stiffness and mass distribution of most airplanes is such that only a very few free vibration modes have natural frequencies that are sufficiently low to participate dynamically. However, there is motion due to the higher frequency modes. This motion is quasi-static in nature and can have a significant effect on airplane stability and control.

Without the residual flexibility formulation of the equations of motion the stability and control engineer is faced with two alternatives. He may include the free vibration modes that contribute the major quasi-static elastic deflections as dynamically participating. Or, he may ignore all structural dynamics and base his stability and control analysis on the equivalent elastic airplane representation. Either of these alternatives carries a penalty. In the first case, there is a loss in numerical accuracy because of the complexity of the equations of motion. In the second case, the mathematical model does not accurately represent the airplane. Residual flexibility theory provides a middle ground between these two alternatives, including the quasi-static deflections of all elastic modes that do not participate dynamically. Thus, the optimal accuracy in predicting dynamic stability of elastic airplanes may be expected by using residual flexibility theory.

The surface representation of the residual elastic airplane is the same as the completely elastic airplane, except that now only a limited number of mode shapes are considered. The boundary condition on $G = 0$ is as written in equation (4.88).

4.3.1.3 The equivalent elastic airplane: The equivalent elastic airplane is characterized by elastic motion of the same frequency and phase as the body's c.g. motion. The elastic surface is assumed to adjust itself instantaneously to any changes in aerodynamic or inertial loading. (S7)

In the case of the equivalent elastic airplane, the only inertial forces considered to act on the lumped masses arise as a consequence of accelerations of the airplane's c.g. Thus, the deflected shape of the airplane, at any instant of time, is due entirely to the applied aerodynamic forces and the inertial forces resulting from acceleration of the airplane as a rigid body. This representation neglects all structural dynamics, i.e., the inertial forces due to motion in the elastic degrees of freedom are ignored.

The differences between the equivalent elastic and completely elastic airplane representations may be illustrated by a simple example. Consider an airplane clamped at its plane of symmetry, as shown by fig. 7. The airplane is subjected to a sinusoidally varying force of frequency ω at its wing tip. The deflection of the tip for the equivalent elastic airplane is given by

$$\Delta = \frac{1}{K} P_o \sin \omega t$$

where K is an elastic constant representing the effective stiffness of the wing. Under these conditions, the deflection is always in phase with the load and is in constant proportion with the load. When the loads are aerodynamic, the problem is complicated by the fact that the load is dependent upon the deflection. However, this complication does not change the essential features illustrated by the example.

When the airplane is completely elastic, the inertia force M must be included (where M is an effective mass of the wing). A differential equation now governs the elastic deflection, i.e.,

$$M\ddot{\Delta} + K\Delta = P_o \sin \omega t$$

The solution to this differential equation is given by

$$\Delta = \frac{1}{K} P_o \frac{1}{1 - \omega^2/\omega_o^2} \left(\sin \omega t - \frac{\omega}{\omega_o} \sin \omega_o t \right)$$

where $\omega_o = \sqrt{\frac{K}{M}}$: natural frequency of the wing.

Note that $\omega_o \to \infty$ as $M \to 0$ and the solution tends to that of the equivalent elastic airplane. Consider what happens if $\omega_o = 2\omega$. Under this circumstance

$$\Delta = 1.33 \frac{1}{K} P_o \left(\sin \omega t - 2 \sin 2 \omega t \right)$$

The deflection now exceeds that of the equivalent elastic airplane and is no longer in phase with the applied load. The excessive deflection is referred to as dynamic overshoot.

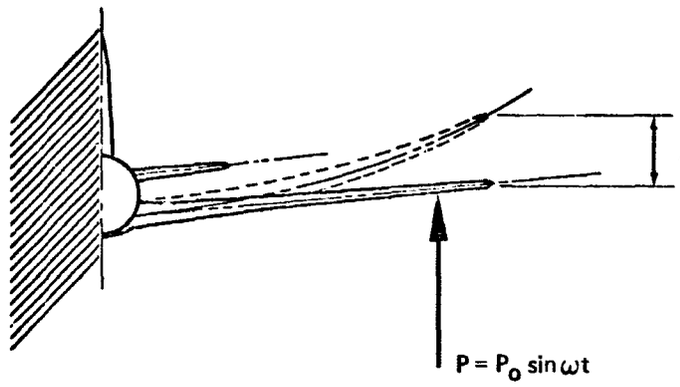

Equivalent elastic airplane

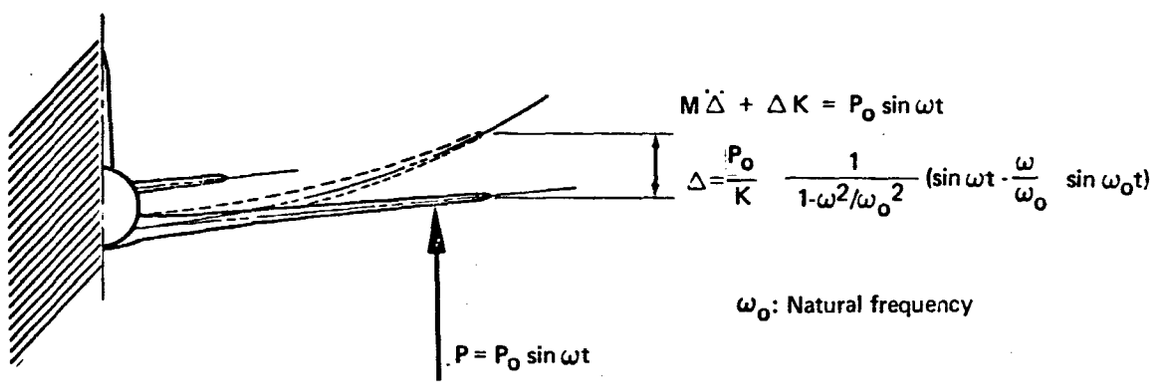

Completely elastic airplane

FIGURE 7.– SIMPLIFIED MODELS FOR AN EQUIVALENT ELASTIC AND A COMPLETELY ELASTIC AIRPLANE

The elastic motion and the c.g. motion are interdependent in the case of the equivalent elastic airplane. The elastic displacement vector field is a known function of the instantaneous values of the airplane's c.g. velocity and acceleration. The functional dependence is shown in app. A to be determined by the internal equilibrium equations for the airplane with all inertial and damping forces directly related to elastic motion set to zero. The c.g. velocities are $\vec{V}_R$ and $\vec{\Omega}$ and the accelerations are $\dot{\vec{V}}_R$ and $\dot{\vec{\Omega}}$. And, analogous to the expressions of app. A, the aerodynamic pressure is

$$\vec{F} = \vec{A}_1 \cdot \vec{V}_R + \vec{A}_1' \cdot \vec{\Omega} + \vec{A}_2 \cdot \dot{\vec{V}}_R + A_2' \cdot \dot{\vec{\Omega}} + \vec{A}_3 \cdot \sum_{i=1}^{n} \vec{\phi}_i u_i + \vec{A}_4 \cdot \sum_{i=1}^{n} \vec{\phi}_i \dot{u}_i + \vec{A}_5 \cdot \sum_{i=1}^{n} \vec{\phi}_i \ddot{u}_i$$

where aerodynamic influence tensors have been introduced in place of the aerodynamic matrices of app. A.

The internal equilibrium equations for the perturbation substitution were given in app. A, par. 6.2.3 as

$$u_j = -\frac{1}{m_j} \int_V \rho_A \vec{\phi}_j \cdot \int_V \vec{G} \cdot \vec{\phi}_j \rho_A \, dV \, dV \, \ddot{u}_j + \int_V \rho_A \vec{\phi}_j \cdot \int_V \vec{G} \cdot \vec{F} \, \delta(\vec{r} - \vec{r}_s) \, dV \, dV \qquad \text{(6.86, app. A)}$$

Setting the inertial and damping associated with u_j to zero it follows by substituting the aerodynamic force expression into the internal equilibrium equations that

$$u_j = \int_V \rho_A \vec{\phi}_j \cdot \int_V \vec{G} \cdot \left(\vec{A}_1 \cdot \vec{V}_R + \vec{A}_1' \cdot \Omega + \vec{A}_2 \cdot \dot{\vec{V}}_R + \vec{A}_2' \cdot \dot{\vec{\Omega}} \, \delta(\vec{r} - \vec{r}_s) \right) dV \, dV + \int_V \rho_A \vec{\phi}_j \cdot \int_V \vec{G} \cdot \vec{A}_3 \cdot \sum_{i=1}^{n} \vec{\phi}_i \, \delta(\vec{r} - \vec{r}_s) \, dV \, dV \, u_i$$

But consider

$$\vec{d} = \sum_{j=1}^{3n-6} \vec{\phi}_j u_j$$

so that the above may be used to write

$$\vec{d} - \sum_{j=1}^{n} \vec{\phi}_j \int_V \rho_A \vec{\phi}_j \cdot \int_V \vec{G} \cdot \vec{A}_3 \cdot \vec{d} \, \delta(\vec{r} - \vec{r}_s) \, dV \, dV = \sum_{j=1}^{3n-6} \vec{\phi}_j \int_V \rho_A \vec{\phi}_j \cdot \int_V \vec{G} \cdot \left(\vec{A}_1 \cdot \vec{V}_R + \vec{A}_1' \cdot \Omega + \vec{A}_2 \cdot \dot{\vec{V}}_R + \vec{A}_2' \cdot \dot{\vec{\Omega}} \right) \delta(\vec{r} - \vec{r}_s) \, dV$$

This is not a very usable result because the elastic displacement vector is involved in an integral. However, this result does prove the assertion that the elastic deformation depends only on the instantaneous velocity and acceleration of the cg. Thus, the vector $\vec{d}$ is not an explicit function of time. Its dependence on time is only through its dependence on $\vec{V}_R$, $\dot{\vec{V}}_R$, $\vec{\Omega}$, $\dot{\vec{\Omega}}$ for the case of the equivalent elastic airplane.

The boundary condition on G = 0 remains written as it is for the completely elastic airplane (4.88) except that now the time dependence is controlled by the motion of the airplane's c.g., i.e.,

$$\left[\dot{\vec{d}}_i + \left(\vec{\omega} + \dot{\vec{\theta}}_{e_i}\right) \times \vec{r}_{e_i} + \vec{\omega} \times \vec{r}_i\right]^T \nabla_s G_s + \left[\left(\frac{\partial \vec{r}_i}{\partial \vec{r}}\right)^T \vec{v}_p - U_\infty\left(\vec{i} + \nabla\phi\right)\right]^T \left(\frac{\partial \vec{r}_i}{\partial \vec{r}}\right)^T \nabla_s G_s = 0 \quad \text{on } G(x,y,z,t) = 0 \tag{4.91}$$

where the time variations of $\dot{\vec{d}}_i(t)$ and $\dot{\vec{\theta}}_{e_i}(t)$ are exactly the same as the c.g. motion instead of being described by the eigenvalues of equation (4.71).

where $G_S(x_S, y_S, z_S, t) = F_S(x_X, y_S, z_S, \vec{v}_R(t), \dot{\vec{v}}_R(t), \vec{\Omega}(t), \dot{\vec{\Omega}}(t))$

The problem of defining the plane of potential-flow singularities, z = 0, simplifies to defining the plane containing the time-averaged c.g. trajectory in the fluid-axis space.

4.3.1.4 The rigid airplane: The rigid airplane is characterized by a lack of elastic deflection from the reference surface description regardless of the load factor or static aerodynamic loading involved during the small-disturbance c.g. motion. (S8)

Changes in the boundary condition in the region S are reflected in the definition of G in equation (4.88) or F_s in equation (4.91). The rigid-airplane-surface description is that of equation (4.88) with elastic deflections equal to zero. The boundary condition on G = 0 becomes,

$$\left(\vec{\omega} \times \left(\vec{r}_i + \vec{r}_{e_i}\right)\right) \cdot \nabla_s f + \left[\left(\frac{\partial \vec{r}_i}{\partial \vec{r}}\right)^T \vec{v}_p - U_\infty\left(\vec{i} + \nabla\phi\right)\right]^T \left(\frac{\partial \vec{r}_i}{\partial \vec{r}}\right)^T \nabla_s f = 0 \quad \text{on } G(x,y,z,t) = 0 \tag{4.92}$$

where $f = f(x_s, y_s, z_s) = 0$ is the description of the surface in some reference flight orientation at time t_o and for all subsequent time afterwards during which the stability and control analysis occurs.

4.3.1.5 The flutter boundary condition: As a check of equation (4.88), it should be possible to generate the boundary conditions applied to the inviscid problem associated with elastic-surface motion (flutter) by setting all c.g. motion equal to zero.

$$\left(\vec{d}_i + \dot{\vec{e}}_{e_i} \times \vec{r}_{e_i}\right) \cdot \nabla_s G_s - \left(U_\infty \left(\vec{i} + \nabla\phi\right)\right) \cdot \left(\frac{\partial \vec{r}_s}{\partial \vec{r}}\right)^T \nabla_s G_s = 0 \quad \text{on } G(x,y,z,t)=0 \tag{4.93}$$

Because the aircraft's rigid-body c.g. motion has been set equal to zero, the c.g. of the aircraft (origin of the stability axis) and the origin of the fluid axis are now synonomous and all axis systems are inertial. The boundary condition on G = 0 can be written,

$$\left[\dot{\vec{d}}_i + \dot{\vec{e}}_{e_i} \times \vec{r}_{e_i} - U_\infty \left(\vec{i} + \nabla\phi\right)\right] \cdot \nabla G = 0 \quad \text{on } G(x,y,z,t) = 0 \tag{4.94}$$

Equation (4.94) is the boundary condition used by Van Dyke (ref. 31) and Miles (ref. 28) for the harmonically vibrating wing.

An additional result is obtained from the boundary condition expressed in equation (4.94). Recall, that in the case of the completely elastic and the residual elastic mathematical models of an elastic airplane, the 9n stability derivatives associated with elastic motion are evaluated for c.g. motion set equal to zero. Therefore, equation (4.94) is also the exact boundary condition applied in the regions to evaluate the elements of the $[A_3]$, $[A_4]$, and $[A_5]$ matrices.

4.3.2 The pressure-force equation. — The solution of equations (4.29), where (4.29b) is replaced by the appropriate boundary condition described by (4.88), gives a velocity potential that is dependent upon the boundary conditions on S , W , and R . The boundary condition on S has been shown to depend upon initial conditions, the small-disturbance c.g. motion, and the airplane elastic motion. The stability derivatives representative of each set of motion variables can be extracted from equation (4.29e) by relating the pressure forces dependent upon velocity potential to the aerodynamic forces of the small-disturbance equations.

Consider equation (4.29e).

$$C_p = \begin{cases} 2\left(\phi_x + \frac{1}{U_\infty}\phi_t\right)_{z=0^+} & \text{upper surface} \\ -2\left(\phi_x + \frac{1}{U_\infty}\phi_t\right)_{z=0^-} & \text{lower surface} \end{cases}$$

where C_p is the pressure coefficient of the pressure force perpendicular to $G = 0$ and $G_S = 0$ at the point of evaluation (x, y, z, t) directly above or below the plane containing the potential singularities.

Since pressure has been defined as normal to the surface $G_S = 0$, the net pressure force can be resolved into force components associated with the stability axis system. Define a surface unit normal in the stability axis system as $\vec{n}_S$, where

$$\vec{n}_s = \frac{\nabla_s G_s}{|\nabla_s G_s|} \tag{4.95}$$

the resultant pressure force at surface point i becomes

$$\vec{C}_{N_i} = \frac{C_{p_i}}{S_{REF}} \left[\frac{\nabla_s G_s}{|\nabla_s G_s|}\right]$$

where i denotes the point of evaluation.

The total pressure force on the aircraft normal to the surface $G_S = 0$ is found by a surface integration to be

$$\vec{C}_N = \frac{2}{S_{REF}} \iint_S \frac{\nabla_s G_s^+}{\nabla_s G_s^+} \left(\phi_x + \frac{1}{U_\infty}\phi_t\right)_{z=0^+} dS + \frac{2}{S_{REF}} \iint_S \frac{\nabla_s G_s^-}{\nabla_s G_s^-} \left(\phi_x + \frac{1}{U_\infty}\phi_t\right)_{z=0^-} dS \tag{4.96}$$

$$\vec{C}_N \doteq \frac{4}{S_{REF}} \iint_S \frac{\nabla_s G_s}{|\nabla_s G_s|} \left(\phi_x + \frac{1}{U_\infty}\phi_t\right)_{z=0^+} dS \tag{4.97}$$

for a near-planar (thin-body) surface.

Define the components of $\vec{C}_n$ as in par. 4.2.1,

$$\begin{aligned} \vec{C}_N &= \vec{C}_{N_1} + \Delta\vec{C}_N(t) \\ &= \left(C_{x_1} + \Delta C_x(t)\right)\vec{i}_s + \left(C_{y_1} + \Delta C_y(t)\right)\vec{j}_s + \left(C_{z_1} + \Delta C_z(t)\right)\vec{k}_s \end{aligned} \tag{4.98}$$

where $\vec{C}_{N_1}$ is the reference state force coefficient and is independent of time.

C_{x_1} is the reference x_s force coefficient

C_{y_1} is the reference y_s force coefficient

C_{z_1} is the reference z_s force coefficient

$\Delta\vec{C}_N(t)$ is the perturbation force coefficient associated with the elastic and c.g. motion variables

$\Delta C_X(t)$ is the perturbation x_s force defined in equation (4.4)

$\Delta C_Y(t)$ is the perturbation y_s force defined in equation (4.3)

$\Delta C_Z(t)$ is the perturbation z_s force defined in equation (4.4)

Rewriting the left side of (4.97) in terms of (4.98) relates the stability derivatives to the inviscid velocity potential satisfying equations (4.29) and (4.88)

$$C_x = C_{x_1} + \Delta C_x(t) = \frac{4}{S_{REF}} \iint_S \frac{\partial G_s/\partial x_s}{|\nabla_s G_s|} \left(\phi_x + \frac{1}{U_\infty}\phi_t\right)_{z=0^+} dS \qquad (4.99a)$$

$$C_y = C_{y_1} + \Delta C_y(t) = \frac{4}{S_{REF}} \iint_S \frac{\partial G_s/\partial y_s}{|\nabla_s G_s|} \left(\phi_x + \frac{1}{U_\infty}\phi_t\right)_{z=0^+} dS \qquad (4.99b)$$

$$C_z = C_{z_1} + \Delta C_z(t) = \frac{4}{S_{REF}} \iint_S \frac{\partial G_s/\partial z_s}{|\nabla_s G_s|} \left(\phi_x + \frac{1}{U_\infty}\phi_t\right)_{z=0^+} dS \qquad (4.99c)$$

The unknowns (stability derivatives) in equations (4.99) are evaluated by considering one time-variant-motion variable at a time; e.g., for α, $\dot{\alpha}$ force derivatives, only $\alpha(t)$ and $\dot{\alpha}(t)$ exist, and p, q, u, v, etc. are zero.

Once the force derivatives have been evaluated, the moment derivatives follow directly.

$$\vec{C}_M = \vec{C}_{M_1} + \Delta\vec{C}_M(t) \qquad (4.100a)$$

$$\vec{C}_{M_1} = \sum_{i=1}^{K} \left(\vec{r}_i/\ell_M \times \vec{C}_{N_{1_i}}\right) \qquad (4.100b)$$

$$\Delta\vec{C}_M(t) = \sum_{i=1}^{K} \left((\vec{r}_i + \vec{d}_i)/\ell_M \times \Delta\vec{C}_{N_i}(t)\right) \qquad (4.100c)$$

where $\vec{r}_i$ - is the distance from the aircraft's c.g. to the point i on the aircraft's surface $G_s = 0$

$\vec{d}_i$ - is the elastic extension vector from the reference aircraft shape

ℓ_M - is a parameter such as span on reference chord used to nondimensionalize the moment coefficients

$\vec{C}_{N_{1_i}}$ - and $\Delta C_N(t)$ are as defined in equation (4.98)

and where i - denotes a summation over the surface of a thin body represented by K points or panels

Summarizing the significant equations required to calculate the small-disturbance stability derivatives,

flow equation:

$$\beta^2 \phi_{xx} - \phi_{yy} - \phi_{zz} + \frac{2M}{a_\infty} \phi_{xt} + \frac{1}{a_\infty^2} \phi_{tt} = 0 \qquad (4.101a)$$

B.C.:

$$\left[\vec{V} - \left. \frac{\partial \vec{r}}{\partial t} \right|_{\vec{R}_s} \right] \cdot \nabla G = 0 \qquad \text{on } S \qquad (4.101b)$$

$$\left(\phi_x + \frac{1}{U_\infty} \phi_t \right)_{z=0} = 0 \qquad \text{on } W \qquad (4.101c)$$

$$\phi \big|_{z=\infty} = 0 \qquad \text{on } R \qquad (4.101d)$$

Force derivatives:

$$\vec{C}_N(t) = \vec{C}_{N_1} + \Delta \vec{C}_N(t) = \frac{4}{S_{REF}} \iint_S \frac{\nabla_s G_s}{|\nabla_s G_s|} \left(\phi_x + \frac{1}{U_\infty} \phi_t \right)_{z=0^+} dS \qquad (4.101e)$$

Moment derivatives:

$$\vec{C}_{M_1} = \sum_{i=1}^{k} \frac{\vec{r}_i}{\ell_M} \times \vec{C}_{N_i} \qquad (4.101f)$$

$$\Delta C_M(t) = \sum_{i=1}^{k} \frac{\vec{r}_i + \vec{d}_i}{\ell_M} \times \Delta \vec{C}_{N_i}(t) \qquad (4.101g)$$

4.4 Applications

This section describes the application of equations (4.101) to several specific problems. Because of the complications involved in applying the boundary conditions on the surface G = 0 and its wake, and the relative lack of prior theoretical work, only a few of the stability derivatives can be evaluated from equations (4.101) using existing techniques.

It is possible to carry the development of equations (4.101) for α, p, q, and u derivatives to a point where several computer techniques have evolved to solve the equations numerically. This section concerns itself primarily with the evaluation of α (t) derivatives for "flat" and "3-D" airplanes. The evaluation of p, q, and u derivatives are indicated and briefly outlined for the flat airplane. The remaining derivatives associated with longitudinal and lateral-directional motion are not theoretically formulated at this time to permit an accurate and exact velocity potential representation.

4.4.1 A "flat" airplane. — The application of equations (4.101) to an airplane that can be represented as a flat surface has been investigated. This representation implies that the airplane's body extension in the z_s direction is of the same order as wing thickness and that wing dihedral angle is zero. Additionally, the effect of elastic-surface deflection is such that the extension from the reference shape is small.

Consider the definition of a completely elastic airplane satisfying all thin-body requirements of size and thickness and with some arbitrary specified wing thickness, camber, and twist distribution.

$$G_s(x_s, y_s, z_s, t_s) = z_s - f(x_s, y_s) - \sum \phi_n(x_s, y_s)\, u_{pn}(t) = 0 \qquad (4.102)$$

where z_S - is the coordinate to the surface from the $z_S = 0$ plane

$f(x_S, y_S)$ - is the reference shape of the flat airplane (thickness, camber, and twist)

$\phi_n(x_S, y_S)$ - is the modal elastic representation (n^{th} mode shape) of the elastic deflection from the reference position $f(x_S, y_S)$

$u_{pn}(t)$ - is the time variation of the n^{th} mode shape

From equation (4.101b) the boundary condition on the completely elastic mathematical model of an elastic flat airplane is written,

$$\left[\vec{d}_i + \left(\vec{\omega} + \vec{\theta}_{e_i}\right) \times \left(\vec{r}_{e_i} + \vec{\omega}\right) \times \vec{r}_i\right]^T \cdot \nabla_s G_s + \left[\left(\frac{\partial \vec{r}_s}{\partial \vec{r}}\right)^T \vec{v}_p - U_\infty \left(\hat{i} + \nabla \phi\right)\right]^T \left(\frac{\partial \vec{r}_s}{\partial \vec{r}}\right)^T \nabla_s G_s = 0 \quad \text{on } G_S(x_s, y_s, z_s, t) = 0$$

where $G_S(x_S, y_S, z_S, t) = 0$ is as defined in equation (4.102).

Performing the indicated operations in equation (4.101b),

$$\left[\left(\vec{\omega} + \vec{\theta}_{e_i}\right) \times \vec{r}_{e_i}\right] = \left[\left(p + \dot{\theta}_{e_{i_x}}\right) \hat{i}_s + \left(q + \dot{\theta}_{e_{i_y}}\right) \hat{j}_s + \left(r + \dot{\theta}_{e_{i_z}}\right) \hat{k}_s \times \left(r_{e_{i_x}} \hat{i}_s + r_{e_{i_y}} \hat{j}_s + r_{e_{i_z}} \hat{k}_s\right)\right]$$

$$\nabla_s G_s = \left(-f_{x_s}\right)\hat{i}_s + \left(-f_{y_s}\right)\hat{j}_s + \hat{k}_s$$

$$\left(\frac{\partial \vec{r}_t}{\partial \vec{r}}\right)^T \hat{V}_\rho - [D]^{-1}\begin{Bmatrix} u(t) \\ v(t) \\ w(t) \end{Bmatrix} = \frac{dx}{dt}\hat{i} + \frac{dy}{dt}\hat{j} + \frac{dz}{dt}\hat{k}$$

$$= \Big[-u\cos\theta\cos\psi - v\left(\sin\phi\sin\theta\cos\psi - \cos\phi\sin\psi\right) - w\left(\cos\phi\sin\theta\cos\psi + \sin\phi\sin\psi\right)\Big]\hat{i} + \Big[u\cos\theta\sin\psi + v\left(\sin\phi\sin\theta\sin\psi + \cos\phi\cos\psi\right) + w\left(\cos\phi\sin\theta\sin\psi - \sin\phi\cos\psi\right)\Big]\hat{j} + \Big[u\sin\theta - v\sin\phi\cos\theta - w\cos\phi\cos\theta\Big]\hat{k}$$

$$U_\infty\left(\hat{i} + \nabla\phi\right) = U_\infty\Big[\left(1+\phi_x\right)\hat{i} + \phi_y\hat{j} + \phi_z\hat{k}\Big]$$

$$\left(\frac{\partial \vec{r}_s}{\partial \vec{r}}\right)^T \nabla_s G_s = [D]^{-1}\begin{Bmatrix} -f_{x_s} \\ -f_{y_s} \\ 1 \end{Bmatrix} = \frac{\partial G}{\partial x}\hat{i} + \frac{\partial G}{\partial y}\hat{j} + \frac{\partial G}{\partial z}\hat{k}$$

$$= \Big[f_{x_s}\cos\theta\cos\psi + f_{y_s}\left(\sin\phi\sin\theta\cos\psi - \cos\phi\sin\psi\right) - \left(\cos\phi\sin\theta\cos\psi + \sin\phi\sin\psi\right)\Big]\hat{i} + \Big[-f_{x_s}\cos\theta\sin\psi - f_{y_s}\left(\sin\phi\sin\theta\sin\psi + \cos\phi\cos\psi\right) + \left(\cos\phi\sin\theta\sin\psi - \sin\phi\cos\psi\right)\Big]\hat{j} + \Big[\left(-f_{x_s}\sin\theta\right) + f_{y_s}\sin\phi\cos\theta - \cos\phi\cos\theta\Big]\hat{k}$$

where G_S has been defined in equation (4.102),

where, as stated in equations (4.90),

$$\psi(t) = \int_0^t \Big(Q\sin\phi(t) + R\cos\phi(t)\Big)\sec\theta(t)\,dt$$

$$\theta(t) = \int_0^t \Big(Q\cos\phi(t) - R\sin\phi(t)\Big)\,dt$$

$$\phi(t) = \int_0^t \Big(P + Q\sin\phi(t)\tan\theta(t) + R\cos\theta(t)\tan\theta(t)\Big)\,dt$$

and where

$$Q = Q_i + q(t), \quad P = P_i + p(t), \quad R = R_i + r(t)$$

Equation (4.101b) with the substitution of the indicated operations gives the exact boundary condition on the surface $G(x,y,z,t) = 0$ for a flat airplane experiencing simultaneously both c.g. small-disturbance motion and elastic-surface deflections. By performing the simplifications indicated in par. 4.3.1, the boundary condition on the completely elastic airplane, residual elastic airplane, equivalent elastic airplane, and rigid airplane mathematical models can be generated.

For illustration, the α derivatives (C_{z_α}, C_{x_α}, C_{y_α}, C_{ℓ_α}, C_{m_α}, C_{n_α}) will be calculated for the completely elastic airplane. For this case, the boundary condition on $G = 0$ (as for all c.g. motion) is identical to that of the mathematical model of a rigid flat airplane. As is usual, it is assumed that all c.g. disturbance motions and elastic motions are small. Stating the boundary condition as equation (4.101b) where all motions other than $w(t) = U_\infty \alpha(t)$ are set equal to zero,

$$\left[\left(\frac{\partial \vec{r}_s}{\partial \vec{r}}\right)^T \vec{v}_p - U_\infty (\hat{i} + \Delta\phi)\right]^T \left(\frac{\partial \vec{r}_s}{\partial \vec{r}}\right)^T \nabla_s G_s = 0 \qquad \text{on } G(x,y,z,t) = 0$$

Note that in the above formulation, the inertial axis system x,y,z is initially oriented with the reference-state orientation of the x_s, y_s, z_s axis system. Relative to an axis system fixed in the flat earth, the x,y,z axis system translates at a velocity u_∞ and at some initial angle of climb θ to the horizon.

Therefore, since $u = v = p = q = r = \phi = \theta = \psi = u_n(t) = 0$, the boundary condition on $G = 0$ becomes:

$$\left[-w\hat{k} - U_\infty(1+\phi_x)\hat{i} - U_\infty\phi_y\hat{j} - U_\infty\phi_z\hat{k}\right]\left[f_{x_s}\hat{i} - f_{y_s}\hat{j} - \hat{k}\right] = 0 \qquad \text{on } G(x,y,z,t) = 0 \tag{4.103}$$

Alternatively,

$$\left[-(1+\phi_x)f_{x_s} + \phi_y f_{y_s} + (\phi_z + \alpha(t))\right] = 0 \qquad \text{on } G = 0 \tag{4.104}$$

It is required that an order of magnitude argument be performed on equation (4.103) to determine which of the terms in the brackets, if any, can be neglected. Define new dimensionless coordinates:

$$\xi = \frac{x}{l} \qquad \eta = \frac{y}{l_o} \qquad \varsigma = \frac{z}{\mu l} \qquad \tau = \frac{K U t}{l}$$

then

$$f(x,y) = \delta l \bar{f}(\xi, \eta) = z$$

$$\phi(x,y,z,t) = \varepsilon l \varphi(\xi, \eta, \varsigma, \tau)$$

$$\alpha(t) = \frac{\dot{z}(t)}{U_\infty} = \mu K \varsigma_\tau(\tau)$$

where μ - is the vertical extent of the neighborhood where order of magnitude arguments hold true

K - ($= \frac{a l}{U_\infty}$) is the reduced frequency (it is a measure of the time rate of change; the quantity a may or may not be a complex number

ϵ - is the perturbation quantity

σ - is proportional to aspect ratio

δ - is proportional to thickness

l - is a characteristic length such as mean aerodynamic chord

Assume, as a consequence of small-disturbance c.g. motion, that surface slopes measured in the stability axis system are proportional to surface slopes in the fluid axis system, i.e., (G8)

$$f_{x_s} \approx f_x \approx \delta \bar{f}_\xi$$

Performing the operations required to nondimensionalize equation (4.104), the boundary condition on G = 0 ($\zeta = \frac{\delta}{\mu} \bar{f}$) becomes,

$$-\left(1 + \varepsilon \varphi_\xi\right)\left(\delta \bar{f}_\xi\right) + \left(\frac{\varepsilon}{\sigma} \varphi_\eta\right)\left(\frac{\delta}{\sigma} \bar{f}_\eta\right) + \left(\mu K \varsigma_\tau + \frac{\varepsilon}{\mu} \varphi_\varsigma\right) = 0 \qquad (4.105)$$

on $\varsigma = \frac{\delta}{\mu} \bar{f}$

where K, ϵ, and μ are to be determined or specified.

For a thin body, for which $\delta << 1$ and $\sigma >> \delta$ and for which $\left\{\begin{matrix}\varphi = O(1)\\ \xi = O(1)\\ \tau = O(1)\end{matrix}\right\}$, the products of small terms, such as $\epsilon\,\delta\,\varphi_\xi F_\xi$ and $\frac{\epsilon\delta}{\sigma^2}\,\bar{f}_\eta\,\varphi_\eta$, are an order of magnitude smaller than the largest terms in equation (4.105). Considering only higher order terms and rearranging equation (4.105),

$$-\delta f_\xi + \mu K \varphi_{\tau\tau} + \frac{\epsilon}{\mu}\varphi_{yy} = 0 \quad \text{on} \quad y = \frac{\delta}{\mu}\bar{f}$$

$$\varphi_y\big/_{y=\frac{\delta}{\mu}\bar{f}} = \frac{\mu}{\Sigma}\left[\delta \bar{f}_\xi - \mu K \bar{f}_\tau\right] \tag{4.106}$$

Expanding this boundary condition in a Maclaurin series about the plane containing the singularities (the plane containing the reference cg trajectory in which the fluid axis system x,y,z is oriented) gives

$$\varphi_S\Big|_{S=\frac{\epsilon}{\mu}\bar{f}} = \varphi_S\Big|_{S=0} + \varphi_{SS}\Big|_{S=0} S + \varphi_{SSS}\Big|_{S=0}\frac{S^2}{2!} + \cdots = \varphi_S\Big|_{S=0} + \text{terms of } O(S^2) \text{ small}$$

(4.107)

$$\varphi_S\Big|_{S=0} \doteq \frac{\mu}{\epsilon}\left[\delta \bar{f}_\xi - \mu K \bar{f}_\tau\right]$$

Returning to the dimensional notation of equation (4.104), equation (4.107) becomes,

$$\phi_z\Big|_{z=0} = +f_{x_s} - \alpha(t) \tag{4.108}$$

in the region S of the plane of singularities z = 0.

The boundary condition on the projected wake and on the "remainder" area of the z = 0 plane can be evaluated in a similar manner.

$$\left(\phi_x + \frac{1}{U}\phi_t\right)_{z=0} = 0 \quad \text{on} \quad W \tag{4.109a}$$

$$\phi\Big|_{z=0} = 0 \quad \text{on} \quad R \tag{4.109b}$$

The partial differential equations required to describe the velocity potential representation of the aerodynamics associated with the α (t) small-disturbance c.g. motion about a reference flight condition can now be summarized.

flow equation: $$\beta^2 \phi_{xx} - \phi_{yy} - \phi_{zz} + \frac{2M}{a_\infty} \phi_{xt} + \frac{1}{a_\infty^2} \phi_{tt} = 0 \qquad (4.110a)$$

B.C.:

$$\phi_z\Big|_{z=0} = f_{x_s} - \alpha(t) \quad \text{on } S \qquad (4.110b)$$

$$\left(\phi_z + \frac{1}{u} \phi_t\right)_{z=0} = 0 \quad \text{on } W \qquad (4.110c)$$

$$\phi\Big|_{z=0} = 0 \quad \text{on } R \qquad (4.110d)$$

where $f = f(x_S, y_S) = f^S(x_S, y_S) + f^a(x_S, y_S)$

and where $f^a(x_S, y_S) = \frac{1}{2}(z_{S_u} + z_{S_\ell})$ is the camber,

and $f^S(x_S, y_S) = \frac{1}{2}(z_{S_u} - z_{S_\ell})$ is the thickness.

Note: For all the thin-body ("flat" airplane) lifting-surface calculations discussed in this appendix, the airplane is assumed to have zero thickness, i.e.,

$$f(x_S, y_S) = f^a(x_S, y_S).$$

Equations (4.110) describe the flow field surrounding a completely elastic airplane and include the effects of reference orientation and small-disturbance α (t) motion. To evaluate each effect separately, from hypothesis it is assumed that the reference forces and motions are time independent. Thus, all effects on ϕ due to time are attributed to small-disturbance motion.

4.4.1.1 The reference velocity potential: Setting the time-dependent quantities in equations (4.110) equal to zero, gives a reference velocity potential called ϕ_1, where

$$\phi(x,y,z,t) = \phi_1(x,y,z) + \phi_p(x,y,z,t) \qquad (4.111)$$

Equations (4.110a through d) reduce to a steady motion form,

flow equation: (4.112a)

$$\beta \phi_{1_{xx}} - \phi_{1_{yy}} - \phi_{1_{zz}} = 0$$

B.C.:

$$\phi_{1_z}\Big|_{z=0} = f_{x_s} \quad \text{on } S \tag{4.112b}$$

$$\phi_{1_z}\Big|_{z=0} = 0 \quad \text{on } W \tag{4.112c}$$

$$\phi_1\Big|_{z=0} = 0 \quad \text{on } R \tag{4.112d}$$

Several techniques exist to solve the partial differential equations describing the reference-flight-velocity "potential", ϕ_1. Lifting-surface influence-coefficient theory was chosen for most of the theoretical calculations because it will represent both high- and low-aspect ratio thin bodies at subsonic and supersonic speeds.

Lifting surface theory: aerodynamic influence coefficients (AIC).— The lifting surface AIC technique is summarized from ref. 35. It is desired to derive the aerodynamic influence coefficients for the simplest, most useful case satisfying equation (4.112). This case will consist of a surface of finite extent whose boundary is a quadrilateral. The surface will be immersed in a uniform flow and there will be a pressure difference across the surface that is constant on the surface. The uniform flow is perturbed by the presence of the surface and the perturbation-velocity field is found by using Green's theorem in conjunction with the linearized flow equation for steady flow. The velocity perturbation at point j, due to a surface with unit pressure force at point i, will give the desired aerodynamic influence coefficient.

The derivation will be carried out in the fluid-fixed-coordinate system, x,y,z. In this development, complete in all details, the c.g. motion has been assumed equal to zero and all results are written in the inertial axis system, x,y,z. The computer mechanization is presented in ref. 35.

Consider the constant pressure surface to be a portion of the mean camber surface of an airplane wing. The x axis is in the freestream direction and the z axis is upward. This is illustrated typically in the following sketch.

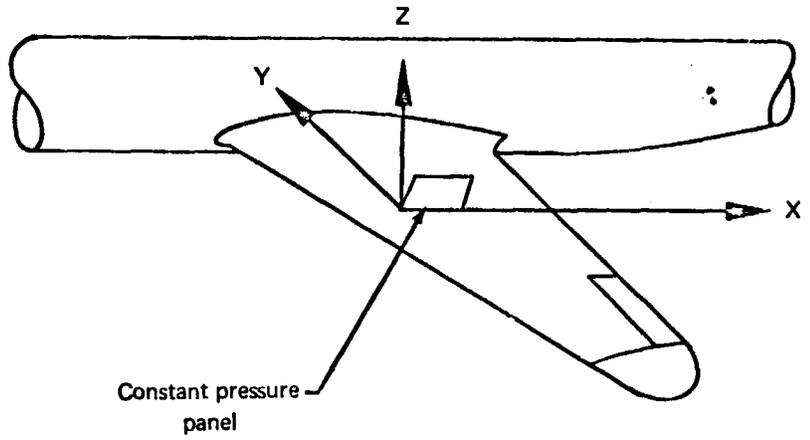

Aerodynamic influence coefficients (subsonic): When the potential function does not contain time explicitly (steady flow), the linearized flow equation reduces to

$$\left(1 - M_\infty^2\right)\frac{\partial^2\phi'}{\partial x^2} + \frac{\partial^2\phi'}{\partial y^2} + \frac{\partial^2\phi'}{\partial z^2} = 0 \tag{4.113}$$

Consider the case when $M_\infty < 1$ and define:

$$\beta^2 = 1 - M_\infty^2$$

On introducing the transformation:

$$\begin{aligned} x' &= x \\ y' &= \beta y \\ z' &= \beta z \end{aligned} \tag{4.114}$$

equation (4.113) becomes:

$$\frac{\partial^2\phi'}{\partial x'^2} + \frac{\partial^2\phi'}{\partial y'^2} + \frac{\partial^2\phi'}{\partial z'^2} = 0 \tag{4.115}$$

and may be recognized as Laplace's partial differential equation.

Consider any two functions σ, Ω that together with their first and second derivatives are finite and single valued in a region R in space surrounded by the surface S. In accordance with Green's theorem (ref. 56):

$$\iint_S \left[\sigma\,\vec{\nabla}\Omega - \Omega\,\vec{\nabla}\sigma\right]\cdot\vec{n}\,dS = \iiint_R \vec{\nabla}\cdot\left[\sigma\,\vec{\nabla}\Omega - \Omega\,\vec{\nabla}\sigma\right]dV \tag{4.116}$$

where $\vec{n}$ is the inward unit normal vector to S.

Secondly, consider the potential function

$$\phi' = \frac{-Q}{4\pi\sqrt{(x'-\xi')^2+(y'-\eta')^2+(z'-\zeta')^2}} \quad . \tag{4.117}$$

This function satisfies Laplace's equation and is the potential function corresponding to a source of strength Q located at $x' = \xi'$, $y' = \eta'$, $z' = \zeta'$. Defining:

$$r_1 = \left[(x'-\xi')^2 + (y'-\eta')^2 + (z'-\zeta')^2\right]^{1/2} \tag{4.118}$$

it follows that:

$$r_1 = -\frac{Q}{4\pi\phi'} \tag{4.119}$$

Now, let:

$$\sigma \equiv \frac{1}{r_1}$$

and require Ω to be a second function that satisfies Laplace's equation. The point where $r_1 = 0$ is excluded from the region R by enclosing the point by a sphere of surface Σ and radius ϵ. For this case, equation (4.116) becomes:

$$\iint_S \left[\frac{1}{r_1}\vec{\nabla}\Omega - \Omega\vec{\nabla}\frac{1}{r_1}\right]\vec{n}\,dS - \iint_\Sigma \left[\frac{1}{r_1}\vec{\nabla}\Omega - \Omega\vec{\nabla}\frac{1}{r_1}\right]\vec{n}'\,dS = 0 \tag{4.120}$$

where $\vec{n}'$ is a unit outward normal vector to Σ. But, as shown by ref. 56,

$$\iint_\Sigma \left[\frac{1}{r_1}\vec{\nabla}\Omega - \Omega\vec{\nabla}\frac{1}{r_1}\right]\vec{n}'\,dS = -4\pi\Omega \tag{4.121}$$

so that equation (4.110) may be written as

$$\Omega = -\frac{1}{4\pi}\iint_S \left[\frac{1}{r_1}\vec{\nabla}\Omega - \Omega\vec{\nabla}\frac{1}{r_1}\right]\vec{n}\,dS \tag{4.122}$$

Further, it may be noted that

$$\vec{n}\cdot\vec{\nabla} = \frac{\partial}{\partial n}$$

so that equation (4.122) may be written as

$$\Omega = -\frac{1}{4\pi}\iint_S \left[\frac{1}{r_1}\frac{\partial\Omega}{\partial n} - \Omega\frac{\partial}{\partial n}\frac{1}{r_1}\right]dS \tag{4.123}$$

Equation (4.123) is fundamental to the following development of aerodynamic influence coefficient theory for the subsonic case. It should be noted that $-1/4\pi r_1$ is the potential function for a source of unit strength, while $-1/4\pi\left[\partial/\partial\eta\ (1/r_1)\right]$ is the potential function for a doublet of unit strength with axis aligned with the normal to S. It is essential to recognize the functional dependence of the terms appearing in equation (4.123). It may be illustrated by writing equation (4.123) as:

$$\Omega(x';y';z') = -\frac{1}{4\pi}\iint_S\left[\frac{1}{r_1}(x';y';z';\xi';\eta';\zeta')\frac{\partial}{\partial\eta}\Omega(\xi';\eta';\zeta') - \Omega(\xi';\eta';\zeta')\frac{\partial}{\partial\eta}\frac{1}{r_1}(x';y';z';\xi';\eta';\zeta')\right]dS \tag{4.124}$$

Note that S is a closed surface with sources and doublets continuously distributed over it. The distributed sources are given by

$$\frac{1}{r_1}(x';y';z';\xi';\eta';\zeta')$$

where ξ', η', ζ' is a point on S. The distributed doublets are given by

$$-\frac{\partial}{\partial\eta}\ \frac{1}{r_1}(x';y';z';\xi';\eta';\zeta')$$

where ξ', η', ζ' is a point on S. Then it should be clear that equation (4.124) may be written as $\Omega(x',y',z') = \iint_S d\Omega$ where

$$d\Omega = -\frac{1}{4\pi}\left[\frac{1}{r_1}\frac{\partial}{\partial\eta}(\Omega) - \Omega\frac{\partial}{\partial\eta}\left(\frac{1}{r_1}\right)\right]dS \tag{4.125}$$

is the differential potential function for a source of strength $[\partial/\partial\eta\ \Omega(\xi',\eta',\zeta')]dS$ and a doublet of strength $\Omega(\xi',\eta',\zeta')\,dS$ located at the surface point ξ', η', ζ'. Hence, equations (4.124) and (4.125) give the potential function for sources and doublets continuously distributed over the surface S.

To continue, let the region R be bound by the surface S, which consists of the x'y' plane and a hemispheric surface of infinite radius over this plane. The surface, S, then consists of two parts, S_1 (the x'y' plane) and S_2 (the hemispherical surface), as illustrated by the following sketch:

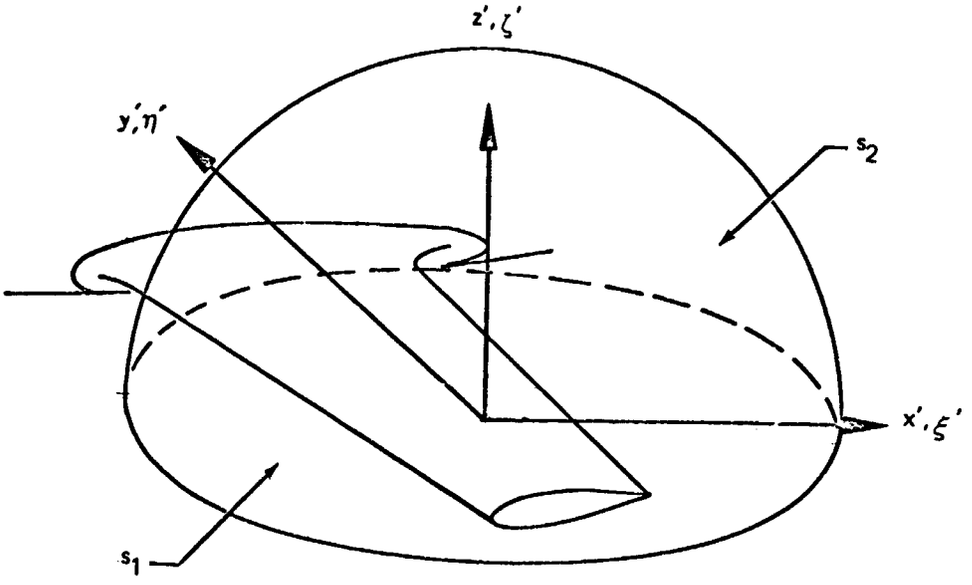
z', ζ'
y', η'
S2
x', ξ'
S1

On S_1 the derivative $\frac{\partial}{\partial \eta}$ is equal to $\frac{\partial}{\partial \zeta'}$. Now, Ω and $\frac{\partial \Omega}{\partial \eta}$ are set equal to zero on S_2. Under these conditions, equation (4.123) becomes

$$\Omega = -\frac{1}{4\pi} \iint_{S_1} \left[\frac{1}{r_1'} \frac{\partial \Omega}{\partial \zeta'} - \Omega \frac{\partial}{\partial \zeta'} \left(\frac{1}{r_1'} \right) \right] dS \qquad (4.126)$$

Introduce a special notation that will permit consideration of functions that are discontinuous across the surface. To this end equation (4.126) is written as:

$$\Omega(x', y', z') = -\frac{1}{4\pi} \iint_{S_1} \left[\left(\frac{1}{r_1} \right)_{\zeta'=0^+} \left(\frac{\partial \Omega}{\partial \zeta'} \right)_u - \Omega_u \left(\frac{\partial}{\partial \zeta'} \frac{1}{r_1} \right)_{\zeta'=0^+} \right] d\xi' d\eta' \qquad (4.127)$$

where

$$\left(\frac{\partial \Omega}{\partial \zeta'} \right)_u = \left(\frac{\partial \Omega}{\partial \zeta'} \right)_{\zeta'=0^+} \qquad \text{and} \qquad \Omega_u \equiv \Omega \big|_{\zeta'=0^+}$$

and $\zeta' = 0^+$ denotes the limiting value found by approaching from $+\zeta'$.

This notation is of value when there is a surface of discontinuity in an otherwise continuous field as, for example, a shock surface in supersonic flow field. The situation arises here from the wing having been replaced by the mean camber surface. This surface does not have thickness. The values of the functions Ω and $\frac{\partial \Omega}{\partial \zeta}$ at the surface are not defined. But the values are defined at all other points, including the very near neighborhood of both sides of the surface, especially the limiting values as the surface is approached from either side. If these two values differ as the same surface point is approached, then a jump in the function is said to exist at that surface point and the surface is a surface of discontinuity. The jump in Ω is denoted by symbol $[\Omega]$. This quantity, i.e., $[\Omega]$, is also a function, but it is only defined on the surface, and is a function of the surface coordinates.

Now, in deriving equation (4.126) it was necessary to assume that the sources $(\frac{1}{r_1})$ and doublets $\frac{\partial}{\partial n}$ $(\frac{1}{r_1})$ are interior to the region R. If not, the integral over the surface vanishes as noted by equation (4.120). Thus, the sources and doublets must be distributed in the neighborhood above and adjacent to the x'y' plane. If we take R as the region below the x'y' plane so that S_2 is a hemispherical surface of infinite radius below, then

$$-\frac{1}{4\pi} \iint_{S_1} \left[\left(\frac{1}{r_1} \right)_{\zeta'=0^-} \left(\frac{\partial \Omega}{\partial \zeta'} \right)_l - \Omega_l \left(\frac{\partial}{\partial \zeta'} \frac{1}{r_1} \right)_{\zeta'=0^-} \right] d\xi' d\eta' \qquad (4.128a)$$

where

$$\left(\frac{\partial \Omega}{\partial \zeta}\right)_\ell \equiv \left(\frac{\partial \Omega}{\partial \zeta'}\right)_{\zeta'=0^-} \qquad \text{and} \qquad \Omega_\ell = \Omega|_{\zeta'=0^-}$$

and $\zeta' = 0^-$ denotes the limiting value found by approach from $-\zeta'$.

Subtracting equation (4.128a) from equation (4.127) gives

$$\Omega(x', y', z') = -\frac{1}{4\pi}\iint_{S_1}\left\{\left(\frac{1}{r_1}\right)_{\zeta'=0}\left[\left(\frac{\partial \Omega}{\partial \zeta'}\right)_u - \left(\frac{\partial \Omega}{\partial \zeta'}\right)_\ell\right] - (\Omega_u - \Omega_\ell)\left(\frac{\partial}{\partial \zeta'}\frac{1}{r_1}\right)_{\zeta'=0}\right\} d\xi' d\eta' \tag{4.128b}$$

Introduce the definitions $[\Omega] \equiv \Omega_u - \Omega_\ell$ and

$$\left[\frac{\partial \Omega}{\partial \zeta'}\right] \equiv \left(\frac{\partial \Omega}{\partial \zeta'}\right)_u - \left(\frac{\partial \Omega}{\partial \zeta'}\right)_\ell \tag{4.129}$$

Also, note that

$$\left(\frac{\partial}{\partial \zeta'}\frac{1}{r_1}\right)_{\zeta'=0} = \frac{z}{r_2^3}$$

where

$$r_2 = \left[(x'-\xi')^2 + (y'-\eta')^2 + z'^2\right]^{1/2} \tag{4.130}$$

so that, after using the inverse of the transformation given by equation (4.114) equation (4.128) may be written as

$$\Omega(x, y, z) = -\frac{1}{4\pi}\int_{-\infty}^{\infty}\int_{-\infty}^{\infty}\left(\left[\frac{\partial \Omega}{\partial \zeta}\right]\frac{1}{r_2} - \frac{[\Omega]}{r_2^3}\beta^2 z\right) d\xi\, d\eta \tag{4.131}$$

The function Ω is as yet arbitrary except for the requirements on continuity previously stated and the requirement that Ω be harmonic (i.e., a solution to Laplace's equation). The components of the perturbation velocity satisfy these requirements. Thus, choose $\Omega \equiv u$ and write equation (4.131) as

$$u(x, y, z) = -\frac{1}{4\pi}\int_{-\infty}^{\infty}\int_{-\infty}^{\infty}\left(\left[\frac{\partial \Omega}{\partial \zeta}\right]\frac{1}{r_2} - [\Omega]\frac{\beta^2 z^2}{r_2^3}\right) d\xi\, d\eta \tag{4.132}$$

Now, introduce the boundary condition requiring the flow must be tangent to the surface. Thus, $\frac{\partial w}{\partial x}$ is equal to the surface slope. Also, the surface is infinitesimally thin so that $\left(\frac{\partial w}{\partial x}\right)_u = \left(\frac{\partial w}{\partial x}\right)_\ell$. Thus, it follows that

$\left[\frac{\partial w}{\partial x}\right] = 0$ on S_1. Then from the assumed irrotationality of the flow, equation (4.9), i.e., $\frac{\partial w}{\partial x} - \frac{\partial u}{\partial x} = 0$, it follows that

$$\left[\frac{\partial u}{\partial x}\right] = \left[\frac{\partial w}{\partial x}\right] = 0 \qquad \text{on } S_1 \tag{4.133}$$

Application of equation (4.133) to equation (4.132) gives

$$u(x,y,z) = -\frac{1}{4\pi}\int_{-\infty}^{\infty}\int_{-\infty}^{\infty}\left[u(\xi,\eta)\right]\frac{\beta^2 z}{r_2^3}\,d\xi\,d\eta \tag{4.134}$$

the perturbation velocity component u is related to the perturbation potential function by

$$u = \frac{\partial \phi'}{\partial x}$$

Now, noting that the flow is unperturbed at $x = -\infty$, $\phi' \to 0$ as $x \to \infty$. Hence, it follows that

$$\phi'(x,y,z) = \int_{-\infty}^{x} u(\bar{x},y,z)\,d\bar{x} \tag{4.135}$$

and equation (4.134) may be written as

$$\phi(x,y,z) = -\frac{1}{4\pi}\int_{-\infty}^{\infty}\int_{-\infty}^{\infty}\left[u(\xi,\eta)\right]\beta^2 z\int_{-\infty}^{x}\frac{1}{r_2^3}\,d\bar{x}\,d\xi\,d\eta \tag{4.136}$$

But,

$$\int_{-\infty}^{x}\left(\frac{1}{r_2}\right)^3 d\bar{x} = \frac{1}{\beta^2\left[(y-\eta)^2+z^2\right]}\frac{x-\xi}{r_2}\Bigg|_{-\infty}^{x}$$

$$= \frac{1}{\beta^2\left[(y-\eta)^2+z^2\right]}\left(1+\frac{x-\xi}{r_2}\right)$$

so that

$$\phi'(x,y,z) = -\frac{1}{4\pi}\int_{-\infty}^{\infty}\int_{-\infty}^{\infty}\frac{z\left[u(\xi,\eta)\right]}{(y-\eta)^2+z^2}\left(1-\frac{x-\xi}{r_2}\right)d\xi\,d\eta \tag{4.137}$$

The jump in perturbation velocity, $[u]$, is now taken to be zero everywhere except over the semi-infinite triangular region (see sketch) bounded by $y = C_i$ (C_i = constant) and $y = M_i x$. Hence, equation (4.137) becomes

$$\phi'(x,y,z) = -\frac{1}{4\pi}\int_{x=\frac{C_i}{M_i}}^{\infty}\int_{y=C_i}^{y=M_i x}\frac{z\left[u(\xi,\eta)\right]}{(y-\eta)^2+z^2}\left(1+\frac{x-\xi}{r_2}\right)d\xi\,d\eta \tag{4.138}$$

The perturbation velocity component w is given by $w = \frac{\partial \phi}{\partial z}$ so that equation (4.138) may be used to find

$$\frac{w(x,y,z)}{U_\infty} = -\frac{1}{4\pi}\int_{x=\frac{C_i}{M_i}}^{\infty}\int_{y=C_i}^{y=M_i x}\frac{[u(\xi,\eta)]}{U_\infty}\frac{\partial}{\partial z}\left[\frac{z}{(y-\eta)^2+z^2}\left(1+\frac{x-\xi}{r_2}\right)\right]d\xi\,d\eta$$

If the jump in velocity component is set equal to a constant, and it is noted that

$$[C_p] = -\frac{2[u]}{U_\infty}$$

then

$$\frac{w(x,y,z)}{U_\infty} = \frac{[C_p]}{8\pi}\int_{x=\frac{C_i}{M_i}}^{\infty}\int_{y=C_i}^{y=M_i x}\frac{\partial}{\partial z}\left[\frac{z}{(y-\eta)^2+z^2}\left(1+\frac{x-\xi}{r_2}\right)\right]d\xi\,d\eta \qquad (4.139)$$

The result $\frac{w(x,y,z)}{U_\infty}$ is the downwash angle at an arbitrary point in the flow due to a constant pressure on the semi-infinite triangular region. If equation (4.139) is evaluated at $z = 0$, the $\frac{w(x,y,0)}{U_\infty}$ is the downwash angle in the plane of the surface. Since the flow must be parallel to the surface S, the downwash angle over the surface must be equal to the surface slope. Also, since $w(x,y,0)/U_\infty$ is a function of x and y, the surface is warped and not planar.

The region of integration is shown in the following sketches:

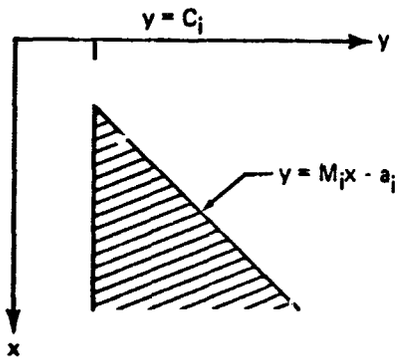

If a second region is chosen with $y = C_{i+1}$ where $C_{i+1} > C_i$ and the pressure coefficient is constant and equal to the negative of the original region, the combined solutions will give the downwash angle for the strip shown in the following sketch:

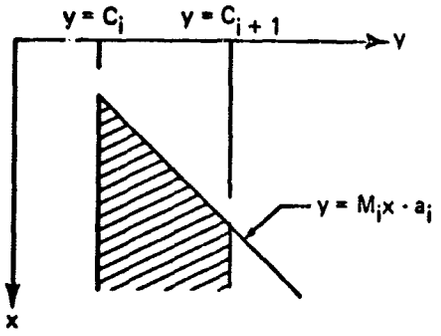

The semi-infinite strip of constant pressure jump may be modified into a finite region of constant-pressure jump that is quadrilateral. This is accomplished by adding a second semi-infinite strip having a constant pressure jump of opposite sign:

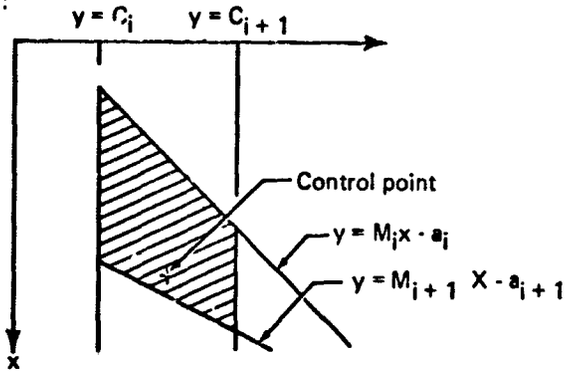

The downwash angle found by superimposing the integrals; equation (4.139), may be denoted by

$$\alpha(x,y,z) = \frac{w(x,y,z)}{U_\infty} = [C_{p_i}]\, f_i(x_i, y_i, x, y, z) \qquad (4.140)$$

In this development the region of constant pressure jump ("panel" when the region is a quadilateral) is confined to the xy plane. By an affine transformation of coordinates, the plane of the panel of constant pressure jump may be shifted from the xy plane and reoriented. This feature allows one to treat arbitrary camber and twist. Equation (4.140) will continue to hold provided the parallel edges $y = C_i$ and $y = C_{i+1}$ continue to be aligned with the direction of the freestream velocity. The form of equation (4.140) will remain unchanged but the spatial variables will be replaced by the affinely transformed spatial variables. To remain brief, the details of these operations are not discussed here.

The downwash angle for the panel is chosen to be the value of $\alpha(x,y,z)$ found by evaluating equation (4.140) at the point that corresponds to midspan and 95 percent of the mean chord of the panel, as shown above. This point is termed the control point. If the downwash angle is evaluated at the control point of the j^{th} panel, equation (4.140) may be written as

$$\alpha_j(x_j, y_j, z_j) = C_{p_i} f_{ji}(x_i, y_i, z_i, x_j, y_j, z_j) \tag{4.141}$$

Thus, the coefficient f_{ji} represents the downwash angle at the control point of panel j due to a unit pressure coefficient at panel i. The total downwash angle at panel j due to constant pressure distributions at all panels is given by

$$\alpha_j = \sum_{i=1}^{n} f_{ji} C_{p_i}$$ for a total of n panels.

This result may be written as a matrix equation

$$\{\alpha_j\} = [f_{ji}]\{C_{p_i}\} = [f_{ji}]\{P_{w_i}\} \tag{4.142}$$

where f_{ji} is the velocity component normal to control point j induced by a unit pressure jump on panel i

P_{w_i} is the strength of the singularity located on panel i and is unknown

If one is given the panel slope at each control point, α_j, the unknown panel strengths can be determined by inverting equation (4.142).

$$\{P_{w_i}\} = [f_{ji}]^{-1}\{\alpha_j\} = [f_{ij}]\{\alpha_j\} \tag{4.143}$$

The pressure at each panel due to all the panels in the flow field is calculated from the pressure coefficient given in equation (4.143).

$$C_{p_i} = \begin{cases} -2u_i & \text{- first order thin body} \\ -2u_i - v_i^2 - w_i^2 & \text{- second order thin body or slender body} \end{cases}$$

In the case of a thin body represented solely by vortex panels, the net pressure force on panel i is P_{w_i}

Note. Reference 35 defines aerodynamic influence coefficient to be the terms f_{ji} in equation (4.142). However, throughout this appendix "aerodynamic influence coefficient" is taken to mean the terms of the matrix $[\, a_{ij} \,]$ in equation (4.143).

Aerodynamic influence coefficients (supersonic): When the freestream Mach number is greater than unity, $M_\infty > 1$, and the perturbation potential function is not an explicit function of time, the linearized flow equation may be written as

$$\beta^2 \frac{\partial^2 \phi'}{\partial x^2} = \frac{\partial^2 \phi'}{\partial y^2} + \frac{\partial^2 \phi'}{\partial z^2} \tag{4.144}$$

where

$$\beta^2 = M_\infty^2 - 1$$

Equation (4.144) may be written more conveniently by introducing the coordinate transformation

$$\begin{aligned} X &= x \\ Y &= \beta y \\ Z &= \beta z \end{aligned} \tag{4.145}$$

such that

$$\frac{\partial^2 \phi}{\partial X^2} = \frac{\partial^2 \phi'}{\partial Y^2} + \frac{\partial^2 \phi'}{\partial Z^2} \tag{4.146}$$

If the operator L (ϕ') is defined such that

$$L(\phi) = \frac{\partial^2 \phi'}{\partial X^2} - \frac{\partial^2 \phi'}{\partial Y^2} - \frac{\partial^2 \phi'}{\partial Z^2} \tag{4.147}$$

then Green's theorem for equation (4.146) has the form

$$\iiint_R \left[\sigma L(\Omega) - \Omega L(\sigma)\right] dV = \iint_S \left(\sigma \frac{\partial \Omega}{\partial \nu} - \Omega \frac{\partial \sigma}{\partial \nu}\right) dS \tag{4.148}$$

where $\frac{\partial}{\partial \nu}$ is the directional derivative

$$\frac{\partial}{\partial \nu} = \vec{\nu} \cdot \vec{\nabla} = \nu_x \frac{\partial}{\partial x} - \nu_y \frac{\partial}{\partial y} - \nu_z \frac{\partial}{\partial z} \tag{4.149}$$

and $\vec{\nu}$ is the unit vector termed the "co-normal", having the components

$$\begin{aligned} \nu_x &= -n_x \\ \nu_y &= n_y \\ \nu_z &= n_z \end{aligned} \tag{4.150}$$

where $\bar{n}$ is the unit inward normal vector to the surface S surrounding the volume R.

If the functions σ, Ω are required to satisfy equation (4.146) (analogous to the harmonic functions in the subsonic case), then equation (4.148) reduces to

$$\iint_S \sigma \frac{\partial \Omega}{\partial \nu} \, dS = \iint_S \Omega \frac{\partial \sigma}{\partial \nu} \, dS \tag{4.151}$$

Consider, now, a surface S which, for present purposes, is taken to be coincident with the xy plane. The value of the function Ω at some arbitrary point (x, y, z) will be found from boundary values specified on S. The solution is suggested by the form of equation (4.151). Neglecting the details contained in ref. 59, the function Ω evaluated at x, y, z is given by

$$\Omega(x,y,z) = -\frac{1}{2\pi} \frac{\partial}{\partial x} \iint_S \left[\left(\frac{\partial \Omega}{\partial \nu} \right)_u + \left(\frac{\partial \Omega}{\partial \nu} \right)_\ell \right] \sigma \, dS \tag{4.152}$$

$$+ \frac{1}{2\pi} \frac{\partial}{\partial x} \iint_S \left(\Omega_u - \Omega_\ell \right) \frac{d\sigma}{d\nu} \, dS$$

when

$$\sigma = \cosh^{-1} \frac{x-\xi}{\sqrt{(y-\eta)^2 + (z-\zeta)^2}} \tag{4.153}$$

which is the potential function for a source of unit strength in a supersonic flow. The subscripts written as u and ℓ, again, refer to the limiting values of the subscripted function on the surface in the manner noted in equations (4.127) and (4.128).

Because of the nature of solutions to the partial differential equation, equation (4.146), which is hyperbolic in form, the function Ω depends on the boundary conditions specified on only a particular region of the surface S. This region is denoted by τ and is the region of S included interior to a cone with axis parallel to the x axis and apex at the point P where Ω is evaluated. This is indicated by the following figure.

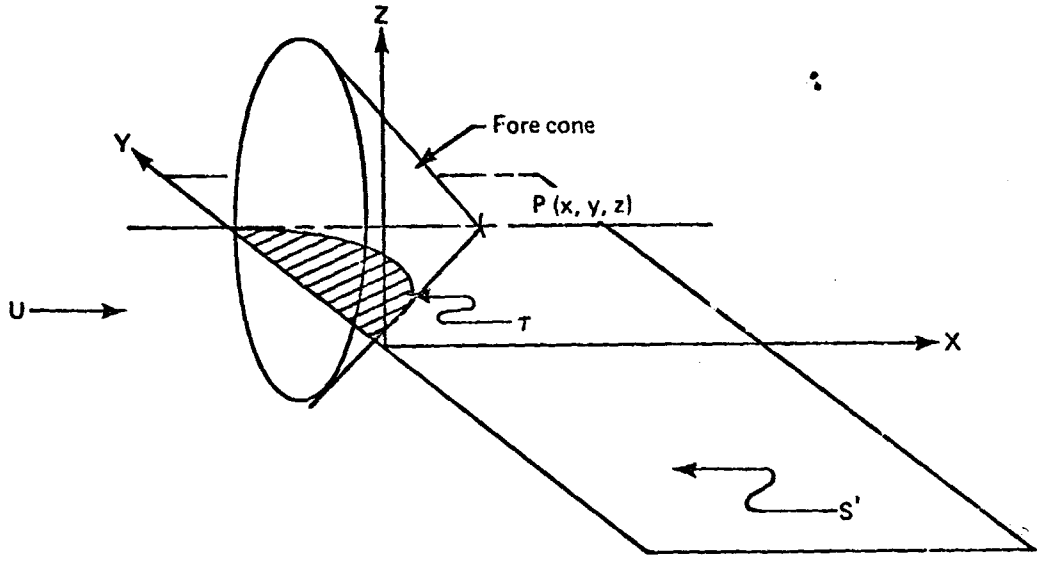

This cone is termed the force cone and τ is the "domain of dependence" of Ω at point P. Equation (4.152) may, therefore, be written as

$$\Omega(x,y,z) = -\frac{1}{2\pi}\frac{\partial}{\partial x}\iint_{\tau}\left[\left(\frac{\partial\Omega}{\partial\nu}\right)_u + \left(\frac{\partial\Omega}{\partial\nu}\right)_\ell\right]\sigma\, dS$$

$$+\frac{1}{2\pi}\frac{\partial}{\partial x}\iint_{\tau}\left(\Omega_u - \Omega_\ell\right)\frac{\partial\sigma}{\partial\nu}\, dS \qquad (4.154)$$

Only the particular case when $\left(\frac{\partial\Omega}{\partial\nu}\right) = -\left(\frac{\partial\Omega}{\partial\nu}\right)_\ell$ will be considered here so that equation (4.154) reduces to

$$\Omega(X,Y,Z) = \frac{1}{2\pi}\frac{\partial}{\partial x}\iint_{\tau}\left[\Omega_u - \Omega_\ell\right]\frac{\partial\sigma}{\partial\nu}\, dS \qquad (4.155)$$

This will be seen to hold for the case when the component of perturbation velocity normal to the surface S is continuous, i.e., when $w_u = w_\ell$. The surface is required to be infinitesimally thin.

On substituting equation (4.152) into (4.155), the result is

$$\Omega(X,Y,Z) = \frac{1}{2\pi}\iint_{\tau}\frac{(\Omega_u - \Omega_\ell)(x-\xi')(z-\zeta')\, d\xi\, d\eta}{\left[(Y-\eta')^2 + (z-\zeta')^2\right]\sqrt{(x-\xi')^2 - (Y-\eta')^2 - (z-\zeta')^2}}$$

(4.156)

By using the inverse form of the transformation given by equation (4.147) it follows that

$$\Omega(X,Y,Z) = \frac{1}{2\pi}\frac{\partial}{\partial Z}\iint_{\tau}\frac{(\Omega_u - \Omega_\ell)(X-\xi)\,Z\,d\xi\,d\eta}{[(Y-\eta)^2+Z^2]\sqrt{(X-\xi)^2-\beta^2[(Y-\eta)^2+Z^2]}} \qquad (4.157)$$

Now, consider the surface S to be the semi-infinite triangular region with boundaries y = 0 and y = mx. The equation for the curve formed by the intersection of this region with the surface of the fore cone is given by

$$(x-\xi)^2 = \beta^2(y-\eta)^2 + \beta^2 z^2 \qquad (4.158)$$

and is denoted by QR in the following sketch:

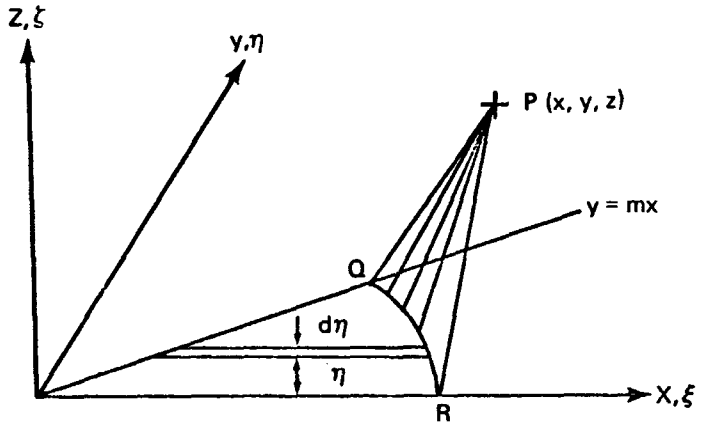

The infinitisimal strip of width dy extends from $\xi = \eta/m$ to ξ_{QR} where equation (4.158) is satisfied, i.e.,

$$\xi_{QR} = x - \sqrt{\beta^2(y-\eta)^2 + \beta^2 z^2} \qquad (4.159)$$

The variable of integration η ranges from zero to

$$\eta_Q = \frac{(x-\beta^2 y) \pm \sqrt{(x-\beta^2 y)^2 - (x^2 - \beta^2 y^2 - \beta^2 z^2)\left(\frac{1}{m^2}-\beta^2\right)}}{\left(\frac{1}{m^2}-\beta^2\right)} \qquad (4.160)$$

so definite limits of integration may be introduced into equation (4.157). The result is

$$\Omega(x,y,z) = \frac{1}{2\pi}\frac{\partial}{\partial x}\int_{\eta=0}^{\eta=\eta_Q}\int_{\xi=\frac{\eta}{m}}^{\xi_{QR}} \frac{z(\Omega_u - \Omega_\ell)(x-\xi)\, d\xi\, d\eta}{\left[(y-\eta)^2+z^2\right]\sqrt{(x-\xi)^2-\beta^2\left[(y-\eta)^2+z^2\right]}} \qquad (4.161)$$

Now, let the function Ω be the x-component of perturbation of velocity, u. Further, let the limiting values on the surface be constant so that $[u] = u_u - u_\ell$ = constant. Equation (4.161) becomes

(4.162)

$$\Omega(x,y,z) = \frac{[u]}{2\pi}\frac{\partial}{\partial x}\int_{\eta=0}^{\eta=\eta_Q}\int_{\xi=\eta/m}^{\xi_{QR}} \frac{z(x-\xi)\, d\xi\, d\eta}{[(y-\eta)^2+z^2]\sqrt{(x-\xi)^2-\beta^2[(y-\eta)^2-z^2]}}$$

Recalling equation (4.135) and recalling that ϕ' vanishes at points in front of the Mach cones eminating from the leading edge of the domain of influence, equation (4.162) may be integrated to find

(4.163)

$$\phi'(x,y,z) = \frac{[u]}{2\pi}\int_{\eta=0}^{\eta=\eta_Q}\int_{\xi=\eta/m}^{\xi_{QR}} \frac{z(x-\xi)\, d\xi\, d\eta}{[(y-\eta)^2+z^2]\sqrt{(x-\xi)^2-\beta^2[(y-\eta)^2+z^2]}}$$

Noting, again, that

$$[C_{p_i}] = -2\frac{[u]}{u_\infty} = \{p_{w_j}\}$$

and

$$\alpha(x,y,z) = \frac{w(x,y,z)}{u_\infty} = \frac{1}{u_\infty}\frac{\partial\phi}{\partial z}(x,y,z)$$

it follows that

(4.164)

$$\alpha(x,y,z) = \frac{[C_p]}{4\pi}\frac{\partial}{\partial z}\int_{\eta=0}^{\eta=\eta_Q}\int_{\xi=\eta/m}^{\xi_{QR}} \frac{z(x-\xi)\, d\xi\, d\eta}{\left[(y-\eta)^2+z^2\right]\sqrt{(x-\xi)^2-\beta\left[(y-\eta)^2+z^2\right]}}$$

This result corresponds with equation (4.139) obtained for the subsonic case except for the range of integration in the positive x-direction. Here panels that are aft of the fore cone from the point P where α is evaluated, have no influence. They are outside of the domain of influence. Triangular regions may, again, be combined to form quadrilateral panels. For the quadrilateral panels, equation (4.164) may be used to find

$$\alpha_j(x,y,z) = [C_{p_i}]\, g_{ij}(x_i, y_i, x, y, z) \qquad (4.165)$$

Evaluation of equation (4.165) at the panel control points leads to

$$\alpha_j(x_j, y_j, 0) = \left[C_{p_i}\right] g_{ji}(x_i, y_i, x_j, y_j, 0) \qquad (4.166)$$

and in matrix form

$$\{\alpha_j\} = [g_{ji}]\{C_{p_i}\} = [g_{ji}]\{P_{w_i}\} \qquad (4.167)$$

where P_{w_i} is the strength of the i^{th} singularity

α_j is the surface slope of the j^{th} panel

It should be noted that $g_{ji} = 0$ for panels j, which are not in the domain of influence of the i^{th} panel. The aerodynamic influence coefficients are, again, obtained by equating the downwash angle to the panel slope. Then the change in pressure at the j^{th} panel due to a unit change in slope of the i^{th} panel is required. The desired result is obtained by writing equation (4.167) in terms of the panel pressure forces acting at the centroid of the panel areas and solving the system of equations for the panel-pressure forces. In the case of a thin body represented solely by vortex panels, the net pressure is P_{w_i} on each panel.

(A12) Briefly, in application of aerodynamic influence coefficient theory, the airplane is divided into a large number of panels. An aerodynamic influence coefficient is defined as the pressure induced on one panel (at the panel-control point) by a unit incidence at another panel. The boundary condition used to solve for these influence coefficients is the requirement that the downwash combined with the freestream flow must produce a resultant that is parallel to each panel. The influence coefficients are assembled in an n-by-n aerodynamic influence coefficient matrix where n is the number of panels. This square matrix depends only on the planform geometry of the panels and on the Mach number. It is not influenced by camber, twist, or incidence.

Practical solutions to these influence coefficients can only be obtained through the use of high-speed digital computers. In a program identified as TA 67A (ref. 35), the wing-body-tail is divided into not more than 80 panels (per airplane side). There is considerable freedom in how these are distributed. The usual technique is to make panels coincide with movable surfaces, such as ailerons, elevators, spoilers, and flaps. It is important to arrange the panels more closely spaced where the pressure distribution is changing rapidly, such as near the wing leading edge. Typical examples of paneling are shown for the 707-320B in Sec. 7.

The influence coefficient matrix can be used to solve for the lift distribution over the airplane for any desired camber, twist, and incidence:

$$\{L_i\} = \bar{q}[S_i][a_{ij}]\{\alpha_j\} \qquad (4.168)$$

where L_i is the load on panel i and ${}^{\alpha}J_j$ is the j^{th} panel incidence angle.

There is no thickness representation in the TA 67A program. The airplane is treated as a thin surface. Also, all panel control points are assumed to be coplanar. This means that as far as the computer program TA 67A is concerned, the airplane looks as indicated in fig. 8.

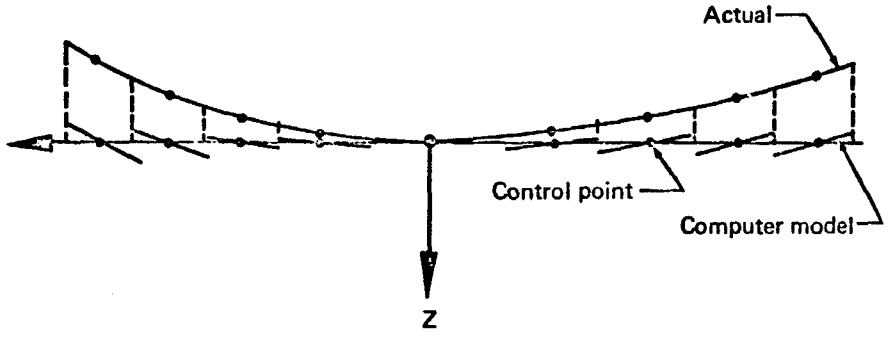

FIGURE 8.– EXAMPLE OF AIRPLANE REPRESENTATION IN PROGRAM TA 67A

Observe that the geometry of fig. 8 implies that the program only sees the downwash field of the lifting surface in the xy plane. Deformation (rolling up, vertical displacement, etc.) of the downwash sheet are, therefore, not accounted for in the current method.

The primary printout of the program consists of lift and drag coefficients and centers of pressure. These quantities are all that are needed to calculate the rigid airplane stability derivatives using finite differencing techniques.

A significant shortcoming of lifting surface theory is that it does not calculate total drag correctly. There are two reasons for this. One, a theory limitation, is that friction drag is not included. The other is that the program leaves out leading edge suction and, hence, the pressure part of drag is overestimated by a considerable margin in the subsonic regime. The physical interpretation of this anomaly is that a thin-plate representation of a wing has

a singularity at the leading edge. The stagnation line is on the lower surface, which means there is a theoretical infinite suction at the leading edge. Because there is zero thickness, no 'thrust' term is generated. One possible way of overcoming the singularity would be to use the Trefftz plane solution to the leading edge pressures as indicated in ref. 60.

Lifting surface theory: vortex-lattice method: This theory allows the determination of potential-flow aerodynamic characteristics of most three-dimensional surfaces in steady incompressible flow. Using Gothert's rule, it may be applied to compressible flow (ref. 61). The three-dimensional surface is represented by a network of horseshoe vortices, distributed on the surface and trailing behind. The strength of these vortices is determined by requiring the flow to be parallel to the surface at a number of control points. The force on each vortex segment is computed as the vector product of the local velocity and the vortex strength multiplied by the density. The forces and moments on the entire surface are obtained by summing the forces and moments created on each vortex segment. The pressure coefficients are computed on both sides of the surface at the boundary points from considerations of the velocity induced at the boundary points, together with the local vorticity density.

A computer program identified in ref. 62 is an application of vortex-lattice theory, which promises to be important in the near future. It computes lift, drag, and side-force coefficients on almost all lifting or nonlifting, planar or nonplanar surfaces. The pitching, yawing, and rolling moment coefficient and surface-pressure distribution are also computed. Dihedral, camber, twist, control surfaces, and end plates can be simulated. Complete configurations (wing + body + tail) indicating asymmetric configurations can be treated. The program is presently restricted to incompressible (i.e., low-subsonic) flow.

Lifting line theory: Lifting line theory, as used in this study, has been documented in ref. 63 for steady incompressible flow. The theory is based on the work by Weissinger as published in ref. 64. In this theory, the airplane lifting surfaces are represented by systems of horseshoe vortices located at the quarter chord.

The theory is restricted by the following assumptions:

(A1) Potential-flow theory; i.e., boundary-layer effects, separation and compressibility shock are neglected

(A2) Thin wings

Lifting line theory, as presently programmed and identified as computer program TS 70, is capable of predicting lift and pitching-moment derivatives for wing-body combinations and for isolated surfaces (such as a horizontal tail). Expressions for these lift and pitching-moment coefficients are documented in ref. 64. The component data are then manipulated into airplane derivatives using formulas such as:

$$C_{L_{\alpha_A}} = C_{L_{\alpha_{WB}}} + \eta_H C_{L_{\alpha_H}} \left(1 - \frac{d\epsilon}{d\alpha}\right) \frac{S_H}{S_W} \tag{4.169}$$

where $(1 - \frac{d\epsilon}{d\alpha})$ and η_H (efficiency factor) are to be determined from separate methods or from wind tunnel data. In that sense, this method is partly a handbook method. However, there is no reason why a lifting line program could not be written that computes derivatives for complete configurations. The method, as currently programmed, cannot deal very well with irregular wing planforms such as occur with variable-sweep designs.

4.4.1.2 The $\alpha(t)$ velocity potential: Having evaluated the reference velocity potential ϕ_1 by equations (4.112), it can be eliminated from equations (4.110) to give the small disturbance velocity potential ϕ_p. Assume that the total velocity potential, ϕ, can be written $\phi = \phi_1 + \phi_p$ as has been done in ref. 31. Equations (4.112) separate from equations (4.110) leaving the small disturbance aerodynamic equations,

flow equation: $$\beta^2 \phi_{p_{xx}} - \phi_{p_{yy}} - \phi_{p_{zz}} + \frac{2M}{a_\infty} \phi_{p_{xt}} + \frac{1}{a_\infty^2} \phi_{p_{tt}} = 0 \tag{4.170a}$$

B.C.: $$\phi_{p_z}\Big|_{z=0} = -\alpha(t) \qquad \text{on } S \tag{4.170b}$$

$$\left(\phi_{p_z} + \frac{1}{U} \phi_{p_t}\right)_{z=0} = 0 \qquad \text{on } W \tag{4.170c}$$

$$\phi_p\Big|_{z=0} = 0 \qquad \text{on } R \tag{4.170d}$$

From equations (4.101e) and (4.101f), the stability derivatives are related to ϕ_p by

(4.171a)

force derivatives: $$\Delta \vec{C}_N(t) = \vec{C}_{N_\alpha}\alpha(t) + C_{N_{\dot\alpha}}\dot\alpha(t) = \frac{4}{S_{REF}}\iint_S \frac{\nabla G_s}{|\nabla G_s|}\left(\phi_{P_z} + \frac{1}{U}\phi_{P_t}\right)_{z=0} dS$$

moment derivatives: $$\Delta \vec{C}_M(t) = \vec{C}_{M_\alpha}\alpha(t) + \vec{C}_{M_{\dot\alpha}}\dot\alpha(t) = \sum_{i=1}^{k} \frac{\vec{r}_i}{l_M} \times \Delta \vec{C}_{N_i}(t) \qquad (4.171b)$$

The general form of $\alpha(t)$ was given in equation (4.5):

$$\alpha(t) = \alpha_0 e^{at} \qquad (4.172)$$

where α_0 is some initial small disturbance amplitude from the reference value $\alpha_{ref.}$.

a is a complex number ($a = a_1 + ia_2$) representing frequency and damping of the small disturbance motion.

Substituting equation (4.172) into equation (4.170),

$$\phi_{P_z}\Big|_{z=0} = -\alpha_0 e^{at} \qquad (4.173a)$$

Consider the form that ϕ_p must have to satisfy the differential equations (4.170abcd) and to satisfy the left side of equations (4.171a,b). From (4.171a),

$$\vec{C}_{N_\alpha}\alpha(t) + \vec{C}_{N_{\dot\alpha}}\dot\alpha(t) = \frac{4}{S_{REF}}\iint_S \frac{\nabla_s G_s}{|\nabla_s G_s|}\left(\phi_{P_z} + \frac{1}{U}\phi_{P_t}\right)_{z=0^+} dS \qquad (4.173b)$$

when (4.172) is substituted,

$$\left(\vec{C}_{N_\alpha} + a\vec{C}_{N_{\dot\alpha}}\right)\alpha_0 e^{at} = \frac{4}{S_{REF}}\iint_S \frac{\nabla_s G_s}{|\nabla_s G_s|}\left(\phi_{P_z} + \frac{1}{U}\phi_{P_t}\right)_{z=0^+} dS \qquad (4.173c)$$

It is concluded that the time variation of the left side of (4.173c) requires $\phi_p(x, y, z, t)$ to be of the form,

$$\phi_p(x, y, z, t) = \phi^*(x, y, z)e^{at} \qquad (4.174)$$

Equations (4.170) may now be simplified to a time-independent form by substituting equation (4.174) into (4.170). Eliminating the common factors of e^{at} that result,

flow equation: $$\beta^2\phi^*_{xx} - \phi^*_{yy} - \phi^*_{zz} + \frac{2Ma}{a_\infty}\phi^*_x + \frac{a^2}{a_\infty^2}\phi^* = 0 \qquad (4.175a)$$

B.C.:

$$\phi_z^*\Big|_{z=0} = -\alpha_o \qquad \text{on } S \tag{4.175b}$$

$$\left(\phi_x^* + \frac{a}{U}\phi^*\right)_{z=0} = 0 \qquad \text{on } W \tag{4.175c}$$

$$\phi^*\Big|_{z=0} = 0 \qquad \text{on } R \tag{4.175d}$$

force derivatives:

$$\Delta \vec{C}_N(t) = \vec{C}_{N_\alpha}\alpha_o + \vec{C}_{N_{\dot\alpha}}\alpha_o a = \frac{4}{S_{REF}}\iint_S \frac{\nabla_s G_s}{|\nabla_s G_s|}\left(\phi_x^* + \frac{a}{U}\phi^*\right)_{z=0} dS \tag{4.175e}$$

moment derivatives:

$$\Delta \vec{C}_M(t) = \vec{C}_{M_\alpha}\alpha_o + \vec{C}_{M_{\dot\alpha}}\alpha_o a = \sum_{i=1}^{k} \frac{\vec{r}_i}{l_M} \times \Delta \vec{C}_{N_i}(t) \tag{4.175f}$$

Note: Usually C_{Y_α}, C_{ℓ_α}, and C_{n_α} are zero.

$$C_{z_\alpha}\alpha_o + C_{z_{\dot\alpha}}\alpha_o a = \frac{4}{S_{REF}}\iint_S \frac{\partial G_s/\partial z_s}{|\nabla_s G_s|}\left(\phi_x^* + \frac{a}{U}\phi_x^*\right)_{z=0^+} dS \tag{4.176a}$$

$$C_{x_\alpha}\alpha_o + C_{x_{\dot\alpha}}\alpha_o a = \frac{4}{S_{REF}}\iint_S \frac{\partial G_s/\partial x_s}{|\nabla_s G_s|}\left(\phi_x^* + \frac{a}{U}\phi^*\right)_{z=0^+} dS \tag{4.176b}$$

Moment derivatives follow from (4.175f).

Redefining equation (4.175) in terms of reduced frequency, $k = \frac{a\ell}{U_\infty}$,

flow equation: $$\beta^2\phi_{xx}^* - \phi_{yy}^* - \phi_{zz}^* + \frac{2M^2K}{\ell}\phi_x^* + \frac{k^2M^2}{\ell^2}\phi^* = 0 \tag{4.177a}$$

B.C.:

$$\phi_z^*\Big|_{z=0} = -\alpha_o \qquad \text{on } S \tag{4.177b}$$

$$\left(\phi_x^* + \frac{kM}{\ell}\phi^*\right)_{z=0} = 0 \qquad \text{on } W \tag{4.177c}$$

$$\phi^*\Big|_{z=0} = 0 \qquad \text{on } R \tag{4.177d}$$

Consider the perturbation normal force equation (4.176a)

$$C_{z_\alpha}\alpha_o + C_{z_{\dot\alpha}}\dot\alpha_o\,\frac{kU_\infty}{\ell} = \frac{4}{S_{REF}}\iint_S \frac{\partial G_s/\partial z_s}{|\nabla_s G_s|}\left(\phi_x^* + \frac{kM}{\ell}\phi^*\right)_{z=0^+} dS$$

From the form of equations (4.177), the evaluation of ϕ^* is by a series expansion of ϕ^* in terms of reduced frequency k (ref. 31). Following the notation of Miles (ref. 28)

$$\phi^* = \phi^{(0)} + k\phi^{(1)} + k^2\phi^{(2)} + k^3\phi^{(3)} + \cdots \tag{4.178}$$

Substituting equation (4.178) into equations (4.177) and collecting like order terms in k,

flow equation:

$$\left[\beta^2\phi^{(0)}_{xx} - \phi^{(0)}_{yy} - \phi^{(0)}_{zz}\right] + k\left[\beta^2\phi^{(1)}_{xx} - \phi^{(1)}_{yy} - \phi^{(1)}_{zz} + \frac{2M^2}{\ell}\phi^{(0)}_x\right] + k^2\left[\beta^2\phi^{(2)}_{xx} - \phi^{(2)}_{yy} - \phi^{(2)}_{zz} + \frac{2M^2}{\ell}\phi^{(1)}_x + \frac{M^2}{\ell^2}\phi^{(0)}\right] + k^3\left[\quad\right] + \cdots = 0 \tag{4.179a}$$

B.C.: $$\phi^{(0)}_z\Big|_{z=0} + k\phi^{(1)}_z\Big|_{z=0} + k^2\phi^{(2)}_z\Big|_{z=0} + \cdots = -\alpha_0 \qquad \text{on } S \tag{4.179b}$$

$$\phi^{(0)}_x\Big|_{z=0} + k\left(\phi^{(1)}_x + \frac{M}{\ell}\phi^{(0)}\right)\Big|_{z=0} + \cdots = 0 \qquad \text{on } W \tag{4.179c}$$

$$\phi^{(0)}\Big|_{z=0} + k\phi^{(1)}\Big|_{z=0} + \cdots = 0 \qquad \text{on } R \tag{4.179d}$$

normal force:

$$C_{z_\alpha} + \frac{kU_\infty}{\ell}C_{z_{\dot\alpha}} = \frac{4}{\alpha_0 S_{REF}}\iint_S \frac{\partial G_s/\partial z_s}{|\nabla_s G_s|}\chi\left[\phi^{(0)}_x\Big|_{z=0} + k\left(\phi^{(1)}_x + \frac{M}{\ell}\phi^{(0)}\right)\Big|_{z=0} + \cdots\right]dS \tag{4.179e}$$

It is known from the properties of series solution of partial differential equations (ref. 41) that if ϕ^* is a solution of (4.173) and (4.175), then each term in the series for ϕ^* must satisfy (4.173) and (4.175). Since k is a small number less than unity, the series will converge, provided $\phi^{(i)}$ remains finite. This implies that (4.177) can be split into a number of differential equation sets that can be solved in a step-by-step process. Terms of k^0 are first separated and solved for $\phi^{(0)}$, then k^1 terms separated is $\phi^{(1)}$ and solved in terms of $\phi^{(0)}$, etc.

For zero order terms in k (k^0):

flow equation: $$\beta^2 \phi^{(0)}_{xx} - \phi^{(0)}_{yy} - \phi^{(0)}_{zz} = 0 \qquad (4.180a)$$

B.C.: $$\phi^{(0)}_z\Big|_{z=0} = -\alpha_0 \qquad \text{on } S \qquad (4.180b)$$

$$\phi^{(0)}_x\Big|_{z=0} = 0 \qquad \text{on } W \qquad (4.180c)$$

$$\phi^{(0)}\Big|_{z=0} = 0 \qquad \text{on } R \qquad (4.180d)$$

normal force: $$C_{z_\alpha} = \frac{4}{\alpha_0 S_{REF.}} \iint_S \frac{\partial G / \partial z_s}{|\nabla_s G|} \left(\phi^{(0)}_x\right)_{z=0^+} dS \qquad (4.180e)$$

A comparison of equations (4.180) with equations (4.112) indicates they are similar in form and the computer programs developed for equations (4.112) can now be used to evaluate $\phi^{(0)}$ and, thus, C_{z_α}.

Given a solution, $\phi^{(0)}$, of equations (4.180), the next order term in k, $\phi^{(1)}$, can be evaluated from the first order terms of k in equation (4.177).

flow equation: $$\beta^2 \phi^{(1)}_{xx} - \phi^{(1)}_{yy} - \phi^{(1)}_{zz} + \frac{2M^2}{l} \dot{\phi}^{(0)}_x = 0 \qquad (4.181a)$$

B.C.: $$\phi^{(1)}_z\Big|_{z=0} = 0 \qquad \text{on } S \qquad (4.181b)$$

$$\left(\phi^{(1)}_x + \frac{M}{l}\phi^{(0)}\right)_{z=0} = 0 \qquad \text{on } W \qquad (4.181c)$$

$$\phi\Big|_{z=0} = 0 \qquad \text{on } R \qquad (4.181d)$$

normal force: $$C_{z_{\dot\alpha}} = \frac{4}{S_{REF}\frac{\alpha_0 l}{U_\infty}} \iint_S \frac{\partial G / \partial z_s}{|\nabla_s G|} \left(\phi^{(1)}_x + \frac{M}{l}\phi^{(0)}\right)_{z=0^+} dS \qquad (4.181e)$$

No computer program exists at the present time to numerically solve the differential equations in (4.181). However, a literature search indicated the equations are common in the field of engineering and both Miles (ref. 28) and Tekhonov and Samarskii (ref. 65) have formulated a solution.

The calculation of C_{X_α} and $C_{X_{\dot{\alpha}}}$ follows (4.180e) and (4.181e) when $\frac{\partial G_S}{\partial z_S}$ is replaced by $\frac{\partial G_S}{\partial x_S}$ by an expansion technique similar to that used to arrive at equations (4.180) and (4.181). Note that the effects of leading edge suction have not been evaluated in this analysis. The evaluation of C_{m_α} and $C_{m_{\dot{\alpha}}}$ proceeds directly from (4.175) once the C_X, C_y, and C_Z force derivatives are known.

For example, to determine C_{m_α} with the aid of computer program TA 67A, it is necessary to compute the pitching moment coefficient from:

$$C_m = C_L \frac{x_{c.p.} - x_{REF}}{\bar{c}} \tag{4.182}$$

By evaluating C_m in this manner at two angles of attack, the derivative C_{m_α} is found from:

$$C_{m_\alpha} = \frac{C_{m_1} - C_{m_2}}{\alpha_1 - \alpha_2} \tag{4.183}$$

where the meaning of the quantities C_{m_i} and α_i are illustrated in fig. 9

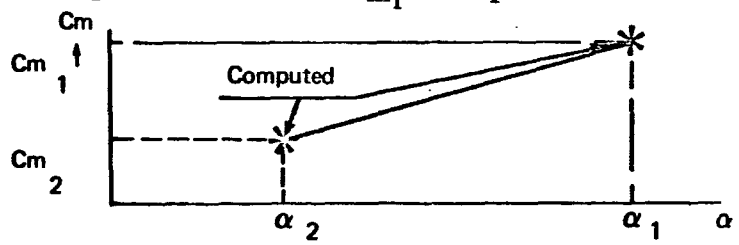

FIGURE 9.–EXAMPLE OF $C_{M\alpha}$ CALCULATION FROM PROGRAM TA 67A

4.4.1.3 The q(t) stability derivatives: The q(t) derivatives can be evaluated from equations (4.29) and (4.88) by setting all small-disturbance c.g. motion and elastic motions, other than q(t), equal to zero. The boundary condition on G(x,y,z,t) = 0 becomes

$$\left[\vec{\omega} \times \left(\vec{r}_i + \vec{r}_{e_i}\right) - U_\infty \left(\vec{i} + \Delta\phi\right)\right] \cdot \nabla G \qquad \text{on } G = 0 \tag{4.184}$$

Evaluating the terms of (4.184):

$$\vec{\omega} \times \left(\vec{r}_i + \vec{r}_{e_i}\right) = \vec{\omega} \times \vec{r}_i = \left(qz_i' - ry_i'\right)\hat{i}_s + \left(rx_i' - pz_i'\right)\hat{j}_s + \left(py_i' - qx_i'\right)\hat{k}_s$$

(4.185a)

$$\nabla G = \left(\frac{\partial \vec{r}_s}{\partial r}\right)^T \nabla_s G_s$$

$$= \Big[f_{x_s} \cos\Theta \cos\Psi + f_{y_s} \left(\sin\phi \sin\Theta \cos\Psi - \cos\phi \sin\Psi\right) :$$

$$- \left(\cos\phi \sin\Theta \cos\Psi + \sin\phi \sin\Psi\right) \Big] \hat{i}$$

$$+ \Big[- f_{x_s} \cos\Theta \sin\Psi - f_{y_s} \left(\sin\phi \sin\Theta \sin\Psi + \cos\phi \cos\Psi\right)$$

$$+ \left(\cos\phi \sin\Theta \sin\Psi - \sin\phi \cos\Psi\right) \Big] \hat{j}$$

$$+ \Big[- f_{x_s} \sin\Theta + f_{y_s} \sin\phi \cos\Theta - \cos\phi \cos\Theta \Big] \hat{k} \qquad (4.185b)$$

By definition,

$$\Psi(t) = \int_0^t \left(q \sin\phi(t) + f^0 \cos\phi(t) \right) \sec\Theta(t)\, dt \doteq 0$$

$$\phi(t) = \int_0^t \left(p^0(t) + q(t) \sin\phi(t) \tan\Theta(t) + f^0 \cos\phi(t) \tan\Theta(t) \right) dt \doteq 0 \qquad (4.185c)$$

$$\Theta(t) = \int_0^t \left(q \cos\phi(t) - f^0 \sin\phi(t) \right) dt \doteq \int_0^t q\, dt$$

Substituting (4.185) into (4.184) and performing the indicated vector operation gives the exact boundary condition on the surface G = 0. After simplification the boundary condition for q(t) c.g. motion becomes

$$- \frac{q x_i'}{U_\infty} - f_{x_s} \cos\Theta(t) - \sin\Theta(t) \left(1 + \phi_x\right) + f_{y_s} \phi_y$$

$$+ \phi_z \left(f_{x_s} \sin\Theta(t) + 1 \right) = 0 \quad \text{on } G = 0 \qquad (4.186a)$$

$$- \left(f_{x_s} - \Theta(t) \right) \left(1 + \phi_x\right) + \phi_y f_{y_s} + \phi_z \left(f_{x_s} \Theta(t) + 1 \right) - \frac{q x_i'}{U_\infty} = 0$$

$$\text{where} \quad \Theta(t) = \int_0^t q\, dt \quad \text{on } G = 0 \qquad (4.186b)$$

After an order-of-magnitude analysis and a Maclaurin series expansion about the plane z = 0, the boundary condition becomes

$$\phi_z \Big|_{z=0} = + f_{x_s} - \Theta + \frac{q x_i'}{U_\infty} \qquad (4.187)$$

where $+f_{x_S}$ is the boundary condition associated with the reference flight orientation

$\frac{qx_j'}{U_\infty}$ is the boundary condition associated with the q(t) small-disturbance velocity potential

$\theta(t)=\int_0^t q\,dt$ is the boundary condition associated with the rotation of the stability axis system due to q(t)

By definition the quantity θ(t) is made zero when evaluating q(t) derivatives

The partial differential equations describing the perturbation velocity potential associated with q(t) motion are written,

flow equation:

$$\beta^2\phi_{p_{xx}}-\phi_{p_{yy}}-\phi_{p_{zz}}+\frac{2M}{a_\infty}\phi_{p_{xt}}+\frac{1}{a_\infty^2}\phi_{p_{tt}}=0 \qquad (4.188a)$$

B.C.:

$$\phi_{p_z}\Big|_{z=0}=\frac{q\,x_i'}{U_\infty} \qquad \text{on } S \qquad (4.188b)$$

$$\left(\phi_{p_z}+\frac{1}{U}\phi_{p_t}\right)_{z=0^+}=0 \qquad \text{on } W \qquad (4.188c)$$

$$\phi_p\Big|_{z=0}=0 \qquad \text{on } R \qquad (4.188d)$$

force derivatives:

$$\Delta\vec{C}_N(t)=\vec{C}_{N_q}q(t)+\vec{C}_{N_{\dot q}}\dot q(t)=\frac{4}{S_{REF}}\iint_S\frac{\nabla_s G_s}{|\nabla_s G_s|}\left(\phi_{p_z}+\frac{1}{U}\phi_{p_t}\right)_{z=0^+}dS \qquad (4.188e)$$

moment derivatives:

$$\Delta C_M(t)=\vec{C}_{M_q}q(t)+\vec{C}_{M_{\dot q}}\dot q(t)=\sum_{i=1}^{k}\frac{\vec{r}_i}{l_M}\times\Delta\vec{C}_{N_i}(t) \qquad (4.188f)$$

The solution of equations (4.188) for q(t) and $\dot q$(t) derivatives proceeds via the frequency expansion and aerodynamic influence coefficient techniques of par. 4.4.1.3.

4.4.1.4 The p(t) stability derivatives: The stability derivatives associated with a steady roll rate, p(t), are evaluated from equations (4.29) and (4.88) with all motion variables other than p(t) set equal to zero. The boundary condition on the surface G = 0 is

$$\left[\vec{\omega}\times(\vec{r}_{o_i}\times\vec{r}_i)-u_\infty(\vec{i}+\nabla\phi)\right]\cdot\nabla G=0 \qquad \text{on } G=0 \qquad (4.189a)$$

Performing the indicated operations;

$$\nabla G = f_{x_s}\,\hat{i} - \left(f_{y_s} + \sin\theta(t)\right)\hat{j} + \left(f_{y_s}\sin\phi(t) - 1\right)\hat{k} \qquad (4.189b)$$

where by definition of small disturbances,

$$\psi(t) = \int_0^t \left(\cancel{q}^{\,0}\sin\theta(t) + \cancel{r}^{\,0}\cos\theta(t)\sec\theta(t)\right)dt = 0 \qquad (4.189c)$$

$$\phi(t) = \int_0^t \left(p(t) + \cancel{q}^{\,0}(t)\sin\phi(t)\tan\theta(t) + \cancel{r}^{\,0}\cos\phi(t)\tan\theta(t)\right)dt = \int_0^t p\,dt \qquad (4.189d)$$

$$\theta(t) = \int_0^t \left(\cancel{q}^{\,0}\cos\phi(t) - \cancel{r}^{\,0}\sin\phi(t)\right)dt = 0 \qquad (4.189e)$$

Substituting the results of equations (4.189c), (4.189d), and (4.189e) into equation (4.189c) and performing the indicated vector operations results in the exact, small-disturbance boundary condition on G = 0.

$$\frac{py_i'}{U_\infty} - f_{x_s}\left(1 + \phi_x\right) + \phi_y\left(f_{y_s} + \sin\phi(t)\right) - \phi_z\left(f_{y_s}\sin\phi(t) - 1\right) = 0 \quad \text{on } G=0 \qquad (4.190)$$

Apply the small angle approximation for ϕ,

$$-f_{x_s}\left(1 + \phi_x\right) + \left(f_{y_s} + \phi\right)\phi_y - \left(f_{y_s}\phi - 1\right)\phi_z + \frac{py_i}{U_\infty} = 0 \quad \text{on } G=0 \qquad (4.191)$$

The boundary condition on the region S is developed by an order-of-magnitude argument and Maclaurin series expansion of equation (4.191).

$$\phi_z\Big|_{z=0} = f_{x_s} - \frac{py_i'}{U_\infty} \quad \text{on } S \qquad (4.192)$$

where $+f_{x_s}$ is the boundary condition associated with the reference flight orientation

$\frac{-py_i'}{U_\infty}$ is the boundary condition associated with the p(t) small disturbance velocity

Finally, the partial differential equations describing the velocity potential associated with p(t) small-disturbance c.g. motion are written,

flow equation:

$$\beta^2 \phi_{p_{xx}} - \phi_{p_{yy}} - \phi_{p_{zz}} + \frac{2M}{a_\infty} \phi_{p_{xt}} + \frac{1}{a_\infty^2} \phi_{p_{tt}} = 0 \qquad (4.193a)$$

B.C.:

$$\phi_{p_z}\Big|_{z=0} = -\frac{py_i'}{U_\infty} \qquad \text{on } S \qquad (4.193b)$$

$$\left(\phi_{p_z} + \frac{1}{U} \phi_{p_t}\right)_{z=0} = 0 \qquad \text{on } W \qquad (4.193c)$$

$$\phi_p\Big|_{z=0} = 0 \qquad \text{on } R \qquad (4.193d)$$

force derivatives: (4.193e)

$$\Delta \vec{C}_N(t) = \vec{C}_{N_p} p(t) + \vec{C}_{N_{\dot{p}}} \dot{p}(t) = \frac{4}{S_{REF}} \iint_S \frac{\nabla_3 G_s}{|\nabla_3 G_s|} \left(\phi_{p_x} + \frac{1}{U} \phi_{p_t}\right)_{z=0'}$$

moment derivatives: $$\Delta \vec{C}_M(t) = \vec{C}_{M_p} p(t) + \vec{C}_{M_{\dot{p}}} \dot{p}(t) = \sum_{i=1}^{K} \frac{\vec{r}_i}{\ell_M} \times \Delta \vec{C}_{N_i}(t) \qquad (4.193f)$$

Solution of equations (4.193e, f) for the p(t) and $\dot{p}$(t) small-disturbance stability derivatives is again by the frequency expansion and aerodynamic influence coefficient techniques of par. 4.4.1.3.

4.4.1.5 The u(t) derivatives: The stability derivatives associated with a change in forward velocity can be calculated by finite differencing the lifting surface program denoted as TA 67A. For instance, the speed derivative C_{m_u} can be determined from the following equation:

$$C_{m_u} = \frac{C_m(\text{at } M = M_1 + \Delta M) - C_m(\text{at } M = M_1 - \Delta M)}{2\,\Delta M} \qquad (4.194)$$

where M_1 is the steady state Mach number at which C_{m_u} is to be found $\Delta M = 0.02$.

4.4.1.6 The equivalent elastic stability derivatives: An equivalent elastic airplane is a descriptive term used when the dynamic properties of the structure viewed as separate degrees of freedom are neglected. In other words, for an equivalent elastic airplane, it is assumed that aerodynamic loads and structural deflections are always in phase with the airplane motion. It turns out that the aerodynamic forces on an equivalent elastic airplane can be expanded in terms of equivalent elastic stability derivatives. (S7)

In formulating aerodynamic forces in terms of motion variables using the derivative concept, app. A showed that a distinction must be made between steady-state and perturbed-state formulations. Even though the aerodynamic-derivative concept is valid only for the perturbed state, it has been used with success in solving steady-state problems. Appendix A also showed that for a rigid airplane, the major difference between perturbed- and steady-state formulations is the occurrence of C_{L_o}, C_{m_o}, and C_{D_o} in the case of steady-state aerodynamic-force expansions. The remaining parts of this section will show how aerodynamic derivatives can be made for perturbed and steady-state flight.

Equivalent elastic derivatives for the perturbed state: It was already explained in app. A that the dynamic analysis of the elastic airplane simplifies to six degrees of freedom. Because of this, it seems reasonable to expect that the stability derivatives of the equivalent elastic airplane (table 2) will be similar in form to those of the rigid airplane. That this is not quite the case is the consequence of the fact that there are two types of loads acting on an elastic airplane: aerodynamic and inertial (including gravitational). The inertial loads cause the deflections of the structure that induce changes in aerodynamic loading. The aerodynamic loading itself does the same thing. In general, airplane derivatives represent the change in aerodynamic loading due to changes in the motion variables. In Formulation I the stability derivatives are split into two categories: those due to aeroelastic effects in the absence of inertial forces (called zero-mass derivatives) and those due to aeroelastic effects caused solely by inertial forces (called inertial derivatives). The following inertial effects must be accounted for: linear and angular accelerations, as well as changes of airplane orientation with respect to the earth's gravitational field. Consider, for example, the longitudinal derivatives.

TABLE 2. – EQUIVALENT ELASTIC AIRPLANE STABILITY DERIVATIVES

$$F_{A_{X_S}} = -\Big\{ \underbrace{C_{D_{\alpha_E}}\alpha + C_{D_{\dot{\alpha}_E}}\frac{\dot{\alpha}\bar{c}}{2V_c} + C_{D_{u_E}}\frac{u}{V_c} + C_{D_{q_E}}\frac{q\bar{c}}{2V_c}}_{\text{zero mass derivatives}} \text{ (negligible, negligible)} + \underbrace{C_{D_{\dot{w}_I}}\dot{w} + C_{D_{q_I}}q + C_{D_{\theta_I}}\theta + C_{D_{\ddot{\theta}_I}}\ddot{\theta}}_{\text{negligible inertial derivatives}} \Big\} \bar{q} S_w$$

$$F_{A_{Y_S}} = \Big\{ \underbrace{C_{Y_{\beta_E}}\beta + C_{Y_{p_E}}\frac{pb}{2V_c} + C_{Y_{r_E}}\frac{rb}{2V_c}}_{\text{zero mass derivatives}} + \underbrace{C_{Y_{\phi_I}}\phi + C_{Y_{\ddot{y}_I}}\ddot{y} + \boxed{C_{Y_{\dot{p}_I}}\dot{p} + C_{Y_{\dot{r}_I}}\dot{r}}}_{\text{inertial derivatives}} \Big\} \bar{q} S_w$$

$$F_{A_{Z_S}} = -\Big\{ \underbrace{C_{L_{\alpha_E}}\alpha + C_{L_{\dot{\alpha}_E}}\frac{\dot{\alpha}\bar{c}}{2V_c} + C_{L_{u_E}}\frac{u}{V_c} + C_{L_{q_E}}\frac{q\bar{c}}{2V_c}}_{\text{zero mass derivatives}} + \underbrace{C_{L_{\dot{w}_I}}\dot{w} + C_{L_{q_I}}q + C_{L_{\theta_I}}\theta + \boxed{C_{L_{\ddot{\theta}_I}}\ddot{\theta}}}_{\text{inertial derivatives}} \Big\} \bar{q} S_w$$

$$m_{A_{X_S}} = \Big\{ \underbrace{C_{l_{\beta_E}}\beta + C_{l_{p_E}}\frac{pb}{2V_c} + C_{l_{r_E}}\frac{rb}{2V_c}}_{\text{zero mass derivatives}} + \underbrace{C_{l_{\phi_I}}\phi + C_{l_{\ddot{y}_I}}\ddot{y} + C_{l_{\dot{p}_I}}\dot{p} + C_{l_{\dot{r}_I}}\dot{r}}_{\text{inertial derivatives}} \Big\} \bar{q} S_w b$$

$$m_{A_{Y_S}} = \Big\{ \underbrace{C_{m_{\alpha_E}}\alpha + C_{m_{\dot{\alpha}_E}}\frac{\dot{\alpha}\bar{c}}{2V_c} + C_{m_{u_E}}\frac{u}{V_c} + C_{m_{q_E}}\frac{q\bar{c}}{2V_c}}_{\text{zero mass derivatives}} + \underbrace{C_{m_{\dot{w}_I}}\dot{w} + C_{m_{q_I}}q + C_{m_{\theta_I}}\theta + C_{m_{\ddot{\theta}_I}}\ddot{\theta}}_{\text{inertial derivatives}} \Big\} \bar{q} S_w \bar{c}$$

$$m_{A_{Z_S}} = \Big\{ \underbrace{C_{n_{\beta_E}}\beta + C_{n_{p_E}}\frac{pb}{2V_c} + C_{n_{r_E}}\frac{rb}{2V_c}}_{\text{zero mass derivatives}} + \underbrace{C_{n_{\phi_I}}\phi + C_{n_{\ddot{y}_I}}\ddot{y} + C_{n_{\dot{p}_I}}\dot{p} + C_{n_{\dot{r}_I}}\dot{r}}_{\text{inertial derivatives}} \Big\} \bar{q} S_w b$$

In addition to the regular stability derivatives due to α, u, q, and $\dot{\alpha}$ aerodynamic effects shown in table 2, there appear inertial derivatives due to $\left.\begin{matrix}\dot{u}\\ \dot{w}\end{matrix}\right\}$ linear acceleration, $\left.\begin{matrix}q\\ \end{matrix}\right\}$ centrifugal acceleration, $\left.\begin{matrix}\dot{q}\\ \end{matrix}\right\}$ angular acceleration, and $\left.\begin{matrix}\theta\\ \end{matrix}\right\}$ gravity perturbation. Except for $\dot{u}$ all inertial perturbations are accounted for in Formulation I of table 3. Forward accelerations ($\dot{u}$) are assumed to be negligible.

Observe that the equations of table 2 contain derivatives marked "zero mass" and derivatives marked "inertial." They physical significance of this is that zero-mass derivatives are independent of the mass distribution of the equivalent elastic airplane. However, the inertial derivatives are very much dependent on the mass distribution of the equivalent elastic airplane. Observe that the inertial derivatives as used here have no relation to unsteady flow phenomena. The inertial derivatives simply occur because of elastic distortions of the airplane caused by inertial forces.

The boxed terms in table 2 are responsible for changes in the perturbed equations of motion of the rigid airplane as presented in app. A. All nonboxed derivatives of table 2 already have a "home" in these equations. For example, the derivative $C_{m_{\ddot{\theta}}}$ can be pulled together with I_{yy_1} to form:

$$\left\{ I_{yy_1} - C_{m_{\ddot{\theta}_1}} \bar{q} S_w \bar{c} \right\} \ddot{\theta}$$

Similarly, because of the identity

$$\dot{w} = \dot{\alpha} V_e$$

it is possible to combine $\dot{w}$ inertial derivatives with the $\dot{\alpha}$ acceleration (unsteady aerodynamic) derivatives.

There exists another way of accounting for inertial effects in the study of equivalent elastic airplane dynamics. This is the way identified as Formulation II in table 3. It represents what has been the standard method of accounting for inertial effects, or as it is frequently called, inertial relief. In this method, longitudinal linear acceleration terms are combined in so-called load-factor derivatives $\frac{\partial C_n}{\partial n}$ and $\frac{\partial C_m}{\partial n}$.

TABLE 3. – UNCOUPLED SMALL PERTURBATION EQUATIONS OF MOTION FOR AN EQUIVALENT ELASTIC AIRPLANE

Formulation 1

$$M\dot{u} + MQ_1 w + (Mg\cos\theta_1 + C_{p_{\theta_1}}^{\approx 0}\bar{q}S_w)\theta$$
$$+\left\{C_{DU_E}\frac{u}{V_{c_1}} + (C_{D_{\alpha_E}} - C_{L_1})\alpha + (C_{p_{\dot{\alpha}_E}}^{\approx 0} + C_{p_{\dot{w}_I}}^{\approx 0}\frac{2V_{c_1}^2}{\bar{c}})\frac{\dot{\alpha}\bar{c}}{2V_c}\right\}qS_w$$
$$+\left\{(C_{p_{q_E}}^{\approx 0} + C_{p_{q_I}}^{\approx 0}\frac{2V_{c_1}}{\bar{c}})\frac{q\bar{c}}{2V_{c_1}} + C_{p_{\ddot{\theta}_I}}^{\approx 0}\ddot{\theta}\right\}\bar{q}S_w = 0$$

$$(M + C_{L_{\dot{w}_I}}\bar{q}S_w)\dot{w} - M(Q_1 u + U_1 q)$$
$$+(Mg\sin\theta_1 + C_{L_{\theta_1}}\bar{q}S_w)\theta + (C_{L_{U_E}}\frac{u}{V_{c_1}})\bar{q}S_w$$
$$+\left\{C_{L_{\alpha_E}}\alpha + (C_{L_{\dot{\alpha}_E}} + C_{L_{\dot{w}_I}}\frac{2V_{c_1}^2}{\bar{c}})\frac{\dot{\alpha}\bar{c}}{2V_{c_1}}\right\}\bar{q}S_w$$
$$+\left\{(C_{L_{q_E}} + C_{L_{q_I}}\frac{2V_{c_1}}{\bar{c}})\frac{q\bar{c}}{2V_{c_1}} + \boxed{C_{L_{\ddot{\theta}_I}}\ddot{\theta}}\right\}\bar{q}S_w = 0$$

$$\left\{I_{yy_1} - C_{m_{\ddot{\theta}_I}}\bar{q}S_w\bar{c}\right\}\dot{q} - \left\{C_{m_{U_E}}\frac{u}{V_{c_1}} + C_{m_{\alpha_E}}\alpha\right.$$
$$\left.+(C_{m_{\dot{\alpha}_E}} + C_{m_{\dot{w}_I}}\frac{2V_{c_1}^2}{\bar{c}})\frac{\dot{\alpha}\bar{c}}{2V_{c_1}}\right\}\bar{q}S_w\bar{c}$$
$$+\left\{C_{m_\theta}^{\substack{=0 \text{ for } \theta_1=0 \\ \approx 0 \text{ otherwise}}}\theta\right\}\bar{q}S_w\bar{c} = 0$$

TABLE 3. – UNCOUPLED SMALL PERTURBATION EQUATIONS OF MOTION FOR AN EQUIVALENT ELASTIC AIRPLANE (CONTINUED)

Formulation I (con't)

$$(M - C_{y_{\dot I}}\,\bar q\,S_W)\,\dot v - M(g\,\phi\cos\theta_1 - U_1 r)$$

$$- \left\{ C_{y_{\beta_E}}\beta + C_{y_{\dot\beta_E}}\frac{\dot\beta b}{2V_{c_1}} + C_{y_{p_E}}\frac{pb}{2V_{c_1}} \right\}\bar q\,S_W \qquad \text{(usually neglected)}$$

$$- \left\{ C_{y_{r_E}}\frac{rb}{2V_{c_1}} + \boxed{C_{y_{\dot p_I}}\dot p + C_{y_{\dot r_I}}\dot r} \right\}\bar q\,S_W = 0$$

$$(I_{xz_1} - C_{l_{\dot p_I}}\,\bar q\,S_W b)\,\dot p$$

$$- I_{xz_1} + C_{l_{\dot r_I}}\,\bar q\,S_W b)\,\dot r - I_{xz_1} Q_1 p + (I_{zz_1} - I_{yy_1})\,Q r$$

$$- \left\{ C_{l_{\beta_E}}\beta + C_{l_{\dot\beta_E}}\frac{\dot\beta b}{2V_{c_1}} + C_{l_{p_E}}\frac{pb}{2V_{c_1}} \right\}\bar q\,S_W b \qquad \text{(usually neglected)}$$

$$- \left\{ C_{l_{r_E}}\frac{rb}{2V_{c_1}} + \boxed{C_{l_{\ddot y_I}}\ddot v} \right\}\bar q\,S_W b = 0$$

$$(I_{zz_1} - C_{n_{\dot r_I}}\,\bar q\,S_W b)\,\dot r$$

$$- (I_{xz_1} + C_{n_{\dot p_I}}\,\bar q\,S_W b)\,\dot p + I_{xz_1} Q_1 r + (I_{yy_1} - I_{xx_1})\,Q_1 p$$

$$- \left\{ C_{n_{\beta_E}}\beta + C_{n_{\dot\beta_E}}\frac{\dot\beta b}{2V_{c_1}} + C_{n_{p_E}}\frac{pb}{2V_{c_1}} \right\}\bar q\,S_W b \qquad \text{(usually neglected)}$$

$$- \left\{ C_{n_{r_E}}\frac{rb}{2V_{c_1}} + \boxed{C_{n_{\ddot y_I}}\ddot v} \right\}\bar q\,S_W b = 0$$

TABLE 3. – UNCOUPLED SMALL PERTURBATION EQUATIONS OF MOTION FOR AN EQUIVALENT ELASTIC AIRPLANE (CONCLUDED)

Formulation II

Alternate formulation for appendix A eq. 6.12 and 6.31:

$$M\dot{w} - M(Q_1 u + U_1 q) + Mg(\sin\theta_1)\theta$$

$$+\left\{C_{L_{u_E}} \frac{u}{2V_{c_1}} + C_{L_{\alpha_E}} \alpha + C_{L_{\dot{\alpha}_E}} \frac{\dot{\alpha}\bar{c}}{2V_{c_1}}\right\} \bar{q} S_w$$

$$+\left\{C_{L_{q_E}} \frac{q\bar{c}}{2V_{c_1}} + \boxed{C_{L_{\dot{\theta}_I}} \dot{\theta}}\right\} \bar{q} S_w = 0$$

$$\left\{I_{yy_1} - C_{m_{\dot{\theta}_I}} \bar{q} S_w \bar{c}\right\} \dot{q}$$

$$+\left\{C_{m_{u_E}} \frac{u}{V_{c_1}} + C_{m_{\alpha_E}} \alpha + C_{m_{\dot{\alpha}_E}} \frac{\dot{\alpha}\bar{c}}{2V_{c_1}}\right\} \bar{q} S_w \bar{c}$$

$$+\left\{C_{m_{q_E}} \frac{q\bar{c}}{2V_{c_1}}\right\} \bar{q} S_w \bar{c} = 0$$

NOTES:
1. Stability axes
2. Steady-state wings, level flight ($\Phi_1 = 0$)
3. Control and thrust derivatives omitted
4. For derivation of all equivalent elastic derivatives

It is then possible to write the aerodynamic Z_s-force and Y_s-moment expansion as follows:

$$C_{L_{(PERTURBED)}} = C_{L_{\alpha_{\bar{E}}}} + C_{L_{\dot{\alpha}_{\bar{E}}}} \frac{\dot{\alpha}\bar{c}}{2V_c} + C_{L_{u_{\bar{E}}}} \frac{u}{V_c} + C_{L_{q_{\bar{E}}}} \frac{q\bar{c}}{2V_c} + \frac{\partial C_L}{\partial \eta} \eta_{(PERTURBED)} + C_{L_{\ddot{\theta}_I}} \ddot{\theta} \tag{4.195}$$

$$C_{m_{(PERTURBED)}} = C_{m_{\alpha_{\bar{E}}}} + C_{m_{\dot{\alpha}_{\bar{E}}}} \frac{\dot{\alpha}\bar{c}}{2V_c} + C_{m_{u_{\bar{E}}}} \frac{u}{V_c} + C_{m_{q_{\bar{E}}}} \frac{q\bar{c}}{2V_c} + \frac{\partial C_m}{\partial \eta} \eta_{(PERTURBED)} + C_{m_{\ddot{\theta}_I}} \ddot{\theta} \tag{4.196}$$

Comparing equation (4.195) with the equations of table 2 shows that the inertial effects of $\dot{w}$, q, and θ have been lumped together in n_p, the perturbation load factor which is defined by:

$$\eta \equiv 1 + \eta_p \equiv \frac{C_{L_1} + C_{L_p}}{C_{L_1}} \equiv 1 + \frac{C_{L_p}}{C_{L_1}} \tag{4.197}$$

where n is the total load factor and $C_{L_1} = C_{L_{trim}}$, the equilibrium (steady-state) lift coefficient. It is not difficult to realize that for perturbations about rectilinear steady-state flight:

$$\frac{C_{L_p}}{C_{L_1}} = \eta_p = -\left(\frac{\dot{W}}{g} - \frac{V_{c_1} q}{g} + \theta \sin \theta_1\right) \tag{4.198}$$

where V_{c_1} = speed along X

θ_1 = steady-state initial attitude

This implies, therefore:

$$C_{L_{\dot{w}_I}} \dot{W} + C_{L_{q_I}} q + C_{L_{\theta_I}} \theta \equiv \frac{\partial C_L}{\partial \eta}\left(\frac{\dot{W}}{g} + \frac{V_{c_1} q}{g} - \theta \sin \theta_1\right) \tag{4.199}$$

so that the following identities must be satisfied:

$$\begin{aligned} C_{L_{\dot{w}_I}} &= -\frac{1}{g}\frac{\partial C_L}{\partial \eta} \\ C_{L_{q_I}} &= \frac{u_1}{g}\frac{\partial C_L}{\partial \eta} \\ C_{L_{\theta_I}} &= -\frac{\partial C_L}{\partial \eta} \sin \theta_1 \end{aligned} \tag{4.200}$$

(Observe that the latter term vanishes for perturbations about steady-state level flight because then: $\theta_1 = 0$.) Similarly, it may be shown that:

$$C_{m_{\dot{w}_1}}\dot{w} + C_{m_{q_1}}q + C_{m_{\theta_1}}\theta \equiv \frac{\partial C_m}{\partial n}\left(\frac{\dot{w}}{g} + \frac{V_{c_1}q}{g} - \theta \sin\theta_1\right) \quad (4.201)$$

from which:

$$C_{m_{\dot{w}_1}} = -\frac{1}{g}\frac{\partial C_m}{\partial n}$$

$$C_{m_{q_1}} = \frac{V_{c_1}}{g}\frac{\partial C_m}{\partial n} \quad (4.202)$$

$$C_{m_{\theta_1}} = -\frac{\partial C_m}{\partial n}\sin\theta_1$$

As will be shown, it is possible to compute $\frac{\partial C_L}{\partial n}$, $\frac{\partial C_m}{\partial n}$, and the inertial derivatives of equations (4.201) and (4.202) individually so that these equations can be used as a cross-check.

Now, by substituting $n_p \frac{C_{L_p}}{C_{L_{trim}}}$ from equation (4.198) in equation (4.195) and solving for C_{L_p} it is found that:

$$C_{L_p} = \frac{1}{1 - \frac{\partial C_L}{\partial n}\frac{1}{C_{L_{TRIM}}}}\left\{C_{L_{\alpha_{\bar{E}}}}\alpha + C_{L_{\dot{\alpha}_{\bar{E}}}}\frac{\dot{\alpha}\bar{c}}{2V_c} + C_{L_{u_{\bar{E}}}}\frac{u}{V_c} + C_{L_{q_{\bar{E}}}}\frac{q\bar{c}}{2V_c} + C_{L_{\ddot{\theta}_{\bar{E}}}}\ddot{\theta}\right\} \quad (4.203)$$

Or upon defining:

$$C_{L_{\alpha_E}} = \frac{C_{L_{\alpha_{\bar{E}}}}}{1 - \frac{\partial C_L}{\partial n}\frac{1}{C_{L_{TRIM}}}} \quad (4.204a)$$

$$C_{L_{\dot{\alpha}_E}} = \frac{C_{L_{\dot{\alpha}_{\bar{E}}}}}{1 - \frac{\partial C_L}{\partial n}\frac{1}{C_{L_{TRIM}}}} \quad (4.204b)$$

$$C_{L_{u_E}} = \frac{C_{L_{u_{\bar{E}}}}}{1 - \frac{\partial C_L}{\partial n}\frac{1}{C_{L_{TRIM}}}} \quad (4.204c)$$

$$C_{L_{q_E}} = \frac{C_{L_{q_{\bar{E}}}}}{1 - \frac{\partial C_L}{\partial n}\frac{1}{C_{L_{TRIM}}}} \quad (4.204d)$$

$$C_{L_{\ddot{\theta}_E}} = \frac{C_{L_{\ddot{\theta}_{\bar{E}}}}}{1 - \frac{\partial C_L}{\partial n}\frac{1}{C_{L_{TRIM}}}} \quad (4.204e)$$

it is possible to write:

$$C_{L_{(PERTURBED)}} = C_{L_{\alpha_E}}\alpha + C_{L_{\dot{\alpha}_E}}\frac{\dot{\alpha}\bar{c}}{2V_c} + C_{L_{u_E}}\frac{u}{V_c} + C_{L_{q_E}}\frac{\bar{q}\bar{c}}{2V_c} + \boxed{C_{L_{\ddot{\theta}_E}}\ddot{\theta}} \quad (4.205)$$

The boxed term, if not negligible, still causes a change in the small perturbation equations of motion as compared with the rigid case, but at least the other terms are quite analogous to those of the rigid case. By now substituting $n_p = \frac{C_{L_p}}{C_{L_{trim}}}$ and equation (4.205) into (4.196) it follows that:

$$C_{m_{(PERTURBED)}} = \left\{ C_{m_{\alpha_{\bar{E}}}} + \frac{\partial C_m}{\partial \eta} \frac{C_{L_{\alpha_{\bar{E}}}}}{C_{L_{TRIM}} - \partial C_L/\partial \eta} \right\} \alpha + \left\{ C_{m_{\dot{\alpha}_{\bar{E}}}} + \frac{\partial C_m}{\partial \eta} \frac{C_{L_{\dot{\alpha}_{\bar{E}}}}}{C_{L_{TRIM}} - \partial C_L/\partial \eta} \right\} \frac{\dot{\alpha}\bar{c}}{2V_c}$$
$$+ \left\{ C_{m_{u_{\bar{E}}}} + \frac{\partial C_m}{\partial \eta} \frac{C_{L_{u_{\bar{E}}}}}{C_{L_{TRIM}} - \partial C_L/\partial \eta} \right\} \frac{u}{V_c} + \left\{ C_{m_{q_{\bar{E}}}} + \frac{\partial C_m}{\partial \eta} \frac{C_{L_{q_{\bar{E}}}}}{C_{L_{TRIM}} - \partial C_L/\partial \eta} \right\} \frac{q\bar{c}}{2V_c} \quad (4.206)$$
$$+ \left\{ C_{m_{\ddot{\theta}_S}} + \frac{\partial C_m}{\partial \eta} \frac{C_{L_{\ddot{\theta}_S}}}{C_{L_{TRIM}} - \partial C_L/\partial \eta} \right\} \ddot{\theta}$$

Or upon defining:

$$C_{m_{\alpha_E}} = C_{m_{\alpha_{\bar{E}}}} + \frac{\partial C_m}{\partial \eta} \frac{C_{L_{\alpha_{\bar{E}}}}}{C_{L_{TRIM}} - \frac{\partial C_L}{\partial \eta}} \quad (4.207a)$$

$$C_{m_{\dot{\alpha}_E}} = C_{m_{\dot{\alpha}_{\bar{E}}}} + \frac{\partial C_m}{\partial \eta} \frac{C_{L_{\dot{\alpha}_{\bar{E}}}}}{C_{L_{TRIM}} - \frac{\partial C_L}{\partial \eta}} \quad (4.207b)$$

$$C_{m_{u_E}} = C_{m_{u_{\bar{E}}}} + \frac{\partial C_m}{\partial \eta} \frac{C_{L_{u_{\bar{E}}}}}{C_{L_{TRIM}} - \frac{\partial C_L}{\partial \eta}} \quad (4.207c)$$

$$C_{m_{q_E}} = C_{m_{q_{\bar{E}}}} + \frac{\partial C_m}{\partial \eta} \frac{C_{L_{q_{\bar{E}}}}}{C_{L_{TRIM}} - \frac{\partial C_L}{\partial \eta}} \quad (4.207d)$$

$$C_{m_{\ddot{\theta}_S}} = C_{m_{\ddot{\theta}_S}} + \frac{\partial C_m}{\partial \eta} \frac{C_{L_{\ddot{\theta}_S}}}{C_{L_{TRIM}} - \frac{\partial C_L}{\partial \eta}} \quad (4.207e)$$

it is possible to write:

$$C_{m_{(PERTURBED)}} = C_{m_{\alpha_E}} \alpha + C_{m_{\dot{\alpha}_E}} \frac{\dot{\alpha}\bar{c}}{2V_c} + C_{m_{u_E}} \frac{u}{V_c} + C_{m_{q_E}} \frac{q\bar{c}}{2V_c} + C_{m_{\ddot{\theta}_E}} \ddot{\theta} \quad (4.208)$$

With this expression it is seen that the rigid and equivalent elastic derivative formulations for pitching moment coefficient are quite similar. The $\ddot{\theta}$ term again can be pulled together with the I_{yy_1} inertia term. Observe, however, that using the concept of derivatives corrected for inertial (load factor) effects does <u>not</u> eliminate the occurrence of inertial θ terms. This fact is not always recognized.

Notice that Formulation I of the third and fifth equations of table 2 is physically completely identical to Formulation II of equations (4.203) and (4.208). The only difference is in the interpretation of the equivalent elastic derivatives. For example, $C_{L_{\alpha\bar{E}}}$ is the lift curve slope of the equivalent elastic but 'zero-mass' airplane. This is the same as saying the $C_{L_{\alpha\bar{E}}}$ is the lift-curve slope at constant load factor. It will be pointed out in Sec. 7 that it is precisely this quantity that is measurable on an elastic wind tunnel model.

On the other hand, $C_{L_{\alpha E}}$ is the lift curve slope of the equivalent elastic airplane for varying load factor.

The results of using equations (4.205) and (4.208) (Formulation II) in the small perturbation equations of motion is indicated also in table 4 by the last two equations.

There has been no reason for developing a Formulation II in the case of lateral-directional stability derivatives. All derivatives of table 4 are called equivalent elastic stability derivatives and are defined in the stability axis system.

<u>Equivalent elastic derivatives for the steady state</u>: For the purpose of steady-state trim calculations, it is again possible to use Formulation I or II, the end result being identical. As a typical example of a steady-state problem, consider the case where for steady-state level flight the trim angle-of-attack α_{trim} and elevator δ_E are desired. This problem can be solved by computing α_{trim} and $\delta_{E_{trim}}$ from:

TABLE 4. – METHODS USED IN DETERMINING EQUIVALENT ELASTIC DERIVATIVES

Equivalent elastic derivatives		Methods				
		Theory			Experiment	
Formulation I ○	Formulation II □	Lifting surface (TA 67A)		Lumped (handbook)	Tunnel (SST only)	Flight test (707-320B)
$C_{L_{\alpha_{\bar{E}}}}$	$C_{L_{\alpha_E}}$	○	□	□	○	□
$C_{m_{\alpha_{\bar{E}}}}$	$C_{m_{\alpha_E}}$	○	□	□	○	□
$C_{D_{\alpha_{\bar{E}}}}$	$C_{D_{\alpha_E}}$		□			
$C_{Lq_{\bar{E}}}$	C_{Lq_E}	○	□	□		
$C_{m_{q_{\bar{E}}}}$	$C_{m_{q_E}}$	○	□	□		
$C_{D_{q_{\bar{E}}}}$	$C_{D_{q_E}}$					
$C_{L_{u_{\bar{E}}}}$	$C_{L_{u_E}}$	○	□		○	
$C_{m_{u_{\bar{E}}}}$	$C_{m_{u_E}}$	○	□		○	
$C_{D_{u_{\bar{E}}}}$	$C_{D_{u_E}}$					
$C_{L_{\dot{\alpha}_{\bar{E}}}}$	$C_{L_{\dot{\alpha}_E}}$			□		
$C_{m_{\dot{\alpha}_{\bar{E}}}}$	$C_{m_{\dot{\alpha}_E}}$			□		
$C_{D_{\dot{\alpha}_{\bar{E}}}}$	$C_{D_{\dot{\alpha}_E}}$					
C_{L_n} $C_{L_{\dot{w}_I}}$						
C_{L_n} $C_{L_{q_I}}$			□			
C_{L_n} $C_{L_{\theta_I}}$						
C_{L_n} $C_{L_{\phi_I}}$						
C_{m_n} $C_{m_{\dot{w}_I}}$						
C_{m_n} $C_{m_{q_I}}$			□			
C_{m_n} $C_{m_{\theta_I}}$						
C_{m_n} $C_{m_{\phi_I}}$						
$C_{L_{\ddot{\theta}_I}}$	$C_{L_{\ddot{\theta}_E}}$	○				
$C_{m_{\ddot{\theta}_I}}$	$C_{m_{\ddot{\theta}_E}}$	○				

zero mass derivatives — varying load factor — inertial derivatives

TABLE 4. – METHODS USED IN DETERMINING EQUIVALENT ELASTIC DERIVATIVES (CONCLUDED)

Equivalent elastic derivatives		Methods			
		Theory		Experiment	
Formulation I ○	Formulation II □	Lifting surface (TA 67A)	Lumped (handbook)	Tunnel (SST only)	Flight test (707-320B)
$C_{\ell_{p_{\bar{E}}}}$	Formulation II has not been used for lateral-directional derivatives	○	○		○
$C_{n_{p_{\bar{E}}}}$			○		
$C_{Y_{p_{\bar{E}}}}$			○		
$C_{\ell_{r_{\bar{E}}}}$			○		
$C_{n_{r_{\bar{E}}}}$			○		○
$C_{Y_{r_{\bar{E}}}}$			○		
$C_{\ell_{\beta_{\bar{E}}}}$			○		○
$C_{n_{\beta_{\bar{E}}}}$			○		○
$C_{Y_{\beta_{\bar{E}}}}$			○		○
$C_{\ell_{\dot{p}_I}}$			○		
$C_{n_{\dot{p}_I}}$			○		
$C_{Y_{\dot{p}_I}}$			○		
$C_{\ell_{\dot{r}_I}}$			○		
$C_{n_{\dot{r}_I}}$			○		
$C_{Y_{\dot{r}_I}}$			○		
$C_{\ell_{\ddot{y}_I}}$			○		
$C_{n_{\ddot{y}_I}}$			○		
$C_{Y_{\ddot{y}_I}}$			○		
$C_{L_{\delta E_{\bar{E}}}}$	$C_{L_{\delta E_E}}$	□		○	○
$C_{m_{\delta E_{\bar{E}}}}$	$C_{m_{\delta E_E}}$	□		○	○

Note: Restrictions and limitations of tables 7, 8, and 9 apply.

$$C_{L_{0_E}} + C_{L_{\alpha_E}}\alpha + C_{L_{\delta E_E}}\delta E = C_{L_{TRIM}}$$
$$C_{m_{0_E}} + C_{m_{\alpha_E}}\alpha + C_{m_{\delta E_E}}\delta E = 0 \qquad (4.209)$$

or from:

$$C_{L_{0_{\bar{E}}}} + C_{L_{\alpha_{\bar{E}}}}\alpha + C_{L_{\delta E_{\bar{E}}}}\delta E + \frac{\partial C_L}{\partial \eta}\Delta\eta = C_{L_{TRIM}}$$
$$C_{m_{0_{\bar{E}}}} + C_{m_{\alpha_{\bar{E}}}}\alpha + C_{m_{\delta E_{\bar{E}}}}\delta E + \frac{\partial C_L}{\partial \eta}\Delta\eta = 0 \qquad (4.210)$$

The defining equations for relating zero-mass derivatives (subscript $\bar{E}$) to derivatives corrected for inertial effects (subscript E) are similar to those of equations (4.204) and (4.207).

Influence coefficient method: The influence coefficient method used in this chapter in calculating equivalent elastic stability derivatives employs two types of influence coefficients:

(1) aerodynamic influence coefficients.

(2) structural influence coefficients.

The aerodynamic theory used to compute aerodynamic influence coefficients was discussed in Par. 4.3.1. Structural influence coefficients used in this study have all been obtained from beam theory, the prime restriction of which was the neglect of camber bending. (S12)

Thin-body lifting surface theory was used to calculate equivalent elastic derivatives. This program solves for elastic equilibrium lift (C_L), drag (C_D), and moment (C_m) coefficients for prescribed steady-state flight conditions. To obtain stability derivatives from C_L, C_D, and C_m data thus obtained, it was necessary to apply the finite difference methods as used for the rigid and completely elastic airplanes and explained in par. 4.3.1. For illustration purposes, it will now be shown how $C_{L_{\alpha E}}$, $\frac{\partial C_L}{\partial n}$, and $C_{m_{u_E}}$ were determined in this manner. Other derivatives were computed in a similar manner.

$C_{L_{\alpha E}}$ - The derivative $C_{L_{\alpha E}}$ was determined from the following equation:

$$C_{L_{\alpha_E}} = \left.\frac{C_L|_{\alpha_{TR}} - C_{L_0}}{\alpha_{TRIM}}\right| \begin{array}{l}\text{elastic airplane}\\ \text{with mass}\end{array} \qquad (4.211)$$

By computing the terms of this equation for the zero-mass case it was possible to find $C_{L_{\alpha_E}}$. The terms of equation (4.211) were computed in the same way that their rigid counterparts were computed.

$\frac{\partial C_L}{\partial n}$ - The load-factor derivative $\frac{\partial C_L}{\partial n}$ was determined from the following equation:

$$\frac{\partial C_L}{\partial \eta} = \frac{C_{L\,(AT\ \alpha_{TRIM}\ WITH\ MASS)} - C_{L\,(AT\ \alpha_{TRIM}\ WITHOUT\ MASS)}}{1.0} \tag{4.212}$$

Both terms in equation (4.212) were determined by computing C_L for $\alpha = \alpha_{trim}$ (elastic airplane) with and without mass.

$C_{m_{u_E}}$ - The speed derivative $C_{m_{u_E}}$ was determined from the following equation:

$$C_{m_{u_E}} = \frac{C_{m\,(AT\ M=M_1+\Delta M)} - C_{m\,(AT\ M=M_1-\Delta M)}}{2\,\Delta M} \tag{4.213}$$

where M_1 is the steady-state Mach number at which $C_{m_{u_E}}$ is to be found and $\Delta M = 0.02$. By recomputing the terms of equation (4.213) for the zero mass, it was possible to find $C_{m_{u_E}}$.

All terms in equation (4.213) were computed at the corresponding trim angles of attack and in a manner identical to that used in par. 4.4.1.1

4.4.2 A 3-D airplane (wing-body interference). — As a consequence of the thin-body assumptions discussed in par. 4.3.1, the inviscid fluid dynamic equations solved by computer program TA 67A can only estimate stability derivatives for a flat airplane. Thus, the coplanar representation of an airplane such as the 707-320B treats the horizontal tail as though it were in the plane of the wing. Also, the airplane's body induced upwash on the wing and its lift carryover must be estimated by an "equivalent" flat-plate representation of the body's thickness.

In order to correct some of the deficiencies of TA 67A several techniques combining thin body, lifting surface theory, and slender-body theory have been developed. One computer mechanization used to estimate noncoplanar and wing-body interference effects, referred to as TA 176 (ref. 35) in this appendix, modifies TA 67A with slender-body results. The surface of the aircraft's body is divided into panels. The function of TA 176 is then to compute the change in the pressure force coefficient at each surface panel due to a unit change in

inclination to the flow at each panel. The AIC's include the effects of a slender body, thin wing, and tail as well as wing-body-tail interference.

This method represents the perturbation of a uniform irrotational flow (due to the presence of the airplane) by line singularities (along an axis of the fuselage) and surface singularities (at inner surfaces of the wing and tail). Body thickness, camber, and incidence are represented by line sources and line doublets on the body axis. The wing- and tail-surface-thickness slopes are represented by surface distributions of sources with linearly varying strengths. The effects of wing and tail surface incidence and camber, as well as body interference on the wing and tail surfaces is represented by vorticity distributions. The vorticity distributions are such that their effect on the wake is included.

Theoretical justification of the general approach is given in ref. 35. TA 176 is Mach-number dependent, but is programmed for both the subsonic and supersonic flow regimes. In this study, computer program TA 176 was used to check only $C_{L_{\alpha}}$ for the 707-320B. No elastic or lateral-directional capability is included in the program at this time.

5. SEMI-EMPIRICAL METHODS FOR CALCULATING STABILITY DERIVATIVES

5.1 Handbook Methods

5.1.1 Rigid aircraft. — Handbook methods represent a combination of theoretical and experimental information on stability derivatives. Examples of the reports written on the subject are refs. 63, 64, and 66 through 71. When the derivatives in question was amenable to such treatment, equations and design charts have been put together. Theories used in these charts are generally applications of the linearized flow equation to simple wings or wing-bodies. These applications give the change in surface aerodynamic characteristics due to geometric properties such as aspect ratio, taper ratio, and sweep angle.

A correlation of theoretical data with wind tunnel results has led to the incorporation of empirical relationships into the design charts. These empirical results, together with the theoretical applications in handbook form, represent the state of the art and are invaluable in preliminary design work. The handbook technique is the only technique presently available that can be used to estimate nonlinear effects in the viscous-fluid dynamic equations.

The USAF Handbook (ref. 6) develops expressions for derivatives based on the principle of superposition, generally of the form:

(total derivative) = (wing-body contribution) + (horizontal-tail contribution) + (vertical-tail contribution) + (interference) (5.1)

Interference effects between the three basic airplane components are accounted for by empirical factors.

Detailed expressions for the derivatives appear in Sec. 7. For this section one example will be given. Consider the expression for C_{L_α}:

$$\underbrace{C_{L_\alpha}}_{(4.5.1.1)} = \underbrace{\underbrace{\left(C_{L_\alpha}\right)'_e}_{(4.1.3.2)} \frac{S'_e}{S'} \underbrace{\left[K'_N + K'_{w(b)} + K'_{b(w)}\right]}_{(4.3.1.2)}}_{\text{Wing-Body Contribution}} + \underbrace{\underbrace{\left(C_{L_\alpha}\right)''_e}_{(4.1.3.2)} \underbrace{\left[K''_{w(b)} + K''_{b(w)}\right]}_{(4.3.1.2)} \underbrace{\left[1 - \frac{\partial \varepsilon}{\partial \alpha}\right]}_{(8.1.1)} \underbrace{\frac{q''}{q_\infty}}_{(9.4.1)} \frac{S''}{S'} \frac{S'_e}{S''}}_{\text{Horizontal Tail Contribution}} \tag{5.2}$$

Numbers refer to sections in ref. 6.

where $(C_{L_\alpha})_e'$ is the lift-curve slope for the wing of appropriate aspect ratio, taper ratio, section profile (camber, thickness), twist distribution, etc.

K_N' is the ratio of aircraft nose lift to aircraft wing lift

$K_{W'(B)}$ is the effect of lift carryover on the wing due to the body

$K_{B'(W)}$ is the effect of lift carryover on the body due to the wing

$(C_{L_\alpha})_e''$ is the lift-curve slope of a tail with the appropriate geometric parameters

$K''_{W(B)}$ is the effect of lift carryover on the tail due to the body

$K''_{B(W)}$ is the effect of lift carryover on the body due to the tail

$\frac{\partial \epsilon}{\partial \alpha}$ is the change in downwash on the tail due to the change in angle of attack of the airplane

$\frac{\bar{q}''}{\bar{q}_\infty}$ is the ratio of dynamic pressure at the tail to freestream dynamic pressure

$\frac{S'}{S_e''}$ is the ratio of wing area to the "effective area" of the tail

$\frac{S_e''}{S''}$ is the ratio of effective tail area to the actual tail area

Equation (5.2) represents the summed knowledge due to personal experience of the handbook authors (ref. 6). It should be emphasized that the approximation of C_{L_α} in equation (5.2) is not unique because of the experience factor involved. Therefore, there is no guarantee that the approximation is correct for all configurations. The accuracy of this technique is a function of the ingenuity, insight, and experience of the engineer performing the analysis.

5.1.2 Equivalent elastic aircraft. — The USAF Handbook (ref. 6) and other similar handbooks do not give a direct method of calculating equivalent elastic stability derivatives. At most, they present an elastic ratio to be evaluated at each individual engineer's discretion.

The superposition of terms, as in equations (5.1) and (5.2), can give reasonable accuracy if the interference terms are properly evaluated. This same superposition technique can be adapted to give equivalent elastic derivatives. It is the purpose of this section to present the superposition technique used to calculate equivalent elastic longitudinal and lateral-directional stability derivatives for the SST and 707-320B airplanes of this study.

The existing handbook techniques do not present a method to evaluate changes in lift-curve slope and aerodynamic-center location due to elastic distortion of the aircraft's surface. The technique to be presented in this section uses the computer methods of par. 4.4.1.6 to calculate the stability derivatives. The use of the methods of par. 4.4.1.6 will offer no new advantage in calculating the longitudinal stability derivatives, but will offer a suitable method for the lateral-directional derivatives. At the present time this is the only theoretical or semi-empirical technique available to calculate equivalent elastic lateral-directional stability derivatives.

5.1.2.1 Longitudinal derivatives: The lift coefficient for the flexible airframe is expressed as:

$$C_{L_A} = C_{L_{O_E}} + a_{T_O}\Big|_{n=0}\alpha + \frac{\partial C_{L_{T_O}}}{\partial n}\, n + \frac{\partial C_{L_{T_O}}}{\partial \frac{q\bar{c}}{2V_c}}\Bigg|_{n=0}\left(\frac{q\bar{c}}{2V_c}\right) + \frac{S_H}{S_W}\, C_{L_H} \qquad (5.3)$$

In a similar manner, define:

$$C_{L_H} = K''_{W(B)}\left(\frac{\bar{q}''}{\bar{q}_\infty}\right)\left[a_H\Big|_{n=0}\alpha + \frac{\partial C_{L_H}}{\partial \delta_E}\delta e + \frac{\partial C_{L_H}}{\partial \frac{q\bar{c}}{2V_c}}\Bigg|_{n=0}\left(\frac{q\bar{c}}{2V_c}\right) + \frac{\partial C_{L_H} n}{\partial n}\right] \qquad (5.4)$$

The tail angle of attack is defined as:

$$\alpha_H = \alpha - \varepsilon + i_H + \Delta\alpha_E + \Delta\alpha_n \qquad (5.5)$$

where

$$\Delta\alpha_E = \bar{K}\, C_{L_H}\, \bar{q}\, S_H \qquad (5.6)$$

is the change in angle of attack of the horizontal tail due to elasticity, and:

$$\Delta\alpha_n = \frac{\partial \alpha_H}{\partial n}\, n \qquad (5.7)$$

is the change in angle of attack of the horizontal tail due to load factor. Also,

$$n = \frac{C_{L_A} \bar{q} S_w}{W} = \frac{C_{L_A}}{C_{L_{TR}}} \tag{5.8}$$

Combining equations (5.3) through (5.8) gives:

$$\begin{aligned} C_{L_A} = {} & C_{L_0} + a_{T0}\Big|_{n=0}\alpha + \frac{\partial C_{L_{T0}}}{\partial n}\frac{C_{L_A}}{C_{L_{TR}}} + \frac{\partial C_{L_{T0}}}{\partial\left(\frac{q\bar{c}}{2V_c}\right)}\Bigg|_{n=0}\left(\frac{q\bar{c}}{2V_c}\right) \\ & + \frac{S_H}{S_w} K\left\{a_H\Big|_{n=0}(\alpha - \varepsilon + i_H) + \frac{\partial C_{L_H}}{\partial \delta E}\delta E + \frac{\partial C_{L_H}}{\partial\left(\frac{q\bar{c}}{2V_c}\right)}\Bigg|_{n=0}\left(\frac{q\bar{c}}{2V_c}\right)\right. \\ & \left. + \frac{C_{L_A}}{C_{L_{TR}}}(a_H)_{n=0}\left(\frac{\partial \alpha_H}{\partial n} + \frac{\partial C_{L_H}}{\partial n}\right)\right\} \end{aligned} \tag{5.9}$$

where $$K = \frac{K''_{\omega(B)}\left(\frac{\bar{q}''}{\bar{q}_\infty}\right)}{1 - \bar{K}\bar{q}\, S_H K''_{\omega(B)}\left(\frac{\bar{q}''}{\bar{q}_\infty}\right) a_H\Big|_{n=0}}$$

Solving equation (5.9) for C_{L_A} gives:

$$\begin{aligned} C_{L_A} = {} & \frac{C_{L_{0_E}} + a_{T0}\Big|_{n=0}\alpha + \frac{\partial C_{L_{T0}}}{\partial\left(\frac{q\bar{c}}{2V_c}\right)}\Bigg|_{n=0}\left(\frac{q\bar{c}}{2V_c}\right) + \frac{S_H}{S_w}K\left[a_H\Big|_{n=0}(\alpha + i_H - \varepsilon)\right]}{\left\{1 - \frac{1}{C_{L_{TR}}}\left[\frac{\partial C_{L_{T0}}}{\partial n} + \frac{S_H}{S_w}K\left(a_H\Big|_{n=0}\frac{\partial \alpha_H}{\partial n} + \frac{\partial C_{L_H}}{\partial n}\right)\right]\right\}} \\ & + \frac{\frac{S_H}{S_w}K\left[+\frac{\partial C_{L_H}}{\partial \delta E}\delta E + \frac{\partial C_{L_H}}{\partial\left(\frac{q\bar{c}}{2V_c}\right)}\Bigg|_{n=0}\left(\frac{q\bar{c}}{2V_c}\right)\right]}{\left\{1 - \frac{1}{C_{L_{TR}}}\left[\frac{\partial C_{L_{T0}}}{\partial n} + \frac{S_H}{S_w}K\left[\left(a_H\Big|_{n=0}\frac{\partial \alpha_H}{\partial n} + \frac{\partial C_{L_H}}{\partial n}\right)\right]\right]\right\}} \end{aligned} \tag{5.10}$$

From equation (5.10) the lift derivatives can be evaluated. Define the lift-curve slope for the airplane as:

$$C_{L_{\alpha_E}} = \frac{\partial C_L}{\partial \alpha}\Big|_r \tag{5.11}$$

Applying (5.11) to (5.10) gives:

$$C_{L_{\alpha_E}} = \frac{a_{T0}\Big|_{A=0} + K\frac{S_H}{S_w}a_H\Big|_{n=0}\left(1 - \frac{d\varepsilon}{d\alpha}\right)}{1 - \frac{1}{C_{L_{TR}}}\left[\frac{\partial C_{L_{T0}}}{\partial n} + K\frac{S_H}{S_w}\left(a_H\Big|_{n=0}\frac{\partial \alpha_H}{\partial n} + \frac{\partial C_{L_H}}{\partial n}\right)\right]} \tag{5.12}$$

For $C_{L_{q_E}}$, take $\dfrac{\partial}{\partial\left(\frac{q\bar{c}}{2V_c}\right)}$ [equation (5.10)]

$$C_{L_{q_E}} = \frac{\left.\frac{\partial C_{L_{TO}}}{\partial\left(\frac{q\bar{c}}{2V_c}\right)}\right|_{n=0} + K\frac{S_N}{S_W}\left.\frac{\partial C_{L_N}}{\partial\left(\frac{q\bar{c}}{2V_c}\right)}\right|_{n=0}}{1-\frac{1}{C_{L_{TR}}}\left[\frac{\partial C_{L_{TO}}}{\partial n} + K\frac{S_N}{S_W}\left(a_N\Big|_{n=0}\frac{\partial \alpha_N}{\partial n} + \frac{\partial C_{L_N}}{\partial n}\right)\right]} \qquad (5.13)$$

Inspection of equations (5.12) and (5.13) shows they may be easily written in finite difference form and applied to matrix-method component values or other data.

In calculating the moment coefficient, it is necessary to identify the aerodynamic center associated with each lift component. However, the lift on the zero-mass airplane and the lift on the airplane with inertial distortions have different centers of action. Generating analytical expressions and then using them for finite difference equations creates problems in the pitching-moment derivatives not encountered in the lift-coefficient derivatives. This approach requires a knowledge of $i_{H_{trim}}$, ϵ, etc. in advance. Treating the problem from the finite difference approach eliminates that requirement. For the tail-off airplane the pitching-moment variation with angle of attack may be written as:

$$C_{m_{\alpha_{T.a_E}}} = C_{m_{\alpha_{T.a.}}}\Big|_{n=0} + C_{m_{n_{T.O.}}}\frac{C_{L_{\alpha_E}}}{C_{L_{TR}}} \qquad (5.14)$$

where:

$$C_{m_{\alpha_{T.a.}}}\Big|_{n=0} = \frac{1}{\alpha_2-\alpha_1}\left[\left(x_{c.g.}-x_{c.p.}\Big|_{\alpha_2}\right)C_L\Big|_{\alpha_2} - \left(x_{c.g.}-x_{c.p.}\Big|_{\alpha_1}\right)C_L\Big|_{\alpha_1}\right]_{T.O.}\Big|_{n=0} \qquad (5.15)$$

$$C_{m_{n_{T.O.}}} = \frac{1}{n\big|_{\alpha_2}}\left[\left(x_{c.g.}-x_{c.p.}\Big|_{n,\alpha_2}\right)C_L\Big|_{n,\alpha_2} - \left(x_{c.g.}-x_{c.p.}\Big|_{n=0,\alpha_2}\right)C_L\Big|_{n=0,\alpha_2}\right]_{T.O.} \qquad (5.16)$$

$$n\big|_{\alpha_2} = \frac{C_{L_{T.a.}}\big|_{\alpha_2}}{C_{L_{T.O.}}\big|_{\alpha_1}} \qquad C_{L_{T.O.}}\Big|_{n=1} = \frac{W_{T.O.}}{\bar{q}\,S_W} \qquad (5.17)$$

The horizontal-tail contribution to $C_{m_{\alpha E}}$ can be obtained using equations (5.4) and (5.5), with appropriate moment arms. Combining the horizontal-tail and tail ff contributions, $C_{m_{\alpha E}}$ is given by:

$$C_{m_{\alpha_E}} = C_{m_{\alpha_{TO}}}\Big|_{n=0} + C_{m_{n_{TO}}} \frac{C_{L_{\alpha_E}}}{C_{L_{TR}}} + K \frac{S_H}{S_W} \left\{ C_{m_{\alpha_H}}\Big|_{n=0} \left(1 - \frac{d\varepsilon}{d\alpha}\right) + \bar{K}\bar{q}\, S_W K C_{m_{\alpha_H}}\Big|_{n=0} \frac{\partial C_{L_H}}{\partial \alpha} + C_{m_{\alpha_H}}\Big|_{n=0} \frac{\partial \alpha_H}{\partial n} \frac{C_{L_{\alpha_E}}}{C_{L_{TR}}} + C_{m_{n_H}} \frac{C_{L_{\alpha_E}}}{C_{L_{TR}}} \right\} \tag{5.18}$$

where, in $\frac{\partial C_{L_H}}{\partial \alpha}$, C_{L_H} is obtained from equations (5.4) and (5.5) and $C_{m_{\alpha H}}|_{n=0}$, $C_{m_{\alpha H}}|_{n=0}$, $C_{m_{n_H}}$, and $n|_{\alpha_p}$ are analogous to equations (5.15), (5.16), and (5.17) with 'T.O.' subscripts replaced by 'H' subscripts.

Using the same finite difference approach and considering the tail-off airplane and equations (5.4) and (5.5) generates the following equation for $C_{M_{q_E}}$:

$$C_{m_{q_E}} = C_{m_{q_{TO}}}\Big|_{n=0} + C_{m_{TO}}\Big|_q \frac{C_{L_{q_E}}}{C_{L_{TR}}} + K \frac{S_H}{S_W} \left\{ C_{m_{n_H}}\Big|_q \frac{C_{L_{q_E}}}{C_{L_{TR}}} + \bar{K}\bar{q}\, S_W K C_{m_{\alpha_H}}\Big|_{n=0} \frac{C_{L_{q_E}}}{C_{L_{TR}}} \left(a_H\Big|_{n=0} \frac{\partial \alpha_H}{\partial n} + \frac{\partial C_{L_H}}{\partial n} \right) + C_{m_{q_H}}\Big|_{n=0} \right\} \tag{5.19}$$

where $C_{m_{q_{T.O.}}}\Big|_{n=0}$, $C_{m_{n_{T.O.}}}\Big|_q$, $n_{TO}|_q$ and $C_{m_{q_H}}\Big|_{n=0}$, $C_{m_{n_H}}\Big|_q$, $n_H|_q$

are defined analogous to the α terms with $\alpha_2 - \alpha_1$ replaced by $\frac{q\bar{c}}{2V_c}$ and α_2 by q in equations (5.15), (5.16), and (5.17).

5.1.2.2 Lateral-directional derivatives: In accordance with ref. 72, the side-force coefficient is assumed to be equal to the sum of the wing-body component and the vertical-tail component:

$$C_Y = C_{Y_{WB}} + C_{Y_V} \tag{5.20}$$

Aeroelastic effects on $C_{y_{WB}}$ will be neglected. In that case, the conventional and side-force definition can be used:

$$C_{Y_{WB}} = C_{Y_{p_{WB}}} \frac{pb}{2V_c} + C_{Y_{r_{WB}}} \frac{rb}{2V_c} + C_{Y_{\beta_{WB}}} \beta \tag{5.21}$$

Extending the superposition principle to allow for aeroelastic effects, and considering the contribution due to the vertical tail:

$$C_{Y_V} = \frac{S_V}{S_W}\frac{\bar{q}_V}{\bar{q}_\infty}\left[a_V\Big|_{\ddot{Y}_V=0}\beta_V - \frac{\partial C_{L_V}}{\partial \ddot{Y}_V}\ddot{Y}_V\right] \tag{5.22}$$

where

$$\beta_V = \left(\beta + \sigma + \bar{K}_\beta C_{Y_V}\bar{q}_\infty S_W + \frac{p z_V}{V_c} - \frac{r l_V}{V_c} + K_{\dot{\beta}}\dot{\beta} + K_{\dot{r}}\dot{r} + K_{\ddot{Y}}\ddot{Y}\right) \tag{5.23}$$

and

$$\ddot{Y}_V = \ddot{Y} + z_V\dot{p} - l_V\dot{r} \tag{5.24}$$

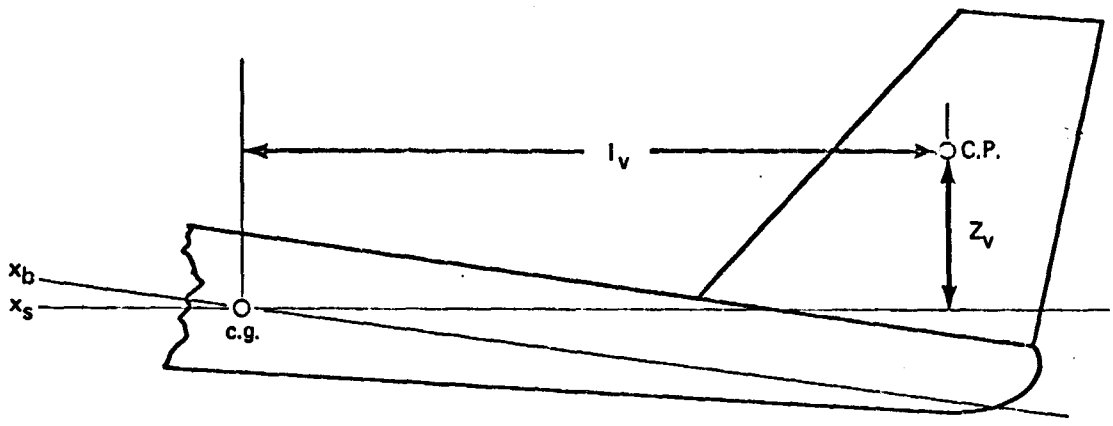

The above sketch defines l_V and Z_V. Combining equations (5.22), (5.23), and (5.24) and solving for C_{Y_V} gives:

$$C_{Y_V} = \frac{1}{1+\bar{K}_\beta S_V \bar{q}_V a_V\Big|_{\ddot{Y}_V=0}}\left[\frac{S_V}{S_W}\frac{\bar{q}_V}{\bar{q}_\infty}\left(-a_V\Big|_{\ddot{Y}_V=0}\right)\left(\beta+\sigma+\frac{pz_V}{V_c}-\frac{rl_V}{V_c}\right.\right.$$
$$\left.\left. + K_{\dot{\beta}}\dot{\beta} + K_{\dot{r}}\dot{r} + K_{\ddot{Y}}\ddot{Y}\right) - \frac{S_V}{S_W}\frac{\bar{q}_V}{\bar{q}_\infty}\frac{\partial a_V}{\partial \ddot{Y}_V}\left(\ddot{Y} + z_V\dot{p} - l_V\dot{r}\right)\right] \tag{5.25}$$

Since C_{y_V} depends on acceleration terms, it is not possible to define conventional partial derivatives. However, it is entirely feasible to define terms that are analogous to derivatives, as will be shown.

The equation for the side-force coefficient of the entire airplane is now:

$$C_Y = \left[C_{Y_{\beta_{WB}}} + K\bar{a}_v\Big|_{\ddot{Y}_v=0}\left(1+\frac{\partial\sigma}{\partial\beta}\right)\right]\beta + \left[C_{Y_{r_{WB}}}\frac{b}{2V_c} + K\frac{z_v}{V_c}\bar{a}_v\Big|_{\ddot{Y}_v=0}\right]p$$
$$+\left[C_{Y_{r_{WB}}}\frac{b}{2V_c} - K\frac{l_v}{V_c}\bar{a}_v\Big|_{\ddot{Y}_v=0}\right]r + \left[K\bar{a}_v\Big|_{\ddot{Y}_v=0}K_{\dot{Y}} + K\frac{\partial C_{L_v}}{\partial\ddot{Y}_v}\right]\ddot{Y} \qquad (5.26)$$
$$+\left[K\bar{a}_v\Big|_{\ddot{Y}_v=0}K_{\dot{p}} + Kz_v\frac{\partial C_{L_v}}{\partial\ddot{Y}_v}\right]\dot{p} + \left[K\bar{a}_v\Big|_{\ddot{Y}_v=0}K_{\dot{r}} - Kl_v\frac{\partial C_{L_v}}{\partial\ddot{Y}}\right]\dot{r}$$

where
$$K = \frac{-\frac{S_v}{S_w}\frac{\bar{q}_v}{\bar{q}_\infty}}{1+K_\beta\bar{q}_v S_v\bar{a}_v\Big|_{\ddot{Y}_v=0}} \quad \text{and} \quad \bar{a}_v\Big|_{\ddot{Y}_v=0} = \left(\frac{L_{v_E}\Big|_{\ddot{Y}_v=0}}{L_{v_R}}\right)a_v\Big|_{\text{USAF HANDBOOK}} \qquad (5.27)$$

Inspection indicates that for a rigid vertical tail, all elastic constants are zero. In that case, only the first three terms of equation (5.26) remain, and the coefficients of β, p, and r are then identical to the conventional and lumped stability derivatives C_{y_β}, C_{y_p} and C_{y_r}.

Now define the following equivalent elastic derivatives:

$$C_{Y_{\beta_E}} = \left[C_{Y_{\beta_{WB}}} + K\bar{a}_v\Big|_{\ddot{Y}_v=0}\left(1+\frac{d\sigma}{d\beta}\right)\right]$$
$$C_{Y_{p_E}} = \left[C_{Y_{p_{WB}}} + K\frac{2z_v}{b}\bar{a}_v\Big|_{\ddot{Y}_v=0}\right] \qquad (5.28)$$
$$C_{Y_{r_E}} = \left[C_{Y_{r_{WB}}} - K\frac{2l_v}{b}\bar{a}_v\Big|_{\ddot{Y}_v=0}\right]$$

The remaining terms in equation (5.26) are defined as inertial derivatives and can be identified as follows:

$$C_{Y_{\ddot{Y}_I}} = K\left[\bar{a}_v\Big|_{\ddot{Y}_v=0}K_{\ddot{Y}} + \frac{\partial C_{L_v}}{\partial\ddot{Y}_v}\right]$$
$$C_{Y_{\dot{p}_I}} = K\left[\bar{a}_v\Big|_{\ddot{Y}_v=0}K_{\dot{p}} + \frac{\partial C_{L_v}}{\partial\ddot{Y}_v}z_v\right] \qquad (5.29)$$
$$C_{Y_{\dot{r}_I}} = K\left[\bar{a}_v\Big|_{\ddot{Y}_v=0}K_{\dot{r}} + \frac{\partial C_{L_v}}{\partial\ddot{Y}_v}l_v\right]$$

Now turn to the rolling-moment coefficient. In accordance with general handbook theory, the rolling-moment coefficient is assumed to be equal to the sum of a wing-body, a vertical-tail, and a horizontal-tail component.

$$C_l = C_{l_{WB}} + C_{l_v} + C_{l_H} \qquad (5.30)$$

First, consider the wing-body contribution. The sideslip contribution $C_{\ell_{\beta_{WB}}}$ is affected by aeroelasticity in two ways: (a) through wing-lift-curve slope (C_{ℓ_β}/C_L) and (b) through wing bending (C_{ℓ_β}/Γ). Whether or not these effects oppose each other depends on the load factor of the airplane. It is assumed $C_{\ell_{\beta_{WB}}}$ can be computed. The roll-damping contribution $C_{\ell_{p_{WB}}}$ is affected by aeroelasticity in two ways: (a) through wing-lift-curve slope (C_{ℓ_p}/C_L) and (b) through the inertial effect induced by roll acceleration $C_{\ell_{\dot{p}}}$.

The yaw-rate contribution $C_{\ell_{r_{WB}}}$ is affected by aeroelasticity primarily through lift-curve slope. It is assumed that an elastic value for $C_{\ell_{r_{WB}}}$ can be computed. So:

$$C_{\ell_{WB}} = C_{\ell_{\beta_{WB_E}}}\beta + C_{\ell_{p_{WB_E}}}\frac{pb}{2V_c} + \left.\frac{\partial C_\ell}{\partial \dot{p}}\right|_{WB}\dot{p} + C_{\ell_{r_{WB_E}}}\frac{rb}{2V_c} \qquad (5.31)$$

Second, consider the contribution due to the vertical tail. Using the same approach as used in the side-force coefficient:

$$C_{\ell_V} = -\frac{S_V}{S_W}\frac{\bar{q}_V}{\bar{q}_\infty}\frac{z_V}{b}\left[\bar{a}_V\Big|_{\ddot{y}=0}\beta_V + \frac{\partial C_{L_V}}{\partial \ddot{y}}\ddot{y}_V\right] \qquad (5.32)$$

where β_V is given by equation (5.23) and $\ddot{y}_V$ is given by equation (5.24).

Finally, consider the contribution of the horizontal tail. This will be restricted to contributions due to C_{ℓ_p} and $C_{\ell_{\dot{p}}}$, although a contribution due to C_{ℓ_β} may be important for very large tails.

$$C_{\ell_H} = C_{\ell_{p_{H_E}}}\frac{pb}{2V_c} + \left.\frac{\partial C_\ell}{\partial \dot{p}}\right|_H\dot{p} \qquad (5.33)$$

When added together, these components give the rolling-moment coefficient for the total airplane as:

$$C_\ell = \left[C_{\ell_{\beta_{WB_E}}} + K\frac{z_V}{\rho}\bar{a}_V\Big|_{\ddot{y}_V=0}\left(1+\frac{d\sigma}{d\beta}\right)\right]\beta \qquad (5.34)$$

$$+\left[C_{\ell_{p_{WB_E}}}\frac{b}{2V_c} + C_{\ell_{p_{H_E}}}\frac{b}{2V_c} + \frac{K_{\ddot{y}_V}}{b}\frac{z_V}{V_c}\bar{a}_V\Big|_{\ddot{y}_V=0}\right]p + \left[C_{\ell_{r_{WB_E}}}\frac{b}{2V_c} - K\frac{z_V}{b}\frac{\ell_V}{b}\bar{a}_V\Big|_{\ddot{y}_V=0}\right]r$$

$$+\left[K\left(\bar{a}_V\Big|_{\ddot{y}_V=0}K\cdot\frac{\partial C_{L_V}}{\partial \ddot{y}_V}z_V\right)\frac{z_V}{b} + \left.\frac{\partial C_\ell}{\partial \dot{p}}\right|_{WB} + \left.\frac{\partial C_\ell}{\partial \dot{p}}\right|_H\right]\dot{p} + \left[K\left(\bar{a}_V\Big|_{\ddot{y}_V=0}K_{i_V} - \frac{\partial C_{L_V}}{\partial \ddot{y}_V}\ell_V\right)\frac{z_V}{b}\right]\dot{r}$$

For a rigid airplane, all elastic constants are zero. In that case, only the first three terms of equation (5.34) remain, and it is again seen that the coefficients of β, p, and r are identical to the conventional stability derivatives C_{ℓ_β}, $C_{\ell_p}\frac{b}{2V_c}$, and $C_{\ell_r}\frac{b}{2V_c}$. For an elastic airframe, equation (5.34) results in an effective modification of various terms in the equation of motion because of the occurrence of the $\ddot{y} = \dot{v}$ term.

Now define the following equivalent elastic derivatives:

$$
\begin{aligned}
C_{\ell_{\beta_E}} &= \left[C_{\ell_{\beta_{WB_E}}} + K \frac{Z_v}{b} \bar{a}_v \Big|_{\ddot{Y}_v=0} \left(1 + \frac{d\sigma}{d\beta} \right) \right] \\
C_{\ell_{r_E}} &= \left[C_{\ell_{r_{WB_E}}} + K \frac{2Z_v^2}{b^2} \bar{a}_v \Big|_{\ddot{Y}_v=0} \right] \\
C_{\ell_{\dot{r}_E}} &= \left[C_{\ell_{\dot{r}_{WB_E}}} - K \frac{2Z_v \ell_v}{b^2} \bar{a}_v \Big|_{\ddot{Y}_v=0} \right]
\end{aligned}
\tag{5.35}
$$

The remaining terms in equation (5.34) are defined as inertial derivatives and can be identified as follows:

$$
\begin{aligned}
C_{\ell_{\ddot{Y}_s}} &= K \left[\bar{a}_v \Big|_{\ddot{Y}_v=0} + \frac{\partial C_{L_v}}{\partial \ddot{Y}_v} \right] \frac{Z_v}{b} \\
C_{\ell_{\dot{p}_s}} &= \left[K \left(\bar{a}_v \Big|_{\ddot{Y}_v=0} K_{\dot{p}} + \frac{\partial C_{L_v}}{\partial \ddot{Y}_v} Z_v \right) \frac{Z_v}{b} + \frac{\partial C_\ell}{\partial \dot{p}} \Big|_{WB} + \frac{\partial C_\ell}{\partial \dot{p}} \Big|_{H} \right] \\
C_{\ell_{\dot{r}_s}} &= K \left[\bar{a}_v \Big|_{\ddot{Y}_v=0} K_{\dot{r}} - \frac{\partial C_{L_v}}{\partial \ddot{Y}_v} \ell_v \right] \frac{Z_v}{b}
\end{aligned}
\tag{5.36}
$$

Finally, consider the yawing-moment coefficient. In accordance with ref. 72, the yawing-moment coefficient is assumed to be equal to the sum of the wing-body component and the vertical-tail component.

$$
C_n = C_{n_{WB}} + C_{n_v} \tag{5.37}
$$

Aeroelastic effects on the body will be neglected except where they contribute to a change in the vertical-tail angle of attack. The wing sideslip is proportional to C_L^2. For large dynamic pressures, where aeroelastic effects are important, C_L values are usually low; hence, the wing will be considered rigid. Thus,

$$C_{n_{WB}} = C_{n_{\beta_{WB}}}\beta + C_{n_{r_{WB}}}\frac{rb}{2V_c} + C_{n_{p_{WB}}}\frac{pb}{2V_c} \tag{5.38}$$

For the contribution of the vertical tail, the same approach as for the side-force coefficient is applied and the following expression is obtained:

$$C_{n_v} = \frac{S_v}{S_w}\frac{\bar{q}_v}{\bar{q}_\infty}\frac{l_v}{b}\left[\bar{a}_v\Big|_{\ddot{y}_v=0}\beta_v + \frac{\partial C_{L_v}}{\partial \ddot{y}_v}\ddot{y}_v\right] \tag{5.39}$$

where β_v is given by equation (5.23) and $\ddot{y}_v$ is given by equation (5.24).

The equation for the yawing-moment coefficient of the entire airplane is then:

$$\begin{aligned} C_n = &\left[C_{n_{\beta_{WB}}} - K\frac{l_v}{b}\bar{a}_v\Big|_{\ddot{y}_v=0}\left(1+\frac{d\sigma}{d\beta}\right)\right]\beta + \left[C_{n_{p_{WB}}}\frac{b}{2V_c} - K\frac{l_v}{b}\frac{z_v}{V_c}\bar{a}_v\Big|_{\ddot{y}_v=0}\right]p \\ &+\left[C_{n_{r_{WB}}}\frac{b}{2V_c} + K\frac{l_v}{b}\frac{l_v}{V_c}\bar{a}_v\Big|_{\ddot{y}_v=0}\right]r - \left[K\bar{a}_v\Big|_{\ddot{y}_v=0}K_{\ddot{y}} + K\frac{\partial C_{L_v}}{\partial \ddot{y}_v}\right]\frac{l_v}{b}\ddot{Y} \\ &-\left[K\bar{a}_v\Big|_{\ddot{y}_v=0}K_{\dot{\beta}} + K\frac{\partial C_{L_v}}{\partial \ddot{y}_v}z_v\right]\frac{l_v}{b}\dot{p} + \left[K\bar{a}_v\Big|_{\ddot{y}_v=0}K_{\dot{r}} + K\frac{\partial C_{L_v}}{\partial \ddot{y}_v}l_v\right]\frac{l_v}{b}\dot{r} \end{aligned} \tag{5.40}$$

For a rigid airplane, all elastic constants are zero. In that case, only the first three terms of equation (5.40) remain and the coefficients of β, p, and r are then identical to the conventional stability derivatives C_{l_β}, $C_{l_p}\frac{b}{2V_c}$, $C_{l_r}\frac{b}{2V_c}$. For an elastic airframe, equation (5.40) results in an effective modification of various terms in the equation of motion through the occurrence of the $\ddot{y} = \dot{v}$ term.

Define the following equivalent elastic derivatives:

$$C_{n_{\beta_E}} = \left[C_{n_{\beta_{WB}}} - K\frac{l_v}{b}\bar{a}_v\Big|_{\ddot{y}_v=0}\left(1+\frac{d\sigma}{d\beta}\right)\right]$$

$$C_{n_{p_E}} = \left[C_{n_{p_{WB}}} - K\frac{2l_v z_v}{b^2}\bar{a}_v\Big|_{\ddot{y}_v=0}\right]$$

$$C_{n_{r_s}} = \left[C_{n_{r_{wb}}} + K \frac{2 l_v^*}{b^2} \bar{a}_v \Big|_{\ddot{Y}_v = 0} \right] \tag{5.41}$$

The remaining terms in equation (5.40) are defined as inertial derivatives and can be identified as follows:

$$\begin{aligned} C_{n_{\ddot{Y}_s}} &= -K \left[\bar{a}_v \Big|_{\ddot{Y}_v = 0} K_{\ddot{Y}} + \frac{\partial C_{L_v}}{\partial \ddot{Y}_v} \right] \frac{l_v}{b} \\ C_{n_{\dot{p}_s}} &= -K \left[\bar{a}_v \Big|_{\ddot{Y}_v = 0} K_{\dot{p}} + \frac{\partial C_{L_v}}{\partial \ddot{Y}_v} Z_v \right] \frac{l_v}{b} \\ C_{n_{\dot{r}_s}} &= K \left[\bar{a}_v \Big|_{\ddot{Y}_v = 0} K_{\dot{r}} + \frac{\partial C_{L_v}}{\partial \ddot{Y}_v} l_v \right] \frac{l_v}{b} \end{aligned} \tag{5.42}$$

5.2 Corrector Matrix

5.2.1 Introduction. — The solution provided by the aerodynamic influence coefficient program TA 67A is the solution to the linearized, isentropic, steady-flow equations. Under the present state of the art, there is no method of including theoretical nonlinear effects in the analysis using aerodynamic influence coefficients. However, it is possible using semi-empirical methods to incorporate corrections for certain nonlinearities. This section is a study to investigate the possibility of allowing for nonlinear effects by a corrector matrix used in conjunction with the matrix of aerodynamic influence coefficients. (A7) (A8)

For the study, the computer program called TA 67A was used with a corrector matrix and the results were compared with those obtained from a wind tunnel test of an early SST model. The wind tunnel test was carried out in the NASA Ames Unitary Wind Tunnel using a 0.032-scale model of a supersonic transport. The following section will deal with the method of incorporating the corrector matrix into the theory. Paragraph 5.2.3 will discuss the results and conclusions of the study.

5.2.2 Corrector matrix theory. — It has been shown in par. 4.4.1 that, according to aerodynamic influence coefficient theory, the panel pressure forces on a rigid, flat airplane are given by:

$$\{P\} = \bar{q}\,[A]\,\{\alpha_R\} \tag{5.43}$$

Without altering the above equation, it is possible to insert the identity matrix. For the purpose of this study, consider the identity matrix inserted between the aerodynamic influence coefficient matrix and the column matrix of panel incidences. If we now relax the solution by allowing the identity matrix to become a general n x n matrix, we obtain an expression containing the corrector matrix:

$$\{P\} = \bar{q}\,[A][K]\,\{\alpha_R\} \tag{5.44}$$

where K_{ij} is the ij^{th} element of the corrector matrix and will be small for $i \neq j$, and approximately unity for $i = j$. At this point note that the number of panels used to represent the airplane is n.

Equation (5.44) can represent a change in the influence of any panel on any other panel. It is also possible, at least conceptually, to make each element of the corrector matrix a function of angle of attack. Equation (5.44) will then give nonlinear variations of pressure distribution with angle of attack.

The general n x n corrector matrix [K] must be considered an idealization. At present, there are no methods for determining corrector matrices with complications such as functional dependence. Much work has gone into the development of diagonal corrector matrices in which all components are constants.

The nature of the diagonal corrector matrix suggests some possible uses. For example, if one has prior knowledge that the predicted influence of the leading edge panels is going to be affected in a certain way, the diagonal correction matrix may be used to adjust the influence of these panels on all other panels.

5.2.3 Corrector matrix use and results. — As an example of adjusting influence coefficients, a diagonal corrector matrix was used to make TA 67A

predicted pressure distributions match experimental pressure data. From experiment the panel pressure forces be expressed as:

$$\{P\} = \bar{q}\,[S]\,\{\Delta C_p\} \tag{5.45}$$

where

$$\Delta C_p = C_{p_L} - C_{p_u} = [C_p] \tag{5.46}$$

where C_{p_L} and C_{p_u} are the pressure coefficients on the lower and upper surfaces, respectively. We can now relate experimental and predicted pressures by combining equations (5.44) and (5.45) to get:

$$[S]\,\{\Delta C_p\} = [A]\,[k]\,\{\alpha_R + \alpha_{exp}\} \tag{5.47}$$

where the corrector matrix $[k]$ is used here as a matrix of slope-correction constants and $\{\alpha_{exp}\}$ is a column matrix of intercept-correction constants. The following procedures may now be used to determine $[k]$ and $\{\alpha_{exp}\}$. Assume that $[k]$ and $\{\alpha_{exp}\}$ are invariant with $\{\alpha_{ref}\}$ for some range $\alpha_{ref_{(1)}} < \alpha_{ref} < \alpha_{ref_{(2)}}$ (see sketch below).

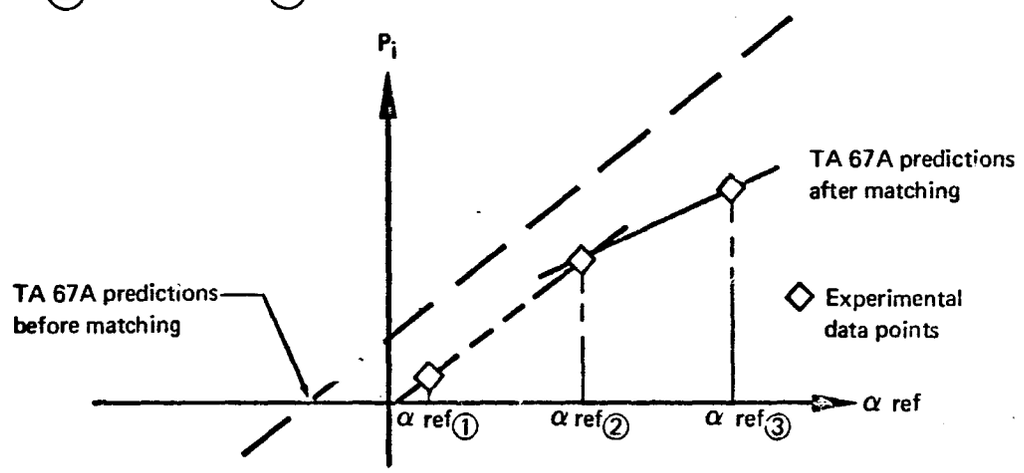

Typical Panel Pressure Curve

This assumption implies a local linearization. If experimental data are available for $\alpha_{ref_{(1)}}$ and $\alpha_{ref_{(2)}}$, then it follows that $\{\alpha_{exp}\}$ can be eliminated to yield:

$$[S]\{\Delta C_{p_{①}} - \Delta C_{p_{①}}\} = [A][k]\left(\alpha_{REF_{②}} - \alpha_{REF_{①}}\right)\{1\} \qquad (5.48)$$

This equation represents n linear algebraic equations in the unknown coefficients K_{ij}. Knowing $[k]$, it is now possible to solve for $\{\alpha_{exp}\}$ from:

$$[S]\{AC_{p_{①}}\} = [A][k]\{\alpha_{R_{①}} + \alpha_{exp}\} \qquad (5.49)$$

This solution is not unique, however, as it is also possible to write:

$$[S]\{\Delta C_{p_{②}}\} = [A][k]\{\alpha_{R_{②}} + \alpha_{exp}\} \qquad (5.50)$$

As a more accurate method for calculating $\{\alpha_{exp}\}$ write:

$$\{\alpha_{exp}\} = \frac{1}{2}\{\alpha_{exp_{(5.49)}} + \alpha_{exp_{(5.50)}}\} \qquad (5.51)$$

Repeating this process between $\alpha_{ref\,②}$ and $\alpha_{ref\,③}$ and so on, will give slope and intercept corrector matrices for all α_{ref}.

The method used in calculating slope- and intercept-corrector matrices for the TA 67A program representation of the SST model is a modification of the piecewise linearization method. Because of the random nature of the experimental data, a straight line between the data points at $\alpha_{ref\,①}$ and $\alpha_{ref\,②}$ may not represent the true experimental trends. For data points that are close together, an average over three data points should give a better approximation to actual trends. This would then give equation (5.48) as:

$$[S]\{\Delta(\Delta C_p)\} = [A][k]\left(\Delta\alpha_{REF}\right)\{1\} \qquad (5.52)$$

where

$$\{\Delta(\Delta C_p)\} = \left\{\frac{1}{2}\left(\frac{\Delta C_{p_{②}} - \Delta C_{p_{①}}}{\alpha_{REF_{②}} - \alpha_{REF_{①}}} + \frac{\Delta C_{p_{③}} - \Delta C_{p_{②}}}{\alpha_{REF_{③}} - \alpha_{REF_{②}}}\right)\Delta\alpha_{REF}\right\} \qquad (5.53)$$

and

$$\Delta\alpha_{REF} = \alpha_{REF_{③}} - \alpha_{REF_{①}} \qquad (5.54)$$

The $\{\alpha_{exp}\}$ used in this modified method is obtained from equation (5.50).

There is available a computer program that will generate $[k]$ and $\{\alpha_{exp}\}$ as used in equations (5.50) and (5.52). This program was developed for a structures group and is designated TS 167 in this appendix. The inputs for this program are the experimental panel pressure coefficients, $\{\Delta C_p\}$, for each Mach number and $\{\alpha_{ref}\}$ at which data was taken.

As a check for this method, experimental panel pressure coefficients for six α_{ref}'s and two Mach numbers were calculated for the SST model. The correction matrices obtained from TS 167 were included in the input for TA 67A which has a provision for slope- and intercept-correction factors. Program TA 67A then generated the desired experimental panel pressure coefficients.

If corrector matrices are needed for a large number of conditions, the process of calculating these matrices can be completely automated using a series of existing programs. These programs take raw wind tunnel data from magnetic tapes, interpolate to obtain experimental panel-pressure coefficients, and output slope- and intercept-correction matrices.

In conclusion:

(1) Correction matrices may be used to force the aerodynamic influence coefficient matrix to give experimental pressure distribution. However, the calculations are long and involved.

(2) Correcting the nonlinearity and/or other effects without employing experimental data requires an "experience factor" (prior knowledge about the desired effect).

6. EXPERIMENTAL METHODS FOR CALCULATING STABILITY DERIVATIVES

The two experimental techniques used to extract the stability derivatives are: (1) wind tunnel tests of scaled models of the proposed aircraft and (2) flight tests of similar aircraft or the actual aircraft. Both techniques have the advantage of being potentially more accurate than either the theoretical technique or semi-empirical techniques. The disadvantages of both techniques are the high costs of each data point and the difficulty of correcting collected data for errors due to experimental procedure. Additionally, neither offers a useful and convenient way of optimizing a configuration for good stability and control characteristics.

Needless to say, the derivatives generated by flight test techniques have a mixture of rigid and elastic effects. Consequently, the extraction of single-motion derivatives is difficult, if not impossible.

6.1 Wind Tunnel Tests

6.1.1 Rigid model technique. — Wind tunnel tests of rigid models are a reliable means of measuring rigid aircraft static or quasi-static stability derivatives, provided the implied assumptions of aircraft modeling are correct. The modeling parameters required to simulate the proper wake effects depend upon the test Reynolds number. Thus, the size and location of trip strips required to duplicate the nonlinear viscous effects can affect the values of the measured stability derivatives.

Additional experimental errors are introduced by wind tunnel geometry. Some tests are plagued by high wind tunnel turbulence levels or tunnel wall boundary layer effects that can affect the force and moment data. Once the force and moment data are collected, the correction of the data for wall effects and model-support effects must be made. The techniques of ref. 60 have been applied with success to eliminate the effects on the model of the wall or support constrained flow.

Note: For most wind tunnel tests the effects of the tunnel walls are minimized by testing "small" models in "large" tunnels.

In order to adequately compare the stability derivatives for the SST and 707-320B calculated by the theoretical and semi-empirical techniques, a base point measured by experiment is required. In the case of the rigid stability derivative comparisons, wind tunnel tests of rigid models are used. The following wind tunnel data for the 707-320B and an SST have been selected:

(1) The 707-320B models.

(a) High-speed test — Boeing Transonic Wind Tunnel, BTWT 866, $0.4 \leq M \leq 0.975$, $1.8 \times 10^6 < R_e < 3.0 \times 10^6$, scale = 0.035 (TC-814).

(b) Low-speed test — University of Washington Aeronautical Laboratory, UWAL 837, $M < 0.4$, $0.8 \times 10^6 < R_e < 1.4 \times 10^6$, scale = 0.05 (TC-229E).

(2) The SST models.

(a) Supersonic test — Boeing Supersonic Wind Tunnel, BSWT 366, $1.33 < M < 2.7$, $15 \times 10^6 < R_e < 21 \times 10^6$, $\Lambda_{LE} = 72°$, scale = 0.015 (SA-984).

(b) High-speed test — Boeing Transonic Wind Tunnel, BTWT 989, $0.5 < M < 1.0$, $6 \times 10^6 < R_e < 10 \times 10^6$, $\Lambda_{LE} = 42°$ and $72°$, scale = 0.015 (SA-984).

(c) Low-speed test — University of Washington Aeronautical Laboratory, UWAL 864, $0.1 < M < 0.26$, $4 \times 10^6 < R_e < 7 \times 10^6$, $\Lambda_{LE} = 30°$, scale = 0.03668 (SA-981).

6.1.2 Elastic model technique. — Wind tunnel tests of rigid models (scaled to the elastic deflections at some Mach number and dynamic pressure) and of equivalent elastic models have proven to be a useful tool to predict full-scale aeroelastic effects. However, the data from such wind tunnel tests must be corrected for the experimental errors noted for rigid models and for "elastic" errors.

The purpose of this section is to discuss the procedure that should be followed in using elastic-model wind tunnel data to predict full-scale-airplane characteristics. Methods for cross-checking are also indicated. The prediction of full-scale elastic lift-curve slope is discussed in par. 6.2.1.1. This is followed in par. 6.2.1.2 by a discussion of the data reduction technique to derive the full-scale elastic pitching moment versus lift coefficient. Prediction of full-scale drag from tunnel data is not discussed.

6.1.2.1 Prediction of lift coefficient versus angle of attack from elastic model data

Design flight condition. — This paragraph describes the four steps needed to predict the full-scale-airplane $C_{L_A} - \alpha$ curve for a design flight condition.

It is assumed that the shape of the airplane for the design flight condition is known (cruise shape) and that a rigid model has been constructed that is a scaled duplication of this shape. It should be realized that rigid models cannot be perfectly rigid and the consequence of this is discussed later in this paragraph.

The idea of building rigid models of the cruise shape relies on the assumption that one particular flight condition is of major importance or that the demonstration of analytical accuracy at one flight condition is sufficient to validate estimates for other conditions. It is impractical to construct rigid models for each important flight condition.

When using the word "airplane," the true (elastic) airplane is meant. When using the words "rigid airplane," an airplane shape is meant that results from freezing the airplane (true, elastic) in some equilibrium flight condition.

Making the assumptions that the wind tunnel model is a perfectly scaled duplication of the airplane, that Reynolds number effects and power effects are negligible, and that shock formations are properly simulated, the rigid-airplane $C_{L_A} - \alpha$ curve should be identical to the measured rigid-model $C_{L_M} - \alpha$ curve. This is indicated in fig. 10 by the curves marked 'rigid'.

It is also assumed that an elastic model has been constructed that, when tested at cruise Mach number, cruise dynamic pressure, and cruise angle of attack, deflects to the desired cruise shape. This implies that the rigid and the elastic model have, for the design flight condition, identical values of C_L, C_m (and C_D) at the design α. Figure 10 reflects this fact at point P_1. The result of wind tunnel measurements is the establishment of $C_{L_M} - \alpha$ curves for the rigid and elastic model. This completes step 1 of the procedure.

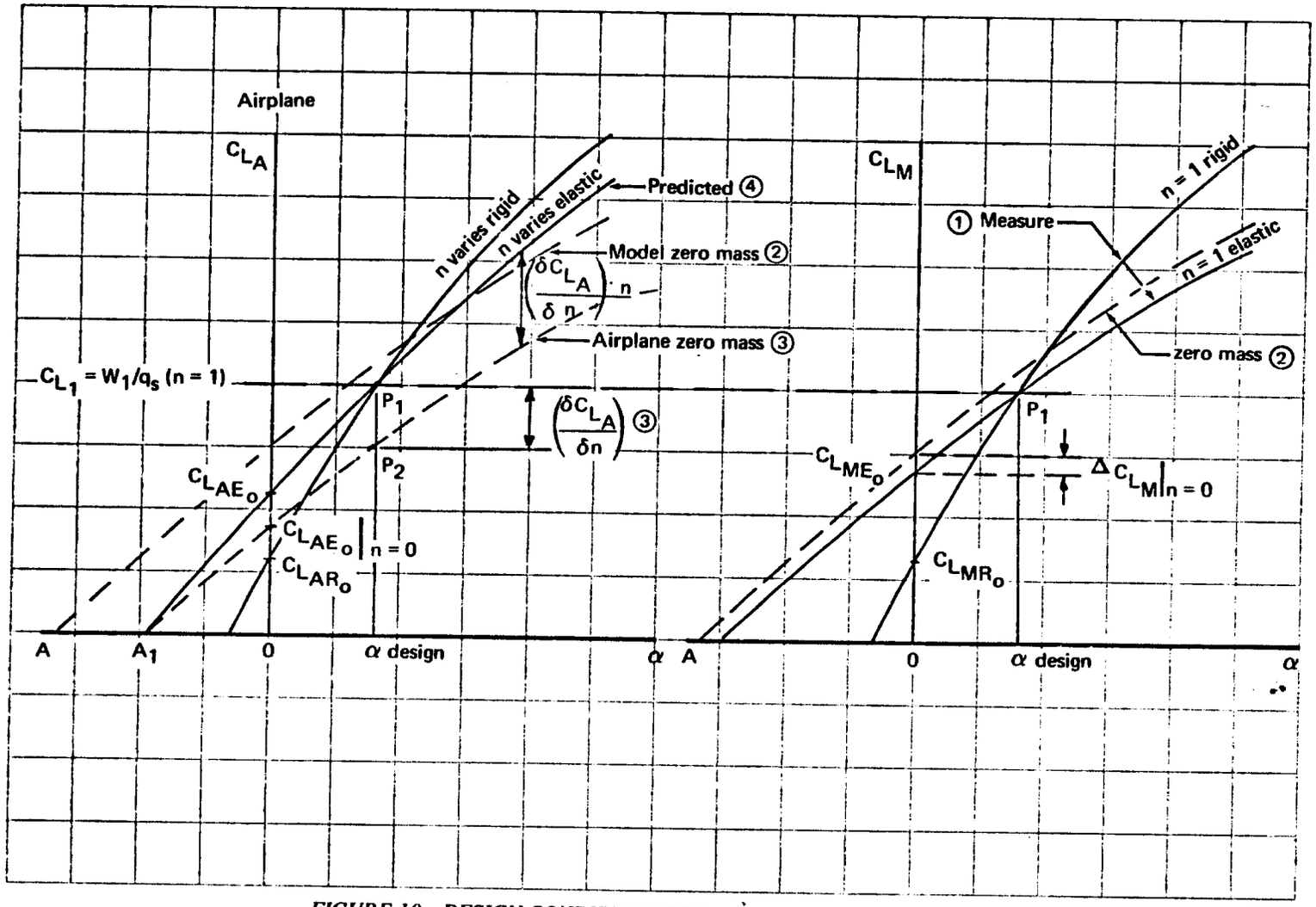

FIGURE 10.–DESIGN CONDITION (RIGID): $P_1, \bar{q}_1, M_1$, AND W_1

B-205

Observe that in the case of the real airplane, a variation of α at constant dynamic pressure implies a varying load factor. This is not the case for the wind tunnel model, where the load factor simulated is always 1. Even though this fact is of no consequence to the rigid case, in the case of the elastic airplane it has an important consequence because inertial forces participate in deforming the airplane. It is not feasible to simulate real airplane total mass and mass-distribution effects in a wind tunnel test and, at the same time, test at full-scale dynamic pressures. However, the varying effects of gravity on the model can be estimated from model data by introducing the concept of zero model mass and assuming a massless model has the effect of shifting the $n = 1$ elastic model $C_{L_M} - \alpha$ curve (vertically) over a small amount $\Delta C_{L_M}\big|_{m=0}$. This amount can be computed (from the known model mass and stiffness distribution), but it is expected to be very small. A typical value computed for an elastic SST model is $\Delta C_{L_M}\big|_{m=0} = 0.00031$ at $M = 2.7$ and $\bar{q} = 456$ psf (21 840 N/m^2). This value is small compared with the flight C_L at this Mach number and dynamic pressure which is $C_{L_{design}} \approx 0.085$. It is assumed that the effect of model mass on model elasticity (deflection) is constant over the α-range. This assumption is reasonable, particularly in view of the smallness of $C_{L_M}\big|_{m=0}$. The zero mass model $C_{L_M} - \alpha$ curve is now replotted on the left (i.e., airplane) side of fig. 10. This completes step 2.

For the airplane at the design α, it is possible to use TA 67A to compute $\frac{\partial C_{L_A}}{\partial n}$, the incremental lift coefficient due to the unit load. This yields point P_2. Assuming that the elastic model is perfectly scaled (dimensional and stiffness) and that local shocks and Reynolds effects are negligible, it follows that the zero-mass-airplane $C_{L_A} - \alpha$ curve should be identical to the zero-mass and mass-elastic-model $C_{L_M} - \alpha$ curve, but shifted vertically so that it intercepts point P_2. This provides the first anchor point for prediction of full-scale characteristics and represents step 3.

Because the airplane in reality has mass and because load factor varies with α, it is necessary to correct the full-scale zero-mass $C_{L_A} - \alpha$ curve. Load factor is defined as

$$\eta = \frac{C_{L_A} \bar{q} S}{W} \qquad (6.1)$$

Notice that n = 0 for $C_{L_A} = 0$. Because of this it is possible to consider the line $C_{L_A} = 0$ as corresponding to a zero-gravity environment. For that reason, the airplane $C_{L_A} - \alpha$ curves for full and zero mass intersect at $C_{L_A} = 0$ (point A_1), providing still another anchor point in the process of predicting full-scale-airplane characteristics. The effect of load factor on the $C_{L_A} - \alpha$ curve is expressed by the increment

$$\Delta C_{L_{A_n}} = \frac{\partial C_{L_A}}{\partial n} \cdot n \qquad (6.2)$$

where $\frac{\partial C_{L_A}}{\partial n}$ must be computed for the airplane using its known mass and stiffness distribution at constant dynamic pressure and Mach number in TA 67A. It is assumed that the partial derivative $\frac{\partial C_{L_A}}{\partial n}$ has a value independent of α. In other words, it is assumed that the incremental aerodynamic loading due to mass distribution $\Delta C_{L_{A_n}}$ is not a function of the variation of lift distribution with angle of attack. A typical value for $\frac{\partial C_{L_A}}{\partial n}$ is 0.0050 which, although small compared with the design C_{L_A} at n = 1, is not negligible. Adding the correction $\Delta C_{L_{A_n}}$, the full-scale $C_{L_A} - \alpha$ curve of the (elastic) airplane has finally been found. Notice that both points A_1 and P_1 are on the elastic airplane $C_{L_A} - \alpha$ curve. The correction $\Delta C_{L_{A_n}}$ varies from zero to A_1 to $\frac{\partial C_{L_A}}{\partial n}$ at P_2, but in a linear manner. This completes step 4.

It will be observed that the process of predicting full-scale airplane $C_{L_A} - \alpha$ characteristics from elastic model data involves computer applications because of the fact that it is not feasible to simulate mass and mass-distribution while at the same time testing at full-scale Mach numbers and dynamic pressures.

The following cross-check is proposed. It is possible to measure $C_{L_{ME_o}} - C_{L_{MR_o}}$ as indicated in fig. 10. This quantity corrected to zero mass becomes $(C_{L_{ME_o}} - \Delta C_{L_M}\big|_{m=0} - C_{L_{MR_o}})$. If the airplane load factor at $\alpha = 0$ would be n = 1, it would follow that $(C_{L_{ME_o}} - \Delta C_{L_M}\big|_{m=0} - C_{L_{MR_o}}) = (C_{L_{AE_o}}\big|_{m=o} - C_{L_{AR_o}})$. However, the true load factor at $\alpha = 0$ is $n = C_{L_{AE_o}}/C_{L_1}$. Therefore, the condition to be satisfied is

$$\left(C_{L_{ME_o}} - \Delta C_{L_M}\big|_{m=o} - C_{L_{MR_o}}\right) = \frac{C_{L_1}}{C_{L_{AE_o}}}\left(C_{L_{AE_o}}\big|_{m=o} - C_{L_{AR_o}}\right) \qquad (6.3)$$

This ends the cross-check.

NOTES: (1) The procedures indicated here depend on a number of assumptions, of which the essential are:

(a) Power, shock, and Reynolds number effects are negligible (or accounted for separately).

(b) $\Delta C_{L_M}\big|_{m=o}$, $\frac{\partial C_{L_A}}{\partial n}$ are independent of α.

(2) The procedures indicated here can be applied at only one flight condition if, as is usually the case, only one rigid and elastic model are available. For any other flight condition the rigid model has actually the wrong shape. The correction procedure to be followed in that case is outlined shortly.

(3) Notice that (elastic) airplane lift-curve slope is made up of two components as indicated by the following equation

$$C_{L_{\alpha_A}} = \frac{\partial C_{L_A}}{\partial \alpha}\bigg|_{\bar{q}} = \frac{\partial C_{L_A}}{\partial n}\bigg|_{\bar{q}} \frac{\partial n}{\partial \alpha}\bigg|_{\bar{q}} \tag{6.4}$$

Observe the subscripts for constant $\bar{q}$ and n. Now, it is seen that

$$\frac{\partial n}{\partial \alpha}\bigg|_{\bar{q}} = \frac{\partial n}{\partial C_{L_A}}\bigg|_{\bar{q}} \frac{\partial C_{L_A}}{\partial \alpha}\bigg|_{\bar{q}} = \frac{C_{L_{\alpha_A}}}{C_{L_{TRIM}}} \tag{6.5}$$

so

$$C_{L_{\alpha_A}} = \frac{C_{L_{TRIM}} C_{L_\alpha}\big|_n}{C_{L_{TRIM}} - \frac{\partial C_{L_A}}{\partial n}\big|_{\bar{q}}} \tag{6.6}$$

This equation indicates that if the effect of mass distribution on C_L is negligible, then $C_{L_{\alpha_A}} = C_L\big|_n$ which is to be expected. The equation also demonstrates the fact that $C_{L_{\alpha_A}}$ can be increased or decreased due to the inertial effects, depending on the sign of $\frac{\partial C_L}{\partial n}\big|_{\bar{q}}$. The sign of $\frac{\partial C_L}{\partial n}\big|_{\bar{q}}$ depends on the relative locations of center-of-mass loci to elastic axes.

(4) Lift coefficients at zero angle of attack for the rigid and elastic airplane are a fallout of the procedure described.

(5) Observe that equation (6.6) accounts for nonlinear effects provided $C_{L_\alpha}\big|_n$ is measured at the proper trim angle of attack on the elastic model.

(6) In view of the smallness of $\Delta C_{L_M}\big|_{m=0}$, step 2 can be eliminated.

Arbitrary flight condition: For arbitrary (other than cruise or design) flight conditions, the rigid model still has a shape corresponding to the cruise shape. Therefore, this model shape no longer corresponds to that of the airplane if it were frozen at the new flight condition. It seems reasonable to assume that this change in shape does not affect C_{L_α} to an appreciable extent. In other words, this shape change effects the camber and twist distribution but not C_{L_α}. Therefore, the rigid model still has the correct lift-curve shape. The change in camber and twist distribution on the airplane can be estimated by computing the equilibrium shape of the airplane at the new flight condition. By subtracting the camber and twist distribution from the known one at the design flight condition, the incremental camber, twist distribution is found. This incremental camber, twist distribution can, in turn, be used to estimate $\Delta C_{L_{CTW}}$ as indicated in fig. 11. The corrected rigid model (and, therefore, rigid airplane) C_{L_M} - α curve can now be obtained by shifting the measured curve vertically over $\Delta C_{L_{CTW}}$. Observe that knowing C_{L_2} at the new flight condition now allows the establishment of α_2. This completes step 1.

Correcting the elastic model data at the new flight condition, to the zero-mass environment, a C_{L_M} - α curve is obtained, the general shape of which (barring shock and viscous effects) should be the same as the zero-mass C_{L_A} - α curve of the airplane. This represents step 2. The zero-mass-airplane C_{L_A} - α curve can now be obtained by shifting vertically to point P_3. Point P_3 is found by computing $\frac{\partial C_{L_A}}{\partial n}$ for the new flight condition and the new mass distribution. This way point A_2 is established and step 3 is completed.

The elastic airplane C_{L_A} - α curve can be obtained by adding the computed increment to the zero-mass curve as shown in fig. 11, making sure that this curve passes through points A_2 and P_2. This completes the prediction of full-scale airplane C_{L_A} - α for an arbitrary flight condition and represents step 4.

A cross-check identical to the one described in the preceding paragraphs can now be made. However, it is necessary to first determine the value of $C_{L_{ME_0}}$ by extrapolation (step 5) as indicated in fig. 11.

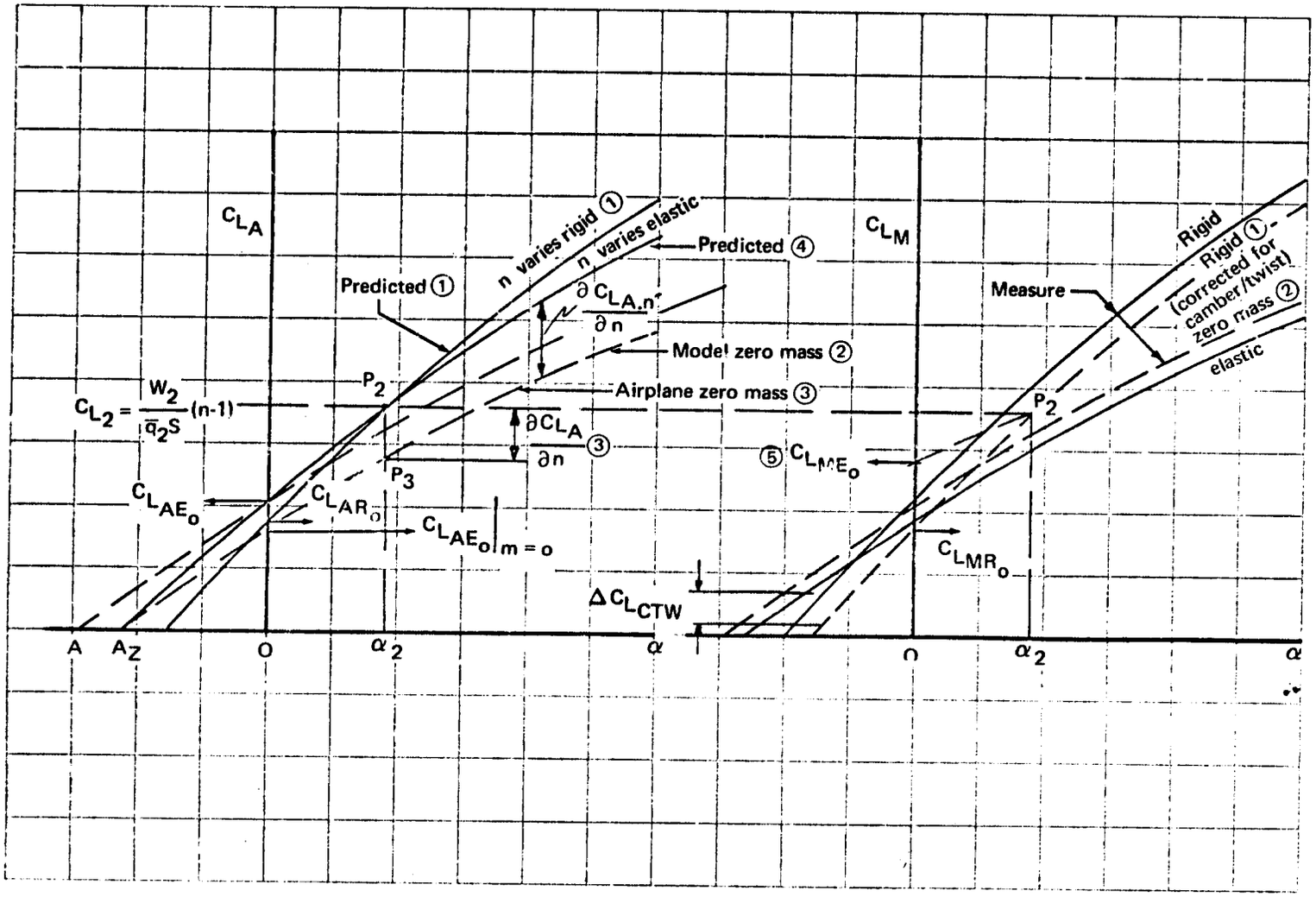

FIGURE 11.– ARBITRARY (OFF-DESIGN) CONDITION: P_2, $\bar{q}_2$, M_2, AND W_2

NOTES: (1) The prediction of airplane $C_{L_A} - \alpha$ for an arbitrary flight condition involves an extra computer step to compute $\Delta C_{L_{CTW}}$. This was not necessary at the design condition.

(2) If merely the (elastic) airplane lift-curve slope is needed, this can be obtained from equation (6.6), where now

$C_{L_{trim}} \Longrightarrow C_{L_2}$

$C_{L_\alpha}\big|_n \Longrightarrow C_{L_{\alpha ME}}$ (measured elastic model lift-curve slope)

$\frac{\partial C_{L_A}}{\partial n}\Big|_{\bar{q}} \Longrightarrow \frac{\partial C_{L_A}}{\partial n}\Big|_{\bar{q}_2}$ computed at M_2 and for the weight distribution corresponding to W_2

What to do when the "rigid" model is not really rigid: The purpose of this paragraph is to discuss what should be done to correct for flexibility effects on the so-called "rigid" model.

In general, such corrections are expected to be small. Therefore, theoretically obtained aeroelastic model corrections should be accurate. Such corrections, in the form of $\Delta C_{L_{MR_o}}$ and $\Delta C_{L_{MR_\alpha}}$ can be computed as soon as a flexibility matrix is obtained for the model. Such a matrix can be computed as follows.

(1) Directly from the known model structure (this means an enormous amount of work and is probably not worth it).

(2) Indirectly from measurements of EI and GJ distributions and application of beam theory. (This has been done with elastic models.)

(3) Indirectly by measuring influence coefficients at specified control points. (This is used when assumptions of beam theory are of doubtful validity.)

Ideally then, all model $C_{L_M} - \alpha$ data should be corrected for the above mentioned flexibility effects after which the data can be used as representative of a truly rigid model in the manner described in preceding paragraphs.

6.1.2.2 Prediction of pitching moment versus lift coefficient curve from elastic model data:

Design flight condition: The measured rigid and elastic model pitching moment curves are shown in fig. 12, step 1. By computing $\Delta C_{L_M}\big|_{m=o}$

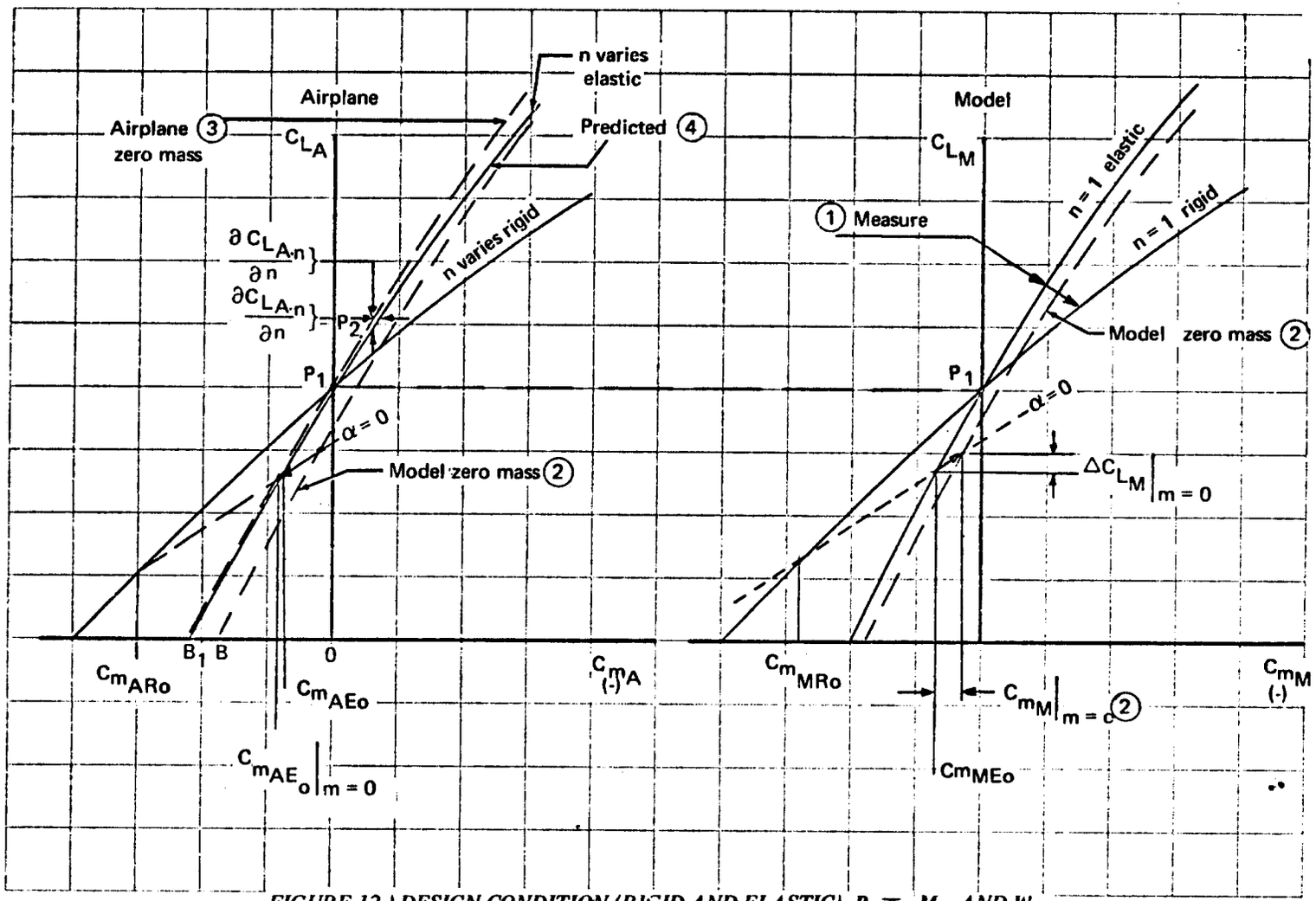

FIGURE 12.) DESIGN CONDITION (RIGID AND ELASTIC) P_1,$\bar{q}_1$, M_1, AND W_1

(as before) and $\Delta C_{m_M}\big|_{m=o}$ for the elastic model, it is possible to construct the zero-mass model pitching moment curve. In par. 6.2.1.1 it was already shown that $\Delta C_{L_M}\big|_{m=o}$ can be expected to be negligible. The same is true for $\Delta C_{m_M}\big|_{m=o}$, a typical value for which is -0.00010 at M = 2.7 and $\bar{q}$ = 456 psf (21 840 N/m^2). This number is indeed small compared with the corresponding airplane value at the same flight condition, which is

$$\frac{\partial C_{m_A}}{\partial n} = \Delta C_{m_M}\Big|_{m=o} = -0.00305$$

Anyway, the zero-mass-model curve in fig. 12 can now be obtained by shifting along a constant α line. This assumes that the increments $\Delta C_{L_M}\big|_{m=o}$ and $\Delta C_{m_M}\big|_{m=o}$ are constant with α which, particularly in view of their smallness, is justified. This terminates step 2.

For the elastic airplane the zero-mass pitching moment curve can be found by establishing point P_2 from calculations of $\frac{\partial C_{L_A}}{\partial n}$ and $\frac{\partial C_{m_A}}{\partial n}$. Neither of these values are negligible. By shifting the zero-mass model curve along a constant α line until it intersects P_2, it is possible to find Point B_1, step 3. At Point B_1 the true airplane has zero load factor and, as shown in fig. 12, the elastic zero-mass and full-mass lines intersect here. By adding the increment $\frac{\partial C_{m_A}}{\partial n}$ to the zero-mass curve, it is now possible to draw in the predicted airplane pitching moment curve, which will go through points B_1 and P_1. This completes step 4.

An elastic model of a variable sweep SST configuration (fig. 13) has been built and tested in the Boeing Supersonic Wind Tunnel. An elastic wind tunnel model of the 707-320B was not available. Only α, angle of attack derivatives, and elevator, δ_E, control derivatives were measured. In the wind tunnel, only zero-mass derivatives can be measured.

The wind tunnel model is a 0.015-scale model of an SST configuration with a wing sweep of 72 degrees. The shape of the model in the unloaded condition represents the theoretical jig shape. When loaded at the design point Mach number, dynamic pressures, and angle of attack, the model coincides with the 1-g cruise shape of the full-scale airplane. The Mach number range was 1.6 to 2.7 and the dynamic-pressure range was 1300 to 1800 psf (62 100 to 83 200 N/m^2). The wind tunnel tests are documented in Boeing wind tunnel test summary BSWT 386. The theoretical jig shape for the model was determined (S12)

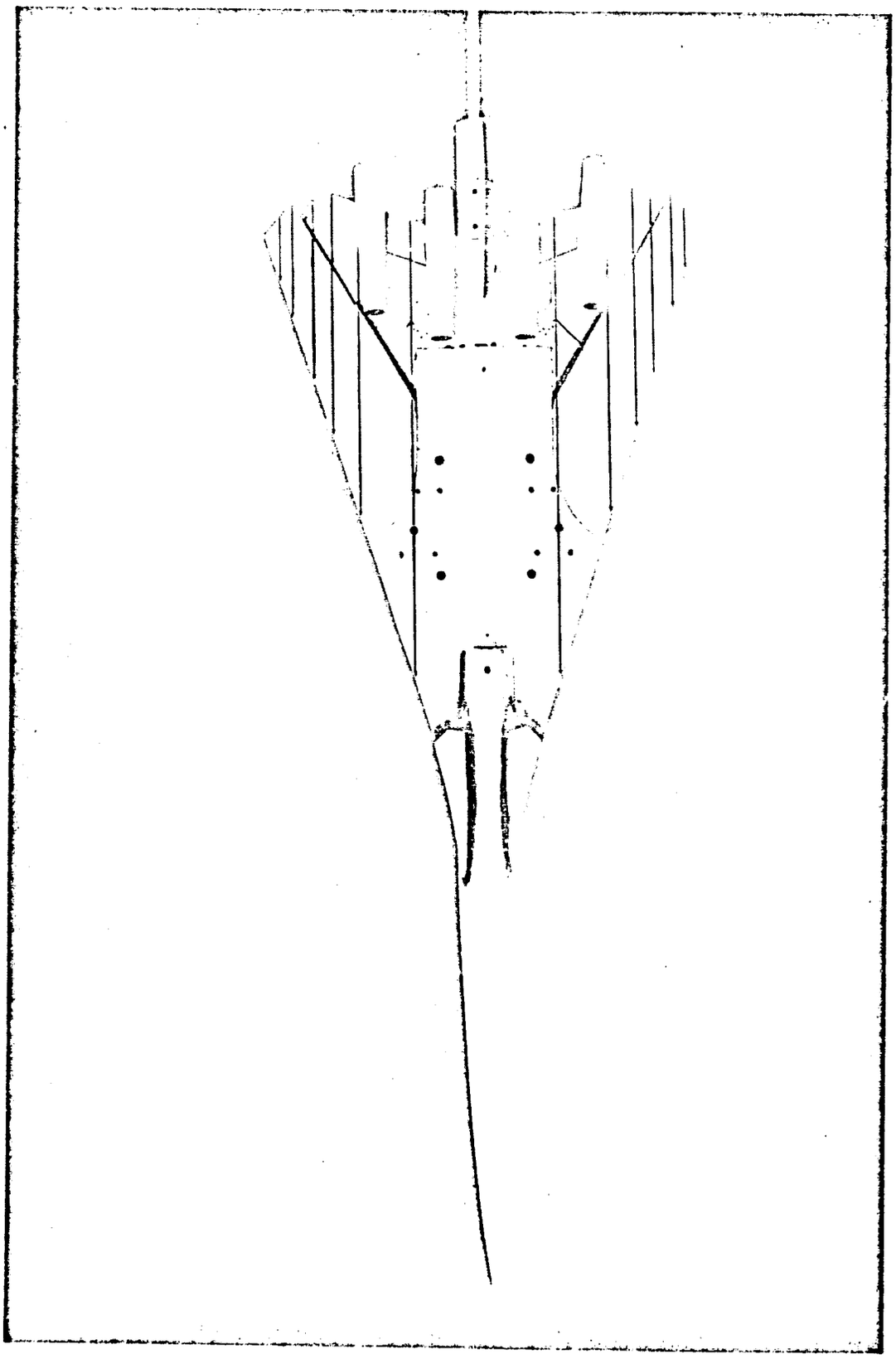

FIGURE 13.– ELASTIC SST MODEL

by using beam theory as the basis for computing the structural influence coefficient matrix.

It has been noted in par. 4.2.3 that structural beam theory has limitations in airplane applications. This is not so in the case of elastic wind tunnel models. These models are nearly always constructed so they accurately reflect the basic ideas of beam theory: all elastic properties are concentrated in one elastic axis and the wing portions forward and aft of this axis are rigidly attached to this elastic axis. Examples of the elastic model construction technique used on the SST model are shown in figs. 14 and 15.

6.2 Flight Test Data

The evaluation of stability derivatives from flight test data, by definition, should give the most accurate elastic values. The flight test values can then be used in handbook analysis, provided independent component contributions to each stability derivative can be extracted from the flight test data.

The primary difficulty associated with stability derivative evaluation from flight test data is the difficulty of performing a maneuver holding all motion variables, except one, equal to zero. Obviously, even if it were possible to fly only at an angle-of-attack variation, the aircraft would elastically deform at some other frequency determined by the structural properties and aerodynamic loads. The force and moment data measured at the aircraft's c.g. would contain both α and structural motion $u_n(t)$.

6.2.1 The 707-320B longitudinal derivative. — The available flight test data for the 707-320B are not ideal for extracting stability derivatives. The data used were generated during certification flight tests of the airplane. The fundamental difficulty of finding derivatives from flight test data is that they cannot be measured directly during any maneuver. Only special maneuvers, described in detail in ref. 11, lend themselves readily to the determination of stability derivatives. Due to the nature of the flight tests and the limited number of maneuvers available, only C_{m_α} and C_{L_α} could be extracted. Further, C_{L_α} and C_{m_α} could only be evaluated by assuming values for some other longitudinal derivatives. Both C_{L_α} and C_{m_α} were deduced from analyses of elevator hardover maneuvers; C_{m_α} was also evaluated from windup turn data.

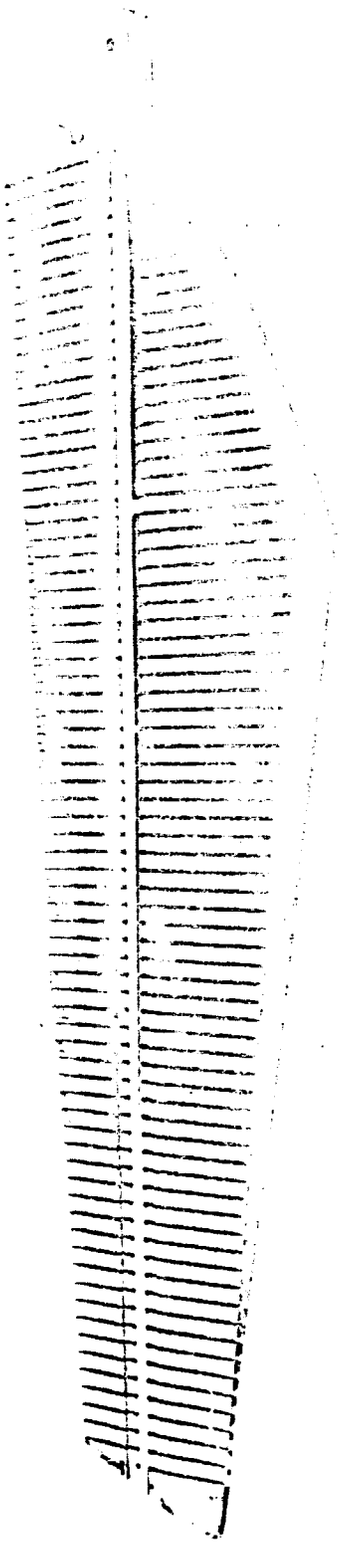

FIGURE 14.– EXAMPLE OF BEAM METHOD OF ELASTIC SST MODEL CONSTRUCTION

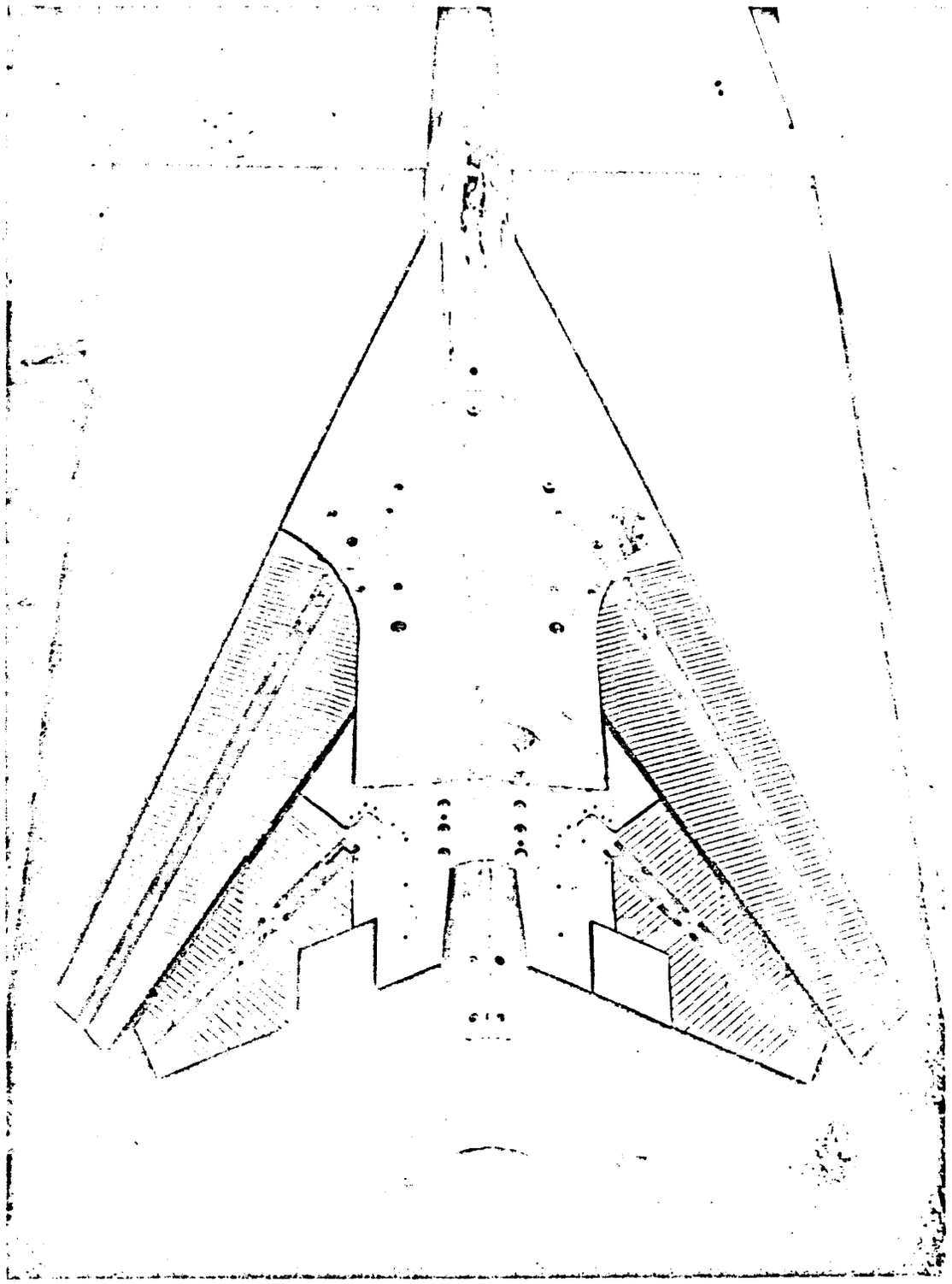

FIGURE 15.–ELASTIC SST MODEL–WING CONSTRUCTION

In addition, it was found that steady-state data could yield a more direct comparison between flight test data and the theoretical analysis. Such a comparison is shown in terms of the quantity $(\frac{dC_m}{dC_L})^*_E$ of constant altitude and load factor, and varying Mach number. Each method is described below.

6.2.1.1 Elevator hardover maneuvers:

$$C_{L_{\alpha_E}} = \frac{\partial C_L}{\partial \alpha}\Big|_V :$$

Using existing flight test recordings for the 707-320B, $C_{L_{\dot{\delta}e_E}}$, $C_{L_{qE}}$, and $C_{L_{\dot{\alpha}_E}}$ must be estimated from theory. From the flight test recordings of pitch attitude and norma acceleration, the angle of attack is deduced. The following relations are deduced, using the sketch below:

$$n_{z_s} = n_{z_B} \cos\alpha - n_{x_B} \sin\alpha \qquad (6.7a)$$

$$n_{x_s} = n_{x_B} \cos\alpha + n_{z_B} \sin\alpha \qquad (6.7b)$$

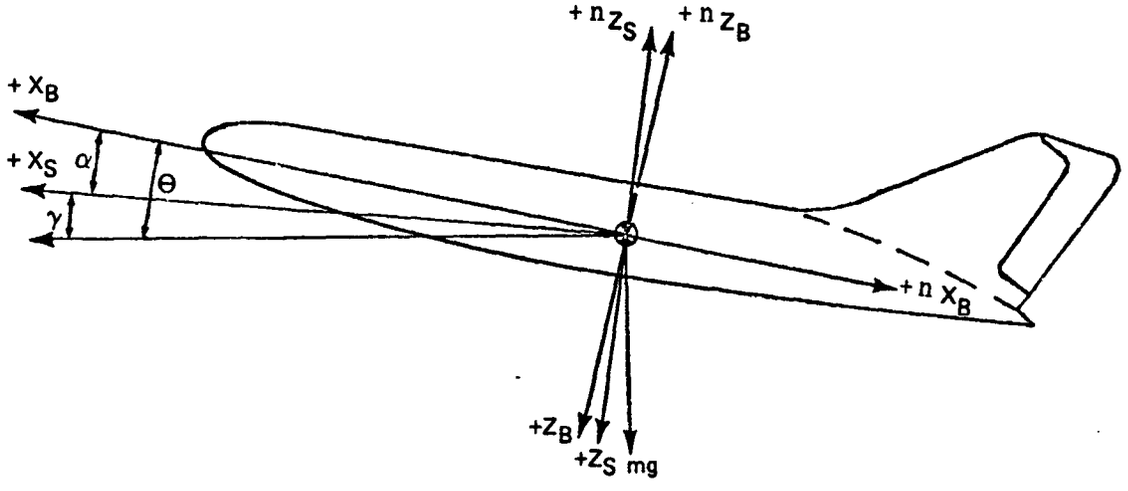

Axis System for Hardover Maneuver

If the maneuver is at constant speed, then $n_{x_s} = 0$ and a relation for n_{z_s}, the perturbation load factor in the z stability axis follows:

$$n_{x_B} = -n_{z_B} \frac{\sin\alpha}{\cos\alpha} \qquad (6.8a)$$

$$n_{z_s} = n_{z_B} \frac{1}{\cos\alpha} \qquad (6.8b)$$

An accelerometer will measure the combination of the body acceleration and the gravity component. If n_z^1 is the measured value of load factor along $-z_B$, the stability axis load factor is given by:

$$n_{z_s} = \left(n'_z - \cos\Theta\right)\frac{1}{\cos\alpha} \qquad (6.9)$$

The angle-of-attack variation during the hardover maneuver is deduced from the relation

$$\alpha = \theta - \gamma = \theta - \int \dot{\gamma}\, dt \tag{6.10}$$

The airplane lift coefficient can now be found from

$$C_L = \left(n_{z_s} + \cos\gamma\right)\frac{W}{\bar{q}S} \tag{6.11}$$

Writing this in terms of derivatives:

$$C_L = C_{L_\alpha}\left(\alpha_{TRIM} + \Delta\alpha\right) + C_{L_q}\hat{q} + C_{L_{\dot{\alpha}}}\hat{\dot{\alpha}} + C_{L_{\delta_E}}\delta_E \tag{6.12}$$

where $\Delta\alpha$ is the perturbed angle of attack.

The quantity $(n_{z_s} + \cos\gamma)\frac{W}{\bar{q}S} - (C_{L_q}\hat{q} + C_{L_{\dot{\alpha}}}\hat{\dot{\alpha}} + C_{L_{\delta_E}}\delta_E)$ can be determined as a function of time from time history measurements of n_z^1, α, θ, $\dot{\theta}$, and δ_E. This quantity is plotted against $\Delta\alpha$ in fig. 16 where $\Delta\alpha$ is calculated by equation (6.10). It is emphasized that C_{L_q}, $C_{L_{\dot{\alpha}}}$, and $C_{L_{\delta E}}$ used in this process are theoretical estimates, but are judged to be of the right magnitude. The slope of the curve in fig. 16 is then $C_{L_{\alpha_E}}$.

$$C_{m_\alpha} = \left.\frac{\partial C_m}{\partial \alpha}\right|_V$$

A similar technique has been applied to the pitching moment data using a value of $C_{m_{\zeta_E}}$ generated from flight test elevator-stabilizer trades and from a theoretical prediction of the stabilizer effectiveness. At constant speed the following relationship is used to determine the elevator effectiveness from predicted values of elastic $C_{m_{i_H}}$ and the measured elevator stabilizer trades,

$$C_{m_{\delta_R}} = -C_{m_{i_H}}\left(\frac{di_H}{d\delta_e}\right)_E \quad , \quad \left(\frac{di_H}{d\delta_R}\right)_E \tag{6.13}$$

The resultant $C_{m_{\zeta_E}}$ is plotted against dynamic pressure for various altitudes in fig. 17.

Using these values of $C_{m_{\zeta_E}}$ and theoretical values of I_{yy}, C_{m_q} and $C_{m_{\dot{\alpha}}}$, the C_{m_α} derivative is deduced from flight records as follows. The angle-of-attack variation for C_{m_α} is determined the same way it is determined for C_{L_α}

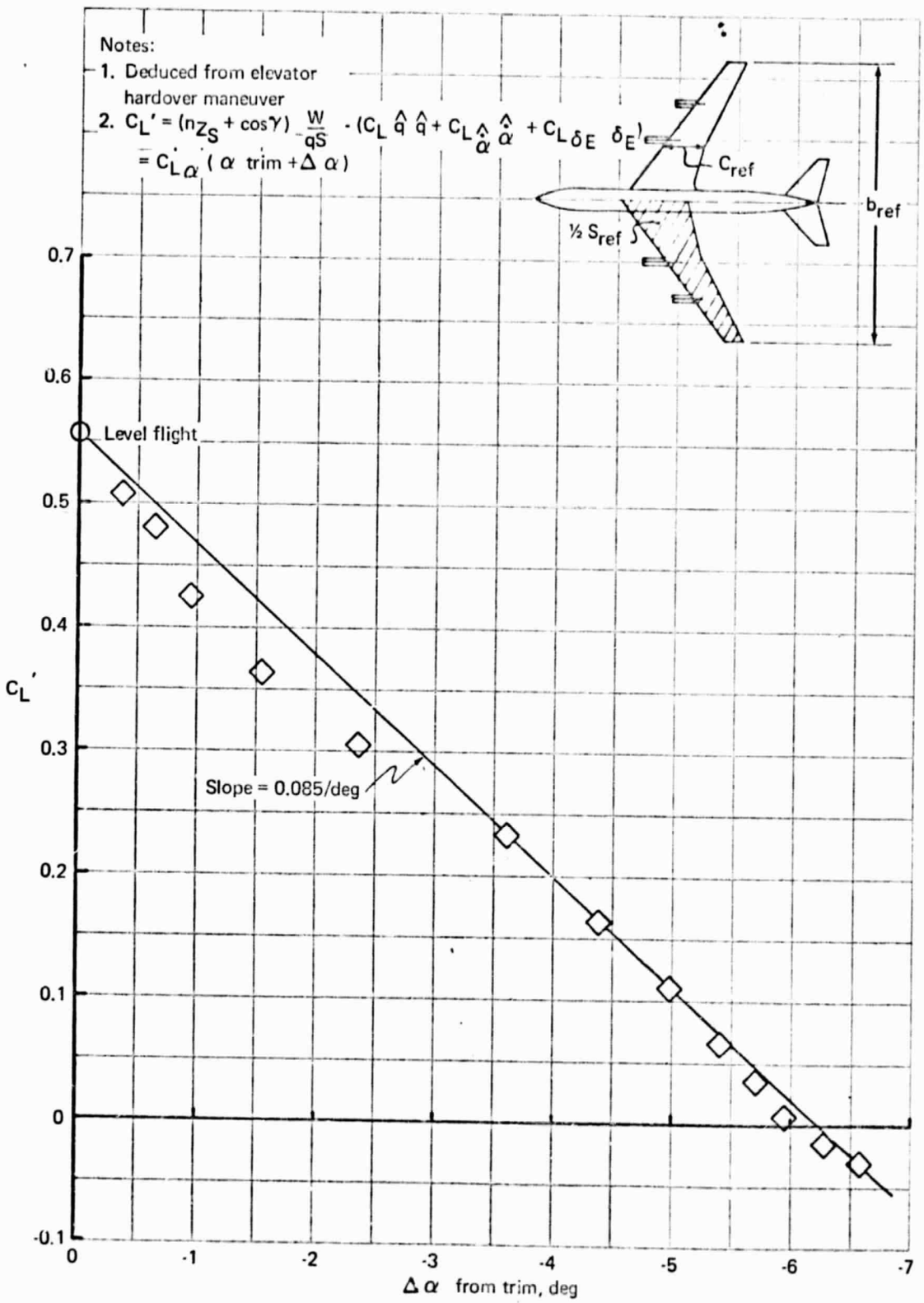

FIGURE 16.– DETERMINATION OF C_{L_α} FROM FLIGHT TEST DATA

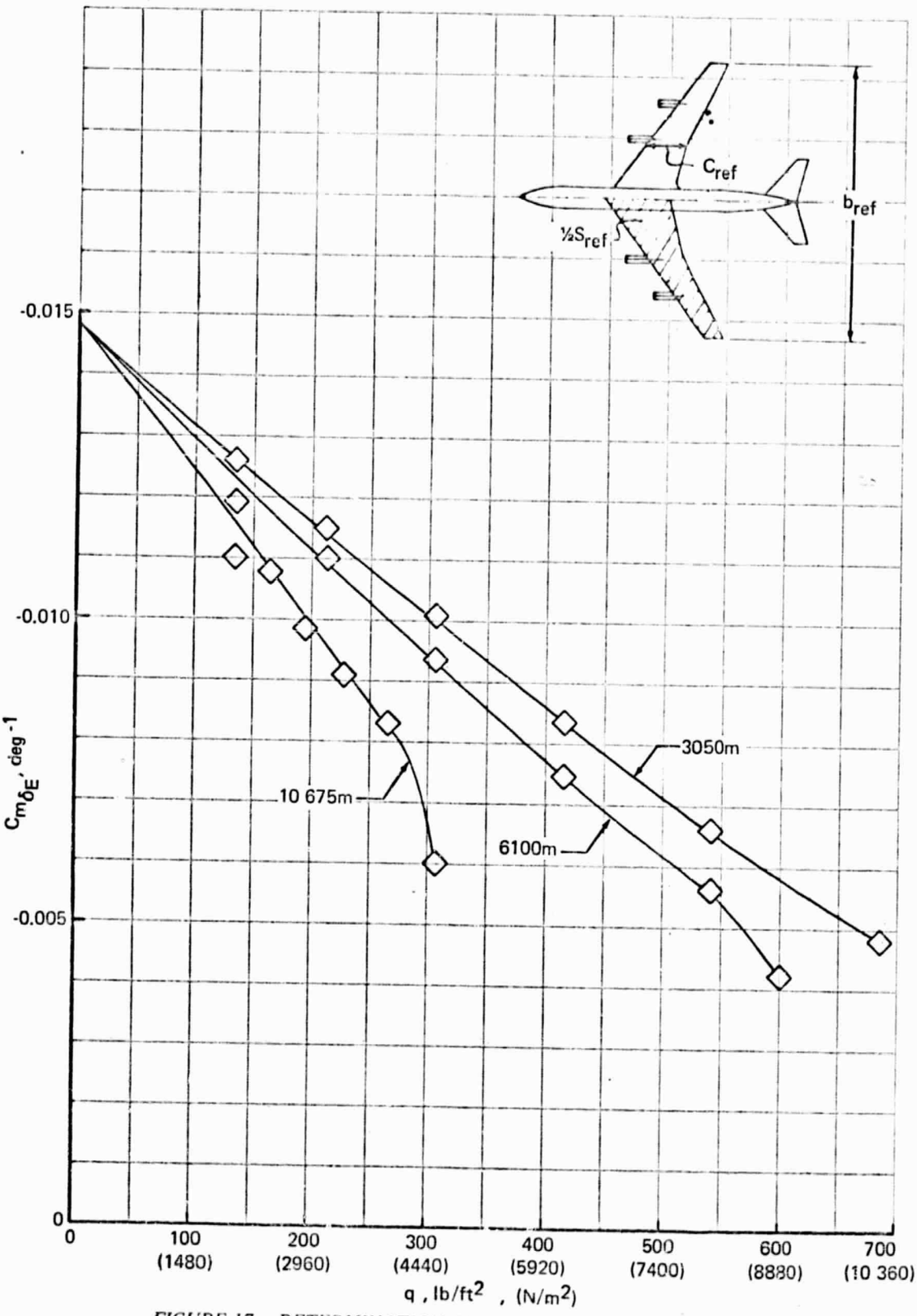

FIGURE 17.– DETERMINATION OF $C_{m_{\delta_E}}$ FROM FLIGHT TEST DATA

in equation (6.10). The pitching moment variation during the motion is determined from the relation:

$$\Delta C_m = C_{m_\alpha}(\alpha_{TRIM} + \Delta\alpha) = \frac{I_{yy}\ddot{\theta}}{\bar{q}S\bar{c}} - (C_{m_{\delta_E}}\delta_E + C_{m_{\hat{q}}}\hat{q} + C_{m_{\dot{\hat{\alpha}}}}\dot{\hat{\alpha}}) \tag{6.14}$$

where values for $\ddot{\theta}$, δ_E, $\hat{q}$, and $\hat{\alpha}$ are measured from flight records. This ΔC_m is shown plotted versus $\Delta\alpha$ in fig. 18. Pitch acceleration and elastic transients appear to dominate the maneuver for the first 1 to 1-1/2 seconds, but when $\ddot{\theta}$ has dropped to zero, a constant C_m versus α relationship is established.

The C_m in the latter part of the maneuver follows a linear relationship that can be extrapolated back to intersect the trim point. The effect of the elastic transient is very pronounced in fig. 18. The pitching moment is heavily dependent on the accuracy with which the pitch acceleration is deduced, which in this case comes from a double differentiation. The slope of fig. 18 gives $C_{m\alpha_E}$ about the center of gravity that is then referenced to $0.25\bar{c}$ using $C_{L\alpha_E}$ (from flight test) by the relation

$$C_{m\alpha_{E_{.25\bar{c}}}} = C_{m\alpha_{E_{c.g.}}} - \frac{(x_{c.g.} - x_{.25\bar{c}})}{\bar{c}} C_{L\alpha_E} \tag{6.15}$$

6.2.1.2 Windup turns: Windup turn tests are carried out at forward and aft c.g. as part of the airworthiness certification. The data are presented as curves of elevator angle per g and stick force per g against speed. The problem in using this data for finding stability derivatives is that there is no readily available gyro reference angle from which the angle of attack can be deduced. Nevertheless, it is possible to make some useful cross-checks on the pitching moment characteristics. By assuming a value of C_{m_q} and subtracting its effect from the pitching moment (produced by the elevator), an elastic $\frac{dC_m}{dC_L}$ for varying load factor and constant speed could be obtained. Multiplying this by $C_{L\alpha_E}$, the $C_{m\alpha_E}$ is obtained.

The data reduction process used the following lift and moment equations

$$C_L = \frac{n_{z_s} W}{qS} = C_{L_\alpha}\Delta\alpha + C_{L_{\hat{q}}}\hat{q} + C_{L_{\delta_E}}\delta_E \tag{6.16}$$

and

$$C_m = 0 = C_{m_\alpha}\Delta\alpha + C_{m_{\hat{q}}}\hat{q} + C_{m_{\delta_E}}\delta_E \tag{6.17}$$

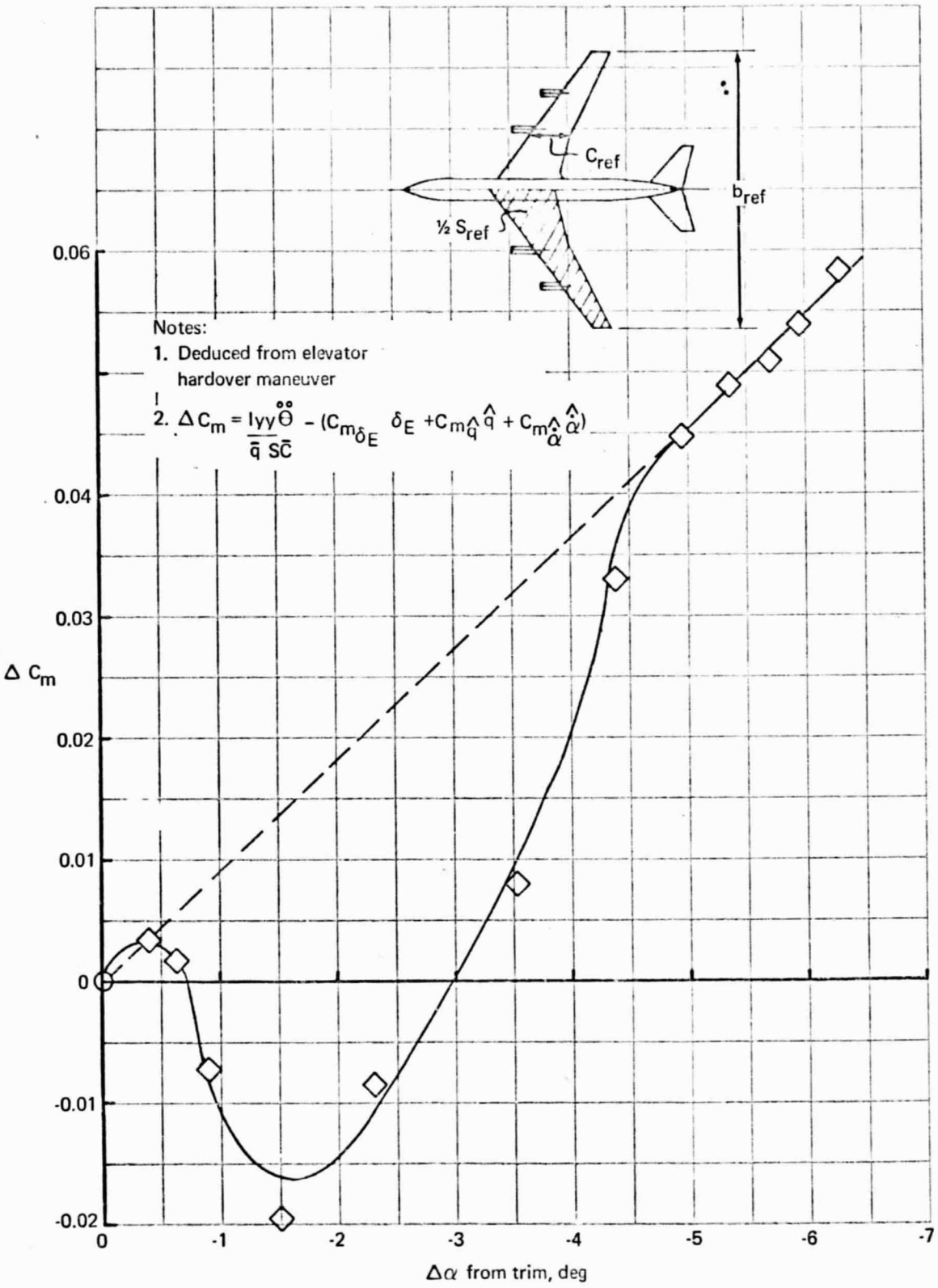

FIGURE 18.– DETERMINATION OF C_{m_α} FROM FLIGHT TEST DATA

$\hat{q}$ was found from

$$\hat{q} = \frac{\bar{c}\,\eta_{t_s}}{2V^2}\,q \qquad (6.18)$$

Theoretical values were used for C_{L_α}, C_{L_q}, $C_{L_{\delta_E}}$, and $\dot{C}_{m_{\hat{q}}}$. The $\dot{C}_{m_{\delta_E}}$ used was based on the theoretical stabilizer effectiveness and the stabilizer/elevator trades as described earlier.

Equation (6.16) was solved for $\Delta\alpha$ and equation (6.17) for C_{m_α} which, in turn, has been corrected to a c.g. of 0.25c by equation (6.15). The results showed quite good agreement between the hardover elevator maneuver and the windup turns at forward c.g., but poor agreement with windup turns at aft c.g. This might be accounted for by the deadweight bending effect due to the ballast necessary for an aft c.g. A concentration of ballast in the aft fuselage would give an apparent increase in C_{m_α}.

Steady state $\left(\frac{dC_m}{dC_L}\right)_E^*$:

$$\left(\frac{dC_m}{dC_L}\right)_E^* = \left.\frac{\partial C_m}{\partial C_L}\right|_n \qquad \text{(Mach number varies)}$$

This derivative can be obtained from flight test data by plotting trimmed values of $C_{m_{.25\bar{c}}}$ and C_L for several different c.g. positions. This implies a different Mach number for each c.g. position.

The reciprocal of the slope of the i_H = constant line connecting the test points gives the desired $\left(\frac{dC_m}{dC_L}\right)_E^*$ value.

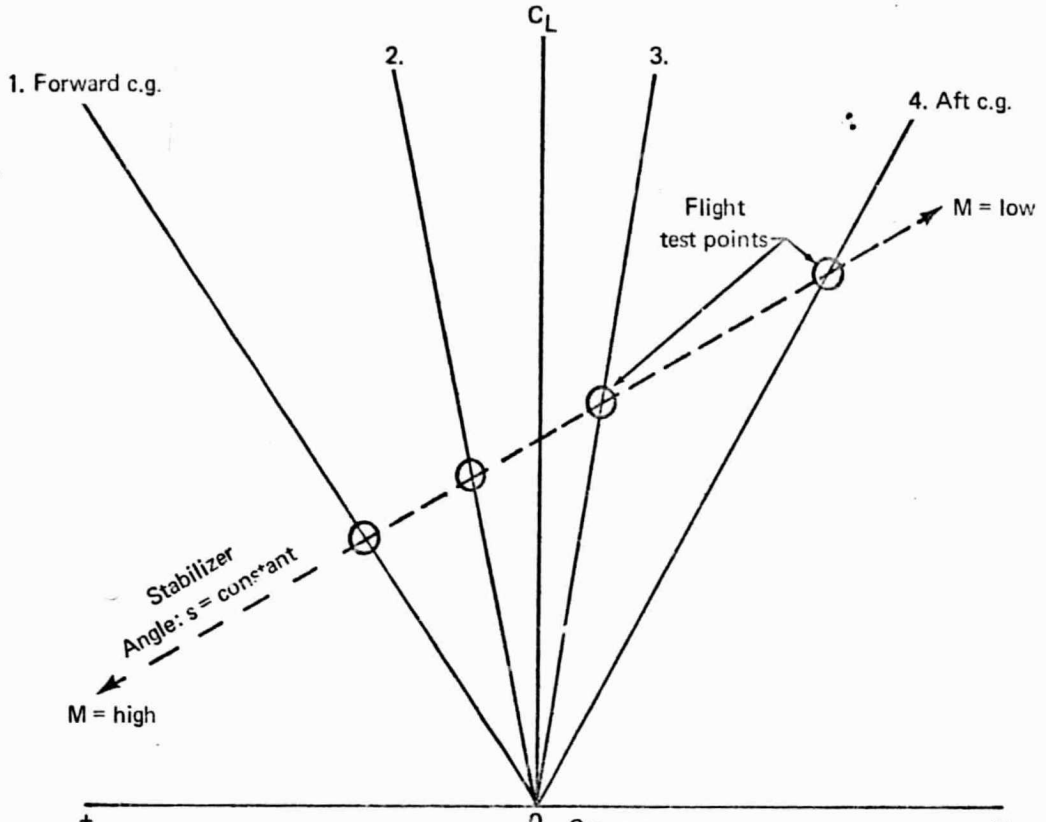

Method of Determining $\left(\frac{dCm}{dC_L}\right)^*_E$ From

Flight Test Data

6.2.2 The 707-320B lateral-directional derivatives.— Four maneuvers were chosen for extracting lateral and directional derivatives. These were as follows:

(1) Aileron hardover from which aileron effectiveness ($C_{\ell\,\delta_A}$) and roll damping ($C_{\ell\,p}$) were deduced.

(2) Rudder hardovers from which rudder effectiveness ($C_{n_{\delta_R}}$), yawing moment due to sideslip (C_{n_β}), and yaw damping (C_{n_r}) were found.

(3) Steady roll rates where the roll damping was equated to the aileron effectiveness found in (1). Appropriate flexibility factors ($\frac{Re}{R_R}$) were used in this derivation.

(4) Steady sideslip where the rolling moment due to sideslip ($C_{\ell\,\beta}$) was related to the $C_{\ell_{\delta A}}$ found in (1). C_{Y_β} was also found, but due to lack of sensitivity of the instrumentation there is little confidence in the value determined.

Three of these maneuvers were conducted at 35 000 to 37 000 feet (10 675 to 11 285 meters); the roll rates were done at 10 000 feet (3050 meters). The hardover maneuvers were made during autopilot testing, which ensures an initial steady-state condition and a smooth control application.

6.2.2.1 Aileron hardovers: Gyro recordings of roll angle and roll rate were available. Roll acceleration was found from the slope of the roll-rate gyro trace. The aileron effectiveness was evaluated during the initial part of the maneuver before the roll rate had time to build up. The roll damping was evaluated where the roll rate was approaching a steady-state value. Both derivatives were found from the one-degree-of-freedom roll equation:

$$C_{\ell_{\delta_T}} \delta_T + C_{\ell_{\delta_A}} \delta_A + C_{L_{\delta_{sp}}} \delta_{sp} + C_{\ell_{\dot{\phi}}} \dot{\phi} - \frac{I_{xx}}{\bar{q} S_w b} \ddot{\phi} = 0 \tag{6.19}$$

The ratios of $C_{\ell\,\delta\,T}$, $C_{\ell\,\delta\,A}$, $C_{\ell\,\delta_{sp}}$ were taken from theory. The final distribution of rolling moment as a function of time is shown on fig. 19.

6.2.2.2 Rudder hardovers: A similar approach was used in the rudder hardover maneuvers. The time history is shown on fig. 20 and up to the 2.5-second point, roll angle was less than 1°. Sideslip was not recorded and, hence, it had to be deduced from the following relationship:

$$\beta = -\int \dot{\psi}\, dt + \int \frac{a_y}{V}\, dt \tag{6.20}$$

This is found by integrating the basic stability axes relationship $\frac{\partial y}{V} = \dot{\beta} + \dot{\psi}$. The lateral acceleration is related to C_{Y_β}, which leads to the expression:

$$\beta = -\int \dot{\psi}\, dt + g \frac{C_{y_\beta}}{V c_1} \int \beta\, dt \tag{6.21}$$

This is an integral equation that in this instance is cumbersome to solve. However, in a manner such as this, it will be found that the additional side force makes the magnitude of β approximately 10 percent larger than ψ. Hence, equation (6.21) can be approximated by:

$$\beta = -\int \dot{\psi}\, dt - \frac{1.1 g C_{y_\beta}}{V c_1} \int \dot{\psi}\, dt \tag{6.22}$$

The resulting sideslip is plotted against time on fig. 21.

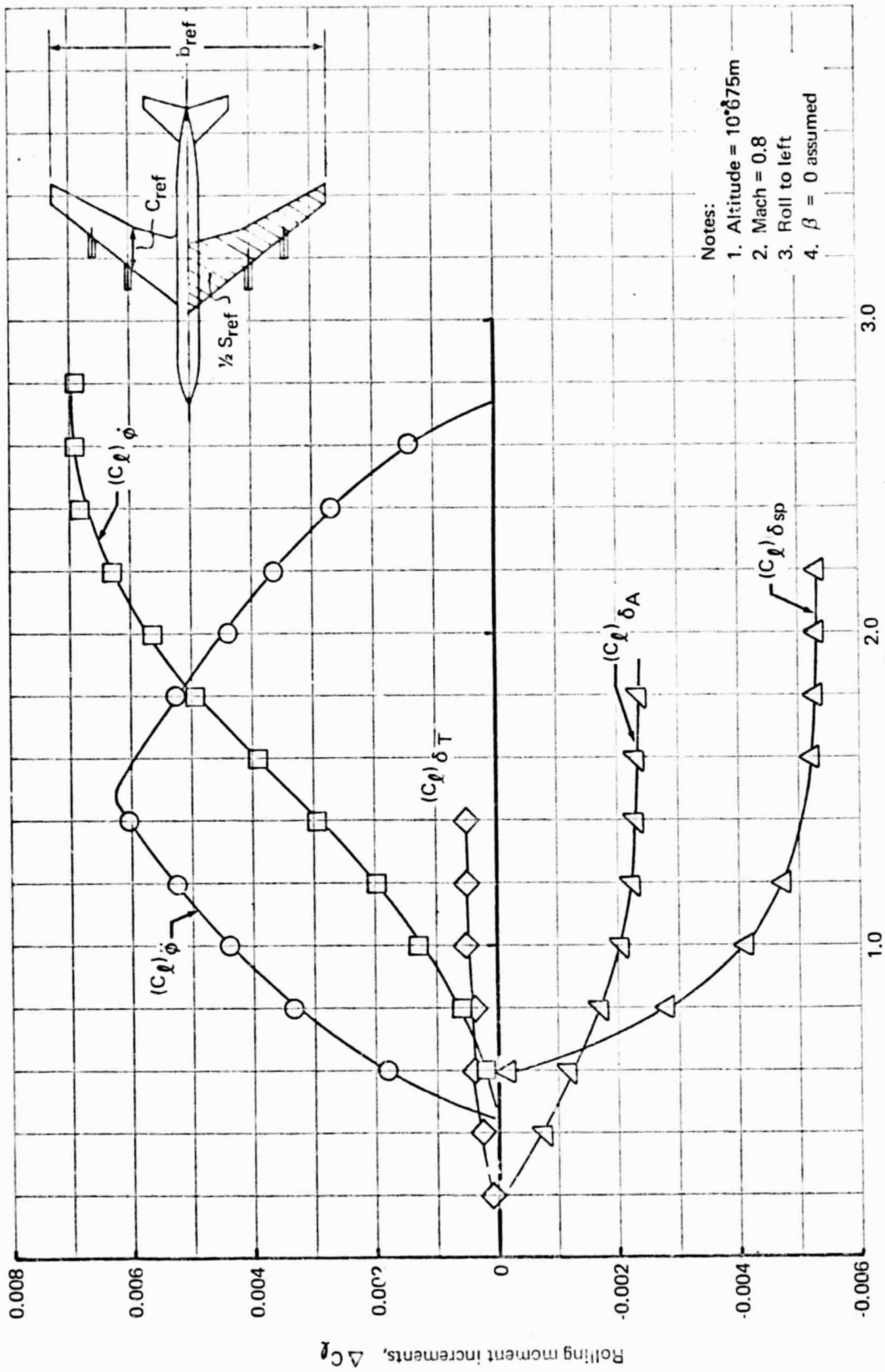

FIGURE 19.– DISTRIBUTION OF ROLLING MOMENT AS A FUNCTION OF TIME

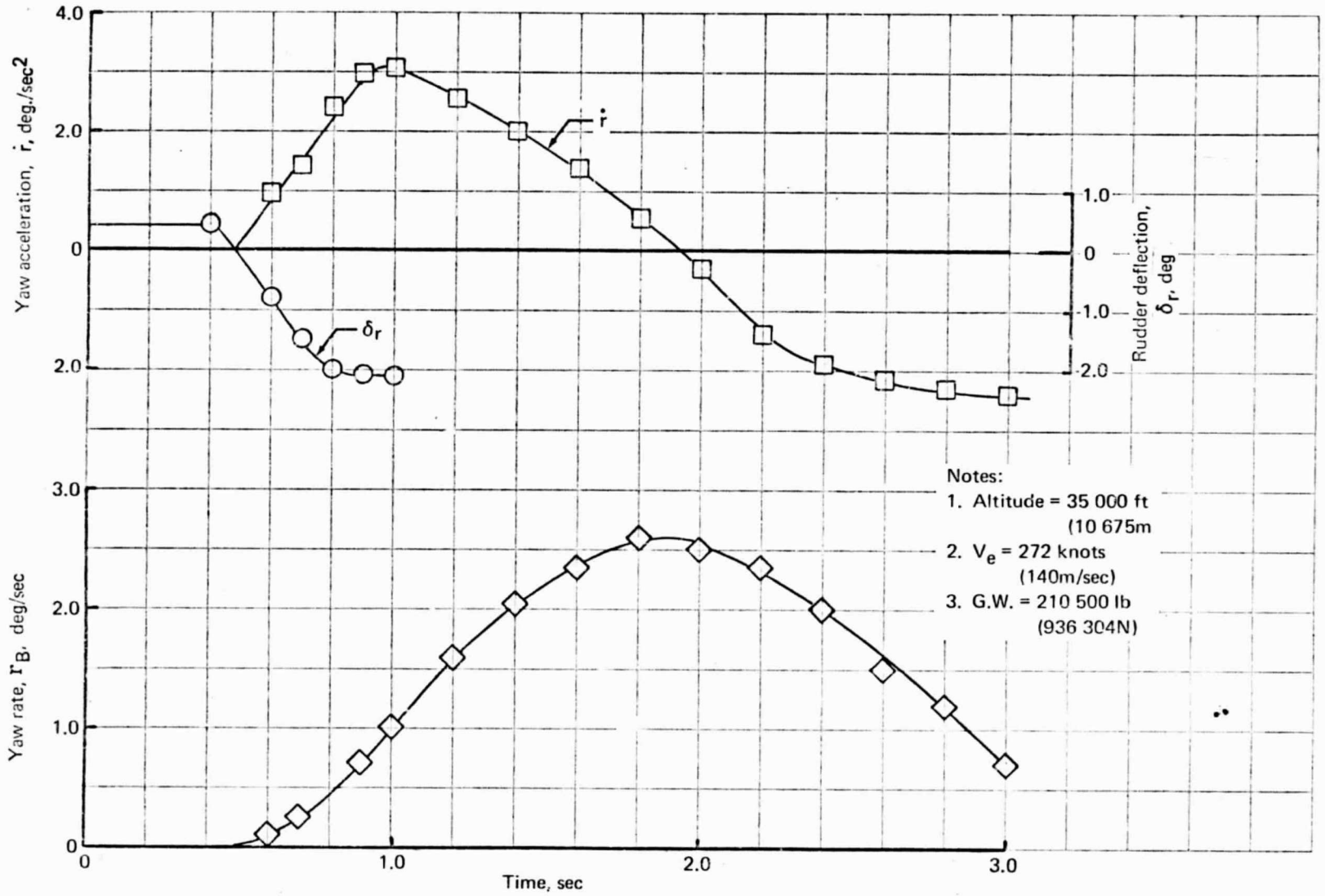

FIGURE 20.– RESPONSE OF THE 707-320B TO A RUDDER HARDOVER

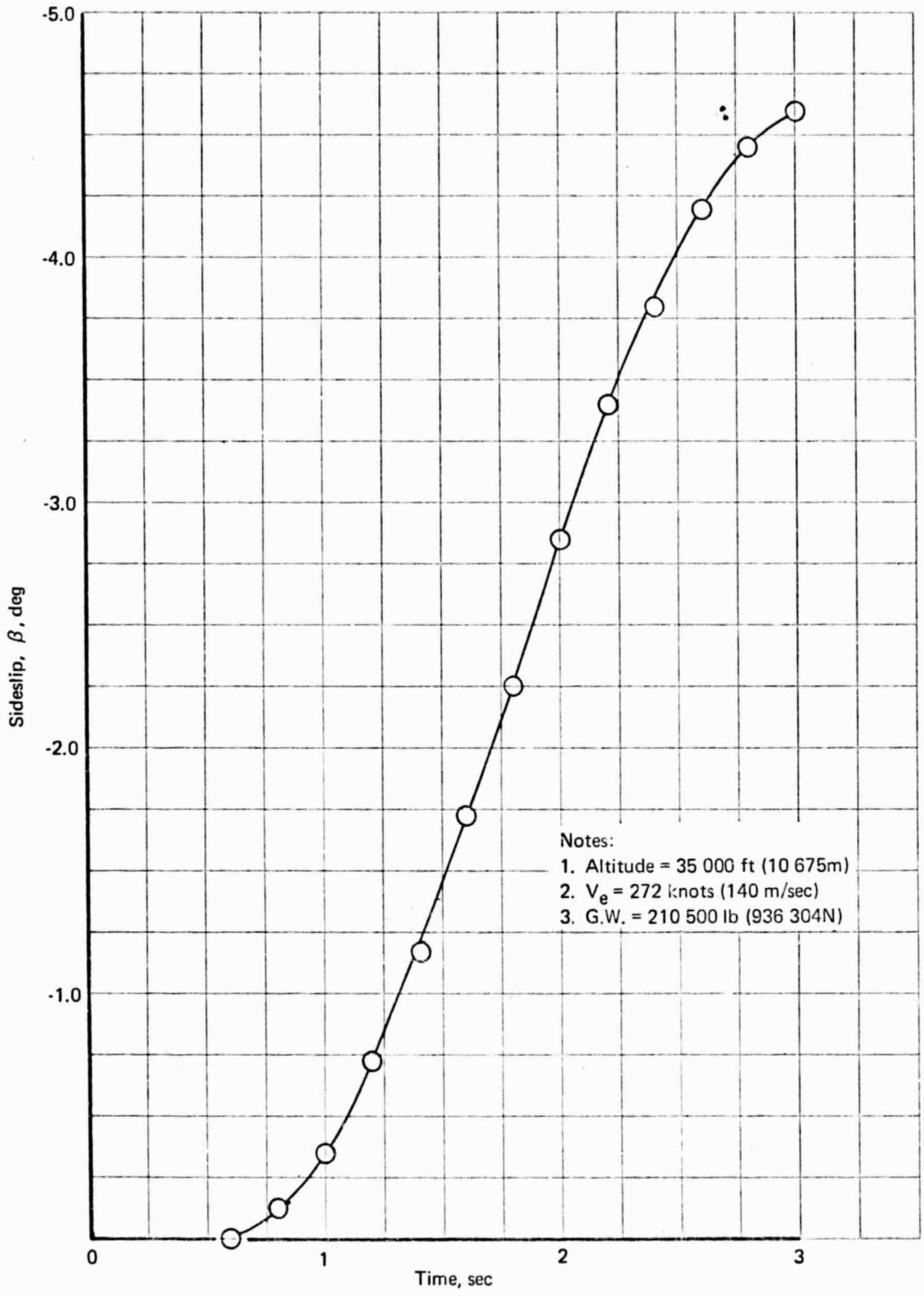

FIGURE 21.– SIDESLIP DURING RUDDER HARDOVER (707-320B FLIGHT TEST)

Finally, the yawing-moment derivatives are found from the three-degrees-of-freedom yawing equation:

$$C_{n_\beta}\beta + C_{n_{\dot\psi}}\dot\psi + C_{n_{\dot\phi}}\dot\phi + C_{n_{\delta_R}}\delta_R - \frac{I_{zz}}{\bar q S_w b}\ddot\psi = 0 \qquad (6.23)$$

As in the case of the rolling maneuver, control effectiveness is found from the early part of the maneuver before either yaw rate or sideslip have become significant. Values for C_{n_β} and $C_{n_{\ddot\psi}}$ were found from a form of best fit from the later part of the maneuver. The final distribution of yawing moment is plotted as a function of time on fig. 22. It can be seen that $C_{n_{\ddot\psi}}$ has only a minor contribution to the yawing moment and, hence, no great accuracy for the derivative is expected from this maneuver.

6.2.2.3 Steady roll rate: Figure 23 summarizes a series of roll-rate tests at 10 000 feet (3050m). These tests were conducted such that δ_A and ϕ were measured at $\phi = 0$, so that the data can be used in a one-degree-of-freedom roll equation:

$$C_{l_{\delta_A}}\delta_A + C_{l_{\dot\phi}}\dot\phi = 0 \qquad (6.24)$$

The $C_{l\,\delta A}$ was found by applying the proper $(\frac{R_e}{R_R})$ factor to the $C_{l\,\delta A}$ from the 'hardover' tests at 35 000 feet (10 675 meters). The resulting $C_{l\,p}$ is plotted on fig. 24.

6.2.2.4 Steady sideslip: The flight test data are shown on fig. 25. The sideslip was found from calibrated static vents on both sides of the body. The rolling derivatives were found from:

$$C_{l_{\delta_A}}\delta_A + C_{l_{\delta_R}}\delta_R + C_{l_\beta}\beta = 0 \qquad (6.25)$$

by differentiating with respect to β, which gives:

$$C_{l_\beta} = -C_{l_{\delta_A}}\frac{d\delta_A}{d\beta} - C_{l_{\delta_R}}\frac{d\delta_R}{d\beta} \qquad (6.26)$$

Used in this form the best average of the data points is obtained. Similarly, for the side force equation:

$$C_{y_\beta} + C_L\frac{d\phi}{d\beta} + C_{y_{\delta_R}}\frac{d\delta_R}{d\beta} = 0 \qquad (6.27)$$

The roll resolution was very poor in these data and, therefore, there is not much reliance in the resultant value of C_{y_β}.

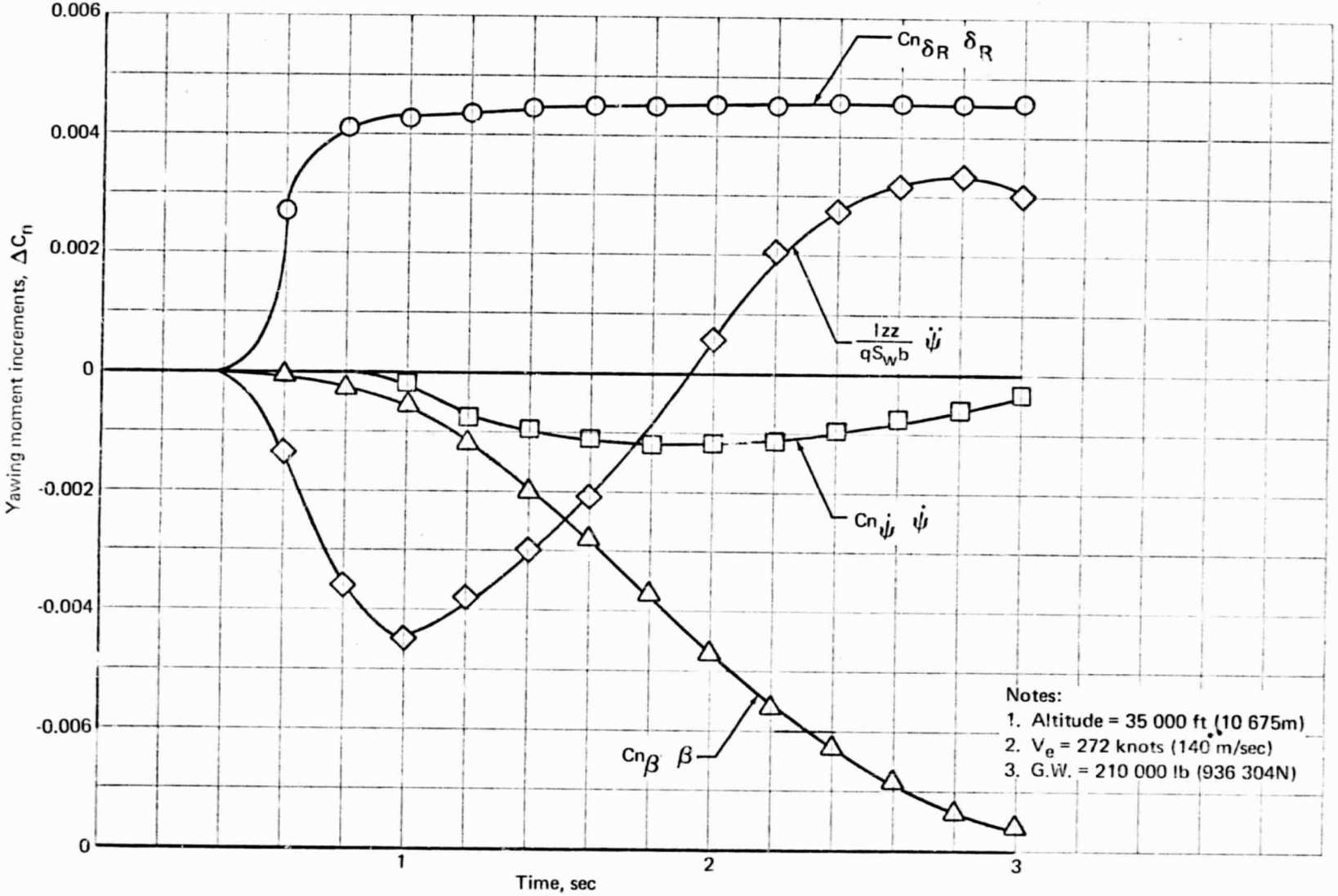

FIGURE 22.– DISTRIBUTION OF YAWING MOMENT DURING RUDDER HARDOVER (707-320B FLIGHT TEST)

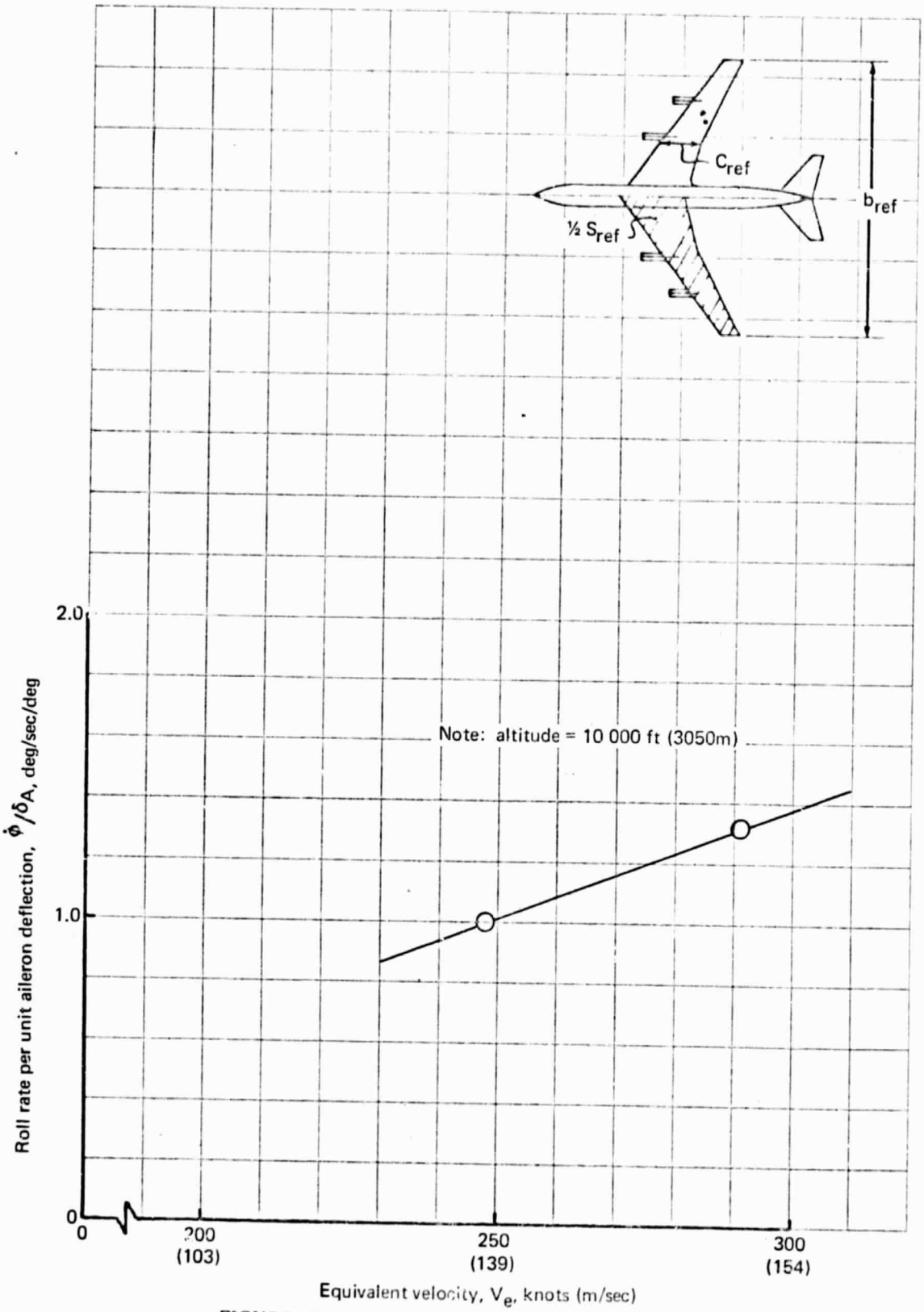

FIGURE 23.– STEADY ROLL-RATE SUMMARY – 707-320B

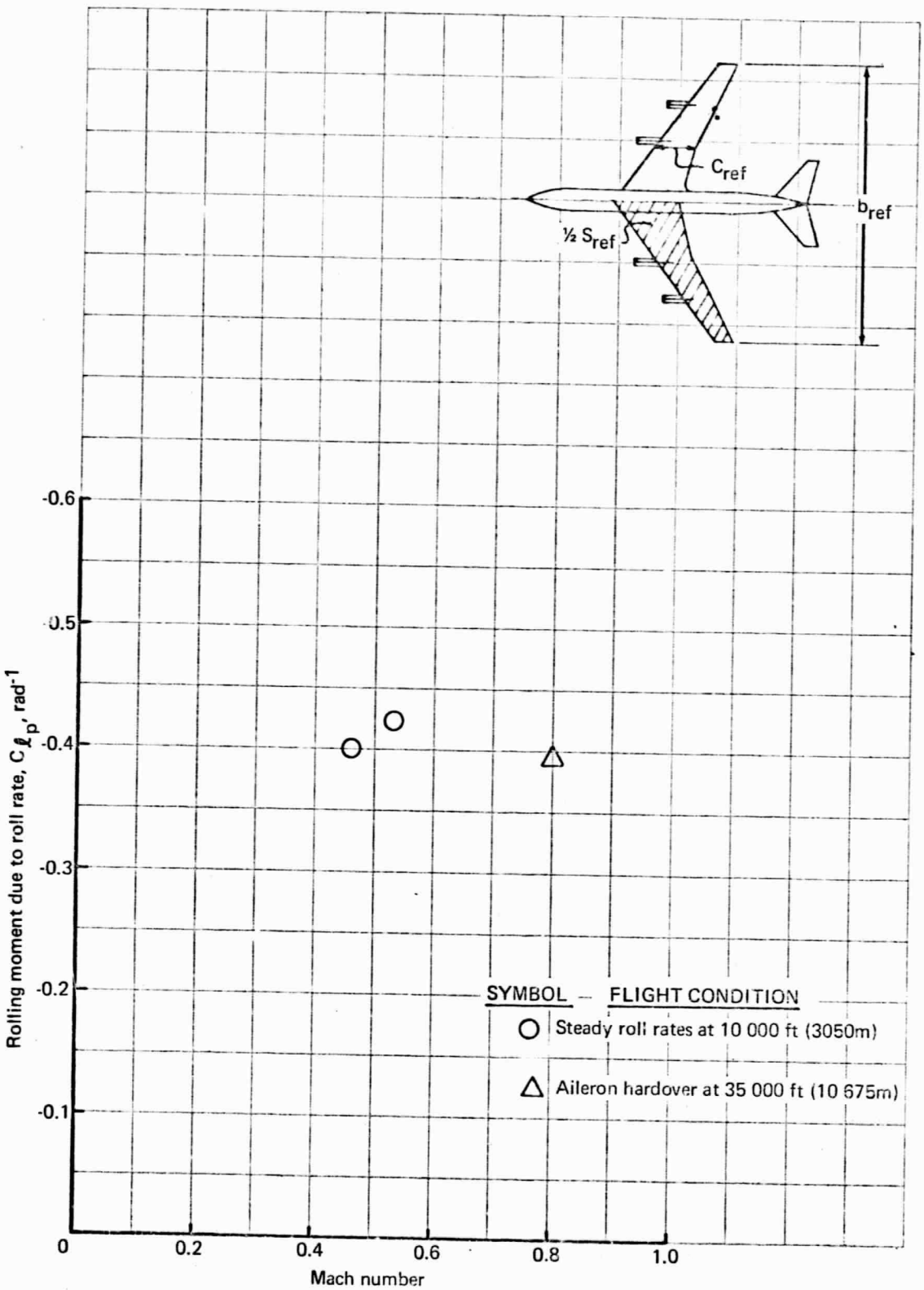

FIGURE 24.– ROLL DAMPING DERIVED FROM 707-320B FLIGHT TEST DATA

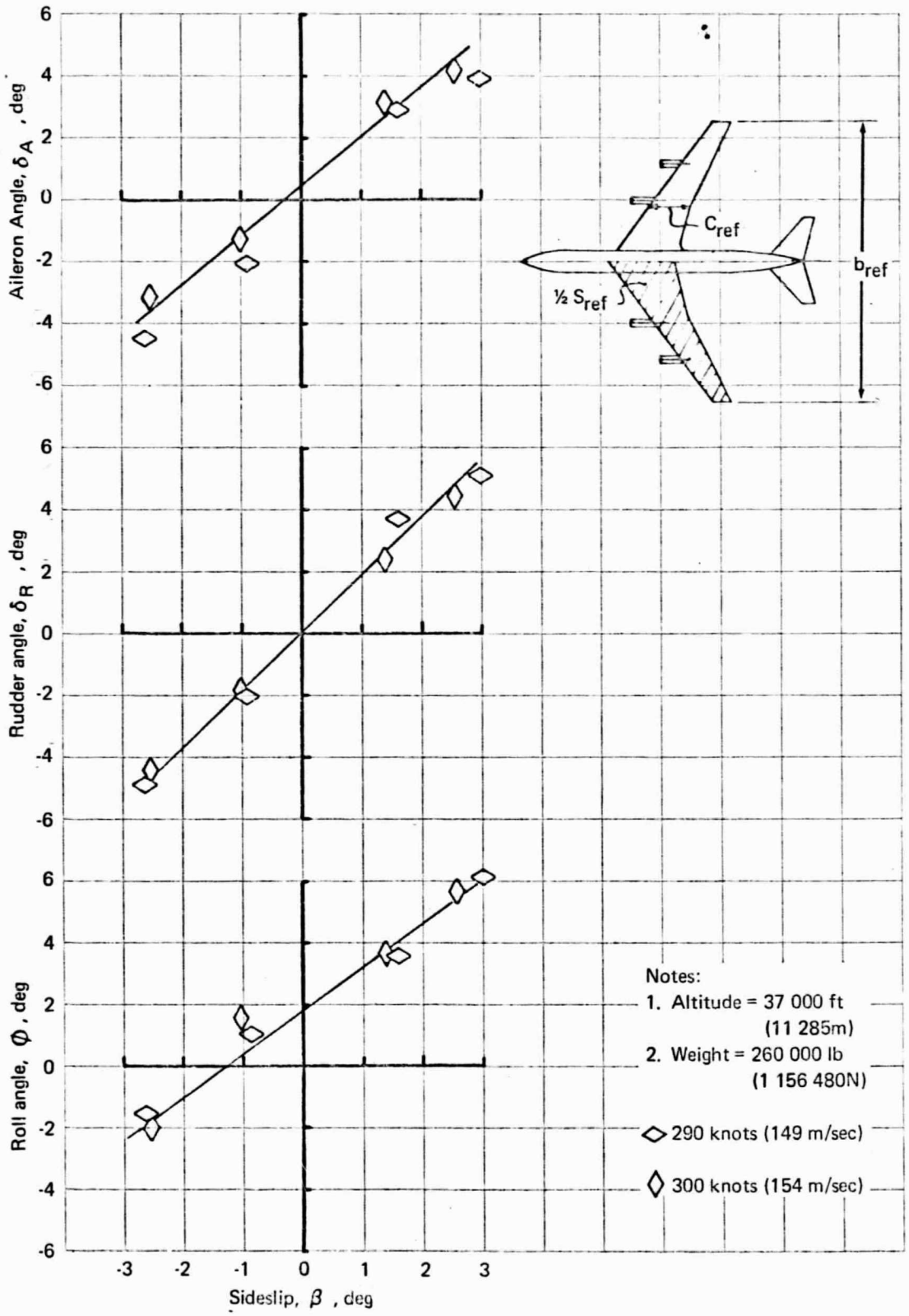

FIGURE 25.–STEADY SIDESLIP SUMMARY FOR THE 707-320B

7. COMPARISON OF METHODS

7.1 Introduction

A comparison of calculated values of stability derivatives of the 707-320B and a representative SST, evaluated by theoretical methods of Sec. 4 and semi-empirical methods of Sec. 5, has been made with experimental data measured by the methods of Sec. 6. The 707 and SST rigid wind tunnel models provide the experimental base points for the α, β, and u rigid stability derivatives. The 707 flight test certification data provide the experimental base points for the C_{L_α}, C_{m_α}, and C_{ℓ_p} elastic stability derivative estimates. Wind tunnel tests of an elastic wind tunnel model of a variable-sweep SST configuration at $\Lambda_{LE} = 72°$ provide the experimental base points for the α, β, and u elastic stability derivatives. The final results of the comparisons are presented in a qualitative fashion in tables 5 and 6 for the stability derivatives listed in table 1.1 of the introduction.

Experimental data are only available for the limited number of derivatives discussed above. Consequently, the results presented in tables 5 and 6 for derivatives that do not have accompanying experimental data are "best guesses" based on the results from available comparisons. For instance, lifting surface theory can treat the leading edge sweep discontinuity on the 30° and 42° SST cases and, thus, gives better rigid C_{L_α} values than the handbook techniques. Similar results are expected for the other rigid and elastic derivatives influenced by the leading edge sweep discontinuity.

In some cases it is not possible to calculate stability derivatives by all the theoretical and semi-empirical methods. This difficulty is also reflected in tables 5 and 6. To emphasize the problem areas encountered in lifting surface, lifting line, and the handbook techniques, tables 7, 8, and 9 were constructed. These tables outline the limitations of each technique in representing non-coplanar surfaces, thick fuselages, etc. Some areas in which "no capability exists" may, in fact, be workable if a large effort in terms of man-hours is extended. However, since this report is a comparison of techniques, such effort would not have been productive.

TABLE 5. – LONGITUDINAL STABILITY DERIVATIVES

Derivative		Lifting surface (computer) rigid and eq. elastic			Lifting line (computer) rigid and eq. elastic			Handbook rigid only			Handbook + lifting surface eq. elastic		
		Sub		Super	Sub		Super	Sub		Super	Sub		Super
		707	SST	SST	707	SST	SST	707	SST	SST	707	SST	SST
α	C_{D_α}	P	P	P	P	P		P	P				
	C_{L_α}	F	G	G	G	G		G	P	G	G	P	P
	C_{m_α}	G	P	F	F	F		P	P	G	P	P	
$\dot{\alpha}$	$C_{D_{\dot{\alpha}}}$							P	P	P			
	$C_{L_{\dot{\alpha}}}$							P	P	P			
	$C_{m_{\dot{\alpha}}}$							P	P	P			
u	C_{D_u}	P	P	P									
	C_{L_u}	G	G	G				P	P	P			
	C_{m_u}	G	G	G									
q	C_{D_q}	P	P	P									
	C_{L_q}	F	F	F				P	P	P	P	P	P
	C_{m_q}	F	F	F				P	P	F	P	P	P

G = good: method compares favorably with experiment with some exception.
F = fair: method compares favorably with experiment with exception of some M, Λ_{LE}, etc.
P = poor: method does not compare favorably with experiment.
Blank: not calculated

TABLE 6. – LATERAL-DIRECTIONAL STABILITY DERIVATIVES

Derivative		Lifting surface (computer) rigid and eq. elastic			Lifting line (computer) rigid and eq. elastic			Handbook * rigid only			Handbook + lifting surface eq. elastic		
		Sub		Super	Sub		Super	Sub		Super	Sub		Super
		707	SST	SST	707	SST	SST	707	SST	SST	707	SST	SST
β	C_{Y_β}							F	F	F			
	C_{ℓ_β}							P	P	P			
	C_{n_β}							P	F	P			
$\dot{\beta}$	$C_{Y_{\dot{\beta}}}$							P	P	P			
	$C_{\ell_{\dot{\beta}}}$							P	P	P			
	$C_{n_{\dot{\beta}}}$							P	P	P			
p	C_{Y_p}							P	P		P	P	P
	C_{ℓ_p}	F	F	F	F	F		P	P		P	P	P
	C_{n_p}							P	P		P	P	P
r	C_{Y_r}							P	P	P			
	C_{ℓ_r}							P	P	P			
	C_{n_r}							P	P	P			

G = good: method compares favorably with experiment with some exception.
F = fair: method compares favorably with experiment with exception of some M, Λ_{LE}, etc.
P = poor: method does not compare favorably with experiment.
Blank: not calculated

TABLE 7. – APPLICABILITY AND LIMITATIONS OF LIFTING SURFACE THEORY

Derivative		Thin-body formulation thickness ratio $\delta \ll \bar{c}, b/2$						Non-coplanar, thick-body formulation														
		Wing			Wing-body			non-coplanar surfaces			Thick surfaces			Thick body			W-B-HT vert tail			Wing+tail dihedral		
		Sub	Tran	Sup	Sub	Tran	Sup	Sub	Tran	Sup	Sub	Tran	Sup	Sub	Tran	Sup	Sub	Tran	Sup	Sub	Tran	Sup
α	C_{D_α} C_{L_α} C_{m_α}	√	√	√	√	√	√	√		√	√		√	√		√	√		√	N	N	N
$\dot{\alpha}$	$C_{D_{\dot{\alpha}}}$ $C_{L_{\dot{\alpha}}}$ $C_{m_{\dot{\alpha}}}$	√		√	√		√	?		?	√		√	√		√				N	N	N
u	C_{Du} C_{L_u} C_{m_u}	√		√	√		√	√		√	√		√	√		√	√		√	N	N	N
q	C_{D_q} C_{L_q} C_{m_q}	√		√	√		√	√		√	√		√	?		?	?		?	N	N	N
β	C_{Y_β} C_{ℓ_β} C_{n_β}	?		?	?		?	?		?	?		?	?		?	?		?	?		?
$\dot{\beta}$	$C_{Y_{\dot{\beta}}}$ $C_{\ell_{\dot{\beta}}}$ $C_{n_{\dot{\beta}}}$	?		?	?		?															
p	C_{Yp} C_{ℓ_p} C_{n_p}	√		√	√		√	√		√	√		√									
r	C_{Y_r} C_{ℓ_r} C_{n_r}	?		?	?		?															

Ability to calculate various flow conditions	
Flow	Capability
Compressible	Yes
Steady	Yes
Quasi-steady	Yes
Unsteady	Yes
Viscous	No
Separated	No

√ = Capability exists or can be developed from existing theory.
N = Not applicable to first-order approximations of this derivative.
Blank = No capability exists.
? = Capability may exist, but further development is required.

TABLE 8. – APPLICABILITY AND LIMITATIONS OF LIFTING-LINE THEORY

Derivative		Wing			Wing-body horz tail			Non-coplanar surfaces			Thick surfaces			Thick body			W-B-HT vert tail			Wing-tail dihedral		
		Sub	Tran	Sup	Sub	Tran	Sup	Sub	Tran	Sup	Sub	Tran	Sup	Sub	Tran	Sup	Sub	Tran	Sup	Sub	Tran	Sup
α	C_{D_α} C_{L_α} C_{m_α}	√			√			√												N	N	N
$\dot{\alpha}$	$C_{D_{\dot{\alpha}}}$ $C_{L_{\dot{\alpha}}}$ $C_{m_{\dot{\alpha}}}$	√			√			√												N	N	N
u	C_{D_u} C_{L_u} C_{m_u}	√			√			√												N	N	N
q	C_{D_q} C_{L_q} C_{m_q}	√			√			?												N	N	N
β	C_{Y_β} C_{ℓ_β} C_{n_β}	√			√			?												?		
$\dot{\beta}$	$C_{Y_{\dot{\beta}}}$ $C_{\ell_{\dot{\beta}}}$ $C_{n_{\dot{\beta}}}$	?			?			?														
p	C_{Y_p} C_{ℓ_p} C_{n_p}	?			?			?														
r	C_{Y_r} C_{ℓ_r} C_{n_r}	?			?																	

Ability to calculate various flow conditions	
Flow	Capability
Compressible	Yes
Steady	Yes
Quasi-steady	Yes
Unsteady	Yes
Viscous	No
Separated	No

√ = Capability exists or can be developed from existing theory.
N = Not applicable to first-order approximations of this derivative.
Blank = No capability exists.
? = Capability may exist, but further development is required.

TABLE 9. – APPLICABILITY AND LIMITATIONS OF THE HANDBOOK METHODS

Derivative		Wing			Wing-body			Non-coplanar surfaces			Thick surfaces			Thick body			W-B-HT vert tail			Wing+tail dihedral		
		Sub	Tran	Sup	Sub	Tran	Sup	Sub	Tran	Sup	Sub	Tran	Sup	Sub	Tran	Sup	Sub	Tran	Sup	Sub	Tran	Sup
α	C_{D_α}																					
	C_{L_α}	√	√	√	√	√	√	√	√	√	√	√	√	√	√	√	√	√	√	N	N	N
	C_{m_α}																					
$\dot{\alpha}$	$C_{D_{\dot\alpha}}$										√		√									
	$C_{L_{\dot\alpha}}$	√	√	√	√	√	√	√	√	√		√		√	√	√	√	√	√	N	N	N
	$C_{m_{\dot\alpha}}$	√	√	√	√	√	√	√	√	√	√	√	√	√	√	√	√	√	√			
u	C_{Du}																					
	C_{L_u}																			N	N	N
	C_{m_u}																					
q	C_{D_q}																					
	C_{L_q}	√	√	√	√	√	√	√	√	√		√		√	√	√	√	√	√	N	N	N
	C_{m_q}	√	√	√	√	√	√	√	√	√		√		√	√	√	√	√	√			
β	C_{Y_β}																					
	C_{ℓ_β}	√	√	√	√	√	√	√	√	√	√	√	√	√	√	√	√	√	√	√	√	√
	C_{n_β}																					
$\dot{\beta}$	$C_{Y_{\dot\beta}}$																					
	$C_{\ell_{\dot\beta}}$										√	√	√	√	√		√	√				
	$C_{n_{\dot\beta}}$																					
p	C_{Y_p}						?									?				?		?
	C_{ℓ_p}	√	√	√			√				√	√	√			√	√	√	√	√	√	√
	C_{n_p}						√									√						√
r	C_{Y_r}	?		?																?		?
	C_{ℓ_r}	√		√							√	√	√				√	√	√	√		√
	C_{n_r}	√	√	√																?		?

Ability to calculate various flow conditions	
Flow	Capability
Compressible	Yes
Steady	Yes
Quasi-steady	Yes
Unsteady	Yes
Viscous	Yes
Separated	No

√ = Capability exists.

N = Not applicable to first-order approximations of this derivative.

Blank = No capability exists.

? = Capability may exist, but further development is required.

The flight conditions considered for the 707-320B and SST rigid and elastic stability derivatives are listed in table 10. General configuration arrangement and significant dimensions are shown in figs. 26 and 27. Tables 11 through 13 contain the 707 and SST inertial properties and also list the lateral-directional inertial derivatives discussed in Sec. 4. A comparison of the inertial derivative $C_{m\ddot{\theta}_I}$ with pitch inertia is presented in table 14.

Graphical comparisons of the derivatives and stability characteristics calculated appear in figures later in this section. The methods used are noted on the plots together with any other pertinent information. The elastic data shown are functions of both Mach number and dynamic pressure. Consequently, the interconnecting lines between values for the elastic data are for visual purposes only. Interpolation for intermediate values is not possible.

7.1.1 Application of lifting surface method. —

7.1.1.1 Introduction: Matrix expressions for the determination of aerodynamic derivatives and steady-state coefficients for rigid and equivalent elastic airplanes based on aerodynamic influence coefficient theory have been derived in par. 4.2. Some of these have been presented at appropriate places in this appendix. The accomplishment of a digital program capable of calculating these stability and control parameters would improve, supplement, and streamline current techniques. The programming of all of the derivative and coefficient expressions in one package is currently in the general flow chart stage. However, some of the longitudinal parameters have already been programmed and details of some preliminary calculations (subroutines) already exist in the programs designated TA 67A and TA 176, discussed in Sec. 4.

Presentation of the following flow charts for these parameters will serve a two-fold purpose. It will illustrate both current technology and the general approach for a proposed expansion and improvement. In particular, there are three charts subsequently presented and discussed. These charts cover the general approach, the jig-shape calculation, and the derivative and coefficient package.

TABLE 10.– FLIGHT CONDITIONS FOR EVALUATION OF METHODS FOR PREDICTING STABILITY DERIVATIVES OF RIGID AND ELASTIC AIRPLANES

[a]707-320				
Altitude, ft	Dynamic pressure, $\bar{q}$, psf	Reynolds number[b] ReX 10^{-6}	Mach number	Weight, lb
10 000	66.7	31.0	0.255	268 000
	136.0	44.3	0.365	
	306.0	66.5	0.548	
35 000	223.0	43.4	0.800	
	251.0	46.1	0.850	
	283.0	48.8	0.900	

[a]SST					
Altitude, ft	Dynamic pressure, $\bar{q}$, psf	Reynolds number[c] ReX 10^{-6}	Mach number	Weight lb	Wing L. E. sweep, deg
8 500	98	265.1	0.3	370 000	30
9 500	260	413.5	0.5		
11 000	470	739.5	0.7		
32 500	98	206.9	0.5	675 000	42
26 000	260	360.5	0.7		
23 500	470	502.9	0.9		
47 500	98	147.8	0.7	668 000	72
37 000	260	314.1	0.9		
33 000	470	447.4	1.1		
30 000	750	586.9	1.3	520 000	
24 000	1300	824.9	1.5		
60 500	500	249.3	2.2		
49 000	1300	532.0	2.7		

[a]All conditions for clean airplane (gear up, flaps up)

[b]Based on C_{ref} = 22.7 ft

[c]Based on C_{ref} = 158.1 ft

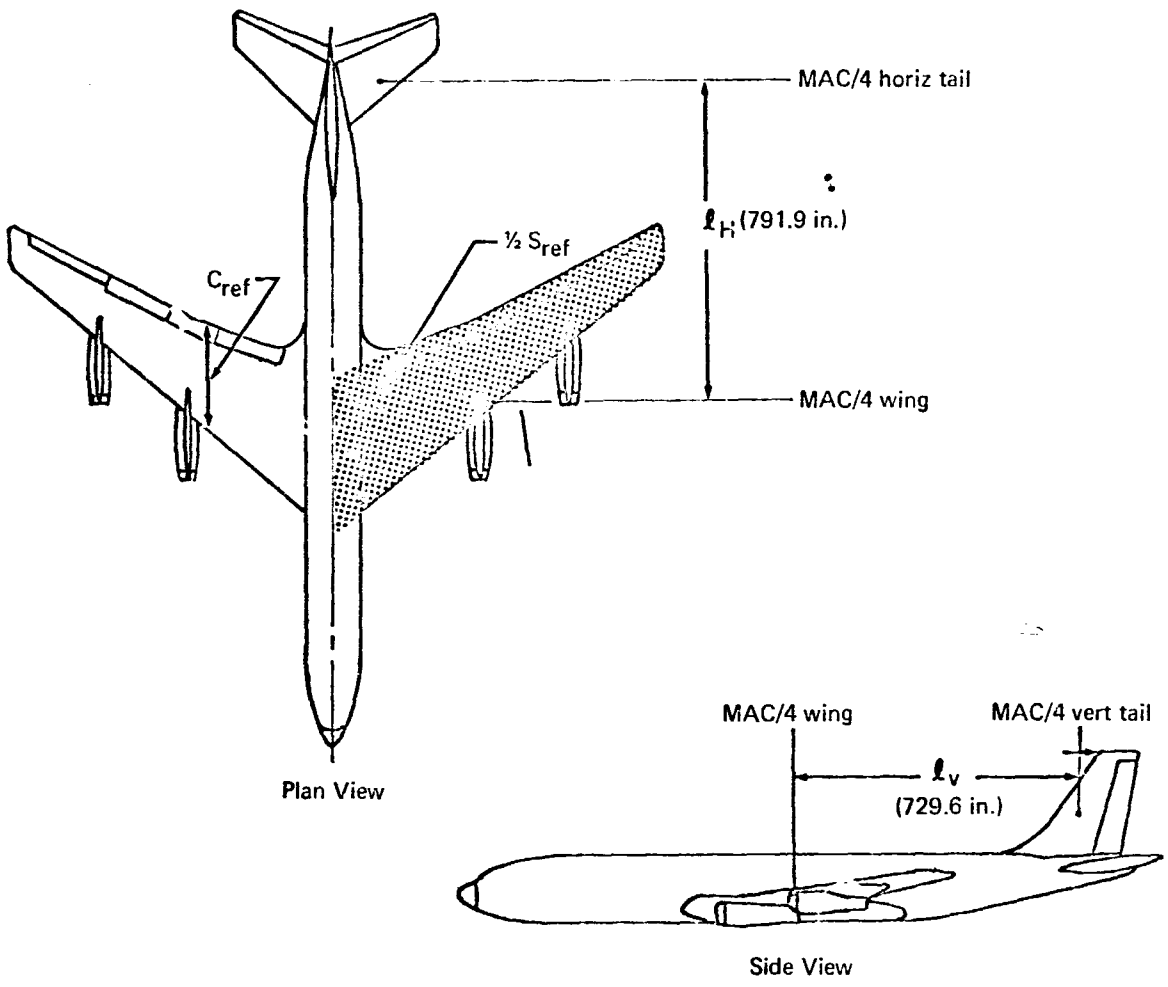

Notes:

1. L.E. sweep = 37.5 deg
2. Total wing area S_{ref} = 2892 ft^2
3. Wing span = b_{ref} = 142 ft 5 in.
4. Reference chord = C_{ref} = 272.3 in.
5. Fuselage length = 145 ft 6 in.

FIGURE 26.– BOEING MODEL 707-320B GENERAL ARRANGEMENT

Notes:

1. L.E. sweep = 72 deg (42 deg, 30 deg)
2. Reference wing area = S_{ref} = 9000 ft^2
3. Reference wing span = b_{ref} = 105.75 ft^2
4. Reference chord = C_{ref} = 1897 in.
5. Fuselage length = 306 ft 9 in.

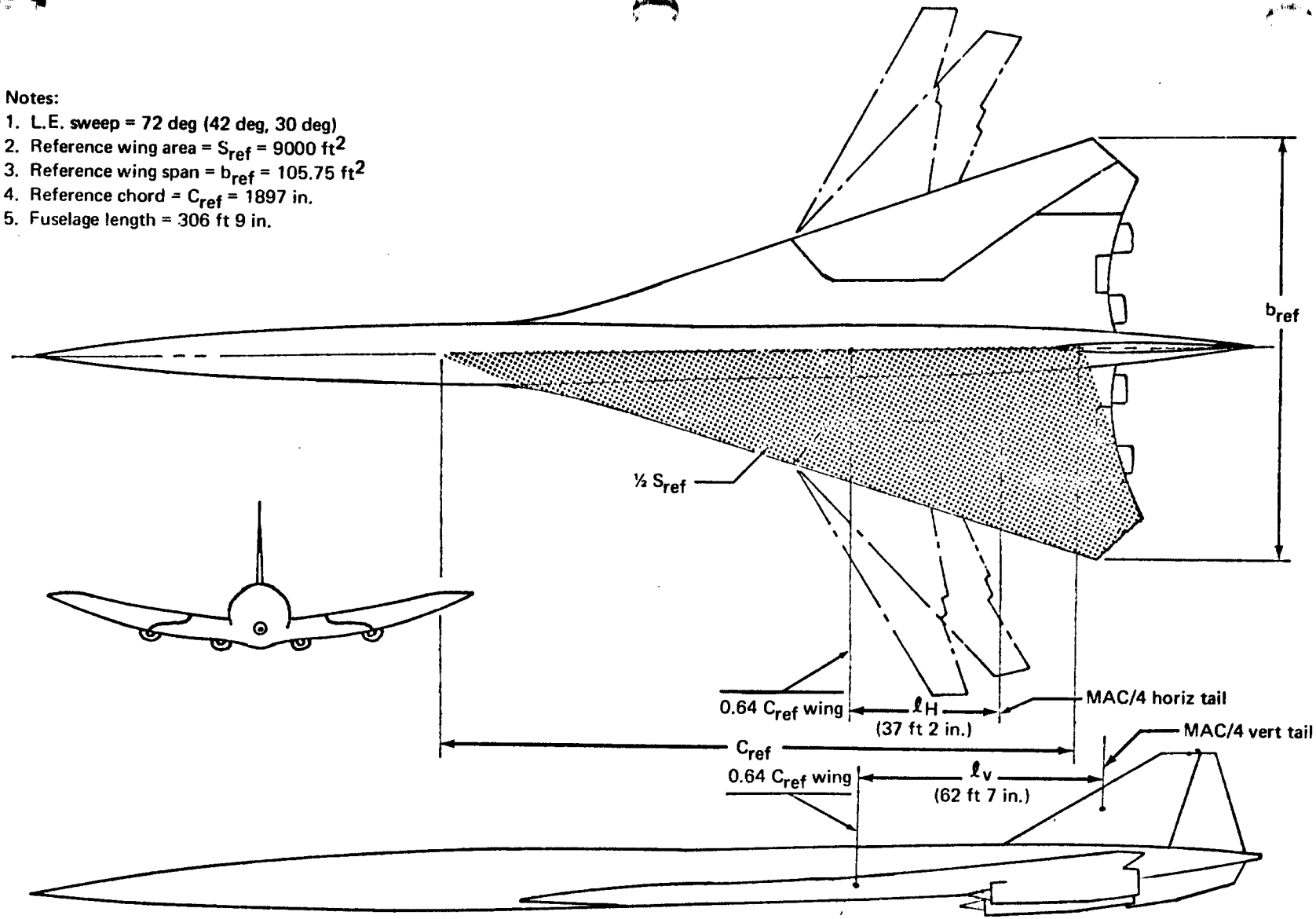

FIGURE 27.– TYPICAL SST GENERAL ARRANGEMENT

TABLE 11.–INERTIAL LATERAL-DIRECTIONAL STABILITY DERIVATIVES

707-320B b = 142 ft 5 in. = 142.42 ft*										
Mach no.		Altitude, ft*	W, lb*	M, slugs*	I_{XX}, slug ft^{2*}	I_{ZZ}, slug ft^{2*}	I_{XZ}, slug ft^{2*}	$C_{Y_{\dot{Y}_I}}$, sec^2/ft*	$M\text{-}C_{Y_{\dot{Y}_I}}\frac{qS_w}{}$	$\frac{qS_w}{}$ slugs*
0.255		10 000	268 000	8335	5.1156 x 10^6	9.7094 x 10^6	-2.1412 x 10^6	0.463 x 10^{-4}	1.928 x 10^5	8316
0.365		↓	↓	↓	4.9362	9.888	-0.8375	0.421	3.931	8308
0.548		↓	↓	↓	4.9167	9.9083	-0.1098	0.368	8.850	8292
0.800		35 000	↓	↓	4.9162	9.9088	-0.2127	0.385	6.434	8300
0.850		↓	↓	↓	4.9166	9.9084	-0.1203	0.371	7.259	8298
0.900		↓	↓	↓	4.9176	9.9074	-0.0361	0.278	8.183	8302
Λ_{LE}, deg	Mach no.	SST b = 105 ft 9 in.= 105.75 ft*								
30	0.3	8 500	370 000	11 491	4.9866	45.3234	-5.6898	-0.1793	8.813	11 475
↓	0.5	9 500	↓	↓	4.3427	45.9673	-2.4590	-0.1768	23.41	11 450
↓	0.7	11 000	↓	↓	4.2696	46.0404	-1.7184	-0.1763	42.30	11 416
42	0.5	32 500	675 000	20 963	14.6202	62.2798	-16.2639	-0.4025	8.813	20 928
↓	0.7	26 000	↓	↓	10.6123	66.2095	-7.5797	-0.4000	23.41	20 869
↓	0.9	23 000	↓	↓	10.0487	66.8513	-5.0754	-0.3901	42.30	20 798
72	0.7	47 500	668 000	20 745	16.8382	44.2118	-19.9762	-0.4019	8.813	20 710
↓	0.9	37 000	↓	↓	8.3694	52.6806	-9.7710	-0.3934	23.41	20 653
↓	1.1	33 000	↓	↓	7.1713	53.8787	-6.3966	-0.5875	42.30	20 496
↓	1.3	30 000	520 000	16 149	4.2488	49.5112	-3.9125	-0.5190	67.50	15 799
↓	1.5	24 000	↓	↓	4.1026	49.6574	-2.9417	-0.4854	117.03	15 581
↓	2.2	60 000	↓	↓	4.2771	49.4829	-4.0718	-0.4915	67.50	15 817
↓	2.7	49 000	↓	↓	4.1493	49.6107	-3.2852	-0.4495	117.03	15 623

*1 ft = 0.305m; 1 lb = 4.448N; 1 slug = 14.594 kg; 1 slug-ft^2 = 1.355 kg-m^2
1 sec^2/ft = 3.281 sec^2/m

TABLE 12. – INERTIAL LATERAL-DIRECTIONAL STABILITY DERIVATIVES

707-320B b = 142 ft 5 in. = 142.42 ft*										
Mach no.	Altitude, ft*	$C_{Y_{\dot{p}_I}}$, sec^2/rad	$C_{Y_{\dot{r}_I}}$, sec^2/rad	$C_{\ell_{\dot{Y}_I}}$, sec^2/ft*	$C_{\ell_{\dot{p}_I}}$ sec^2/rad	$I_{XX}-C_{\ell_{\dot{p}_I}}\bar{q}S_W$		$C_{\ell_{\dot{r}_I}}$, sec^2/rad	$I_{xz}+C_{\ell_{\dot{r}_I}}\bar{q}S_W b$, slug ft^{2*}
						$\bar{q}S_W b$	slug ft^{2*}		
0.255	10 000	0.382 x 10^{-3}	-0.234 x 10^{-2}	.894 x 10^{-6}	0.74 x 10^{-5}	2.746 x 10^7	5.1154 x 10^6	-0.452 x 10^{-4}	-2.1424 x 10^6
0.365		0.101	-0.213	3.05	0.73	5.599	4.9358	-1.545	-0.8462
0.548		-0.050	-0.187	3.98	-0.54	12.603	4.9174	-2.025	-0.1353
0.800	35 000	-0.046	-0.192	3.76	-0.45	9.163	4.9166	-1.876	-0.2299
0.850		-0.075	-0.185	3.80	-0.77	10.338	4.9174	-1.894	-0.1399
0.900		-0.147	-0.134	2.94	-1.56	11.655	4.9194	-1.419	-0.0526
Λ_{LE}, deg	Mach no.	SST b = 105 ft 9 in. = 105.75 ft*							
30	0.3	8 500	0.6389	-0.07616	1.241	-6.167	9.320	4.9923	-0.4407	-5.6939
	0.5	9 500	0.6995	-0.07601	2.112	-10.323	24.752	4.3683	-0.8242	-2.4794
	0.7	11 000	0.6969	-0.07704	1.685	-11.10	44.734	4.3193	-0.9313	-1.7601
42	0.5	32 500	0.4319	-0.20878	4.300	-0.2406	9.320	14.6204	0.3654	-16.2605
	0.7	26 000	0.6323	-0.20821	3.210	-6.3541	24.752	10.6280	-1.6072	-7.6195
	0.9	23 000	0.6712	-0.20808	4.232	-8.6921	44.734	10.0876	-2.1383	-5.1711
72	0.7	47 500	0.2125	-0.20409	-5.218	2.4502	9.320	16.8359	3.2796	-19.9456
	0.9	37 000	0.5323	-0.49928	1.029	-2.4639	24.752	8.3755	-0.4482	-9.7821
	1.1	33 000	0.7147	-0.30715	2.275	-5.5368	44.734	7.1961	-1.0220	-6.4423
	1.3	30 000	1.7207	-0.22015	2.569	-16.831	71.377	4.3689	-0.9991	-3.9838
	1.5	24 000	1.5231	-0.21214	3.077	-16.722	123.758	4.3095	-1.3112	-3.1040
	2.2	60 000	1.6113	-0.21623	3.115	-16.723	71.377	4.3965	-1.3528	-4.1683
	2.7	49 000	1.4496	-0.20214	3.584	-16.825	123.758	4.3575	-1.6245	-3.4862

*1 ft = 0.305m; 1 slug-ft^2 = 1.355 kg-m^2; 1 sec^2/ft = 3.281 sec^2/m

TABLE 13.–INERTIAL LATERAL-DIRECTIONAL STABILITY DERIVATIVES

707-320B b = 142 ft 5 in. = 142.42 ft*							
Mach no.		Altitude, ft*	$C_{n_{\dot{Y}_I}}$, sec^2/ft*	$C_{n_{\dot{r}_I}}$, sec^2/rad	$I_{zz}-C_{n_{\dot{r}_I}}\bar{q}S_w b$, slug ft^{2*}	$C_{n_{\dot{p}_I}}$, sec^2/rad	$I_{xz}+C_{n_{\dot{p}_I}}\bar{q}S_w b$, slug ft^{2*}
0.255		10 000	-1.98 x 10^{-5}	0.999 x 10^{-3}	9.6820 x 10^6	-1.63 x 10^{-4}	-2.1457 x 10^6
0.365		↓	-1.80	0.909	9.8379	-0.431	-0.8399
0.548		↓	-1.57	0.798	9.8077	+0.213	-0.1071
0.800		35 000	-1.64	0.820	9.8337	+0.196	-0.2109
0.850		↓	-1.58	0.790	9.8267	+0.320	-0.1170
0.900		↓	-1.19	0.572	9.8407	+0.628	-0.0288
Λ_{LE}, deg	Mach no.	SST b = 105 ft 9 in. = 105.75 ft*					
30	0.3	8 500	-1.112	0.4796	45.2787	3.821	-5.6542
↓	0.5	9 500	-1.098	0.4786	45.8488	4.182	-2.3555
↓	0.7	11 000	-1.094	0.4846	45.8236	4.168	-1.5319
42	0.5	32 500	-2.473	1.2883	62.1597	2.590	-16.2398
↓	0.7	26 000	-2.458	1.2848	65.8915	3.781	-7.4861
↓	0.9	23 000	-2.400	1.2543	66.2902	4.014	-4.8958
72	0.7	47 500	-2.470	1.2600	44.0944	1.283	-19.9[illegible]2
↓	0.9	37 000	-2.419	1.2315	52.3758	3.187	-9.692
↓	1.1	33 000	-3.768	1.9841	52.9911	4.359	-6.2016
↓	1.3	30 000	-3.424	1.4598	48.4692	10.676	-3.7505
↓	1.5	24 000	-3.209	1.4051	47.9185	9.501	-1.7659
↓	2.2	60 000	-3.184	1.4022	48.4821	9.915	-3.3640
↓	2.7	49 000	-2.895	1.3006	48.0011	8.911	-2.1824

*1 ft = 0.305m; 1 slug-ft^2 = 1.355 kg-m^2; 1 sec^2/ft = 3.281 sec^2/m

TABLE 14.–COMPARISON OF $C_{m_{\ddot{\theta}_I}}$ DERIVATIVE WITH PITCH INERTIA

707-320B			
Mach no.	Altitude, ft	I_{yy}, 10^6 slug ft^2 (approximate)	$\frac{\lvert C_{m_{\ddot{\theta}_I}} \rvert}{I_{yy}/\bar{q}S_w\bar{C}}$
0.255	10 000	5.025	0.027
0.365	↓	↓	0.052
0.548	↓	↓	0.105
0.800	35 000	↓	0.094
0.850	↓	↓	0.106
0.900	↓	↓	0.121

SST					
Mach no.	Altitude, ft	Gross weight, lb	Wing sweep deg	I_{yy}, 10^6 slug ft^2 (approximate)	$\frac{\lvert C_{m_{\ddot{\theta}_I}} \rvert}{I_{yy}/\bar{q}S_w\bar{C}}$
0.3	8 500	370 000	30	40.2	0.0080
0.5	9 600	↓	↓	↓	0.0248
0.7	11 000	↓	↓	↓	0.0217
0.5	32 500	675 000	42	47.2	0.0050
0.7	26 000	↓	↓	↓	0.0125
0.9	23 500	↓	↓	↓	0.0198
0.7	47 500	668 000	72	48.3	0.0020
0.9	37 000	↓	↓	↓	0.0031
1.1	33 000	↓	↓	↓	0.0097
1.3	30 000	520 000	↓	47.6	0.0425
1.5	24 000	↓	↓	↓	0.182
2.2	60 500	↓	↓	↓	0.0939
2.7	49 000	↓	↓	↓	0.263

7.1.1.2 The general flow chart: Figure 28 presents a general flow chart that illustrates a proposed aerodynamic derivative and coefficient calculation program based on aerodynamic and structural influence coefficient theory. The top three boxes, and the bottom one not included in the dashed box, do not represent new concepts in the influence coefficient approach since they are in current use for some of the longitudinal coefficients and derivatives. Implicit in this representation is the calculation of both aerodynamic and structural influence coefficient matrices. Concepts foreign to current programs, enclosed in the dashed box, are the internal calculation of inertias and slopes of aerodynamic influence coefficients. Also, there will be the addition of some additional longitudinal and lateral-directional parameters.

7.1.1.3 Jig shape calculation flow chart: As a preliminary step to the calculation of the final steady-stage shape for an arbitrary flight condition, it is necessary to determine the initial unloaded shape. This unloaded shape has been conventionally called the jig shape. A flow chart illustrating the general approach to this problem is given in fig. 29.

The first set of boxes (those on the left under the general heading "Design point airplane") are only necessary for the jig-shape calculations or for "rigid" airplane calculations ("rigid" in this sense may refer to the cruise shape that usually defines the so-called "rigid" wind tunnel model). It is of particular importance to note that virtually any shape or paneling can be input by the geometry input and, therefore, a variety of known shapes can be handled. At this time, only detailed data, such as the mass distribution (designated A), can be conveniently used in subsequent derivative and coefficient calculations.

The second set of boxes, under the heading "Detailed geometry calculations," is self-explanatory. These items are to be used in subsequent calculations directly associated with derivatives or coefficients and are numbered (1) and (2). The calculations in (1) are associated with subsequent calculation of aerodynamic influence coefficients for any flight condition. They are items such as panel leading edge and trailing edge sweep angles, local edge lengths, local chord lengths, local thickness distribution, etc. Those in (2) are used for "rigid" airplane calculations later. The remaining box contains "Panel centroid coordinates." Currently, these values do not have much value beyond the jig-shape calculations.

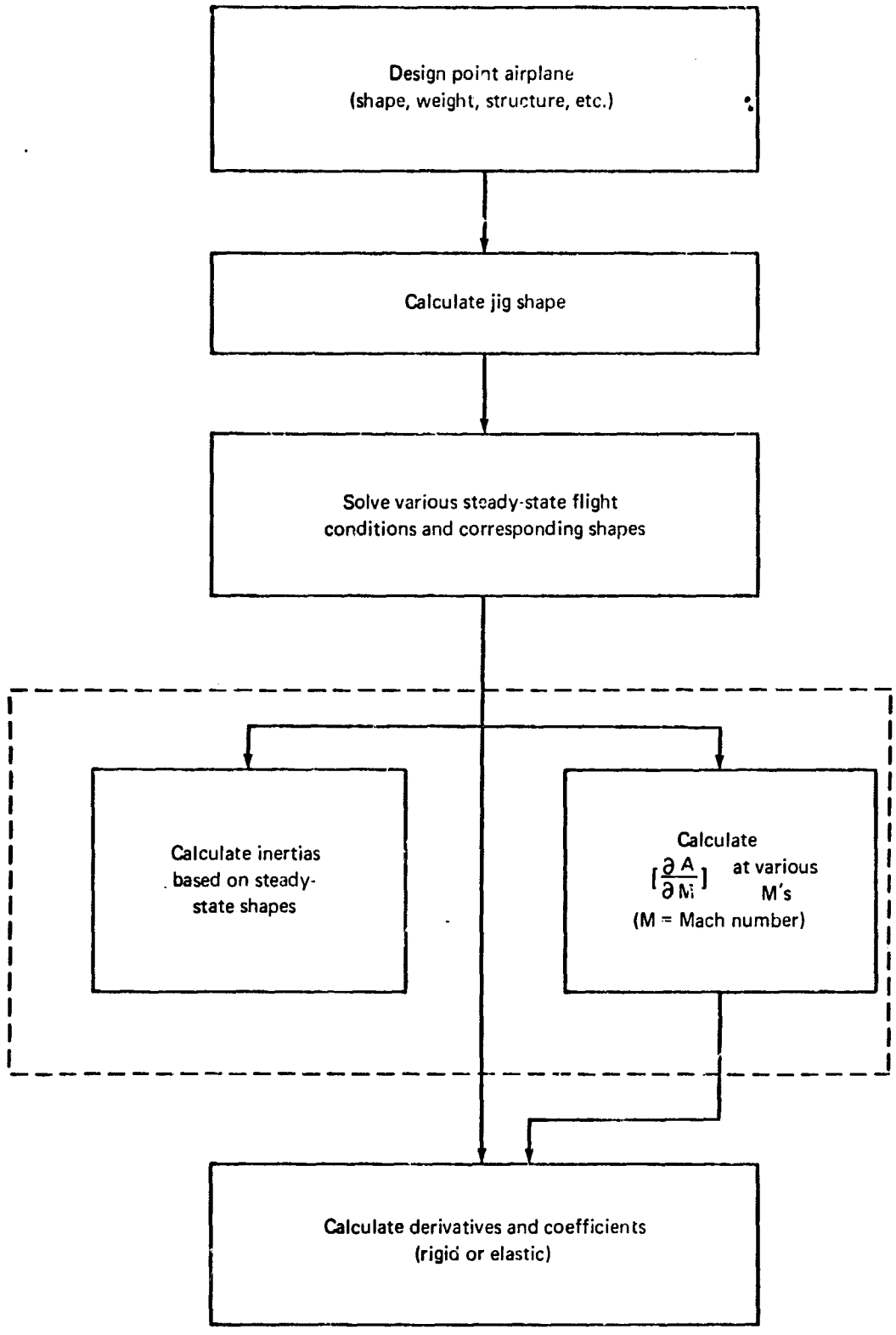

FIGURE 28.– GENERAL FLOW CHART FOR DERIVATIVE PROGRAM

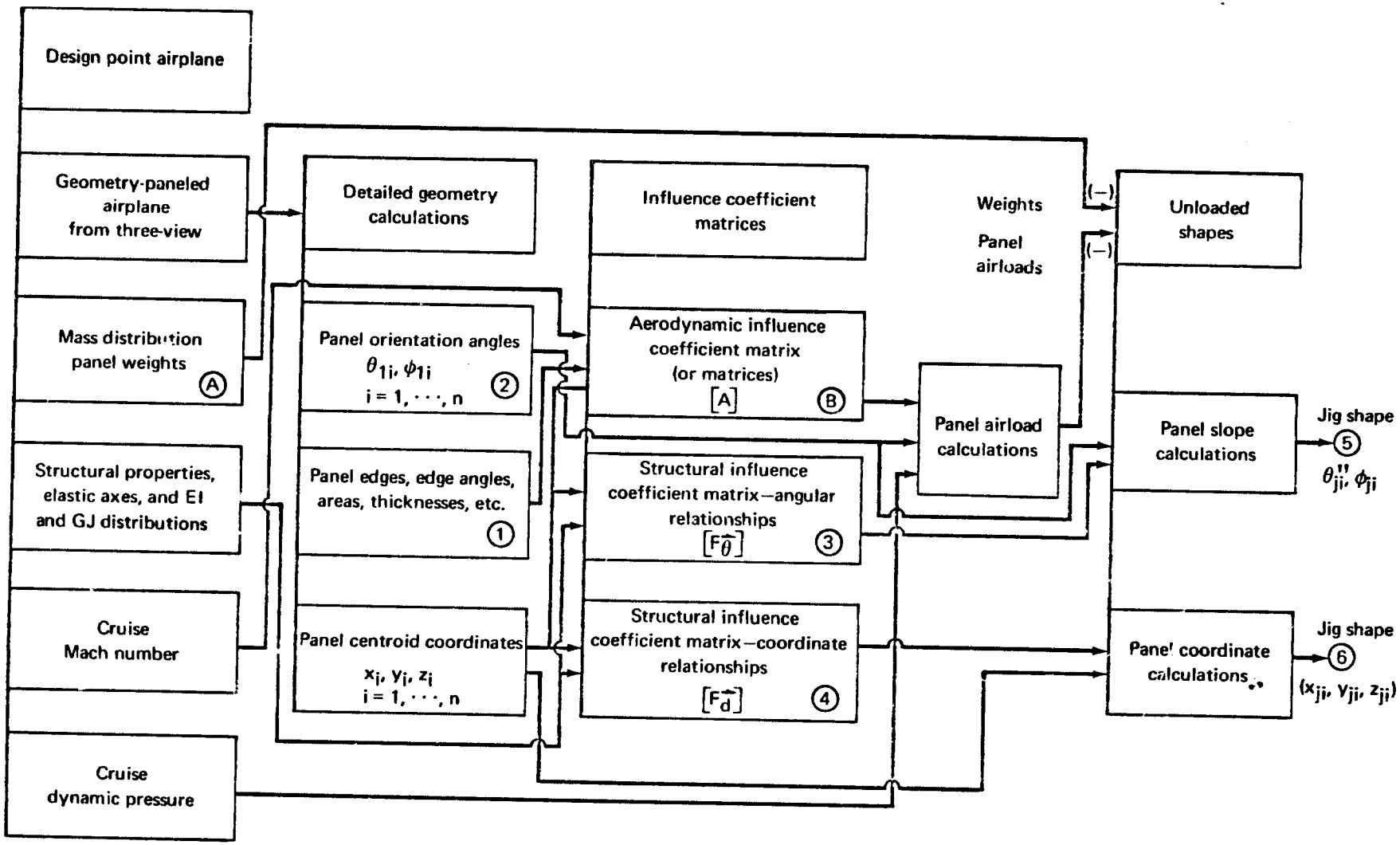

FIGURE 29.– FLOW CHART FOR DERIVATIVE CALCULATIONS (JIG SHAPE CALCULATIONS)

The "Influence coefficients" are indicated in the third set of boxes. The aerodynamic influence coefficient matrix, [A], has been labeled with a (B) because it can be used to solve other problems at the same Mach number. The structural influence coefficient matrices $[F_{\vec{\theta}}]$ and $[F_{\vec{d}}]$, labeled (3) and (4) respectively, can be used for any other problem involving the same structure and paneling. The flexibility matrix $[F_{\vec{\theta}}]$ relates the changes in panel slopes due to unit loads, and $[F_{\vec{d}}]$ relates the changes in centroid coordinates (x_i, y_i, z_i) due to unit loads. More precise and detailed definitions for influence coefficient matrices have been given in app. A and at other points herein for the longitudinal problem. Detailed definitions of these matrices for lateral-directional cases have not been developed.

The next step is to generate the panel airloads based on the design-point shape. This is labeled "Panel airload calculations" and the techniques for the longitudinal case have been covered in Sec. 4. Some of the lateral-directional details have been attacked from the theoretical viewpoint in Sec. 4.

Finally, the two unloaded jig shapes are calculated in terms of panel slopes and centroid locations in the last two boxes. As indicated by the "Unloaded shape" titles and the (-) signs applied to weights and air loads, the jig shape is determined by subtracting the mass and airload in such a way that the airplane returns (unloads/relaxes) to its hypothetical jig shape. The slopes and locations marked (5) and (6) on the output are then available for subsequent analyses and are applicable to all other flight conditions, provided the structure and paneling are not changed.

This completes the general approach to jig-shape calculations. The next general set of calculations are those directly associated with the steady-state coefficients and aerodynamic derivatives.

7.1.1.4 Aerodynamic derivative and steady-state-coefficient flow chart: The general approach to calculating aerodynamic derivatives and steady-state coefficients is illustrated in the flow chart of fig. 30. There are two general paths traced: one solid for equivalent elastic parameters and one dashed for rigid parameters. Note that items (1) through (6) and (A) and (B) from the jig-shape calculations (fig. 29) are applicable in these calculations and appropriately noted in fig. 30. For each Mach number variation from the

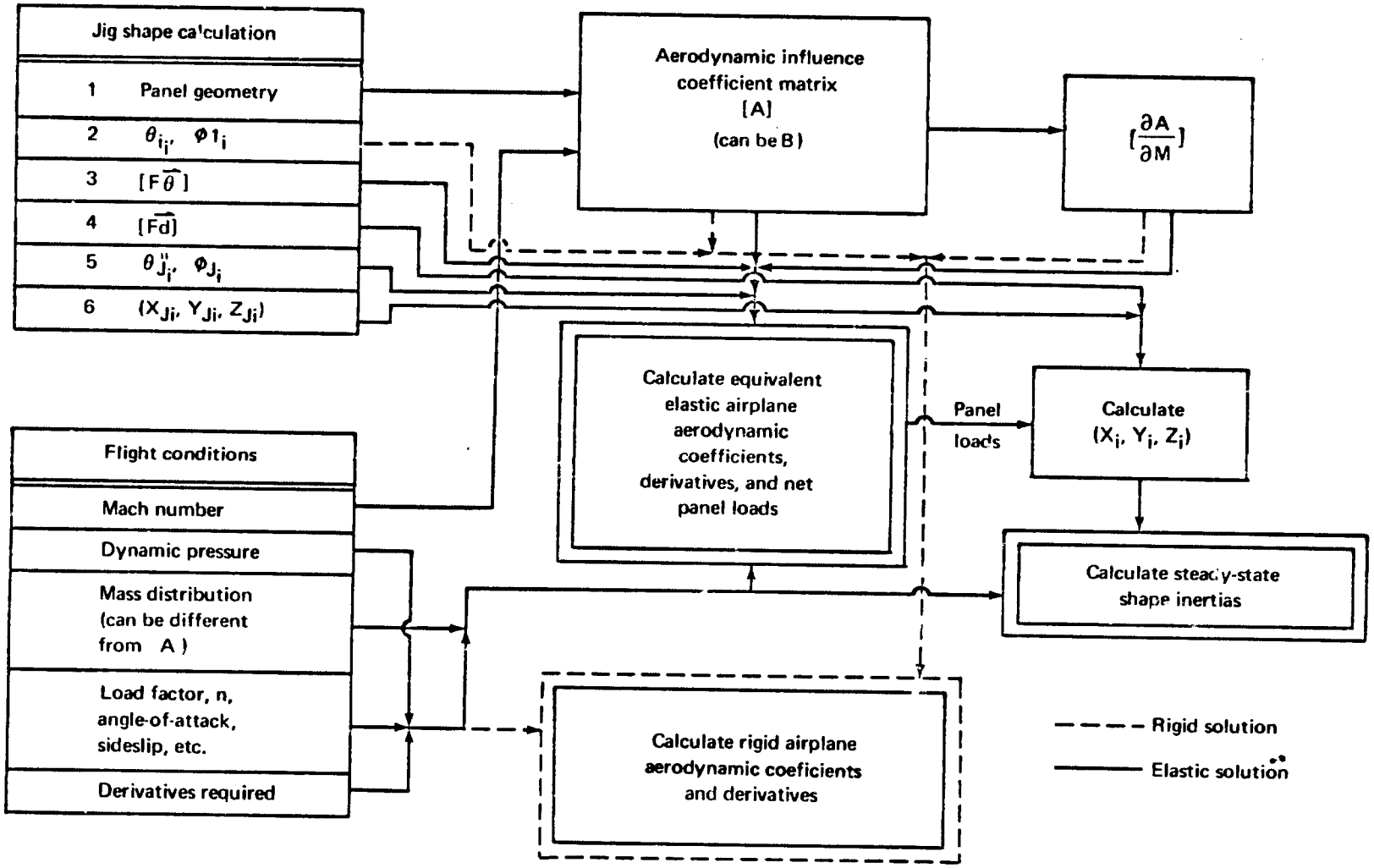

FIGURE 30.– FLOW CHART FOR DERIVATIVE CALCULATIONS (AERODYNAMIC COEFFICIENT AND DERIVATIVE CALCULATIONS)

design-point airplane a new [A] matrix and a $\left[\frac{\partial A}{\partial M}\right]$ matrix must be calculated. Using these and the other items indicated in fig. 30, the rigid or equivalent-elastic aerodynamic derivatives and steady-state coefficients can be calculated. Also, as indicated, the steady-state shape inertias can be calculated using the the net panel loads and $[\overline{F_d}]$ to determine the mass locations (panel centroid coordinates, x_i, y_i, z_i).

It should be noted that the flow charts presented in this section are to illustrate the general approach to the calculation of aerodynamic derivatives and steady-state coefficients. Implementation of these parameters in the form of a digital program, and the details thereof, are areas for future study.

Figures 31 through 34 show the geometric paneling scheme used in the TA 67A program to represent the 707 and SST to the inviscid flow field. The rigid and elastic stability derivatives noted in table 1 were calculated by this scheme.

7.1.2 Application of the lifting line method. — Lifting line theory was discussed in Sec. 4. As noted, programming limitations in the computer program (designated as TS 70 in this report) permit only C_{L_α} and C_{m_α} to be calculated. Additionally, program TS 70 can treat only subsonic cases and cannot be applied to irregular planforms such as occur for a variable-sweep SST design. Consequently, TS 70 was used to analyze the rigid values of C_{L_α} and C_{m_α} for the 707-320B and not the SST. It serves primarily as a check of the lifting surface and handbook methods.

Table 15 contains the formulas used to calculate the rigid values of C_{L_α} and C_{m_α} for the 707-320B by the lifting line method.

7.1.3 Application of the handbook methods. — The values of the stability derivatives for the 707-320B and the SST were calculated using the formulas of Sec. 5 and the various handbook methods presently available. The results are summarized in Tables 16 through 29. The longitudinal stability derivatives were calculated by the methods contained in ref. 6 and ref. 67. The appropriate formulas from that reference are listed in table 16 and 17 for the rigid and equivalent elastic mathematical models of the elastic airplane. The numbers below each term refer to the section in ref. 6 that was used to calculate that term.

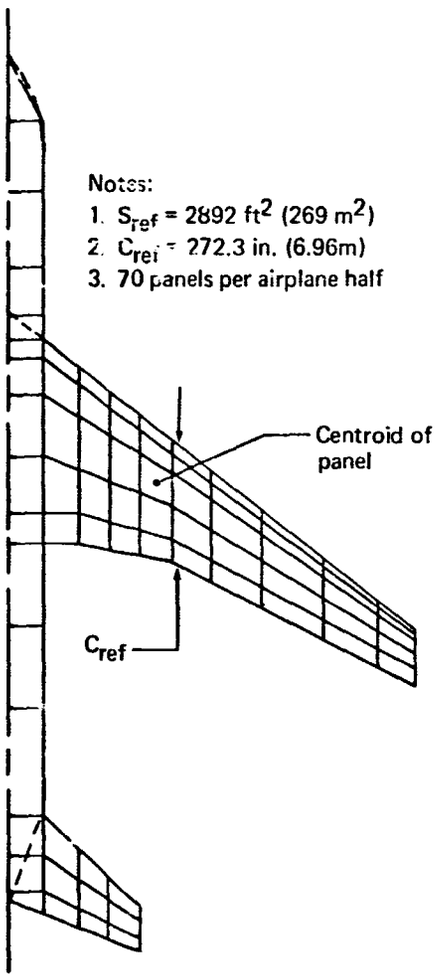

FIGURE 31.– PANELING FOR BOEING 707-320B

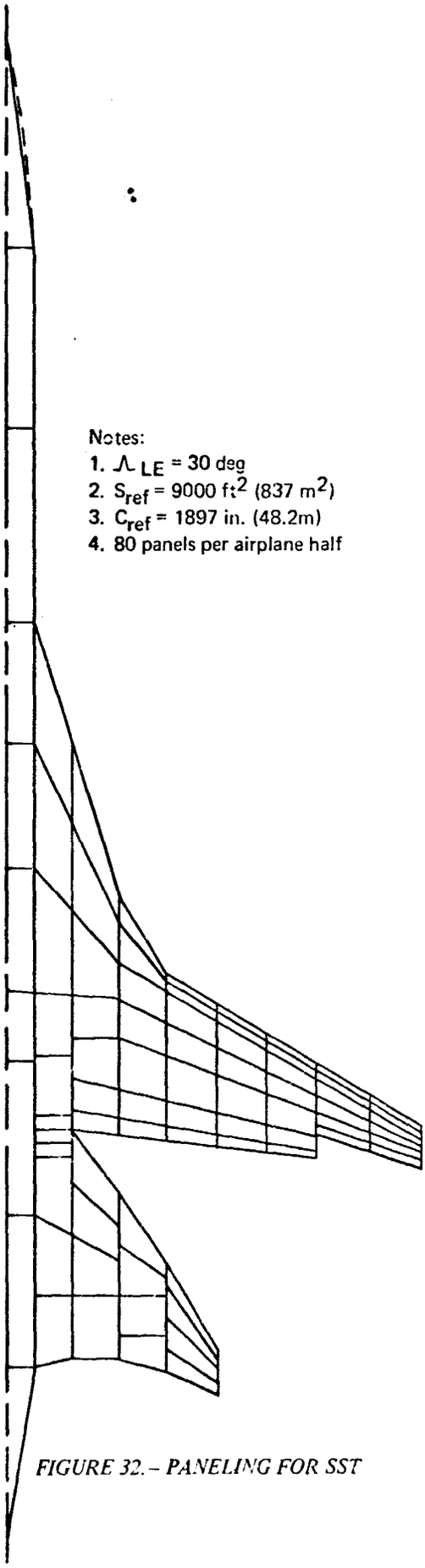

FIGURE 32.– PANELING FOR SST

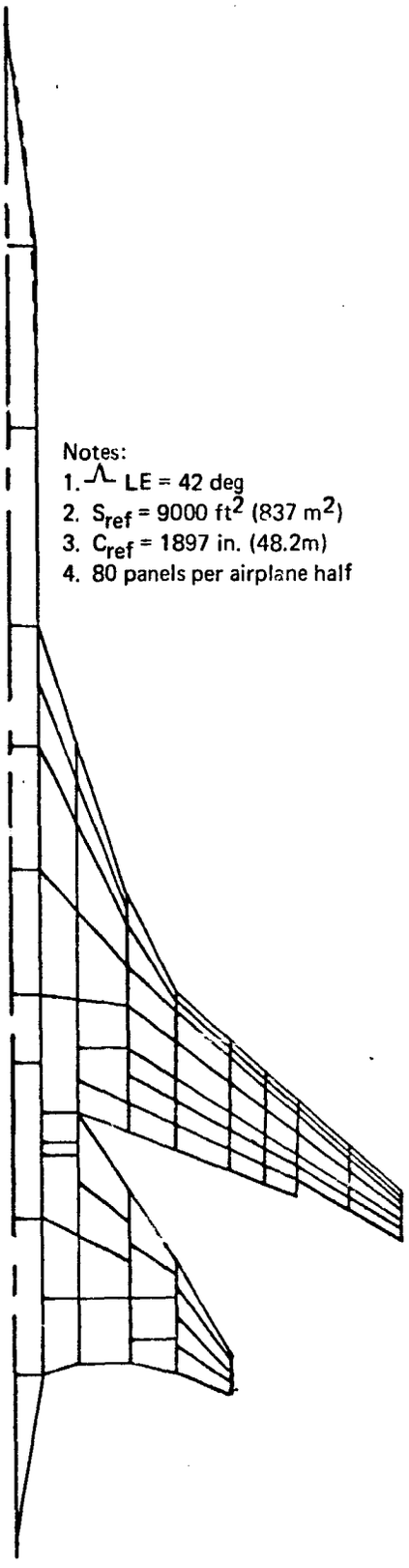

FIGURE 33.– PANELING FOR SST

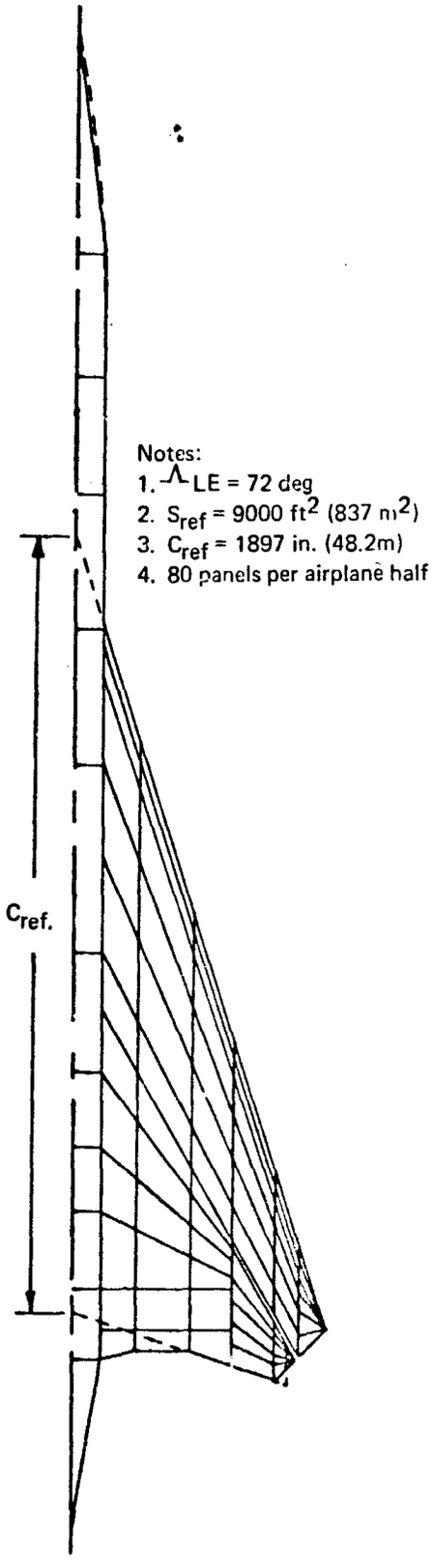

FIGURE 34.–PANELING FOR SST

TABLE 15.–CALCULATION OF STABILITY DERIVATIVES BY THE LIFTING LINE METHOD

$$C_{L_\alpha}\Big|_{\text{tail-on}} = \underbrace{C_{L_\alpha}\Big|_{\text{tail-off}}}_{\text{TS-70}} + \frac{S_H}{S_W}\underbrace{C_{L_{\alpha_H}}\left(1 - \frac{\partial \epsilon}{\partial \alpha}\right)}_{\text{Ref. 6}}$$

$$C_{m_\alpha}\Big|_{\text{tail-on}} = \underbrace{C_{m_\alpha}\Big|_{\text{tail-off}}}_{\text{TS-70}} - \underbrace{\bar{V}_H\, C_{L_{\alpha_H}}\left(1 - \frac{\partial \epsilon}{\partial \alpha}\right)}_{\text{Ref. 6}}$$

TABLE 16. – LONGITUDINAL HANDBOOK DERIVATIVES (RIGID)

Equations from the USAF Stability and Control Handbook

$$\underbrace{C_{L_\alpha}}_{4.5.1.1} = \underbrace{(C_{L_\alpha})'_e}_{4.1.3.2} \underbrace{\left[K_W + K_{W(B)} + K_{B(W)}\right]'}_{4.3.1.2} \frac{S'_e}{S'} + \underbrace{(C_{L_\alpha})''_e}_{4.1.3.2} \underbrace{\left[K_{W(B)} + K_{B(W)}\right]''}_{4.3.1.2} B$$

$$\underbrace{C_{m_\alpha}}_{4.5.2.1} = -\left(\frac{x_{c.g.} - x'}{\bar{c}'}\right)\left[K_W + K_{W(B)} + K_{B(W)}\right]'(C_{L_\alpha})'_e \frac{S'_e}{S'} - \left(\frac{x_{c.g.} - x''}{\bar{c}'}\right)\left[K_{W(B)} + K_{B(W)}\right]''(C_{L_\alpha})''_e B \frac{\bar{c}''}{\bar{c}'}$$

where $B = \underbrace{\left(1 - \frac{\partial \epsilon}{\partial \alpha}\right)}_{8.1.1} \underbrace{\frac{q''}{q_\infty}}_{4.4.1} \frac{S''}{S'} \frac{S''_e}{S''}$

$$\underbrace{C_{L_{\dot\alpha}}}_{7.4.4.1} = \underbrace{(C_{L_{\dot\alpha}})_{WB}}_{7.3.4.1} + 2\left[K_{W(B)} + K_{B(W)}\right]''\frac{S''_e}{S'_e}\left(\frac{x_{c.g.} - x''}{\bar{c}'}\right)\frac{q''}{q_\infty}\frac{\partial \epsilon}{\partial \alpha}(C_{L_\alpha})''_e$$

$$\underbrace{C_{m_{\dot\alpha}}}_{7.4.4.2} = \underbrace{(C_{m_{\dot\alpha}})_{WB}}_{7.3.4.2} - 2\left[K_{W(B)} + K_{B(W)}\right]''\frac{S''_e}{S'}\left(\frac{x_{c.g.} - x''}{\bar{c}'}\right)^2\frac{q''}{q_\infty}\frac{\partial \epsilon}{\partial \alpha}(C_{L_\alpha})'_e$$

$$\underbrace{C_{L_q}}_{7.4.1.1} = \underbrace{(C_{L_q})_{WB}}_{7.3.1.1} + 2\left[K_{W(B)} + K_{B(W)}\right]''\frac{S''_e}{S'}\left(\frac{x_{c.g.} - x''}{\bar{c}'}\right)\frac{q''}{q_\infty}(C_{L_\alpha})''_e$$

$$\underbrace{C_{m_q}}_{7.4.1.2} = \underbrace{(C_{m_q})_{WB}}_{7.3.1.2} - 2\left[K_{W(B)} + K_{B(W)}\right]''\frac{S''_e}{S'}\left(\frac{x_{c.g.} - x''}{\bar{c}'}\right)^2\frac{q''}{q_\infty}(C_{L_\alpha})''_e$$

$$\underbrace{C_{L_{\delta_E}}}_{6.1.4.1} = \underbrace{\Delta C_l}_{6.1.1.1}\underbrace{\left(\frac{C_{L_\alpha}}{C_{l_\alpha}}\right)}_{4.1.1.2}\underbrace{\left[\frac{(a_\delta)_{C_L}}{(a_\delta)_{C_l}}\right]}_{6.1.1.1}\underbrace{K_b}_{6.1.4.1\text{-}2b} \qquad \underbrace{C_{m_{\delta_E}}}_{6.1.5.1} = -\frac{l''}{\bar{c}'}C_{L_{\delta_E}}$$

where

$$l'' = x_{c.g.} - x_{\frac{\bar{c}}{4}}\Big|_H$$

Equations from Etkin (ref. 4)

$$C_{D_\alpha} = \frac{2C_{L_i}}{\pi A e}C_{L_\alpha}$$

(e is the induced drag factor determined from wind tunnel drag polars)

$$C_{L_u} = \frac{M^2}{1 - M^2}C_{L_i}$$

$C_{D_{\dot\alpha}}$, C_{D_u}, and C_{m_u} are not evaluated.

TABLE 17. – LONGITUDINAL HANDBOOK DERIVATIVES (EQUIVALENT ELASTIC)

$$C_{L\alpha_E} = \frac{a_{T_O}|_{n=0} + K\frac{S_H}{S_W}a_H|_{n=0}\left(1-\frac{\partial\epsilon}{\partial\alpha}\right)}{1-\frac{1}{C_{L_{TR}}}\frac{\partial C_{L_{TO}}}{\partial n}+K\frac{S_H}{S_W}\left(a_H|_{n=0}\frac{\partial\alpha_H}{\partial n}+\frac{\partial C_{L_H}}{\partial n}\right)}$$

$$C_{m\alpha_E} = C_{m\alpha_{TO}}|_{n=0} + C_{mn_{TO}}\frac{C_{L\alpha_E}}{C_{L_{TR}}} + K\frac{S_H}{S_W}\left\{C_{m\alpha_H}|_{n=0}\left(1-\frac{\partial\epsilon}{\partial\alpha}\right)\right.$$

$$\left. + \bar{K}\bar{q}S_W K C_{m\alpha_H}|_{n=0}\frac{\partial C_{L_H}}{\partial\alpha} + C_{m\alpha_H}|_{n=0}\frac{\partial\alpha_H}{\partial n}\frac{C_{L\alpha_E}}{C_{L_{TR}}} + C_{mn_H}\frac{C_{L\alpha_E}}{C_{L_{TR}}}\right\}$$

$$C_{Lq_E} = \frac{\frac{\partial C_{L_{TO}}}{\partial(qc/2V_c)}\Big|_{n=0} + K\frac{S_H}{S_W}\frac{\partial C_{L_H}}{\partial(q\bar{c}/2V_c)}\Big|_{n=0}}{1-\frac{1}{C_{L_{TR}}}\left[\frac{\partial C_{L_{TO}}}{\partial n}+K\frac{S_H}{S_W}\left(a_H|_{n=0}\frac{\partial\alpha_H}{\partial n}+\frac{\partial C_{L_H}}{\partial n}\right)\right]}$$

$$C_{mq_E} = C_{mq_{TO}}|_{n=0} + C_{mn_{TO}}|_q\frac{C_{Lq_E}}{C_{L_{TR}}} + K\frac{S_H}{S_W}\left\{C_{mn_H}|_q\frac{C_{Lq_E}}{C_{L_{TR}}}\right.$$

$$\left. + \bar{q}\bar{K}KS_W C_{m\alpha_H}|_{n=0}\frac{C_{Lq_E}}{C_{L_{TR}}}\right\}$$

$C_{D\alpha}$, C_{Dq}, C_{Lu}, C_{mu}, C_{Du}, $C_{L\dot{\alpha}}$, $C_{m\dot{\alpha}}$, $C_{D\dot{\alpha}}$, $C_{L\delta_E}$, and $C_{m\delta_E}$ are not evaluated.

TABLE 18.–SUMMARY OF HANDBOOK METHODS USED IN COMPUTING THE RIGID SIDESLIP DERIVATIVES FOR 707-320B

Derivative	Method	Ref	Wing-body	Horizontal tail	Vertical tail	Total airplane
C_{y_β}	USAF	6	5.2.1.1	Neglected	5.3.1.1	$C_{y_\beta}=C_{y_{\beta WB}}+C_{y_{\beta V.T.}}$
	TR 1098	72	Not used →			
C_{ℓ_β}	USAF	6	5.2.2.1	Neglected ↓	5.3.1.1 5.6.2.1 ↓	$C_{\ell_\beta}=C_{\ell_{\beta WB}}+C_{\ell_{\beta V.T.}}$
	Comb. of Kohlman's method & USAF	73 + 6	Ref. 73, p. 6 (Kohlman method)			
C_{n_β}	USAF	6	5.1.3.1 5.2.3.1		5.3.1.1 5.6.3.1	$C_{n_\beta}=C_{n_{\beta WB}}+C_{n_{\beta V.T.}}$
	TR 1098	72	Not used →			

TABLE 19. – SUMMARY OF HANDBOOK METHODS USED IN COMPUTING THE RIGID SIDESLIP DERIVATIVES FOR SST

Derivative	Speed range	Method	Ref.	Wing-body	Horizontal tail	Vertical tail	Ventral	Total airplane
C_{y_β}	Subsonic	USAF	6	5.2.1.1	Neglected	5.3.1.1	5.3.1.1	$Cy_\beta = Cy_{\beta\,WB} + Cy_{\beta\,vert} + Cy_{\beta vent}$
		TR 1098	72	Not used →				
	Supersonic	USAF	6	5.2.1.1	Considered to be part of wing	5.3.1.1 5.4.1	5.3.1.1 5.4.1	$Cy_\beta = Cy_{\beta\,WB,HT} + Cy_{\beta vert} + Cy_{\beta\,vent}$
		TR 1098	72	No method available	No method available	No method available	No method available	Not applicable
C_{ℓ_β}	Subsonic	USAF	6	5.2.2.1	Neglected	5.3.1.1 5.6.2.1	5.3.1.1 5.6.2.1	$C_{\ell_\beta} = C_{\ell_\beta WB} + C_{\ell_\beta vert} + C_{\ell_\beta vent}$
		TR 1098	72	Not used →				
	Supersonic	USAF	6	5.2.2.1	Considered to be part of wing	5.3.1.1 5.6.2.1 5.4.1	5.3.1.1 5.6.2.1 5.4.1	$C_{\ell_\beta} = C_{\ell_\beta WB,HT} + C_{\ell_\beta vert} + C_{\ell_\beta vent}$
		TR 1098	72	No method available	No method available	No method available	No method available	Not applicable
C_{n_β}	Subsonic	USAF	6	5.2.3.1	Neglected	5.6.3.1 5.3.1.1	5.6.3.1 5.3.1.1	$Cn_\beta = Cn_{\beta\,WB} + Cn_{\beta vert} + Cn_{\beta vent}$
		TR 1098	72	Not used →				
	Supersonic	USAF	6	5.2.3.1	Considered to be part of wing	5.6.3.1 5.3.1.1 5.4.1	5.6.3.1 5.3.1.1 5.4.1	$Cn_\beta = Cn_{\beta\,WB,HT} + Cn_{\beta vert} + Cn_{\beta vent}$
		TR 1098	72	No method available	No method available	No method available	No method available	No applicable

TABLE 20.–SUMMARY OF HANDBOOK METHODS USED IN COMPUTING THE RIGID ROLL-RATE DERIVATIVES FOR 707-320B

Derivative	Method	Ref	Wing-body	Horizontal tail	Vertical tail	Total airplane
C_{y_p}	USAF	6	Method for wing only $(C_{\ell_p})_{r=0}$ from TR 1098	Neglected	4.1.3.2	$C_{y_p}=C_{y_{p_W}}+C_{y_{p_{V.T.}}}$
	TR 1098	72	Method for wing only used to generate $(C_{\ell_p})_{r=0}=C_{\ell_{p\,wing}}$	↓	p. 21 based on $C_{L_{\alpha V.T.}}$ USAF	↓
C_{ℓ_p}	USAF	6	7.3.2.2 d/b = 0	7.3.2.2 Handled as a wing	4.1.3.2	$C_{\ell_p}=C_{p_{WB}}+C_{\ell_{p_{V.T.}}}$
	TR 1098	72	Method for wing only (p. 20); effect of body neglected	p. 20 Handled as a wing	p. 20 based on USAF $C_{\ell_{\alpha VT}}$	↓
C_{n_p}	USAF	6	7.3.2.3 Subsonic body effect neglected	Neglected	4.1.3.2	$C_{n_p}=C_{n_{p_W}}+C_{n_{p_{V.T.}}}$
	TR 1098	72	Method for wing only (p. 18); body neglected	↓	p. 19 based on USAF C_{L_α}	↓

TABLE 21. – SUMMARY OF HANDBOOK METHODS USED IN COMPUTING THE RIGID ROLL-RATE DERIVATIVES FOR SST

Derivative	Speed range	Method	Ref.	Wing-body	Horizontal tail	Vertical tail	Ventral	Total airplane
C_{y_p}	Subsonic	USAF	6	7.3.2.1: wing only using $C_{\ell_p}\|_{r=0}$ TR 1098	Neglected	4.1.3.2	4.1.3.2	$C_{y_p}=C_{y_{PW}}+C_{y_{Pvert}}+C_{y_{Pvent}}$
		TR 1098	72	Method available for wing only (p. 21)	↓	p. 21 based on $C_{L_{\alpha_{V.T.}}}$ USAF	p. 21 based on $C_{L_{\alpha vent}}$ USAF	
	Supersonic	USAF	6	7.3.2.1 wing only	Considered to be part of wing	4.1.3.2	4.1.3.2	$C_{y_p}=C_{y_{PW,HT}}+C_{y_{Pvert}}+C_{y_{Pvent}}$
		TR 1098	72	No method available	No method available	No method available	No method available	Not applicable
C_{ℓ_p}	Subsonic	USAF	6	7.3.2.2	7.3.2.2 Handled as a wing	4.1.3.2	4.1.3.2	$C_{\ell_p}=C_{\ell_{PWB}}+C_{\ell_{Pvert}}+C_{\ell_{Pvent}}$
		TR 1098	72	Method for wing only (p. 20)	Handled as a wing (p. 20)	p. 20 based on $C_{L_{\alpha_{V.T.}}}$ USAF	p. 20 based on $C_{L_{\alpha vent}}$ USAF	↓
	Supersonic	USAF	6	7.3.2.2	Considered to be part of wing	4.1.3.2	4.1.3.2	
		TR 1098	72	No method available	No method available	No method available	No method available	Not applicable
C_{n_p}	Subsonic	USAF	6	7.3.2.3 body neglected	Neglected	4.1.3.2	4.1.3.2	$C_{n_p}=C_{n_{PW}}+C_{n_{Pvert}}+C_{n_{Pvent}}$
		TR 1098	72	Method for wing only (p. 18)	Neglected	p. 19 based on $C_{L_{\alpha_{V.T.}}}$ USAF	p. 19 based on $C_{L_{\alpha vent}}$ USAF	↓
	Supersonic	USAF	6	7.3.2.3	Considered to be part of wing	4.1.3.2	4.1.3.2	$C_{n_p}=C_{n_{PW,HT}}+C_{n_{Pvert}}+C_{n_{Pvent}}$
		TR 1098	72	No method available	No method available	No method available	No method available	Not applicable

TABLE 22.–SUMMARY OF HANDBOOK METHODS USED IN COMPUTING THE RIGID YAW-RATE DERIVATIVES FOR 707-320B

Derivative	Method	Ref	Wing-body	Horizontal tail	Vertical tail	Total airplane
C_{y_r}	USAF	6	No method available	No method available	5.3.1.1 4.1.3.2	$C_{y_r}=C_{y_{r_{V.T.}}}$
	TR 1098	72	↓	↓	p. 24 based on C_{y_β}~USAF	↓
C_{ℓ_r}	USAF	6	Method available for wing only (7.1.3.2)	Neglected	5.3.1.1	$C_{\ell_r}=C_{\ell_{r_W}}+C_{\ell_{r_{V.T.}}}$
	TR 1098	72	Method available for wing only (p. 23)	↓	p. 23 based on C_{y_β}~USAF	↓
C_{n_r}	USAF	6	Method available for wing only (7.1.3.1)	Neglected	5.3.1.1	$C_{n_r}=C_{n_{r_W}}+C_{n_{r_{V.T.}}}$
	TR 1098	72	Method available for wing only (p. 21)	↓	p. 21 (C_{y_β} used, based on C_{y_β} USAF)	↓

TABLE 23. – SUMMARY OF HANDBOOK METHODS USED IN COMPUTING THE RIGID YAW-RATE DERIVATIVES FOR SST

Derivative	Speed range	Method	Ref.	Wing-body	Horizontal tail	Vertical tail	Ventral	Total airplane
C_{y_r}	Subsonic	USAF	6	No method available	No method available	5.3.1.1	5.3.1.1	$C_{y_r}=C_{y_{r_{vert}}}+C_{y_{r_{vent}}}$
		TR 1098	72	↓	↓	p. 24 (C_{y_β} in eq. obtained from USAF	p. 24	↓
	Supersonic	USAF TR 1098	6	↓	↓	5.3.1.1 No method available	5.3.1.1 No method available	Not applicable
C_{ℓ_r}	Subsonic	USAF	6	Method available for wing only (7.1.3.2)	Neglected	5.3.1.1	5.3.1.1	$C_{\ell_r}=C_{\ell_{r_W}}+C_{\ell_{r_{vert}}}+C_{\ell_{r_{vent}}}$
		TR 1098	72	Method available for wing only (p. 23)	↓	p. 23 (C_{y_β} in eq. obtained from USAF)	p. 23	↓
	Supersonic	USAF	6	Method available for wing only (7.1.3.2)	$\Lambda_{LE}=72°$, HT. considered to be part of wing	5.3.1.1	5.3.1.1	$C_{\ell_r}=C_{\ell_{r_{W,HT}}}+C_{\ell_{r_{vert}}}+C_{\ell_{r_{vent}}}$
		TR 1098	72	No method available	No method available	No method available	No method available	Not applicable
C_{n_r}	Subsonic	USAF	6	Method available for wing only (7.1.3.1)	Neglected	5.3.1.1	5.3.1.1	$C_{n_r}=C_{n_{r_W}}+C_{n_{r_{vert}}}+C_{n_{r_{vent}}}$
		TR 1098	72	Method available for wing only (p. 21)	↓	p. 21 (C_{y_β} in eq. obtained from USAF)	p. 21	↓
	Supersonic	USAF	6	Method available for wing only (7.1.3.1)	Considered to be part of wing	5.3.1.1	5.3.1.1	$C_{n_r}=C_{n_{r_{W,HT}}}+C_{n_{r_{vert}}}+C_{n_{r_{vent}}}$
		TR 1098	72	No method available	No method available	No method available	No method available	Not applicable

TABLE 24.–SUMMARY OF HANDBOOK METHODS USED IN COMPUTING EQUIVALENT ELASTIC SIDESLIP DERIVATIVES FOR 707-320B

Derivative	Wing-body	Horizontal tail	Vertical tail	Total airplane
$C_{y_{\beta_{\bar{E}}}}$	Ref. 6, USAF Handbook, Sec. 5.2.1.1 (wing-body considered rigid)	Neglected	As per V.T. contribution to $C_{Y_{\beta_{\bar{E}}}}$	$C_{y_{\beta_{\bar{E}}}}=C_{y_{\beta_{WB}}}+C_{y_{\beta_{V.T.}}}$
$C_{\ell_{\beta_{\bar{E}}}}$	Ref. 72, p. 6 (Kohlman method) Wing tip deflection considered	Neglected	As per V.T. contribution to $C_{\ell_{\beta_{\bar{E}}}}$	$C_{\ell_{\beta_{\bar{E}}}}=C_{\ell_{\beta_{WB}}}+C_{\ell_{\beta_{V.T.}}}$
$C_{n_{\beta_{\bar{E}}}}$	Ref. 6, USAF Handbook, Secs. 5.1.3.1 and 5.2.3.1 (body contribution included) WB considered rigid	Neglected	As per V.T. contribution to $C_{n_{\beta_{\bar{E}}}}$	$C_{n_{\beta_{\bar{E}}}}=C_{n_{\beta_{WB}}}+C_{n_{\beta_{V.T.}}}$

TABLE 25.–SUMMARY OF HANDBOOK METHOD USED IN COMPUTING EQUIVALENT ELASTIC SIDESLIP DERIVATIVES FOR SST

Derivative	Speed range	Method	Ref.	Wing-body	Horizontal tail	Vertical tail	Ventral	Total airplane
$C_{y_{\beta_{\bar{E}}}}$	Subsonic	USAF	6	Considered rigid (5.2.1.1)	Neglected		Treated same as vertical tail but $a\|_{vent}$ rigid	$C_{y_{\beta_{\bar{E}}}}=C_{y_{\beta_{WB}}}+C_{y_{\beta_{vert}}}+C_{y_{\beta_{vent}}}$
	Supersonic	USAF	6	Considered rigid (5.2.1.1)	Considered to be part of wing planform	Term $(1+d\sigma/d\beta)$ replaced by K_v (BU) factor (5.3.1.1, 5.4.1)		$C_{y_{\beta_{\bar{E}}}}=C_{y_{\beta_{WB,HT}}}+C_{y_{\beta_{vert}}}+C_{y_{\beta_{vent}}}$
$C_{\ell_{\beta_{\bar{E}}}}$	Subsonic	USAF	6	Considered rigid (5.2.2.1)	Neglected			$C_{\ell_{\beta_{\bar{E}}}}=C_{\ell_{\beta_{WB}}}+C_{\ell_{\beta_{vert}}}+C_{\ell_{\beta_{vent}}}$
	Supersonic	USAF	6	Considered rigid (5.2.2.1)	Considered to be part of wing planform	Term $(1+d\sigma/d\beta)$ replaced by K_v (BU) factor (5.3.1.1, 5.4.1)		$C_{\ell_{\beta_{\bar{E}}}}=C_{\ell_{\beta_{WB,HT}}}+C_{\ell_{\beta_{vert}}}+C_{\ell_{\beta_{vent}}}$
$C_{n_{\beta_{\bar{E}}}}$	Subsonic	USAF	6	Considered rigid (5.2.3.1)	Neglected			$C_{n_{\beta_{\bar{E}}}}=C_{n_{\beta_{WB}}}+C_{n_{\beta_{vert}}}+C_{n_{\beta_{vent}}}$
	Supersonic	USAF	6	Considered rigid (5.2.3.1)	Considered to be part of wing planform	Term $(1+d\sigma/d\beta)$ replaced by K_v (BU) factor (5.3.1.1, 5.4.1)		$C_{n_{\beta_{\bar{E}}}}=C_{n_{\beta_{WB,HT}}}+C_{n_{\beta_{vert}}}+C_{n_{\beta_{vent}}}$

TABLE 26.–SUMMARY OF HANDBOOK METHODS USED IN COMPUTING EQUIVALENT ELASTIC ROLL-RATE DERIVATIVES FOR 707-320B

Derivative	Wing-body	Horizontal tail	Vertical tail	Total airplane
$C_{y_{p_{\bar{E}}}}$	Ref. 6, USAF Handbook, par. 7.1.2.1 Wing only (considered rigid)	Neglected	As per V.T. contribution $C_{y_{p_{\bar{E}}}}$	$C_{y_{p_{\bar{E}}}} = C_{y_{p_W}} + C_{y_{p_{V.T.}}}$
$C_{\ell_{p_{\bar{E}}}}$	$C_{\ell_{p_{WB}}}$ rigid $\cdot \frac{C_{\ell_p}\ \text{elastic}}{C_{\ell_p}\ \text{rigid}}$ Ref. 72, TR 1098 (wing only); TA 67A (wing-body-H.T. combination)	$C_{\ell_{p_H}} \cdot \frac{C_{\ell_p}\ \text{elastic}}{C_{\ell_p}\ \text{rigid}}$ Ref. 72, Horiz. tail, TR 1098 TA 67A	As per V.T. contribution $C_{\ell_{p_{\bar{E}}}}$	$C_{\ell_{p_{\bar{E}}}} = C_{\ell_{p_W}} + C_{\ell_{p_V}}$
$C_{n_{p_{\bar{E}}}}$	Ref. 72, TR 1098, p. 18 (no wing drag increment used); no body effect indicated (wing considered rigid)	Neglected	As per V.T. contribution $C_{n_{p_{\bar{E}}}}$	$C_{n_{p_{\bar{E}}}} = C_{n_{p_W}} + C_{n_{p_{V.T.}}}$

TABLE 27. – SUMMARY OF HANDBOOK METHODS USED IN COMPUTING EQUIVALENT ELASTIC ROLL-RATE DERIVATIVES FOR SST

Derivative	Speed range	Method	Ref.	Wing-body	Horizontal tail	Vertical tail	Ventral	Total airplane
$C_{y_{p_{\bar{E}}}}$	Subsonic	TR 1098	72	Considered rigid (wing only) (p. 21)	Neglected		Treated same as vertical tail ($a\|_{vent}$ rigid)	$C_{y_{p_{\bar{E}}}}=C_{y_{p_{WB}}}+C_{y_{p_{vert}}}+C_{y_{p_{vent}}}$
	Supersonic	USAF	6	Considered rigid (wing only) (7.3.2.1)	When $\Lambda_{LE}=72°$, horiz. tail is considered as part of wing; its contribution is included in WB.	Term $(1+\delta\sigma/\delta\beta)$ replaced by K_V (BU) factor (5.3.1.1, 5.4.1)		$C_{y_{p_{\bar{E}}}}=C_{y_{p_{WB,HT}}}+C_{y_{p_{vert}}}+C_{y_{p_{vent}}}$
$C_{\ell_{p_{\bar{E}}}}$	Subsonic	As noted		$C_{\ell_p}\cdot\left(\frac{C_{\ell_{p_{elastic}}}}{C_{\ell_{p_{rigid}}}}\right)$ Source: TR 1098 p. 20, TA 67A	$C_{l_p}\left(\frac{C_{l_{p_{elastic}}}}{C_{l_{p_{rigid}}}}\right)$ TR 1098 TA 67A Source: TR 1098, p. 20, TA 67A			$C_{\ell_{p_{\bar{E}}}}=C_{\ell_{p_{WB}}}+C_{\ell_{p_{HT}}}+C_{\ell_{p_{vert}}}+C_{\ell_{p_{vent}}}$
	Supersonic	As noted		$C_{\ell_p}\cdot\left(\frac{C_{\ell_{p_{elastic}}}}{C_{\ell_{p_{rigid}}}}\right)$ TR 1098 & TA 67A Source: USAF 7.3.2.2 & TA 67A	Considered as part of wing; its contribution is included in WB.	$(1+\delta\sigma/\delta\beta)$ replaced by K_V (BU) factor (USAF: 5.3.1.1, 5.4.1)		$C_{\ell_{p_{\bar{E}}}}=C_{\ell_{p_{WB,HT}}}+C_{\ell_{p_{vert}}}+C_{\ell_{p_{vent}}}$
$C_{n_{p_{\bar{E}}}}$	Subsonic	TR 1098	72	Considered rigid (wing only)(p. 18)	Neglected			$C_{n_{p_{\bar{E}}}}=C_{n_{p_{WB}}}+C_{n_{p_{vert}}}+C_{n_{p_{vent}}}$
	Supersonic	USAF	6	Considered rigid (7.3.2.3)	At supersonic speeds H.T. is a part of wing; its contribution is accounted for in WB.	$(1+\delta\sigma/\delta\beta)$ replaced by K_V (BU) factor (5.3.1.1, 5.4.1)		$C_{n_{p_{\bar{E}}}}=C_{n_{p_{WB,HT}}}+C_{n_{p_{vert}}}+C_{n_{p_{vent}}}$

TABLE 28.–SUMMARY OF HANDBOOK METHODS USED IN COMPUTING EQUIVALENT ELASTIC YAW-RATE DERIVATIVES FOR 707-320B

Derivative	Wing-body	Horizontal tail	Vertical tail	Total airplane
$C_{y_{r_{\bar{E}}}}$	Not available	Not available	As per V.T. contribution $C_{y_{r_E}}$	$C_{y_{r_{\bar{E}}}}=C_{y_{r_{V.T.}}}$
$C_{\ell_{r_{\bar{E}}}}$	Ref. 72, TR 1098, p. 23 (assumed to be midwing) Body effects neglected	Neglected	As per V.T. contribution $C_{\ell_{r_E}}$	$C_{\ell_{r_{\bar{E}}}}=C_{\ell_{r_W}}+C_{\ell_{r_{V.T.}}}$
$C_{n_{r_{\bar{E}}}}$	Ref. 72, TR 1098, p. 21 Fuselage effects neglected	Neglected	As per V.T. contribution $C_{n_{r_{\bar{E}}}}$	$C_{n_{r_{\bar{E}}}}=C_{n_{r_W}}+C_{n_{r_{V.T.}}}$

TABLE 29.–SUMMARY OF HANDBOOK METHODS USED IN COMPUTING EQUIVALENT ELASTIC YAW-RATE DERIVATIVES FOR SST

Derivative	Speed range	Method	Ref.	Wing-body	Horizontal tail	Vertical tail	Ventral	Total airplane
$C_{y_{r_{\bar{E}}}}$	Subsonic	As noted		No method available	No method available		Treated same as vertical tail but $a\|_{vent}$ rigid	$C_{y_{r_{\bar{E}}}}=C_{y_{r_{vert}}}+C_{y_{r_{vent}}}$
	Supersonic	As noted				Term $(1+\delta\sigma/\delta\beta)$ replaced by K_V (BU) factor (USAF: 5.3.1.1, 5.4.1)		$C_{y_{r_{\bar{E}}}}=C_{y_{r_{vert}}}+C_{y_{r_{vent}}}$
$C_{\ell_{r_{\bar{E}}}}$	Subsonic	TR 1098	72	Method available for wing only; considered rigid (p. 23)	Neglected			$C_{\ell_{r_{\bar{E}}}}=C_{\ell_{r_W}}+C_{\ell_{r_{vert}}}+C_{\ell_{r_{vent}}}$
	Supersonic	USAF	6	Method available for wing only; considered rigid (7.1.3.2)	Considered to be part of wing	Term $(1+\delta\sigma/\delta\beta)$ replaced by K_V (BU) factor (5.3.1.1, 5.4.1)		$C_{\ell_{r_{\bar{E}}}}=C_{\ell_{r_{W,HT}}}+C_{\ell_{r_{vert}}}+C_{\ell_{r_{vent}}}$
$C_{n_{r_{\bar{E}}}}$	Subsonic	TR 1098	72	Method for wing only; considered rigid (p. 21)	Neglected			$C_{n_{r_{\bar{E}}}}=C_{n_{r_W}}+C_{n_{r_{vert}}}+C_{n_{r_{vent}}}$
	Supersonic	USAF	6	Considered rigid (available for WB) (7.1.3.1)	Considered to be part of wing	Term $(1+\delta\sigma/\delta\beta)$ replaced by K_V (BU) factor (5.3.1.1, 5.4.1)		$C_{n_{r_{\bar{E}}}}=C_{n_{r_{WB,HT}}}+C_{n_{r_{vert}}}+C_{n_{r_{vent}}}$

The lateral-directional rigid stability derivatives for the 707-320B and SST were calculated by the techniques outlined in tables 18 through 23. In several cases two or more handbook methods were used to overcome insufficiencies in the USAF Handbook. Aeroelastic effects were included in the lateral-directional derivatives by the techniques outlined in tables 24 through 29. In the case of the 707-320B, a variation of aft-body flexibility ($K\beta$) from 21×10^{-8} to 56.1×10^{-8}, holding vertical tail elasticity (L_E/L_R) equal to 0.813, was performed. The effect of varying L_E/L_R from 0.813 to 1.0, holding $K_\beta = 21 \times 10^{-8}$, was also investigated for C_{n_β} of the 707 at Mach number equal to 0.85.

7.2 Angle-of-Attack (α) Derivatives

The angle-of-attack derivatives for the 707-320B and a representative, variable-sweep SST configuration have been calculated by several methods. From the results shown in figures that follow, experimental data in predicting the derivatives C_{L_α}, C_{D_α}, and C_{m_α} are obtained by the theoretical lifting surface methods. The main shortcomings in the method are:

(1) The transonic case is not treated.

(2) The drag correlation is unsatisfactory.

The simplified, thin-body, coplanar version of the aerodynamic influence coefficients, designated as TA 67A in this report, does a good job of predicting the α stability derivatives.

7.2.1 $C_{L_\alpha} = \frac{\partial C_L}{\partial \alpha}$; Variation of lift with angle of attack. — This stability derivative was calculated by the following methods:

(1) Lifting surface (TA 67A).

(2) Lifting surface-slender body (TA 176).

(3) Lifting line (TS 70).

(4) Handbook (refs. 6 and 67).

(5) Wind tunnel.

(6) Flight test.

Results for the 707-320B and the SST are presented in figs. 35, 36, and 37. The effect of dynamic pressure on the accuracy of the lifting surface method (TA 67A) is shown in fig. 38.

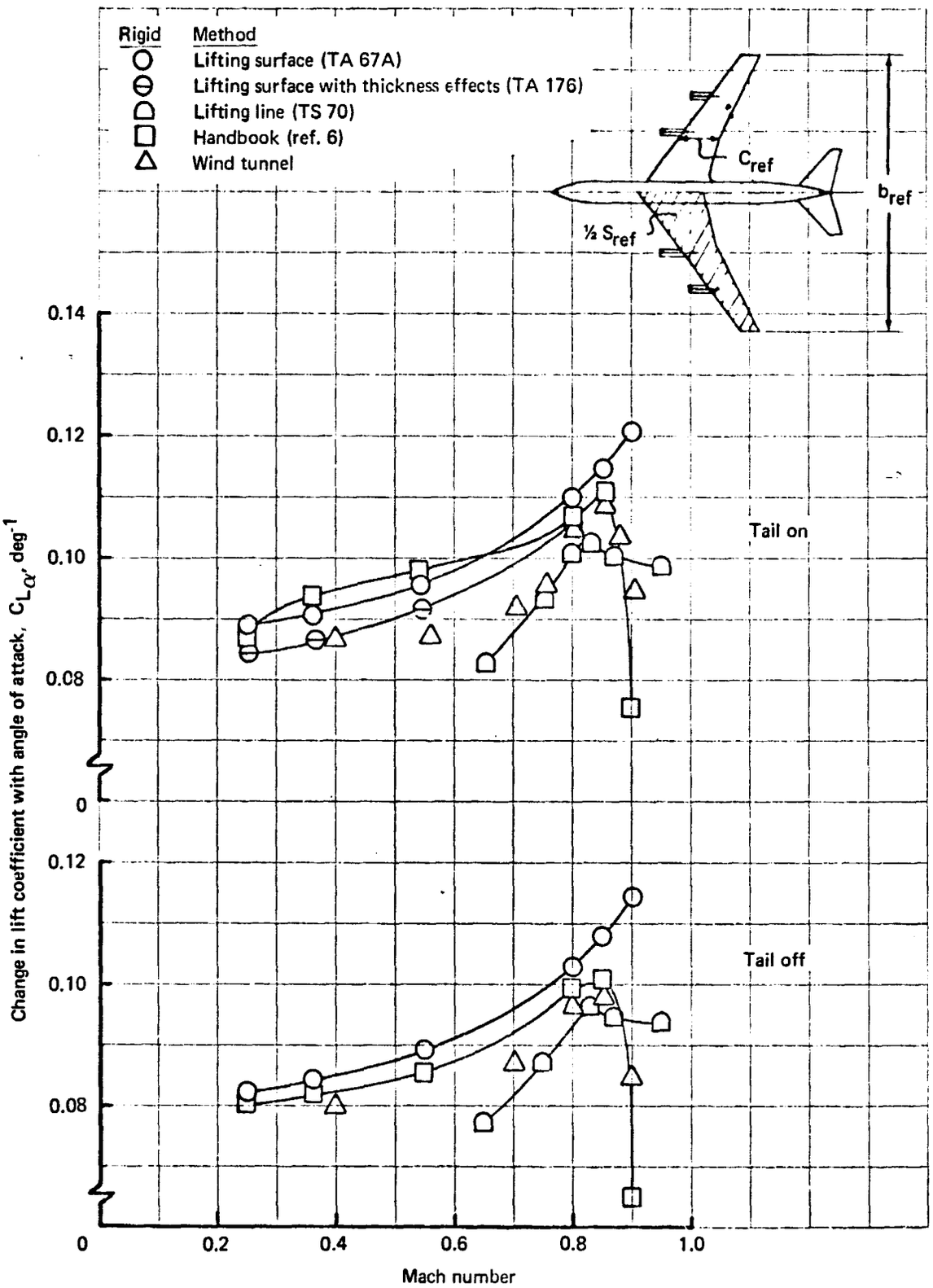

FIGURE 35.– COMPARISON OF ESTIMATION METHODS FOR C_{L_α} – 707-320B (RIGID)

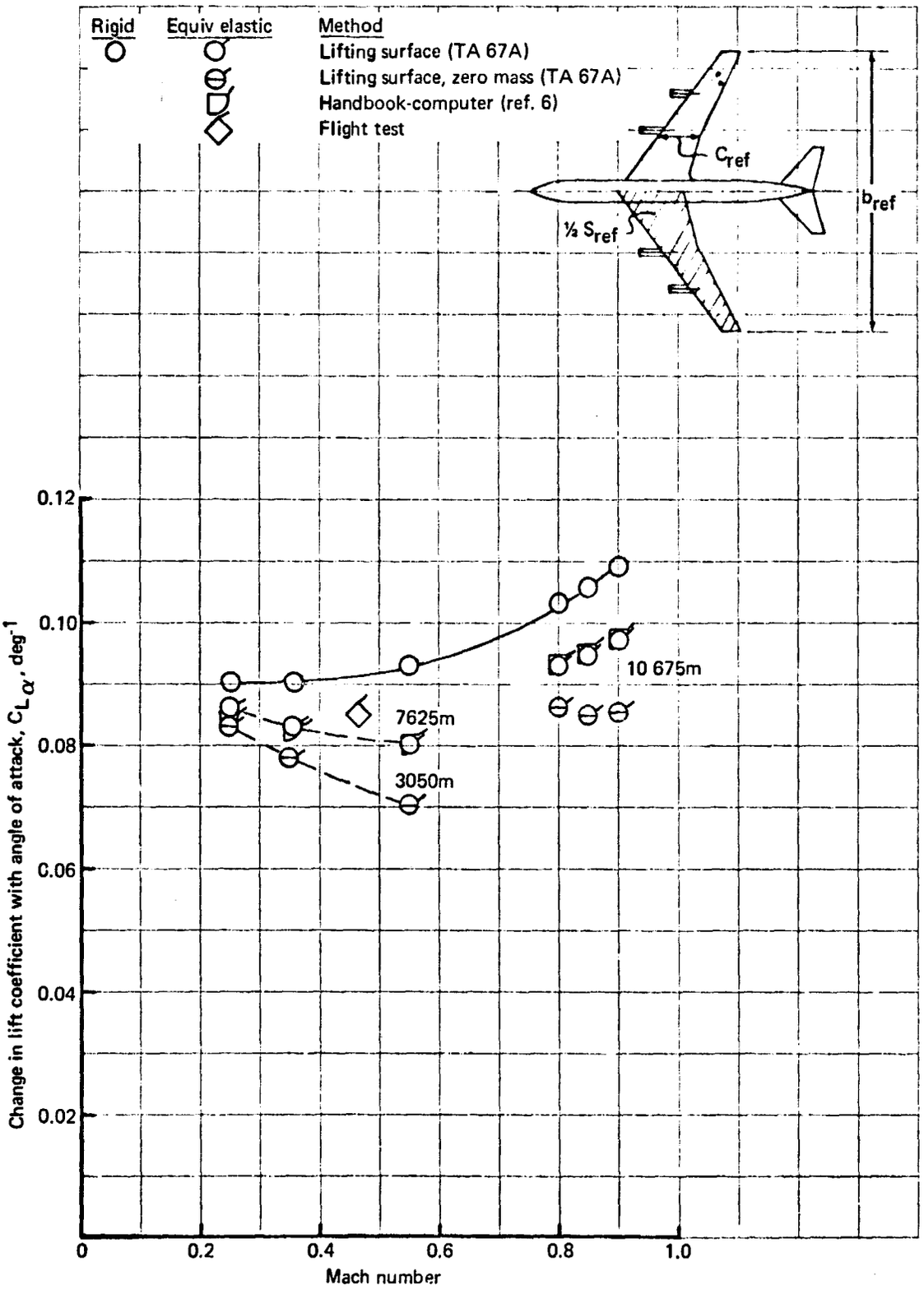

FIGURE 36.– COMPARISON OF ESTIMATION METHODS FOR C_{L_α} – 707-320B (EQUIV ELAS)

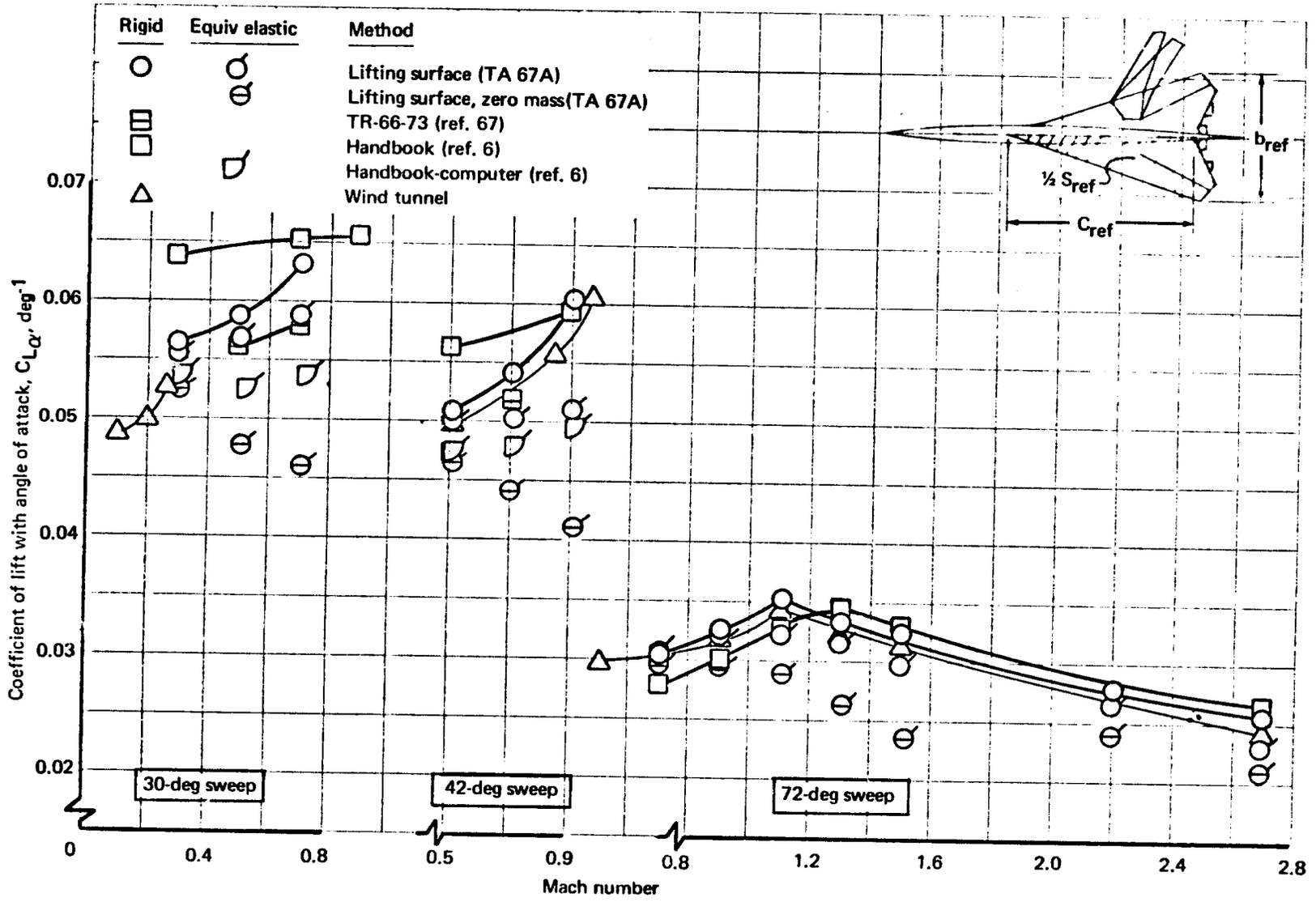

FIGURE 37.– COMPARISON OF ESTIMATION METHODS FOR C_{L_α} – SST

7.2.1.1 Rigid results: The comparison of the results for a rigid 707-320B C_{L_α} analysis is shown in fig. 35. The lifting surface method (TA 67A) compares only in a fair manner to the rigid wind tunnel data. The lifting line method (TS 70) and handbook method (ref. 6) correlate best with the rigid wind tunnel data, particularly at large subsonic Mach numbers ($M > 0.80$). In fact, the handbook predicts the C_{L_α} break at large subsonic Mach numbers that is characteristic for high-aspect-ratio configurations. This is because the handbook uses a "force-break" Mach number empirically determined from wind tunnel data to form a more realistic compressibility factor associated with the onset of localized supersonic flow. In this respect, the handbook technique is superior to other techniques when applied to high-aspect-ratio configurations.

The TA 67A program essentially uses a Prandtl-Glauert correction for compressibility effects. However, it may be possible to develop a corrector matrix to properly account for shock-induced, localized pressure effects. It would appear, assuming the necessary pressure data are available, that a corrector matrix can be predicted purely from knowledge of the geometry, wing thickness, camber, angle of attack, and Mach number. It is expected that with the incorporation of a corrector matrix to compensate for nonlinear effects, an accurate prediction of the transonic stability derivatives is possible with influence coefficient theory.

It is shown in fig. 35 that the lifting surface method TA 67A estimates are more accurate for a tail-off than a tail-on 707-320B configuration. The reason for this is that TA 67A is restricted to coplanar wing-body-tail configurations with zero thickness. In order to investigate the effect of these limitations in TA 67A, the more sophisticated lifting surface-slender body method (TA 176) was applied to the tail-on 707-320B configuration. Figure 35 shows the values from the theoretical methods of TA 176 correlated better with the rigid wind tunnel data than those values of TA 67A.

The comparison of methods for a rigid SST configuration, shown in fig. 37, indicates that the lifting surface method (TA 67A) is superior to the handbook methods. The largest discrepancy between the handbook (ref. 6) and the rigid wind tunnel numbers occurs for the 30° and 42° leading edge sweep cases. In order to improve the handbook estimation, ref. 67 was employed to accurately calculate the effects of the leading edge crank. Reference 67 gave improved correlation over that of ref. 6.

The reason for the superior lifting surface accuracy with the SST is the more accurate representation of the SST planform, including the leading edge crank. Additionally, the SST, with a near coplanar wing-tail and a large body-fineness ratio, better satisfies the approximations made in the thin-body, lifting surface methods of TA 67A.

7.2.1.2 Elastic results: The results of an elastic analysis for C_{L_α} of the 707-320B are shown in fig. 36. Since elastic wind tunnel data are not available for the 707, flight test data are used for the experimental base point. The effect of aeroelasticity on C_{L_α} is seen to be significant even for a subsonic airplane, such as the 707. There are no essential differences between the values of the handbook plus computer method and the lifting surface method (with mass).

The lifting surface calculations were done both by Formulations I and II to show the effects of mass on the value of C_{L_α}. The corresponding lift-curve slopes are defined as $C_{L_{\alpha_{\bar{E}}}}$-and $C_{L_{\alpha_{\bar{E}}}}$, respectively (see Sec. 4). The slope $C_{L_{\alpha_{\bar{E}}}}$-(zero mass) is equivalent to the lift-curve slope for constant load factor and dynamic pressure. The slope $C_{L_{\alpha_{\bar{E}}}}$ (with mass) is equivalent to the lift-curve slope for varying load factor (constant dynamic pressure). The two lift-curve slopes are related to one another through the formulas contained in Sec. 4.

A comparison between lifting surface theory and handbook methods for the elastic SST is shown in fig. 37. The importance of inertia-induced aeroelastic effects is demonstrated by the difference in 'zero-mass' and 'with-mass' lift-curve slopes. Elastic model data were available for a slightly different SST configuration. These data are compared with corresponding lifting surface theory predictions in fig. 38. The Mach number and dynamic pressure conditions used during these tests were different from those corresponding to the flight conditions of table 10. For purposes of comparing theory and data, this was felt to be acceptable.

The handbook derivatives are seen to agree reasonably well with the influence coefficient derivatives for sweep angles of 30° and 42°. In the case of 72°, the handbook methods fail because the elastic SST airplane in that case cannot be logically broken up into components. For that reason, no handbook data are presented for the 72° sweep case.

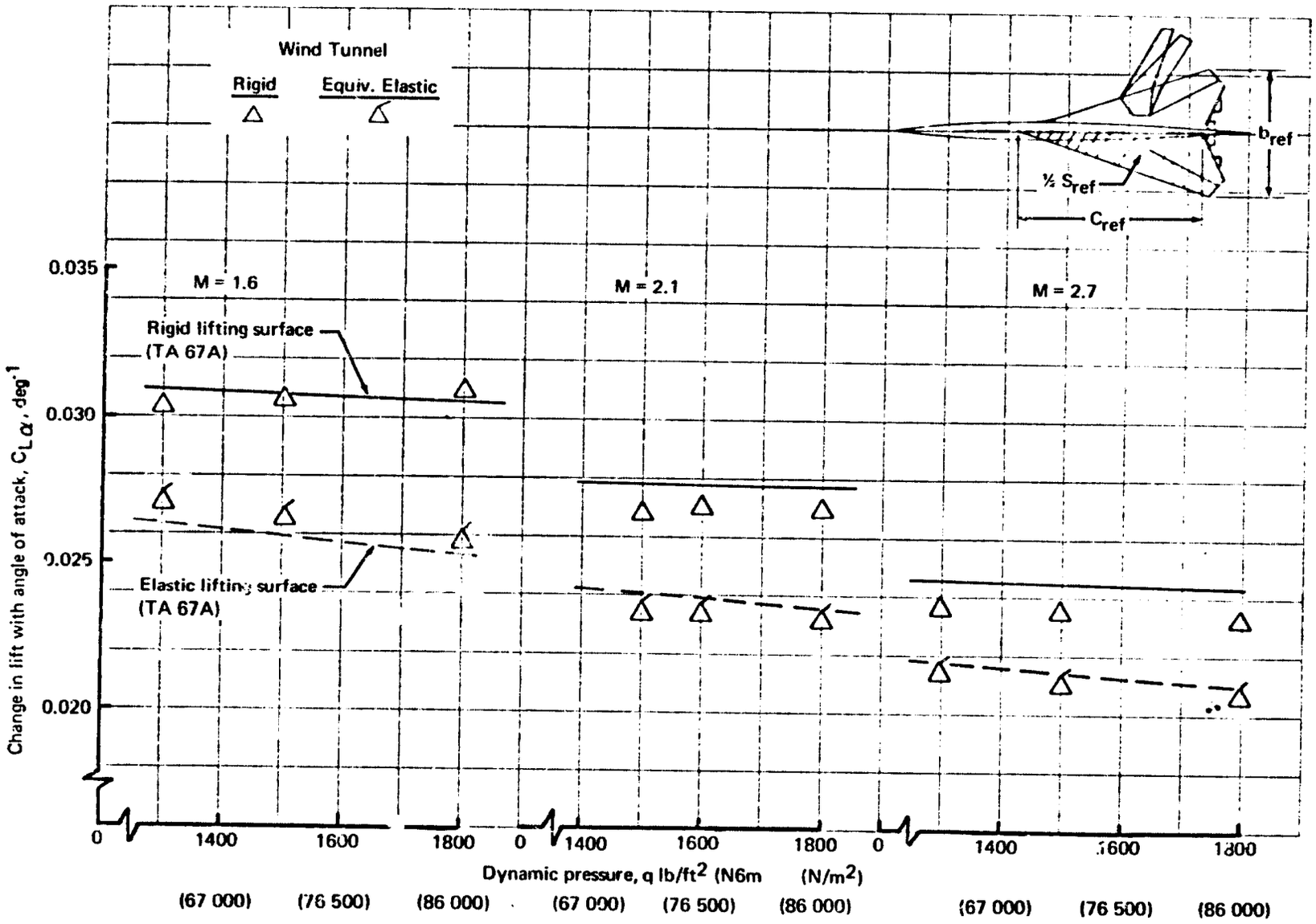

FIGURE 38.– EFFECT OF DYNAMIC PRESSURE ON ACCURACY OF $C_{L\alpha}$ – SST

Figure 38 demonstrates that values of C_{L_α} predicted from influence coefficient theory agree quite well with those obtained from elastic model tunnel data. The fact is observed that the C_{L_α} correlation between tunnel data and influence coefficient theory is better elastic than it is rigid. This may be due to wing-tail seal arrangement used on the elastic model providing a more accurate stiffness matrix.

It should be noted that the error increment between wind tunnel and the lifting surface calculated values of C_{L_α} does not increase appreciably between the rigid and elastic cases. In fact, fig. 38 indicates that an empirical correction to rigid wind tunnel data may result in a more accurate elastic value of the stability derivative C_{L_α}. For the SST at 72° sweep, this correction is of the form:

$$C_{L_{\alpha_E}} = \left(C_{L_{\alpha_{TA\text{-}67A}}}\right)_{ELASTIC} - \left(C_{L_{\alpha_{TA\text{-}67A}}} - C_{L_{\alpha_{W.T.}}}\right)_{RIGID} \qquad (7.1)$$

Whether this is a general result or configuration dependent is unknown.

Both handbook and influence coefficient methods are capable of predicting the equivalent elastic airplane C_{L_α} derivative with acceptable accuracy.

7.2.2 $C_{m_\alpha} = \frac{\partial C_m}{\partial \alpha}$; Variation of pitching moment with angle of attack. — This stability derivative was calculated by the following methods:

(1) Lifting surface (TA 67A).

(2) Lifting line (TS 70).

(3) Handbook (refs. 6 and 67).

(4) Wind tunnel.

(5) Flight test.

Results for the 707-320B and the SST are presented in figs. 39, 40, and 41. The effect of dynamic pressure on the accuracy of the lifting surface method (TA 67A) is shown in figs. 42 and 43. The change in pitching moment increment with Mach number for the 707 is presented in fig. 44.

7.2.2.1 Rigid results: Figures 39 and 41 show that the lifting surface method of TA 67A most accurately predicts the rigid value of C_{m_α} for the 707 and SST. The largest discrepancy in the lifting surface method appears in the transonic range ($M > 0.8$) where nonlinear effects of localized, supersonic flow are prevalent.

In the case of the 707-320B, the rigid lifting surface method correlates better with the wind tunnel data than either the handbook or lifting line method. The lifting line method correlates the poorest. The lifting surface method is more accurate for the tail-off than for the tail-on 707 configuration due to the coplanar assumptions inherent to the method.

In the case of the SST, the handbook/tunnel correlation is good for $\Lambda_{L.E.} = 72°$, but poor for the 30° and 42° sweep configurations. Although the handbook does estimate the variation of total force with angle of attack (C_{L_α}) reasonably well. It does poorly in accounting for the distribution of pressures and, therefore, it does poorly in predicting moment derivatives. The USAF Handbook method does not account for strake* effects in the case of variable-sweep airplanes. In the case of the SST at 30° and 42° of sweep, several spot checks were made with the method of ref. 67, which was specifically developed for cranked-wing configurations. Reference 67** does not do much better (fig. 41).

7.2.2.2 Elastic results: Figure 40 presents a correlation between methods of predicting the elastic value of C_{m_α} for the 707-320B. Flight test data for C_{m_α} agree fairly well with theoretical methods, but the validity of the flight test data is subject to question, as explained in Sec. 6. Flight test data were also generated in the form of C_m versus C_L for constant altitude and load factor (varying Mach number). Such data are compared with influence coefficient methods in fig. 44. There is good agreement between theory and flight test.

In the case of the SST, fig. 41 shows good agreement between lifting surface theory and handbook. A handbook value of C_{m_α} was not calculated for the 72° sweep case due to the inability to logically divide the SST configuration into elastic components.

---

*The strake is the triangular shaped area between the leading edge break and the fuselage in the case of the 30° and 42° sweep configurations.

**This reference was written to update the USAF Handbook with regard to cranked leading edge and trailing edge wings.

A comparison of the lifting surface method with elastic model tunnel data is given in fig. 42. There is poor agreement. To lend more meaning to the C_{m_α} results shown, a correlation for the corresponding aerodynamic-center locations is shown in fig. 43. It is observed that influence coefficient predictions compare better with the theory at the flight-lift coefficient (~ 0.08) than at low-lift coefficient (~ 0.02).

It is again noted that the error increments in C_{m_α} and a.c. between wind tunnel and lifting surface values do not increase appreciably between rigid and elastic cases. For the SST configuration tested, it appears an empirical factor may be developed to more accurately predict elastic C_{m_α} and a.c. from rigid wind tunnel data. These factors are:

$$C_{m_{\alpha_E}} = \left(C_{m_{\alpha_{TA\text{-}67A}}}\right)_{ELASTIC} - \left(C_{m_{\alpha_{TA\text{-}67A}}} - C_{m_{\alpha_{W.T.}}}\right)_{RIGID} \qquad (7.2)$$

$$a.c._E = \left(a.c._{TA\text{-}67A}\right)_{ELASTIC} - \left(a.c._{TA\text{-}67A} - a.c._{W.T.}\right)_{RIGID} \qquad (7.3)$$

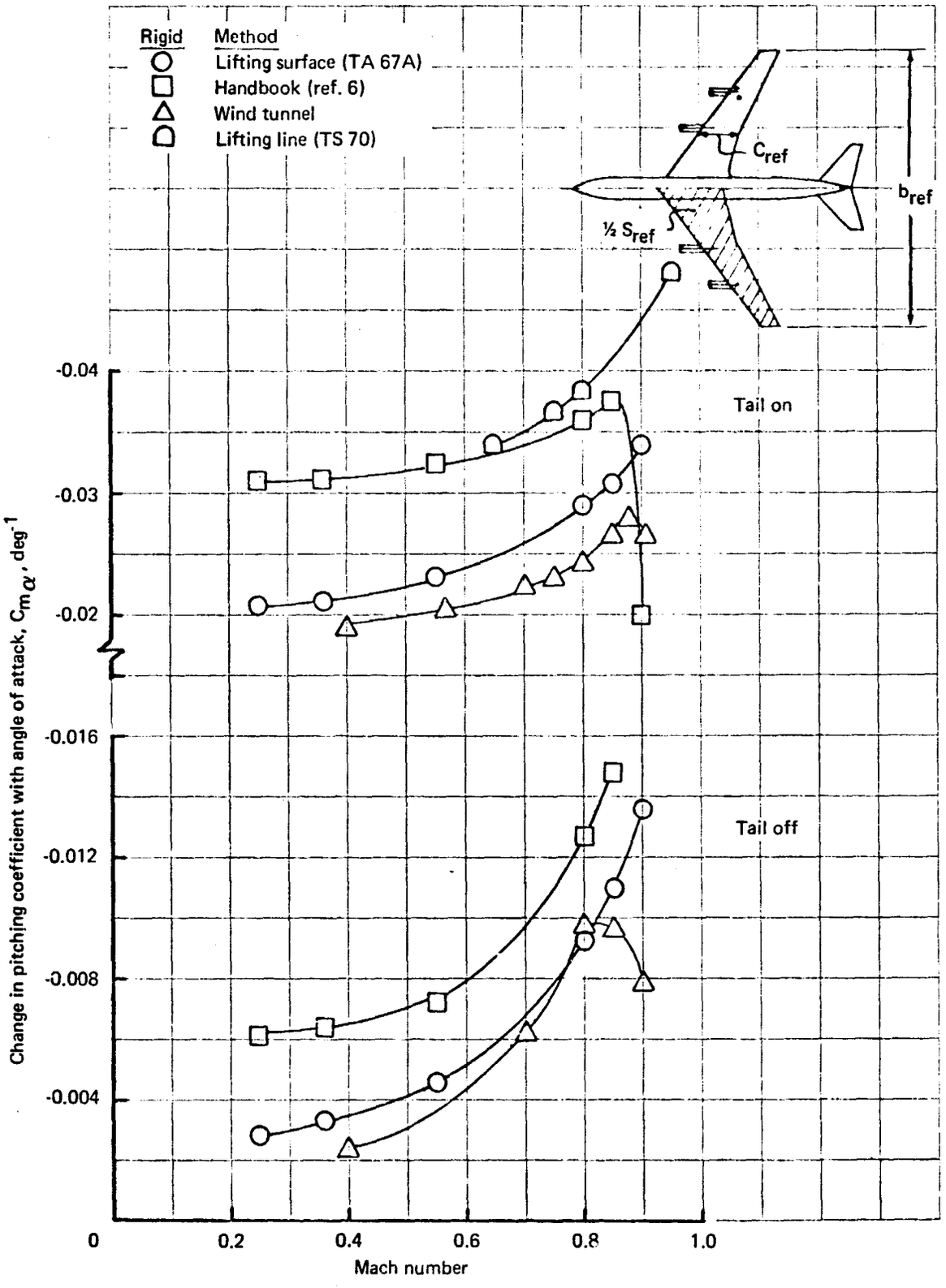

FIGURE 39.– COMPARISON OF ESTIMATION METHODS FOR C_{m_α} – 707-320B (RIGID)

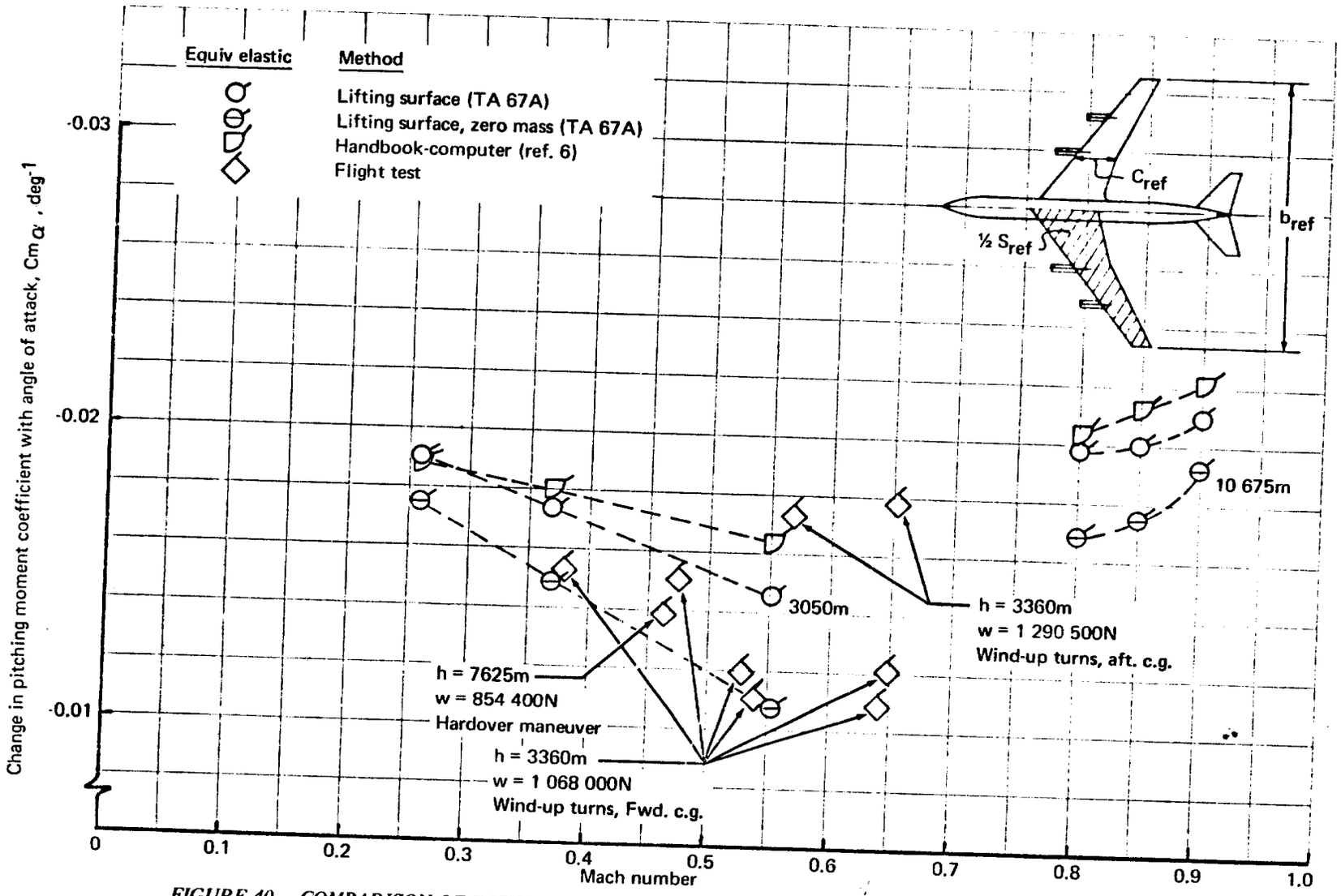

FIGURE 40.– COMPARISON OF ESTIMATION METHODS FOR $C_{m\alpha}$ – 707-320B (EQUIV ELAS)

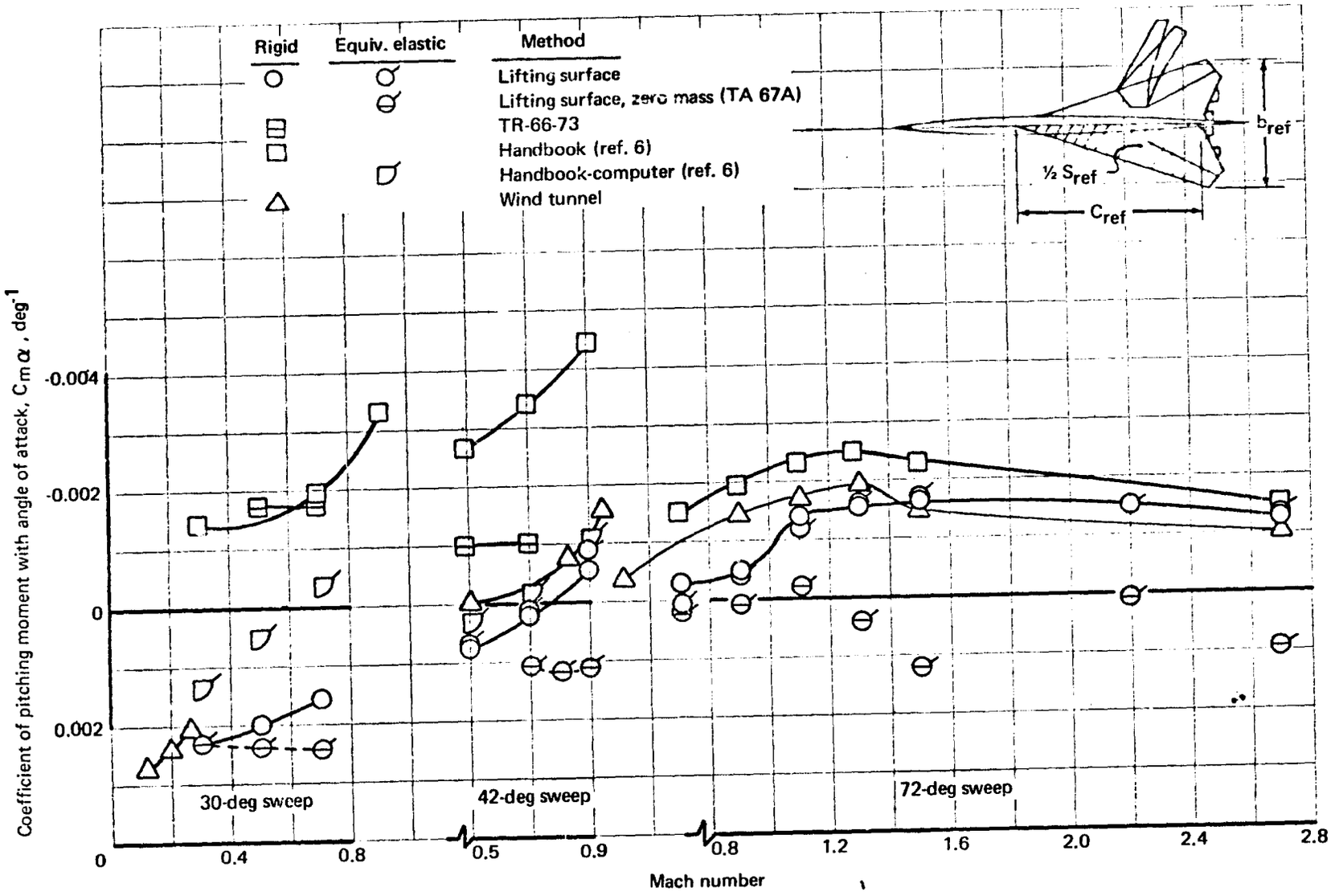

FIGURE 41.– COMPARISON OF ESTIMATION METHODS FOR C_{m_α} – SST

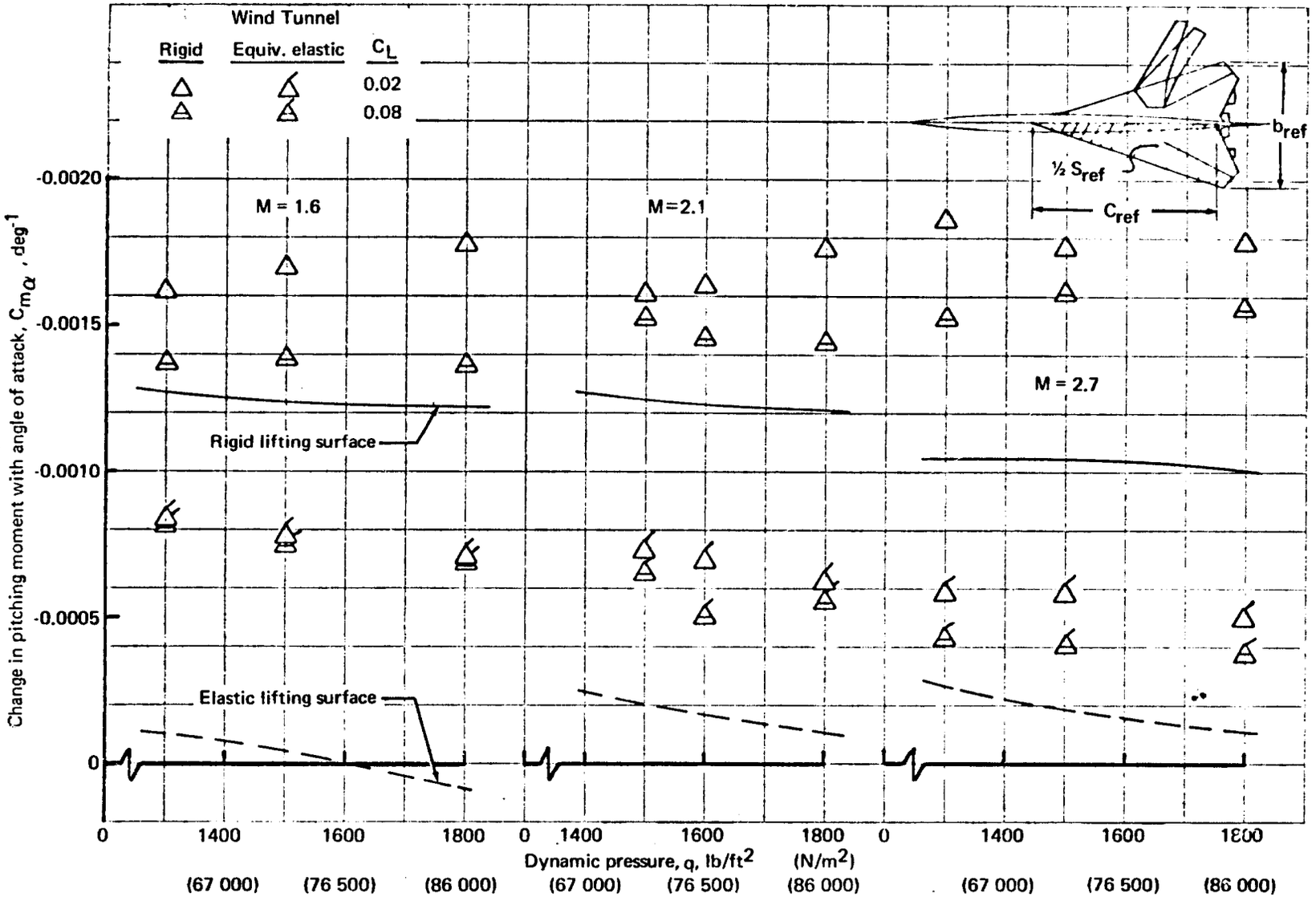

FIGURE 42.– EFFECT OF DYNAMIC PRESSURE ON ACCURACY OF C_{m_α}–SST

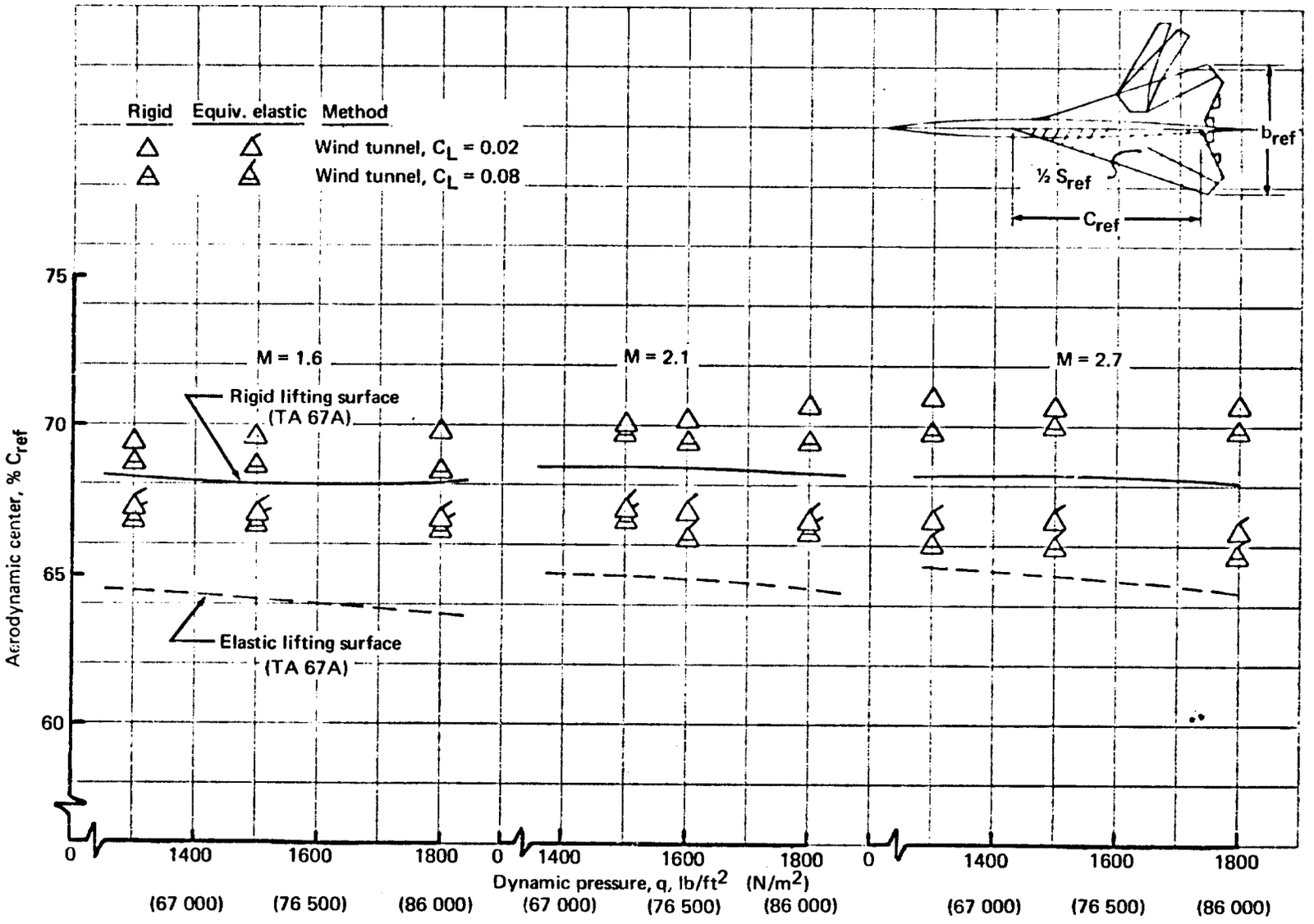

FIGURE 43.– EFFECT OF DYNAMIC PRESSURE ON ACCURACY OF AERODYNAMIC CENTER LOCATION–SST

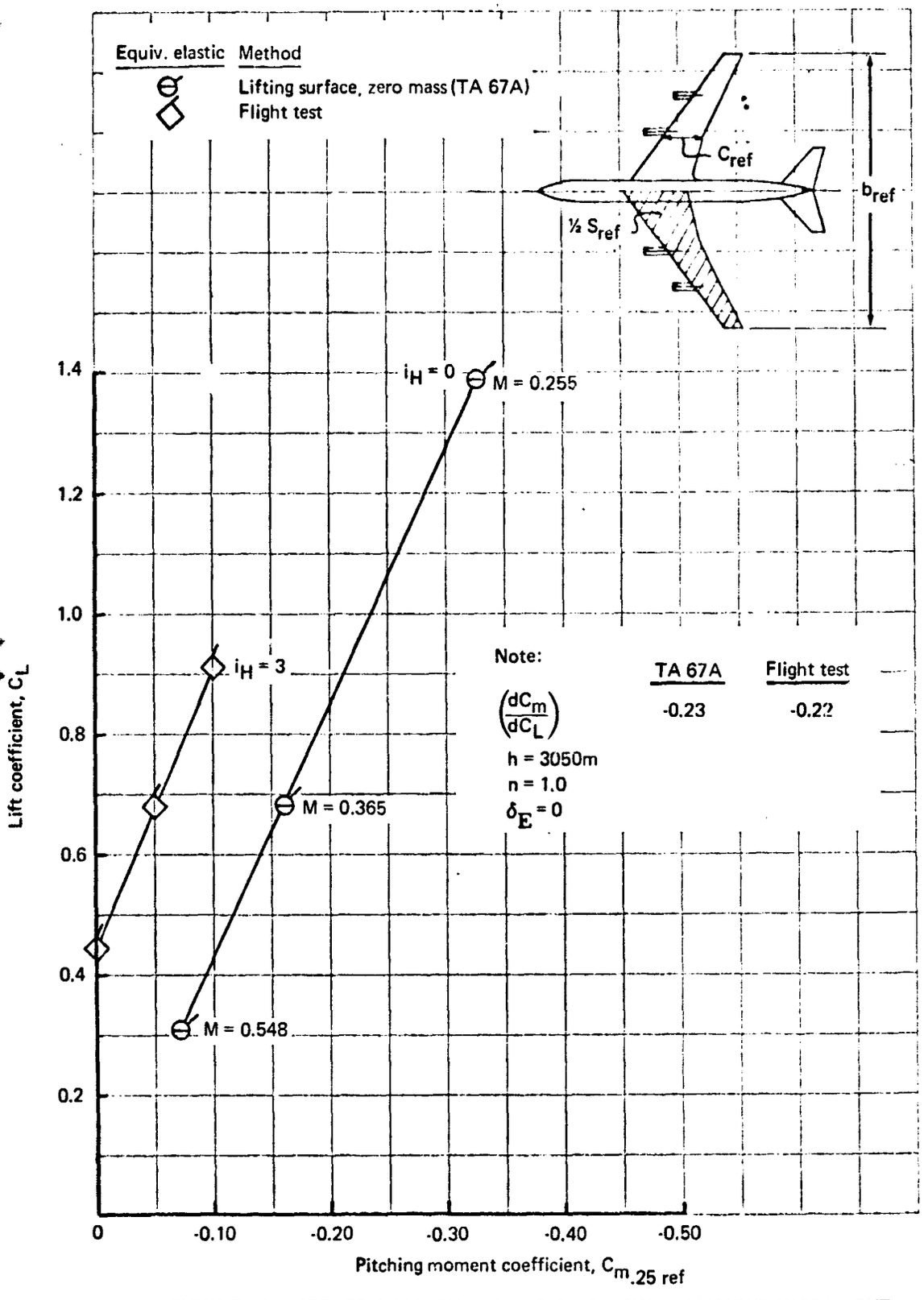

FIGURE 44.– EFFECT OF MACH NUMBER ON PITCHING MOMENT INCREMENT

7.2.3 $C_{D_\alpha} = \frac{\partial C_D}{\partial \alpha}$; Variation of drag with angle of attack. — This stability derivative was calculated by the following methods:

(1) Lifting surface (TA 67A).

(2) Handbook (ref. 4).

(3) Wind tunnel.

(4) Flight test.

The results for the 707-320B and the SST are presented in figs. 46 and 47.

7.2.3.1 Rigid results: Figures 45 and 46 show that the correlation between TA 67A and tunnel data is, in general, not good for the SST but reasonable for the 707-320B. Poor correlation between TA 67A and tunnel data was expected for the following reason. The treatment of the planform leading edge in the current version of TA 67A is not realistic. The difference in leading edge treatment between the mathematical model of TA 67A and the real airplane is illustrated in fig. 45. This is the consequence of the 'thin' surface assumption.

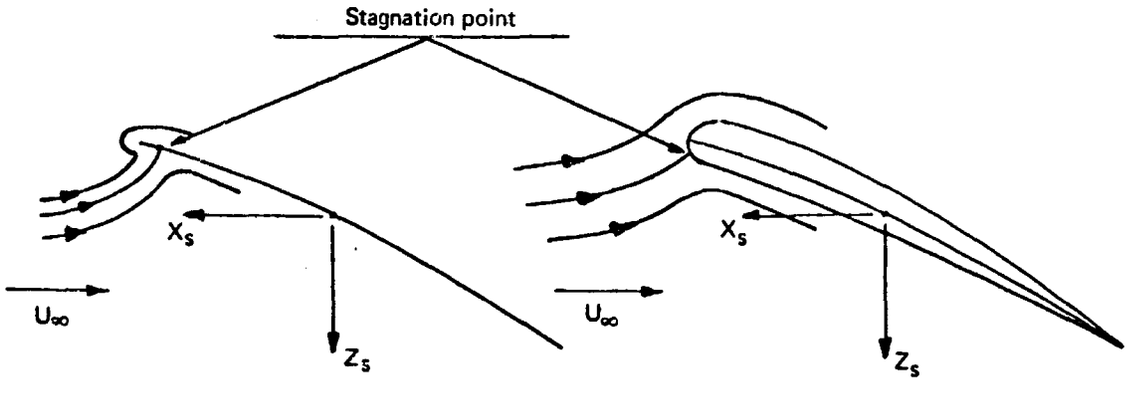

FIGURE 45.-AIRFOIL LEADING-EDGE REPRESENTATION IN COMPUTER PROGRAM TA 67A

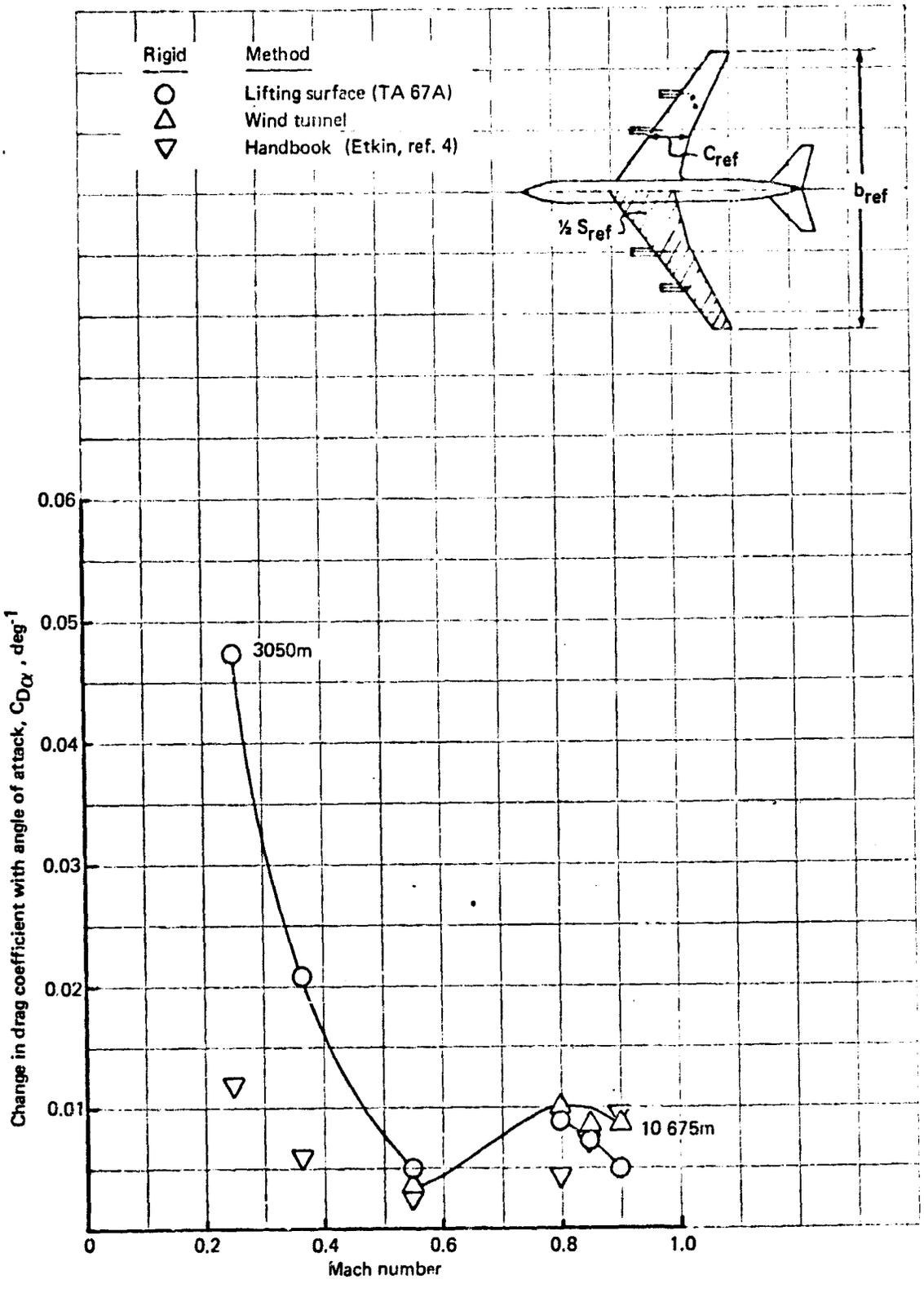

FIGURE 46. – COMPARISON OF ESTIMATION METHODS FOR $C_{D\alpha}$ – 707-320B

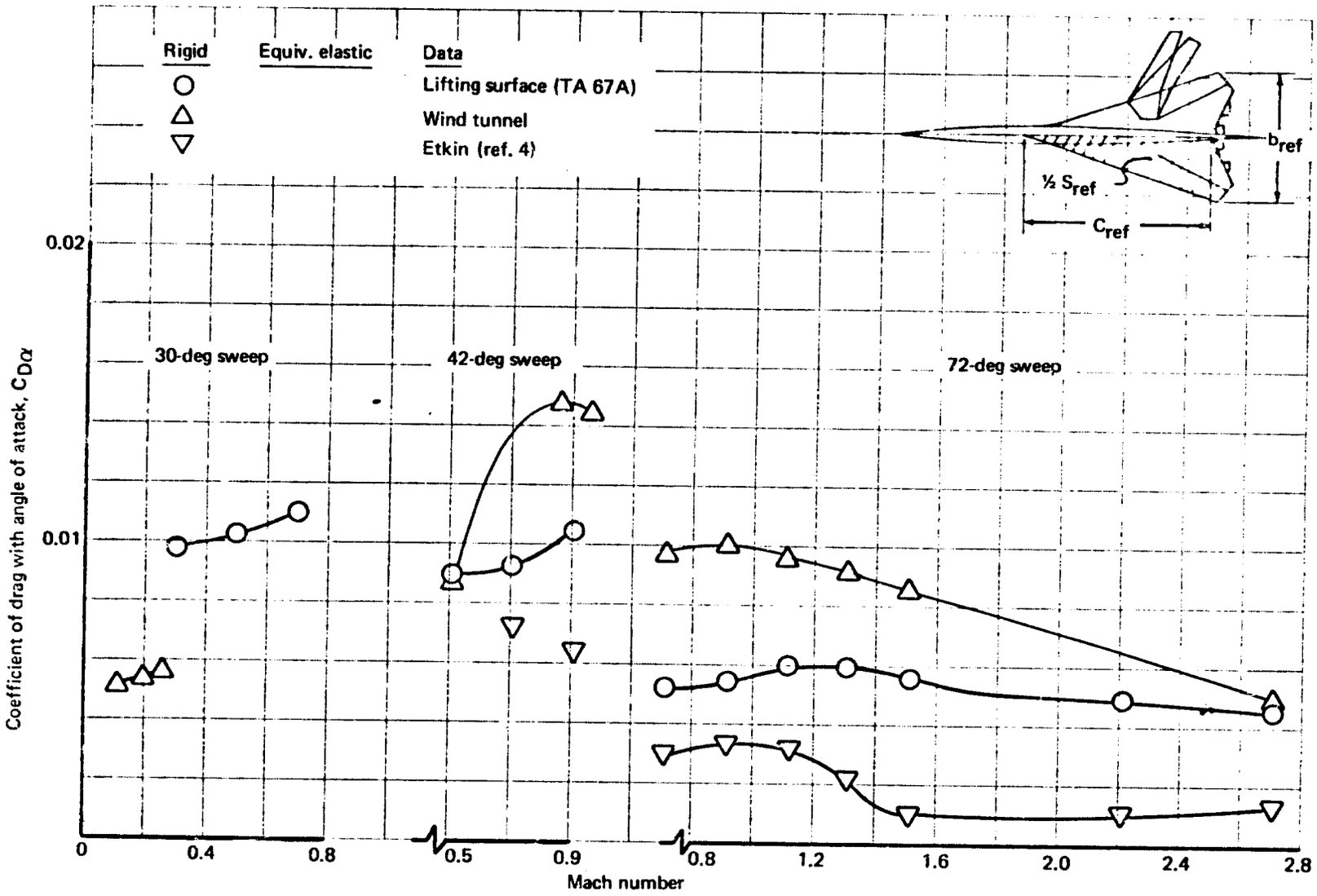

Figure 47. – COMPARISON OF ESTIMATION METHODS FOR C_{D_α} –SST

The handbook values from ref. 4 shown in figs. 45 and 46 do not correlate much better with the rigid wind tunnel values of $C_{D_{\alpha}}$ than TA 67A does. This poor correlation is thought to be due to the gross approximations involved in most handbooks to describe the nonlinearity as a function of geometry features such as aspect ratio, taper ratio, etc.

7.2.3.2 Elastic results: This derivative could not be evaluated from handbook methods in any reasonable manner. Values for $C_{D_{\alpha}}$ were determined from influence coefficient theory but they are not presented here because no comparison with other theoretical or experimental methods is available.

7.3 Angle-of-Attack Rate ($\dot{\alpha}$) Derivatives

The $\dot{\alpha}$ stability derivatives were estimated by the methods of ref. 6 and the only derivatives calculated were $C_{L_{\dot{\alpha}}}$ and $C_{m_{\dot{\alpha}}}$. There is no general method discussed in the handbooks or implemented on the computer to treat the derivative $C_{D_{\dot{\alpha}}}$ with any degree of accuracy. Fortunately, for most configurations, $C_{D_{\dot{\alpha}}}$ does not participate in a stability analysis to a significant degree (ref. 4 and app. C).

The $\dot{\alpha}$ derivatives are a consequence of the fact that the pressure distribution on a lifting surface does not adjust itself instantaneously to its equilibrium value when the angle of attack is suddenly changed. Therefore, unsteady flow is involved in the calculation of such effects. Introduction of the concept of derivatives assumes that this unsteady phenomenon can be treated on a first-order-in-frequency basis. The validity of this assumption is discussed in ref. 28.

The results of the study are presented in figs. 48 through 51 for the 707-320B and the SST. Because only one handbook method (ref. 6) is currently available, no comparison of methods can be made and the equivalent elastic cases cannot be considered.

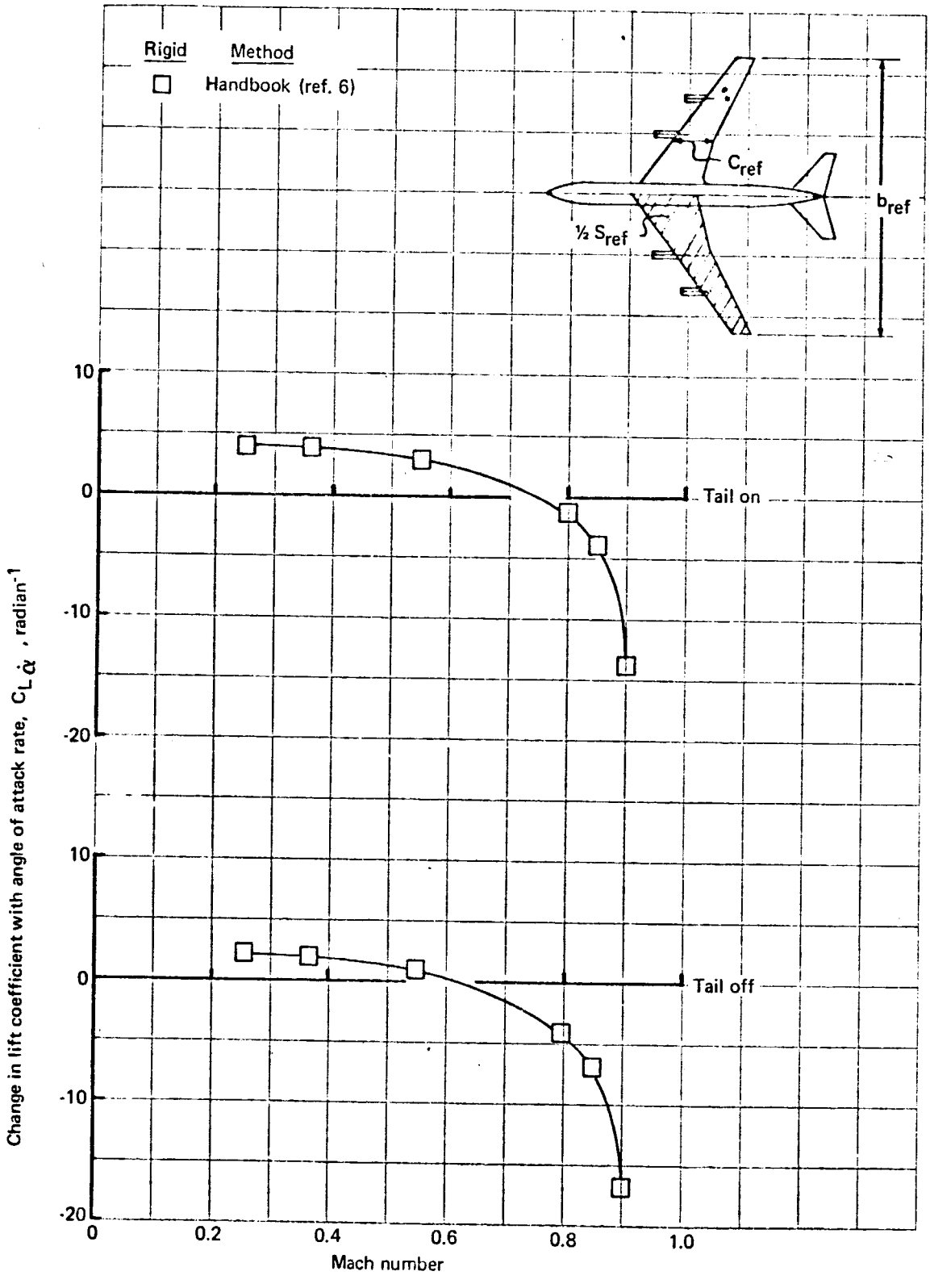

FIGURE 48. – ESTIMATION OF $C_{L_{\dot{\alpha}}}$ – 707-320B

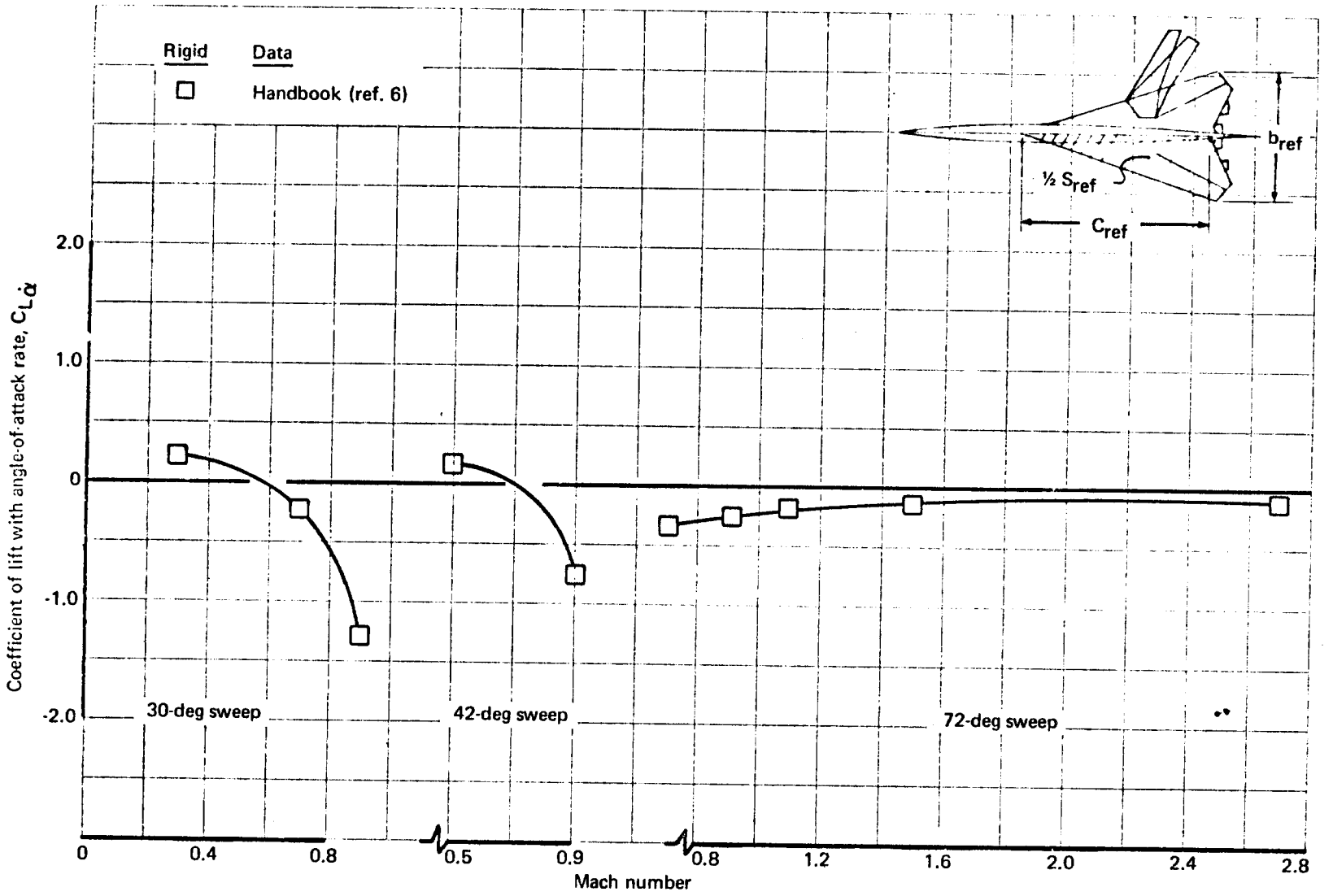

FIGURE 49.– ESTIMATION OF $C_{L\dot{\alpha}}$–SST

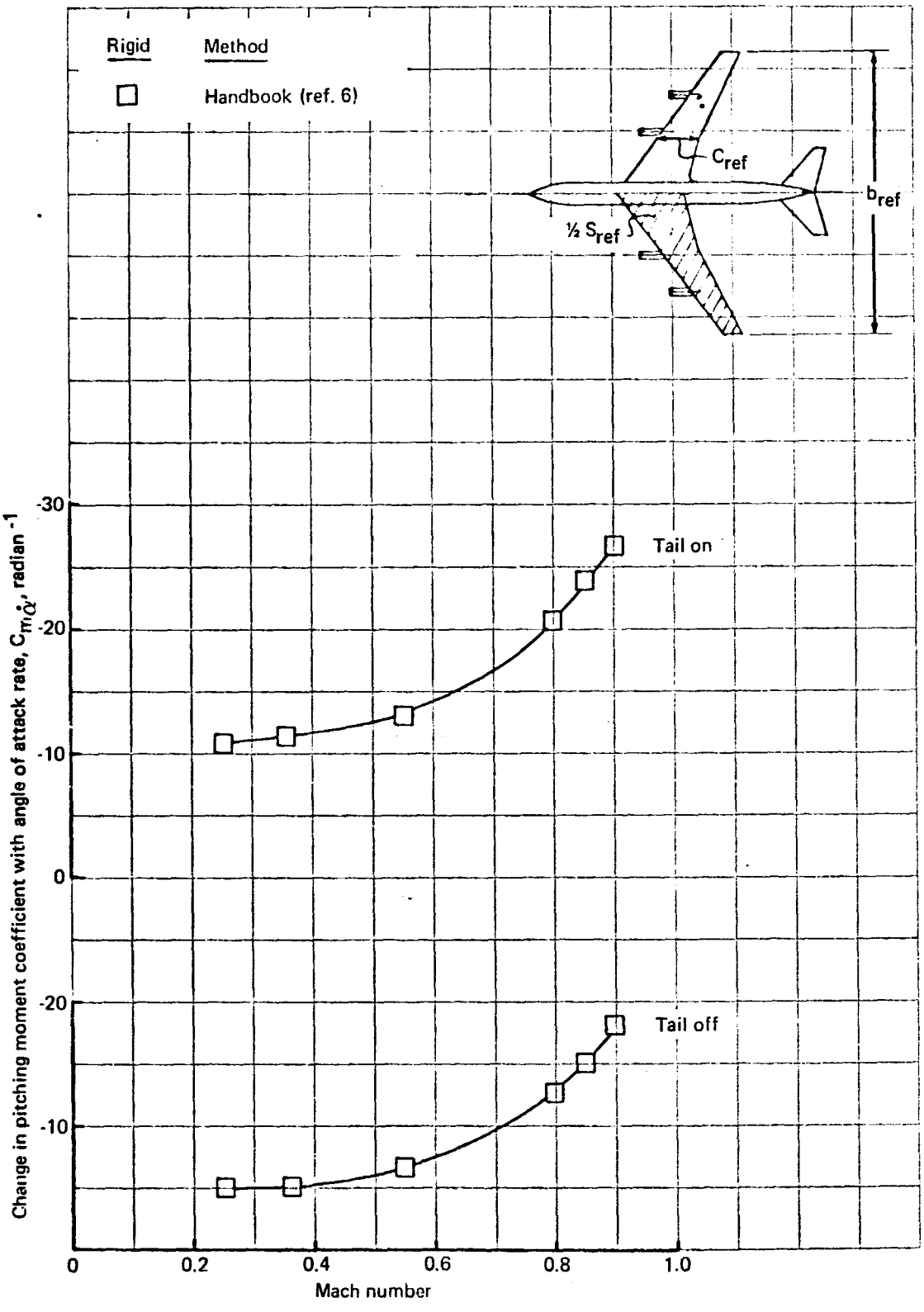

FIGURE 50.-- ESTIMATION OF $C_{m\dot{\alpha}}$ -707-320B

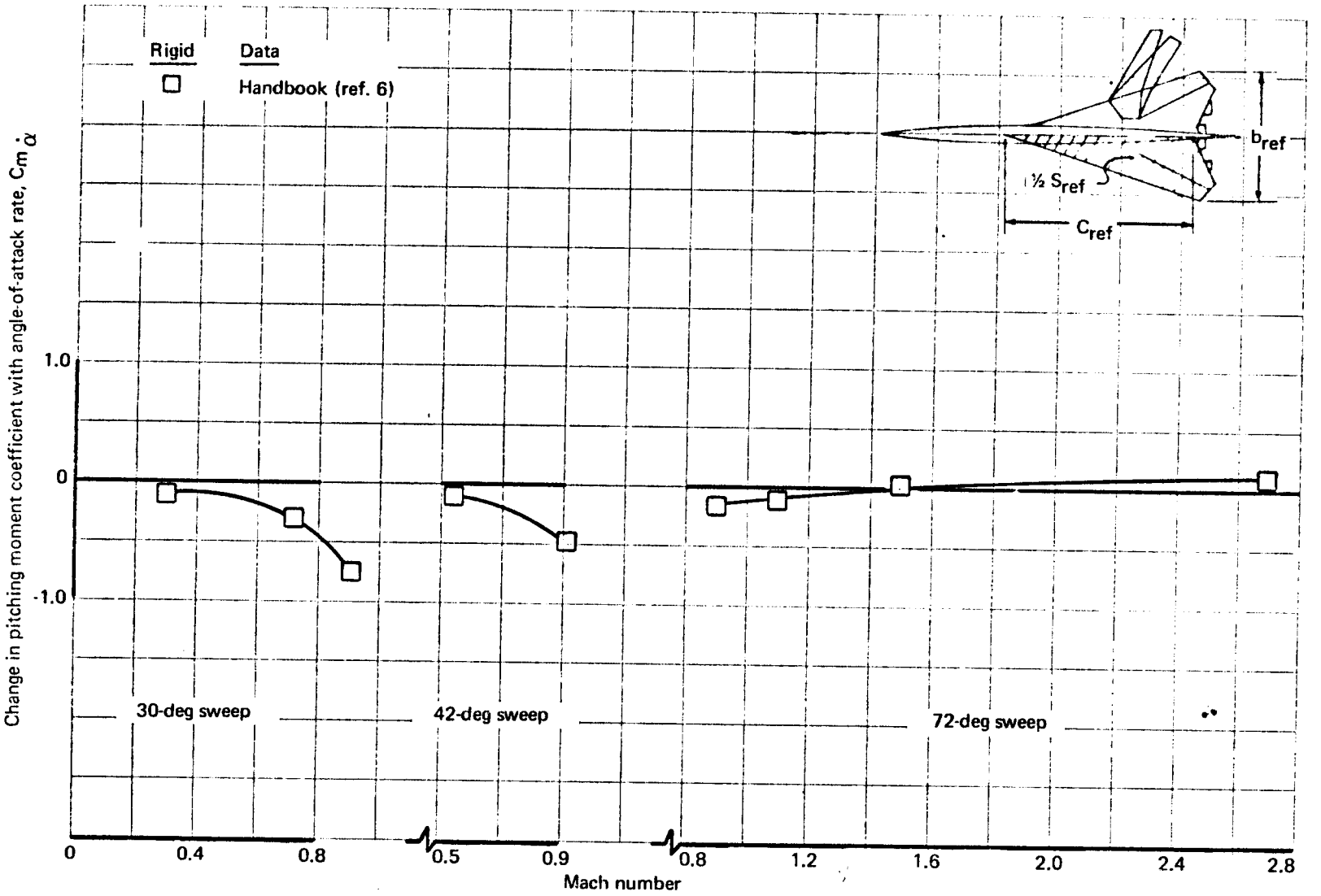

FIGURE 51.– ESTIMATION OF $C_{m_{\dot{\alpha}}}$ –SST

7.4 Speed (u) Derivatives

The derivatives C_{L_u}, C_{D_u}, and C_{m_u} for the 707-320B and SST were calculated by several theoretical and semi-empirical methods. The results of each method were compared to values measured in the wind tunnel. It was found that the method of TA 67A yields C_{L_u} and C_{m_u} values that correlate very well with wind tunnel data; the values of C_{D_u} did not correlate as well. The latter is again due to the poor leading edge representation shown in fig. 47.

The u equivalent elastic stability derivatives were determined by the lifting surface, aerodynamic influence coefficient theory. A handbook method does not exist to evaluate the effect of elasticity on these derivatives. Even though the lifting surface values of the u derivatives cannot be compared against the other methods, the results for C_{L_u} and C_{m_u} are presented because of their relative importance in app. C. No data are shown for elastic effects on C_{D_u} because of difficulty in obtaining this stability derivative by any of the known methods.

In general, it was shown that the effect of mass on the value of the elastic stability derivatives is small. The effect of elasticity, however, was shown to be significant.

7.4.1 $C_{L_u} = \frac{\partial C_L}{\partial U}$; Variation of lift with forward speed. — This stability derivative was calculated by the following methods:

(1) Lifting surface (TA 67A).

(2) Handbook (ref. 4).

(3) Wind tunnel.

The results for the 707-320B and the SST are shown in figs. 52 and 53.

7.4.1.1 Rigid results: Figures 52 and 53 show that the lifting surface method (TA 67A) correlates very well with experiment. It should be noted that C_{L_u} is very sensitive to the wing camber and twist distribution and care for accuracy must be exercised when one uses TA 67A. The handbook method of ref. 4 correlates poorly with the wind tunnel data, possibly because it neglects wing camber and twist. The effect of camber and twist is shown for the SST (fig. 53) by the difference in lifting surface and flat-plate lifting surface theory.

7.4.1.2 Elastic results: As noted, only the lifting surface method could be used to calculate the C_{L_u} elastic stability derivative. However, figs. 52 and 53 do show that the effect of elasticity on C_{L_u} is significant, although the effect of inertia ("zero mass" versus "with mass") is small.

7.4.2 $C_{D_u} = \frac{\partial C_D}{\partial u}$; Variation of drag with forward speed. — This stability derivative was calculated by the following methods:

(1) Lifting surface (TA 67A).

(2) Wind tunnel.

The results for the 707-320B and SST are presented in figs. 54 and 55.

7.4.2.1 Rigid results: The values of C_{D_u} from the lifting surface method (TA 67A) correlate poorly with wind tunnel data for the 707-320B and 42° leading edge sweep SST. However, for the 30° and 72° leading edge sweep SST, the lifting surface method appears to be accurate. The poor wing-leading-edge representation as shown in fig. 47 is again a large source of error and inconsistency.

7.4.2.2 Elastic results: No data are shown for the C_{D_u} elastic stabliity derivative because of the difficulty in obtaining this derivative by existing techniques.

7.4.3 $C_{m_u} = \frac{\partial C_m}{\partial u}$; Variation of pitching moment with forward speed. — This stability derivative was calculated by the following methods:

(1) Lifting surface (TA 67A).

(2) Wind tunnel.

The results for the 707-320B and the SST are shown in figs. 56 and 57.

7.4.3.1 Rigid results: The lifting surface method (TA 67A) correlates well with wind tunnel data except in the transonic speed regime. The transonic error is most evident in the 707-320B case ($M > 0.80$) and 72° leading edge sweep SST case ($0.7 \leq M \leq 1.0$).

7.4.3.2 Elastic results: Figures 56 and 57 also present a comparison of rigid and elastic values of C_{m_u} calculated by the lifting surface method. The effect of inertia ("zero mass" versus "with mass") on the value of C_{D_u} is seen to be small.

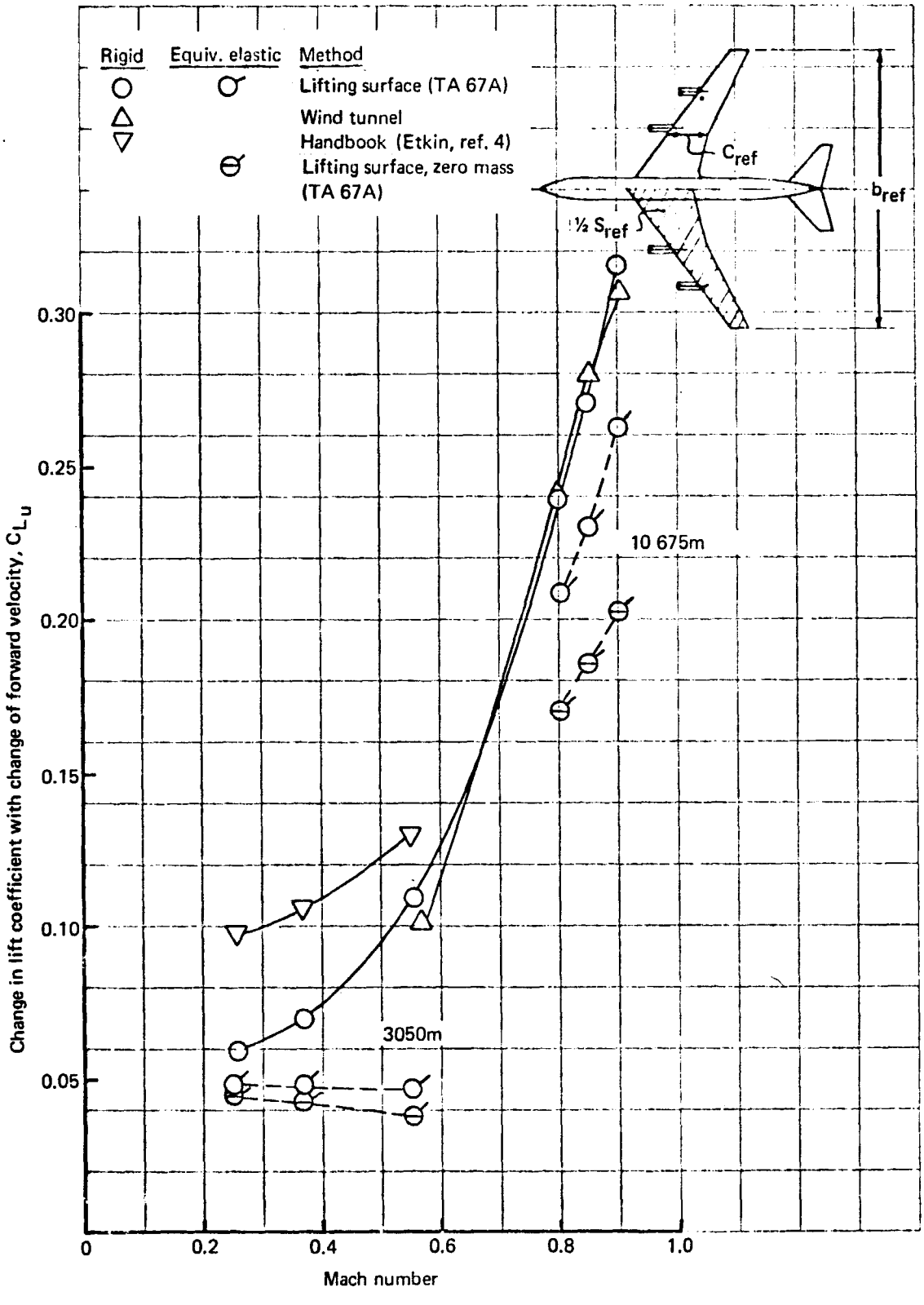

FIGURE 52. – COMPARISON OF ESTIMATION METHODS FOR C_{L_u} – 707-320B

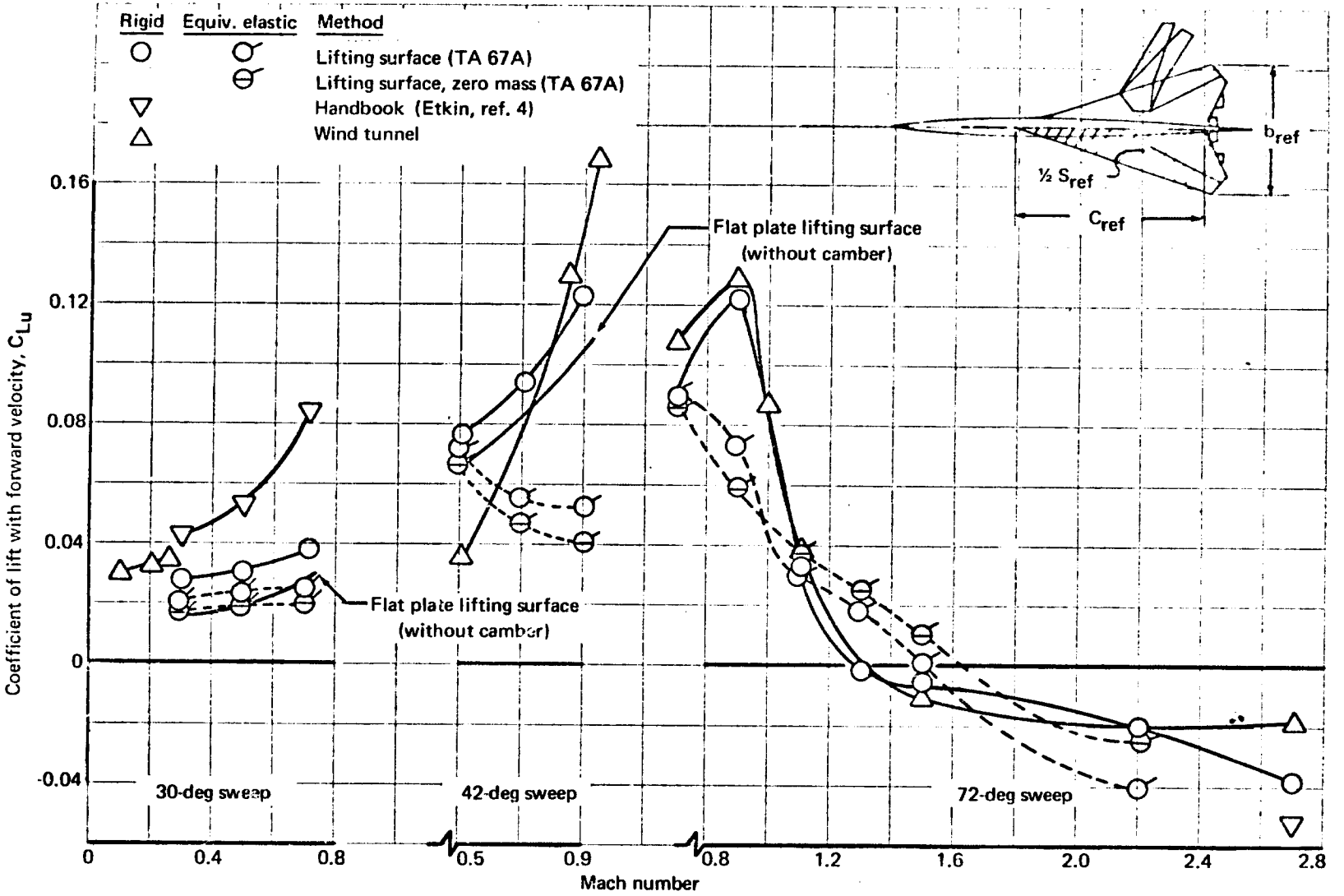

FIGURE 53.– COMPARISON OF ESTIMATION METHODS FOR C_{L_u} –SST

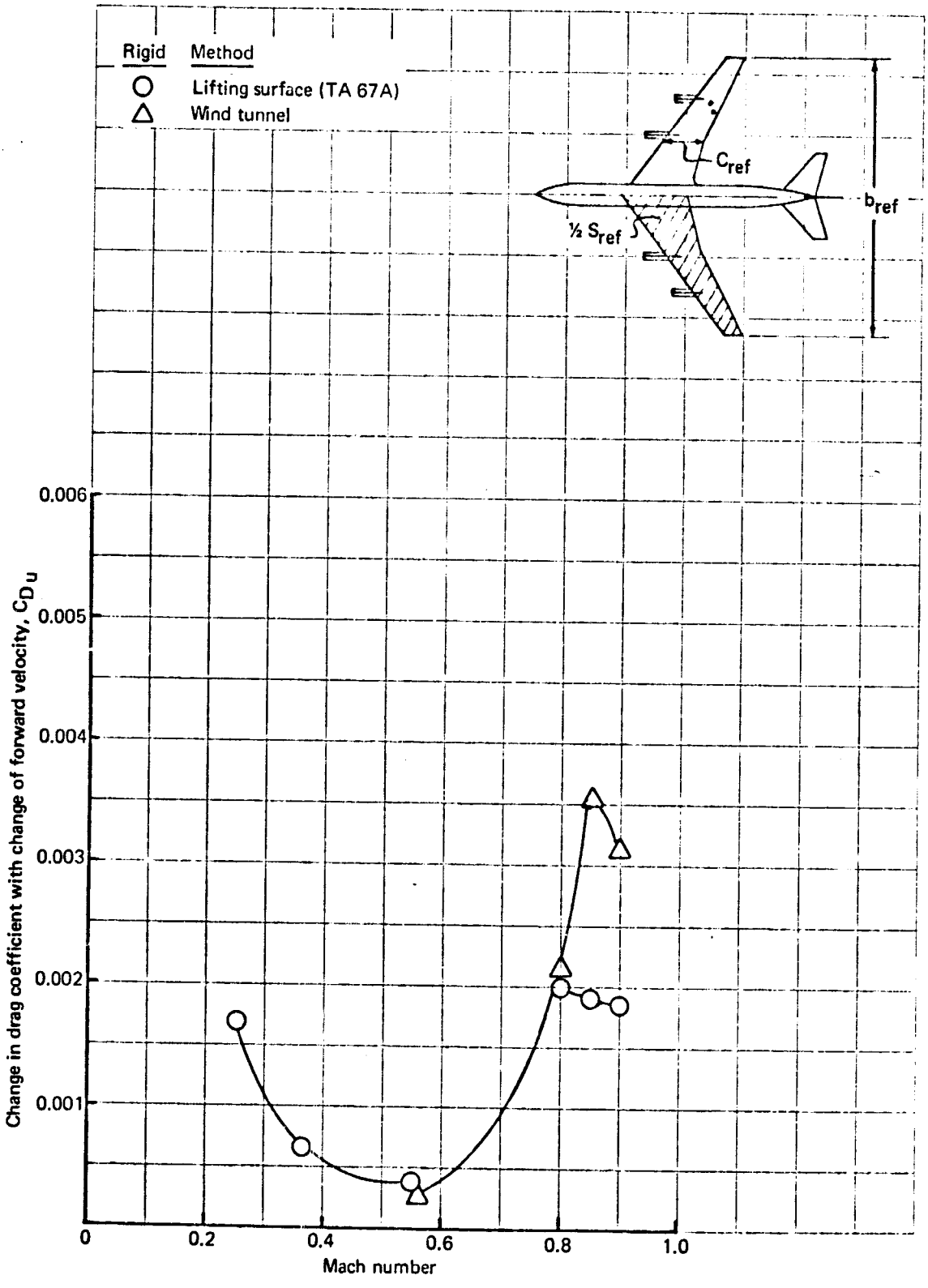

FIGURE 54. – COMPARISON OF ESTIMATION METHODS FOR C_{D_u} – 707-320B

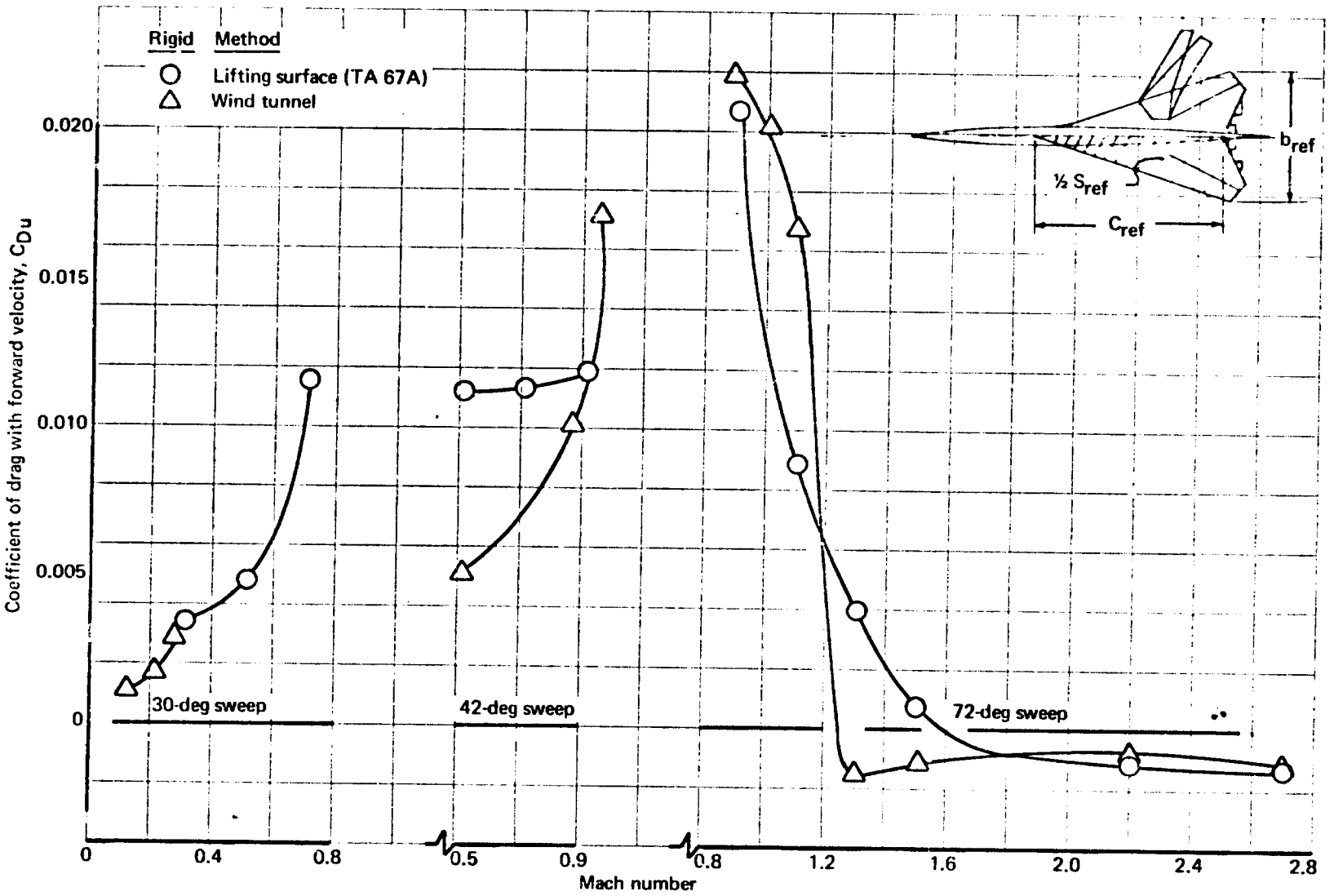

FIGURE 55.– COMPARISON OF ESTIMATION METHODS FOR C_{D_u} –SST

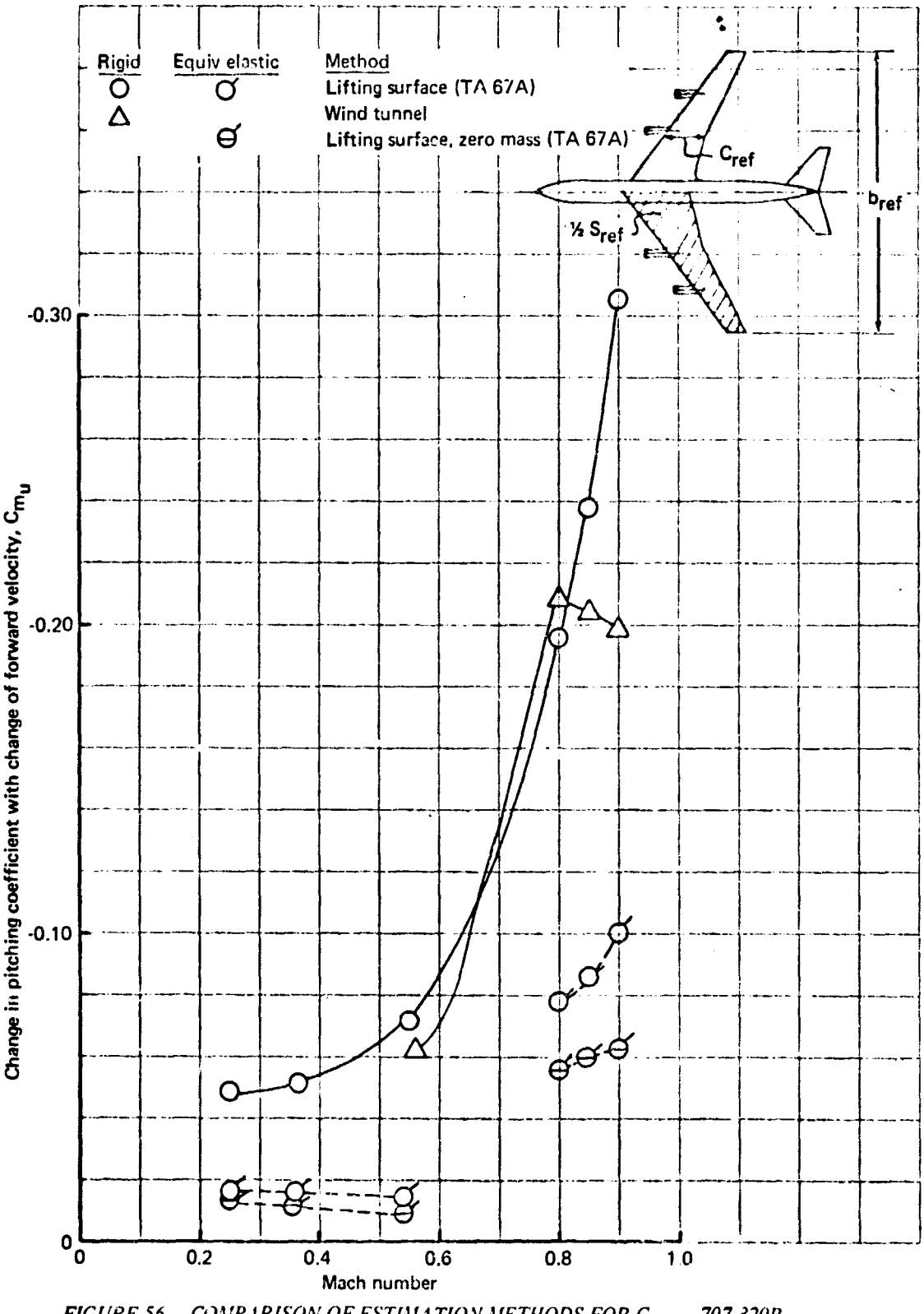

FIGURE 56.- COMPARISON OF ESTIMATION METHODS FOR C_{m_u} – 707-320B

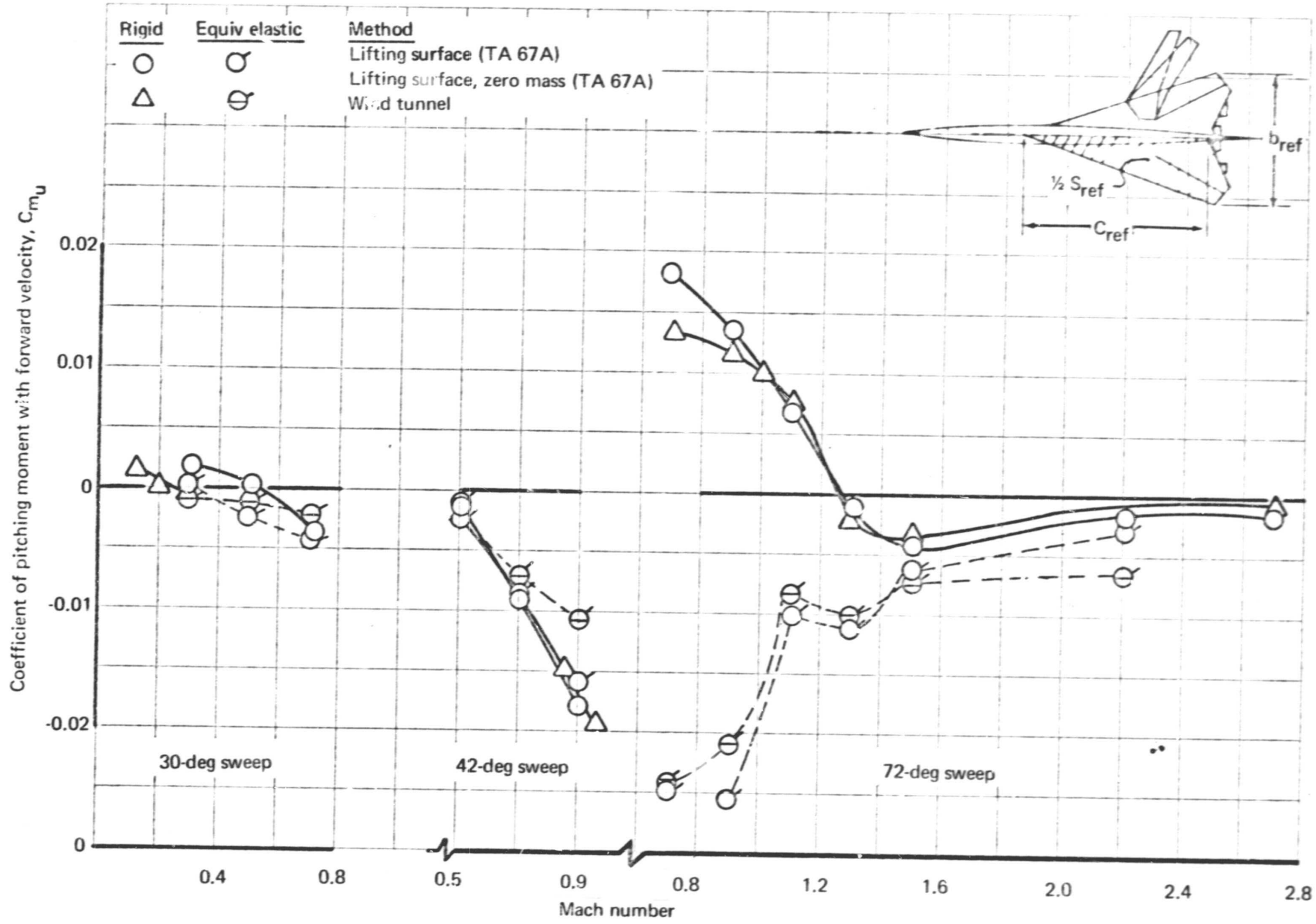

FIGURE 57. – COMPARISON OF ESTIMATION METHODS FOR C_{m_u} – SST

7.5 Pitch-Rate (q) Derivatives

Pitch-rate derivatives belong to the class of rate or dynamic derivatives. For small angles of attack and small values of pitch rate q, the additive aerodynamic-load distribution due to q can be estimated on the basis of assuming steady, attached flow. This assumption is basic to all methods of calculating the q derivatives that are discussed in this section. This usually means that at subsonic speeds, the methods are valid for high-aspect-ratio wings up to stall angle of attack, but are limited for low-aspect-ratio wings to low angles of attack. The following is paraphrased from ref. 6: (G8) (A8)

'For airplanes operating under conditions of partially separated flow, such as with low-aspect-ratio wings at moderate to high angles of attack, experimental data, e.g., refs. 63 and 69, show that substantial nonlinearities exist in the dynamic derivatives.'

In addition, wind tunnel tests by the oscillating mode technique show that the dynamic derivatives are functions of both the amplitude and frequency of oscillation when the frequency of oscillation is large. In general, dynamic derivatives for separated-flow conditions are very nonlinear and, therefore, no tunnel data were available to validate any of the methods for computing q derivatives. However, for attached-flow conditions, the results obtained from lifting surface program TA 67A are most likely to agree with experimental data. It is suggested that this may be checked by applying lifting surface theory to configurations for which known, reliable values of C_{L_q} and C_{m_q} are available.

The results of comparison of methods for calculating the q derivatives showed that agreement between the lifting surface method and handbook method is poor.

7.5.1 $C_{L_q} = \frac{\partial C_L}{\partial q}$; Variation of lift with pitch rate. — This stability derivative was calculated by the following methods:

(1) Lifting surface (TA 67A).

(2) Handbook (ref. 6).

The results for the 707-320B and the SST are presented in figs. 58 and 59.

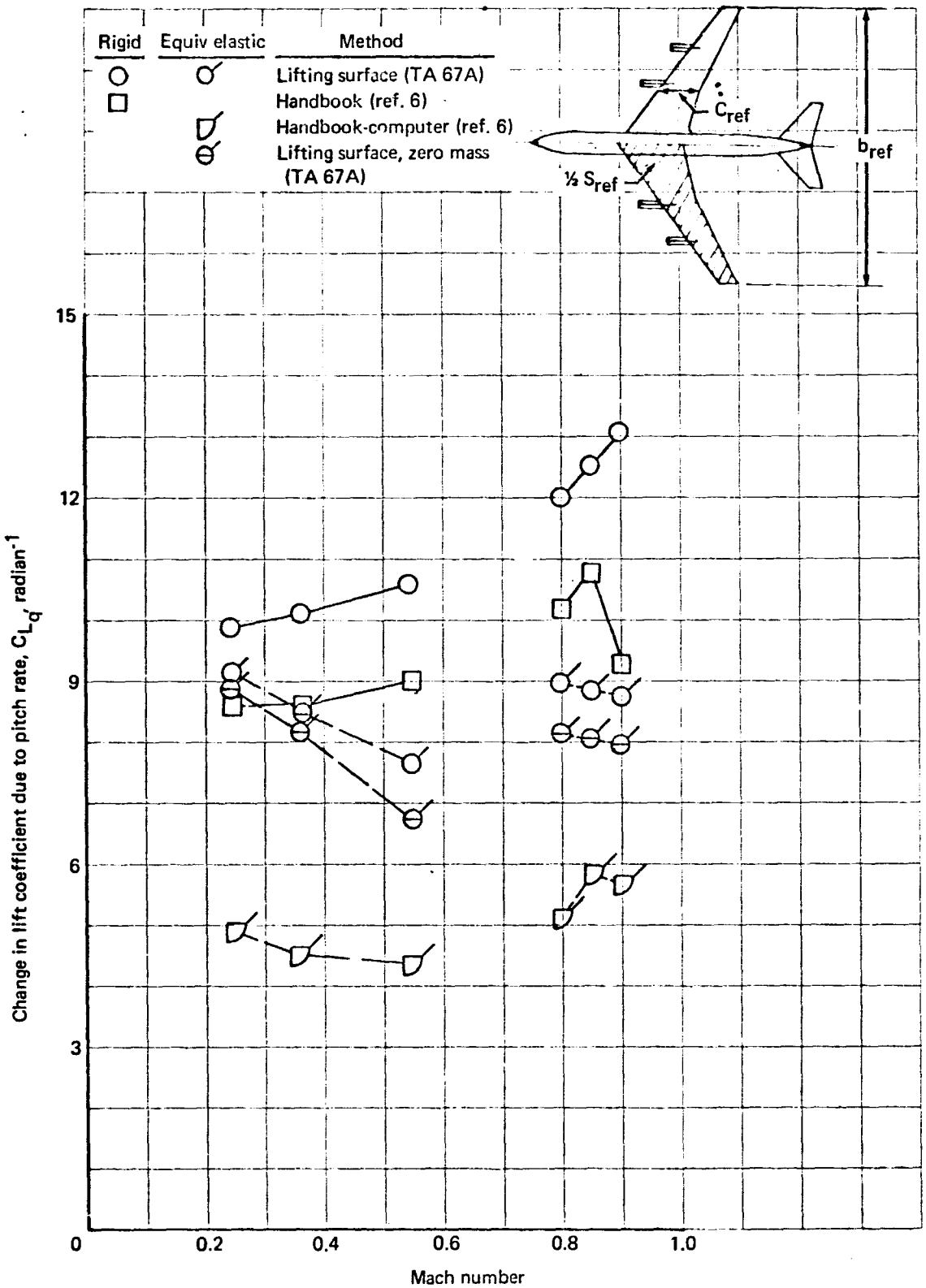

FIGURE 58.– COMPARISON OF ESTIMATION METHODS FOR C_{L_q} –707-320B

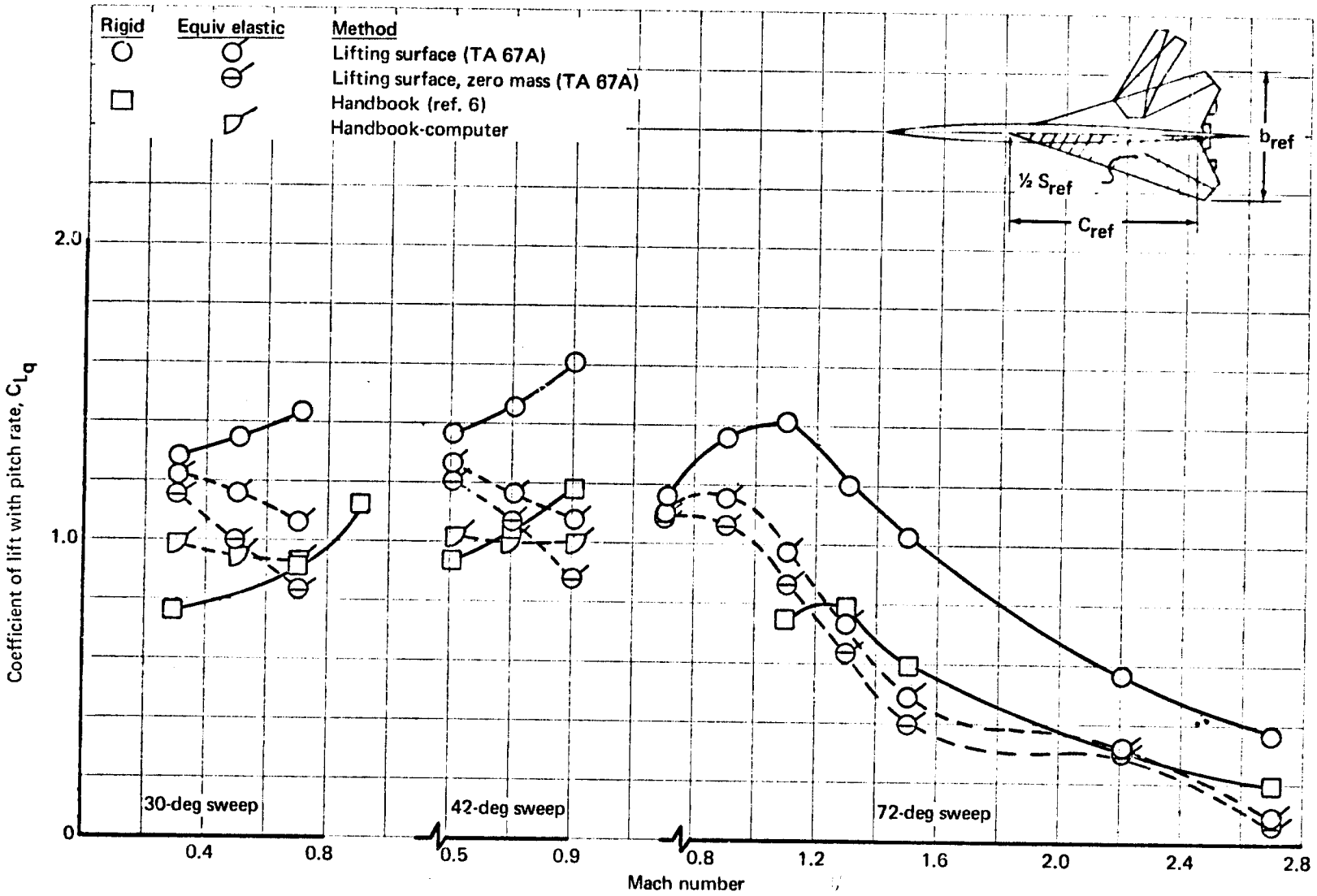

FIGURE 59.– COMPARISON OF ESTIMATION METHODS FOR C_{L_q} –SST

7.5.1.1 Rigid results: Figures 58 and 59 show that there is only fair agreement between lifting surface and handbook-calculated values of C_{L_q}. In view of the good results obtained with TA 67A in the case of α and $\dot{u}$ derivatives, the TA 67A value of C_{L_q} may be more accurate than that of the handbook. However, because the handbook has been shown superior to TA 67A in the transonic range, it is suggested the TA 67A results be "faired" according to handbook transonic trends.

7.5.1.2 Elastic results: An elastic analysis of the 707 and SST generated the values of C_{L_q} shown in figs. 58 and 59. There is poor agreement between the lifting surface and handbook methods; an anticipated result in light of the rigid analysis for C_{L_q}. The effect of elasticity on the value of C_{L_q} is shown to be large. The effect of inertia, shown by the increment of C_{L_q} between the "zero-mass" and "with-mass" lifting surface results, is small

7.5.2 $C_{D_q} = \frac{\partial C_D}{\partial q}$; Variation of drag with pitch rate. — The stability derivative C_{D_q} is normally considered to be small and unimportant to most stability analysis. There is no provision in the USAF Handbook (ref. 6) for calculating this derivative. An explicit expression for C_{D_q} has been developed from lifting surface theory (TA 67A) and results for the 707-320B are presented in fig. 60. The value of C_{D_q} for the SST was not calculated and an elastic analysis for the 707-320B and SST was not attempted.

7.5.3 $C_{m_q} = \frac{\partial C_m}{\partial q}$; Variation of pitching moment with pitch rate. — This stability derivative was calculated by the following methods:

(1) Lifting surface (TA 67A).

(2) Handbook (ref. 6).

The results for the 707-320B and the SST are presented in figs. 61 and 62.

7.5.3.1 Rigid results: Figures 61 and 62 show the lifting surface and handbook values of C_{m_q} are in close agreement for the 707. There is large disagreement between the two methods in the case of the SST. The disagreement for the SST may be due to the leading edge crank problem (discussed for the derivatives). There is again the transonic discrepancy noted for C_{L_q}, and it is suggested that TA 67A be "faired" to reflect the transonic trends calculated by the handbook method.

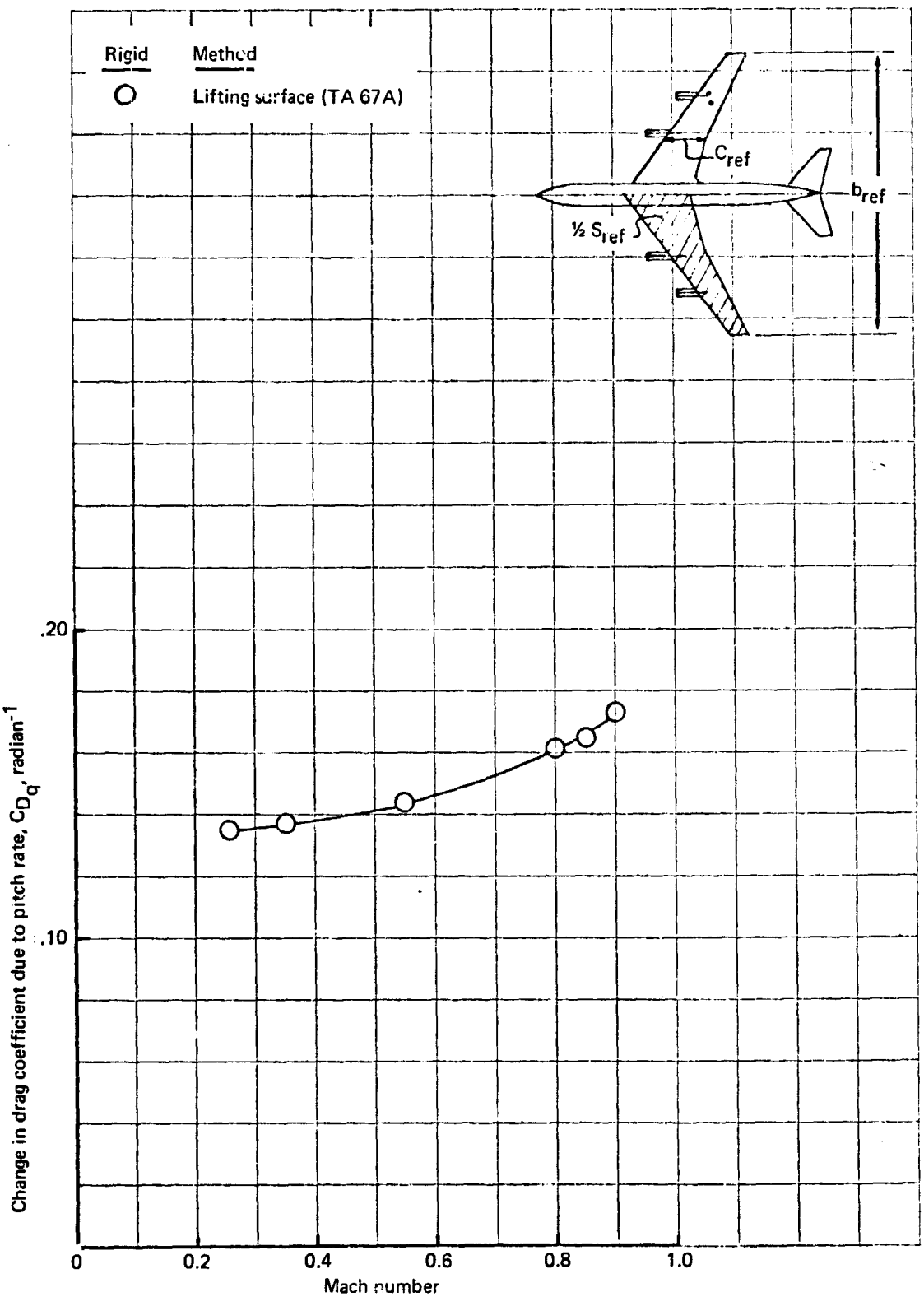

FIGURE 60.– ESTIMATION OF C_{D_q} –707-320B

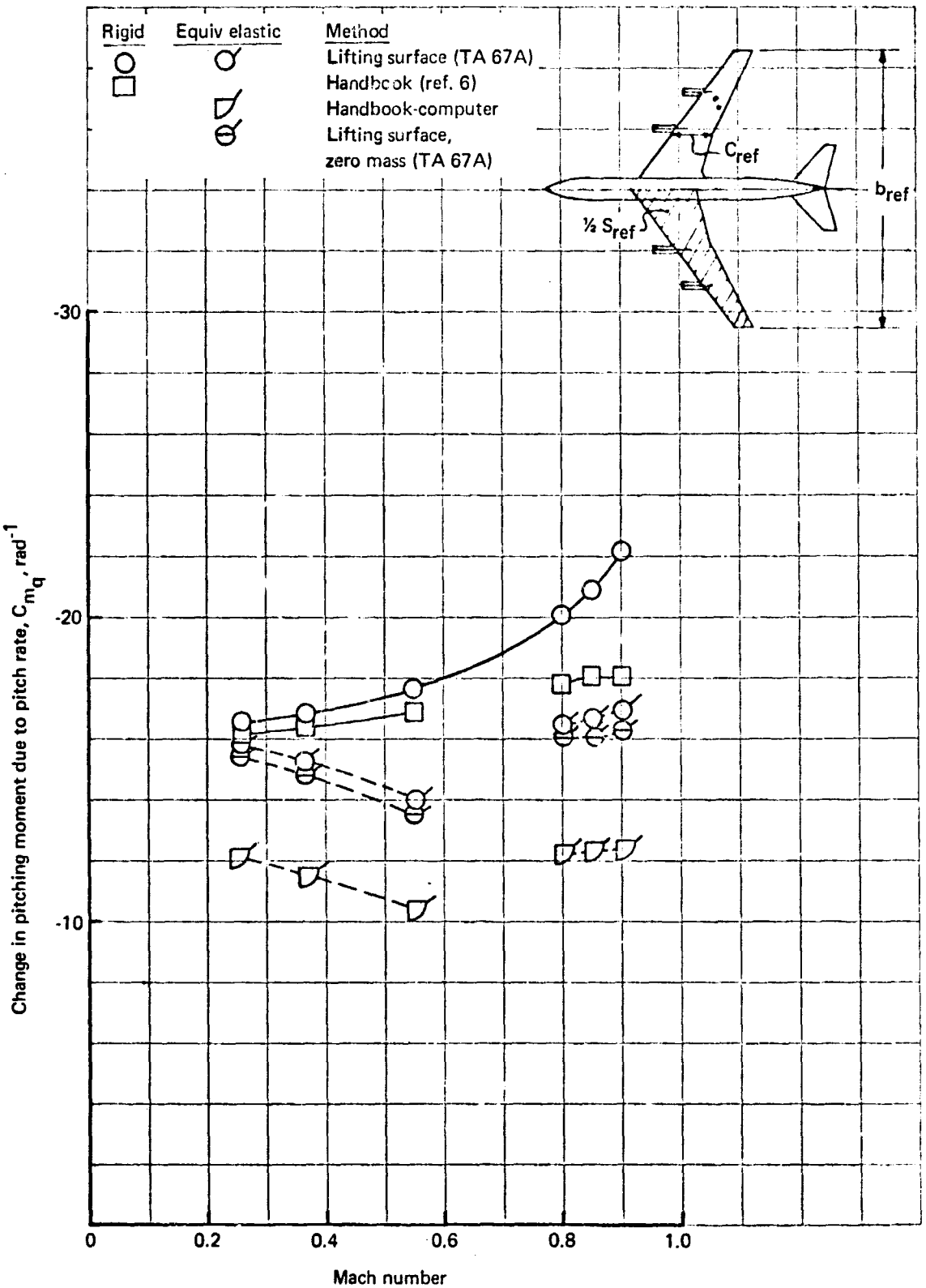

FIGURE 61. - COMPARISON OF ESTIMATION METHODS FOR C_{m_q} - 707-320B

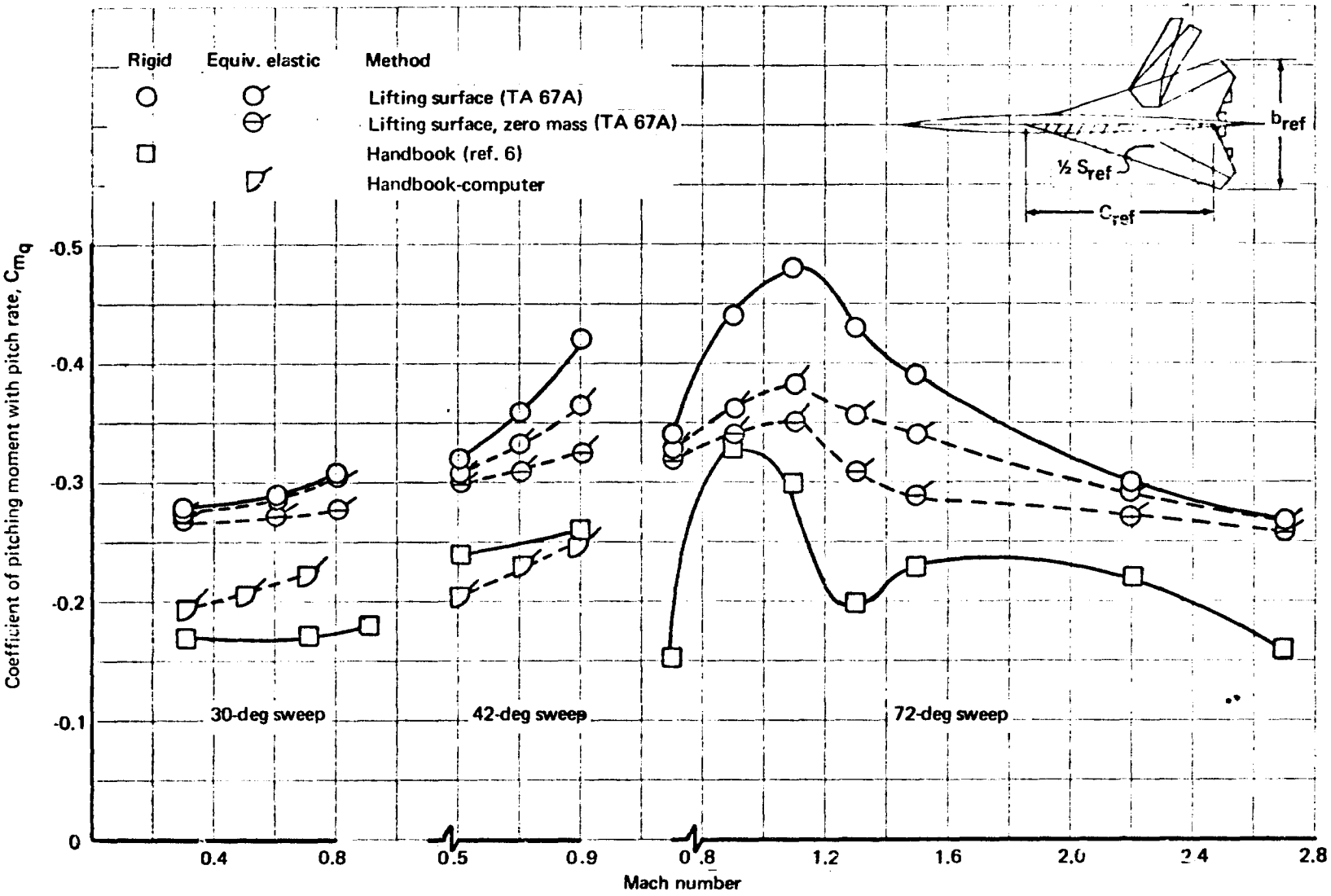

FIGURE 62.– COMPARISON OF ESTIMATION METHODS FOR C_{m_q}–SST

7.5.3.2 Elastic results: The effects of elasticity on the value of C_{m_q} for the 707 and SST are also shown in figs. 61 and 62. The effect of elasticity is large for both airplanes, while the effect of inertia is significant only for the SST. There is only fair agreement between the handbook and lifting surface methods; C_{m_q} from the handbook is always smaller in value.

7.6 Sideslip (β) Derivatives

The sideslip derivatives were predicted by semi-empirical handbook methods only. At the present time, an accurate theoretical method does not exist to predict the flow field around an arbitrary aircraft configuration in sideslip. Several formulations, e.g., Sec. 4, have been proposed. In view of the success in accurately predicting the α and u derivatives via the lifting surface, aerodynamic influence coefficient technique, it is reasonable to expect a similar exact formulation of the inviscid aerodynamic theory will lead to good results for lateral-directional flight.

The methods of refs. 6 and 73 have been applied to the 707-320B and to the SST and compared to wind tunnel data. Handbook methods used are summarized in tables 18, 19, 24, and 25. All wind tunnel data were obtained by reading slopes at the zero sideslip angle. The effects of aeroelasticity were included per the formulas of Sec. 5 in which only aft body bending (K_β) and vertical-tail elasticity (L_E/L_R) are included. The effect of K_β on the β derivatives of the 707 was investigated; the effect of L_E/L_R on C_{n_β} of the 707 was also investigated.

In all cases it was shown that aeroelasticity is important to the β derivatives. It was found that C_{y_β} and C_{n_β} are affected to a significant degree by the K_β and L_E/L_R terms. It should be noted that C_{l_β} does not include its major aeroelastic effect: wing-forebody bending. It is recommended that the future development of aerodynamic and structural theory be oriented to include lateral-directional flight cases.

7.6.1 $C_{y_\beta} = \frac{\partial C_y}{\partial \beta}$; Variation of side force with sideslip. — This stability derivative was calculated using the USAF Handbook (ref. 6). Results for the 707-320B and the SST are presented in figs. 63 and 64.

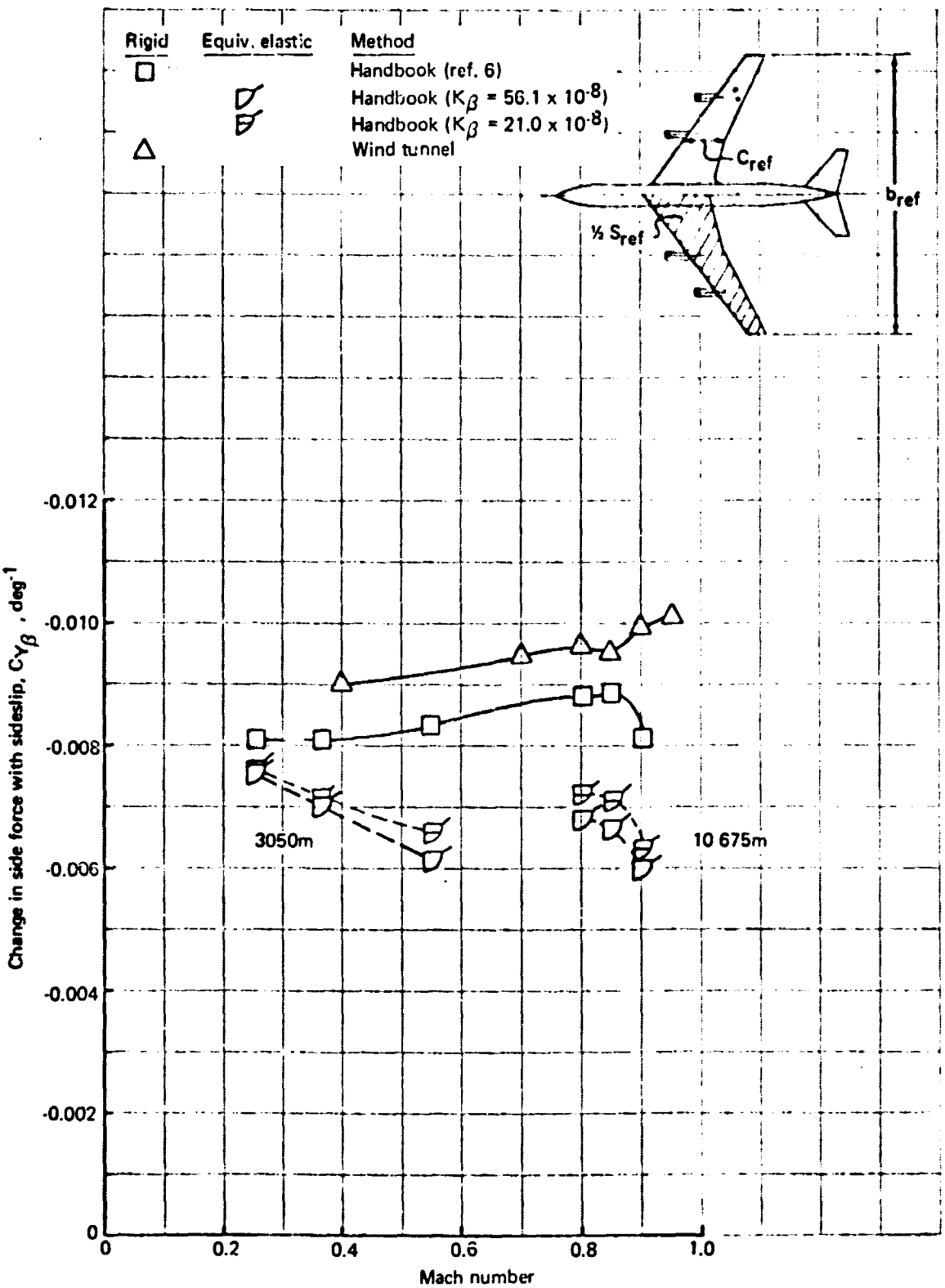

FIGURE 63. – COMPARISON OF ESTIMATION METHODS FOR C_{Y_β} – 707-320B

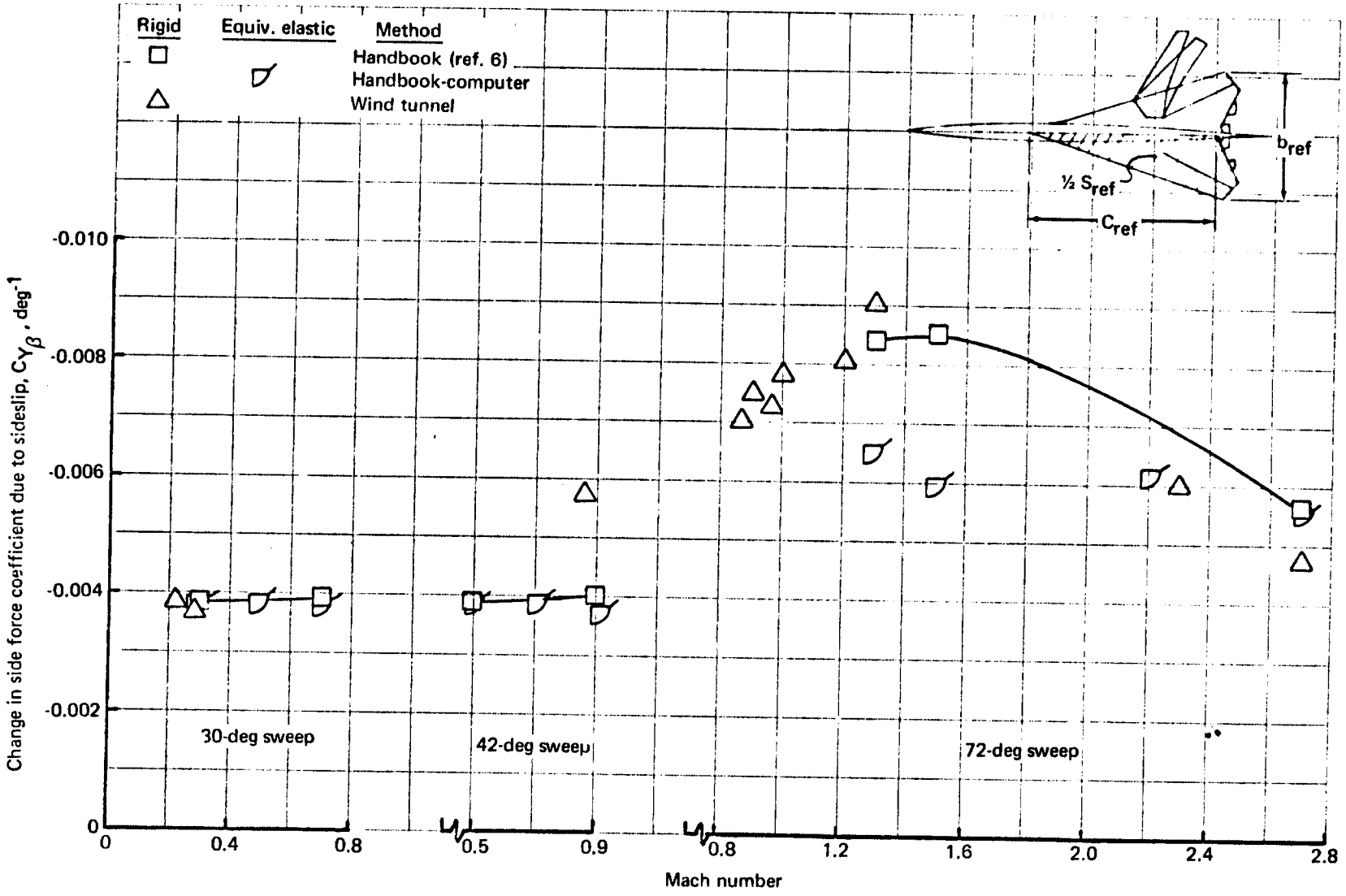

FIGURE 64.– COMPARISON OF ESTIMATION METHODS FOR C_{Y_β} –SST

7.6.1.1 Rigid results: The handbook values of C_{y_β} for the 707 (fig. 63) and the SST (fig. 64) agree very well with wind tunnel data. The accuracy of the handbook decreased slightly in the transonic speed regime for both aircraft.

7.6.1.2 Elastic results: The effect of elasticity on C_{y_β} is also shown in figs. 63 and 64. Aeroelasticity is seen to have a large effect in the case of the 707 and the SST at 72° leading edge sweep. A variation of K_β from 21×10^{-8} to 56.1×10^{-8}, holding $L_E/L_R = 0.813$, had little effect on the value of C_{y_β} for the 707.

7.6.2 $C_{\ell_\beta} = \frac{\partial C_\ell}{\partial \beta}$; Variation of rolling moment with sideslip. — This stability derivative was calculated by the methods of the USAF Handbook (ref. 6) and of Kohlman (ref. 73). The results for the 707-320B and the SST are compared to wind tunnel data in figs. 65 and 66.

7.6.2.1 Rigid results: Estimation of the value of C_{ℓ_β} for the 707 by refs. 6 and 73 is poor in all but the transonic cruise range. The change of C_{ℓ_β} with Mach number for the 707 is incorrect at $M < 0.55$, suggesting fundamental errors in the method. Both methods fail in accuracy but succeed in predicting the correct Mach number trends when applied to the SST configuration.

7.6.2.2 Elastic results: The effect of elasticity on C_{ℓ_β} is also shown in figs. 65 and 66 for the 707 and the SST. Aeroelastic effects are larger for the 707 than the SST, and in the opposite direction. A variation of K_β from 21×10^{-8} to 56.1×10^{-8}, holding $L_E/L_R = 0.813$, had little effect on the value of C_{ℓ_β} of the 707.

7.6.3 $C_{n_\beta} = \frac{\partial C_n}{\partial \beta}$; Variation of yawing moment with sideslip. — This stability derivative was calculated by the USAF Handbook (ref. 6) semi-empirical method. Results for the 707-320B and the SST are compared to wind tunnel data in figs. 67 and 68. The effect on the 707 C_{n_β} at $M = 0.85$ due to variations in vertical-tail elasticity (L_E/L_R) is shown in fig. 67.

7.6.3.1 Rigid results: The estimation of C_{n_β} for the 707 (fig. 67) by the methods of ref. 6 is inadequate when compared to wind tunnel data. Accuracy is poor and the trend with Mach number is incorrect for $M < 0.55$. In the case of the SST (fig. 68) the methods of ref. 6 are adequate for the 30° and 42° sweep cases, but inadequate for the 72° sweep case.

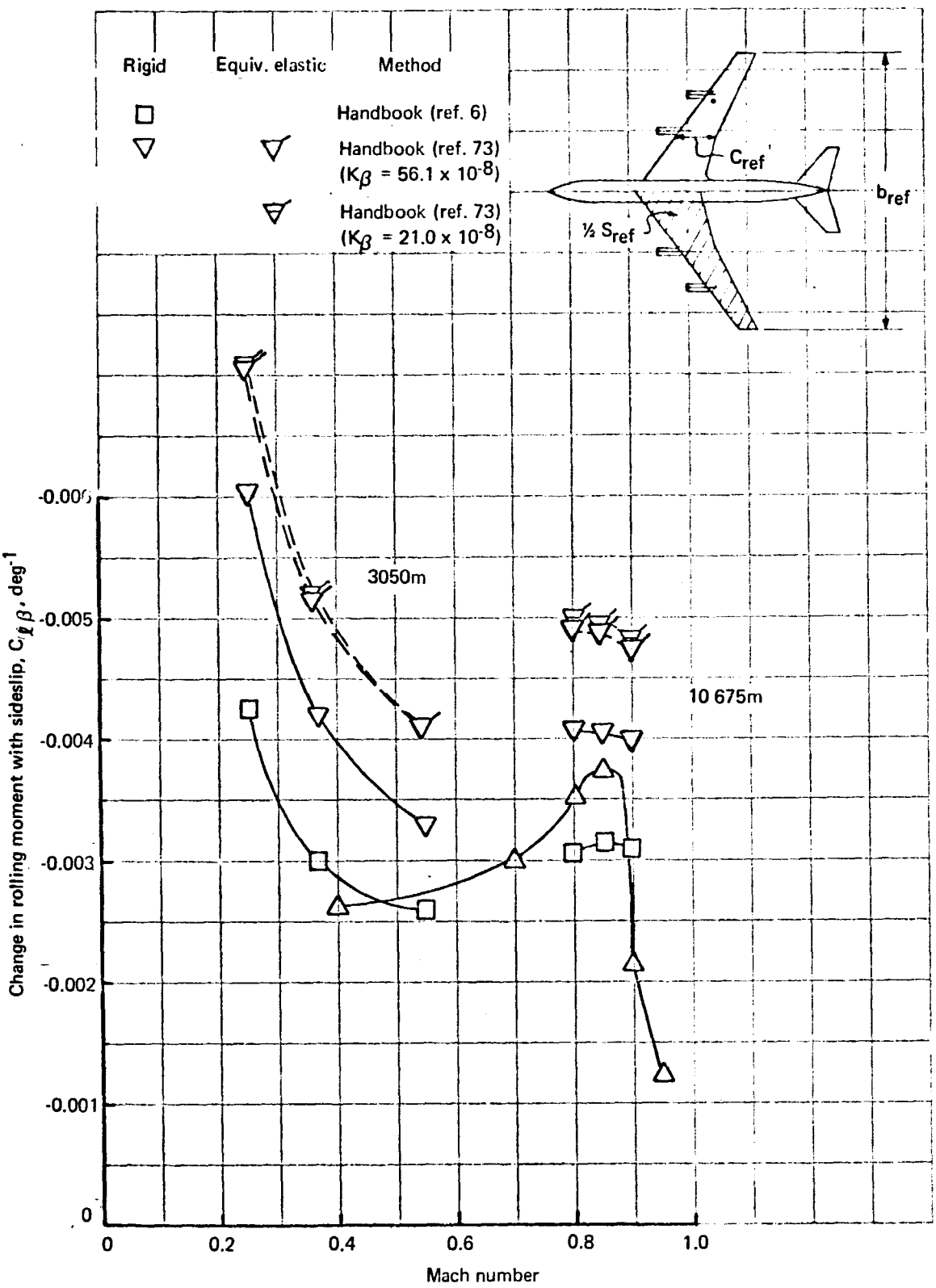

FIGURE 65.– COMPARISON OF ESTIMATION METHODS FOR $C_{\ell\beta}$ – 707-320B

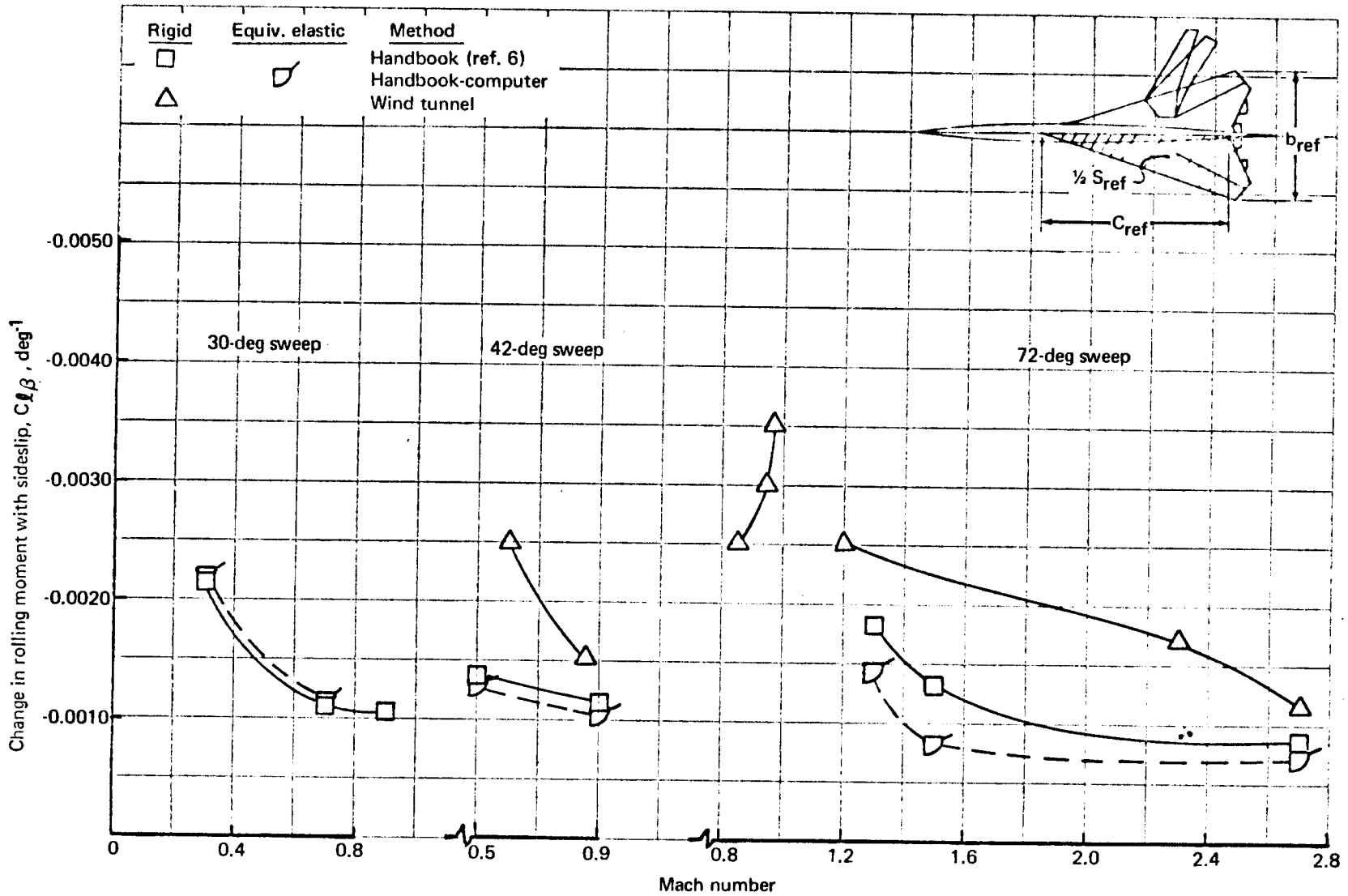

FIGURE 66.– COMPARISON OF ESTIMATION METHODS FOR C_{ℓ_β} –SST

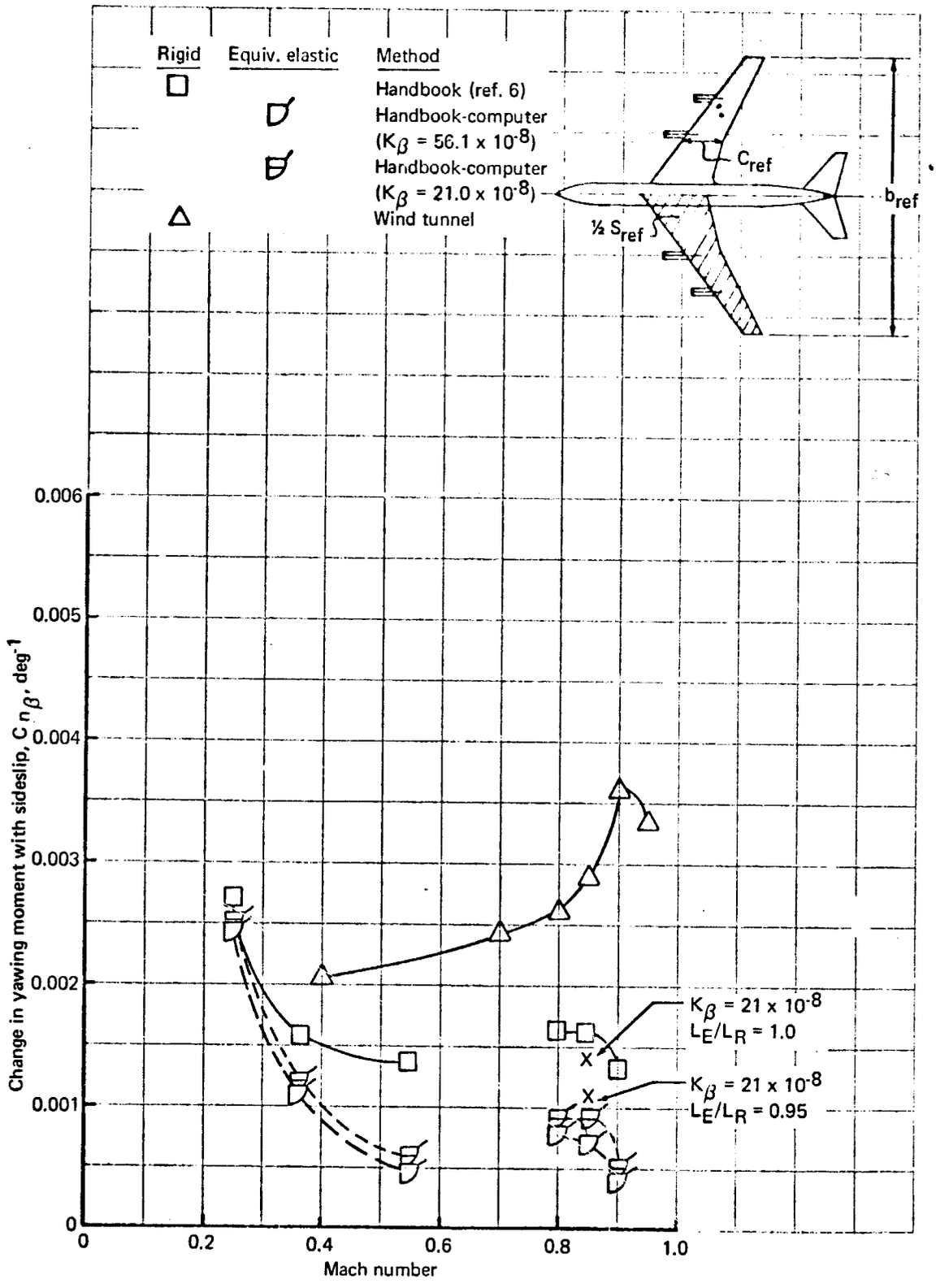

FIGURE 67.-- COMPARISON OF ESTIMATION METHODS FOR C_{n_β} -707-320B

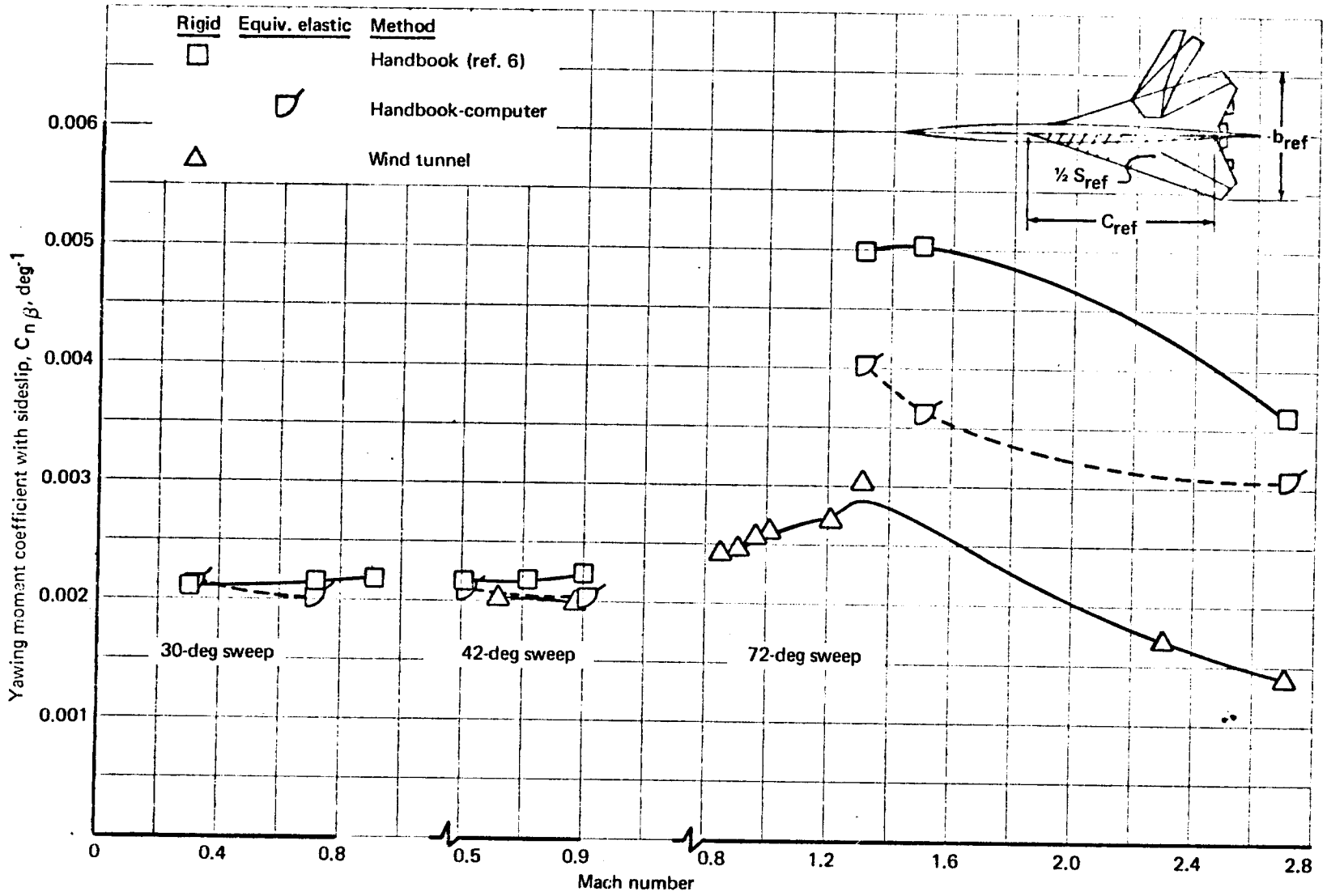

FIGURE 68.– COMPARISON OF ESTIMATION METHODS FOR C_{n_β} –SST

7.6.3.2 Elastic results: The effects of elasticity on C_{n_β} of the 707 (fig. 67) and of the SST at 72° sweep (fig. 68) is large and decreases the rigid value of C_{n_β}. Elasticity has little effect on the 30° and 42° sweep SST cases. A variation of K_β from 21×10^{-8} to 56.1×10^{-8}, holding $L_E/L_R = 0.813$, had little effect on the value of C_{n_β} for the 707 (see fig. 67).

Because the value of C_{n_β} has a strong influence on the Dutch roll frequency (app. C) and because the variation of K_β had little effect on C_{n_β} of the 707, a study of the elastic terms contributing to C_{n_β} of the 707 (K_β and L_E/L_R) was performed. The results are shown in fig. 67 at Mach number 0.85 only. Tabulating the results:

Mathematical model of 707	K_β	L_E/L_R	C_{n_β} (deg^{-1})	C_{n_β} rigid $-C_{n_\beta}$ elas. (deg^{-1})
Rigid	0	1.0	0.001620	----------
Elastic	21.0×10^{-8}	1.0	0.001410	+ 0.000210
Elastic	21.0×10^{-8}	0.95	0.001094	+ 0.000526
Elastic	21.0×10^{-8}	0.813	0.000900	+ 0.000720
Elastic	56.1×10^{-8}	0.813	0.000680	+ 0.000940

Flight test data indicate that the computer value of $L_E/L_R = 0.813$ is too low for the 707 and that $L_E/L_R = 0.95$ is more representative. This error in accuracy generated within the lifting surface elastic program is the most probable cause of the large elastic effects seen in all the 707 lateral-directional derivatives discussed in this report. Thus, it is concluded that this error in vertical-tail elasticity is one of the major shortcomings of the handbook-computer technique.

7.7 Sideslip Rate ($\dot{\beta}$) Derivatives

The physical discussion of par. 7.3 for the $\dot{\alpha}$ derivatives also applies to the $\dot{\beta}$ derivatives. Analogous to the downwash lag, a sidewash lag develops as a result of $\dot{\beta}$ motion. However, no method was found to calculate the $\dot{\beta}$ derivatives for a complete airplane configuration. It was assumed, therefore, that for attached flow conditions the vertical tail would be the largest contributor to $C_{y_{\dot{\beta}}}$ and $C_{n_{\dot{\beta}}}$. By applying a sidewash lag theory in analogy to the

downwash lag theory used in finding $C_{L_{\dot{\alpha}}}$ and $C_{m_{\dot{\alpha}}}$, it is possible to evaluate $C_{y_{\dot{\beta}}}$ and $C_{n_{\dot{\beta}}}$ from the following equations:

$$C_{y_{\dot{\beta}}} \approx C_{y_{\dot{\beta}_{V.T.}}} = -2 a_v V_v \frac{d\sigma}{d\beta} \tag{7.4}$$

$$C_{n_{\dot{\beta}}} \approx C_{n_{\dot{\beta}_{V.T.}}} = -2 a_v V_v \frac{l_v}{b} \frac{d\sigma}{d\beta} \tag{7.5}$$

The results of figs. 69 through 73 were obtained with these formulas. No simple method for computing $C_{\ell_{\dot{\beta}}}$ was found. Wing contribution to $C_{\ell_{\dot{\beta}}}$ may be the most significant. An estimate of the vertical-tail contribution is given by:

$$C_{\ell_{\dot{\beta}_{V.T.}}} = -2 a_v V_v \frac{z_v}{b} \frac{d\sigma}{d\beta} \tag{7.6}$$

This contribution is presented in figure 71 for 707-320B; no value of $C_{\ell_{\dot{\beta}}}$ V. T. was calculated for the SST.

No equivalent elastic $\dot{\beta}$ derivatives have been evaluated.

In conclusion, the state of the art with regard to methods for estimating $\dot{\beta}$ derivatives is poor. In fact, little material is available at the present time to indicate the potential importance of such derivatives.

7.8 Roll-Rate (p) Derivatives

The roll-rate stability derivatives, C_{y_p}, C_{ℓ_p}, and C_{n_p}, belong to the class of dynamic derivatives. The physical discussion of the character of the dynamic derivatives is found in par. 7.4 for the q derivatives and it applies also to the p derivatives.

Section 4 contains the complete derivation of the theoretical method of calculating roll-rate derivatives for a thin body by aerodynamic influence coefficients. However, only C_{ℓ_p} could be evaluated because of present computer programming limitations of TA 67A.

The USAF Handbook (ref. 6) and the technique of TR 1098 (ref. 72) are incomplete with regard to the calculation of p derivatives for wing-body-tail configurations. To as large an extent as possible, the p derivatives were computed by the methods outlined in tables 20, 21, 26, and 27.

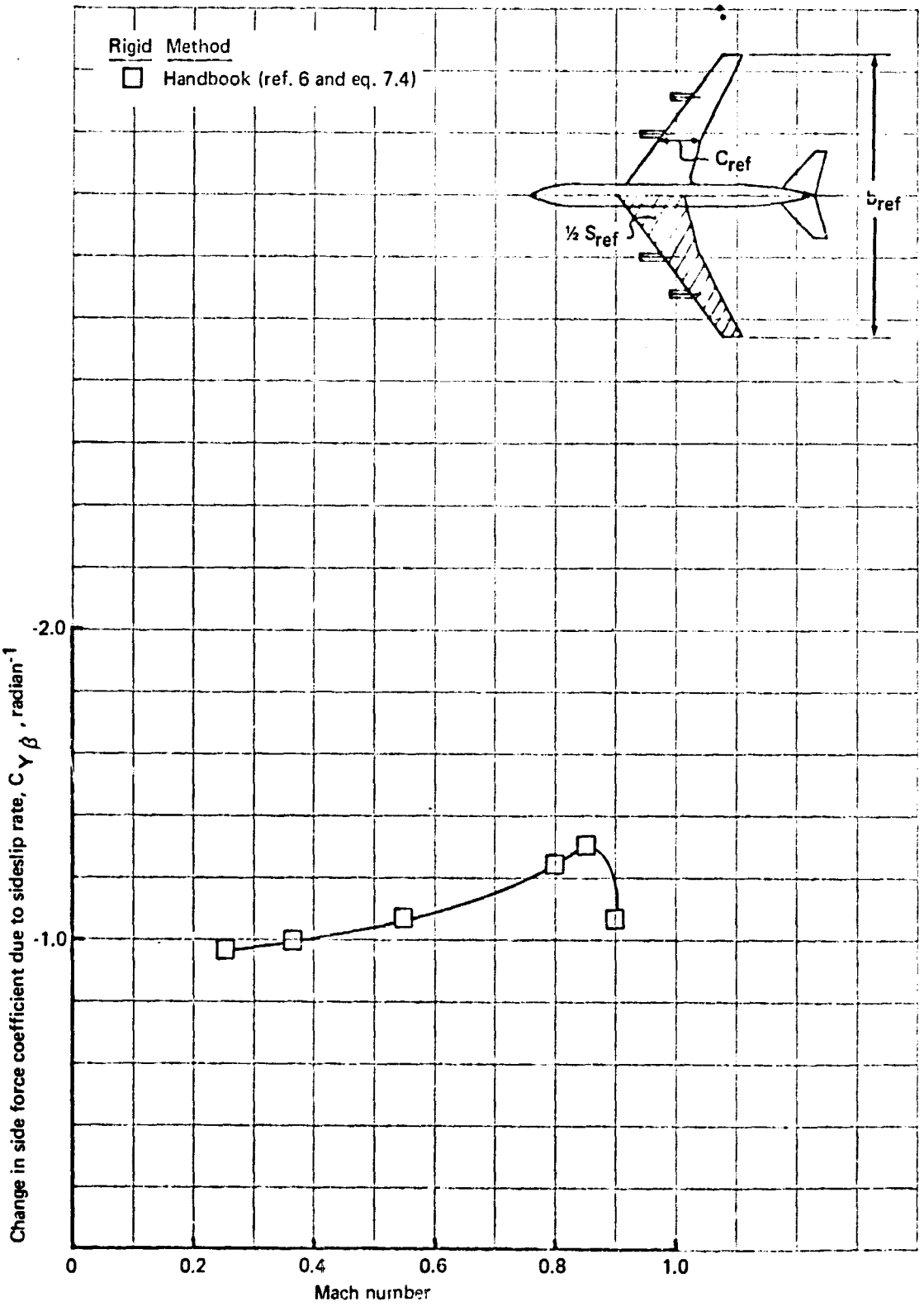

FIGURE 69. – ESTIMATION OF $C_{Y_{\dot{\beta}}}$ – 707-320B

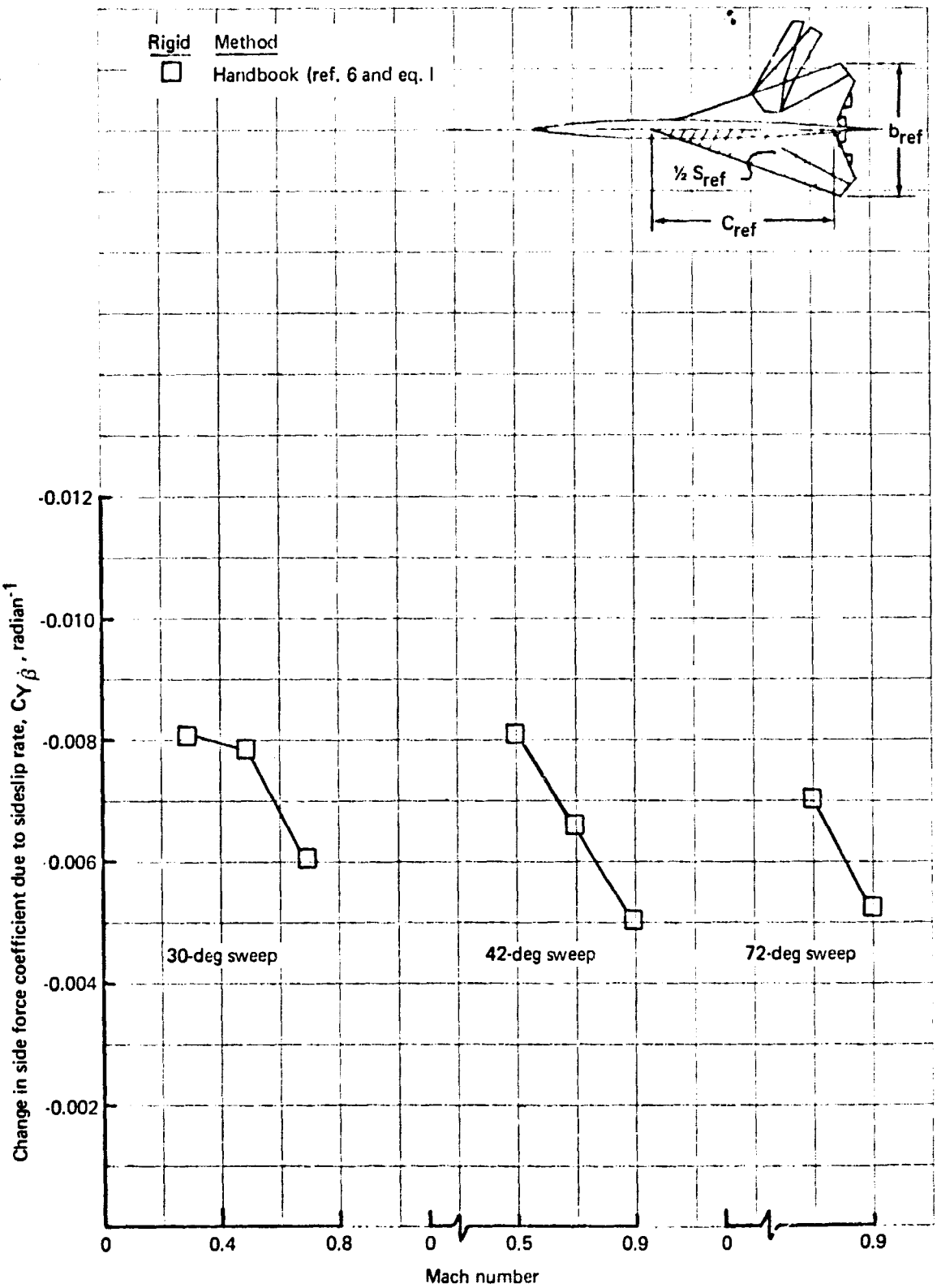

FIGURE 70.--ESTIMATION OF $C_{Y_{\dot{\beta}}}$ -SST

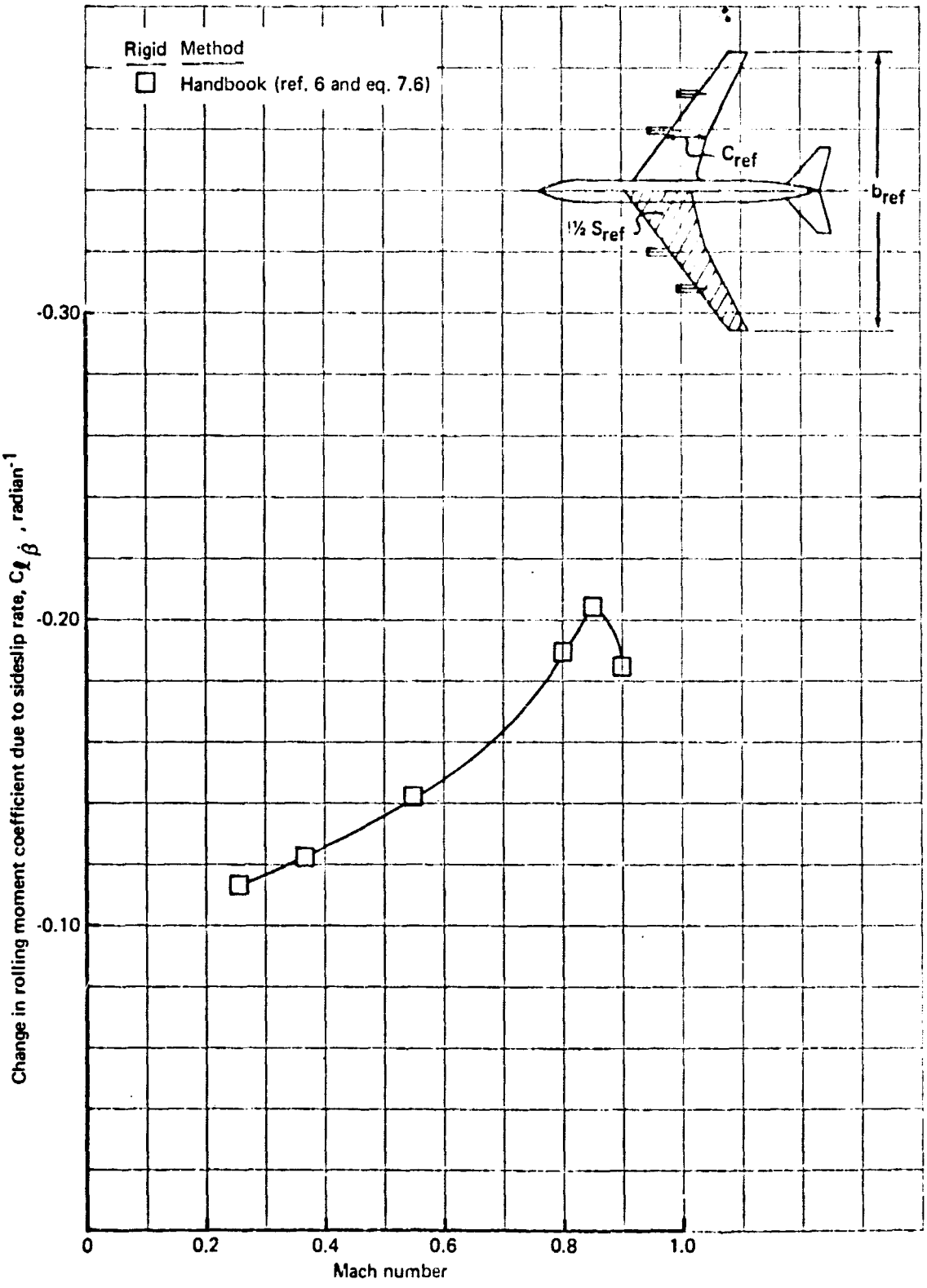

FIGURE 71.– ESTIMATION OF $C_{\ell_{\dot{\beta}}}$ - 707-320B

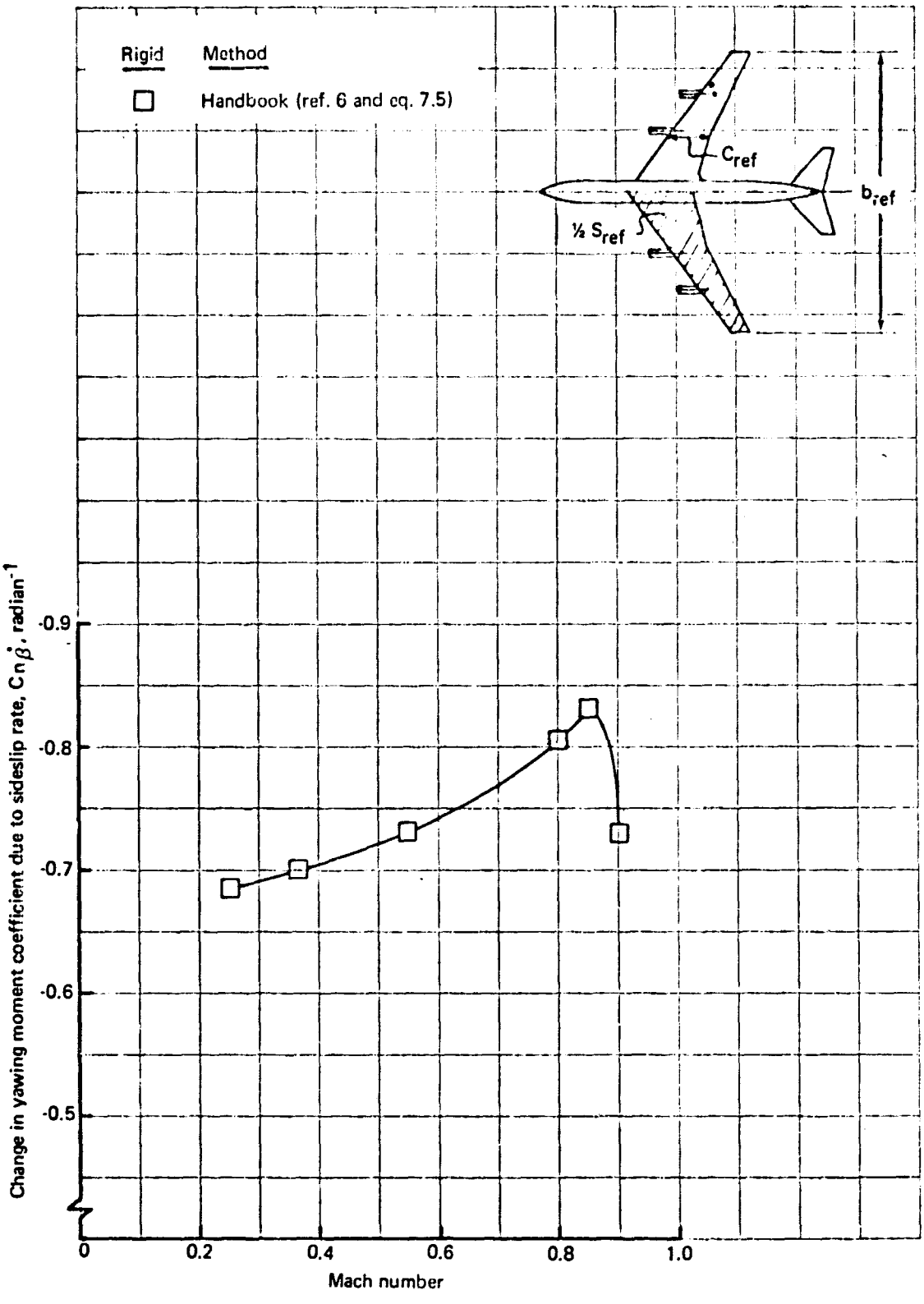

FIGURE 72. – ESTIMATION OF $C_{n\dot{\beta}}$ – 707-320B

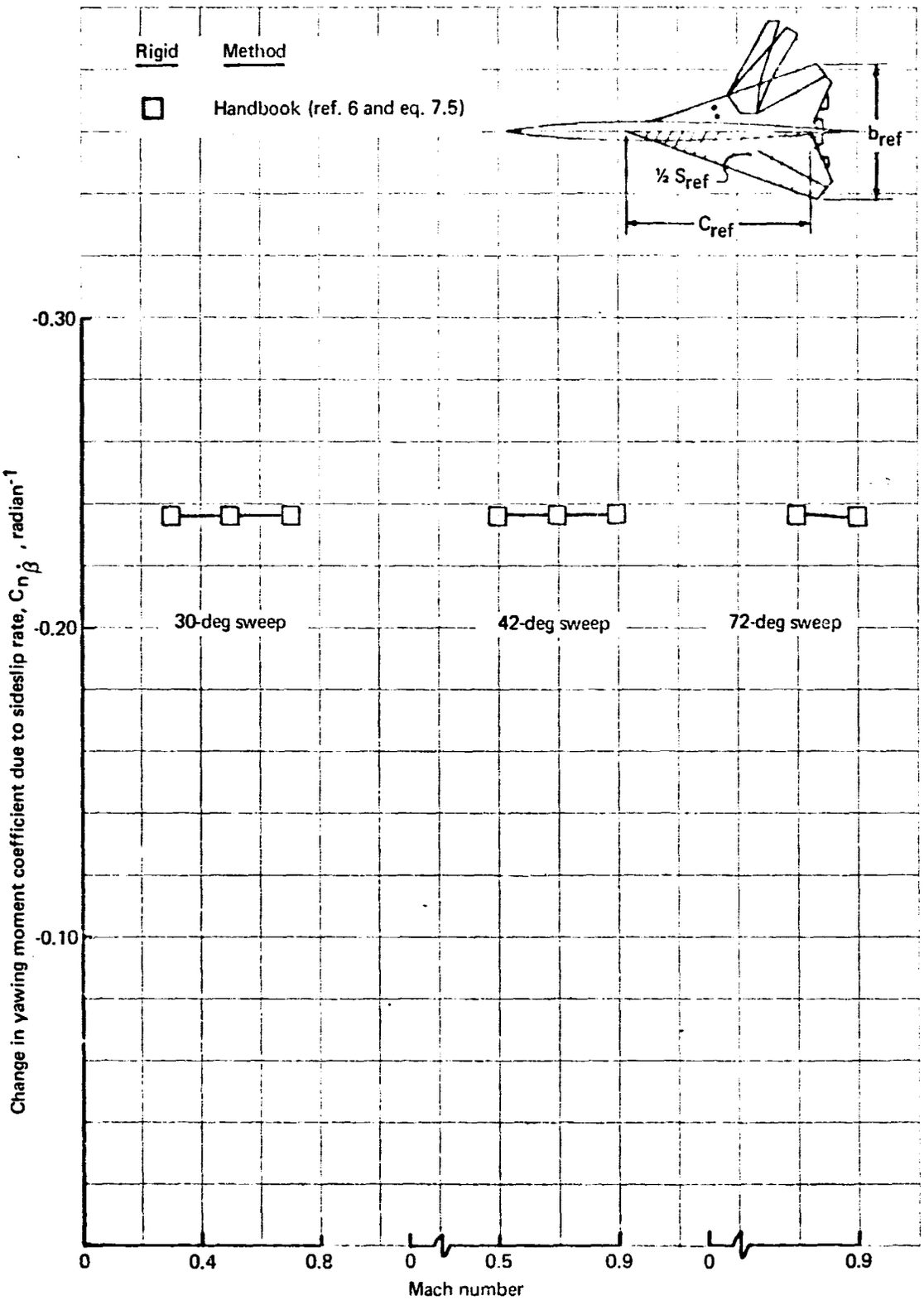

FIGURE 73.- ESTIMATION OF $C_{n_{\dot{\beta}}}$ -SST

Wind tunnel data are not available at the present time to evaluate the methods of calculating the roll-rate derivatives. Consequently, the only experimental values available were from 707 flight test data.

It is concluded from the study that the methods of refs. 6 and 72 give nearly the same values for the roll-rate derivatives at transonic cruise of the 707. The thin-body, lifting surface method appears to overestimate the flight test values of C_{ℓ_p}. A final judgment of the methods awaits the more extensive experimental data being generated by the recently developed wind tunnel, roll-rate test rig.

7.8.1 $C_{y_p} = \frac{\partial C_Y}{\partial\left(\frac{pb}{2V_c}\right)}$; Variation of side force with roll rate. — This stability derivative was calculated by the USAF Handbook (ref. 6) and by the method of Campbell (ref. 72). The results for the 707-320B and the SST are presented in figs. 74 and 75.

7.8.1.1 Rigid results: Figures 74 and 75 indicate that the values of C_{y_p} calculated for the 707 and SST by refs. 6 and 72 are nearly the same. The largest discrepancies occur at low Mach numbers ($M < 0.50$). The method of ref. 72 could not be used for the supersonic flight regime and, therefore, no comparison is shown for the 72° leading edge sweep SST.

7.8.1.2 Elastic results: The effect of elasticity on the value of C_{y_p} of the 707 and the SST is shown in figs. 74 and 75. Aeroelasticity has its largest effect on C_{y_p} at low Mach numbers ($M < 0.50$) for the 707 and 42° sweep SST. It had little effect on the 707 at high-transonic-cruise Mach numbers. The effect of aeroelasticity on the 30° and 72° sweep SST cases is small. A variation of K_β from 21×10^{-8} to 56.1×10^{-8}, holding $L_E/L_R = 0.813$, had no effect on the value of C_{y_p} for the 707.

7.8.2 $C_{\ell_p} = \frac{\partial C_\ell}{\partial\left(\frac{pb}{2V_c}\right)}$; Variation of rolling moment with roll rate. — This stability derivative was evaluated by the following methods:

(1) Lifting surface (TA 67A).

(2) Handbook (refs. 6 and 72).

The results of the 707-320B analysis are compared to flight test data in fig. 76. Figure 77 contains the comparison of methods applied to the SST configurations. It should be noted that the lifting surface method cannot calculate

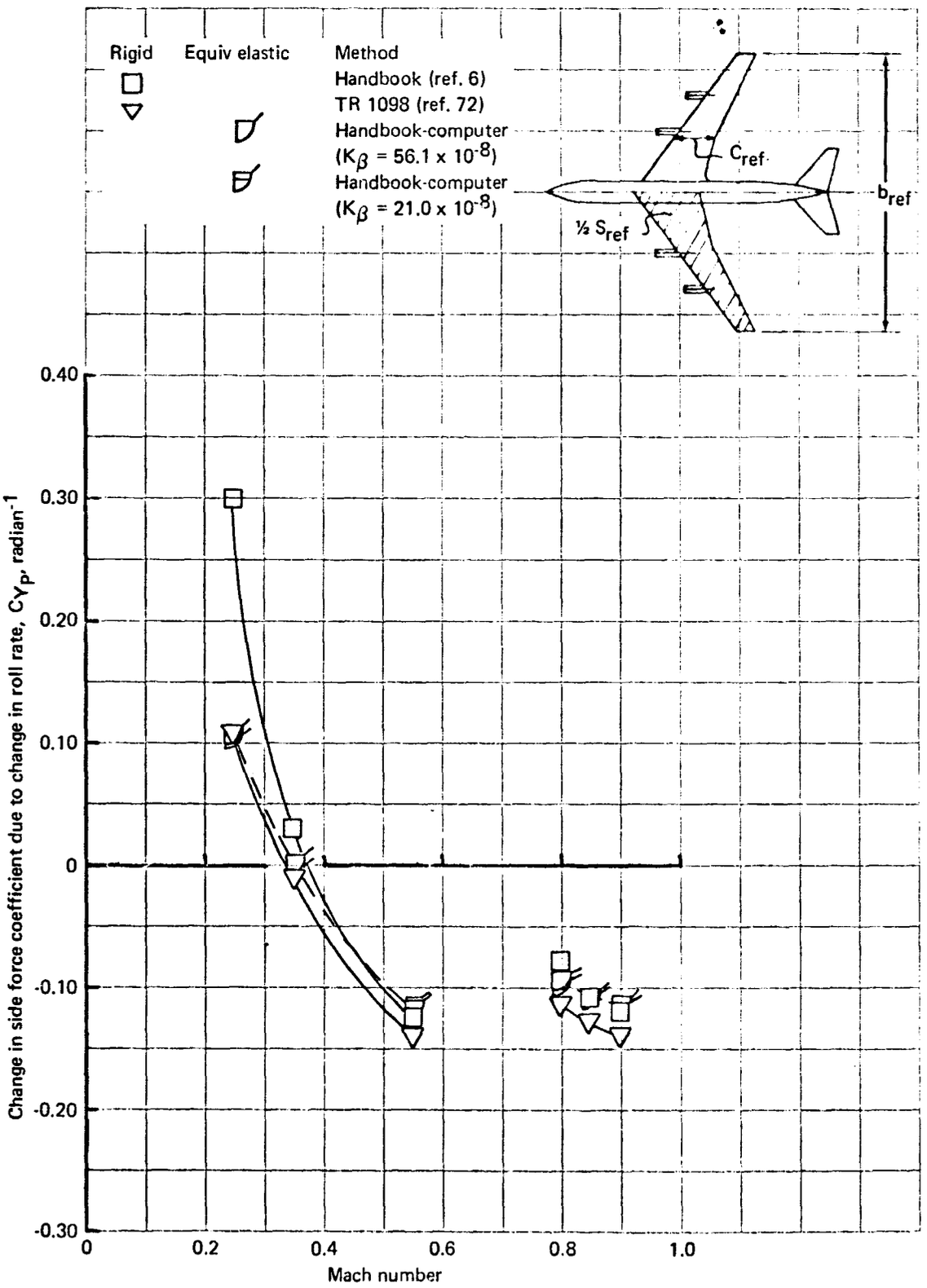

FIGURE 74.– COMPARISON OF ESTIMATION METHODS FOR C_{Y_P} –707-320B

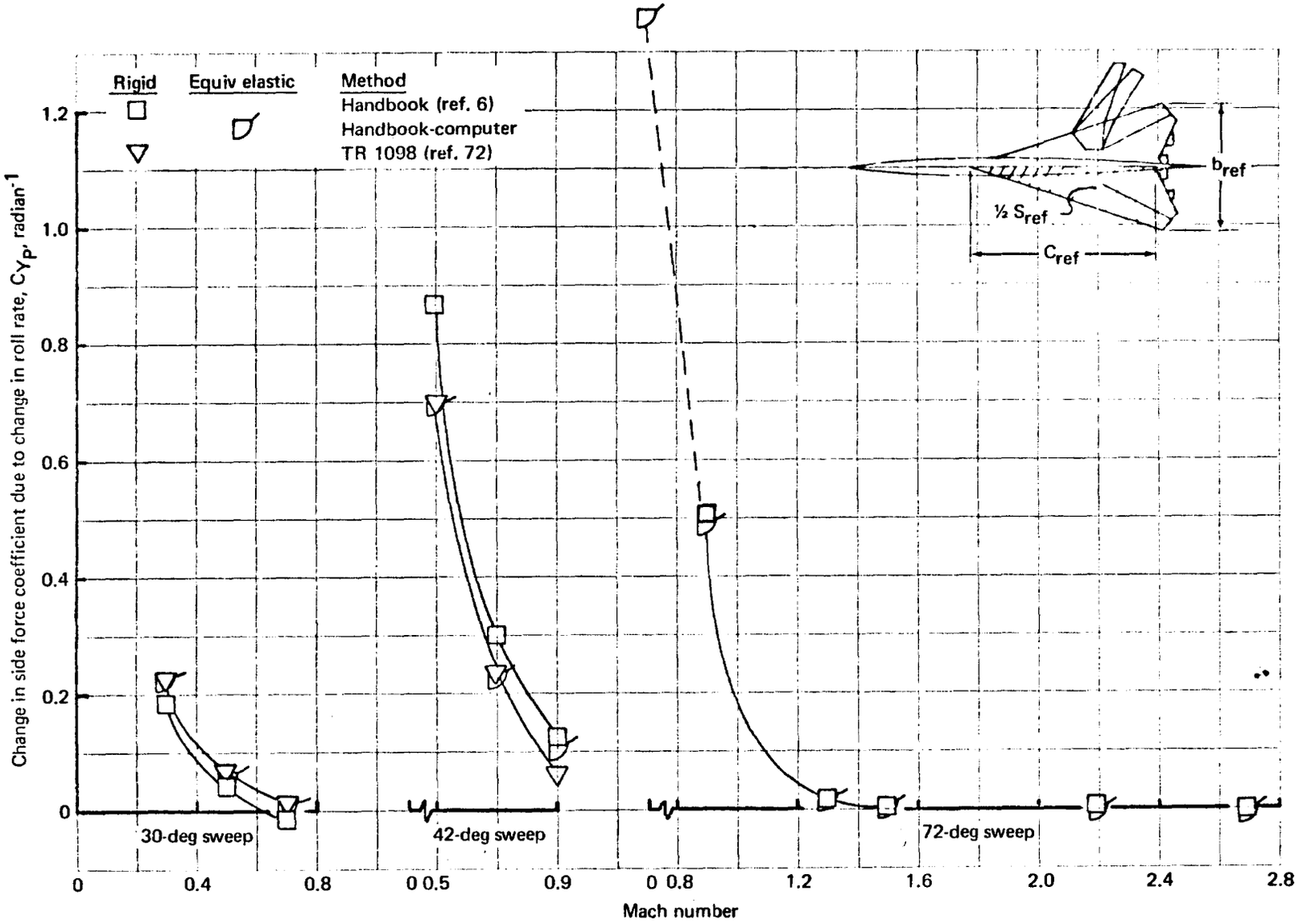

FIGURE 75.– COMPARISON OF ESTIMATION METHODS FOR C_{Y_p} –SST

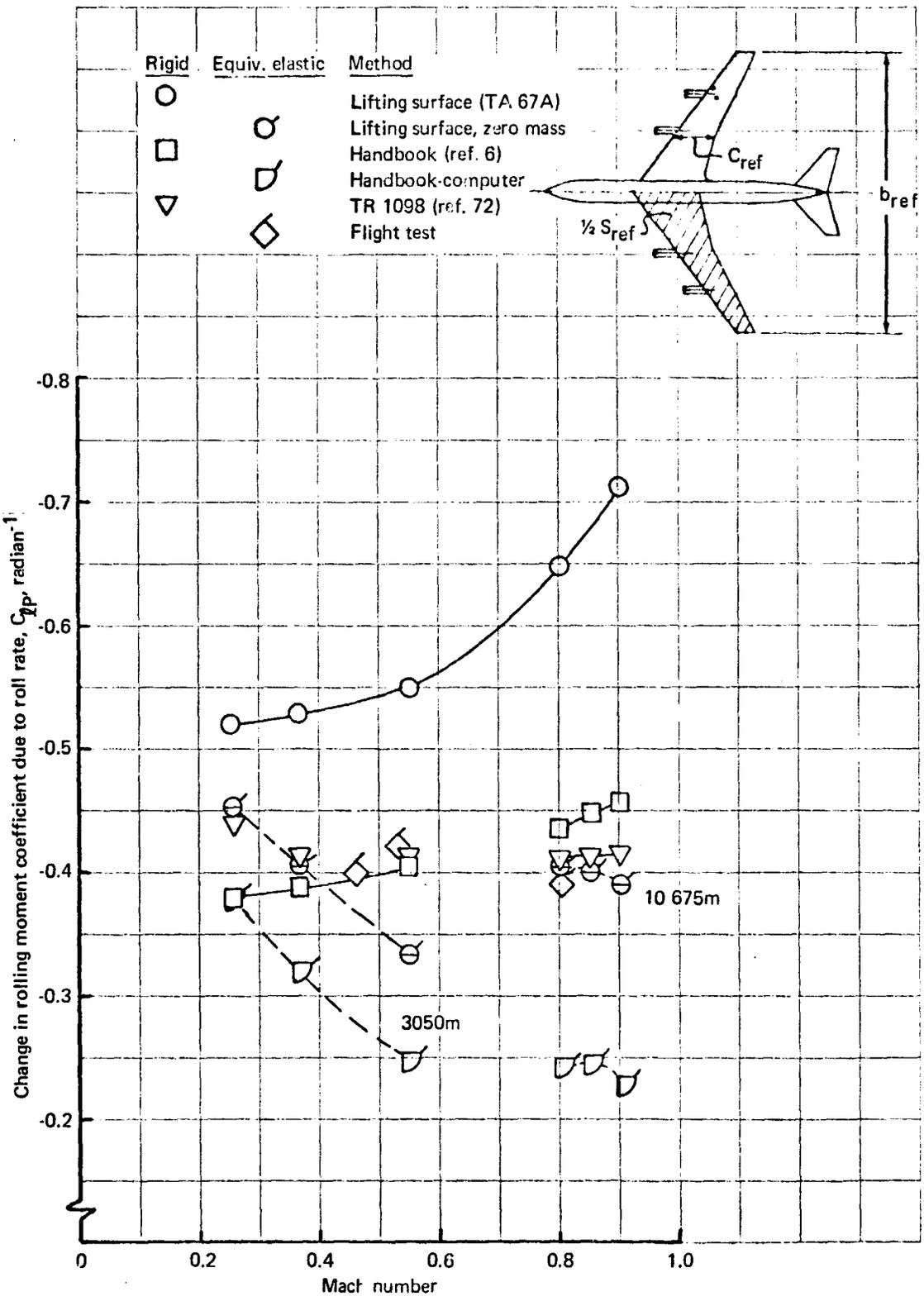

FIGURE 76.– COMPARISON OF ESTIMATION METHODS FOR C_{ℓ_p} – 707-320C

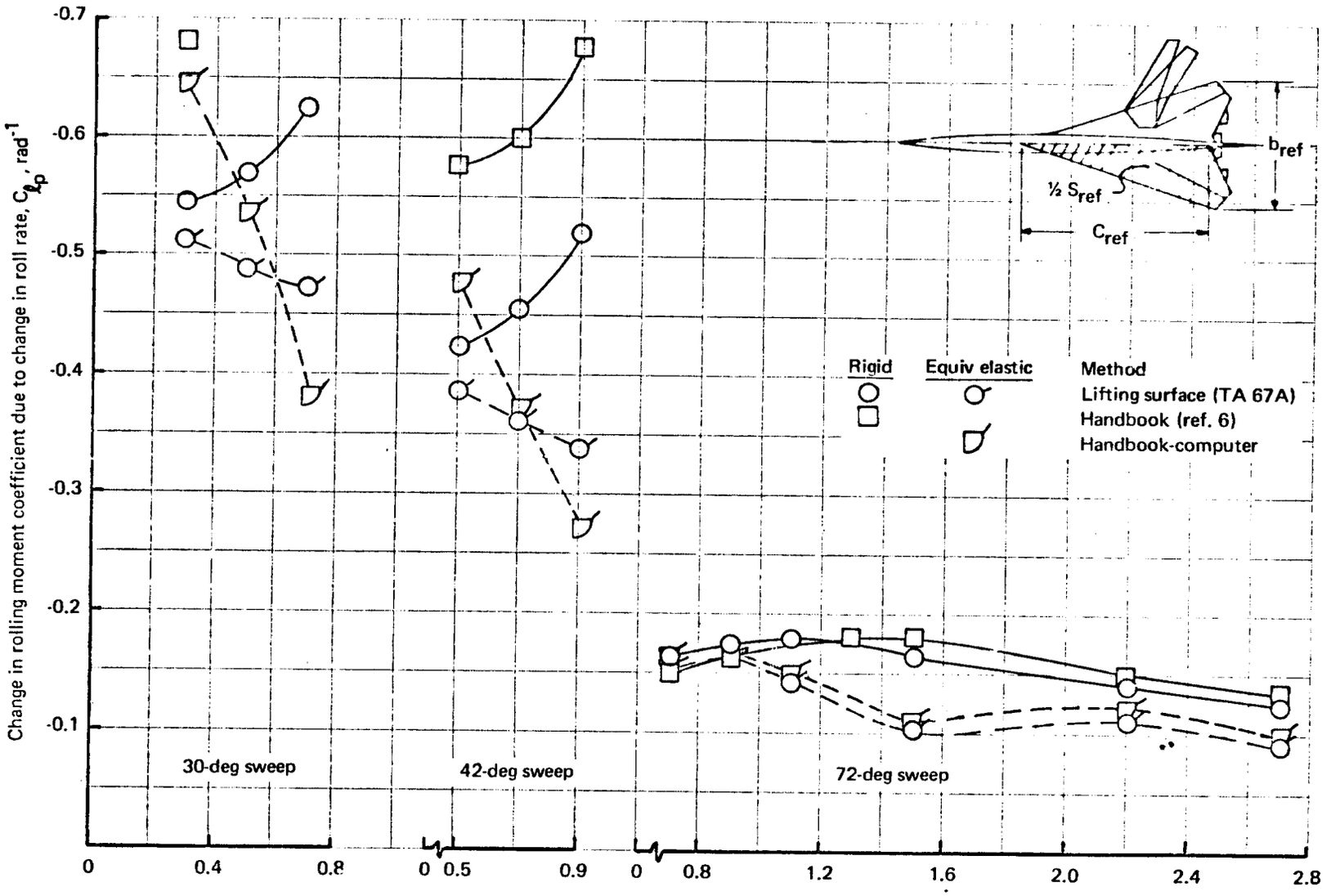

FIGURE 77. – COMPARISON OF ESTIMATION METHODS FOR C_{ℓ_p} – SST

the vertical-tail contribution to C_{ℓ_p} and, thus, the handbook vertical-tail contribution was used.

7.8.2.1 Rigid results: Figure 76 shows that the lifting surface theory of program TA 67A predicts considerably larger values of C_{ℓ_p} for the 707 than the handbook methods of refs. 6 and 72. The opposite is true in the case of the SST at subsonic Mach numbers (fig. 77). Supersonically, there is reasonable agreement between the methods.

7.8.2.2 Elastic results: Figures 76 and 77 present the effect of elasticity on the value of C_{ℓ_p} of the 707 and the SST. In the case of the 707, flight test data were available and the values calculated by the lifting surface method are in fair agreement, while the handbook values are too low. In the case of the SST, there is good agreement between lifting surface methods and ref. 6 at 72° leading edge sweep, but poor agreement at 30° and 42° sweep.

7.8.3 $C_{n_p} = \frac{\partial C_n}{\partial\left(\frac{pb}{2V_c}\right)}$; Variation of yawing moment with roll rate. — This stability derivative was calculated by the semi-empirical methods of the USAF Handbook (ref. 6) and by TR 1098 (ref. 72). The results for the 707-320B and the SST are shown in figs. 78 and 79.

7.8.3.1 Rigid results: The method of TR 1098 gives approximately 40 percent lower values of C_{n_p} for the 707 than those values calculated by the USAF Handbook (fig. 78). In the case of the SST (fig. 79), the methods give nearly the same values of C_{n_p}. Since TR 1098 does not treat supersonic cases, a comparison with the USAF Handbook is not possible for the 72° leading edge sweep SST configuration.

7.8.3.2 Elastic results: The effect of elasticity on the value of C_{n_p} for the 707 and SST is presented in figs. 78 and 79. Aeroelasticity has a minor effect on the value of C_{n_p} calculated by TR 1098 for the 707. A similar result for C_{n_p} calculated from the USAF Handbook for the SST is shown in fig. 79. There was little effect on C_{n_p} of the 707 when K_β was varied from 21×10^{-6} to 56.1×10^{-6}, holding $L_E/L_R = 0.813$.

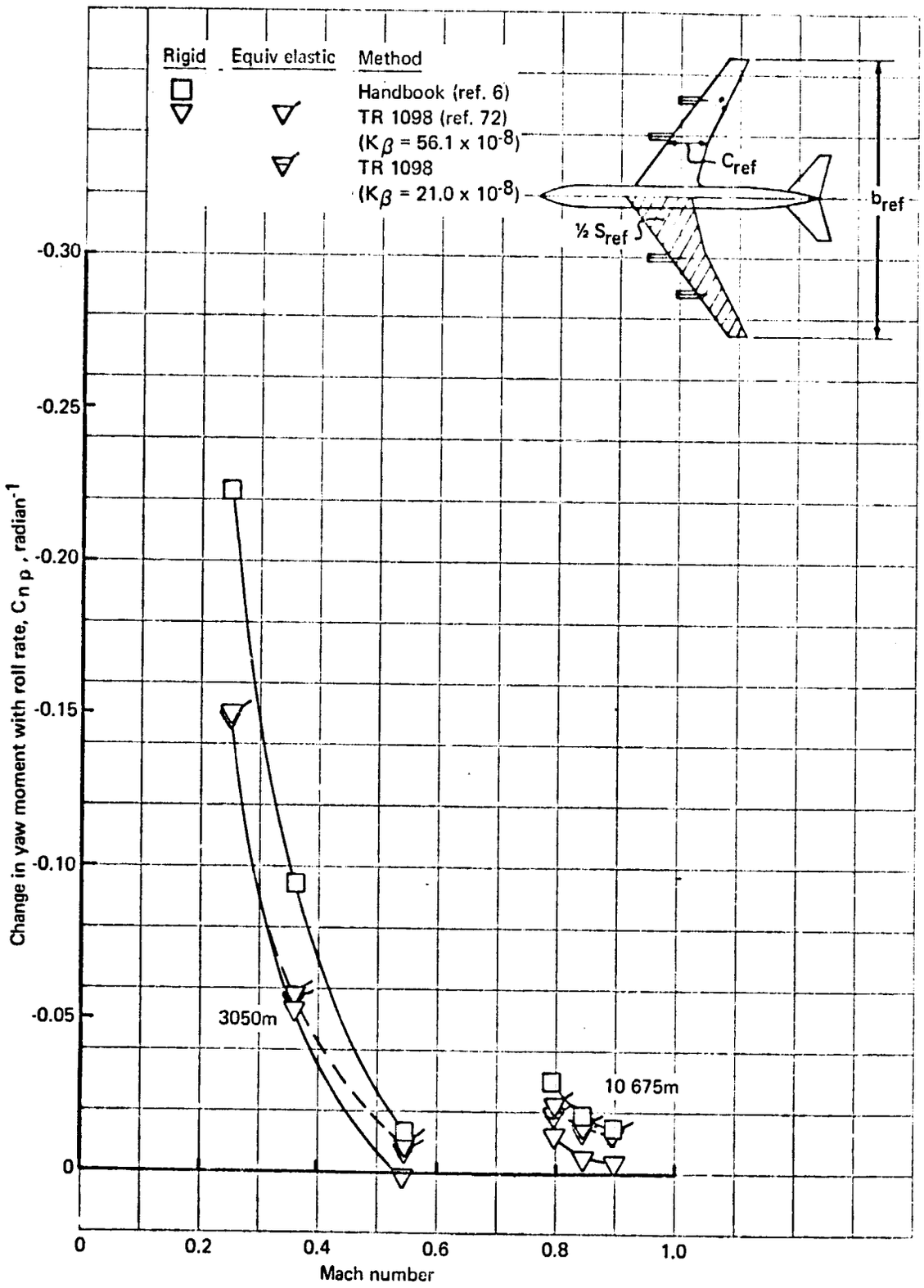

FIGURE 78.– COMPARISON OF ESTIMATION METHODS FOR C_{n_p} – 707-320B

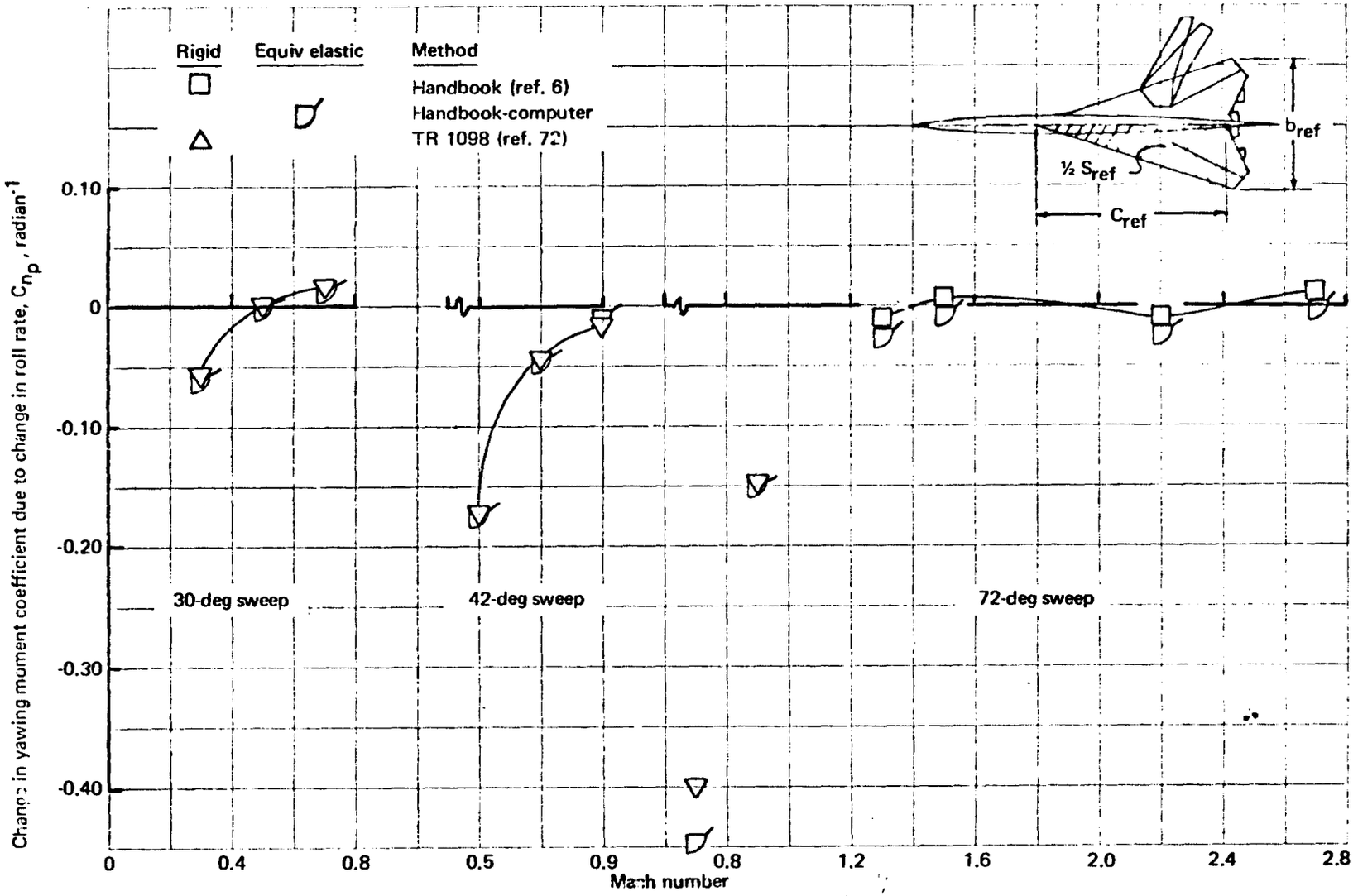

FIGURE 79.– COMPARISON OF ESTIMATION METHODS FOR C_{n_p}–SST

7.9 Yaw-Rate (r) Derivatives

The yaw-rate stability derivatives, C_{y_r}, C_{ℓ_r}, and C_{n_r}, belong to the class of dynamic derivatives. The physical discussion of the character of dynamic derivatives is found in par. 7.4 for the q derivatives and applies equally as well to the r derivatives.

It is not possible to calculate the yaw-rate stability derivatives by the existing mechanization of the thin-body, lifting surface theory. Section 4 does contain the exact set of partial differential equations describing a thin body experiencing yaw rate, but the boundary condition in the region of S of the plane of singularities has not been sufficiently developed.

There were no experimental data available to judge the handbook techniques when applied to the SST and 707 of this study.

It was found that both the USAF Handbook (ref. 6) and TR 1098 (ref. 72) are incomplete with regard to the yaw-rate derivatives. Effects due to aft-body flexibility (K_{ℓ}) and vertical-tail elasticity (L_E/L_R) were the only elastic effects calculated. Handbook methods used are summarized in tables 22, 23, 28, and 29.

It was concluded that the estimation methods available to calculate the yaw-rate derivatives are inadequate for the 707 and the SST aircraft configurations. The effect of this inadequacy on the Dutch-roll damping is discussed in app. C. In light of the importance of the r derivatives, it is recommended that further effort be extended to calculate them by theoretical or semi-empirical means.

7.9.1 $C_{y_r} = \frac{\partial C_Y}{\partial\left(\frac{rb}{2V_c}\right)}$; Variation of side force with yaw rate. — This stability derivative was calculated by the semi-empirical methods of the USAF Handbook (ref. 6) and TR 1098 (ref. 72). The results for the 707-320B and the SST are shown in figs. 80 and 81. Since a handbook technique is not available to estimate the wing-body and horizontal-tail contributions to C_{y_r}, it was assumed that $C_{y_r} = C_{y_r}$ vert. tail. Fortunately, the derivative C_{y_r} is not important to most stability and control analysis. The effect of elasticity on C_{y_r} of the 707 and SST is large.

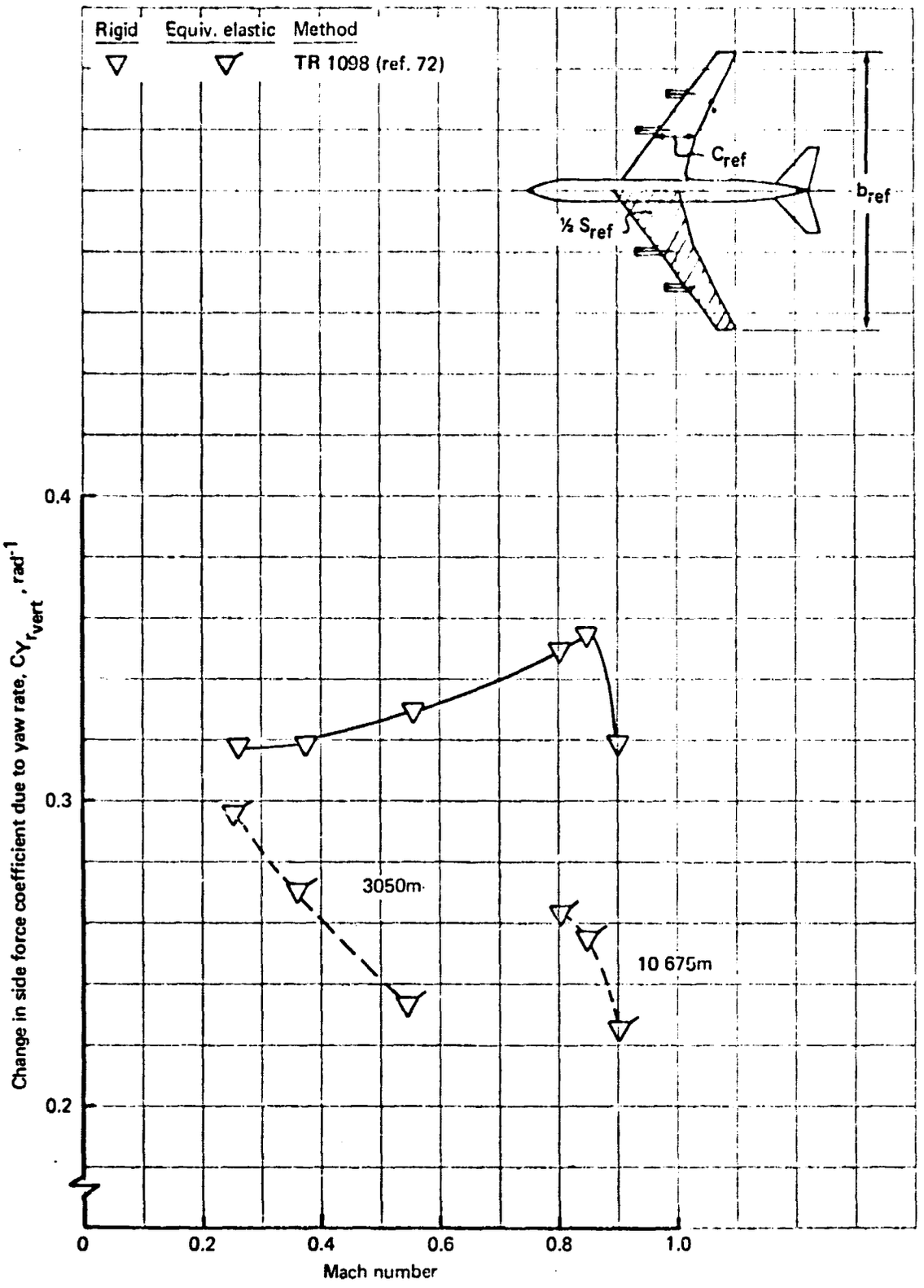

FIGURE 80. – ESTIMATION OF C_{Y_r} – 707-320B

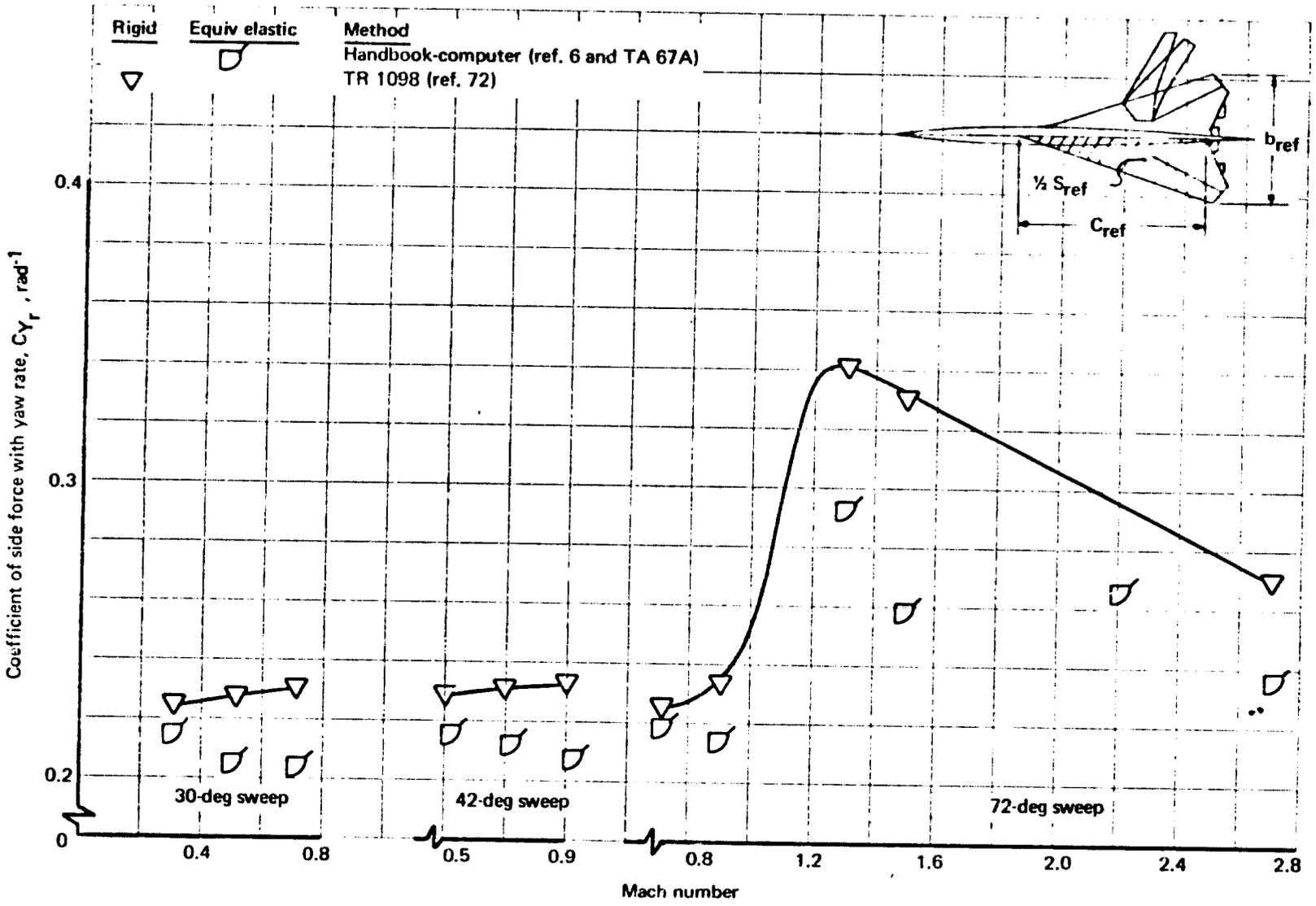

FIGURE 81. – ESTIMATION OF C_{Y_r} FOR –SST

7.9.2 $C_{\ell_r} = \frac{\partial C_\ell}{\partial\left(\frac{rb}{2Vc}\right)}$; Variation of rolling moment with yaw rate. — This stability derivative was calculated by the semi-empirical methods of the USAF Handbook (ref. 6) and TR 1098 (ref. 72). Results for the 707-320B and the SST are presented in figs. 82 and 83. The derivative arises largely from the wing and is caused by changes in dynamic pressure and Mach number. It is considered moderately important in stability and control analysis.

7.9.2.1 Rigid results: Figures 82 and 83 indicate that the values of C_{ℓ_r} calculated from the methods of refs. 6 and 72 are in close agreement at $M > 0.50$ for the 707 and at all Mach numbers for the SST. The value from the method of TR 1098 is 45 percent lower than that of USAF Handbook at $M = 0.25$ for the 707.

7.9.2.2 Elastic results: The effect of elasticity on C_{ℓ_r} of the 707 and SST is shown in figures 82 and 83 and is seen to be small. A variation of K_β from 21×10^{-6} to 56.1×10^{-6}, holding $L_E/L_R = 0.813$, had negligible effect on the value of C_{ℓ_r} for the 707.

7.9.3 $C_{n_r} = \frac{\partial Cn}{\partial\left(\frac{rb}{2Vc}\right)}$; Variation of yaw moment with yaw rate. — This stability derivative was calculated by the semi-empirical methods of TR 1098 (ref. 72). Results are presented in figs. 84 and 85 for the 707-320B and the SST. The values of C_{n_r} are strongly dependent upon the contribution due to the vertical tail. Therefore, the degree of reliability with which this derivative can be calculated is dependent upon the accuracy of the vertical-tail predictions.

Since the values of C_{n_r} were calculated by ref. 72 only, no direct comparison of methods can be made for either the rigid or elastic 707 and SST cases. The effect of elasticity, shown in figs. 84 and 85, is large in all of the 707 and SST cases. A variation of K_β from 21×10^{-8} to 56.1×10^{-8}, holding $L_E/L_R = 0.813$, has a negligible effect on the value of C_{n_r} of the 707, as on all other lateral-directional derivatives.

7.10 Elevator Control (δ_E) Derivatives

Only the longitudinal elevator control surface derivatives, $C_{L_{\delta_E}}$ and $C_{m_{\delta_E}}$, were estimated for the 707-320B and the SST. The methods used in this study are the following:

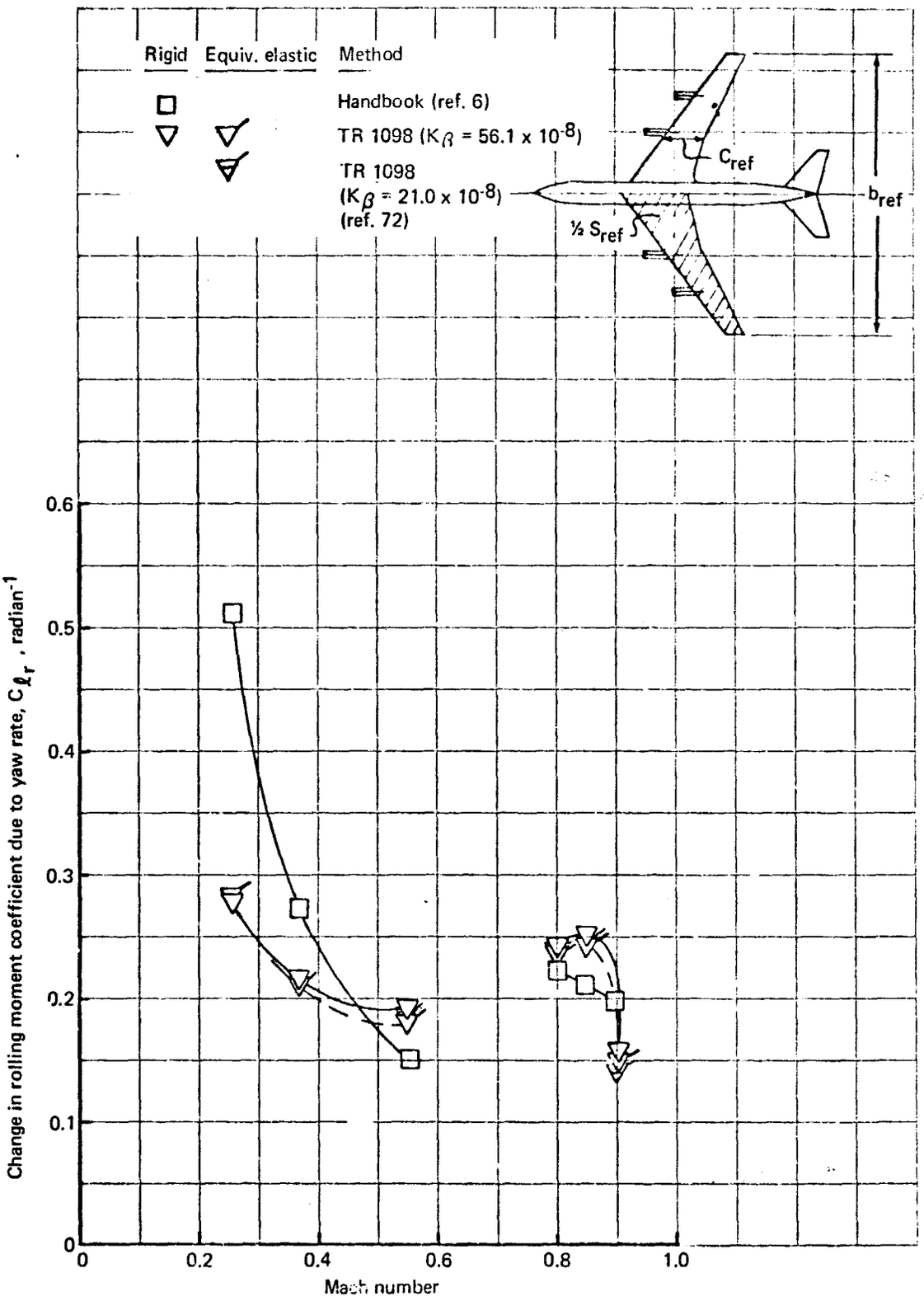

FIGURE 82. – COMPARISON OF ESTIMATION METHODS FOR C_{ℓ_r} –707-320B

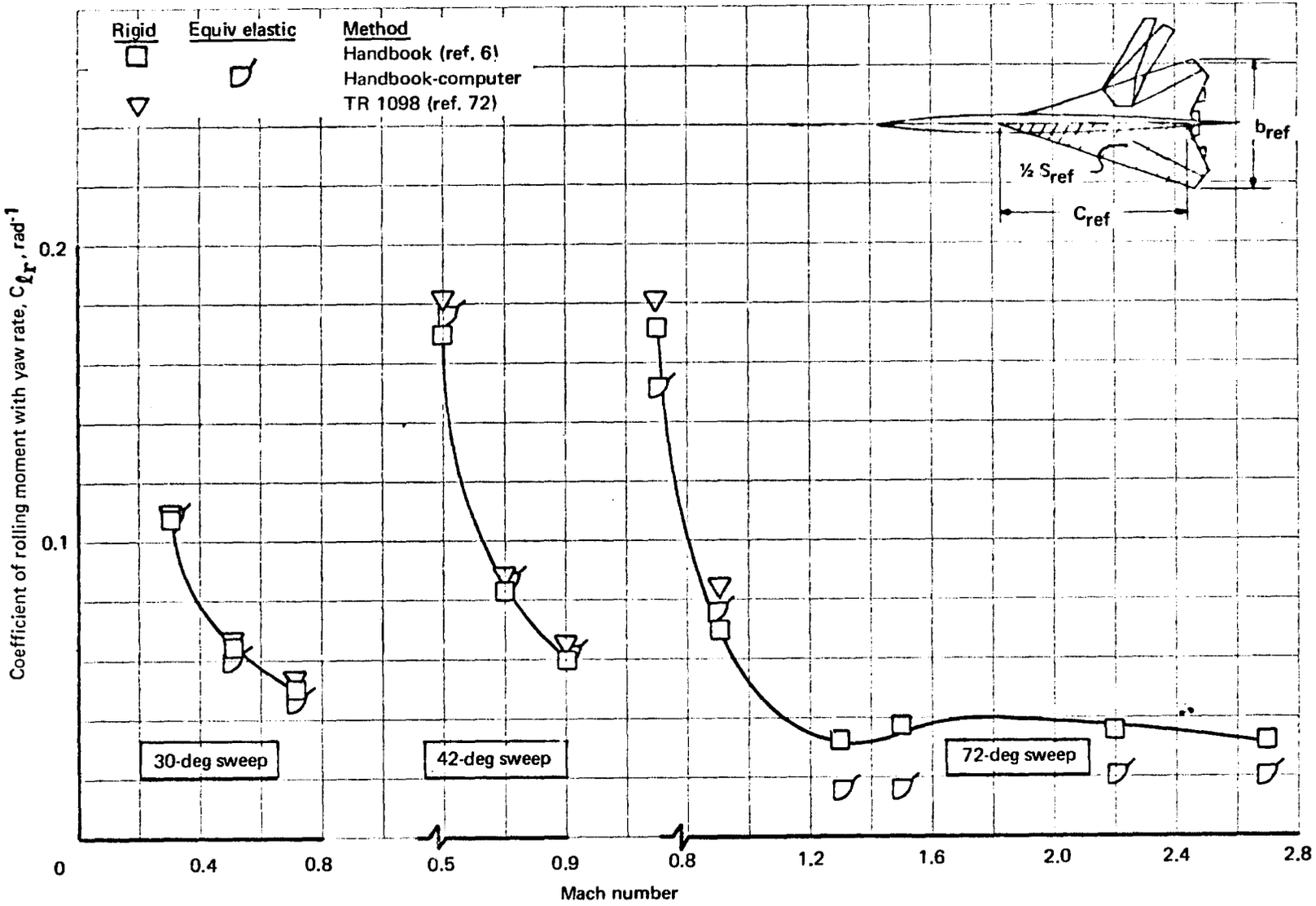

FIGURE 83. – COMPARISON OF ESTIMATION METHODS FOR C_{ℓ_r} – SST

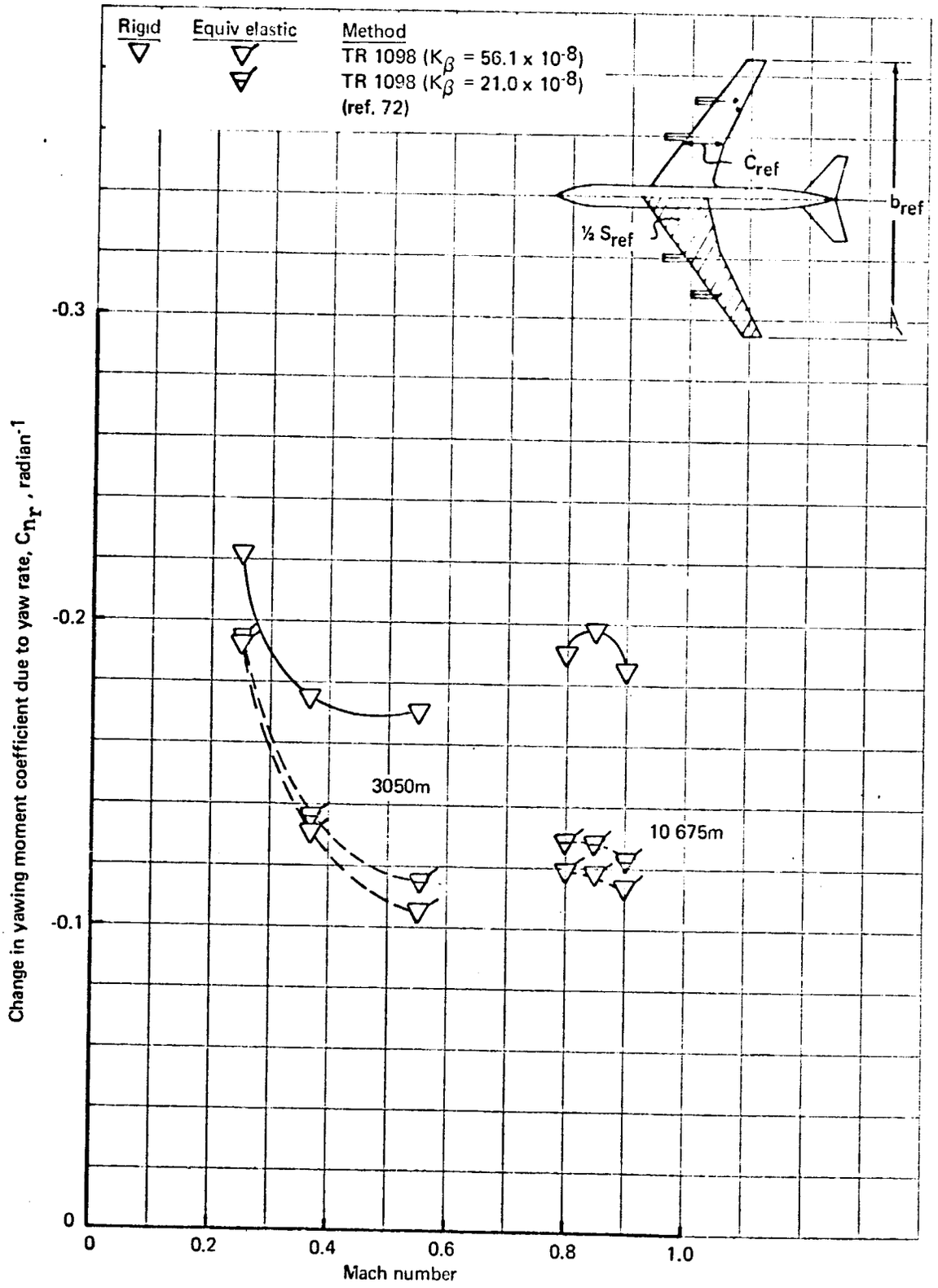

FIGURE 84.– ESTIMATION OF C_{n_r} –707-320B

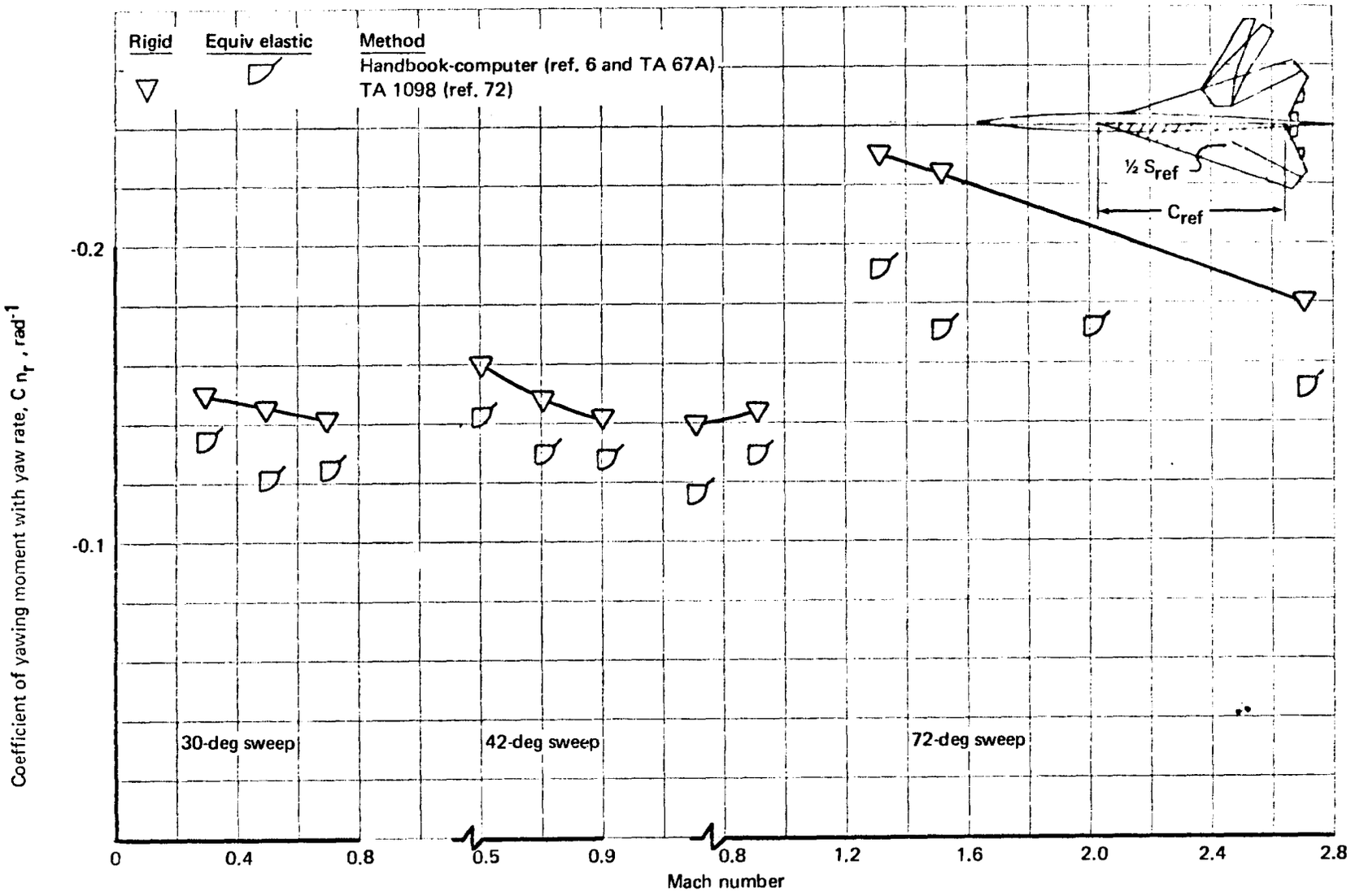

FIGURE 85.– ESTIMATION OF C_{n_r} –SST

(1) Lifting surface (TA 67A).

(2) Handbook (ref. 6).

(3) Wind tunnel.

The computer program TA 67A calculated the control derivatives by inputing wing- or tail-camber slopes that are representative of the control surface deflection angles.

It was concluded that the prediction of the longitudinal elevator control surface derivatives can be estimated in a fair manner by the lifting surface and the USAF Handbook methods. Part of the inaccuracy may be attributable to boundary layer effects It is recommended that further development to viscous and slender-body, lifting surface theory be oriented to include control surface effects.

7.10.1 $C_{L_{\delta_E}} = \frac{\partial C_L}{\partial \delta E}$; Variation of lift with elevator angle. — The estimated magnitude of $C_{L_{\delta_E}}$ is compared with wind tunnel data for the 707 in fig. 86 and for the SST in figs. 87 and 88. The rigid results for the 707 from lifting surface theory compare favorably with those of ref. 6 in all except transonic Mach numbers. Agreement of both methods with wind tunnel measured values of $C_{L_{\delta_E}}$ is good for both the 707 and the SST.

The effect of elasticity on $C_{L_{\delta_E}}$ for the 707 is shown to be significant in fig. 86.

7.10.2 $C_{m_{\delta_E}} = \frac{\partial C_m}{\partial \delta E}$; Variation of pitching moment with elevator angle. — A comparison of $C_{m_{\delta_E}}$ from wind tunnel data with $C_{m_{\delta_E}}$ from the lifting surface method and USAF Handbook method is shown in fig. 89 for the 707 and figs. 90 and 91 for the SST. In the case of the 707, the lifting surface method and handbook method agree quite well, but give a rigid value of $C_{m_{\delta_E}}$ approximately 25 percent too large; there is a large disagreement between the two methods at the 707 transonic cruise speeds. The values of $C_{m_{\delta_E}}$ calculated for a rigid SST agree fairly well with wind tunnel results.

Elastic effects on $C_{m_{\delta_E}}$ for the 707 are shown in fig. 89. These effects appear to be large at high Mach numbers. Figure 91 compares lifting surface results to rigid and elastic wind tunnel model data for the SST. Agreement is good for the rigid SST model but poor for the elastic model.

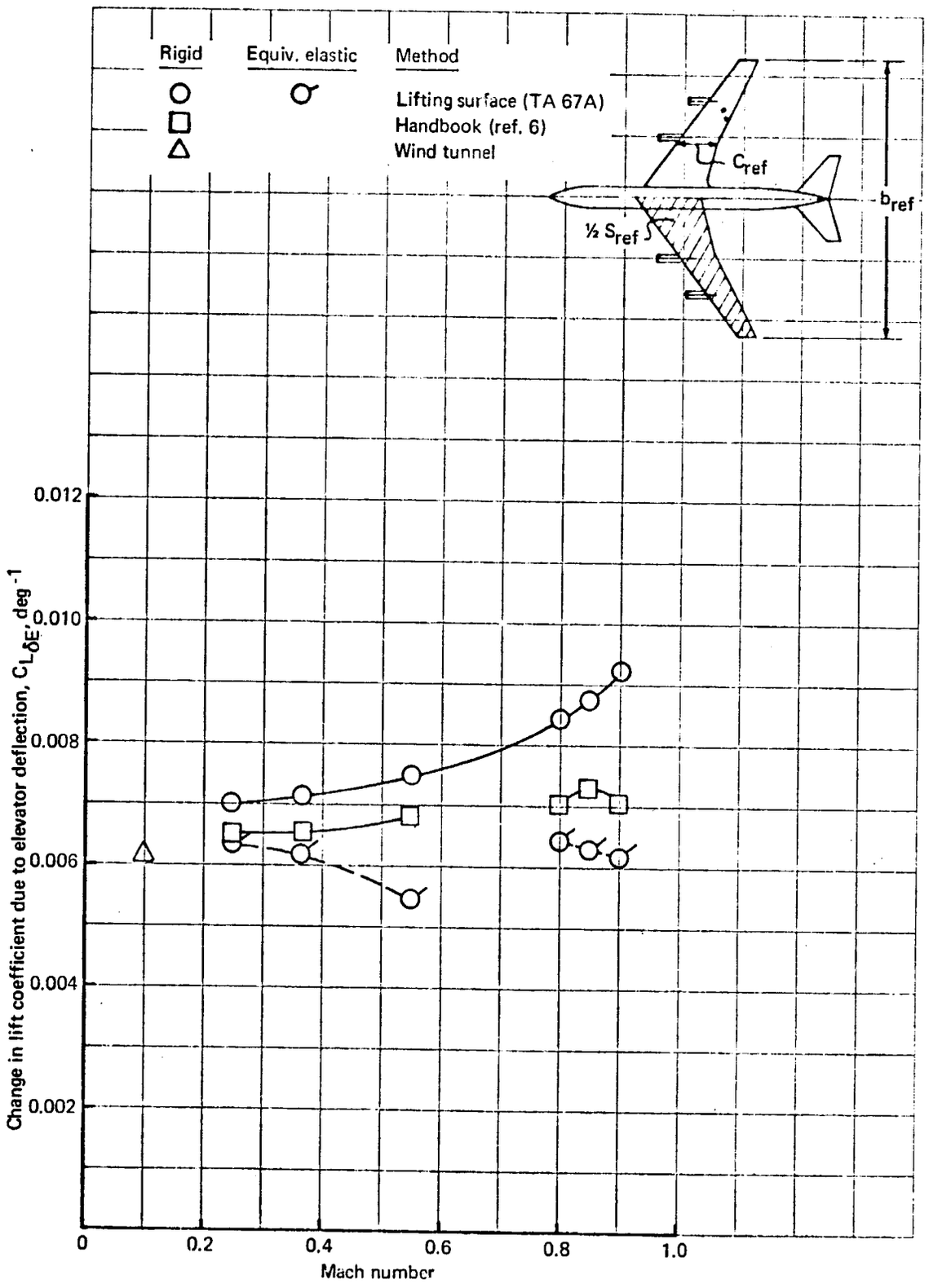

FIGURE 86.– COMPARISON OF ESTIMATION METHODS FOR $C_{L_{\delta_E}}$ – 707-320B

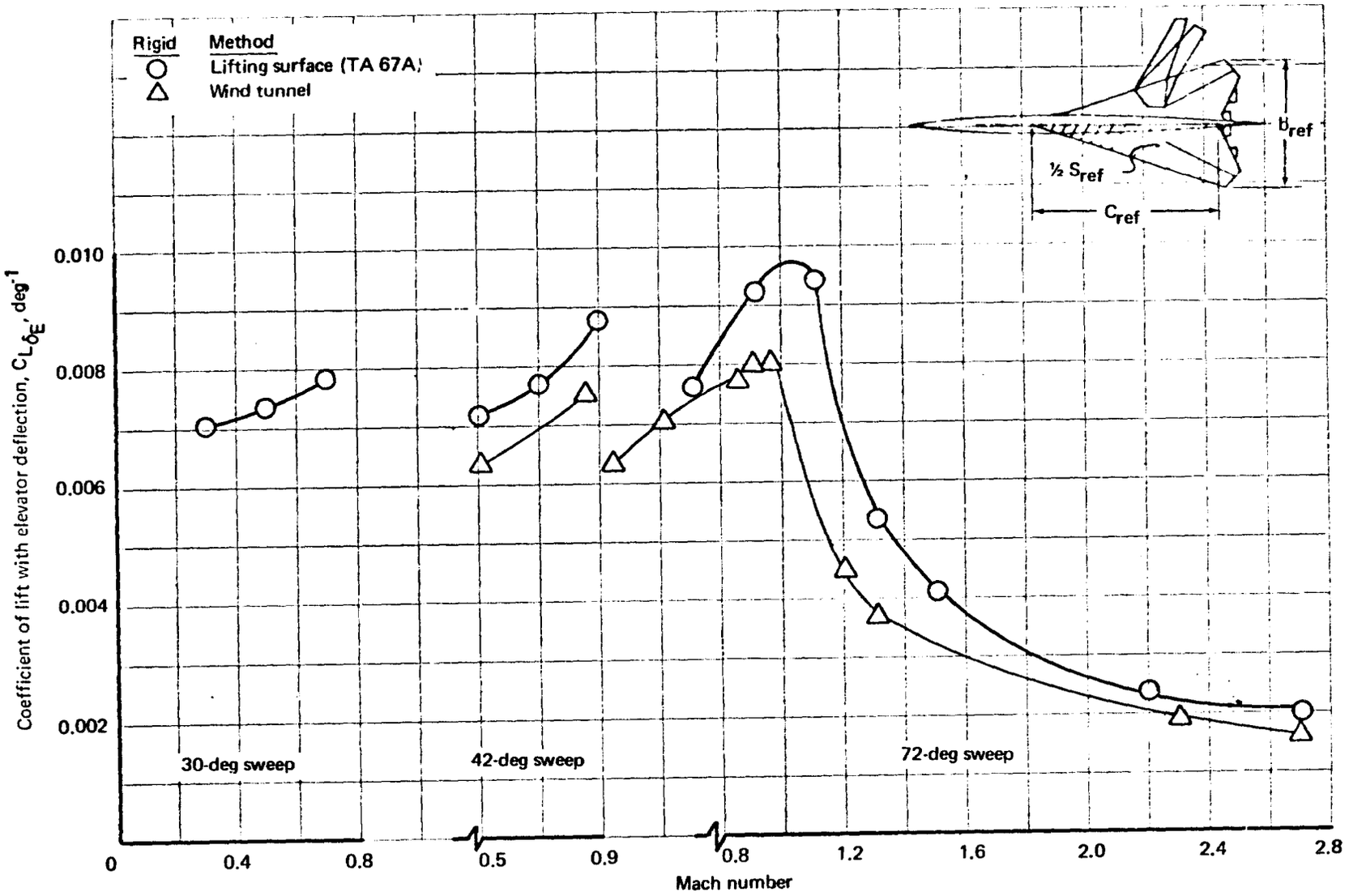

FIGURE 87.– COMPARISON OF ESTIMATION METHODS FOR $C_{L_{\delta_E}}$ –SST

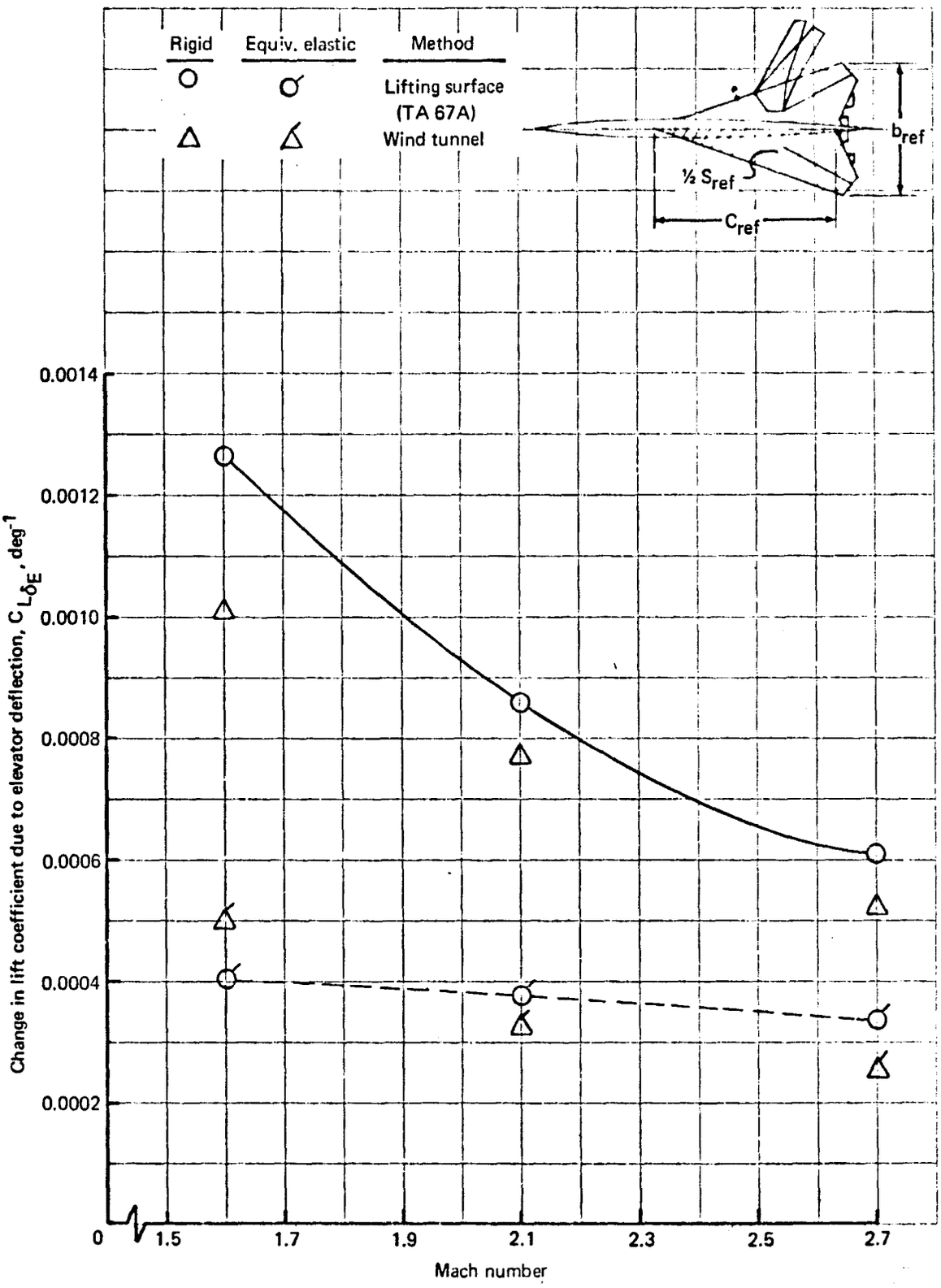

FIGURE 88.- EFFECT OF ELASTICITY ON $C_{L_{\delta_E}}$ -SST

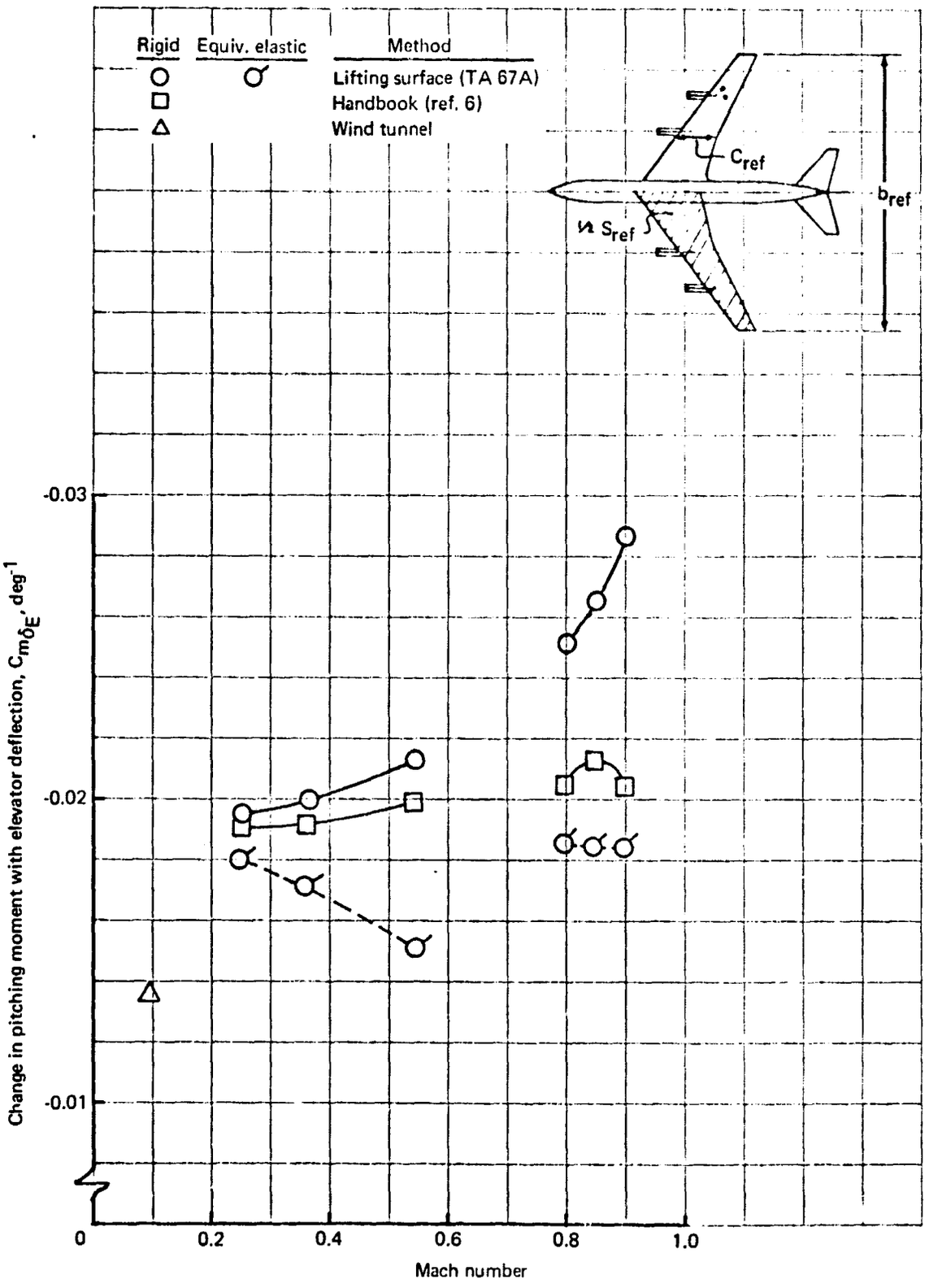

FIGURE 89. – COMPARISON OF ESTIMATION METHODS FOR $C_{m\delta_E}$ – 707-320B

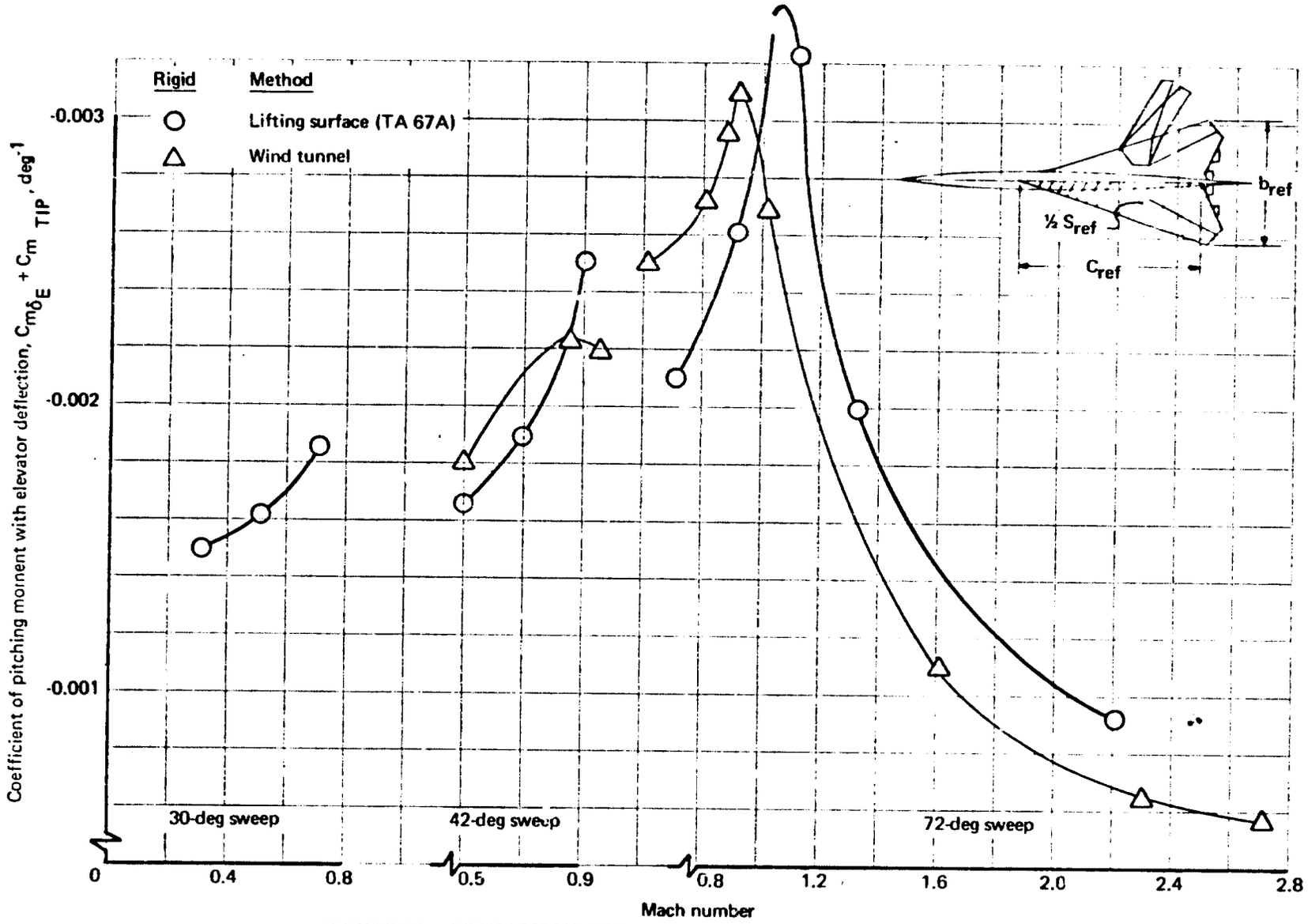

FIGURE 90.– COMPARISON OF ESTIMATION METHODS FOR $C_{m_{\delta_E}}$ –SST

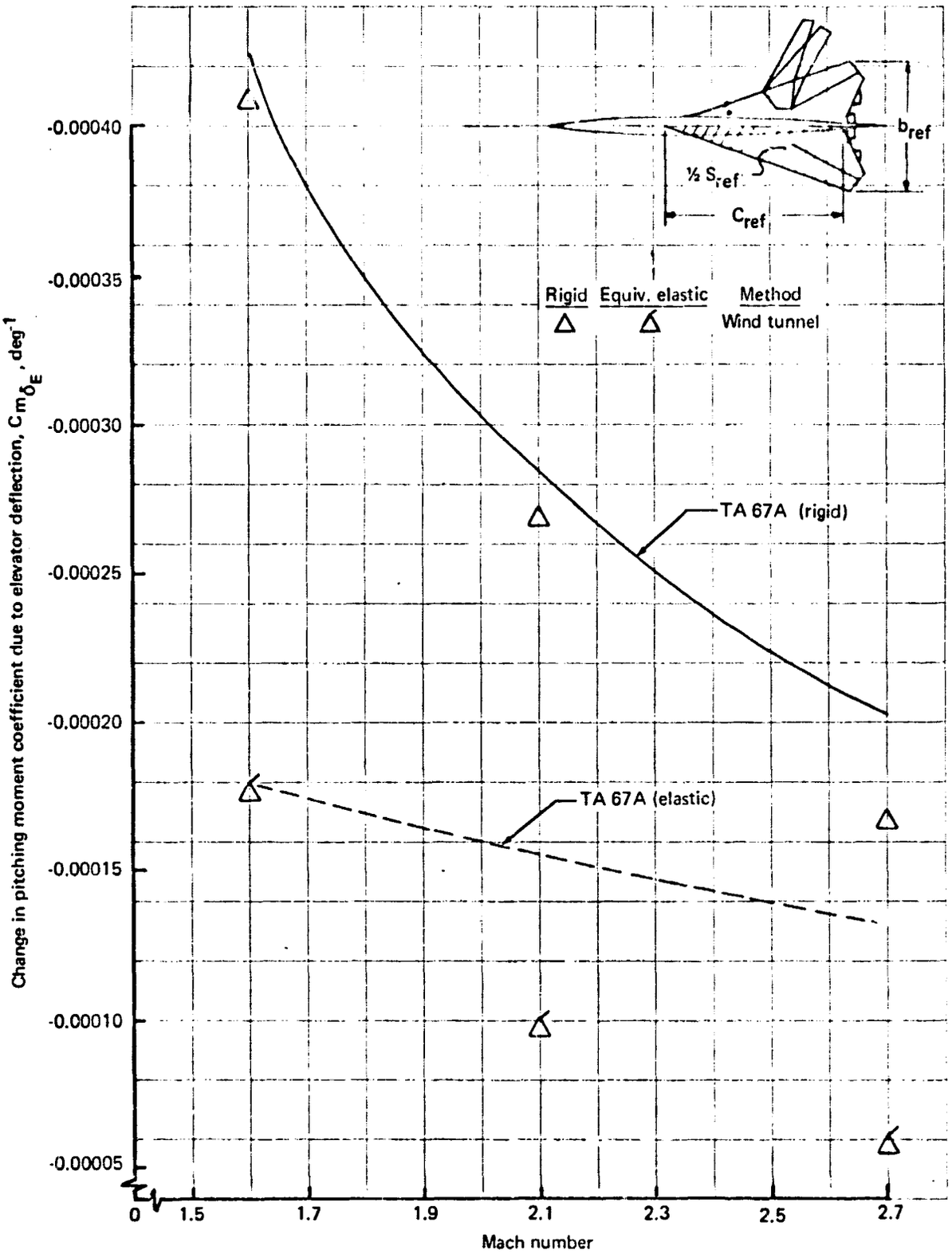

FIGURE 91. - EFFECT OF ELASTICITY ON $C_{m_{\delta_E}}$ -SST

7.11 Inertial Elastic Derivatives

The development of stability derivatives for the equivalent elastic mathematical model of an elastic airplane was outlined in Sec. 4. It was shown in this development that the equivalent elastic formulation of the six-degree-of-freedom motion equations contain the so-called inertial derivatives

$$\frac{\partial C_L}{\partial \dot{W}_s}, \frac{\partial C_m}{\partial \dot{W}_s}, \frac{\partial C_L}{\partial \dot{q}_s}, \frac{\partial C_m}{\partial \dot{q}_s}, \frac{\partial C_L}{\partial n}, \frac{\partial C_m}{\partial n}, \frac{\partial C_L}{\partial \ddot{\theta}_s}, \text{ and } \frac{\partial C_m}{\partial \ddot{\theta}_s}$$

These derivatives can be generated by the lifting surface method computer program designated as TA 67A.

It was also shown in Sec. 4 that a unique relationship exists between the variables q, $\ddot{\theta}$, and $\dot{w}$ and the load factor n. Only the n and θ derivatives were generated in this study; the q and $\dot{w}$ derivatives can then be evaluated using the equations of Sec. 4.

Figures 92 through 99 present the evaluation of the n and $\dot{\theta}$ derivatives for the 707-320B and the SST. The accuracy of the lifting surface method cannot be determined because other methods of estimation do not exist. Their effect on dynamic stability is shown in app. C.

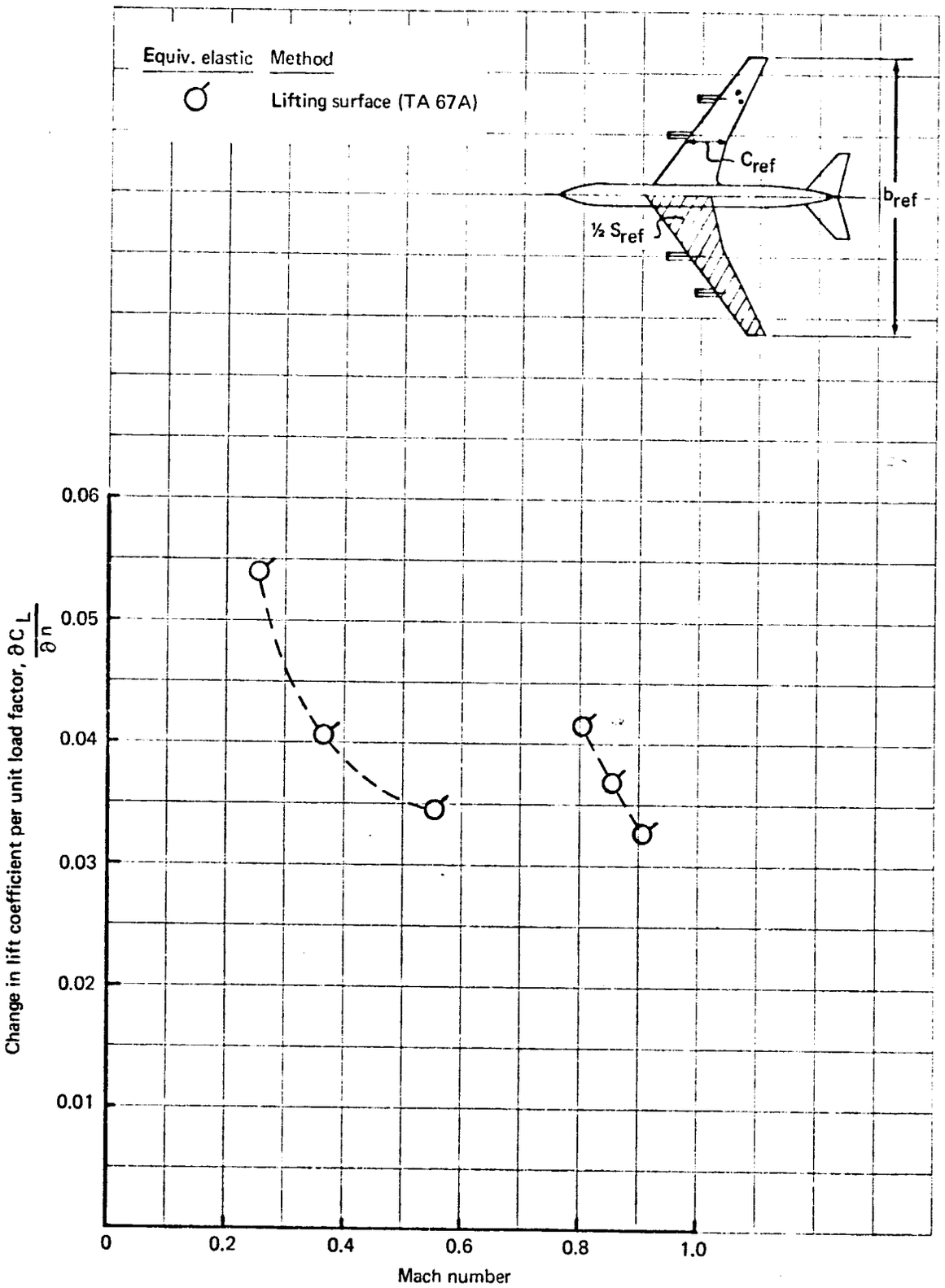

FIGURE 92.– ESTIMATION OF $\frac{\partial C_L}{\partial n}$ *–707-320B*

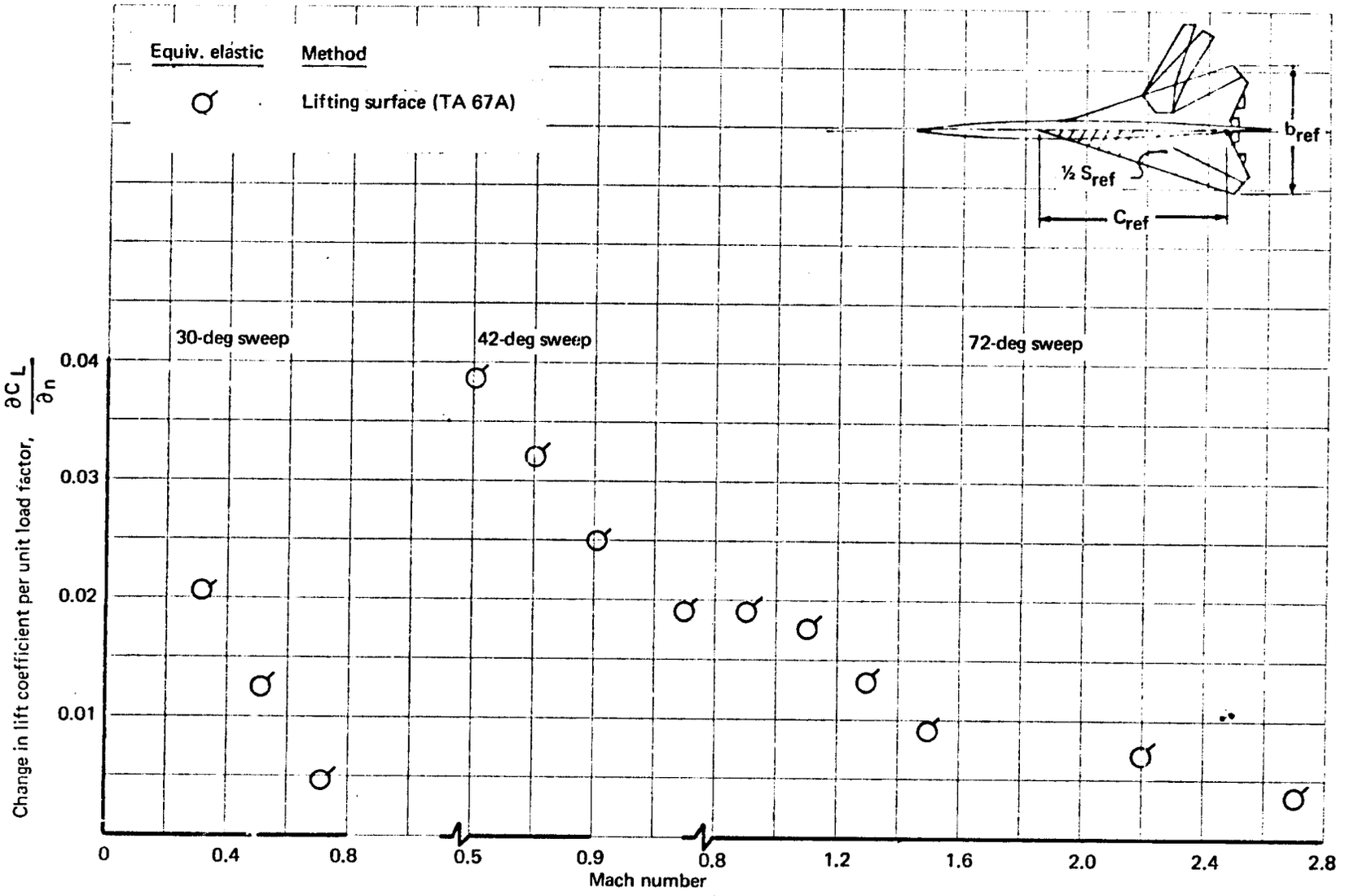

FIGURE 93.– ESTIMATION OF $\frac{\partial C_L}{\partial n}$ *–SST*

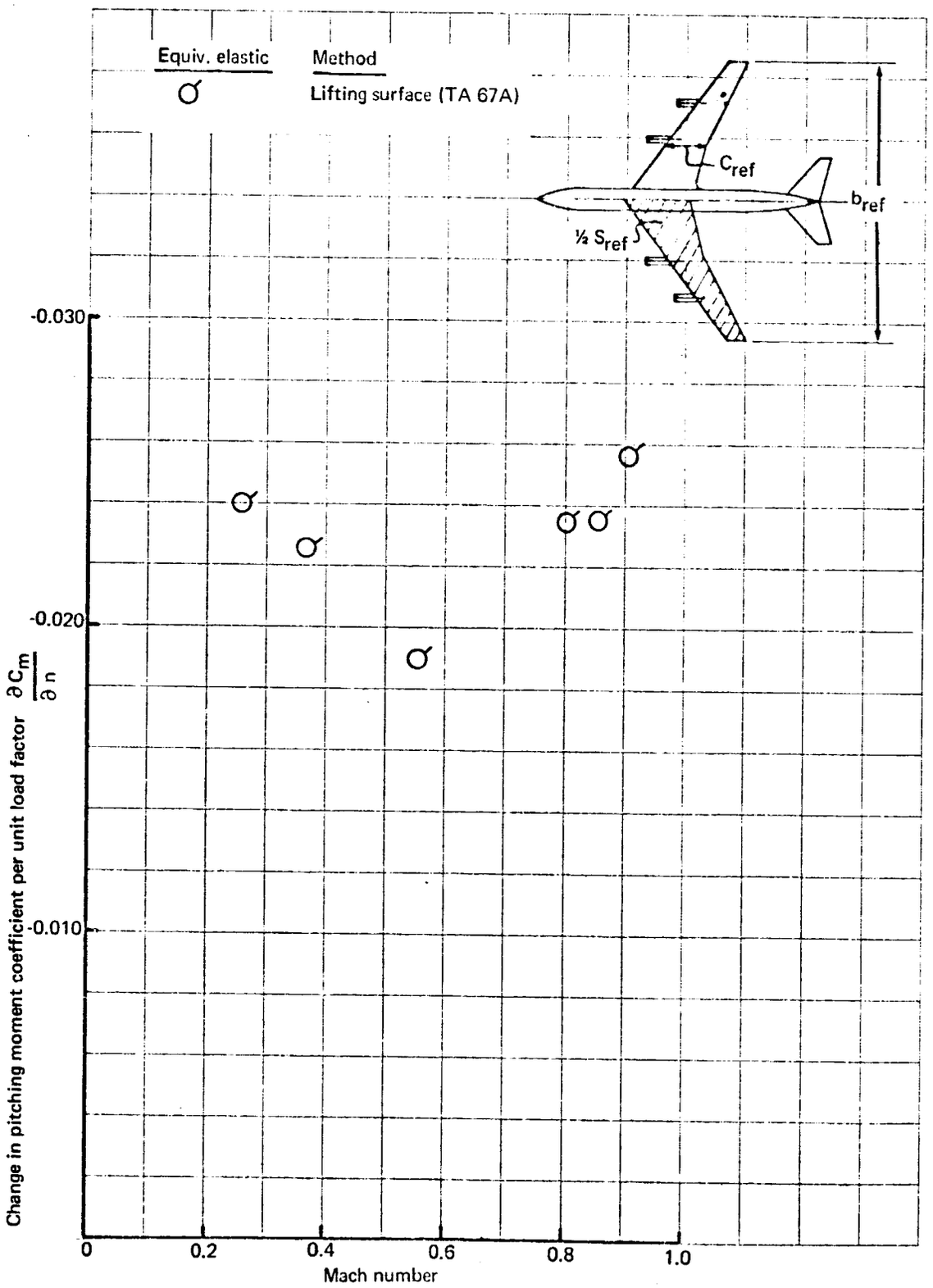

FIGURE 94. - ESTIMATION OF $\frac{\partial C_m}{\partial n}$ *- 707-320B*

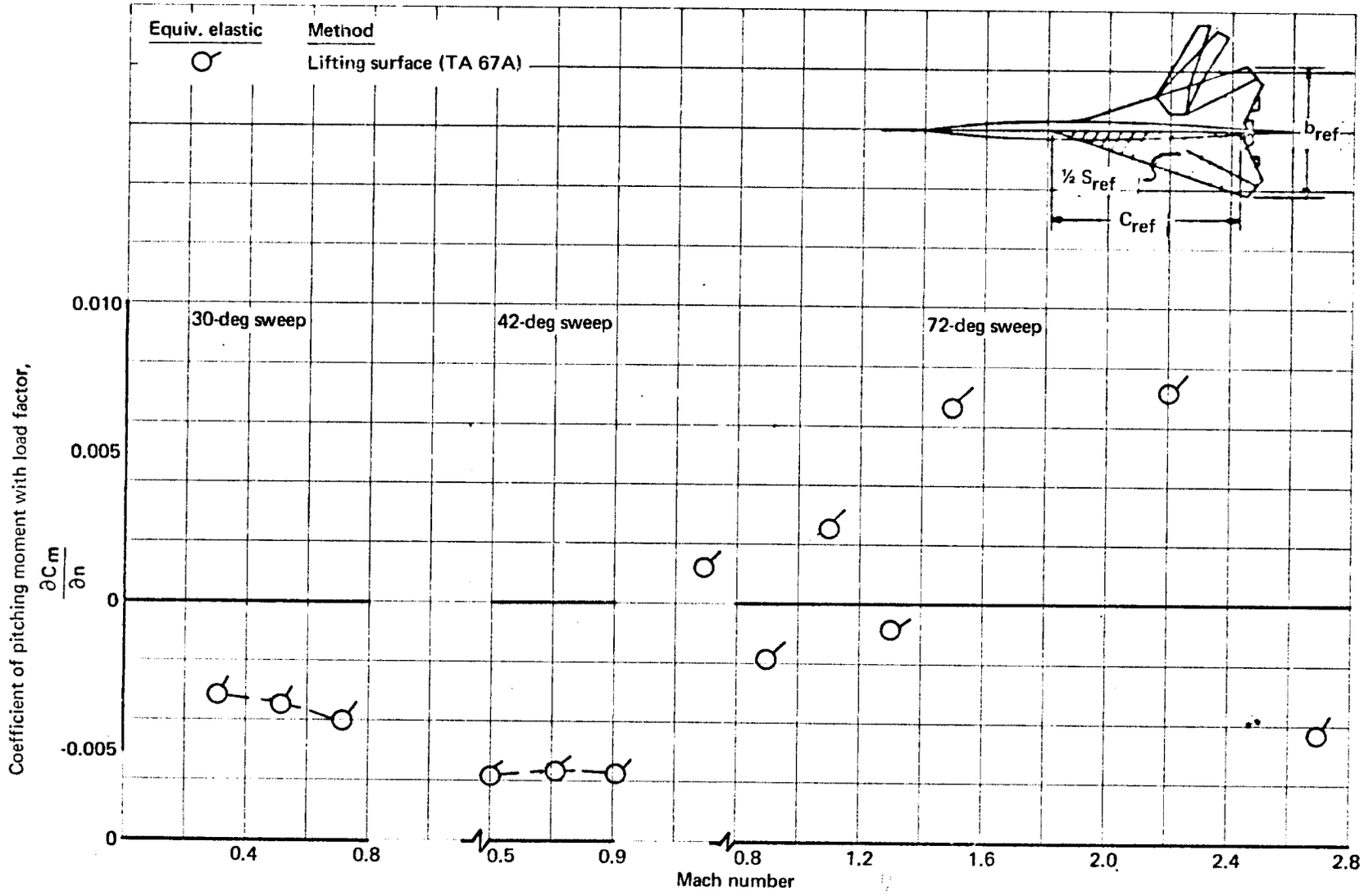

FIGURE 95.– ESTIMATION OF $\frac{\partial C_m}{\partial n}$ *–SST*

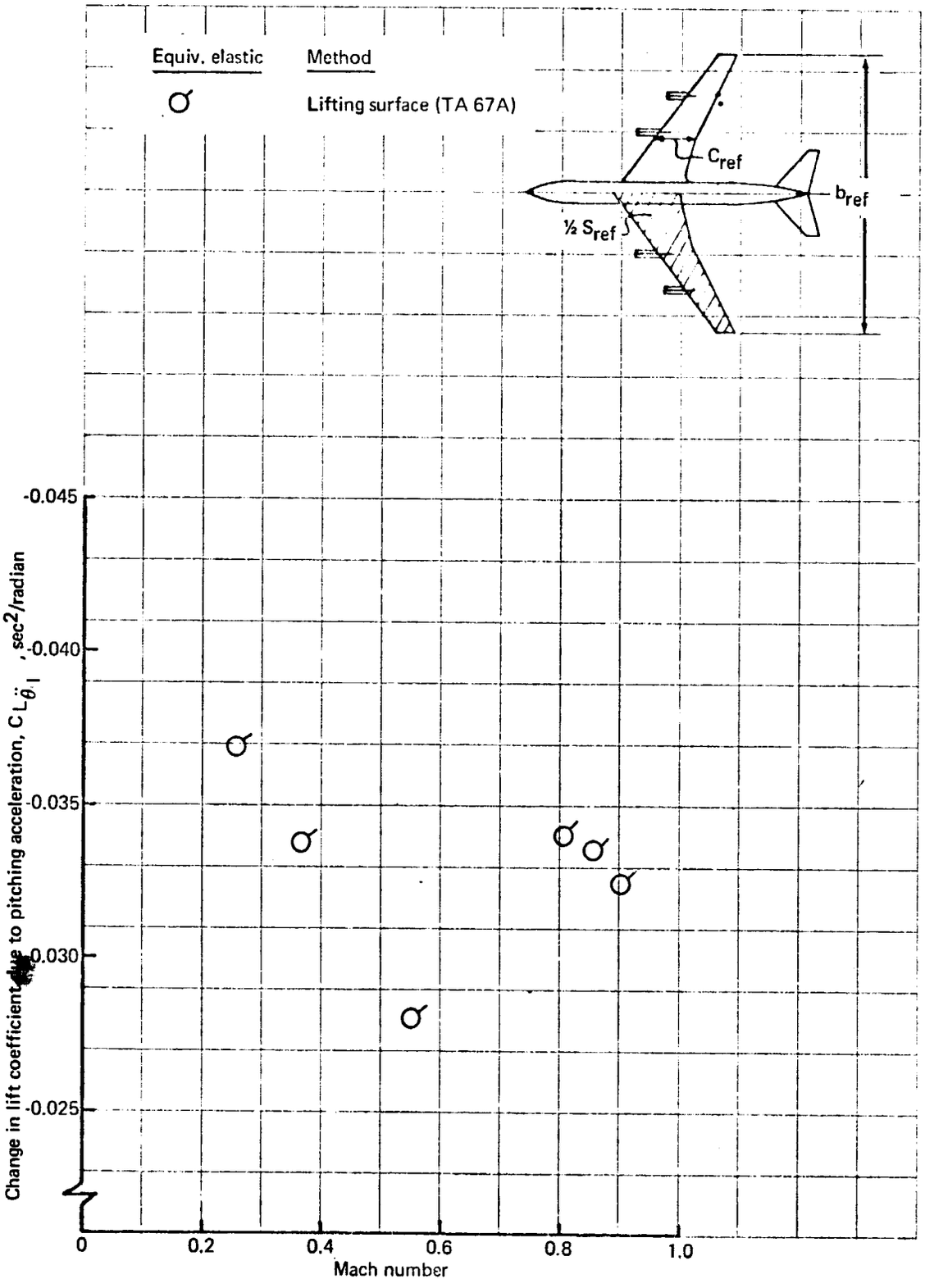

FIGURE 96.– ESTIMATION OF $C_{L_{\ddot{\theta}_I}}$ *–707-320B*

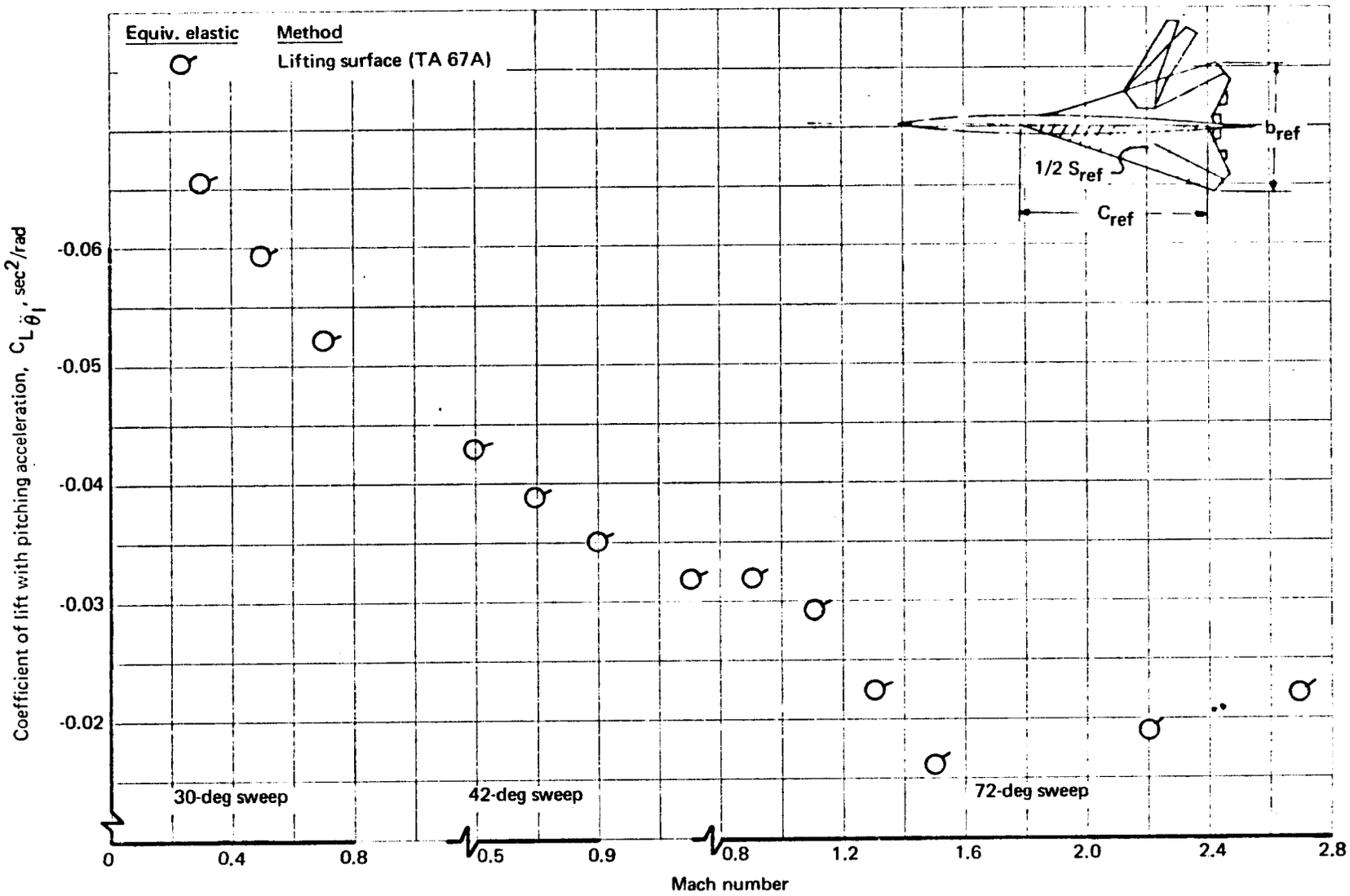

FIGURE 97.– ESTIMATION OF $C_{L_{\ddot{\theta}_I}}$ –SST

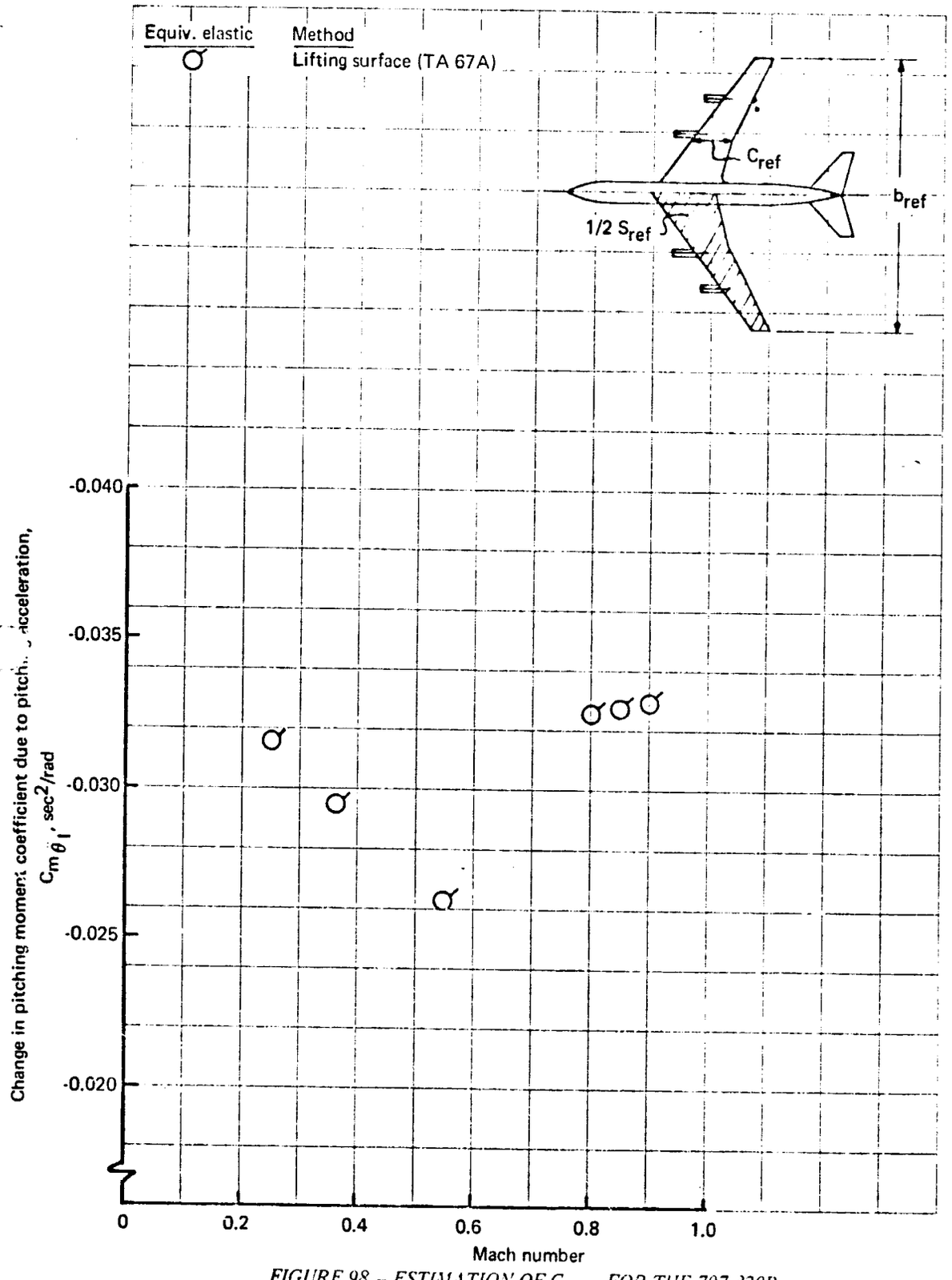

FIGURE 98.- ESTIMATION OF $C_{m_{\dot{\theta}_I}}$ FOR THE 707-320B

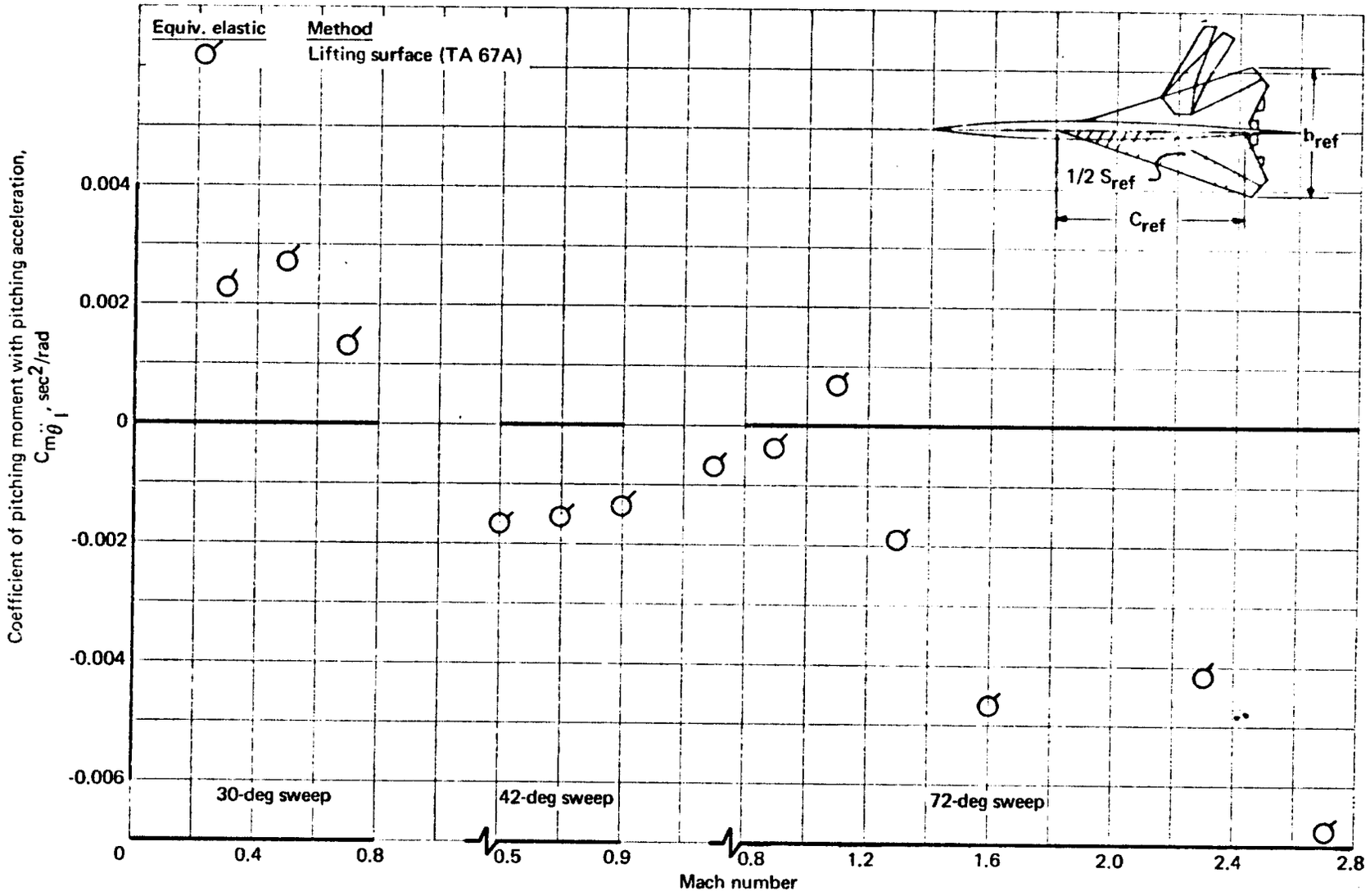

FIGURE 99.– ESTIMATION OF $C_{m_{\ddot{\theta}_I}}$ –SST

8. CONCLUSIONS AND RECOMMENDATIONS

In this appendix an evaluation has been presented of methods for estimating rigid and elastic airplane stability derivatives. Also during this phase of work, investigations were made toward extending and refining the available estimation methods. Conclusions and recommendations concerning specific parts of the investigation are given throughout the report and at the end of each chapter treating the specific areas of work. More general conclusions and recommendations are given below.

8.1 Conclusions

(1) The aerodynamic influence coefficient method using lifting surface theory gives good results for estimation of rigid and equivalent elastic longitudinal stability derivatives.

(2) The aerodynamic influence coefficient method is applicable for generating lateral-directional derivatives; however, because of current computer program limitations and certain aerodynamic representation problems, this method has not yet been put into use for the lateral-directional case.

(3) Handbook methods give generally acceptable results for rigid longitudinal and lateral-directional derivative estimation. However, taken alone, they are inadequate for generating the elastic airplane derivatives.

(4) It is feasible to extend the aerodynamic influence coefficient method to include some nonlinear aerodynamic effects. However, implementation of the procedure may be so involved as to preclude general use.

(5) The residual-flexibility method is a logical approach for solution of dynamic stability and control problems and investigation of ride and handling qualities of elastic airplanes.

(6) Wind tunnel testing of elastic models is very useful in determining elastic stability derivatives. Extreme care in the design and fabrication of models is required to obtain acceptable test data, however.

(7) Explicit expressions can be obtained for the rigid and elastic stability derivatives using lifting surface theory and aerodynamic influence coefficient methods. Implementation of these expressions in computer programs would allow direct computation of the derivatives without the necessity of using the finite differencing procedure required with the the current TA 67A computer program.

8.2 Recommendations for Future Work

(1) The aerodynamic influence coefficient method for estimation of lateral-directional derivatives for rigid and elastic airplanes should be implemented.

(2) Further study should be made of ways to integrate nonlinear aerodynamic effects into the aerodynamic influence coefficient approach. Goal should be to simplify the procedure.

(3) Computer programs should be generated using the explicit stability derivative expressions. Longitudinal and lateral-directional derivatives for rigid and elastic airplanes should be included.

(4) An improved method of calculating vertical-tail elasticity, L_E/L_R, should be developed to eliminate large errors in $C_{n_{\beta E}}$ calculations.

9. REFERENCES

This section includes all of the references for the Summary Report and the three appendixes.

1. Bisplinghoff, R. L.; and Ashley, H.: Principles of Aeroelasticity. John Wiley and Sons, Inc., 1962.

2. Milne, R. D.: Dynamics of the Deformable Airplane, Parts I and II. Her Majesty's Stationery Office, London, 1964.

3. Frazer, R. A.; Duncan, W. J.; and Collar, A. R.: Elementary Matrices. Cambridge University Press, 1952.

4. Etkin, Bernard: Dynamics of Flight. John Wiley and Sons, Inc., 1962.

5. Schwendler, R. G.; and MacNeal, H.: Optimum Structural Representation in Aeroelastic Analysis. ASD-TR-61-680, Computer Engineering Associates, March 1962.

6. Anon.: USAF Stability and Control Handbook. AF33(616)-6460, Douglas Aircraft Company, 1960.

7. Lamb, H.: Hydrodynamics. Second ed., Dover Publications, 1945.

8. Sokolnikoff, I. S.: Mathematical Theory of Elasticity. McGraw-Hill Book Company, Inc., 1956.

9. Hildebrand, F. B.: Advanced Calculus for Engineers. Prentice-Hall, Inc., 1957.

10. Anon.: Military Specification Flying Qualities of Piloted Airplanes. MIL-F-8785 (ASG), April 17, 1959.

11. Anon.: British Civil Airworthiness Requirements. Section D Aeroplanes, Air Registration Board, Issue 8, February 1, 1966.

12. Anon.: Proposal for a Revised Military Specification, Flying Qualities of Piloted Airplanes. MIL-F-8785 (ASG), with Substantiating Text, Bureau of Naval Weapons, Washington, D.C., Report No. NADC-ED-6282, January 18, 1963.

13. Seckel, E.: Stability and Control of Airplanes and Helicopters. Academic Press, Inc., 1964.

14. Babister, A. W.: Aircraft Stability and Control. Pergamon Press, Inc., 1961.

15. Perkins, C. D.: and Hage, R. E.: Airplane Performance, Stability and Control. John Wiley and Sons, Inc., 1957.

16. Kolk, W. R.: Modern Flight Dynamics. Prentice-Hall, Inc., 1961.

17. Abramson, H. N.: The Dynamics of Airplanes. The Ronald Press Company, 1958.

18. Chestnut, H.: and Mayer, R. W.: Servomechanisms and Regulating System Design. Second ed., John Wiley and Sons, Inc., 1963.

19. Graham, D.; and McRuer, D.: Analysis of Nonlinear Feedback Control Systems. John Wiley and Sons, Inc., 1961.

20. Pastel, M. P.: and Thaler, G. J.: Analysis and Design of Nonlinear Feedback Control Systems. McGraw-Hill Book Company, Inc., 1962.

21. Levinson, Emanuel: Nonlinear Feedback Control Systems. Electro-Technology, July through December 1962.

22. Davis, Harold T.: Introduction to Nonlinear Differential and Integral Equations. Government Printing Office, September 1960.

23. Roskam, J.: On Some Linear and Nonlinear Stability and Response Characteristics of Rigid Airplanes and a New Method to Integrate Nonlinear Ordinary Differential Equations. PhD Dissertation, University of Washington, July 1965.

24. Jaffe, Peter: A Generalized Approach to Dynamic-Stability Flight Analysis. JPL Technical Report No. 32-757, July 1965.

25. Hahn, Wolfgang, ed. and trans.: Theory and Application of Liapunov's Direct Method. Prentice-Hall, Inc., 1963.

26. Bisplinghoff; Ashley; and Hoffman: Aeroelasticity. Addison-Wesley Publishing Company, Inc., 1955.

27. Ashley; and Landahl: Aerodynamics of Wings and Bodies. Addison-Wesley Publishing Company, Inc., 1965.

28. Miles, J. W.: The Potential Theory of Unsteady Supersonic Flow. Cambridge University Press, 1959.

29. Chester, W.: Supersonic Flow Past Wing-Body Combinations. The Aeronautical Quarterly, Vol. IV, August 1953, pp. 287-314.

30. Ward, G. N.: Linearized Theory of Steady High-Speed Flow. Cambridge University Press, 1955.

31. Van Dyke, Milton D.: Supersonic Flow Past Oscillating Airfoils Including Nonlinear Thickness Effects. NACA Report 1183, 1954.

32. Bryson, Arthur E.: Stability Derivatives for a Slender Missile with Application to a Wing-Body-Vertical Tail Configuration. J. Aeron. Sci., Vol. 20, May 1953.

33. Landau; and Lifshitz (J. B. Sykes and J. S. Ball, trans.): Mechanics. Addison-Wesley Publishing Company, Inc., 1960.

34. Hayes, W. D.; and Probstein, R. F.: Hypersonic Flow Theory. Academic Press, Inc., 1959.

35. Woodward, F.; LaRowe, E.; and Love, J. E.: Analysis and Design of Supersonic Wing-Body Combinations, Including Flow Properties in Near Field. Part I and II, NASA Report CR-73107, 1967.

36. Anon.: Flight Control and Fire Control System Manual. Vol. II, AE-61-4 II, Bureau of Aeronautics (prepared by Northrop Corporation), September 1952.

37. Francis, J. G. F.: The QR Transformation. Part I, The Computer Journal, Vol. 4, No. 3, October 1961, pp. 263-271. Part II, IBIO, January 1962, pp. 332-345.

38. Wilkinson, J. H.: The Algebraic Eigenvalue Problem. Clarendon Press, Oxford, 1965.

39. Pearce, B. F.; Johnson, W. A.; and Siskind, R. K.: Analytical Study of Approximate Longitudinal Transfer Functions for a Flexible Airframe. ASD-TDR-62-279, June 1962.

40. Samson, F. J.; and Petersen, Harry E.: MIMIC Programming Manual, SEG-TR-67-31, July 1967.

41. Van Dyke, M.: Perturbation Methods in Fluid Mechanics. Academic Press, Inc., 1964.

42. Fung, Y. C.: An Introduction to the Theory of Aeroelasticity. John Wiley and Sons, Inc., 1955.

43. Milne, R. D.: Some Remarks on the Dynamics of Deformable Bodies. AIAA Journal, Vol. 6, March 1968.

44. Anon.: Air Worthiness Standards, Transport Category Airplanes. FAR, Part 25 Federal Aviation Administration.

45. Kuo, B. C.: Automatic Control Systems. Prentice-Hall, Inc., 1962.

46. Korn, G. A.; and Korn, T. M.: Mathematical Handbook for Scientists and Engineers. McGraw-Hill Book Company, Inc., 1961.

47. Hamming, R. W.: Numerical Methods for Scientists and Engineers. McGraw-Hill Book Company, Inc., 1962.

48. Anon.: International Dictionary of Applied Mathematics. D. van Nostrand Company, Inc., 1960.

49. Duncan, W. J.: The Principles of the Control and Stability of Aircraft. Cambridge University Press, 1956.

50. Rheinfurth, Mario H.; and Swift, Frederick W.: A New Approach to the Explanation of the Flutter Mechanism. NASA TN D-3125, 1966.

51. Haus, F. C.; Czinczenheim, J.; and Moulin, L.: The Use of Analog Computers in Solving Problems of Flight Mechanics. Agardograph 44, June 1960.

52. Chetayev, N. G.: The Stability of Motion. Pergamon Press, Inc., 1961.

53. Malkin, I. G.: Theory of Stability of Motion. AEC-TR-3352, translated from the publication of the State Publishing House of Technological-Theoretical Literature, Moscow-Leningrad, 1952.

54. Lefferts, Eugene J.: A Guide to the Application of the Lyapunov Direct Method to Flight Control Systems. NASA CR-209, 1966.

55. Bryan, G. H.: Stability in Aviation. The Macmillan Company, 1911.

56. Milne-Thomson, L. M.: Theoretical Aerodynamics. The Macmillan Company, 1948.

57. Green, A. E.; and Zerna, W.: Theoretical Elasticity. Clarendon Press, Oxford, 1960.

58. Pearce, B. F.: Topics on Flexible Airplane Dynamics, Part I. ASD-TDR-63-334, Systems Technology, Inc., Inglewood, California, 1963.

59. Heaslet, Max A.; Lanar, Harvard; and Jones, Arthur L.: Volterra's Solution of the Wave Equation as Applied to 3-Dimensional Supersonic Airfoil Problems. NASA Report No. 889, Ames Aeronautical Laboratory, Moffett Field, California, April 14, 1947.

60. Pope, A.: Basic Wing and Airfoil Theory. McGraw-Hill Book Company, Inc., 1952.

61. Nelson, H. C.; and Berman, J. H.: Calculations on the Forces and Moments for an Oscillating Wing-Aileron Combination in Two-Dimensional Potential Flow at Sonic Speeds. NACA TN 2590, 1952.

62. Rubbert, P. E.; et al.: A General Method for Determining the Aerodynamic Characteristics of Fan-in-Wing Configurations. Vol. I -Theory and Application. USAAVLABS Technical Report 67-61A, 1967.

63. Campbell, J. P.; Johnson, J. L., Jr.; and Hewes, D. E.: Low-Speed Study of the Effect of Frequency on the Stability Derivatives of Wings Oscillating in Yaw with Particular Reference to High Angle-of-Attack Conditions. NACA RM L55H05, 1955.

64. Weissinger, J.: The Lift Distribution of Swept Back Wings. NACA TM 1120, 1947.

65. Tekhonov; and Samarskii (A.R.M. Robson and P. Basu, trans.): Equations of Mathematical Physics. Pergamon Press, Inc., 1963.

66. Royal Aeronautical Society Data Sheets, 1955.

67. Anon.: Aerodynamic Characteristics of Non-Straight-Taper Wings. AFFDL-TR-66-73, General Dynamics, Fort Worth Division, October 1966.

68. Gray, W. L.; and Schenk, K. M.: Method for Calculating the Subsonic Steady-State Loading on an Airplane with a Wing of Arbitrary Planform and Stiffness. NACA TN 3030, 1953.

69. Johnson, J. L., Jr.: Low-Speed Measurements of Static Stability, Damping in Yaw, and Damping in Roll of a Delta, a Swept and an Unswept Wing for Angles-of-Attack from 0° to 90°. NACA RM L56B01, 1956.

70. Wiley, H. G.: The Significance of Nonlinear Damping Trends Determined for Current Aircraft Configurations. NASA U-59-15, September 1966.

71. Flack, Nelson D.: AFFTC Stability and Control Techniques. USAF Flight Test Center, Edwards Air Force Base, California, AFFTC-TN-59-21, 1959.

72. Campbell, J. P.; and McKinney, M. O.: Summary of Methods for Calculating Dynamic Lateral Stability and Response and for Estimating Lateral Stability Derivatives. NACA TR 1098, 1952.

73. Kohlman, D. L.; and Drake, L. R.: Handbook for Estimating C_{l_β} for Rigid and Elastic Airplanes at Subsonic and Supersonic Speeds. Center for Research Inc., Engineering Science Division, The University of Kansas, Lawrence, Kansas, 1966.

74. Pearce, B. F.; and Siskind, R. K.: Topics on Flexible Airplane Dynamics, Part II. The Application of Flexible Airframe Transfer Function Approximations and the Sensitivity of Airframe Transfer Functions to Elastic Mode Shapes. ASD-TDR-63-334, Part II, July 1963.

75. Pass, H. R.; Pearce, B. F.; and Wolkovitch, J.: Topics on Flexible Airplane Dynamics, Part III. Coupling of the Rigid and Elastic Degrees of Freedom on an Airframe. ASD-TDR-63-334, Part III, July 1963.

76. Pass, H. R.; and Pearce, B. F.: Topics of Flexible Airplane Dynamics, Part IV. Coupling of the Rigid and Elastic Degrees of Freedom of an Airframe-Autopilot System. ASD-TDR-63-334, Part IV, July 1963.